The University of Nottingham

GIBBERELLIN BIOSYNTHESIS AND SIGNALLING IN ARABIDOPSIS ROOT GROWTH

Richard Barker

2011

PhD: PLANT SCIENCE

Supervisors: Peter Hedden[1], Steve Thomas[1], Andy Philips[1], Simon Vaughan[1], and Malcolm Bennett[2].

1. Rothamsted research 2. The University of Nottingham

PERSONAL STATEMENT

First thanks should be to Yuiko Takebayashi, without her I doubt I would have survived my undergrad degree let alone entertained the thought that I was capable of a PhD! Next I'd like to thank Tanya Curtis, as when times were difficult she told me to "stop being an idiot and work harder" in her usually assertive manner. I have a lot of energy so the next person to help me control this energy was Barbora Ndreca, if it wasn't for her I would never have learn salsa or got Lucia into capoeira! Then my new sister came into my life Aakriti Wanchoo, I've always wanted to be royalty and now I have an Indian princess in my family that goal in life has been achieved. I should also thank the rest of the lab Andy Phillips, Dennise Ward, Ian Prosser, Stephen Pearce, Tully Urnst, Andy Placket, Robert Jackson, Anne Grønlund, Jayne Griffiths, Ellen Colebrook and particularly Simon Vaughan for all the help and advice they gave me. I owe a huge debt of gratitude to Malcolm Bennett for offering me this opportunity, he is a genius but I did try not to always agree with him, which is difficult particularly when he's usually right! I liked it when he did the whole good cop/bad cop thing but in solo, very funny! Zoe Wilson and Ranjan Swarup were both inspirational lecturers when I was an undergraduate and I am very lucky to have continued learning from them as a post-graduate. Now finally I'd like to thank my two mentors, two men so full of love for GA that one couldn't help but be caught up in it, Prof Peter Hedden and Dr Steve Thomas. These are possibly two of the greatest men I'll ever work with and I doubt I'll ever enjoy working for anyone as much as I have for them. Peter's fascination for all things related to GA on every scale imaginable is incredible, but what must be even more amazing is what he must also know about GA on an unimaginable scale!! Steve, is due so much respect not only because of his outstanding research career and beautiful family but also because he's a party animal who made it good in his choice of career. Finally and most importantly, I'd also like to thank my parents and grandparents for bringing me into this world, teaching me the value of plants and then believing in me.

1 ABSTRACT

Using targeted expression of a constitutively active repressor of GA signalling Susana Ubeda-Tomas *et al.,* (2007) demonstrated that GA action in endodermal cells is necessary for correct root growth. However, GUS studies have shown the final and penultimate GA-biosynthetic genes are not expressed in the endodermis, indicating movement of GAs may be required. This study used the targeted mis-expression of GA degrading enzymes in Col-0 and the attempted targeted rescue of GA biosynthetic and signalling mutants, using the corresponding GA metabolic or signalling component, to gain an insight into the localisation of important GA biosynthesis and signalling sites.

This study has demonstrated that GA_{12} can be made by epidermal, cortical and endodermal cells. However, the ground tissue of the elongation zone does not contain GA_{12} due to the early GA biosynthetic enzymes only being expressed within cells with a close proximity to the QC. Subsequently the 20-oxidation converts GA_{12} to GA_{15}, to GA_{24} to GA_9. These reactions mobilise GA allowing it to move from the meristematic region to the elongation zone. GA20ox and GA3ox activity is required in both the meristematic region and the elongation zone for correct root growth to occur. In addition, GA metabolic components are subject to tissue specific GA feedback regulation as a result of post-transcriptional processing and/or post-translational modifications to their protein stability.

GA perception in any tissue of the elongation zone can promote complete cell elongation, suggesting that any one tissue can elongate it neighbours, or that each cell is capable of releasing a signal to ensure they all elongate proportionally. The transcriptional network within the endodermis has a disproportionately important role in GAs regulation of cell division within the root proximal meristem but GA action in other cell types is also required. The cambian and bundle sheath cells in aerial tissue like the endodermis in the root contain an important transcriptional network that promotes GA dependant growth.

1.1 LIST OF FIGURES

1.2 LIST OF TABLES

1.3 ABBREVIATIONS

µM	Micro molar
µg	Micro grams
ABA	Absistic acid
ACC	1-amino-cyclopropane-1-carboxylic acid
ARR	*Arabidopsis response regulator*
At	*Arabidopsis*
BP	Base pair
BR	Brassinosteroids
BRX	*Brevis radix*
CAB	Chlorophyll binding protein
cm	Centimetre
Col-0	Columbia
CoR	Cortical expression elongation zone (At1G09750)
Co2	Cortical expression meristematic zone (At1G62500)
CPS	*ent*-copalyl diphosphate synthase
DNA	Deoxyribonucleic acid
DNAase	Deoxyribonuclease
dNTP	Deoxyribonucleotide triphosphate
DTT	Dithioreitol
ETC	Enhancer of tritychon and caprice
ER	Endoplasmic reticulum
EUI	*Elongated uppermost internode*
ECI	Endodermal/cortical initial
ELRC	Epidermal/lateral root cap initial cells
GA	Gibberellin
GAI	*Gibberellin insensitive*
GA20ox	*Gibberellin 20-oxidase*
ga20ox1,-2,-3	*ga20ox1-3 ga20ox2-1 ga20ox3-1*
GA2ox	Gibberellin 2-oxidase
GA3ox	Gibberellin 3-oxidase
ga3ox1,-2	*ga3ox1-3 ga3ox2-1*
GAMT	*GA methyltransferase*
GID1	Gibberellin insensitive dwarf
gid1a,-b,-c	*gid1a-1 gid1b-2 gid1c-1*
GFP	Green florescent protein
GL2	*Glabra 2*
GC-MS	Gas chromatography mass spectrometry
HRGP	Hydroxyproline-rich glycoproteins
YFP	Yellow florescent protein
HSL	Hormone sensitive lipase
HPLC	High performance chromatography
IPTG	Isopropyl-beta-D-thiogalactopyranoside
JKD	*Jackdaw*
KAO	*Kaurenoic acid oxidase*
Kb	Kilobase
KO	*ent-kaurene oxidase*
KS	*Kaurene synthase*

LSD	Least significant difference
MES	2-(N-Morpho;ino) ethanesulfonic acid
min	Minute
mins	Minutes
mRNA	Messenger ribonucleic acid
MS	Murashige and Skoog Basal Salk Mixture
mm	Millimetres
mM	Milli molar
MGP	*Magpie*
NUC	*Nuttcracker*
OD	Optical density
Os	*Oryza sativa*
PAC	Paclobutrazol
PCD	Programmed cell death
PCR	Polymerase chain reaction
PIL	*Phytochrome interacting factor like*
PIF	*Phytpchrome interacting factor*
Phy	Phytochrome
PM	Proximal meristematic
Ps	*Pisum sativum*
RAM	Root apical meristem
RGA	*Repressor of ga1-3*
RGL-1	*Repressor of ga1-3 like 1*
RGL-2	*Repressor of ga1-3 like 2*
ROS	Reactive oxygen species
RSA	Root system architecture
REML	Residual maximum likelihood
SAM	Shoot apical meristem
SCR	*Scare crow*
SCL3	*Scarecrow like 3*
SED	standard error of the difference
SE	Standard error
SLR	*Slender (rice)*
SLY	*Sleepy*
SOD	Super-oxide dismutase
SHR	*Short root*
TBE	Tris borate EDTA buffer
TZ	Transition zone
UV	Ultraviolet
QC	Quiescent centre

1 INTRODUCTION

1.1 GENERAL INTRODUCTION TO GIBBERELINS (GA)

Gibberellins (GAs) are a large group of tetracyclic diterpenoid carboxylic acids, with 136 different compounds currently known in higher plants, fungi and bacteria (http://www.plant-hormones.info), but only a few of these, including GA_1, GA_3, GA_4 and GA_7 show biological activity. Studies with GA-deficient and signalling mutants have revealed that GAs are plant hormones which are involved in a variety of aspects of plant growth and development, such as seed germination, leaf expansion, stem elongation, flowering initiation, reproductive development and root growth (Achard et al., 2007, Peng and Harberd, 2002, King et al., 2001). GAs were discovered in exudates of the phytopathogenic fungus *Gibberella fujikuroi*, which caused over-growth symptoms in infected rice plants, known as the bakanae or foolish seedling disease (Stowe and Yamaki, 1957). Impure crystals containing three active components were separated from a fungal filtrate and subsequently named gibberellin A_1, A_2 and A_3 (Takahashi et al., 1955). It is now common practice to refer to gibberellin A_n as GA_n and to use GA as a general abbreviation for gibberellin (Macmillan and Takahashi, 1968).

GA metabolism is extremely dynamic (summaried in Figure 1-1): modifications to the rate of synthesis and inactivation have an important role in regulating plant growth in response to an array of biotic and abiotic stimuli. It is now known that many of these external environmental factors regulate plant growth and development by controlling GA signalling, either directly by modifying the metabolic pathway (Achard et al., 2006) or indirectly via hormonal cross talk with IAA (Fu and Harberd, 2003) and ethylene (Dugardeyn et al., 2008, De Grauwe et al., 2008). Mutant plants that are insensitive to GAs or deficient in their production exhibit severe developmental abnormalities including dwarfism. A forward genetic approach in *Arabidopsis* identified a variety of GA-deficient mutant lines (Koornneef and Vanderveen, 1980), one of which, *ga1-3* contains a loss-of-function mutation in the *GA1* gene resulting in the complete abolishment of GA biosynthesis; this GA-

deficient mutant line is now widely used as a positive control for severe GA deficiency (Yamaguchi, 2008).

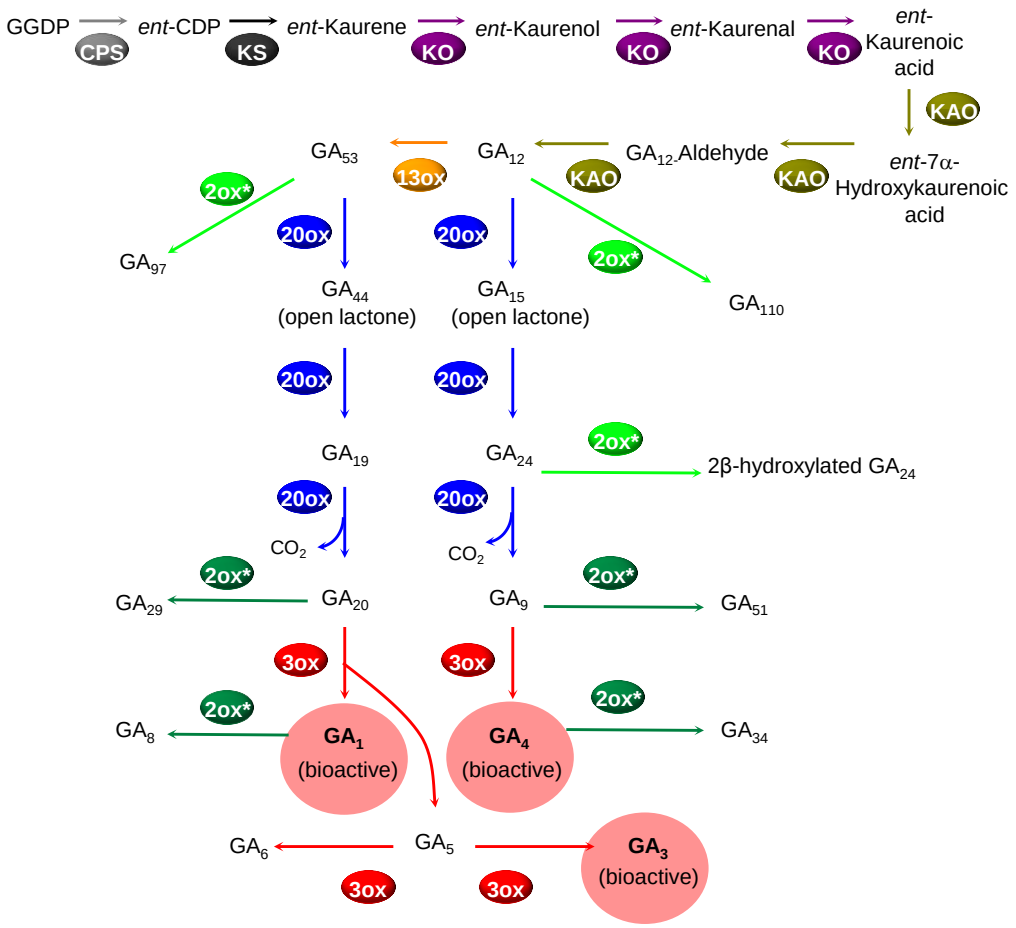

Figure 1-1: **A schematic diagram summarising GA metabolism**. (Adapted with permission from Shinjiro Yamaguchi., (2008)).

Mutants with reduced GA signalling share a wide array of phenotypes such as male-sterility, non-germinating seeds, dark green leaves, shorter roots, compact twisting rosette leaves, short filaments and are generally severely dwarfed due to shorter internodes. If the mutation is in GA biosynthetic genes the plants can be rescued by the application of bioactive GA but not if the mutation is in one of the GA signal transduction components. The crop breeding efforts and large scale industrialisation of food production in developed countries in what is now known as "the green revolution" has been instrumental in preventing widespread food shortages (Hedden, 2003) and may have an important role in the future (Figure 1-2). One of the reasons for the success of the green revolution was the discovery of higher-yielding varieties of wheat and rice that

were resistant to lodging due to their reduced stature. This combined with improved irrigation and the increased application of nitrogen fertilizer resulted in shorter, sturdier, semi-dwarf varieties which had an improved harvest index and higher yields (Hanson et al., 1982). It was later discovered that these dwarfing genes encoded mutant forms of either GA biosynthetic genes or downstream signalling targets. Understanding the mechanisms that modulate GA biosynthesis and/or signalling will help explain how these increased yields occurred during the 'Green Revolution' and may provide novel ways of increasing future crop yields (Hedden, 2003).

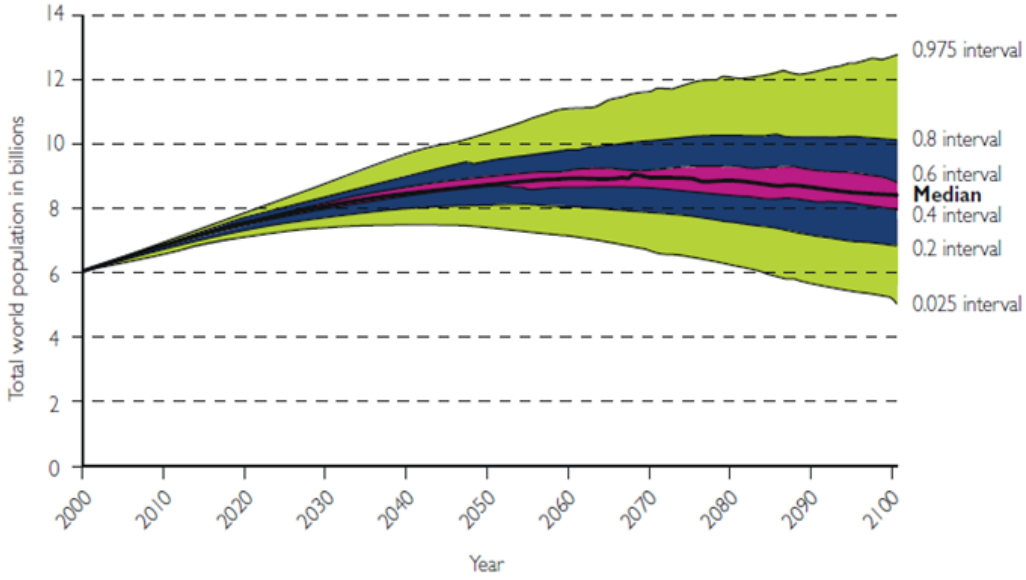

Figure 1-2: **Projected total world population in billions**: probabilistic projections until 2100 (green 98% interval; blue 60% interval; pink 20% interval) (source: The future of food and farming: challenges and choices for global sustainability 2011).

1.2 GA BIOSYNTHESIS

1.2.1 GGPP to GA12

Geranylgeranyl diphosphate (GGDP) is a common precursor of diterpenoids, including the phytol side-chain of chlorophylls, and also of tetraterpenoids, such as the catotenoids. During the biosynthesis of GAs GGPP is converted to *ent*-kaurene via a two-step cyclization reaction that is catalysed first by *ent*-copalyl diphosphate synthase (CPS), which creates the intermediate *ent*-copalyl diphosphate (*ent*-CDP), which is converted to *ent*-kaurene by *ent*-kaurene synthase (KS). *ent*-Kaurene is then converted to *ent*-kaurenoic acid via a three step oxidation reaction that involves two intermediates *ent*-kaurenol and *ent*-kaurenal. This reaction is catalysed by the membrane-bound cytochrome-P450-dependent mono-oxygenase *ent*-kaurene 19-oxidase (KO). Subsequently, *ent*-kaurenoic acid is converted to GA_{12} via two intermediates *ent*-7α-hydroxykaurenoic acid and GA_{12}-aldehyde. All three reactions, 7β-hydroxylation, the contraction of the B-ring to form GA_{12}-aldehyde and oxidation of C-7 from an aldehyde to a carboxylic acid are catalysed by a second cytochrome-P450-dependent mono-oxygenase *ent*-kaurenoic acid oxidase (KAO) (Macmillan, 1997, Hedden, 1997) (Figure 1-3).

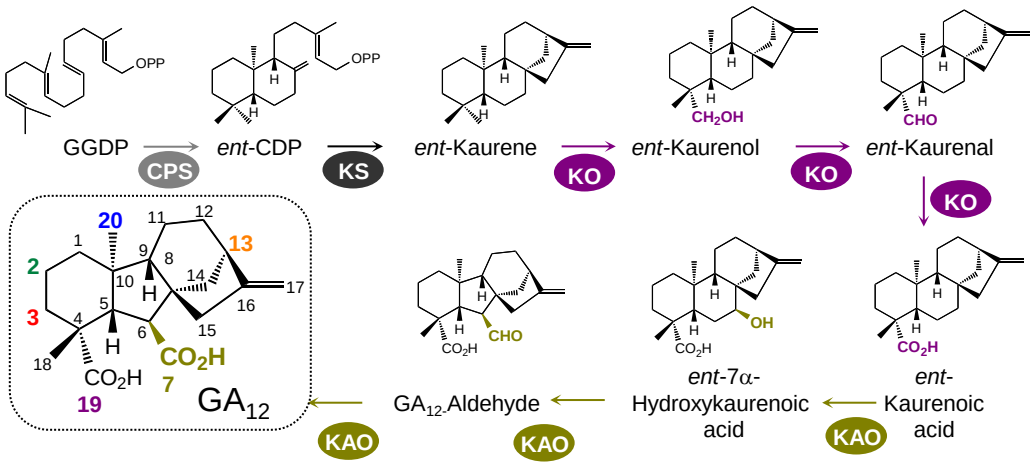

Figure 1-3: **Early GA biosynthetic genes.** GGDP is converted by CPS to *ent*-CDP, which is converted to *ent*-kaurene by KS. *ent*-kaurene is oxidised to *ent*-kaurenoic acid by KO, via the *ent*-kaurenol and ent-kaurenal intermediates. *ent*-Kaurenoic acid is then converted to GA_{12} via ent-7α-hydroxykaurenoic acid and GA_{12}-aldehyde by KAO (Used with permission from Shinjiro Yamaguchi., (2008)).

1.2.2 Oxidation of GA_{12} to GA_9 and GA_{20}

GA_{12} and its 13-hydroxylated analogue GA_{53}, are converted to GA_9 and GA_{20}, respectively, by the GA 20-oxidase (GA20ox) enzyme. The three-step sequential oxidation of C-20 eventually results in the formation of the C_{19} GA_{20} or GA_9 and the release of CO_2 (Figure 1-4). The importance of these later steps in controlling GA levels is illustrated by a study with *Arabidopsis* demonstrating that an increase in the level of *AtGA20ox* expression results in higher levels of bioactive GAs and subsequently increased growth (Coles et al., 1999). In contrast, over-expressing genes that encode earlier GA-biosynthetic enzymes does not have this effect (Fleet et al., 2003), indicating that the later steps are rate limiting. There are five homologues of the GA20ox enzymes in *Arabidopsis*; these enzymes act partially redundantly due to their distinct but overlapping expression patterns. Reverse genetics has revealed that GA20ox activity is required for normal stem internode, hypocotyl, anther filament, and silique elongation and also impacts on fertility, thereby affecting seed numbers (Rieu et al., 2008b).

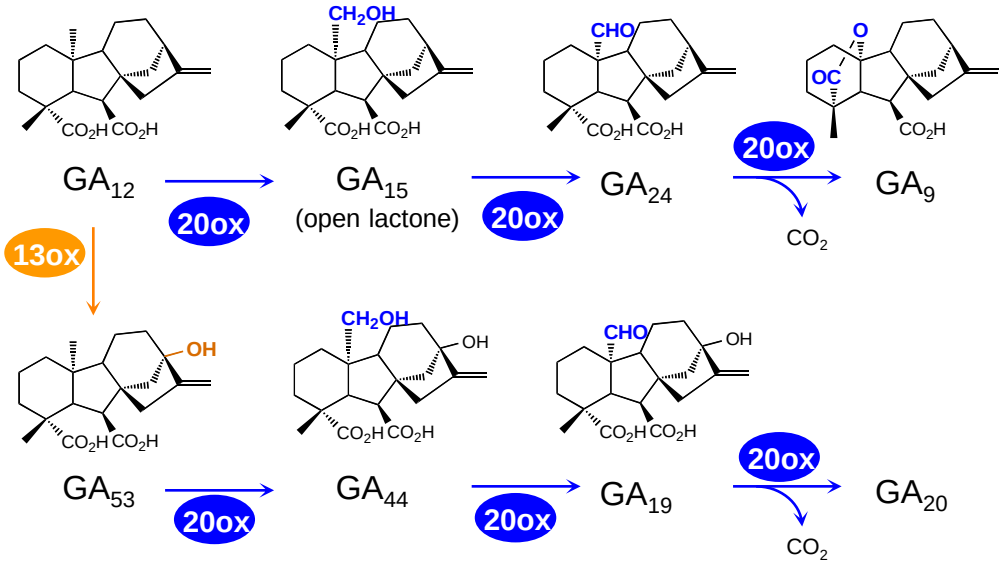

Figure 1-4: **Conversion of C_{20}-GAs to C_{19}-GAs by CO_2 removal via 20-oxidation.** The 13-oxidation results in conversion of GA_{12} to GA_{53}. There are subsequently two parallel sequences of reactions catalysed by GA20ox, the conversion of GA_{12} to GA_9 via the two intermediates GA_{15} and GA_{24} and the conversion of GA_{53} to GA_{20} via the two intermediates GA_{44} and GA_{19} (Adapted with permission from Shinjiro Yamaguchi., (2008)).

1.2.3 GA activation

The final step in GA biosynthesis is catalyzed by the GA 3β-hydroxylase (GA3ox) enzymes and involves the 3β-hydroxylation of GA_9 or GA_{20} to the bioactive products GA_4 and GA_1, respectively (Yamaguchi, 2008, Hedden and Kamiya, 1997). During GA-biosynthesis, the formation of the lactone ring, C-3β hydroxyl group, and C-6β carboxyl group are all essential steps, but the creation of the 3-hydroxyl group by the GA3ox enzyme is the final step in the synthesis of the biologically active hormone. This 3-hydroxyl group is necessary for GA activity due to the hydrogen bond it forms with the GID1 receptor and a bridging water molecule (Shimada et al., 2008, Murase et al., 2008). The GA20ox and GA3ox enzymes appear to be the most highly regulated enzymes involved in GA biosynthesis (Figure 1-5), illustrating their critical role in determining GA concentration. In all plants studied so far the GA20ox and GA3ox enzymes are encoded by multi-gene families, the members of which display distinct spatial and temporal expression patterns, this is in contrast to enzymes earlier in the biosynthetic pathway which are mostly encoded by single genes (Hedden and Phillips, 2000). In *Arabidopsis* the GA3ox family consists of four homologues AtGA3ox1 and AtGA3ox2 primarily regulate vegetative and root growth while AtGA3ox3 and AtGA3ox4 have been shown to coordinate flowering.

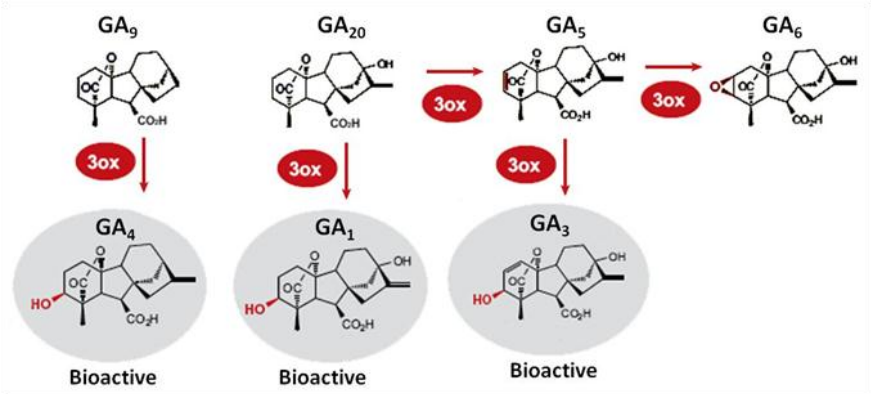

Figure 1-5: **GA activation by 3-oxidation.** GA3ox catalyses the conversion of GA_9 to the biologically active GA_4 and GA_{20} to the biologically active GA_1, GA_{20} can be converted by some GA3ox enzymes to GA_5 and then to GA_6 or the biologically active GA_3 (Adapted with permission from Shinjiro Yamaguchi., (2008)).

1.3 GA DEACTIVATION

1.3.1 GA deactivation by C-2 oxidation

The 2β-hydroxylation and in some cases the subsequent further oxidation of C-2 to a ketone is catalyzed by GA 2-oxidases (GA2ox) (Figure 1-6) and is possibly the best characterized form of GA deactivation. High levels of 2β-hydroxy GAs have been found in many species suggesting that this is a mechanism that is widely used to reduce active GA levels in plants (MacMillan, 2001). The importance of these enzymes in deactivating bioactive GAs and their precursors has been illustrated by studies showing that their over-expression results in a GA-deficient dwarf phenotype and in addition mutations within them affects a wide array of biological processes (Rieu et al., 2008a). As well as deactivating bioactive GAs such as GA_4 and GA_1, the GA 2-oxidases can also hydroxylate GA precursors such as GA_9 and GA_{20}, converting them to products that cannot be reactivated.

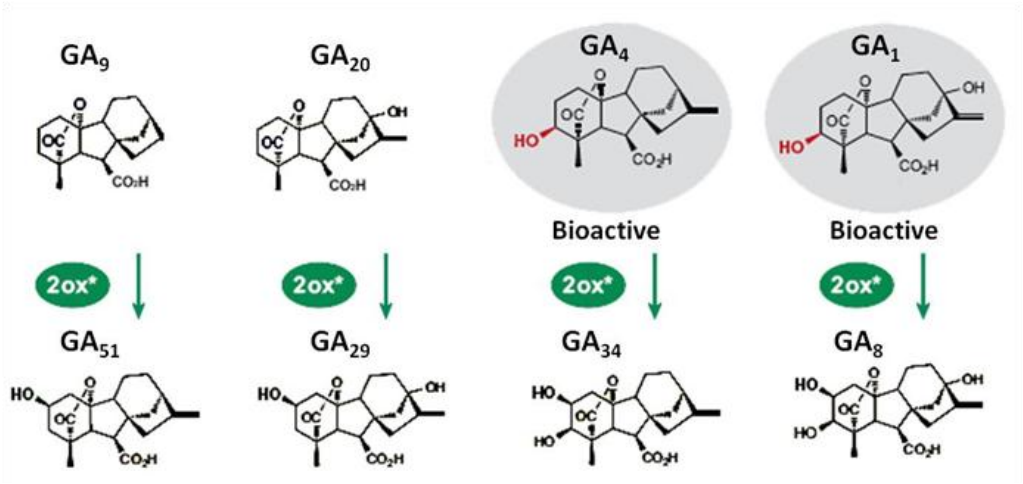

Figure 1-6: **GA deactivation by 2-oxidation.** A group of GA 2-oxidases can catalyse the oxidation of C-2 on C_{19}-GA precursors such as GA_9 and GA_{20} before activation and on C_{19}-GAs such as GA_4 and GA_1 after 3β-oxidation has activated them (Adapted with permission from Shinjiro Yamaguchi., (2008)).

In plants, there are at least two distinct clades of GA 2-oxidase enzymes (Figure 1-7-B) (Huang et al., 2010); The clade containing enzymes that act on C_{19}-GAs is made up of 2 sub-clades, contain the enzymes described above that are able to deactivate bioactive GAs and their C_{19}-GA precursors. Members of the other distinct GA2ox clade act specifically on C_{20}-GA precursors and not on the C_{19}-GAs (Figure 1-7-A) (Schomburg et al., 2003, Thomas et al., 1999). In *Arabidopsis* five C_{19}-GA 2-oxidases have been cloned so far and two C_{20}-GA 2-oxidases (Schomburg et al., 2003, Thomas et al., 1999). The various GA 2-oxidases have been shown to be expressed in all plant tissues, albeit at a wide range of different levels. The phenotype of the *Arabidopsis* C_{19}-GA 2ox quintuple knockout mutant highlights the vital role these enzymes play in regulating GA concentrations in a variety of different tissues and during many different developmental processes from seed germination to the timing of the transition from vegetative to floral growth (Rieu et al., 2008a).

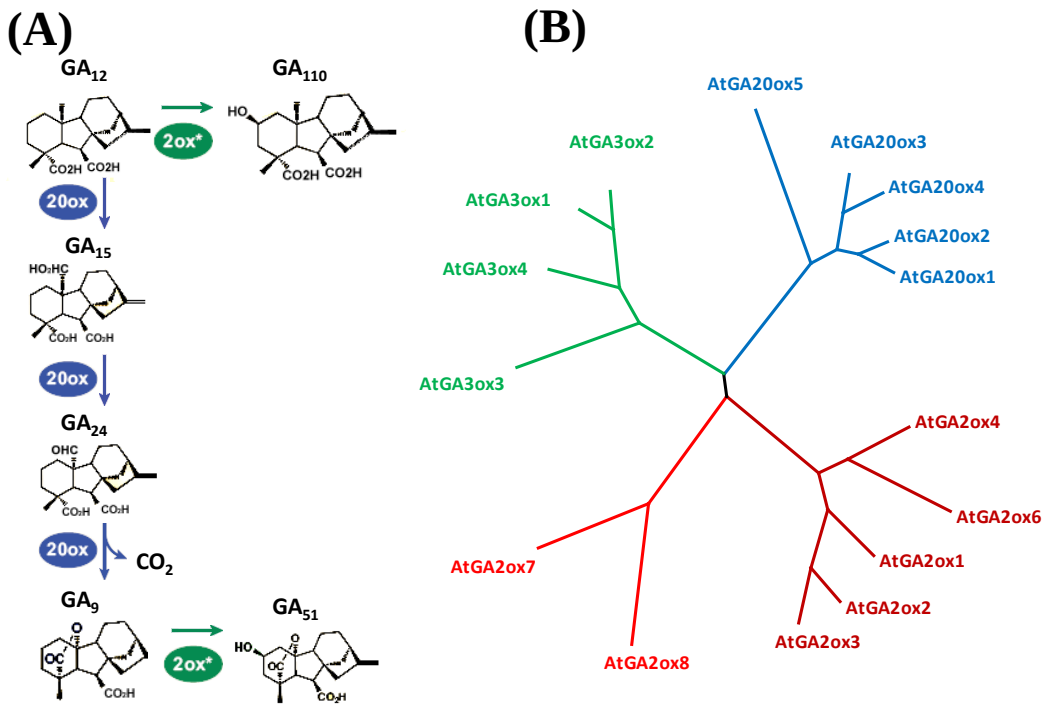

Figure 1-7: **GA deactivation by 2-oxidation is controlled by two distinct clades.** (A) The oxidation of C-2 can take place on C_{20}-GAs such as GA_{12} and C19-GAs such as GA_9 by members of a separate clade of GA 2-oxidases (Adapted with permission from Shinjiro Yamaguchi., (2008)). (B) Unrooted phylogenetic tree for *Arabidopsis* GA-oxidase genes showing the distinct clades responsible for oxidation of C_{20}-GAs and the sub-clades of C_{19}-GA GA2ox genes in red (Courtesy of Peter Hedden).

1.3.2 Other GA inactivation mechanisms

A mutation in the *ELONGATED UPPERMOST INTERNODE* (*EUI*) gene in rice has revealed a cytochrome P450 monooxygenase enzyme that is capable of catalysing the 16α,17- epoxidation of non-13-hydroxylated GAs (Figure 1-8) (Zhu et al., 2006). The 16α,17-$[OH]_2$-GAs products, resulting from hydration of the epoxide, have also been found in GA samples extracted from other plant species such as *Pisum sativum* fruits and developing *Malus domestica* seeds, suggesting that 16α,17- epoxidation of GAs occurs widely and may be a common mechanism for GA deactivation. However it is unclear whether the epoxide hydration is an enzymatic or non-enzymatic reaction (Santes et al., 1995, Hedden et al., 1993). It has also been shown that plants contain GA methyltransferases (GAMTs) that are capable of catalyzing the transfer of a methyl group from S-adenosine-L-methionine to the C-6 carboxyl group creating GA methyl esters. Over-expression of these genes in *Arabidopsis*, tobacco (*Nicotiana tabacum*), and petunia (*Petunia hybrida*) can create a GA-deficient dwarf plant with other typical GA-deficient phenotypes, such as reduced fertility. Examining the expression patterns of the two *Arabidopsis GAMT* homologues from the *SABATH* family revealed that they are differentially expressed and confined to the silique, suggesting that they have a role in seed development and dormancy (Eckardt, 2007, Varbanova et al., 2007). No obvious wheat or rice homologues for GAMTs have been found, possibly indicating that GA methylation does not have a significant role in all plant species (Hirano et al., 2008).

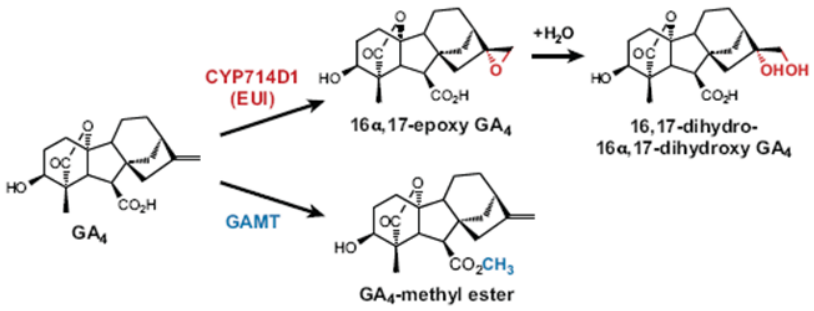

Figure 1-8: **Gibberellins can be deactivated by EUI via 16α,17-epoxidation and GA methyl transferases (GAMTs) due to methylation** (Adapted with permission from Shinjiro Yamaguchi., (2008)).

1.3.3 The sub-cellular localisation of GA metabolism

The various GA metabolic reactions occur in different parts of a cell and involve a variety of different enzymes (Figure 1-9). The CPS and KS terpene cyclase enzymes that catalyse the early biosynthetic steps are located within plastids (Helliwell et al., 1999). Helliwell *et al.*, (2001) showed that the membrane-bound cytochrome P-450 mono-oxygenase KO is attached to the outside of the plastid membrane, and that KAO is also associated with the endoplasmic reticulum (ER). It has also been shown recently that in rice, EUI, another cytochrome P450 monooxygenase, is bound to the ER membrane (Zhu et al., 2006). The final class of enzymes involved in GA biosynthesis, the soluble 2-oxoglutate-dependent dioxygenases GA20ox, GA3ox and GA2ox are located within the cell cytoplasm (Phillips, 1998). It has also been suggested that the GA methylation enzymes are localised within the cytoplasm of *Arabidopsis* cells (Varbanova et al., 2007).

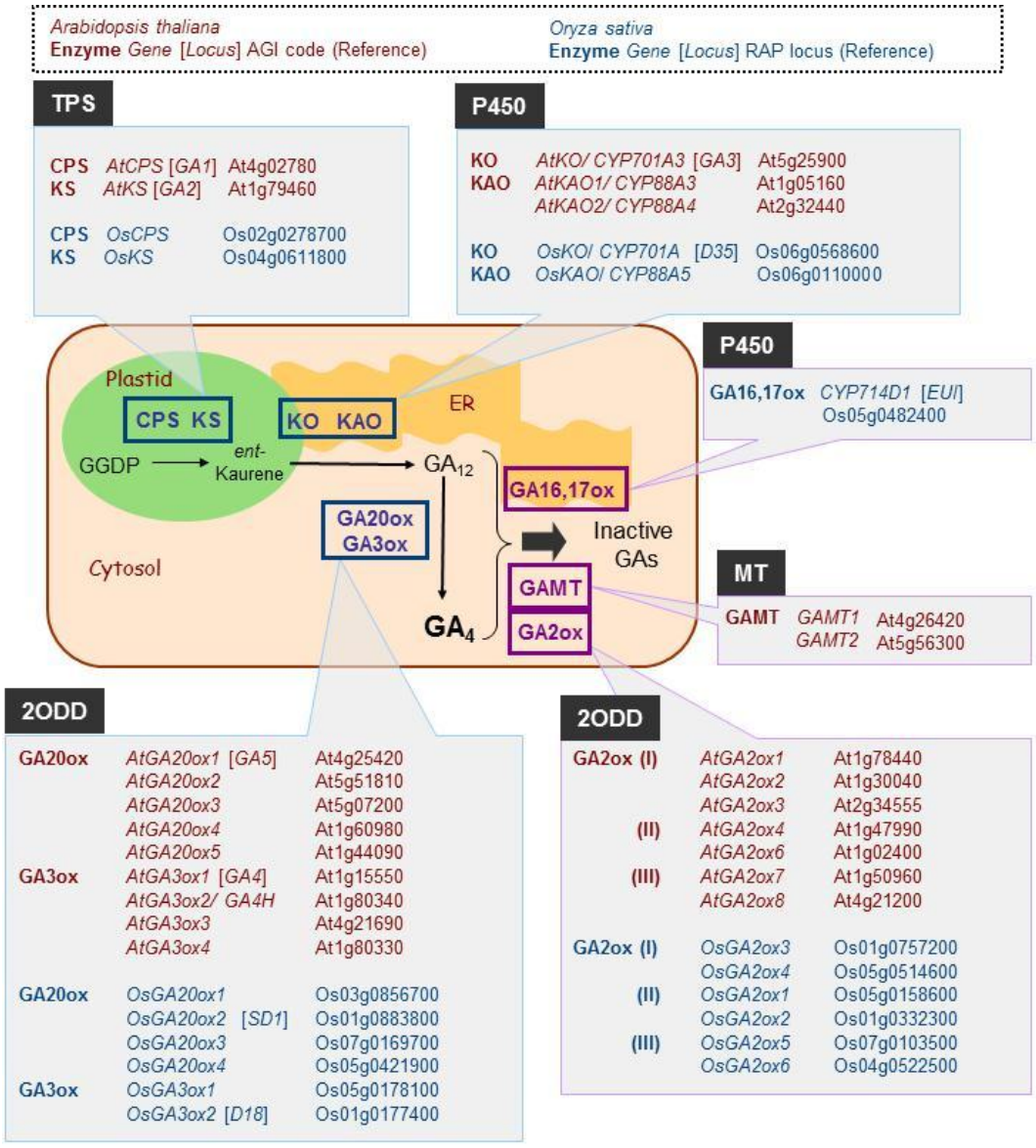

Figure 1-9**: The predicted sub-cellular localisation of GA metabolic genes in *Arabidopsis* (red) and Rice (blue)** (Displayed with permission from Shinjiro Yamaguchi., (2008)).

1.4 GA SIGNALLING

1.4.1 GA binds to the GID1 receptor

The GA receptor *GID1* was first cloned from rice: *gid1* mutants display a severe GA-insensitive dwarf phenotype, which was caused by an inability to degrade the growth repressing DELLA protein SLR (Ueguchi-Tanaka et al., 2005). GID1 is nuclear localized and binds bioactive GAs with a high affinity. In *Arabidopsis* there are three GA receptors *AtGID1a*, *AtGID1b* and *AtGID1c* (Nakajima et al., 2006). They are partially redundant, bind to DELLA proteins in the presence of GA targeting them for degradation and have distinct roles in development (Iuchi et al., 2007, Ueguchi-Tanaka et al., 2007, Griffiths et al., 2006). The GID1 receptor is a monomeric protein that has close homology to hormone-sensitive lipases (HSLs), but with important differences from these proteins in that it has no lipase activity fund in HSLs. GID1 has a pocket-like binding site and when bound to GA it displays a characteristic α/β-hydrolase fold. However, after binding to GA, an amino-terminal lid closes, encapsulating the GA inside (Figure 1-10). The structure of the receptor's pockets ensures the specificity of GA binding, via nucleophilic interaction with the carboxylic acid group on the C-6 and the hydroxyl group on C-3 of the GA molecule. The inside and outside of the N-terminus lid are hydrophobic, the inside interacting with the hydrophobic "upper" face of the GA, which holds the lid in place. The outside surface of the lid interacts with the N-terminal region of the DELLA proteins (Shimada et al., 2008, Murase et al., 2008).

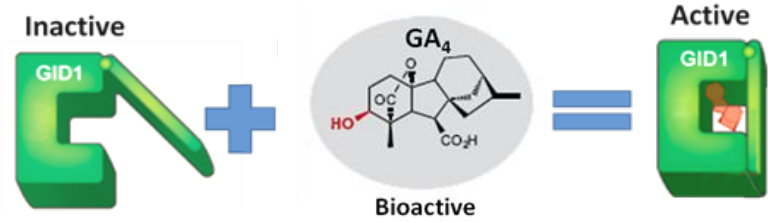

Figure 1-10: **Schematic diagram of GA interacting with the GID1 receptor.** When GA concentrations are low the GID1 receptor remains in its unbound state. When GA binds to GID1 receptor it enters a pocket and is enclosed by the amino-terminal of the protein through a conformational change, trapping the GA molecule inside the GID1 receptor (adapted from with permission from Peter Hedden., (2009)).

1.4.2 The GID1 receptor interacts with DELLA proteins in the presence of GA

The involvement of DELLA proteins in GA-mediated signalling was first indicated in *Arabidopsis* by the identification of a GA-insensitive (*gai*) mutant plant (Koornneef et al., 1985). It was then later demonstrated that mutations in these DELLA proteins were responsible for the dwarf phenotype of the wheat and maize plants that were central to the green revolution (Peng et al., 1999, Harberd and Freeling, 1989). These mutants resembled the GA-deficient plants that had previously been identified, but did not respond to applied GA due to mutations in the DELLA region that prevented the GA-GID1 binding. Murase *et al.*, (2008) have recently presented data regarding the crystal structure of the GA_4-AtGID1a as a ternary complex with the N-terminus of AtGAI. They showed that the GAI N terminus contains four distinct α-helices, αA to αD, one with negatively charged side chains and three containing non-polar side chains that interact with the N-terminus in the GA_4-GID1a. When GA enters the GID1a receptor pocket, allosteric activation allows non-polar interaction to occur between the N-terminal lid of the receptor and the LExLE, VHYNP, and DELLA motifs on the N-terminus of the DELLA proteins. These non-polar interactions cause GA to become more tightly bound within the GID1a receptor pocket and the DELLA protein to undergo a change in conformation (Figure 1-11) (Murase et al., 2008).

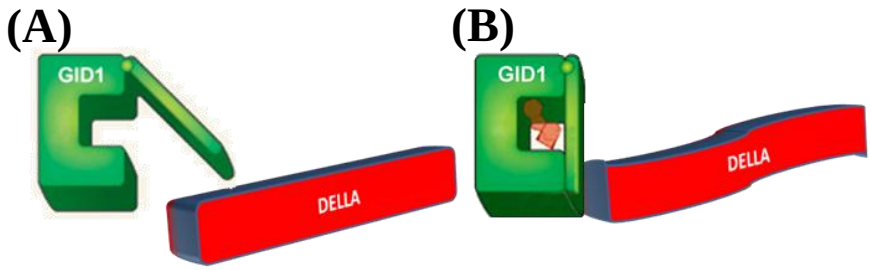

Figure 1-11: **GA binds to its receptor allowing it to bind to DELLA proteins** (A) In the absence of a GA-bound GID1a, DELLA proteins suppress transcription factors that activate GA responsive genes. (B) When GA bound GID1 receptor binds with a DELLA protein it causing a conformational change which leads to its degradation.

1.4.3 Poly-ubiquitination of DELLA proteins via the SCF-E3-ubiquitin ligase complex causing their degradation via 26S proteosome

Binding of GA-GID1a to DELLA proteins initiates their F-box-mediated proteolysis (Ariizumi et al., 2008, Ueguchi-Tanaka et al., 2008), SLY1 has close homology to many other F-box proteins and is a positive regulator of GA signalling, indicating that it may function by targeting proteins for degradation via an SCF complex. There are over 694 putative F-box proteins encoded by the *Arabidopsis* genome; they are able to target proteins for degradation due to a conserved region that allows them to interact with the SKP1 subunit of a SCF complex (Gagne et al., 2002, Kuroda et al., 2002). *Arabidopsis* contains 21 putative SKP1proteins, which function by attaching the F-box to the N terminus of a cullin subunit (Farras et al., 2001). Cullin proteins, of which there are potentially 11 isoforms in *Arabidopsis*, interact with one of two Rbx1 RINGfinger proteins (E1) (Lechner et al., 2002, Shen et al., 2002). The E1 protein is attached to one of the 32 different E2 ubiquitin-conjugating enzymes. The interaction of GA-bound GID1 with DELLA proteins promote their interaction with the SCF^{SLY1} ubitiquitin E3-ligase complex, which catalyzes the transfer of ubiquitin from the E2 protein to the DELLA proteins (Ueguchi-Tanaka et al., 2007, McGinnis et al., 2003, Zheng et al., 2002) (Figure 1-12). The polyubiquitination of DELLA proteins resulting from GA signalling targets them for 26S proteosome-mediated degradation (Zheng et al., 2002, Deshaies, 1999). In this way, GA signalling relieves the DELLA suppression of expression of GA-responsive genes, allowing growth and other GA-mediated processes to occur (Silverstone et al., 2001) (Figure 1-13).

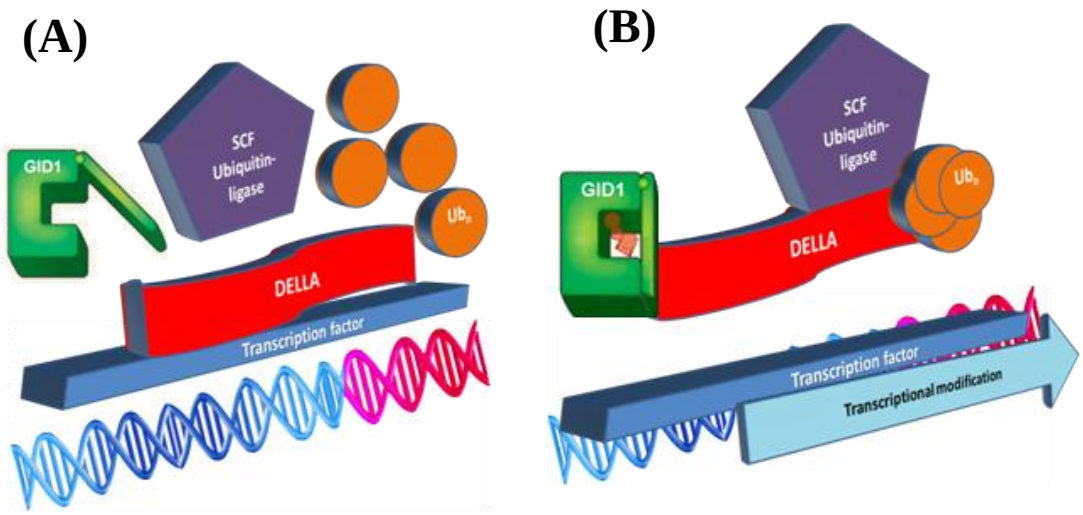

Figure 1-12: **A simplified schematic diagram showing GA targeting DELLA proteins for polyubiquitination.** (A) Without interactions between the GA and GID1, the DELLA proteins cannot be targeted to the SCF-E3 ubiquitin-ligase complex and therefore do not undergo ubiquitination. (B) The binding of GA to GID1 allows it to bind to the DELLA proteins changing their shape in a manner that allows the SCF^{SLY1} ubiquitin E3-ligase complex to bind to them and catalyze their polyubiquitination.

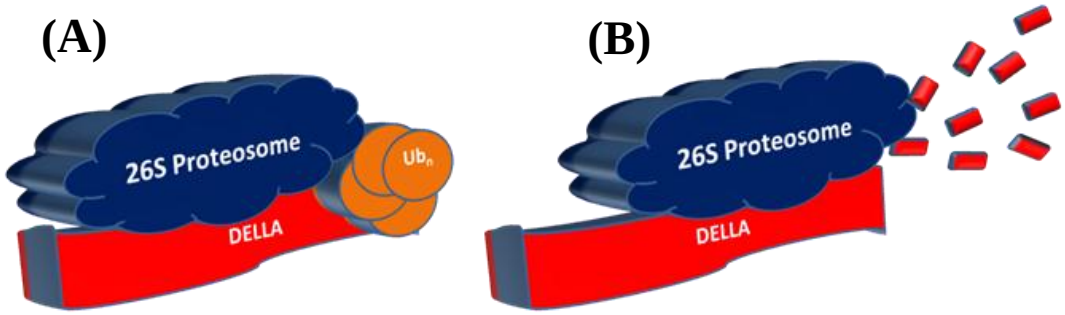

Figure 1-13: **A simplified schematic diagram showing DELLA proteins being degraded due to polyubiquitination.** (A) Polyubiqutination targets DELLA proteins for the 26S proteosome to bind. (B) The 26S proteosome then degrades the DELLA proteins releasing DELLA-induced growth repression.

1.4.4 Homeostatic regulation of GA metabolism

Plants have homeostatic regulatory mechanisms that involve both feedback and feed forward regulation of GA metabolism in order to maintain optimum growth rates (Figure 1-14). This self-regulation is clearly illustrated by comparing GA levels in GA-response mutants with wild type control plants (Hedden and Croker, 1991). The GA-insensitive *gai*, *rht3* and *d8* mutants of *Arabidopsis*, wheat and maize, respectively, have higher levels of the bioactive GAs and reduced levels of GA precursors (Appleford and Lenton, 1991, Talon et al., 1990, Fujioka et al., 1988). The GA3ox-defective maize mutant *d1* has very high levels of GA_{20} and low levels of its precursors GA_{19} and GA_{53} relative to the wild type, indicating that the regulation of *GA20ox* is under feedback regulation (Hedden and Croker, 1991). The application of exogenous bioactive GA reduced the expression of *GA20ox* genes, demonstrating that the increased expression of these GA biosynthesis genes are the result of negative feedback from the low concentration of bioactive GAs (Phillips et al., 1995). However not all GA-biosynthetic enzymes are under feedback control; it has been shown that the *AtGA3ox2,* for example, is not regulated in this way in young seedlings and to date there is no evidence suggesting that early biosynthetic steps are susceptible to feedback control (Yamaguchi et al., 1998).

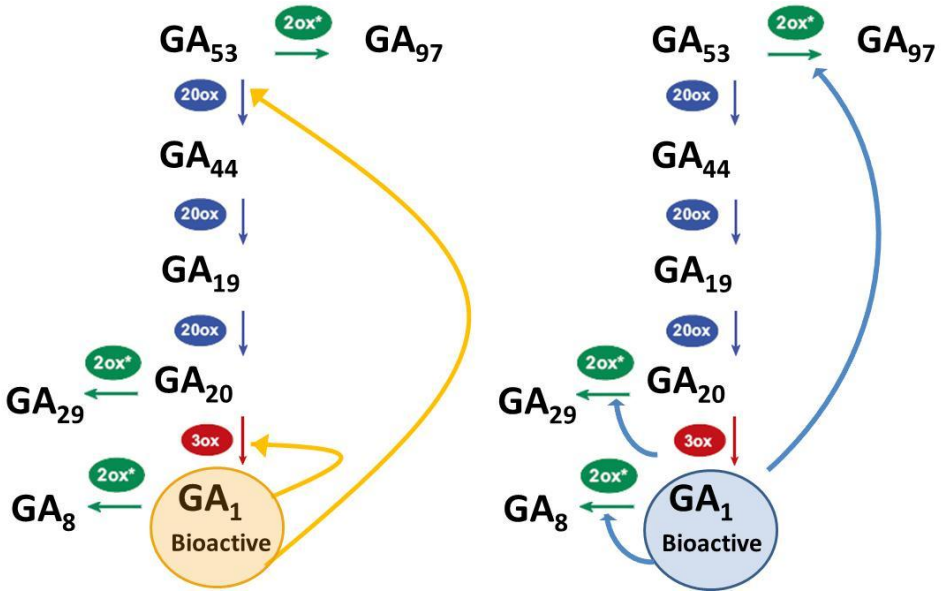

Figure 1-14: **Positive and negative feedback mechanisms maintain GA homeostasis. (A)** High concentrations of bioactive GA activate a negative feedback mechanism that reduces the expression of GA biosynthetic genes. **(B)** High concentrations of bioactive activate a positive feed-forward mechanism that increases the expression of GA catabolic genes. (Adapted from with permission from Shinjiro Yamaguchi., (2008)).

The GA homeostatic mechanism not only involves controlling the expression of GA-biosynthetic genes, but is also heavily dependent on the degradation of bioactive GA and its precursors. For example, in direct contrast to the biosynthetic enzymes the expression of *AtGA2ox1* and *AtGA2ox2* in *ga1-2* plants is increased in response to exogenous GA application (Thomas et al., 1999). This positive feed-forward is not exclusive to *AtGA2ox1* and *AtGA2ox2* and *AtGA2ox4*. *AtGA2ox6* and *AtGA2ox8* are all also up-regulated by GA (Rieu et al., 2008a). This feed-forward regulation of GA2ox enzymes has also been shown in pea illustrating that feed-forward regulation of *GA2ox* expression is a common mechanism (Elliott et al., 2001). When *ga1-3* was treated with GA_4 a decrease in the expression of the *AtGA3ox1* and *AtGA20ox1* genes was observable after just 15-30 minutes, demonstrating the speed at which this self-regulating systems can respond to perturbations in GA levels (Griffiths et al., 2006, Ogawa et al., 2003).

1.5 GROWTH AND DEVELOPMENT OF THE *ARABIDOPSIS* ROOT AND ITS HORMONAL CONTROL

1.5.1 *Arabidopsis* root structure

Root growth is achieved by two main mechanisms: cell replication and cell enlargement. The *Arabidopsis* root can be viewed as a set of concentric cylinders: the epidermis (dermal tissue system), the cortex (ground tissue system), the endodermis (cell layer separating the vasculature and ground tissue systems with its Casparian strip), and the stele (vascular tissue system) (Benfey and Scheres, 2000). The root apical meristem (RAM) is the source of new cells within the root and plays a critical role in defining the lineages of the cell files that result from meristematic divisions. The RAM is located at the distal tip of the root; this meristematic region of initials cells is located next to a non-dividing group of cells known as the quiescent centre (QC) (Dinneny and Benfey, 2008, Nawy et al., 2005). As their neighbouring initial cells divide one of the daughter cells is disconnected from the QC and then differentiates into distinct tissues. The cell files are attached to each other so they cannot move relative to one another, consequentially causing a spatial relationship that is indicative of the cell's age, with the youngest cells near the root tip getting progressively older as their distance from the QC increases (Benfey and Scheres, 2000).

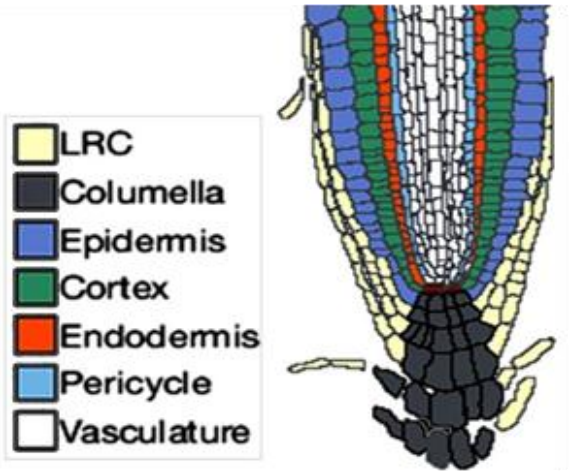

Figure 1-15: **A schematic diagram showing the main root tissues.** The lateral root cap (LRC), the columella cells, the epidermis, the cortex, endodermis, pericycle and vasculature are all shown.

1.5.2 Hormonal control of root growth and development

Roots are highly plastic structures that have architectures that can adapt to both environmental and developmental signals. This morphological flexibility is in part regulated by phytohormones such as GA, Auxin, brassinosteroids, ABA and ethylene (Achard and Genschik, 2009, Greenboim-Wainberg et al., 2005, Leubner-Metzger, 2001). There is cross-talk between the metabolism and signalling pathways of these hormones such that treatment of plant roots with one of them can affect not only the levels of others but also the sensitivity of the downstream signalling components . These hormonal signals are perceived by their various receptors that indirectly interact with transcription factors resulting in gene expression changes and modifications to plant growth and development. The mobility of these internal signals makes them the perfect integrators for a variety of external signals and allow the plant to adjust its growth strategy in response to changes to the environment, such as when exposed to stress. Evidence is now available suggesting that ethylene, auxin, and GA can all affect DELLA function, indicating that DELLA proteins have a key integrative role in the phytohormone signal response network (Achard et al., 2003).

1.5.3 Auxin in root growth & GA crosstalk

Auxin, the most common form of which is indole-3-acetic acid (IAA), has many critical role in regulating plant growth and development. Most auxin is synthesized in the shoot, then transported across adjacent cells in a polar manner throughout the plant, creating a gradient down from the shoot tip to the roots that has been shown to influence a variety of developmental processes (Vieten et al., 2007). These auxin gradients change dynamically during different developmental processes and the molecular components involved in this polarised transport network have been shown to be essential for correct root growth, development and responses to environmental stimuli (Swarup et al., 2005). The directional transport of auxin is mediated by influx and efflux pumps which are modulated by auxin and other signals in a complex pattern of

feedback mechanisms, that guide not only the production and destruction of auxin transporters, but also their sub-cellular localization in order to direct auxin flow (Tanaka et al., 2006).

Recently a high-resolution map showing the distribution of auxin within the *Arabidopsis* root apex has been produced (Petersson et al., 2009) (Figure 1-16-A). These data suggests that an auxin gradient exists and has a distinct maximum in the organizing quiescent centre (QC) of the root apex. The data also demonstrates that all cells in the apex express the genes that encode the enzymes required for synthesising IAA. This indicates that the biosynthesis and polarized distribution of auxin combine to produce auxin gradients with a maximum concentration in the root tip. The auxin distribution map confirmed that an auxin concentration gradient does indeed exist within the root apex and also showed that the highest concentration occurs within the QC cells, while relatively high IAA concentrations were also observed in the cortex, endodermis, and apical parts of the stele. Ultimately the auxin gradient within the root apex is extremely dynamic, and it is believed to be maintained by a combination of biosynthesis, transport, and catabolism/conjugation (Leyser, 2006).

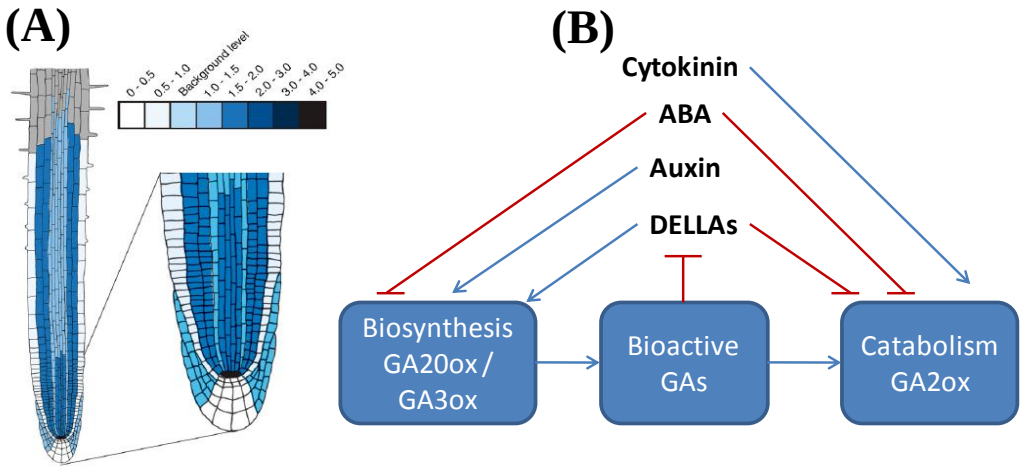

Figure 1-16: **Auxin has a critical role in coordinating root growth in synchrony with many other hormones.** (A) Auxin distribution at the root apex (Petersson et al., 2009) (Reproduced with permission from Karin Ljung). (B) A diagram showing a model of hormonal interactions with GA metabolism and its interaction with DELLA stability (Adapted from Achard and Genschik 2009).

It has also been shown that auxin production in the root apex is positively regulated by ethylene and the auxin is then transported via the lateral root cap to the elongation zone where elongation growth responses occur in multiple tissues (Swarup et al., 2007). Auxin influences root growth partly by modulating the cellular responses to GA. In peas, auxin has been shown to promote stem elongation by increasing the expression of *PsGA3ox1* while simultaneously suppressing the expression of *PsGA2ox1/2* (O'Neill and Ross, 2002). Modification to GA metabolism by auxin in order to promote growth has also been demonstrated in barley, where auxin regulation of *HvGA3ox2* expression has been implicated in the promotion of stem elongation (Wolbang et al., 2004). Auxin is required for the GA-mediated control of root growth, mutations within auxin transport or signalling components delays the GA-induced disappearance of DELLA proteins from root cell nuclei. Thus auxin produced in the shoot apex is able to influence DELLA protein destabilization in the root allowing it to exert long distance control on root growth (Fu and Harberd, 2003).

1.5.4 Ethylene in root growth and GA crosstalk

Many hormones such as ethylene, ABA, cytokinin and auxin have all been shown to interact with GA metabolism. Ethylene has been shown to inhibit root growth, and in *Arabidopsis* this inhibition has been demonstrated to be DELLA-dependent; ethylene delays the GA-induced degradation of DELLA proteins within the root cell nuclei via a constitutive triple response-dependent signalling pathway (Achard et al., 2003). Achard *et al*, (2003) demonstrated that the "apical hook" structure of etiolated seedling hypocotyls, promoted by ethylene, is partially dependent on DELLA degradation. It has also been shown that this ethylene-induced inhibition of growth is also dependent on IAA concentrations (Swarup et al., 2007). In addition, experiments have shown that the application of exogenous ethylene represses the expression of GA metabolism genes, while, conversely, exogenous GA application causes the expression of several ethylene biosynthesis genes to be up-regulated. This

highlights the complexity of how the different hormone metabolism and signalling pathways are interlinked.

Ethylene signalling genes are expressed throughout the entire *Arabidopsis* plant, while its metabolism genes are expressed in the majority of plant organs, thus the ethylene precursor 1-amino-cyclopropane-1-carboxylic acid (ACC) may be synthesized ubiquitously and active ethylene can be perceived universally (Dugardeyn et al., 2008). However transcript meta-analysis at a single cell resolution within the *Arabidopsis* root suggests that ethylene have may have a more localized function in specific developmental zones such as the fast elongation and specialization zones (Dugardeyn et al., 2008). Thus ethylene signalling appears to have a role in regulating root growth when cells have reached their most rapid speed of growth (Le et al., 2001). Interestingly the regulation of ethylene biosynthesis not only relies on modifications to gene expression but also exists at the protein level. ACC synthesis is the penultimate step in ethylene biosynthesis that is catalysed by ACS. This enzyme can be polyubiquitnated by ETO1^{CUL3A} RBX1-E2 ubiquitin ligase complex subsequently leading to its degradation by a 26S proteosome complex (Wang et al., 2004, Chae et al., 2003).

1.5.5 ABA & GA antagonism in root growth

The antagonistic effects of GA and ABA are obvious at many stages during plant growth and development. For example, germination and growth are promoted by GA, but inhibited by ABA (Koornneef et al., 2002). Studies have shown that both the metabolism and downstream signalling targets of these hormones are interlinked. ABA levels have been shown to be positively regulated by DELLA proteins via the up-regulation of the expression of the *XERICO* E3 ubiquitin ligase. Over-expression of *XERICO* has been shown to cause increased levels of ABA, resulting in greater drought tolerance; however the downstream signalling mechanism post-ABA accumulation remains elusive (Ko et al., 2006). ABA pre-treatment inhibited the GA-induced degradation of

GFP-tagged RGA protein (GFP–RGA) suggesting that the presence of ABA stabilizes DELLA proteins, while some evidence also indicates that ABA inhibits GA responses by affecting proteins downstream of DELLA (Ko et al., 2006). DELLAs are known to modify the amount of reactive oxygen species (ROS) that are present in a cell by inducing superoxide dismutase (SOD) (Achard et al., 2008b), while the production of ROS has also been shown to function as secondary messengers in ABA signalling in guard cells. Two NADPH oxidase catalytic subunit genes, *AtRBOHD* and *AtRBOHF* have been shown to be involved in ABA signalling, double mutants having impaired ABA-induced stomatal closure and Ca^{2+} channel activation, which are both rescued by exogenous H_2O_2. ABA inhibition of seed germination and root elongation are also impaired in the rbohD/F double mutant suggesting a general role for ROS and NADPH oxidases in ABA signalling (Kwak et al., 2003). Analysis of the *Arabidopsis* genome has shown that the promoters of many of the GA-down-regulated genes contain ABA response elements (ABRE) (Ogawa et al., 2003).

Microarray experiments investigating the response of DELLA mutants to stress have revealed that DELLAs have a role in moderating the affects of both biotic and abiotic stress, in part by altering the cell's redox potential. Achard *et al* (2008) showed that roots of the *ga1-3* mutant were incapable of accumulating reactive oxygen species (ROS), indicating that DELLA proteins control ROS accumulation. DELLA proteins were found to induce the expression of the Cu/Zn- superoxide dismutase (SODs) genes *CCSD1* and *CSD2*, suggesting a mechanism for suppression of ROS accumulation (Achard et al., 2008b, Kliebenstein et al., 1998). Thus, when plants are subjected to stress, DELLA accumulation up-regulates SOD production, causing a decrease in the amount of ROS, which, as well as relieving stress symptoms, was also suggested to reduce growth of the root (Achard et al., 2008). In the absence of stress, the converse happens; a reduction in the amounts of DELLA proteins causes a decrease in SOD activity resulting in ROS accumulation, thus increasing root growth (Gapper and Dolan, 2006). It is unclear how ROS accumulation causes cell elongation, but they may function as secondary messengers, as H_2O_2 does during ABA signalling in guard cells (Kwak et al., 2003). It is clear that plant

growth rates are related to the degree of environmental stress, and that this maybe mediated via the hormonal (ABA and GA) control of ROS metabolism. These dynamic interactions between ABA and GA regulation of ROS accumulation and the downstream signalling pathways they regulate exemplifies the complexity of plant hormonal antagonism.

1.5.6 Brassinosteroids in root growth

It has been shown that brassinosteroids (BR) and also GA promote root elongation in *Arabidopsis* wild-type plants and that BR acts by increasing cell replication rate and cell elongation (Howell et al., 2007, Mussig et al., 2003) which is a clear example of hormonal synergism. Signalling cross-talk between GA and BR occurs during hypocotyl elongation and seed germination, BR has been shown to promote GA biosynthesis by increasing the expression of *AtGA20ox1*, while BR is also able to rescue the germination of the *ga1-3* mutant indicating that BR can also acts independently of GA (Bouquin et al., 2001). The promotion of germination by BR and subsequent seedling growth is therefore likely to be a vital pathway that is parallel to GA signalling, but with GA acting primarily on the emerging radicle and subsequent roots while the BR promoting germination primarily through the hypocotyl and shoot (Leubner-Metzger, 2001). The exact mechanism of this molecular dialog is unclear, although it has been suggested that signalling between BR and GA may involve a heterotrimeric GTP-binding protein (G-protein) and putative G-protein-coupled receptor during seedling growth (Chen et al., 2004, Ullah et al., 2002). BR signalling is also intimately linked to auxin signalling, partially via the *BREVIS RADIX* transcription factor. Experiments have shown that mutations within this gene reduce the amount of BRs by reducing the expression of the rate-limiting enzyme for brassinosteroid biosynthesis, indicating that IAA potentially positively regulates BR biosynthesis (Mouchel et al., 2006). Recent evidence has shown that BR appears to promote leaf expansion primarily by promoting the enlargement of the epidermis (Savaldi-Goldstein et al., 2007).

1.5.7 Cytokinin in root growth

Cytokinin and auxin act dynamically to operate a self-regulating transcriptional network that maintains the balance between cell division and cellular differentiation in the root (Ioio et al., 2008). It has long been known that during the early stage of root growth the meristematic region enlarges in response to auxin, continually increasing in size until after 5 days, when cytokinin begins to restrict cell division. However GA has only recently been implicated in root meristem growth and the molecular details are just beginning to be revealed (Ubeda-Tomás et al., 2009, Dello Ioio et al., 2007, Achard et al., 2009). Dello loio *et al* (2008) showed that *SHY2*/*IAA3* is activated by the cytokinin-response transcription factor *ARR1*, and, since *SHY2* negatively regulates expression of PIN auxin transporters, this allows cytokinin to influence auxin redistribution and thus modify cell division rates. To prevent *SHY2* completely stopping cell division, auxin promotes the degradation of the SHY2 peptide, consequentially promoting PIN activity, auxin flow and cell division (Ioio et al., 2008). Recently Moubayidin *et el.,* (2010) showed that another cytokinin response factor, *ARR12,* promotes meristem growth after germination, causing the meristem to enlarge until *ARR12* and *ARR1* act together to increase *SHY2* expression, thereby suppressing auxin flow, and producing a balance between cell differentiation and division. Interestingly, during these early stages, *ARR1* expression is suppressed within the proximal meristem by high levels of GA through degradation of RGA, thus allowing the meristem to increase in size (Moubayidin et al., 2010). Thus it is clear that while the balance between cell division and cellular differentiation is determined by the relative auxin and cytokinin concentrations, this balance is subject to regulation by GA levels and their influence on auxin concentrations via the affect of *RGA*, *ARR1* and *SHY2* on *PIN* auxin transporters.

1.5.8 DELLA signalling in root endodermis controls cell elongation and division

Recent studies have revealed the importance of DELLA degradation in the endodermis for the regulation of root growth by GA. The expression of a non-degradable *gai* mutant DELLA protein specifically within endodermal cells blocked expansion of these cells and subsequently retarded root growth (Ubeda-Tomas et al., 2008). Furthermore, Ubeda-Tomas *et al*., (2009) have recently demonstrated that GA-biosynthetic mutants have a smaller meristem through a reduced cell production rate. Recent publications have provided further information on DELLA-regulation of root growth. Zhang *et al.*, (2011) showed that expression of the GRAS protein SCL3 is subject to regulation by GA via DELLA protein stabilisation. Since SCL3 acts as a positive regulator of GA signalling, DELLA and SCL3 antagonise each other's abundance by altering GA concentrations (Zhang et al., 2011).

Work by Heo *et al.,* (2011) indicates that SCL3 has a central role in coordinating GA-dependant cell elongation and is likely to form a conjugate with SCR, which modulates ground tissue cellular divisions and differentiation. Interestingly the stability of DELLAs is altered by a variety of stimuli (Achard et al., 2003), allowing them to function as a convergence point in integrating an array of signals as diverse as phosphate starvation (Jiang et al., 2007), and changes in photoperiods (Achard et al., 2007). Control of cell proliferation rates by GA is not confined to the root, since targeting the non-degradable DELLA protein *gai* to meristematic regions in combination with kinematic analysis revealed reduced cell replication rates in both shoot and root meristems. Achard *et al*., (2009) also showed that DELLA proteins prevent cell division by increasing the expression of the cell cycle inhibitors *KRP2* and *SIM*. Expressing *gai* in the endodermis alone was sufficient to prevent root meristem enlargement, demonstrating that DELLA proteins in the endodermis are a critical target for GA signalling (Ubeda-Tomás et al., 2009). Therefore GAs influence the plant's plasticity by modifying cell elongation (Ubeda-Tomás et al., 2009) and replication (Achard et al., 2009).

1.5.9 Cell-specific hormone action in regulating root growth

It has recently been shown that many hormonal responses appear to be localised to specific cells depending on their temporal and spatial positioning however the precise nature of their tissue specificity remains unclear. As discussed above, in the *Arabidopsis* root, GA seems to act primarily in the endodermis of the (pro)meristematic zone and in the transition zone, while recent research has shown that brassinosteroids and auxins exert their affect at the epidermis. Auxin and cytokinin regulate cell division within the stele and consequently all the hormonal concentration gradients act in combination to drive organ growth (Ubeda-Tomas et al., 2008, Savaldi-Goldstein et al., 2007, Swarup et al., 2005). Supporting this hypothesis, distinct expression patterns can be found in root tissues at different stages of development. Transcript meta-analysis data for specific cell-files in the *Arabidopsis* roots provided evidence that GA, IAA, JA and ethylene have putative action centres based on cluster analysis of important genes that regulate their metabolism and signalling (Dugardeyn et al., 2008, Brady et al., 2007, Birnbaum et al., 2003).

Dugardeyn *et al*., (2008) used published microarray data to describe how the expression of *DELLA* and the *GID1* receptor genes in varies between different *Arabidopsis* root tissues and stages of development. However, this contradicted findings where *RGA::RGA:GFP* is expressed in all tissues and recent evidence, discussed above, suggests that the endodermis is the primary site of GA action. Further complicating matters, expression of the GA-biosynthetic genes *AtGA3ox1*, *AtGA3ox2* and *GA20ox2* do not co-localise within the endodermis throughout the meristem as both *AtGA3ox2-GUS* and *AtGA3ox1-GUS* are expressed within the vasculature (Figure 1-17). AtGA3ox1-GUS was expressed during all stages of development, while AtGA3ox2-GUS was excluded from the meristematic zone (Mitchum et al., 2006). AtGA20ox2-GUS appears to be expressed asymmetrically within the endodermis, while *AtGA20ox1-GUS* was expressed to a much higher level within cortex throughout the promeristematic zone and the beginning of the meristematic zone (Figure 1-17).

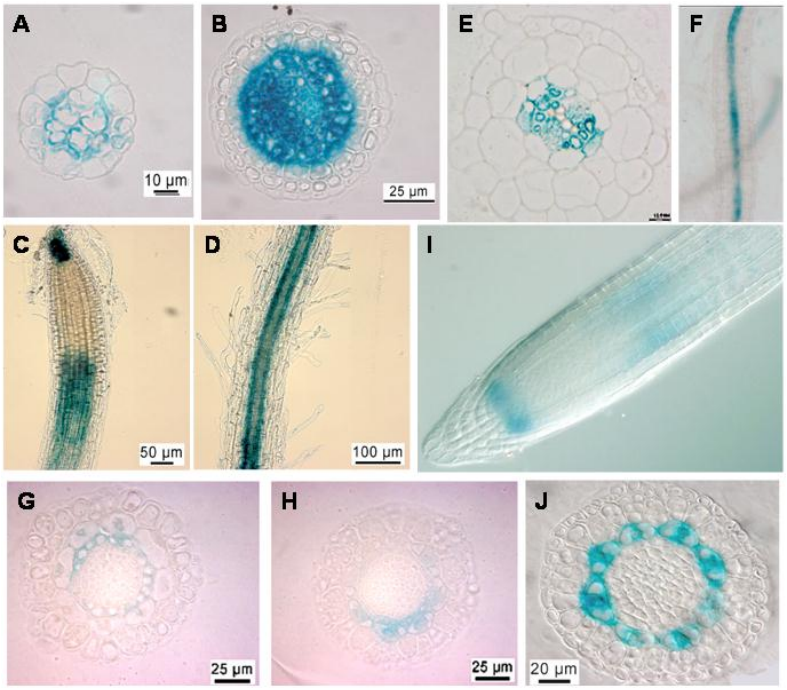

Figure 1-17: **Promoter-GUS expression profiles in the *Arabidopsis* root for GA-biosynthetic genes.** (A-D) TC-AtGA3ox2-GUS expression. (E-F) TL-AtGA3ox1-GUS expression. (I-J) TC-AtGA20ox1-GUS expression. (G-H) TL-AtGA20ox2-GUS expression (Reproduced with permission of Nieves Fernandez., unpublished data).

Meta-analysis of tissue specific transcriptomic data performed by Dugardeyn *et al*, (2008) showed that GA metabolism and signalling genes are expressed in all *Arabidopsis* organs, albeit at varying levels. Thus microarray data implies that GAs may be synthesized, degraded and perceived in all organs, potentially allowing all cells to be GA responsive. Thus the cells position determines its response to GA due to unique and overlapping expression patterns of GA metabolic genes and signalling components interacting in different ratio's depending on the precise tissue and position within hormonal gradients. They also showed that most of the genes belonging to the *AtGA2ox*, *AtGA20ox* and *AtGA3ox* families were differentially expressed and that the majority had highest expression within the endodermis or neighbouring tissues. This also supports the suggestion that a tissue-specific GA response may be primarily regulated by the location of its biosynthesis and action. All this combined with the apparent clustering of hormone related genes, possibly due to co-regulation, indicates that GA and other phytohormones may initiate their respective responses by modifying the growth rate of individual tissues at specific stages of development (Birnbaum et al., 2003).

1.6 AIMS AND OBJECTIVES

The recent groundbreaking studies by Ubeda-Tomas and colleagues (2008 and 2009) have demonstrated that DELLA degradation specifically within the endodermis is essential for the control of GA-induced root elongation. However, the available data on the localisation of expression of key GA-signalling components, including *GID1A, SLY1, RGA* and *GAI,* suggests that they are expressed throughout the root (Dugardeyn et al., 2008, Birnbaum et al., 2005, Birnbaum et al., 2003, Silverstone et al., 2001). The differences observed between the site of action and the varying expression patterns of GA-signalling components implied by microarray data might be reconciled if there are spatial and temporal differences in the localisation of GA metabolism. Expression profiling data from microarray experiments and the analysis of promoter::GUS reporter lines supports the distinct cellular localisation patterns of GA metabolic genes (Figure 1-17). Interestingly, *AtGA20ox1* appears to be expressed exclusively within the cortex whereas *AtGA3ox1* is expressed in the stele and AtGA3ox2 is expressed in similar domains of the meristem and elongation zone as the AtGA20ox1. These differences in expression patterns raise the possibility that the movement of bioactive GA or their precursors is also important for controlling cell growth within the endodermis.

The aim of this project is to expand on these observations by performing experiments designed to finely map the sites of GA metabolism and perception within the *Arabidopsis* root. The main part of this work involves a targeted expression strategy designed to manipulate GA metabolism and signalling in specific cell types to provide insights into GAs role during root growth. Cell-specific deactivation of bioactive GA or its precursors by the targeted miss-expression of *AtGA2ox2* and *AtGA2ox7* will probe the effects of localisation of C_{20}-GA and C_{19}-GA pools. Cell-specific conversion of C_{20}-GAs to C_{19}-GAs using the targeted expression of *AtGA20ox1* in *ga20ox1,-2,-3* triple mutant plants will be employed in an attempt to rescue root growth within these dwarf mutants. A similar approach will be used to determine the site of GA activation via the targeted expression of *AtGA3ox1* in the *ga3ox1,-2* double mutant. Finally the targeted expression of a functional AtGID1a GA receptor in *gid1a,-b,-c* triple mutant plants will be employed to identify which cell layers are important for GA perception. Promoters for genes shown previously to be expressed specifically in different cell-types within the root will be used to drive expression of the effector genes. In addition the *CAB* promoter will be used to drive the expression of the metabolism genes in photosynthetic tissues in order to investigate the contribution of these tissues as a source of GAs or precursors for the root. In order to confirm the expression domains of the transgenes, the effectors will be expressed as fusions with the yellow fluorescent protein (YFP).

2 MATERIALS AND METHODS

2.1 MATERIALS

2.1.1 *Arabidopsis* lines used

Arabidopsis thaliana (*Arabidopsis*) ecotype Col-0 was used in all experiments. *ga3ox2-1* double mutant lines were supplied by Dr Shinjiro Yamaguchi, RIKEN Plant Science Center, Yokohama, Japan. The *ga20ox1 ga20ox2 ga20ox3* triple mutant (*ga20ox1,-2,-3*) was generated by crossing *ga20ox1-3, ga20ox2-1* (Rieu et al., 2008) with *ga20ox3-1* (Andy Plackett, personal communication). The GA-deficient mutant *ga1-3* contains a null mutation in the *CPS* gene that prevents it from making GA, this mutation was originally found in the *Ler* background but was subsequently back crossed to Col-0 six times (Sun et al., 1992).

2.1.2 Bacterial strains

The bacterial host for all cloning work was *Escherichia coli* strain DH5α. For the heterologous expression of GA catabolic enzymes, *E. coli* strain BL21-CodonPlus(DE3)-RIL cells was used. *Agrobacterium tumefaciens* strain GV3101 was used for *Arabidopsis* transformations.

2.1.3 Common chemicals and reagents

2x CTAB DNA extraction buffer: 0.1 M Tris, 2% CTAB, 1.4 M NaCl, 20 mM EDTA. 10x GUS buffer: 1 M Tris pH 7.5 containing 29 mg/ml NaCl, 6.6 mg/ml $K_3Fe(CN)_6$. 0.2% PPM: 0.488g MS salts, 4g sucrose, in 196 ml H_20 at pH 5.8, 4 ml PPM (Plant Persivative Mixture) (Plant Cell Technology). PCRx10 reaction buffer: 500 mM KCl, 100 mM Tris-HCl (pH 9.0 at 25°C), 1% Triton® X-100.

2.2 METHODS

2.2.1 Plant Growth in soil

Arabidopsis plants for seed production, crossing or characterisation were grown in Levington's compost in a controlled environment (CE) cabinet with 16-h days (150 $\mu mol^{-2}.sec^{-1}$) at 24/18ºC (day/night). Seeds to be sown onto compost were imbibed in water or 50µm GA_4 for three days at 4ºC in the dark before being sown and transferred into the CE cabinet. If seeds were required from seedlings that were germinated on either agarose (Sigma) or Gelrite (Duchefa) media, then they were transferred to soil in the CE cabinets after 7-14 day. Plants were tied to stakes during growth and allowed to brown before siliques were harvested. Plants were watered from below as required by glasshouse staff (Jack Turner, Liz Isger, Anthony Griffin and/or Ian Pearman).

2.2.2 Growth of Seedlings in Media

After autoclaving, media was allowed to cool in a 50-55ºC water bath before pouring, if any additional chemicals were required in the media then they were added at this stage, plates were then sealed with 3M Micropore™ surgical tape.

2.2.3 Liquid plant growth media

Seedlings required to undergo treatment were grown in conical flasks in liquid media containing 0.05% MES (Sigma), 0.5x MS (Duchefa), 1% Sucrose (Duchefa) at pH 5.8.

2.2.4 Solid Plant Growth Media

When plants were grown on solid media it contained 0.8% Agar (Sigma), 0.05% MES (Sigma), 1x Murashige and Skoog (MS) (Duchefa), 1% Sucrose (Duchefa) at pH 5.8. However when root growth analysis was performed on plates placed at 80º from the horizontal, the agar was replaced with 0.7% Gelrite (Duchefa), the MS content was ½ strength and no sucrose was added.

2.2.5 Transformant Screening

Primary transformants were selected using a kanamycin resistance screen carried out in Petri dishes containing 0.8% Agar (Sigma), 0.05% MES (Sigma), 1x (MS) (Duchfa Biochemie), 200 µg/ml kanamycin (Sigma). After sterilisation and imbibition, approximately 2000 seeds were re-suspended in 3ml 0.1% agarose and poured evenly and then allowed to grow for 7 days on the selection media.

2.3 PLANT HANDLING

2.3.1 Surface sterilization

All seeds that were grown on solid media or in liquid media were surface sterilised. They were submerged in 70% ethanol and shaken for 3 min, the ethanol was then replaced with 10-20% bleach/0.1% Tween-20 for a further 5-10 min. The bleach was then rinsed off using sterile H_2O for 3-5 washes. T2 and T3 seeds used for segregation analysis were surface sterilized overnight at 4°C in 2% plant preservative mixture (PPM) solution.

2.3.2 Imbibing seeds

All seeds were stratified at 4ºC in the dark for 4 days in order to produce uniform germination. *ga1-3, ga20ox1 ga20ox2 ga20ox3* (*ga20ox1-,2-,3), ga3ox1 ga3ox2 (ga3ox1,-2)* and transgenic or control lines they were being compared with were imbibed in 25 µM GA_4 for 6 days to stimulate germination. Seeds imbibed in GA_4 were rinsed 5 times in H_2O before plating.

2.3.3 Seed dissection

Seeds that would not germinate due GA deficiency could be dissected out of the seed coat to allow germination. Seeds were placed on wet filter paper and, using a dissection microscope, a small incision was made in the seed coat with a syringe needle. The other end of the embryo was gently squeezed using a fine

pair of tweezers and the embryo removed. The embryo was then placed on solid plant growth medium, the plate sealed and transferred to the growth room.

2.3.4 Crossing of *Arabidopsis* lines

Recipient flowers were prepared by removing branches or flowers. All flowers not at stage 11/12 (Smyth et al., 1990) were removed from the chosen inflorescence before emasculating the flower. Subsequently pollen from a mature stamen of the pollen donor was drawn over the stigma of the emasculated flower. Care was taken to ensure that the emasculated flower had not self-pollinated. Cross-pollinated flowers were tagged for subsequent identification. The carpels were then left to develop for 1-2 weeks until they started to turn yellow before harvesting.

2.3.5 Time-lapse imaging of germination and root growth

In order to assess germination rates and root growth rates for up to seven days after germination, time lapse photography was used to record root growth. The time points were either selected manually for measurement with imageJ or all the time-lapse images were measured using RootTrace (French et al., 2009) (data not shown). Initially two plates were photographed simultaneously using a 10 megapixel Canon Powershot 7 camera positioned 10-30 cm from the plates and linked to a PC running "PSRemote Multi Camera" remote imaging software. The PC files were then stored on a 1 Tbyte internal hard drive and backed up regularly onto a 1 Tbyte external hard drive. The plates were held vertically on a black photographic platform. Photographs were taken at 30-min intervals over 7 days, producing 336 JPEG files. Because of the uncertainty as to when the exact moment of germination occurs, timelapse monitoring provides a more accurate and detailed data regarding growth rates. However, due to the large number of transgenic lines generated and the consistent germination rate due to prior GA_4 treatment, it was decided that only one time

point at seven days was required as a representative time point. It was at this point that the distance between the hypocoytle and root tip was recorded

2.3.6 Root imaging and measuring

Plant root lengths were measured after seven days growth using Image-J with the Neuron-J plug-in. When analysing root growth, plants were grown on medium containing 0.5% Gelrite, 1% sucrose, ½ MS at pH of 5.8, except for the *GID1a* lines, which were grown on 0.5% agar, 1% sucrose, ½ MS at pH of 5.8, since the *gid1a,-b,-c* triple mutant cannot survive on Gelrite-containing medium. Plates were placed at 80^{o} angle in continuous light (150 µmol/m^2/sec). Preliminary analysis was performed on 4-8 transgenic lines, from which 3 lines were selected, and the experiment was then repeated for more detailed analysis.

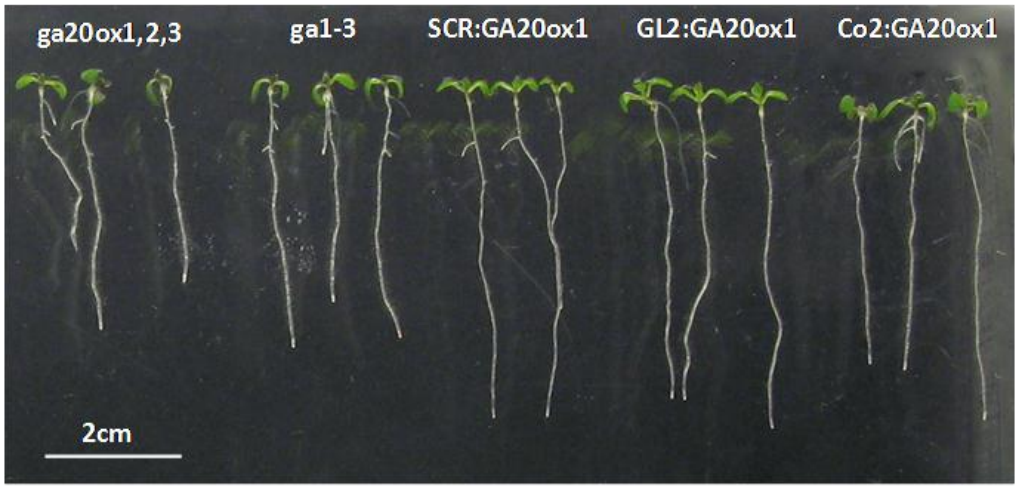

Figure 2-1**: Example image used to generate primary root length.** Scale Bar is 2cm in length.

Plates were photographed with a Fuji S2 Digital Camera 7 days after germination or continually using FUGIFILM hyper-Utility software. Root length was measured using Image J software (Universal Imaging Corporation), EZ-Rhizo (Armengaud et al., 2009) or RootTrace (French et al., 2009) and the data transferred to Excel. To calculate root growth rates, plants were photographed, as above, and the daily root growth was measured. Adobe-Bridge, Image Raw, and Photoshop CS3 were used to enhance the image

contrast on multiple images to improve the recognition during subsequent automated analysis. RootTrace was then used to quantify the dynamics of various characteristics of the primary root during the first 4 days of growth.

2.3.7 Confocal microscopy

Confocal analysis was performed with a Leica TCS-SP confocal microscope (Leica, Milton Keynes, UK). Roots were stained with 10 μg/ml propidium iodide (Sigma) for 10-20s, rinsed, and mounted in water. Enhanced yellow fluorescent protein (EYFP) was excited with at 488 nm from an argon laser and the propidium iodide was excited at 514 nm. Fluorescence emission for the EYFP was collected between 505 and 530 nm. Images were subsequently processed using Leica LAS AF Light and Adobe Photoshop. Subsequently image analysis of images taken using the leica confocal microscope and subsequent analysis using LAS AF lite allowed meristem and cell size to be measured (Figure 2-2-B). The length of the meristematic region was calculated by measuring from the QC to the transition zone (TZ), which was defined as the moment when the cells had reached their maximum width and doubled in length (Figure 2-2-A). The final cortical cell length was calculated by measuring the length of the cortical cells after root hairs had emerged in the differentiation zone (Figure 2-2-B and C). Measurements were taken at 7 days growth as this is when the GA deficient mutant ga1-3 has had its meristem reach its maximum size (Achard et al., 2009).

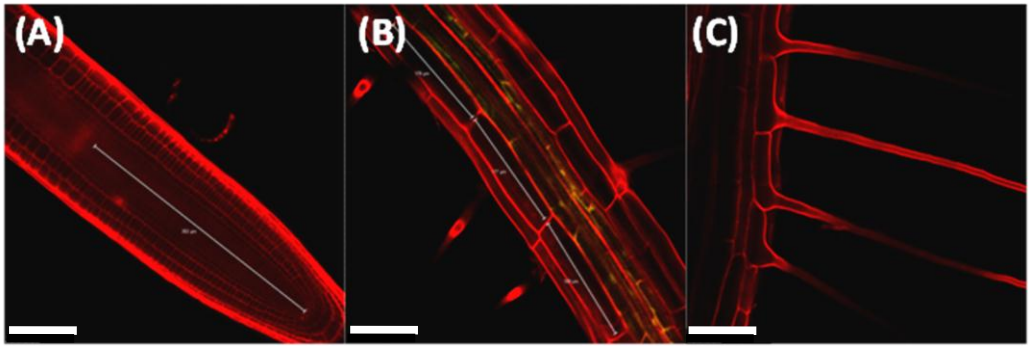

Figure 2-2**: *SHR::YFP:AtGA20ox1* fluorescence in the meristematic region and the differentiation zone of the root. (A)** Meristem measurement from the QC to the transition zone. **(B)** Cortical cell measurements in the differentiation zone (DZ). **(C)** Root hairs define when zone cortical cells have reached their final length. Propidium iodide emission are shown. Bars are 50µm in length.

2.3.8 Statistical analysis

Root growth parameters from the transgenic and control lines were compared using analysis of variance **(**ANOVA): five plates with each genotype having a maximum of five seedlings (technical replicates) per plate. The experimental design structure allowed ANOVA to compare the different genotypes using the F-test, following which the standard error of the difference (SED) and least significant difference (LSD) values for comparison of means were output. However, when ANOVA was unable to be used due to more than 5% of seedlings in a particular experiment being missing, the method of residual maximum likelihood (REML) (Patterson and Thompson, 1971) was employed. This method fits a regression based model, accounts for the design, and outputs predicted means and SEDs/LSDs between means for their comparison. The F-test was again used (as for ANOVA) to assess the overall differences between genotypes. Note that there was now unequal replication though, so each comparison of means has its own SED. The GenStat® (2009) (Twelfth Edition, © Lawes Agricultural Trust (Rothamsted Research), VSN International Ltd., Hemel Hempstead, UK) statistical system was used for both ANOVA and REML analyses.

2.4 GENERAL MOLECULAR BIOLOGY METHODS

2.4.1 Restriction digestion of DNA

Restriction digests of DNA were carried out in 20-µl reactions with 0.5 µl of enzyme and 2µl of the appropriate enzyme buffer (as supplied by the manufacturer) at 37ºC for 2 hours. Some vectors required dephosphorylation post-linearization which was performed by adding 1µl (0.1u) alkaline phosphatase 1 hour after commencing the digest halting the restriction then continuing the incubation for 1 hour at 37°C.

2.4.2 DNA gel electrophoresis

DNA was mixed with 6x loading dye (15% [w/v] ficoll, 0.25% [w/v] bromophenol blue and 0.25% [w/v] xylene cyanol FF in sterile distilled water). It was then loaded into the wells of a 100 ml gel containing 1x Tris/Borate/EDTA (TBE), 1% (w/v) agarose and 0.05 g/ml ethidium bromide which was submerged in 1x TBE buffer. Electrophoresis was performed at 100-120 V for 30-120 min and the DNA fragments were visualised on a UV transilluminator.

2.4.3 Isolation of DNA from agarose gels

DNA fragments that were used for further cloning steps were first viewed using a UV transilluminator and excised using a new razor blade while taking care to remove any unnecessary agarose. The DNA was then extracted using a Promega PCR/Gel clean-up kit following the manufacturer's protocol.

2.4.4 DNA ligations

Ligation of blunt-ended PCR products into pSC-B was carried out using the Stratagene Blunt® PCR Cloning Kit (Stratagene) in 10-µl reactions according to manufacturer's instructions. Fragments were ligated into pET-32a or

pENTR11 vectors in 10µl reactions using 0.5 µl of (0.1u/µl) T4 DNA Ligase, 1µl of T4 buffer and a 3:1 of donor fragment to recipient fragment according to the manufacturer's (Fermentas) protocol.

2.4.5 Transforming *E. coli* and amplifying plasmids in *E. coli*

1-2 µl of plasmid DNA was added to 50 µl of competent DH5α *E. coli* cells. After 30 min on ice the bacteria were put into a 42˚C water bath for 30s before being put back on ice for 2 min. 400 µl of SOC solution (Yeast Extract 0.5%, Tryptone 2%, 10 mM NaCl, 2.5 mM KCl, 10 mM $MgCl_2$, 20 mM $MgSO_4$, 20 mM glucose) was added before placing the *E. coli* into a shaking incubator at 37˚C for 30-90 min. 10 µl and 100 µl were spread onto solid 2YT agar plates containing the appropriate antibiotic selection agent. The plates were then put into an incubator at 37˚C for 12 hours to allow colonies to grow. Single colonies of transformed *E. coli* were then transferred into 2YT liquid broths using sterile wooden toothpicks and allowed to grow overnight.

2.4.6 Preparing agar for selection

Agar medium was melted and then cooled to 55^{o}C allowing addition of kanamycin at 50 ug/ml final concentration. When blue/white screening was used, 1.6 µl of 20 mg/ml X-Gal was added. Medium was mixed before decanting 20 ml into each plate and left to set. When the competent *E. coli* cells of strain BL21-CodonPlus(DE3)-RIL were transformed for *in-vitro* analysis of enzyme activity, 1µl of the pET32a plasmid was taken up using the standard heat shock method. Transformants were then selected on 2YT agar containing 100 mg/ml carbenicillin. Single colonies were selected and grown in 5 ml of 2YT with 100 µg/ml carbenicillin overnight at 37^{o}C.

2.4.7 Gateway cloning, the LR reaction and transferring constructs to the binary vector

All constructs were prepared in pENTR11 using traditional restriction digest and ligation methods (Sections 2.4.1, 2.4.2, 2.4.3 and 2.4.4), the Invitrogen Gateway cloning system was used to transfer constructs into the pGWB7 binary destination vectors. This enables them to be transformed into the GV3101 *Agrobacterium tumefaciens* strain using the standard heat-shock method for subsequent *Arabidopsis* transformation. LR recombination reactions between the pENTR11 cloning vector and pGBW7 binary vector were performed following a simplified Invitrogen protocol. A total volume of 10 ul per reactions was used, 50-150 ng entry plasmid pENTR11was added to each reaction along with 150 ng of the destination vector pGBWB7, 2-8 ul 5xLR Clonase reaction buffer and 2 ul LR clonaseII mix. Finally the reaction was then incubated at 25^{o}C for 2 hours. The whole reaction mix was transformed into DH5α cells, which were selected on plates containing both kanamycin and hygromycin.

2.4.8 Agrobacterium transformation and recovery

50-100 µl of competent *Agrobacterium tumefaciens* GV3101 were thawed on ice before adding 1µg DNA. The mixture was then incubated on ice for 5 min, transferred to liquid nitrogen for 10 seconds and then to a 37ºC water bath for 5 min. 1 ml of LB media was then added before placing the cells in a rocking incubator for 2-4 hours at 28^{o}C. The cells were collected by centrifugation for 30 seconds in a microcentrifuge, and then spread over LB agar plates containing 50 mM kanamycin and 50 mM hygromycin. The plates were then incubated for 2 days at 28^{o}C.

2.4.9 *Agrobacterium*-mediated transformation of *Arabidopsis* by floral dip

The transformed bacteria were incubated in 5 ml liquid 2YT medium containing 25 mg/L kanamycin overnight at 28ºC. Medium (500 ml) was inoculated with the overnight culture (2.5 ml) and grown at 28°C until a final OD_{60} of 4.5 was achieved, when cells were harvested by centrifugation and re-suspended in an infiltration medium consisting of 0.5x MS medium, 5% sucrose and 0.05% Silwet at pH5.8. *Arabidopsis* flowers were then dipped into the bacterial solution for 30 seconds to allow transformation (Clough and Bent, 1998). Plants were then incubated overnight in a propagator.

2.4.10 Genomic DNA extraction for PCR from leaf tissue

For genomic DNA extraction 100mg leaf samples were put into 2ml Eppendorf tubes containing 3mm chrome steel balls, frozen in liquid nitrogen and then ground in the tissue lyser. The ground tissue was then submerged in 200 µl of extraction buffer and incubated at 55ºC for 20 mins. Phenol/chloroform (QBiogene) (200µl) was added to each sample, which was mixed by vortexing for 5 seconds. Samples were then centrifuged for 2 min at 13000 rpm, the supernatant removed and added to 200 µl isopropanol and incubated at room temperature for 2 min before being centrifuged for 5 min at 13000 rpm. The supernatant was discarded and the pellet dried at room temperature for 10 min. The pellet was re-suspended in 100 µl sterile H_2O and 1µl used in 25µl PCR. The primers used for genotyping mutants and demonstrating successful transgene integration are shown in Table 2-1.

Table 2-1: **The primers used for genotyping mutants and demonstrating successful integration of transgene into the genomic DNA.** The table contains the primer names, sequence and size. The melting temperature, annealing temperature and extension temperatures are shown on pages 71 and 72.

Primer name	Primer sequence	Primer size (bp)
RP_2ox2_internal	5'-TATGTGGGGATTAGGGAGATGTGG	24
RP_3ox1_internal	5'-AGGAGATCGTCTTTAGGGGTCCAC	24
RP_20ox1_internal	5'-GTTGATGGAAGGTTTTTCGTCGTC	24
FP_YFP_internal	5'-AGGACGACGGCAACTACAAGACC	23
FP_GA3ox1	5'-ATGTAGAACTTGGGGTGCCTTCC	23
RP_GA3ox1	5'-AGAGGCGATTCAACGGGACTAAC	23
FP_GA3ox2	5'-GTAGCTCGTATTGCTTCGTT	20
RP_GA3ox2	5'-GAAATTCAGTCGGAAGACAG	20
FP_GA2ox2	5'-CACCGGTAGTCTCTTCGGGCTA	22
RP_GA2ox2	5'-AGGTCACCAACGTTAACCACGAG	23
FP_GA2ox7	5'-GGAGGTCAAACGCAAAAGATGTG	23
RP_GA2ox7	5'-CCCAAAGCAATCGATCTCAGTTTC	24
FP_GA20ox1	5'-CGTTCTCGAGCTTGATGTTCCTC	23
RP_GA20ox1	5'-AGCCAATCTGAAAAGGCTTGGAG	23
F_GA20ox1	5'-GCGACGACATGAGCCGCTCAAAATC	25
R_GA20ox1	5'-CTCTCTAAAGTAGTCCCGTTTTACG	25
F2_GA20ox1	5'-CATGAATACACGAGCCGCTTC	22
LBa1	5'-TTTTTCGCCCTTTGACGTTGGA	23
F3_GA20ox2	5'-CGATCTCTCAAGCCAAGACTCG	23
R3_GA20ox2	5'-TCTCTATTCACAACCGCTCTATG	24
GABI-kat LB	5'-CCCATTTGGACGTGAATGTAGACAC	26
F1_GA20ox3	5'-CACTAACCATGGTGTCGATGAGAG	25
R1_GA20ox3d	5'-TTAGAAACAAAGTCTTTAACGGCTT	26
GID1A-1F	5’-GAATTATCGGCGTGCACCA	19
GID1A-1R	5’-TGATTGTTATTAGGCAAGAGGTAAAACC	28
GID1B-1F	5’-TCTCCTGTCCACCAAACATTG	21
GID1B-1R	5’-CTGGGTTTTGGAGACTATGGC	21
SLAT-3’	5’-CTTATTTCAGTAAGAGTGTGGGGTTTTGG	29
GID1C-1F	5’-ATGGCTGGAAGTGAAGAAGTTAATCT	26
GID1C-1R	5’-CAGGGCGACGCAGGAG	16

2.4.11 PCR from genomic DNA and *E coli* colonies

Genotyping of plants and screening of bacterial colonies for successful transformation were carried out by PCR in 25µl reactions containing the following:

Reaction buffer (5x)	5µl
$MgCl_2$ (25mM)	1.5µl
dNTPs (10mM each)	0.5µl
Forward Primer (10µM)	0.75µl
Reverse Primer (10µM)	0.75µl
Promega Taq polymerase (0.1u/µl)	0.2µl
DNA	1µl
H_2O	15.3µl

PCR were assembled on ice and cycled in a Geneamp® PCR system 9700 (PE Applied Biosystems) PCR machine using the following standard conditions:

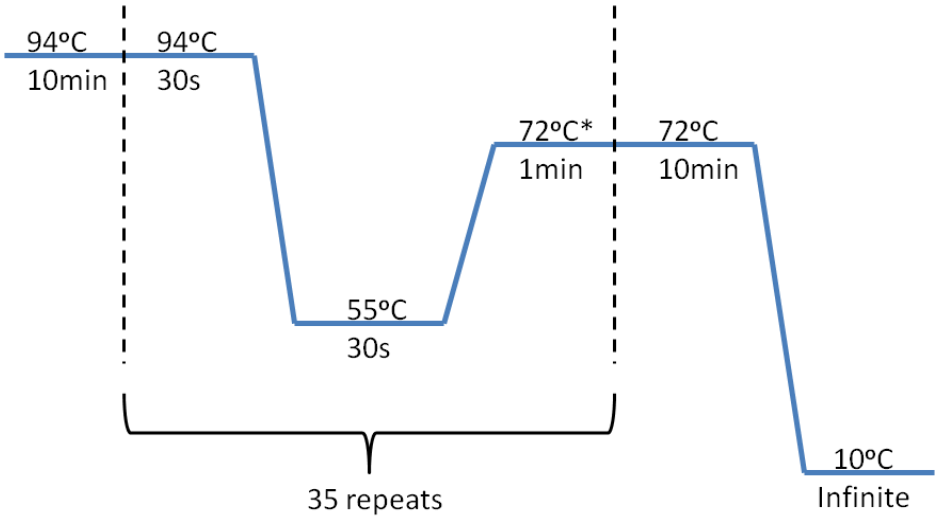

* For PCR products longer than 1-kb an extension time of 1 minute per 1-kb of DNA was used.

2.4.12 Amplifying genes and promoters of interest

When amplifying genes and promoters it was essential that no mutations occurred, so NEB Phusion proof reading taq polymerase was used to ensure PCR with high fidelity. Primers were designed for both the 3' and 5' ends of each gene or promoter incorporating restriction sites required for future cloning steps. The following reaction conditions were used:

Reaction buffer (5x)	10µl
dNTPs (10mM each)	1µl
Forward Primer (10µM)	2.5µl
Reverse Primer (10µM)	2.5µl
NEB Phusion Taq polymerase (0.1u/µl)	0.5µl
DNA	1µl*
H_2O	32.5µl

* Volume varies depending on the concentration of the template plasmid

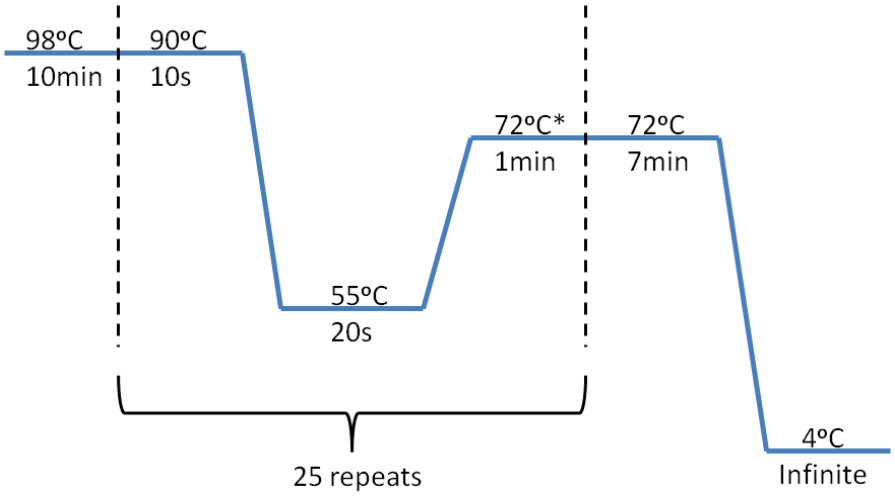

*Time varies depending on the length of the sequence being amplified, an extra 30 seconds was added to the initial 1 minute for every 1-kb of sequence.

Table 2-2: **The primers used to amplify genes and promoters.** The table contains the names, sequence, the restriction site added (restriction sites underlined) and the primer size.

Primers for genes	**Restriction site added**	**Final primer design**	**Primer size (bp)**
C-terminal fusion for *E-coli*			
EYFP F1 for C terminal fusion	*Sal*I	5'-GTCGACATGGTGAGCAAGGGCGAGG	25
EYFP R1 + Stop codon	*Xho*I	5'-CTCGAGCTAAGCCTTGTACAGCTCGT	27
N-terminal fusion			
EYFP F2 for N terminal fusion	*Bgl*II	5'-AGATCTATGGTGAGCAAGGGCGAGG	25
EYFP R2 - stop codon	*Bam*HI	5'-GGATCCAGCCTTGTACAGCTCGTCCA	26
GA oxidase primers			
F1AtGA2ox7	*Bam*H1	5'-AGGATCCATGGCTTCTCAACCTCCCTT	28
R1AtGA2ox7	*Sal*I	5'-GTCGACTCAAATGAGAAACCTGGACA	26
F1AtGA20ox1	*Bam*H1	5'-GGATCCATGGCCGTAAGTTTCGTAAC	26
R1GA20ox1	*Sal*I	5'-GTCGACTTAGATGGGTTTGGTGAGCC	26
F1AtGA3ox2	*Bam*H1	5'-GGATCCATGCCTGCTATGTTAACAGA	27
R1AtGA3ox2	*Xho*1	5'-ACTCGAGTCATTCTTCTCTGTGATTTC	27
F1AtGA2ox2	*Bam*HI	5'-GGATCCATGGTGGTTTTGCCACAGCC	26
R1*AtGA2ox2*- C-fusion	*Xho*I	5'-TCGAGTACAAGGGTTTTATGATTGAG	26
R2*AtGA2ox2* - N-fusion	*Xho*I	5'-ACTCGAGTCATACAAGGGTTTTATGAT	27
Primers for promoters			
Cab_F1 (*Hin*dIII)	*Sal*I	5'-GTCGACGGCTCGCACTTCGCAGATTC	26
Cab_R1(*Bam*HI)	*Bam*HI	5'-GATCCGACTAACTTGTGAGTGAGAGT	26
Co2 F1	*Sal*I	5'-GTCGACGGCTCGCACTTCGCAGATTC	27
Co2 R1	*Bam*HI	5'-AGGATCCCAAACTCTTGTTGCATTA	25
F1*AtGL2* -AT1G79840 -	*Nco*I	5'-ACCATGGCTCTACTTGAGAGATATATC	27
F2*AtGL2* -AT1G79840	*Xho*I	5'-ACTAGAGCTCTACTTGAGAGATATAT	26
R1*AtGL2*-AT1G79840	*Bam*HI	5'-TGGATCCAAAGAAGCTAGCTAGGGAC	26
FPCoR:YFP_*Bam*HI	*Bam*H1	5'-AAGGATCCATGGTGAGCAAGGGCG	24
RPCoR:YFP_*Bgl*II	*Bgl*II	5'-TTAGATCTAGCCTTGTACAGCTCGTCC	27
Primers for GID1a			
FP_GID1a_*Bam*HI	*Bam*HI	5'-TTGGATCCATGGCTGCGAGCGATGAA	26
RP_GID1a_*Eco*R1	*Eco*R1	5'-TGAATTCTTAACATTCCGCGTTTACAA	27

2.4.13 Quantitative PCR

RNA was extracted from 100 root tips using an RNeasy plant RNA isolation kit with on-column DNase treatment (Qiagen), followed by an RNA clean-up using the same kit. 10µg total RNA was treated with Turbo DNA-free kit (Ambion) and 1µg was used as a template to synthesize cDNA using the SuperScript III Platinum Two-Step qRT-PCR Kit with SYBR Green (Invitrogen). PCR was performed on a ABI 7500 Real Time PCR System (Applied Biosystems, Foster City, CA, USA) using Platinum SYBR Green qPCR SuperMix-UDG reagents (Invitrogen), according to the manufacturer's specification, with the cDNA equivalent of 10 ng RNA in a 20 µl reaction volume. Reactions were performed at 65^{o}C in triplicate. Primer dimers were confirmed by analysis of RT-minus and water control samples and by examination of dissociation curves. UBQ10, ACT2 and APT were used as reference genes (Czechowski et al., 2005) when comparing YFP expression. The primers were designed using the Primer 3 website (http://fokker.wi.mit.edu/primer3/input.htm) and are listed in Table 3.

Table 2-3: **Primers for quantitative RT-PCR.**

Gene	Primer name	Primer sequence	Sizes (bp)
Actin 2 AT3G18780	ACT2_LP	5′-TCCCTCAGCACATTCCAGCAGAT-3′	23
	ACT2_RP	5′-AACGATTCCTGGACCTGCCTCATC-3	24
Ubquitin 10 AT4G05320	UBQ10_LP	5′-CACACTCCACTTGGTCTTGCGT-3′	22
	UBQ10_RP	5′-TGGTCTTTCCGGTGAGAGTCTTCA-3′	24
Phosphoribribosyltransferase AT1G27450	APT_LP	5′-GTTGCAGGTGTTGAAGCTAGAGGT-3′	24
	APT_RP	5′-TGGCACCAATAGCCAACGCAATAG-3′	24
YFP	YFP_LP	5′-GACCATHTHATCGCTTCTTCYCGT-3’	24
	YFP_RP	5′-GATCCGCCACAACATCGAGGAC-3’	22

2.5 IN-VITRO EXPRESSION OF *ATGA2OX7, ATGA2OX2:YFP AND YFP:ATGA2OX2*

To investigate if YFP-AtGA2ox2 and AtGA2ox2-YFP function correctly they were created in-situ within BL21 *E-coli*, extracted then tested. In addition, AtGA2ox7 was also incubated with a range of C_{20} and C_{19}-GAs to ensure that it only deactivates C_{20}-GAs.

2.5.1 *E.coli* expression

500 µl of AtGA2ox7, AtGA2ox2-YFP or YFP-AtGA2ox7 overnight 2YT cultures were added to 50 ml of 2YT containing 100 ug/ml carbenicillin and grown in a shaking incubator at 37^{o}C until the optical density was 600 which took between 1-2 hours. Isopropyl β-D-1-thiogalactopyranoside (IPTG) was added to a final concentration of 1 mM and the cultures grown in a shaking incubator for a further 6 hours at 25^{o}C. The cells were pelleted by centrifugation for 5 mins at 4100 rpm. The supernatant was discarded and the cell pellets frozen overnight at -20^{o}C.

2.5.2 Cell lysis for *in-vitro* assays

Cell pellets stored at -80^{o}C (section 2.5.1) were thawed and resuspended in 1.5 ml of freshly prepared lysis buffer (100 mM Tris-HCl pH 7.5, 5 mM DTT, 1 mg/ml lysozyme) and incubated at room temperature for 15 mins. 20 Units of DNase was then added and the incubation continued for 5 min. The lysed cells were centrifuged at 15,000 rpm for 10 min and the supernatant transferred to a fresh tube for future enzymatic studies or freezing at -20^{o}C.

2.5.3 AtGA2ox2 and AtGA2ox7 enzyme assay

The supernatant (section 2.5.2) (90 µL) was incubated at 30°C for 2.5 h with shaking with [^{14}C]GA_9 or [^{14}C]GA_4 (12,500 dpm; 300 Bq/150 pmol) added in 5 µL methanol, and 5 µL cofactor mixture (4 mM 2-oxoglutarate, 4 mM

ascorbate, 0.5 mM $FeSO_4$, 4 mM DTT, 2 mg/ml BSA and 1mg/ml catalase, final concentration). The reaction was stopped by the addition of 10 µL glacial acetic acid, after which the denatured protein was sedimented by centrifugation at 13000 rpm for 2 min.

2.5.4 HPLC Analysis detection of GA post GA2ox incubation

The products remaining post GA incubation with GA2ox2 and GA2ox7 were separated by reversed-phase liquid chromatography using an aqueous methanol gradient mixture of 10% methanol +50µl HAc/L blended with 100% methanol +50µl HAc/L on a Shimadzu Prominence HPLC run for 45 minutes at a ratio dependent on the precise GA being assayed for (methanol gradient average 60%-70%). The oxidation products were detected using an in-line radioactivity monitor (Berthold). The products of oxidation were collected for identification by GC/MS.

3 DESIGN AND CREATION OF CONSTRUCTS AND TRANSGENIC LINES

3.1 INTRODUCTION TO YFP GENE FUSIONS

The main aim of this project was to express GA metabolic enzymes as YFP fusions that will allow their precise location to be determined and then subsequently their effect on root growth to be determined. However, to ensure the presence of an YFP protein fused to either the C or N terminus of the GA metabolic enzymes doesn't affect the function of the enzymes they were first constructed and expressed in *E-coli* for subsequent functional activity testing. AtGA2ox2 was chosen as it has previously been used by the Rothamsted Research Plant Hormone Group, who demonstrated its ability to oxidize the 2-carbon specificity on C_{19}-GAs (Thomas et al., 1999).

3.1.1 Design of N & C *YFP:AtGA2ox2* Expression Constructs

In order to ensure that the YFP fusions are enzymatically active, both C and N terminal *YFP:AtGA2ox2* fusions were generated. They were then expressed in the pET32a vector using BL21-CodonPlus (DE3)-RIL and the expressed YFP:AtGA2ox2 fusions were incubated with GA_{12}, GA_4 and GA_9. The products of the incubation were separated by HPLC and identified from their retention times or by GC-MS.

3.1.2 N-*YFP-AtGA2ox2*::pET-32a

To produce a plasmid construct that allows the expression of YFP fused to the N-terminus of AtGA2ox2, the YFP coding region excluding its stop codon was amplified by PCR (Methods section 2.4 and primer Table 2-2) and cloned into the vector pSC-B (Stratagene). The YFP coding region was then excised from pSC-B using *Nco*I and *Bam*HI and ligated into pET-32a, also cleaved using *Nco*I and *Bam*HI, resulting in the construct YFP:pET-32a. Similarly, the *AtGA2ox2* coding region was amplified by PCR from pYES3/CT35s-2ox2/7-Nos plasmid (provided courtesy of Steve Thomas) and cloned into pSC-B for

confirmatory sequencing. The *AtGA2ox2* coding region was then excised from pSC-B using *Xho*I and *Bam*HI and ligated into N-YFP:pET-32a which had also been cleaved using *Xho*I and *Bam*HI, producing the necessary expression construct N-*AtGA2ox2*:YFP:pET-32a (Figure 3-1-A).

3.1.3 Design of C-*AtGA2ox2-YFP*::pET-32a

To produce a plasmid construct that allows the expression of YFP fused to the C-terminus of *AtGA2ox2*, the YFP coding region was amplified by PCR and cloned into the vector pSC-B (Stratagene) (Methods section 2.4 and primer Table 2-2). The C-terminal-EYFP fusions coding region was then excised from pSC-B using *Sal*I and *Xho*I and ligated into pET-32a, which had also been cleaved using *Sal*I and *Xho*I, resulting in C-YFP:pET-32a. Similarly, the *AtGA2ox2* coding region was amplified without its stop codon by PCR and cloned into pSC-B for confirmatory sequencing. The *AtGA2ox2* coding region was then excised from pSC-B using *Xho*I and *Bam*HI and then ligated into C-YFP:pET-32a which had also been cleaved using *Sal*I and *Bam*HI, producing the expression construct N-*AtGA2ox2*:YFP:pET-32a (Figure 3-1-B).

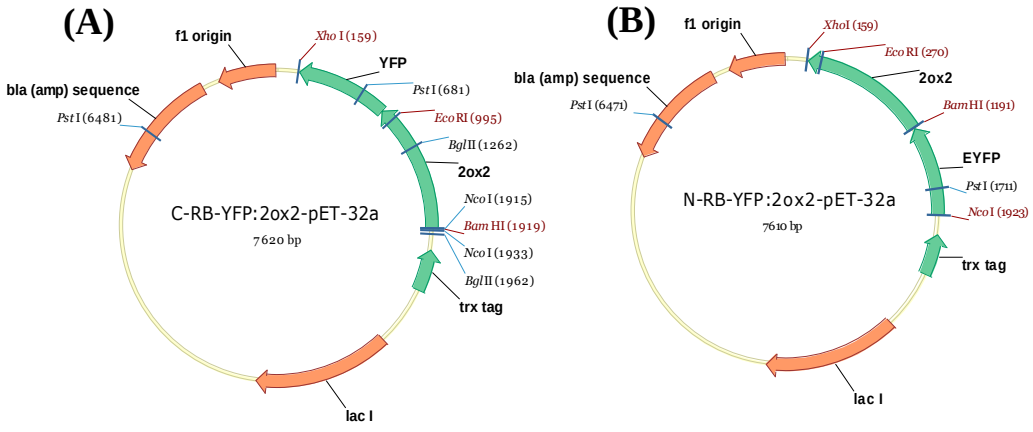

Figure 3-1: **Schematic representations of constructs used for *E-coli* expression. (A)** pET-32a containing the C-terminal *AtGA2ox2:YFP* fusion. **(B)** pET-32a containing the N-terminal *YFP:AtGA2ox2* fusion.

3.1.4 Design of *AtGA2ox7*:pET-32a plasmid

AtGA2ox7 was amplified from plasmids (provided by Steve Thomas, Rothamsted Research) using high fidelity proof reading NEB Phusion Taq polymerases and primers that introduced *Bam*HI and *Sal*I restriction sites (Methods section 2.4 and primer Table 2-2). pET-32a was then cleaved using a *Bam*HI/*Sal*I digest, subsequently allowing *AtGA2ox7* to be ligated into the plasmid, thus creating the bacterial expression vector *AtGA2ox7*:pET-32a (Figure 3-2:).

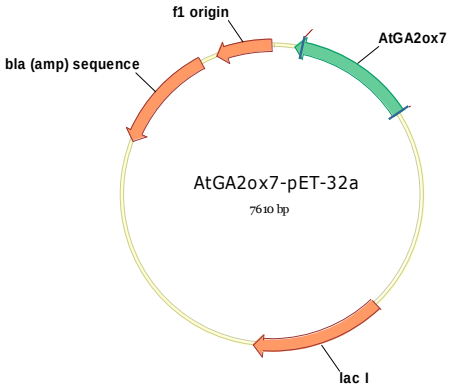

Figure 3-2: **pET-32a containing in-frame *AtGA2ox7* sequence.**

3.2 *IN-VITRO* ASSAY OF *C-YFP:ATGA2ox2* and *N-ATGA2ox2:YFP*

This project required the targeted expression of various enzymes that modify GA metabolism within a variety of different tissues. In order to ensure that the genes were being expressed in the correct tissues they were expressed as YFP fusions, allowing them to be localised by confocal fluorescence microscopy. It has previously been demonstrated that expression of 35S:*GFP:GA2ox8* fusions can reduce the amount of bioactive GAs found within transgenic plants indicating that the fusion is enzymatically active (Zhao et al., 2007). However, it was decided to confirm that this was case by assaying the YFP-AtGA2ox2 fusions *in vitro*. The functionality of both C- and N-terminal YFP fusions was tested by expressing them in *E. coli*, lysing the cells and testing activity *in vitro*. The pET32a expression system allows proteins to be produced from plasmids *in vitro*; the plasmid attaches a thioredoxin tag that increases the

protein solubility, reducing the formation of inclusion bodies, and allowing greater quantities of the active protein to be produced and remain active in solution for functional analysis. They then had their functionality tested with a variety of C_{20}-GA and C_{19}-GA substrates to ensure they only inactivated the correct GAs.

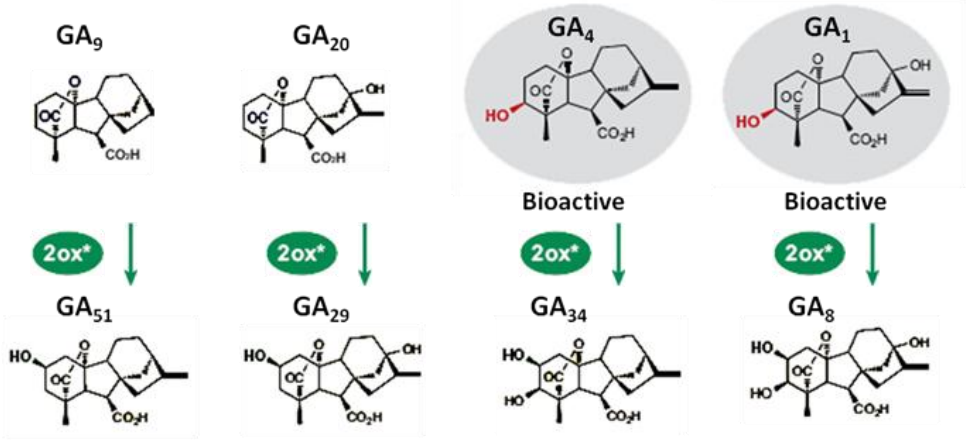

Figure 3-3: **A clade of GA2oxidase enzymes can deactivate both bioactive GA and some of their precursors.** A group of GA 2-oxidases can catalyse the oxidation of C-2 on C_{19}-GA precursors such as GA_9 and GA_{20} before activation by 3β-hydroxylation and on the bioactive products GA_4 and GA_1. (Adapted with permission from Shinjiro Yamaguchi., (2008)).

3.2.1 *In vitro* assay with AtGA2ox2

The *YFP* from pENTR11:*SCR::YFP* and *AtGA2ox2* from pSCB*:AtGA2ox2* were cloned into the pET32a plasmid to produce *C-YFP:AtGA2ox2-pET-32a* and *N-YFP:AtGA2ox2-pET-32a* constructs, which were transformed into the *E. coli* strain BL21. Cell lysates were prepared from both strains and from pET32a containing AtGA2ox2 as a positive control and these were incubated with [^{14}C]GA_9 or [^{14}C]GA_4 to test for 2β-hydroxylase activity. Substrates and products were separated by high performance liquid chromatography (HPLC) and detected using an on-line radioactivity monitor (Figure 3-5). The HPLC radio-chromatogram traces shown in Figure 3-5-B, Figure 3-5-C and Figure 3-5-D are for [^{14}C]GA_4 incubations while the HPLC radio-chromatogram traces shown in Figure 3-5–B, Figure 3-5–C and Figure 3-5–D are for [^{14}C]GA_9 incubations. The products were identified on the basis of their HPLC retention times; Figure 3-5-C and Figure 3-5–D show major peaks at 20min (GA_{51}-catabolite), and 25min (GA_9) indicating that GA_9 was oxidised by both C and N terminal YFP-AtGA2ox2 fusions. Figure 24-C and Figure 24-D show peaks at 22min (GA_{34}), 23.14 min (GA_{34} catabolite) and 24min (GA_4) indicating that GA_4 was also 2β-hydroxylated by both C and N terminal *YFP:AtGA2ox2* fusions. In conclusion it is clear that it is possible to express AtGA2ox2 as a C or N-terminal YFP fusion protein without affecting its functionality in *E-coli*.

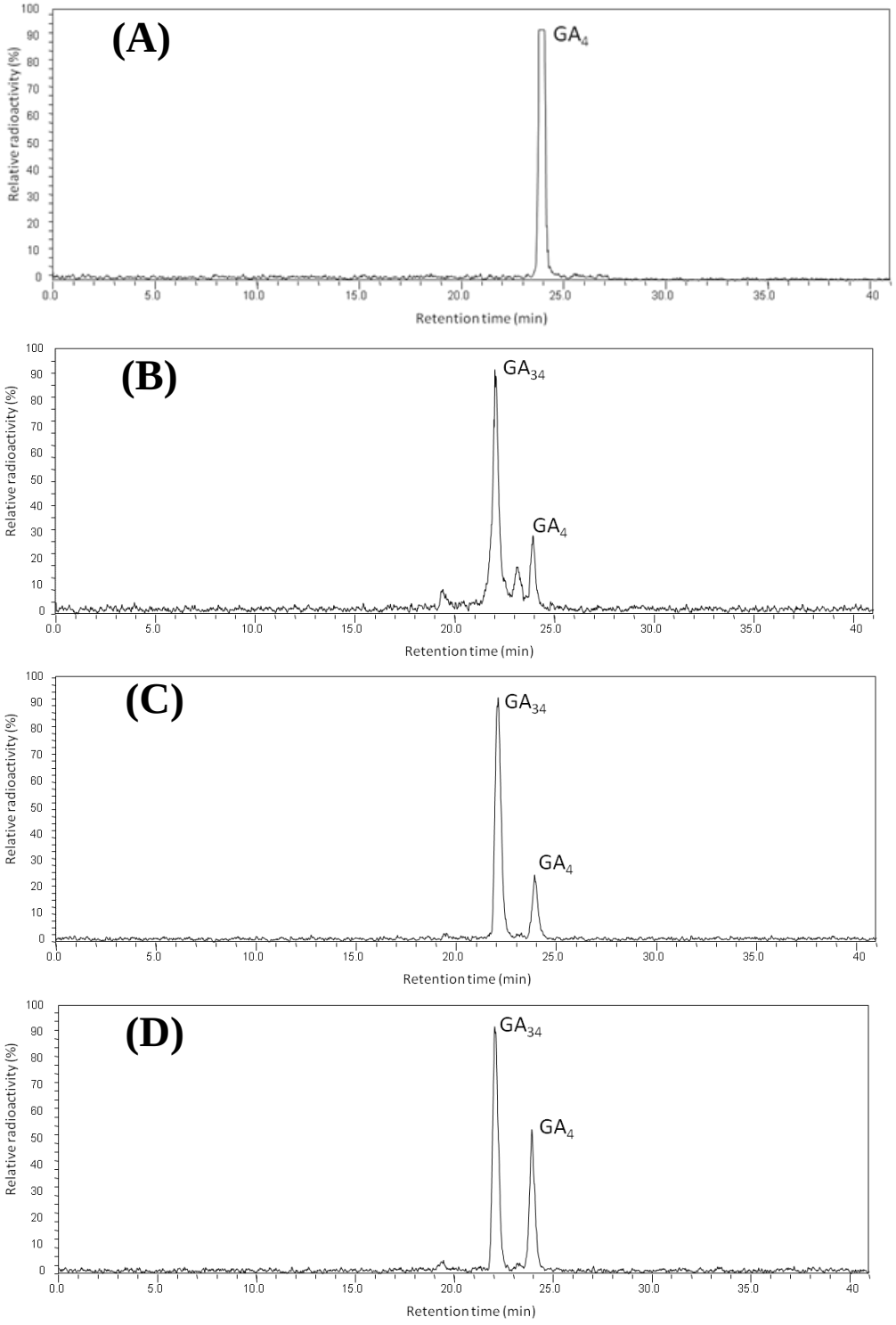

Figure 3-4: ***AtGA2ox2:YFP* degrading GA in vitro.** *In-vitro* catalytic activity of *AtGA2ox2:YFP* fusion proteins with GA_4. HPLC-radioactivity chromatogram traces are shown. **(A)** [^{14}C]GA_4 standard, retention time 24 min. **(B)** Incubation of [^{14}C]GA_4 with *AtGA2ox2*. There were two major peaks: GA_{34} (22 min) and GA_4 (24 min). **(C)** Incubation of [^{14}C]GA_4 with C-terminal *YFP:AtGA2ox2* fusion, there were two major peaks: GA_{34} (22. min) and GA_4 (24 min). **(D)** Incubation of [^{14}C]GA_4 with N-terminal *YFP:AtGA2ox2* fusion, there were two major peaks: GA_{34} (22 min) and GA_4 (24 min).

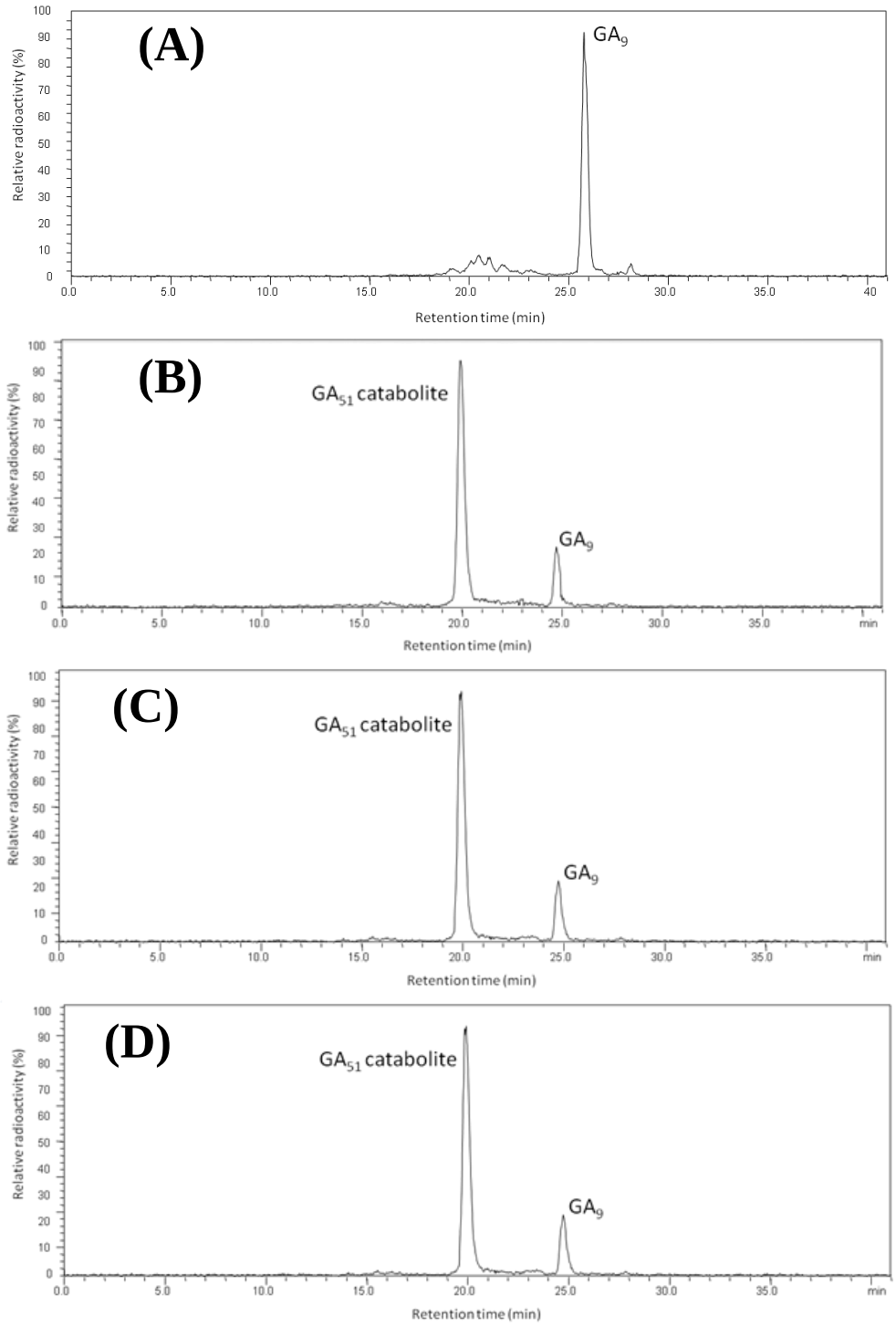

Figure 3-5: ***YFP:AtGA2ox2* degrading GA in vitro.** *In-vitro* catalytic activity of *AtGA2ox2:YFP* fusion proteins. HPLC-radioactivity chromatogram traces are shown. (**A)** [^{14}C]GA_9 standard with a retention time of 25.8 min. **(C)** Incubation of [^{14}C]GA_9 with AtGA2ox2. There were two major peaks: GA_{51}-catabolite (25 min) and GA_{51} (20 min). **(D)** Incubation of [^{14}C]GA_9 with a C-terminal AtGA2ox2:YFP fusion produced two major peaks, identified by HPLC retention time as GA_{51}-catabolite (20 min) and GA_9 (25 min).

3.2.2 In-vitro assay with AtGA2ox7

Two *Arabidopsis* genes, *AtGA2ox7* and *AtGA2ox8*, which form a distinct class of GA 2-oxidases that are capable of catalysing the inactivation of C_{20}-GAs by 2β-hydroxylation, were first identified by an activation-tagging mutant screen. Schomburg *et al* (2003) showed *in vitro* that both were capable of reducing the formation of GA_{24} and GA_{19} via 2β-hydroxylation of the C_{20}-GA precursors GA_{12} and GA_{53} (Figure 3-6). These genes could be used to degrade GA precursors in a tissue specific manner to reveal the site of early 20ox biosynthesis reaction by the 20-oxidisation. In order to ensure that the *AtGA2ox7* enzyme functioned as previously described by Schomburg *et al* (2003), *AtGA2ox7* was cloned into pET32a and the plasmid transformed into the *E. coli* strain BL21 for *in-vitro* analysis. Cell lysates were prepared and incubated with [^{14}C]GA_9, [^{14}C]GA_4 or [^{14}C]GA_{12}. The products were then analysed by HPLC with on-line radiomonitoring and their identity subsequently confirmed by GC-MS. The HPLC radio-chromatogram traces are shown (Figure 3-7, Figure 3-8, Figure 3-9). When AtGA2ox7 was incubated with the C_{19}-GAs [^{14}C]GA_4 and [^{14}C]GA_9 no metabolites were produced. However it did show activity with the C_{20}-GA [^{14}C]GA_{12} which was partially converted to one major metabolite with a retention time of 14 minutes. This was identified by GC-MS as GA_{110} (2β-hydroxy-GA_{12}). Taken together these data have shown that AtGA2ox7 is capable of oxidising the C_{20}-GA GA_{12}, but not C_{19}-GAs, and therefore it is suitable for targeted expression studies that will aim to locate the sites of GA biosynthesis rather than sites of action.

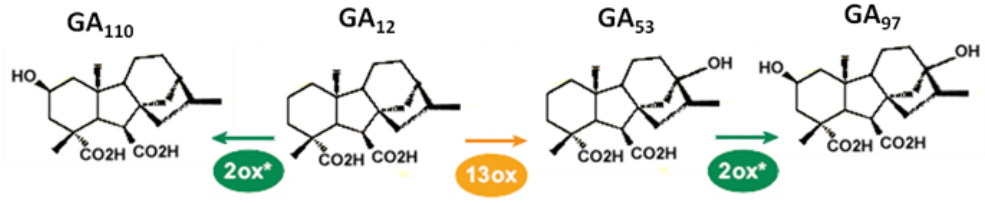

Figure 3-6: **AtGA2ox7 can oxidize the C-2 carbon either before or after 13-hydroxylation.** The oxidation of C-2 can take place on C_{20}-GAs such as GA_{12} and GA_{53} by a separate clade of GA 2-oxidases from those that oxidise C_{19}-GAs. (Adapted with permission from Shinjiro Yamaguchi., (2008)).

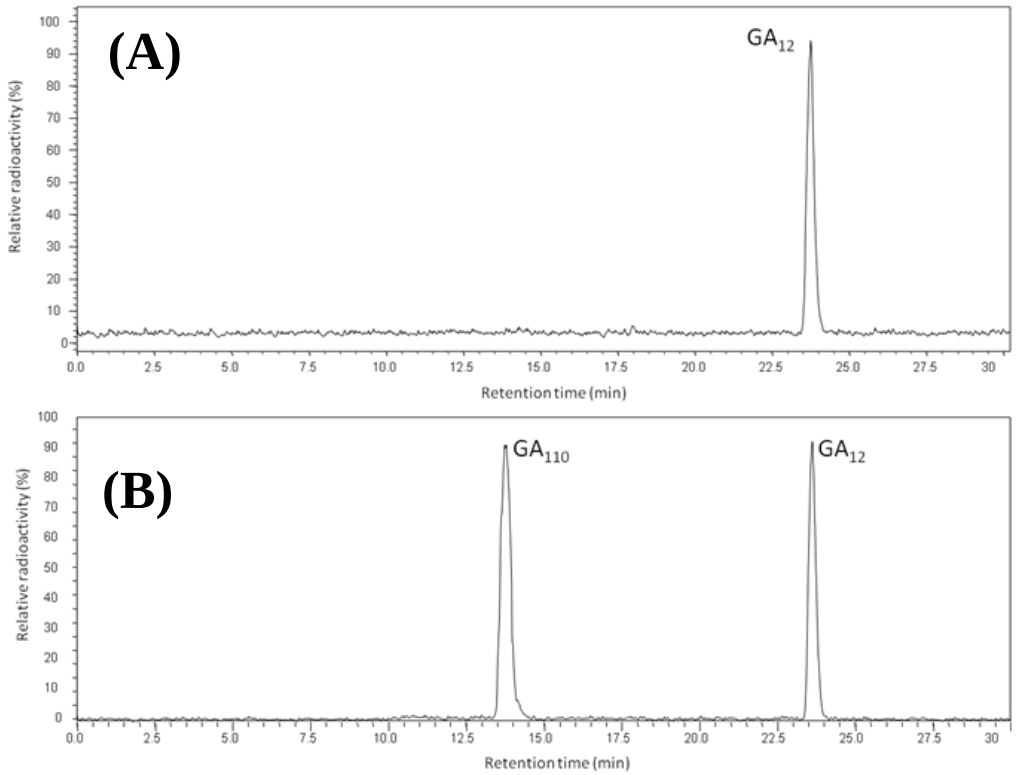

Figure 3-7**: *In-vitro* assay of AtGA2ox7 with GA_{12}. (A)** HPLC-radioactive trace for the [^{14}C]GA_{12} standard that was used for the incubations, **(B)** HPLC-radioactive trace produced after incubating [^{14}C]GA_{12} with AtGA2ox7 for 24 hours. There was one major metabolite with a retention time of 14 minutes that was subsequently identified as [^{14}C]GA_{110}.

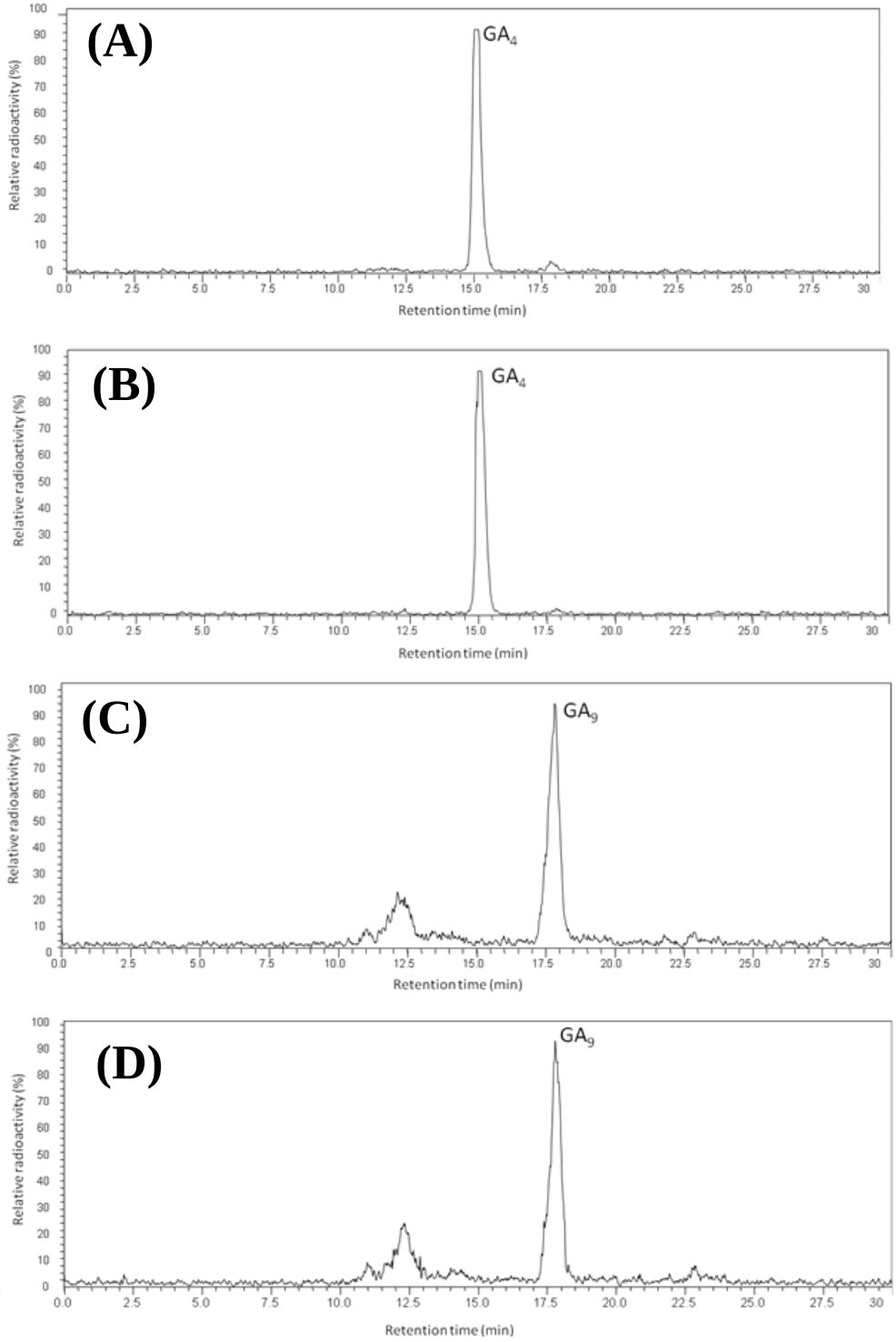

Figure 3-8**: *In-vitro* assay of AtGA2ox7 with GA_4 and GA_9.** **(A)** HPLC-radiochromatogram trace for the [^{14}C]GA_4 standard that was used for the incubations, **(B)** HPLC-radiochromatogram trace produced after incubating [^{14}C]GA_4 with AtGA2ox7 for 24 hours. **(C)** HPLC-radiochromatogram trace for the [^{14}C]GA_9 standard that was used for the incubations, **(D)** HPLC-radioactive trace produced after incubating [^{14}C]GA_9 with *AtGA2ox7* for 24 hours. The small peaks between 10-13 minutes were collected and subsequent analysis by GC-MS revealed that they were not GA metabolites.

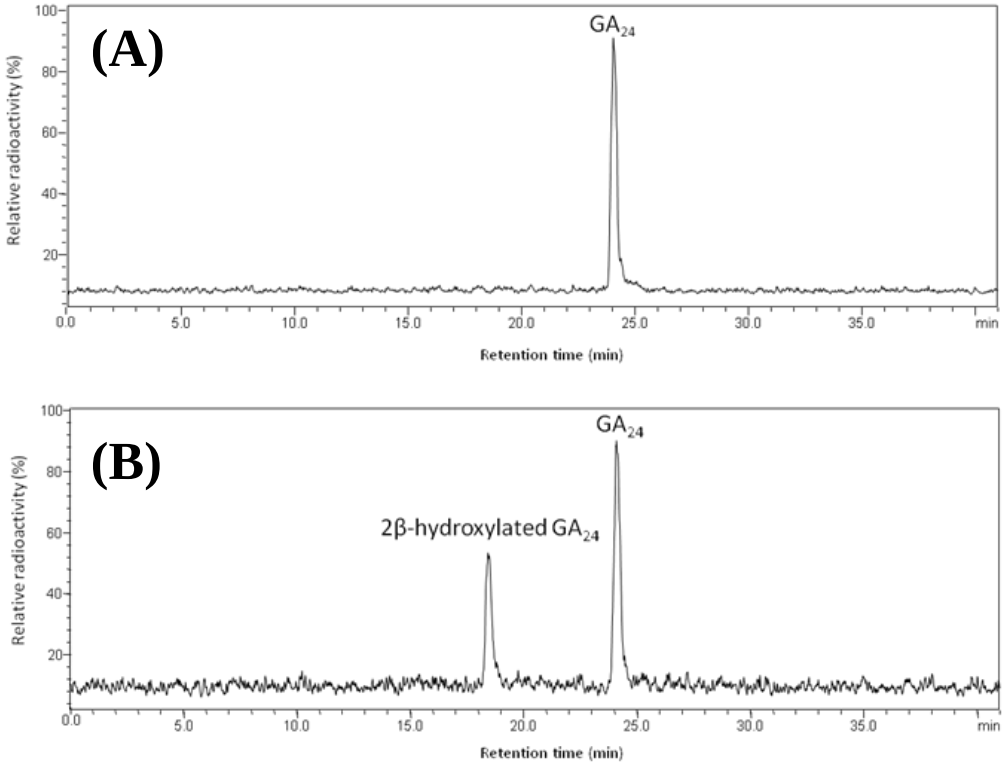

Figure 3-9**: *In-vitro* assay of AtGA2ox7 with GA_{24} (A)** HPLC-radioactive trace for the [^{14}C]GA_{24} standard that was used for the incubations, **(B)** HPLC-radioactive trace produced after incubating [^{14}C]GA_{24} with AtGA2ox7 for 24 hours. There was one major metabolite with a retention time of 18 minutes that was subsequently identified as [^{14}C]2β-hydroxylated GA_{24}.

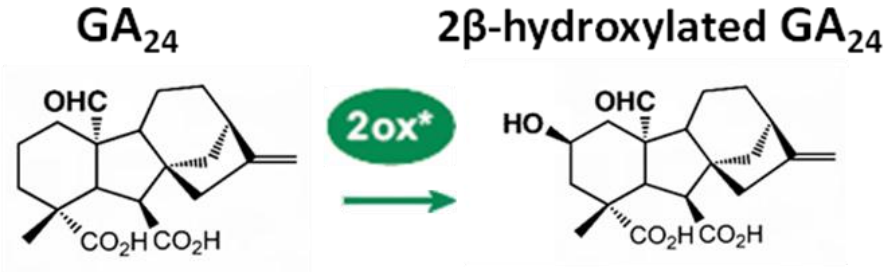

Figure 3-10: **GA_{24} can be inactivated by *AtGA2ox7*.** The oxidation of C-2 can also take place on the C_{20}-GA GA_{24} which is converted to 2β-hydroxylated GA_{24}. (Adapted with permission from Shinjiro Yamaguchi., (2008)).

3.2.3 Summary of results from *in vitro* analysis of GA2ox activity

Attaching YFP to either the N or C terminus of the GA2ox2 protein did not prevent it from performing hydroxylation on C-2 that would deactivate both bioactive GA and GA precursors. This *in-vivo* analysis indicates that YFP fusions to GA oxidase genes can be used as a tool to investigate where they function without disrupting their ability to metabolise GA. This combined with the use of a N-terminal 35S:*GFP*:*AtGA2ox8* fusions in previous studies (Zhao et al., 2007) illustrates that the N-terminal YFP fusions can now be used in conjunction with tissue specific promoters. Assuming that all the GA metabolic oxidase enzymes behave similarly the same methodology could also be used on GA deficient mutants that are lack *AtGA3ox* and *AtGA20ox* genes in order to elicit further information about their sites of action. *In-vivo* analysis of AtGA2ox7 showed that it was capable of 2-β-hydroxylation of the C-2 resulting in the 2β-hydroxylation of GA_{12}, in addition to confirming 2β-hydroxylation of GA_{12}, it was shown that AtGA2ox7 is also capable of 2β-hydroxylation of GA_{24} and therefore preventing it being converted to GA_9 and then activated to GA_4. After confirmation that *YFP:AtGA2ox2* acts only on C_{19}-GAs and AtGA2ox7 is specific for C_{20}-GAs they were used in targeted expression constructs, which were transformed along with the other constructs into Col-0, *ga3ox1,-2*, *ga20ox1,-2,-3* or *gid1a,-b,-c* via *Agrobacterium* mediated floral dip transformation.

3.3 PROMOTERS FOR TISSUE-SPECIFIC EXPRESSION

3.3.1 Promoter introduction

It has long been known that when a gene is transferred from one plant to another one of the same species, correct expression can be achieved provided the appropriate 3' and/or 5' flanking regions are intact (Goldberg, 1986). Since the sequencing of the *Arabidopsis* genome in 2000 (The_Arabidopsis_Initiative, 2000) and the advent of microarrays it has become clear that much of gene regulation is at the transcriptional level and serves to confine expression to specific regions. Expression studies have identified a number of *Arabidopsis* genes for which expression is limited to specific cell types. Table 3-1 lists genes that have been shown to be expressed in specific tissues within the *Arabidopsis* root, and the photosynthetic tissue-specific gene, the promoters of which have been selected for the current study.

Table 3-1: **Genes for which expression is targeted to specific tissues within the *Arabidopsis* root.**

Tissue targeted	Gene with tissue specific expression	ATG code	Reference
Epidermis	GL2 – GLABRA2	At1g79840	Hung et al., (1998)
Cortex – Meristematic region	Co2 – Unknown protein	At1g62500	Heidstra et al., 2004
Cortex – Elongation zone	CoR – Unknown protein	AT1G09750	Dinneny et al., 2008
Endodermis	SCR - SCARECROW	At3g54220	Di Laurenzio et al., 1996
Stele	SHR – SHORTROOT	At4g37650	Di Laurenzio et al., 1996
Green tissue/shoots	CAB – Chlorophyll a/b binding protein	At1g29920	Puente et al., 1996

3.3.2 *SHR* promoter and the vasculature/stele (At4g37650)

SHORTROOT (*SHR*) is a member of the GRAS family of putative transcription factors, and is known to be essential in order to maintain correct *SCR* expression within the endodermis. Interestingly it has been shown that it is not expressed in the cells in which it acts, the translated protein being capable of moving from the stele to the nucleus of neighbouring endodermal and QC cells (Heidstra et al., 2004, Dolan, 2001). *SHR* is expressed in the meristematic region of the root stele, within the vasculature next to the initial cells, in both the central vascular cylinder and the surrounding pericycle cells (Helariutta et al., 2000, Di Laurenzio et al., 1996).

During the late globular stage of embryo development *SHR* is expressed in the lower tier of the procambium cells, which then differentiates into stele tissue. *SHR* is then found within the procambium/stele during the intermediate and later stage of embryogenesis known as the heart stage, torpedo stage and also the final mature embryo. In addition, in the final stages of embryo development, *SHR* expression also extends into the procambium of the cotyledon petiole (Helariutta et al., 2000). Publicly available microarray data (Figure 3-11 and Figure 3-12) suggests that *SHR* is also found in the rosette and inflorescence, but importantly is excluded from the central zone of the SAM and is highly expressed in the peripheral zone (Yadav et al., 2009). Recently Dhondt *et al.* (2010) used *SHR:GUS* data to show that *SHR* expression during leaf development is initially in the apical tip, its expression then appears in the proto-vasculature network until it appears to be expressed uniformly throughout the vasculature of the whole mature leaf. At about 10 days post leaf emergence *SHR* expression is gradually restricted to the vasculature and then finally after 24 days, its expression expands into the bundle sheath cells (Dhondt et al., 2010).

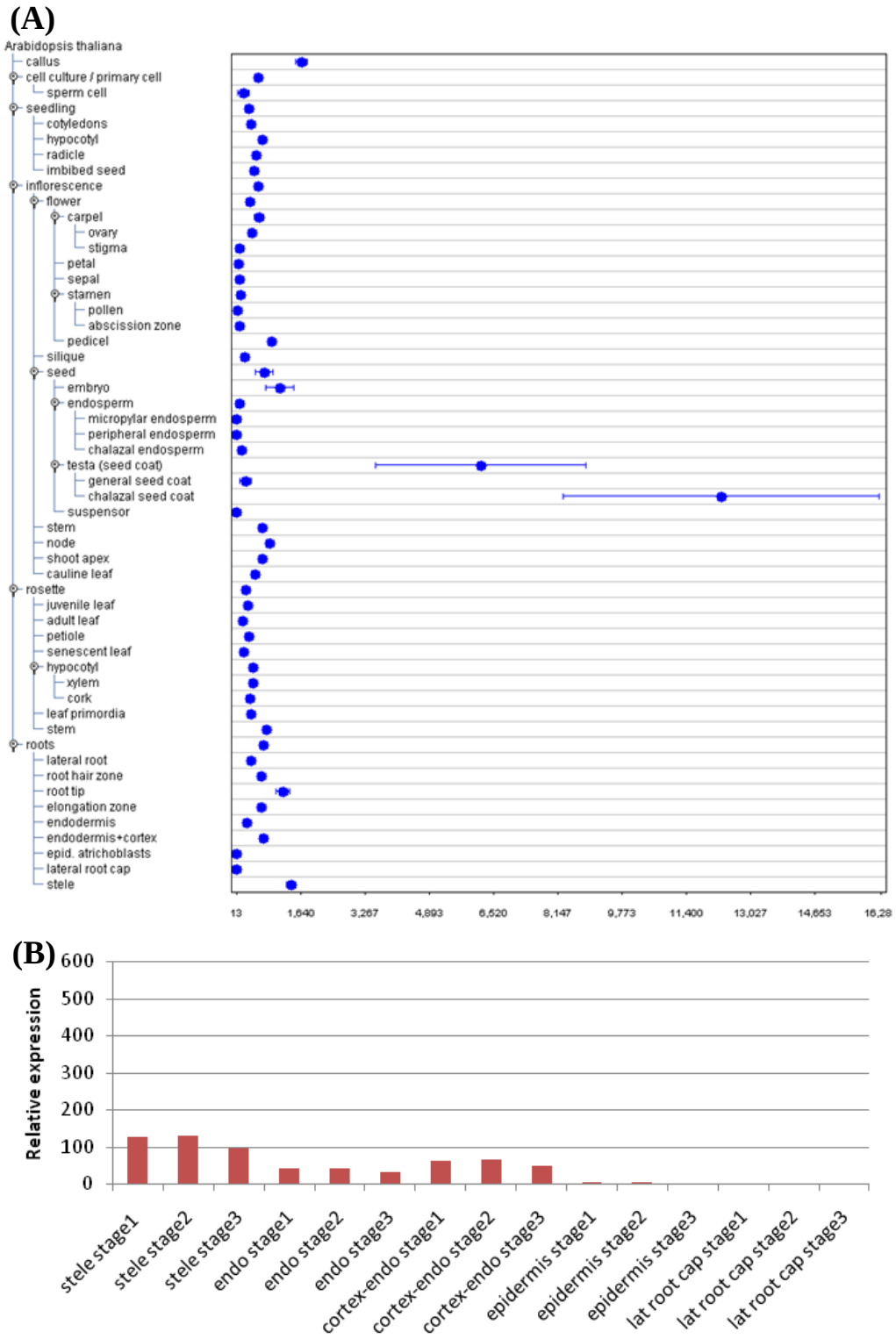

Figure 3-11: ***In silico*** **expression analysis of *SHR* promoter. (A)** *SHR* expression data generated from microarrays and accessed via Genvestigator https://www.genevestigator.com/gv/ (25/10/09). **(B)** Expression data for *SHR* expression in the root apex, taken from the root expression atlas (Birnbaum *et al.*, 2002).

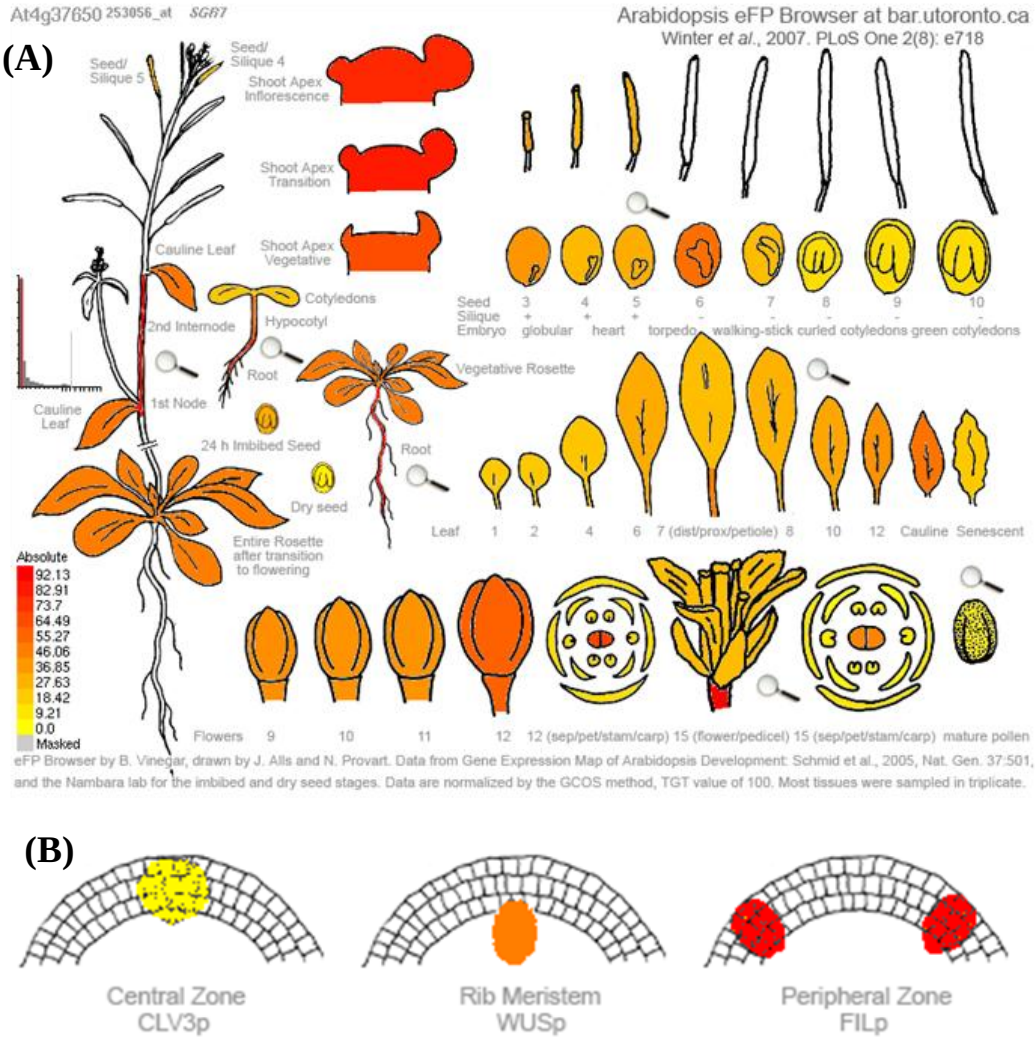

Figure 3-12: ***In silico* expression analysis of *SHR* promoter. (A)** Absolute expression of *SHR* during *Arabidopsis* development. **(B)** Absolute expression of *SHR* within the SAM. Expression profiles were predicted using microarray data and accessed online at http://bar.utoronto.ca/efp/cgi-bin/efpWeb.cgi on the 26/2/11.

3.3.3 SCR promoter and the endodermis (At3g54220)

SCARECROW (*SCR*) is a member of a novel family of proteins that, binds to DNA due to a basic-leucine zipper region. SCR is required for the autonomous distal specification of the quiescent centre, which in turn regulates the fate of the immediately surrounding stem cells and is involved in regulating the radial organization of the root (Benfey and Scheres, 2000). In WT *Arabidopsis* plants *SCR* mRNA can be found in the inflorescence, siliques, leaves, and roots (Figure 3-13 and Figure 3-14).

During embryo development, *SCR* was detected in the ground tissue during the late heart-stage, then after the ground tissues divides the expression was detected solely in the endodermis. Close inspection of specific root tissues in young and old seedlings revealed that in both developing and mature roots *SCR* expression was confined to the endodermis, the cortex/endodermal initial cells and QC demonstrating that after the periclinal division of the initial cells *SCR* expression was restricted to the endodermal daughter cells (Di Laurenzio et al., 1996). *SCR* mutants have hypocotyl and shoot radial pattern defects, and they have an abnormal starch sheath and the shoot is unable to respond to gravity. *SCR* is expressed in the starch sheath cells, which are analogous to the root endodermal cells, in the leaves, hypocotyl and inflorescence stems (Wysocka-Diller et al., 2000). It also appears that the same molecular mechanism that regulates the radial patterning during embryogenesis and post-embryonically functions in ground tissues, not only in roots, but also shoots (Wysocka-Diller et al., 2000).

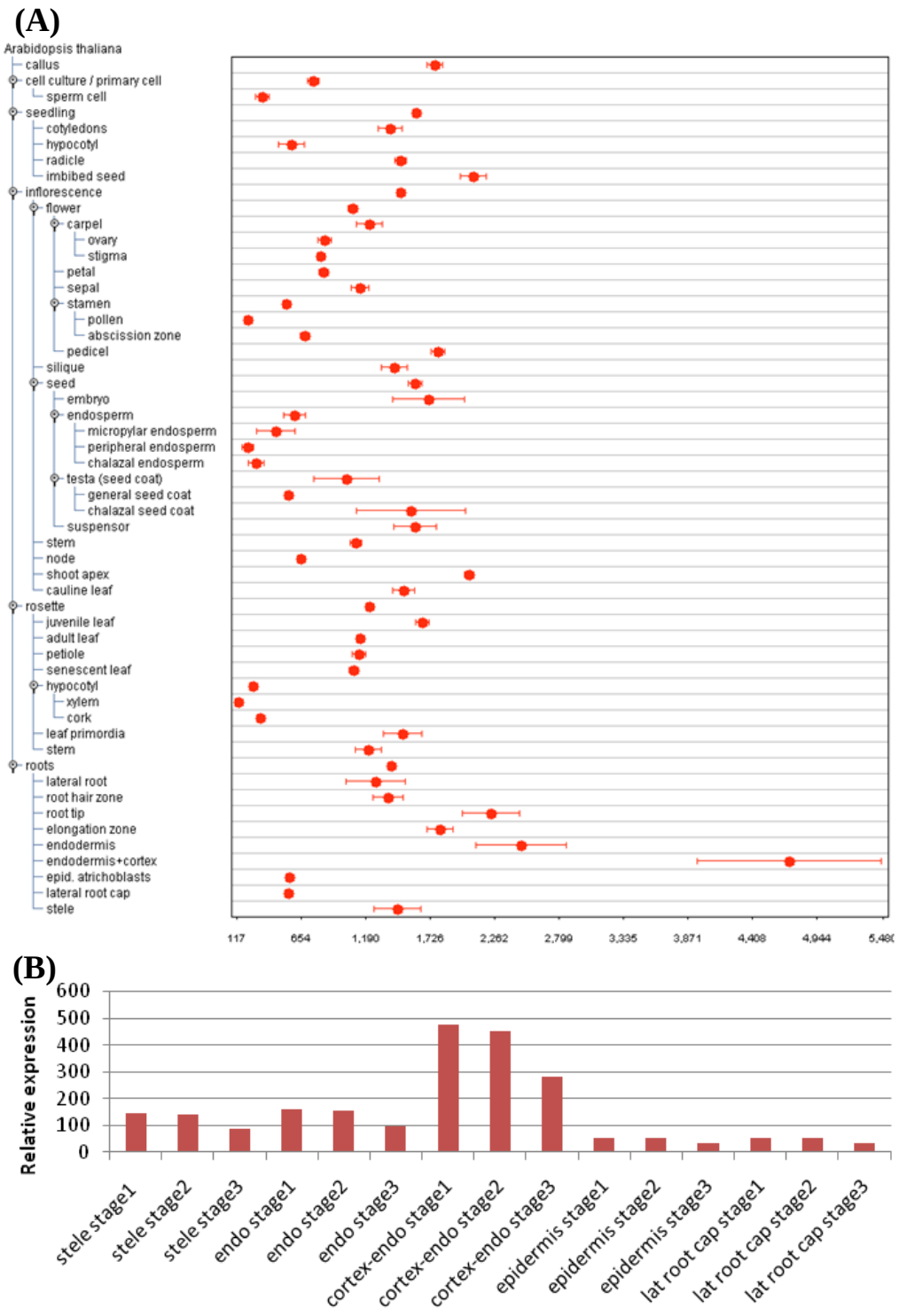

Figure 3-13: ***In silico* expression analysis of *SCR* promoter. (A)** *SCR* expression data generated from microarrays and accessed via Genvestigator (25/11/09). **(B)** Expression data for *SCR* expression in the root apex, taken from root expression atlas (Birnbaum *et al.*, 2002).

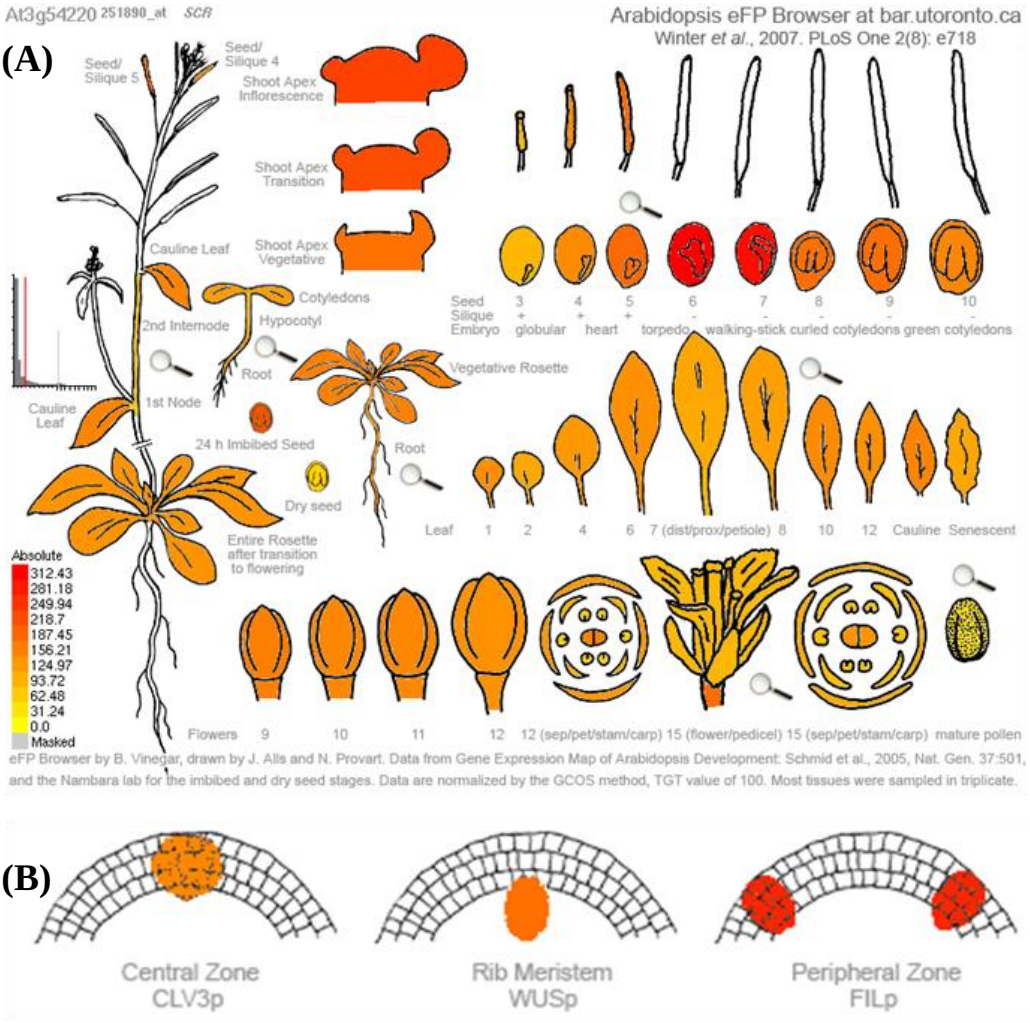

Figure 3-14: ***In silico* expression analysis of *SCR* promoter. (A)** Absolute expression of *SCR* during *Arabidopsis* development. **(B)** *SCR* expression during within the SAM. Expression profiles were predicted using microarray data and accessed online at http://bar.utoronto.ca/efp/cgi-bin/efpWeb.cgi on the 26/2/11.

3.3.4 *CoR* promoter (AT1G09750)

Cell identity varies across the root radial sections. Starting from the outermost tissue, it comprises of epidermal cells, followed by the cortex, the endodermis, and the central stele. It has been shown using fluorescence-activated cell sorting (FACS) (Birnbaum et al., 2005) that each of the different root tissues have distinct transcript profiles that change as the root grows and the cells age (Dugardeyn et al., 2008, Brady et al., 2007, Birnbaum et al., 2003). These cell-type–specific transcriptional profiles identified the *CoR* gene (AT1GO9750), a chloroplast nucleotide DNA-binding protein related to the aspartyl protease family protein, which is expressed specifically within the cortex, and only in the elongation zone (Dinneny et al., 2008).

Microarray data demonstrated that *CoR* is expressed within imbibed seeds, the embryo and developing seedlings (Figure 3-15). Later on in development it is also expressed during rosette growth within the leaf primordia, developing juvenile leaves and gradually increasing in expression before peaking in adult leaves. *CoR* is also expressed during inflorescence development and throughout all parts of the flower, *CoR* is highly expressed in the rib meristem and the peripheral region of the SAM, but is completely excluded from the central zone (Figure 3-16). The *CoR* promoter (provided courtesy of Dr Daniela Dietrich), is a 500 bp sequence upstream of the start codon, and has been used to drive the expression of GFP, confirming its expression pattern and also revealed its responsiveness to ABA (Figure 3-17 (Unpublished data courtesy of the Benfy Lab).

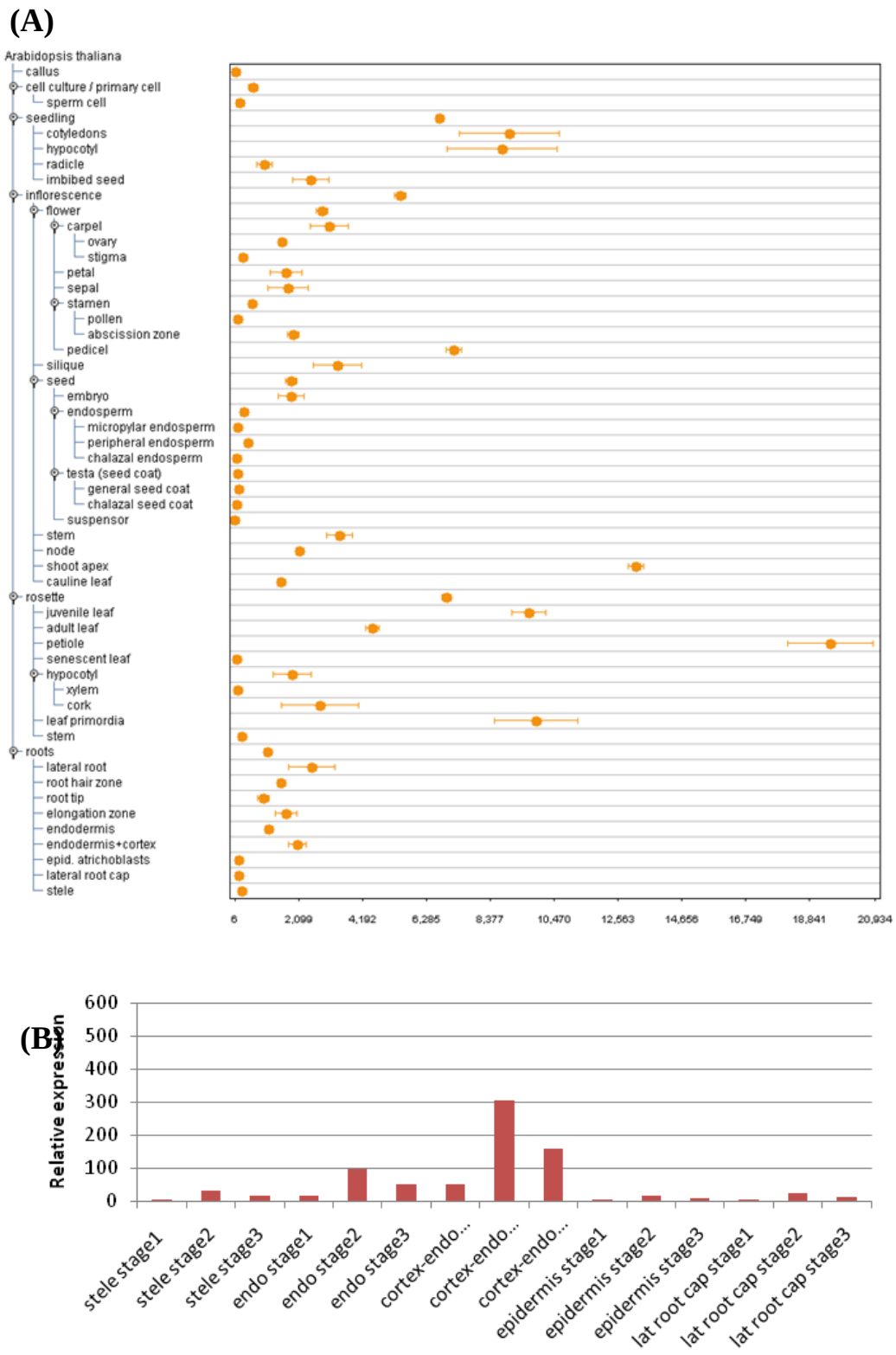

Figure 3-15: ***In silico* expression analysis of *CoR* promoter.** (A) *CoR* expression accessed from Genvestigator on the 25/10/09. (B) Expression data for *CoR* expression in the root apex, taken from the root expression atlas (Birnbaum *et al.*, 2002).

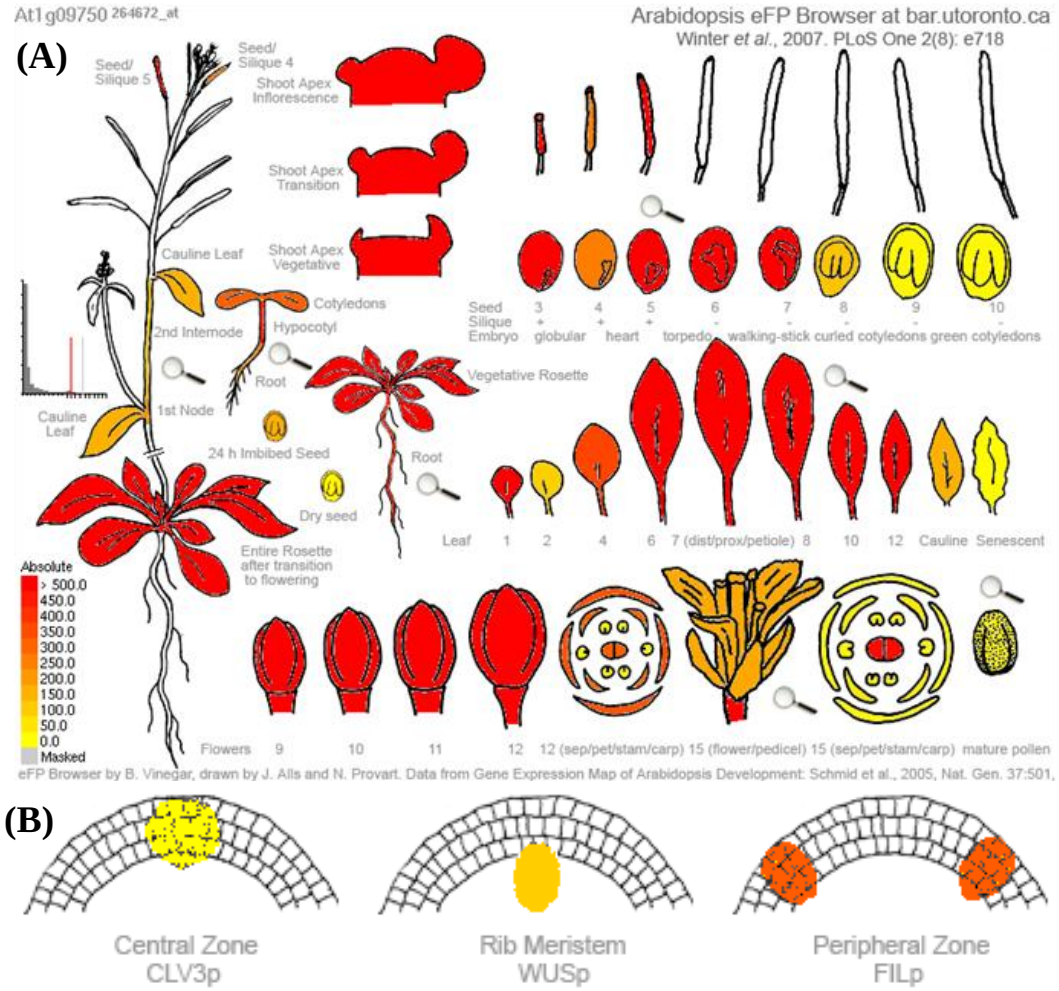

Figure 3-16: ***In silico* expression analysis of *CoR* promoter.** **(A)** Absolute expression of *CoR* during *Arabidopsis* development. **(B)** Absolute expression of *CoR* within the SAM. Absolute expression profile of *CoR* was obtained via http://bar.utoronto.ca/efp/cgi-bin/efpWeb.cgi accessed on the 25/2/11.

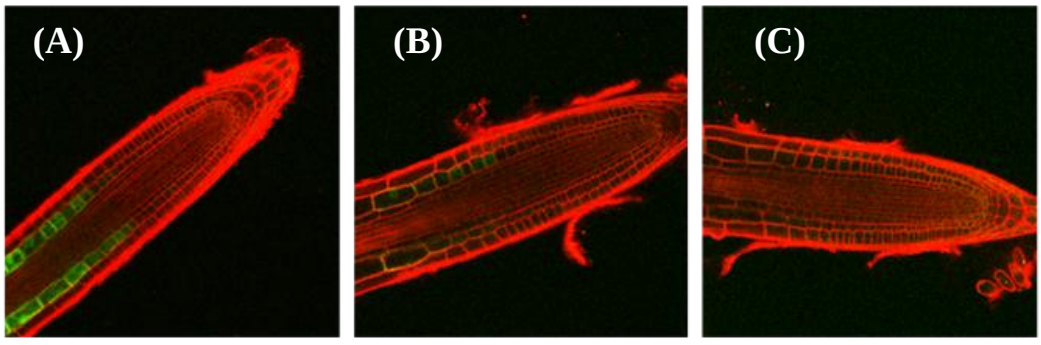

Figure 3-17: ***COR::GFP* expression is reduced one day after ABA treatment** (images courtesy of Dr Daniela Dietrich). **(A)** 0μM ABA . **(B)** 1μM ABA. **(C)** 10μM ABA.

3.3.5 *Co2* promoter (At1g62500)

The *Co2* gene (At1g62500) encodes a protein with similarity to lipid binding, cell-wall plasma-membrane linker proteins. Fluorescent activated cell sorting (FACS) indicated that the *Co2* genes expression is confined specifically to the meristematic region of the cortex, the tissue specificity was conferred by a 0.5-kb non-coding region upstream from the 5' end of the open reading frame (Heidstra et al., 2004). Expression of the *Co2::YFP* reporter gene was confined to the predicted regions of the cortex of transgenic WT roots and was clearly excluded from the QC and ground tissue stem cells (Paquette and Benfey, 2005, Heidstra et al., 2004). FACS and microarray analysis has recently generated a list of the genes expressed within the endodermal/cortical initial cells that included *Co2* (Sozzani et al., 2010). Publically available microarray data suggests that *Co2* is expressed within the seed, the embryo, developing seedling, juvenile rosette leaves and inflorescence, with peaks of expression within the carpel and ovary (Figure 3-18). *Co2* is most highly expressed at the shoot apex during the vegetative, inflorescence and transition stages, more specifically within in the rib meristem and peripheral zone of the SAM (Figure 3-19).

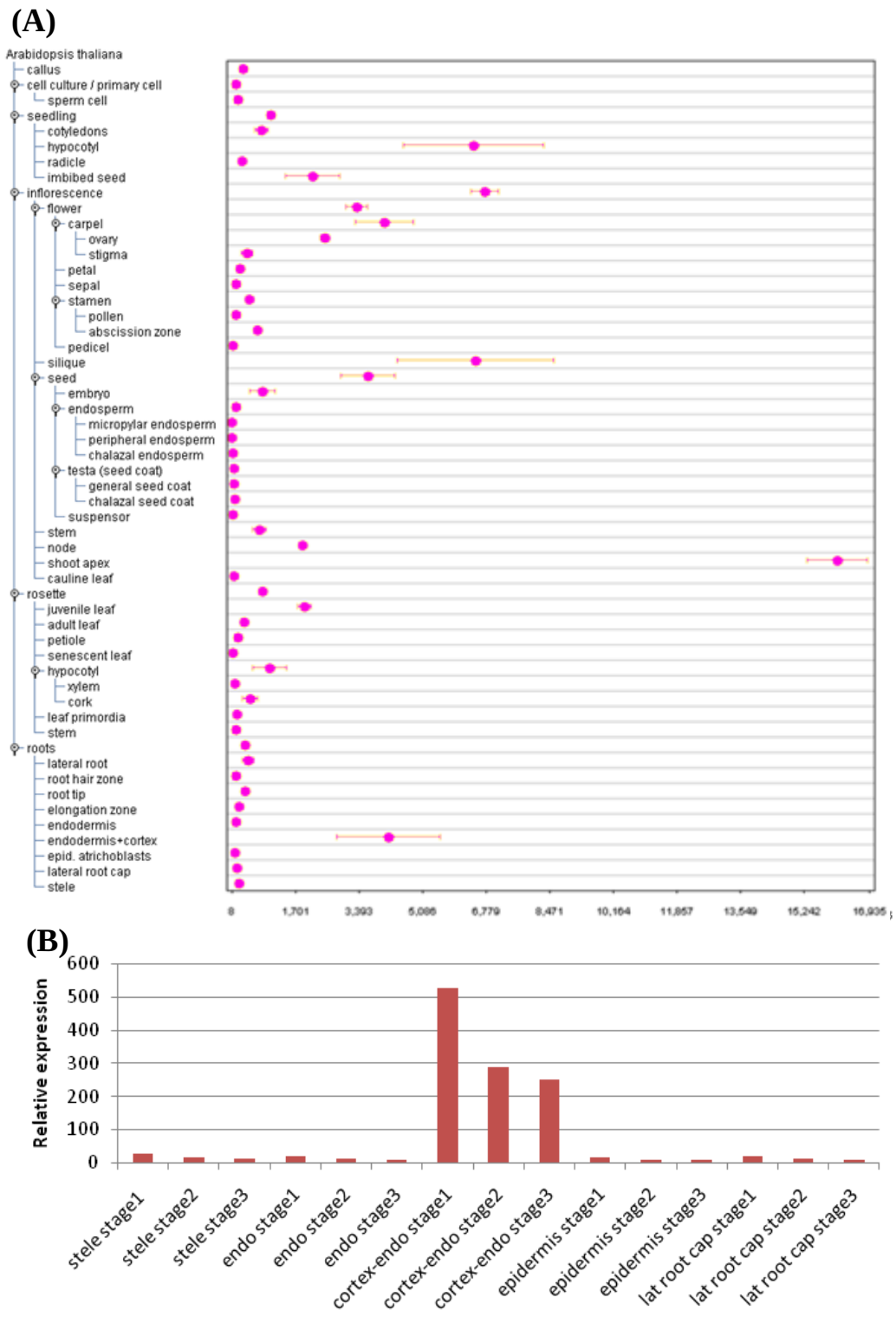

Figure 3-18: ***In silico* expression analysis of *Co2* promoter.** **(A)** *Co2* expression accessed from Genvestigator on the 25/10/09. **(B)** Expression data for *Co2* expression in the root apex, taken from the root expression atlas (Birnbaum *et al.*, 2002).

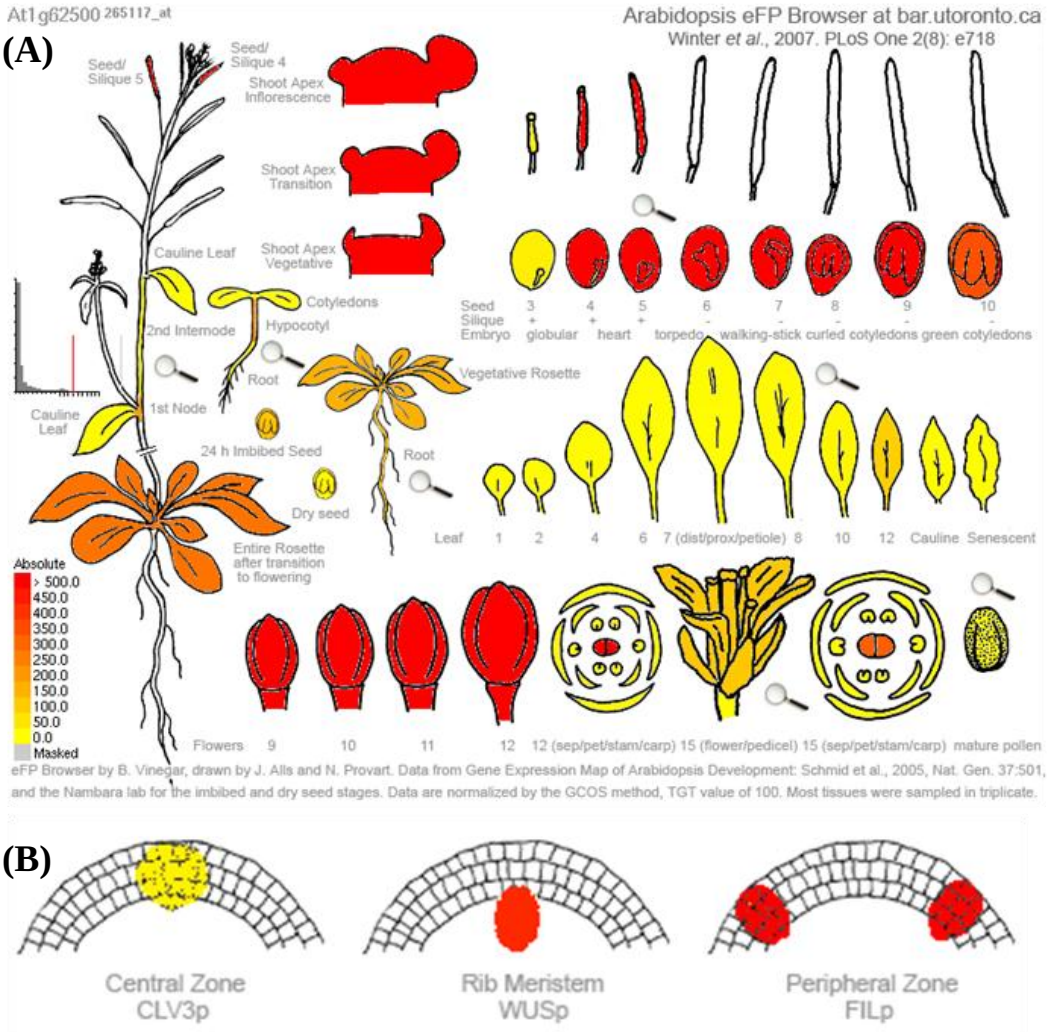

Figure 3-19: ***In silico* expression analysis of *Co2* promoter.** **(A)** Absolute expression of *Co2* during *Arabidopsis* development. **(B)** Absolute expression of *Co2* within the shoot apical meristem. Absolute expression profile of the *Co2* gene was obtained via http://bar.utoronto.ca/efp/cgi-bin/efpWeb.cgi accessed on the 25/10/09.

3.3.6 GL2 promoter (AT1G79840)

GLABRA2 (*GL2*) is a homeodomain protein that was shown by GUS expression studies by Hung *et al.*, (1998) to have a 500-bp region roughly 2-kb upstream of the translational start point that targets its expression throughout atrioblast cell files, in a manner that effects epidermal cell identity throughout the plant (Hung et al., 1998). GL2 is a homeodomain protein of the HD-Zip class that is pivotal in controlling a position-dependent mechanism that regulates epidermal cell-type patterning, the development of trichomes and the formation of seed coat mucilage (Hung et al., 1998, Rerie et al., 1994).

GL2 is expressed preferentially in the differentiating hairless epidermal cells known as atroblasts within both the meristematic and elongation regions of the root, indicating that *GL2* acts as a position-dependent transcriptional regulator that represses root-hair formation (Masucci et al., 1996, Rerie et al., 1994). Early studies used a 4-kb DNA fragment to drive the expression of reporter genes in a cell-position-dependent pattern within the epidermis in a manner that reflects *GL2* RNA accumulation (Masucci et al., 1996). Later studies then showed that a 500-bp fragment located between position -840 and -1340 in the *GL2* promoter was the region necessary to correctly target the expression to differentiating hair cells that are located outside a periclinal cortical cell wall (Hung et al., 1998, Masucci et al., 1996). *In silico* analysis of microarray data implies that *GL2* is also expressed at a relatively low level in developing seedlings but to a slightly higher level in juvenile leaves, stem epidermal tissue and siliques early on during seed development (Figure 3-20 and 3-21).

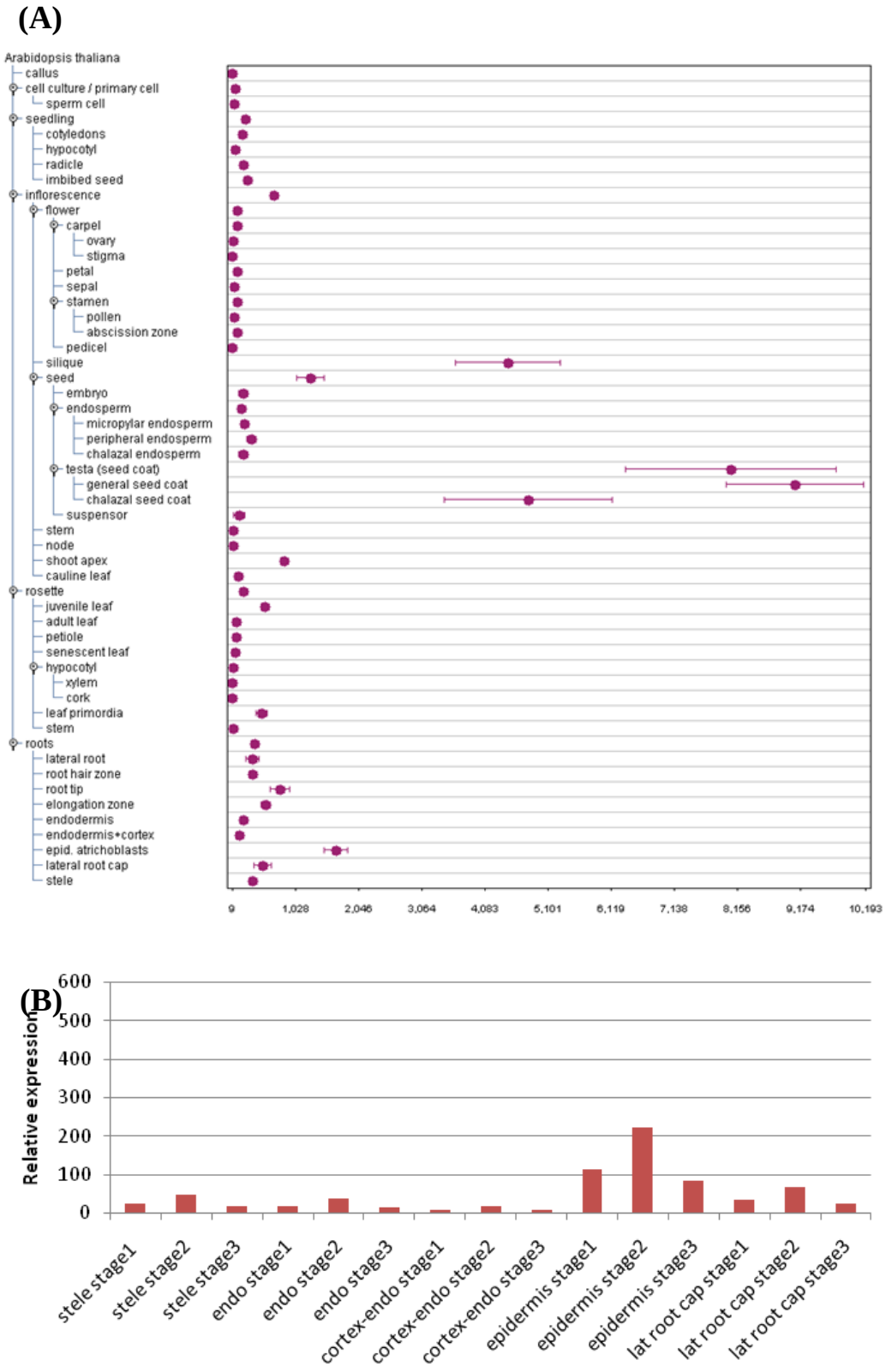

Figure 3-20: ***In silico* expression analysis of *GL2* promoter. (A)** *GL2* expression data generated from microarrays and accessed via Genvestigator (25/10/09). **(B)** Expression data for *GL2* expression in the root apex, taken from the root expression atlas (Birnbaum *et al.*, 2002).

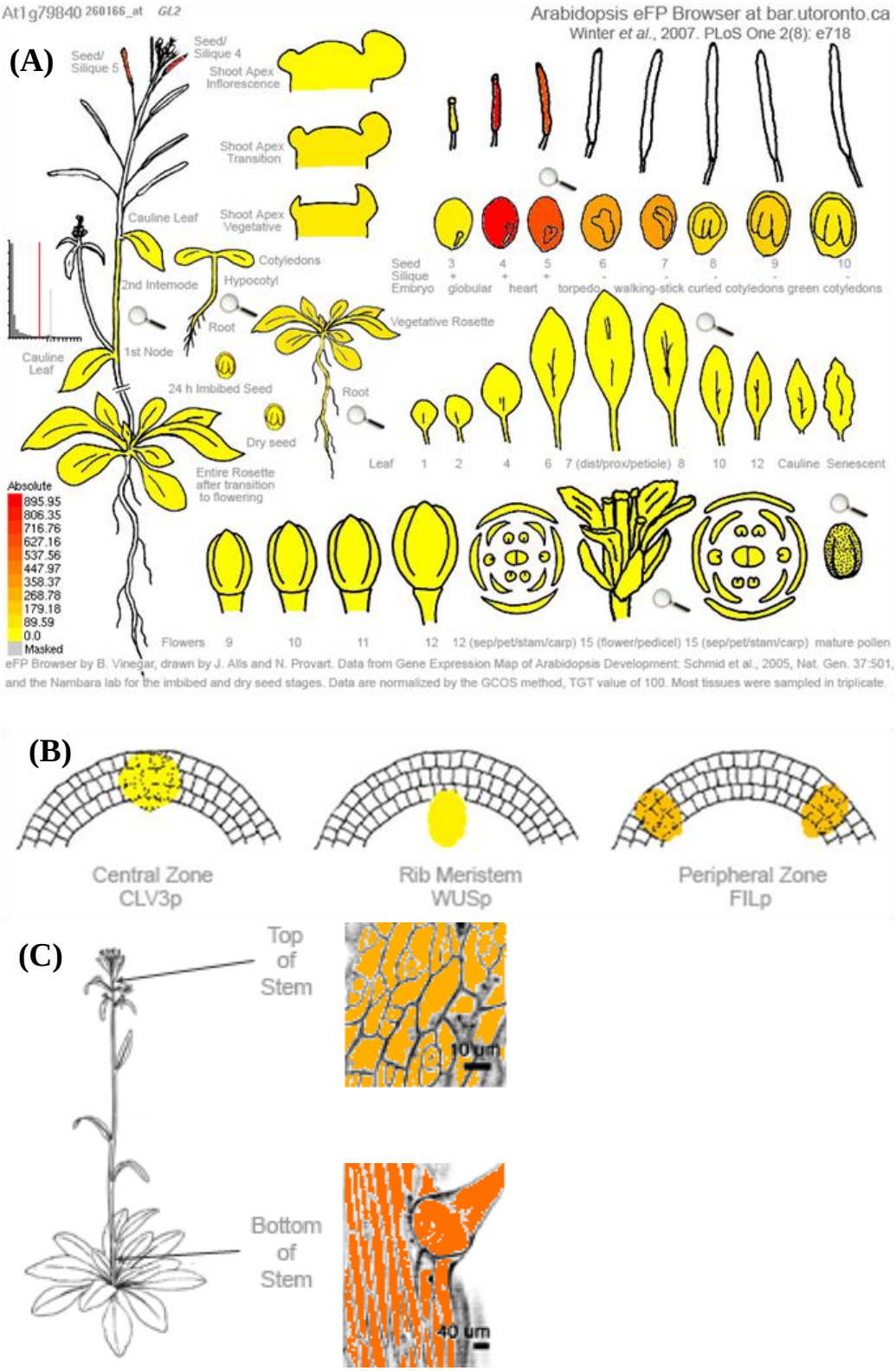

Figure 3-21: ***In silico* expression analysis of *GL2* promoter**. **(A)** Absolute expression of *GL2* during *Arabidopsis* development. **(B)** Absolute expression of *GL2*within the shoot apical meristem. **(C)** Absolute expression of *GL2* within the stem. Absolute expression profile of the *GL2* gene was obtained via http://bar.utoronto.ca/efp/cgi-bin/efpWeb.cgi accessed on the 25/2/11.

3.3.7 CAB promoter (At1g29920)

The chlorophyll a/b binding (*CAB*) protein is one of many nuclear-encoded photosynthesis-related proteins encoded by a light-regulated gene. The *CAB* gene is also capable of responding to many of the developmental signals required for chloroplast development and green tissue specification (Puente et al., 1996). *HY5* facilitates *CAB* up-regulation in response to a wide spectrum of light due to the presence of a light-responsive element (LRE) known as a Z-box. The *CAB* promoter contains three putative Z-box sequences (ATACGTGT), which are essential for the light-dependent developmental expression and are also found in the promoters of a variety of other light inducible genes (Ha and An, 1988). Experiments using *CAB1::GUS* fusions have shown that in WT *Arabidopsis* it is first expressed in the cotyledons in response to light, after further growth, the expression is confined to the photosynthetic tissue (Yadav et al., 2002). Microarray studies have detected *CAB* expression in the seedling, cotyledon, hypocotyl, rosette, inflorescence and the rib meristem of the SAM (Figure 3-22 and Figure 3-23).

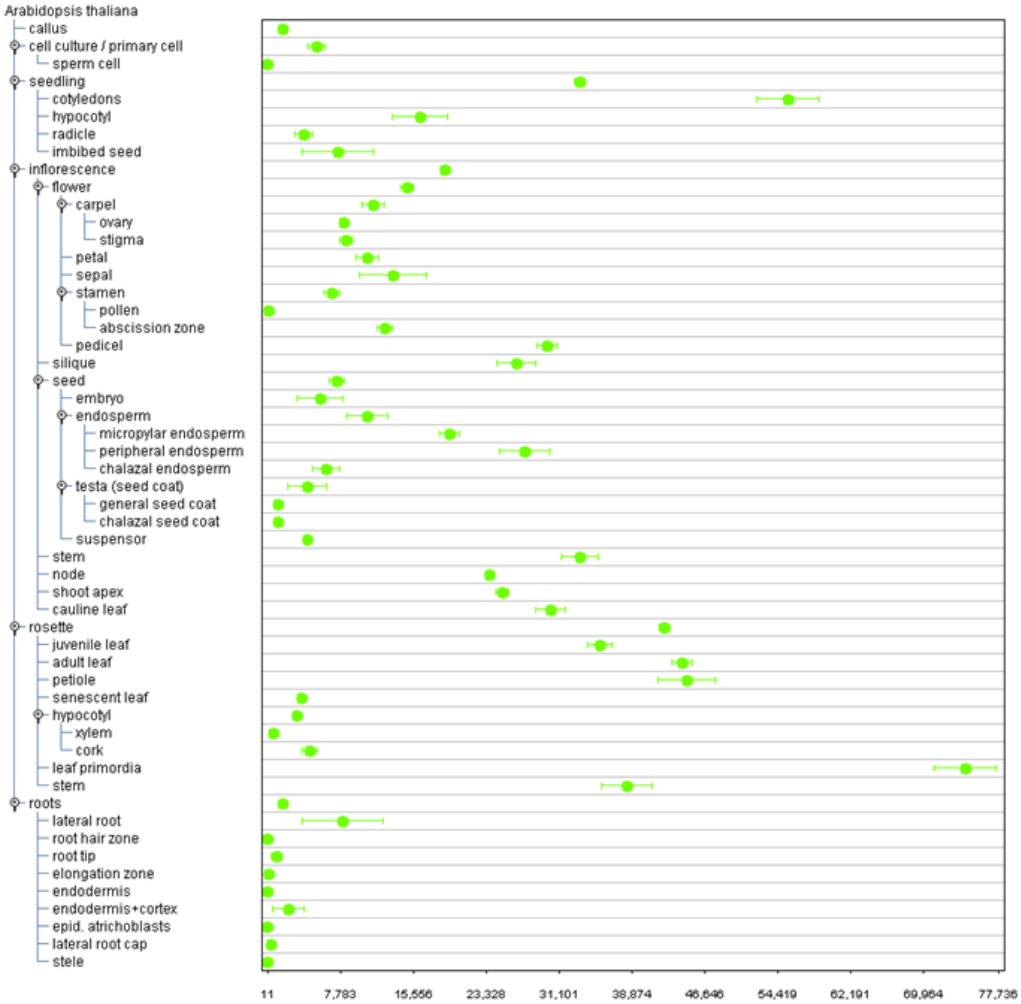

Figure 3-22: ***In silico* expression analysis of *CAB* promoter**. *CAB* expression data generated from microarrays and accessed via Genvestigator (25/10/09).

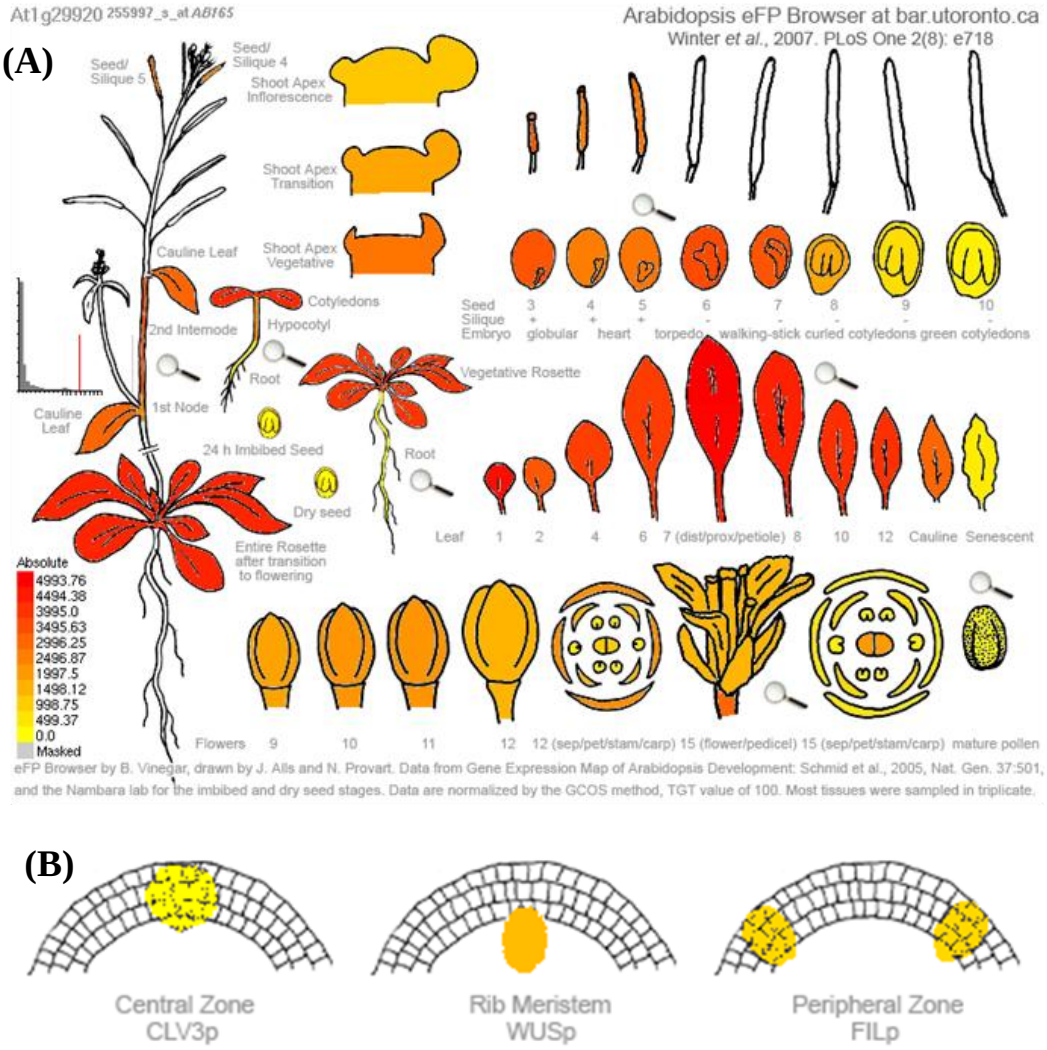

Figure 3-23: ***In silico* expression analysis of *CAB* promoter**. **(A)** Absolute expression of *CAB* during *Arabidopsis* development. **(B)** Absolute expression of *CAB* within the shoot apical meristem. Absolute expression profile of the *CAB* gene was obtained via http://bar.utoronto.ca/efp/cgi-bin/efpWeb.cgi accessed on the 25/2/11.

3.4 CLONING STRATERGY FOR CREATING TARGETED EXPRESSION CONSTRUCTS

Tissue specific promoters (Table 3-2) were attached to the *YFP:AtGA2ox2* fusion within the pENTR11 gateway entry plasmid (Figure 3-24). *AtGA2ox2* was then excised and replaced with *AtGA2ox7*. AtGA2ox2 deactivates C_{19}-GAs, including the bioactive forms, while AtGA2ox7 deactivates C_{20}-GA, but not C_{19}-GAs. Thus, growth inhibition in transgenic plants as a result of cell-specific expression of *AtGA2ox2* should indicate sites of both GA biosynthesis and/or action, while growth of plants expressing *AtGA2ox7* would be affected only when the gene is expressed at the sites of GA biosynthesis.

The *AtGA2ox2* was then replaced in the plasmid with *AtGA3ox1* to produce a *YFP:AtGA3ox1* construct which were used to attempt to rescue the root elongation phenotype of mutants that lack functional *AtGA3ox1* and *AtGA3ox2* genes. This approach was also employed to use the targeted expression of *AtGA20ox1* in a triple mutant line which lacks functional *AtGA20ox1*, *AtGA20ox2* and *AtGA20ox3* genes. In addition, a targeted rescue experiment tried to restore the growth of the triple *Atgid1a,-b,-c* GA-receptor mutant using a C-terminal *GID1a:YFP* fusion with the cell-specific promoters. However, a mistake was made during the construction of the *GID1a:YFP* constructs and the stop codon was left attached to the *GID1a* gene which prevented the YFP sequence from being translated.

Table 3-2: **Constructs created in pENTR11 and targeted tissues.** All *AtGA2ox2*, *AtGA2ox7*, *AtGA20ox1* and *AtGA3ox1* constructs include an enhanced yellow fluorescent (YFP) protein as a fusion in order to allow the expression pattern of the transgene to be verified.

					Cortex	
	Green Tissue	**Epidermis**	**Endodermis**	**Pericycle/ Vasculature**	**Elongation zone**	**Meristematic region**
	CAB	***GL2***	***SCR***	***SHR***	***CoR***	***Co2***
Gene						
GA2ox7	*CAB:2ox7*	*GL2:2ox7*	*SCR:2ox7*	*SHR:2ox7*	*CoR:2ox7*	*Co2:2ox7*
GA2ox2	*CAB:2ox2*	*GL2: 2ox2*	*SCR: 2ox2*	*SHR: 2ox2*	*CoR: 2ox2*	*Co2: 2ox2*
GA3ox1	*CAB:3ox1*	*GL2: 3ox1*	*SCR: 3ox1*	*SHR: 3ox1*	*CoR: 3ox1*	*Co2: 3ox1*
GA20ox1	*CAB: 20ox1*	*GL2: 20ox1*	*SCR: 20ox1*	*SHR: 20ox1*	*CoR: 20ox1*	*Co2: 20ox1*
GID1a	N/A	*GL2:GID1a*	*SCR:GID1a*	*SHR:GID1a*	*CoR:GID1a*	*Co2:GID1a*
All GA metabolic genes have EYFP attached to their N terminus						

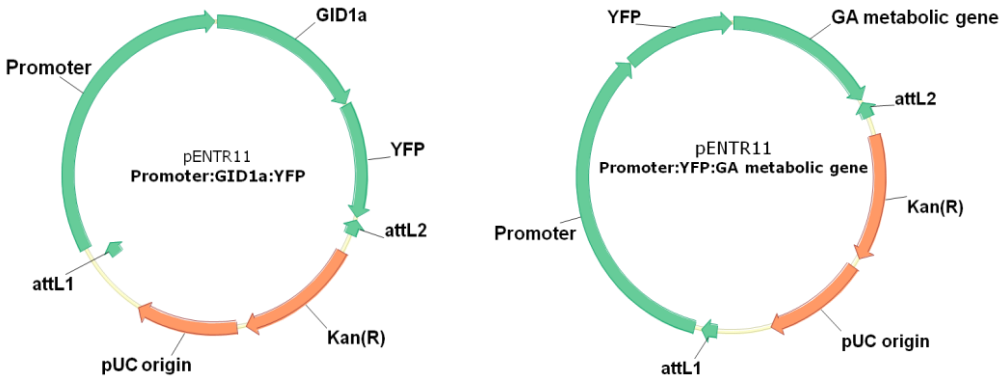

Figure 3-24: **Schematic representations of constructs. (A)** A generic construct showing the design of constructs that will be transformed into the *gid1Aa,bb,cc* mutants. **(B)** A generic construct showing the design of the constructs for rescue of GA-deficient mutants or for GA inactivation in specific cell types. Diagrams describing construction in more detail available in section 11.

3.4.1 Design of pENTR11:*SHR::YFP:AtGA2ox2*

SHR::YFP:AtGA2ox2 was prepared by digesting pENTR11:*SHR*:*GID1a*:*YFP* (provided by Dr Susanna Ubeda-Tomas, The University of Nottingham) with *Xho*I and *Bam*HI to excise *GID1a:YFP*, thus creating pENTR11:*SHR* (Methods section 2.4). The *AtGA2ox2* coding region was excised from pSC-B using *Xho*I and *Bam*HI and ligated into pENTR11:*SHR*, resulting in the pENTR11:*SHR:AtGA2ox2* construct. The YFP coding region was excised from pSC-B using *Bgl*II and *Bam*HI and ligated into pENTR11::*SHR:AtGA2ox2*, which had been cleaved using *Bam*HI and treated with DNA dephosphatase to prevent religation, thus producing the expression construct pENTR11::*SHR::YFP:AtGA2ox2* (Diagrams describing the construction of this and the other targeted expression constructs were produced using VectorNTI and are shown in the appendix, chapter 11).

3.4.2 Design of pENTR11:*SCR::YFP:AtGA2ox2*

SCR::YFP:AtGA2ox2 was prepared by first digesting pENTR11:*SCR:AtGID1a*:YFP (provided by Dr Susanna Ubeda-Tomas, The University of Nottingham) with *Xho*I and *Bam*HI to remove *AtGID1a:YFP* to create pENTR11:*SCR* (Methods section 2.4). The *AtGA2ox2* coding region was excised from pSC-B using *Xho*I and *Bam*HI and ligated into pENTR11:S*CR* to form the construct pENTR11:*SHR:AtGA2ox2*. The YFP coding region was excised from pSC-B using *Bgl*II and *Bam*HI and ligated into pENTR11:*SCR::AtGA2ox2*, which had also been digested with *Bam*HI, to produce the expression construct pENTR11:*SCR::YFP:AtGA2ox2*.

3.4.3 *GID1a* cloned into *SCR:YFP* and *SHR:YFP* plasmids

AtGID1a was amplified from pENTR11:*SCR::GID1:YFP* plasmid (provided by Dr Susanna Ubeda-Tomas, The University of Nottingham) by high-fidelity proof reading Phusion Taq polymerase with primers that introduced *Eco*RI and

*Bam*HI restriction sites (Methods section 2.4 and primer Table 2-2). *SCR::YFP* and *SHR::YFP* fusions in pENTR11 (provided by Dr Susanna Ubeda-Tomas, The University of Nottingham) were digested with *Eco*RI/*Bam*HI allowing ligation of *AtGID1a*, thus creating the pENTR11:*SCR::GID1a:YFP* and pENTR11:*SHR:GID1a:YFP* constructs (B).

3.4.4 Design of pENTR11:*Co2::GID1a:YFP*

To produce *Co2::AtGID1a:YFP* specifically to the cortex; *Xho*I and *Bam*HI were used to excise the 500bp *Co2* promoter region from pGII:*Co2::YFP* (provided by Dr Renze Heidstra, Utrecht University) (Methods section 2.4). *Xho*I and *Bam*HI were used to excise the *SCR* promoter region from pENTR11:*SCR:AtGID1a:YFP* creating pENTR11:*AtGID1a:YFP*. The subsequent ligation resulted in pENTR11:*Co2::AtGID1a:YFP*.

3.4.5 Design of pENTR11:*Co2::YFP:AtGA2ox2*

The *Co2::YFP:AtGA2ox2* construct was prepared by digesting pENTR11:*Co2::AtGID1a:YFP* with *Xho*I and *Bam*HI to excise *AtGID1a*:*YFP* (Methods section 2.4). The *AtGA2ox2* coding region was excised from pSC-B with *Xho*I and *Bam*HI, and the digestion products ligated to produce pENTR11:*Co2:AtGA2ox2*. The *YFP* coding region was then excised from pSC-B by digesting with *Bgl*II and *Bam*HI and ligated into *Bam*HI-digested pENTR11:*Co2::AtGA2ox2* resulting in pENTR11:*Co2::YFP:AtGA2ox2*.

3.4.6 Design of pENTR11:*CAB::YFP:AtGA2ox2*

In order to prepare the *CAB::YFP:AtGA2ox2* construct, 1892-bp of the *CAB* promoter was amplified from pENTR11:*CAB* (provided by Ranjan Swarup, The University of Nottingham) by PCR using a proof reading Phusion taq polymerase (Methods section 2.4 and primer Table 2-2). The PCR product was ligated into pSC-B and sequenced to ensure that no mutations had occurred. The *CAB* promoter region and pENTR11:*SCR::AtGA2ox2* were digested with

*Sal*I and *Bam*HI and ligated to create pENTR11:*CAB:AtGA2ox2*. The *YFP* coding region was excised from pSC-B with *Bam*HI and *Bgl*II and then ligated into pENTR11:*CAB::AtGA2ox2*, which had been previously cleaved with *Bam*HI, resulting in pENTR11:*CAB::YFP:AtGA2ox2*.

3.4.7 Design of pENTR11:*GL2::AtGID1a:YFP*

To produce the *GL2:AtGID1a:YFP* construct, 2kb of the *GL2* promoter was amplified from pENTR11:*GL2* (provided by Dr Siobhan Brady, Duke University) by PCR using proof reading NEB Phusion Taq polymerase (Methods section 2.4 and primer Table 2-2). The PCR product was then cloned into pSC-B for confirmatory sequencing. The *GL2* promoter sequence was excised from pSC-B:*GL2* by digesting with *Xho*I and *Bam*HI. The *SCR* promoter sequence was removed from pENTR11:*SCR:AtGID1a:YFP* by digesting with *Sal*I and *Bam*HI and replaced with the *GL2* promoter to give pENTR11:*GL2::AtGID1a*:*YFP*.

3.4.8 Inserting *AtGA2ox2, AtGA2ox7, AtGA3ox1* and *AtGA20ox1* into pENTR11:*GL2::YFP*

In order to prepare the other GL2 constructs, pSC-B:*GL2* was cleaved by digestion with *Bam*HI and ligated with the *YFP* coding region, which had been excised from pSC-B with *Bgl*II and *Bam*HI (Methods section 2.4). The resulting plasmid pSC-B:*GL2::YFP* was then digested with *Nco*I and *Bam*HI to release the *GL2::YFP* fragment. The *SCR::YFP* fragments were excised from pENTR11:*SCR::YFP:AtGA2ox2*, pENTR11:*SCR::YFP:AtGA2ox7*, pENTR11:*SCR::YFP:AtGA3ox1* and pENTR11:*SCR::YFP:At20ox1* by digesting with *Nco*I and *Bam*HI and replaced with *GL2::YFP* to create pENTR11:*GL2::YFP:AtGA2ox2*, pENTR11:*GL2::YFP:AtGA2ox7*, pENTR11:*GL2::YFP:AtGA3ox1* and pENTR11 *GL2::YFP:AtGA20ox1*, respectively.

3.4.9 Preparation of vectors containing *AtGA2ox7, AtGA20ox1* and *AtGA3ox1* coding sequences

In order to target the expression of *YFP:AtGA2ox7* and *YFP:AtGA20ox1* to specific tissues, a high-fidelity PCR using proof-reading NEB Phusion Taq polymerase was used to amplified their coding region from the pIVO372ox7 and pIVOMOG420ox1 plasmids (Provided by Dr Steve Thomas, Rothamsted Research) (Methods section 2.4 and primer Table 2-2). The PCR products were then cloned into pSC-B for confirmatory sequencing. The *AtGA2ox7* and *AtGA20ox1* coding sequences were then excised using *Sal*I and *Bam*HI and ligated into pENTR11:*SCR::YFP:AtGA2ox2*, pENTR11:*SHR::YFP:AtGA2ox2*, pENTR11:*Co2::YFP:AtGA2ox2*, pENTR11:*GL2::YFP:AtGA2ox2* and pENTR11:*CAB::YFP:AtGA2ox2* from which the *AtGA2ox2* coding sequence had been excised by digestion with *Xho*I and *Bam*HI.. *AtGA3ox1* was amplified from the pMOGIVO3ox1 plasmid (Provided by Dr Steve Thomas, Rothamsted Research) by PCR using proof reading Taq polymerase. The PCR product was ligated into pSC-B and then sequenced to ensure no mutations had occurred. *AtGA3ox1* was then excised using *Xho*I and *Bam*HI and ligated into pENTR11:*SCR::YFP:AtGA2ox2*, pENTR11:*SHR::YFP:AtGA2ox2*, pENTR11:*Co2::YFP:AtGA2ox2*, pENTR11:*GL2::YFP:AtGA2ox2* and pENTR11:*CAB::YFP:AtGA2ox2* from which the *AtGA2ox2* coding sequence had been excised by digestion with *Bam*HI and *Xho*I.

3.4.10 Preparation of constructs with the *CoR* promoter

The *CoR* 1.7-kb promoter was amplified by a high fidelity proof reading NEB Phusion Taq polymerase with primers that included *Bgl*II and *Sal*I restriction sites (Methods section 2.4 and primer Table 2-2). The PCR fragment was then ligated into pSC-B (Stratagene). The *YFP* coding sequence was amplified with primers that created a 5' *Bam*HI restriction site and a 3' *Bgl*II site, and the PCR fragment was then ligated into pSC-B (Stratagene). The *CoR* promoter was then excised from pSC-B with SalI and BglI and ligated into pENTR11 that had been cleaved with *Bam*HI and *Sal*I. *YFP* was excised from pSC-B with *Bam*HI and *Bgl*II, and ligated into *Bgl*II-digested pENTR11:*CoR* creating pENTR11:*CoR::YFP*, which was then digested with *Bgl*II and *Xho*I. The *AtGA2ox2, AtGA2ox7, AtGA3ox1* and *AtGA20ox1* open reading frames were all excised from pSC-B and ligated into the cleaved pENTR11:*CoR::YFP*. The *CoR* promoter was excised from pSC-B with *Sal*I/*Bam*HI and exchanged for the *SHR* promoter in pENTR11*:SHR::GID1a:YFP* after digestion with *Sal*I/*Bam*HI, to produce pENTR11:*CoR::GID1a:YFP*.

3.5 PCR GENOTYPING OF TRANSGENIC LINES

3.5.1 Successful integration transgenes and confirmation of endogenous alleles by gDNA PCR.

After *Agrobacterium*-mediated floral dip transformation, 30-40 T1 transformants were selected on the basis of kanamycin resistance, following segregation analysis of the T2 and T3 by kanamycin resistance. Between 3 and 6 T3 single insertion homozygous kanamycin resistant transgenic lines were generated for further analysis. PCR using gDNA was employed to demonstrate the successful integration of the transgenes and to demonstrate the absence of functional WT alleles in the *ga3ox1,-2*, *ga20ox1,-2,-3* and g*id1a,-b,-c* mutants, the primer combinations are shown in Table 3-3 and the primer sequences are shown in Table 2-1

Table 3-3: **The primer combinations used for genotyping mutants and demonstrating successful integration of transgene into the genomic DNA.** The table contains the gene names, alleles, primer names and size of final product.

Locus	Allele	Forward Primer	Reverse Primer	PCR Product (bp)
GA3ox1	WT	FP_GA3ox1	RP_GA3ox1	1000
GA3ox1	ga3ox1	LBa1	RP_GA3ox1	750
GA3ox2	WT	FP_GA3ox2	RP_GA3ox2	1000
GA3ox2	ga3ox2	LBa1	RP_GA3ox2	750
GA20ox1	WT	F_GA20ox1	R_GA20ox1	350
GA20ox1	ga20ox1-1	F2_GA20ox1	LBa1	600
GA20ox2	WT	F3_GA20ox2	R3_GA20ox2	900
GA20ox2	ga20ox2-3	F3_GA20ox2	GABI-kat LB	1100
GA20ox3	WT	F1_GA20ox3	F1_GA20ox3	93 + 147 (DdeI)
GA20ox3	ga20ox3-016	F2_GA20ox3	R1_GA20ox3d	93 + 121 + 26 (DdeI)
GID1a	WT	GID1A-1F	GID1A-1R	552
GID1a	gid1a-1	LBa1	GID1A-1R	684
GID1b	WT	GID1B-1F	GID1B-1R	897
GID1b	gid1b-1	SLAT-3’	GID1B-1R	700
GID1c	WT	GID1C-1F	GID1C-1R	500
GID1c	gid1c-1	LBa1	GID1C-1R	700
YFP-AtGA2ox2	Transgenic	FP_YFP_internal	RP_GA2ox2	1500
YFP-AtGA2ox7	Transgenic	FP_YFP_internal	RP_GA2ox7	1300
YFP-AtGA3ox1	Transgenic	FP_YFP_internal	RP_GA3ox1	500
YFP-AtGA20ox1	Transgenic	FP_YFP_internal	RP_GA20ox1	600
GID1a-YFP	Transgenic	GID1A-1F	RP_YFP	1300

3.5.2 Successful integration of *YFP:AtGA2ox2* and *YFP:AtGA2ox7* transgenes into Col-0 gDNA

Figure 3-25 (A) shows PCR confirming the successful integration of *YFP:AtGA2ox2* in all the final lines chosen for secondary analysis of transgene expression profiles, root length, meristem length and final cell length (Methods section 2.4 and primer Table 2-2). The successful integration of *YFP:AtGA2ox7* in the final lines chosen for primary growth analysis was confirmed by PCR (Figure 3-25-B). However, Col-0;*GL2::YFP:AtGA2ox7* line A was negative for the presence of the *YFP:AtGA2ox7* fusion, and since this line showed no root or shoot phenotypes, it was discounted for further analysis.

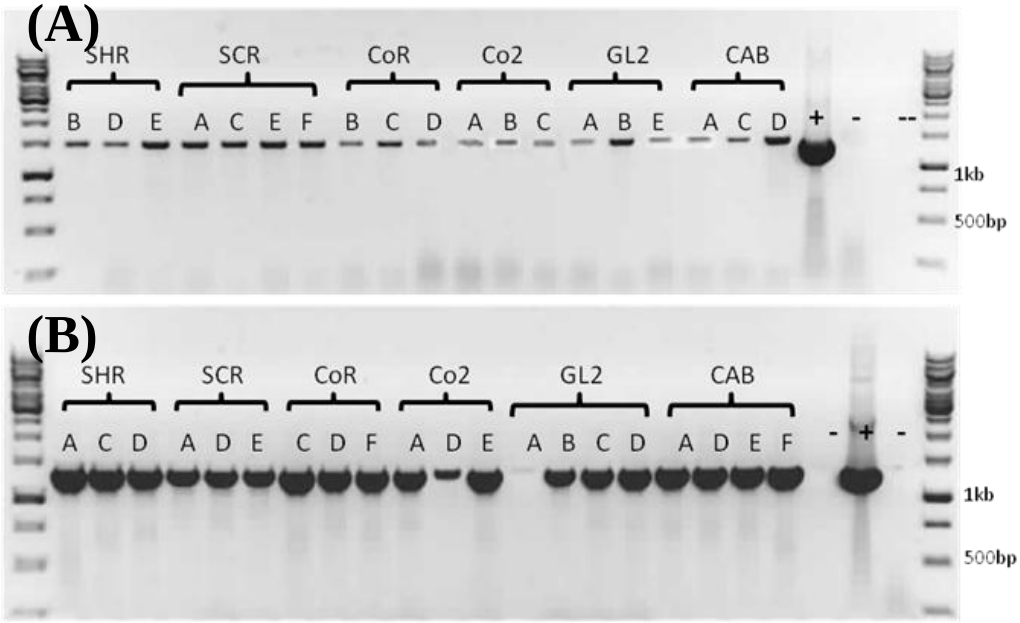

Figure 3-25**: Identification of *YFP:AtGA2ox2* and *YFP:AtGA2ox7* in transgenic lines by gDNA PCR. (A)** Amplification product of 1500-bp confirms integration of *YFP:AtGA2ox2* gene fusion in transgenic lines. **(B)** Amplification product of 1300-bp confirms integration of *YFP:AtGA2ox7* gene fusion in transgenic lines. Positive plasmid control (+), WT Col-0 control (-) and water (--) are also included. For primer sequences used see Table 2-1 and for primer combinations used see Table 3-3

3.5.3 PCR to show successful integration of *YFP:AtGA20ox1* transgenes into *ga20ox1,-2,-3* gDNA and that the wild-type versions of *AtGA20ox1, AtGA20ox2* and *AtGA20ox3* are not present.

After *Agrobacterium*-mediated floral dip transformation of the triple *Atga20ox1,-2,-3* mutant with the YFP-AtGA20ox1 constructs , T1 transformants were selected using kanamycin resistance, to ensure all the mutants produced seeds each generation was sprayed with GA_3 and then segregation analysis was performed on the T2 and T3 generations in order to generate T3 single insertion homozygous lines. The presence of *YFP:AtGA20ox1* in all the lines selected for primary analysis was confirmed by PCR using primers that crossed YFP_AtGA20ox1 boundary (Figure 3-26A). The native *AtGA20ox1* containing a T-DNA insertion that prevents it from functioning, shown by PCR of the transgenic lines and untransformed triple mutant (Figure 3-26-B).

The functional *AtGA20ox1* allele in the transgenic insert was distinguished from the intact native gene by PCR across the two introns, after which the native gene produced a band that was 250-bp larger than that from the transgene (Figure 3-26-C). *ga20ox1,-2,-3;Co2::YFP:AtGA20ox1* line A contained both the transgenic *AtGA20ox1* open reading frame and the wild-type version. The presence of the mutant *atga20ox2* containing a T-DNA insertion was also confirmed by PCR (Figure 3-27-A). The lack of a functional *AtGA20ox2* allele in the transgenic lines was confirmed by PCR, except in the *ga20ox1,-2,-3;Co2::YFP:AtGA20ox1* line A, which contained both *Atga20ox2* and *AtGA20ox2* alleles (Figure 3-27-B). The presence in the transgenic lines of mutant *Atga20ox3* containing a SNP that introduces a stop codon was confirmed by PCR, which revealed that *ga20ox1,-2,-3;Co2::YFP:AtGA20ox1* line A contained both mutant *Atga20ox3* and *AtGA20ox3* alleles (Figure 3-28).

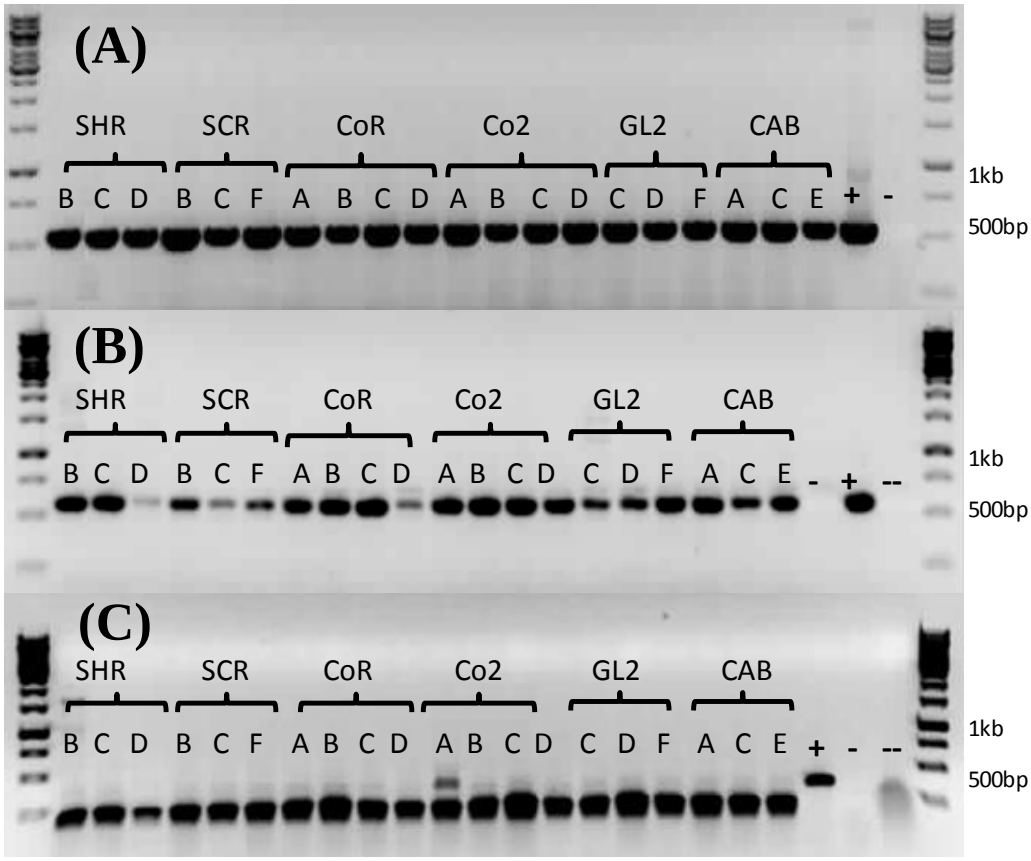

Figure 3-26: **Identification of *YFP:AtGA20ox1*, confirmation of the presence of a T-DNA insertion within the *AtGA20ox1* and the presence of the transgenic *AtGA20ox1* by gDNA PCR. (A)** Amplification product of 600-bp confirms integration of *YFP:AtGA20ox1* gene fusion in transgenic lines. **(B)** Amplification product of 600 bp confirms T-DNA insertion. **(C)** Amplification product of 250 bp confirms integration of *YFP:AtGA20ox1* and the 350-bp band confirms the presence of the WT *GA20ox1* due to the presence of the intron. Positive *ga20ox1*,*-2*,*-3* (+), WT Col-0 (-) and water controls (--) are also included. For primer sequences used see Table 2-1 and for primer combinations used see Table 3-3

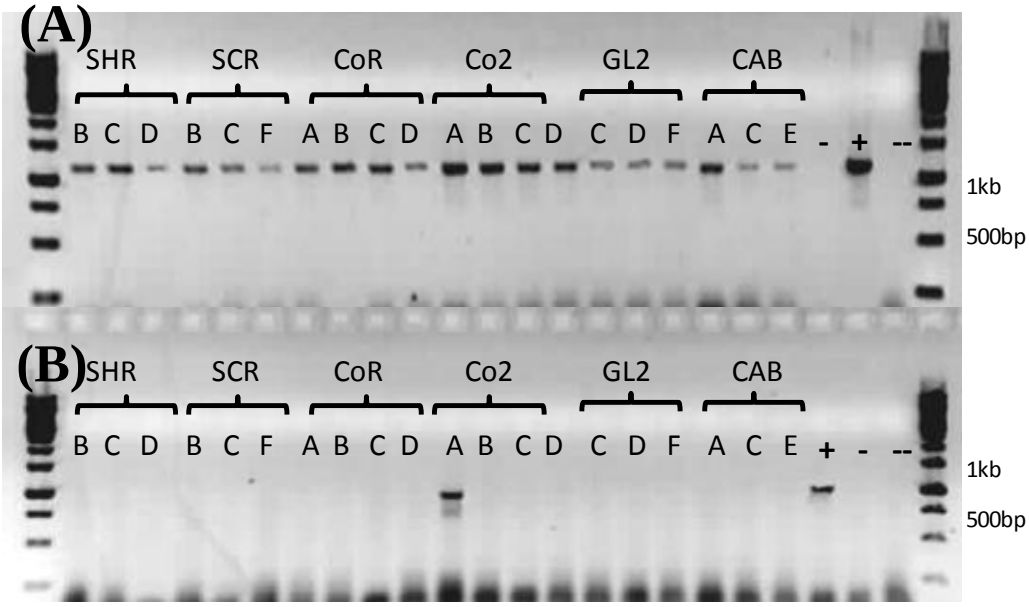

Figure 3-27: **Identification of T-DNA insertion within the *AtGA20ox2*and the absence of a functional wild-type *AtGA20ox2* within transgenic lines by gDNA PCR. (A)** Amplification of a 1300-bp band confirms the presence of a T-DNA insertion within *Atga20ox2* **(B)** Amplification product of 900-bp confirms the presence of WT *AtGA20ox2*. Positive *ga20ox1,-2,-3* (-), WT Col-0 (+) and water controls (--) are also included. For primer sequences used see Table 2-1 and for primer combinations used see Table 3-3

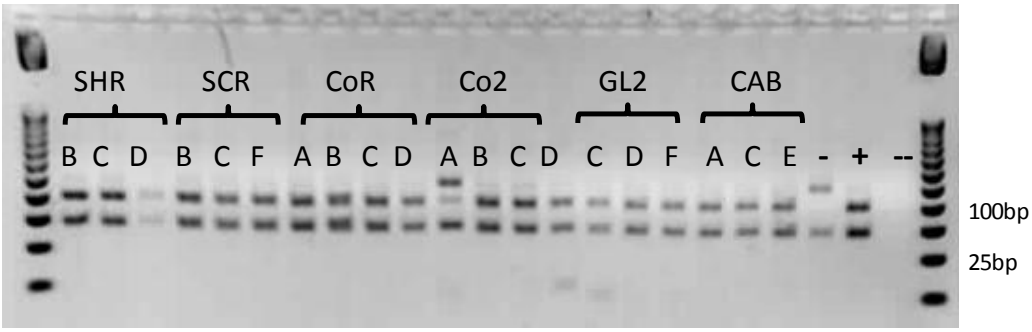

Figure 3-28: **PCR & Ddel digest to confirm presence of a SNP within the *AtGA20ox3* in transgenic lines by gDNA PCR.** Amplification and subsequent digestion products of 93-bp and 147-bp confirms the presence of WT *AtGA20ox3*. Amplification and subsequent digestion products of 93-bp, 121-bp and 26-bp confirm the presence of the SNP. Amplification and subsequent digestion products of 26-bp, 93-bp, 121-bp and 147-bp confirms the presence of *AtGA20ox3* and at*ga20ox3*. Positive *ga20ox1,-2,-3* (+), WT Col-0 (-) and water controls (--) are also included. For primer sequences used see Table 2-1 and for primer combinations used see Table 3-3

3.5.4 PCR to show successful integration of *YFP:AtGA3ox1* transgenes into gDNA and that *AtGA3ox1*, and *AtGA3ox2* are not present.

T1 *Atga3ox1 Atga3ox2* (*ga3ox1,-2*) double mutants transformed with the *YFP:AtGA3ox1* constructs were selected on kanamycin, and segregation analysis was performed on the T2 and T3 generations to produce T3 single insertion homozygous lines. Seeds were imbibed in GA_3 and sprayed with a 100μM GA_3 solution until they set seed. The presence of *YFP:AtGA3ox1* was confirmed by PCR in all the lines selected for primary analysis (Figure 3-29-A). The mutant *AtGA3ox1* containing a T-DNA insertion that prevents it from functioning was also confirmed by PCR in all *YFP:AtGA3ox1* transgenic lines (Figure 3-29-B). Although the presence of a functional *AtGA3ox1* allele was confirmed in the transgenic lines, it was only possible to distinguish between the transgenic *YFP:AtGA3ox1* and endogenous *AtGA3ox1* by the size of the band due to the presence of the WT intron (Figure 3-29-C). The presence of the mutant *AtGA3ox2* containing a T-DNA insertion was confirmed by PCR in all transgenic *YFP:AtGA3ox1* lines (Figure 3-30-A) as was the absence of a functional wild-type *AtGA3ox2* allele (Figure 3-30-B)

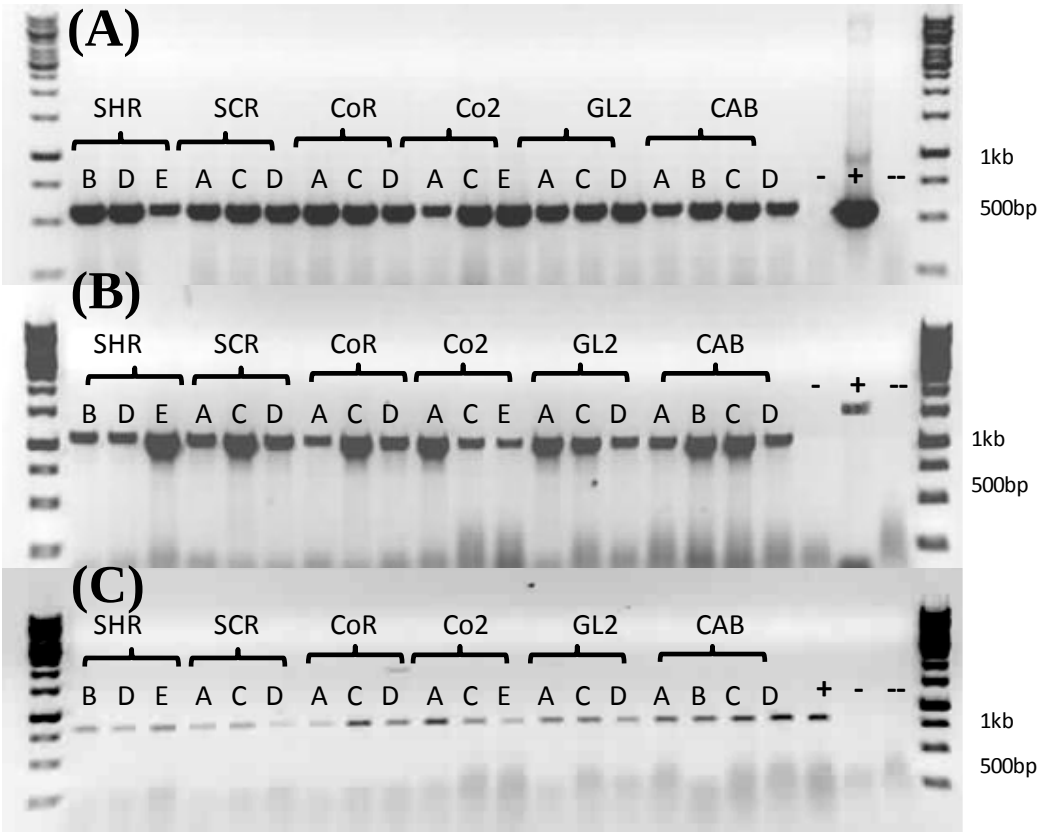

Figure 3-29**: Identification of *YFP:AtGA3ox1* and confirmation of both the presence of the *Atga3ox1* allele and a functional AtGA3ox1 in transgenic liens by gDNA PCR. (A)** Amplification product of 500-bp confirms integration of the *YFP:AtGA3ox1* gene fusion in transgenic lines. **(B)** Amplification product of 1-Kb confirms the presence of a functional *AtGA3ox1* gene either endogenously or due to the integration of *YFP:AtGA3ox1* gene fusion in transgenic lines. **(C)** Amplification product of 750-bp confirms the presence of the *ga3ox1* allele within transgenic lines. Positive *ga3ox1,-2* control (+), Negative WT Col-0 control (-), and water (--) are also included. For primer sequences used see Table 2-1 and for primer combinations used see Table 3-3

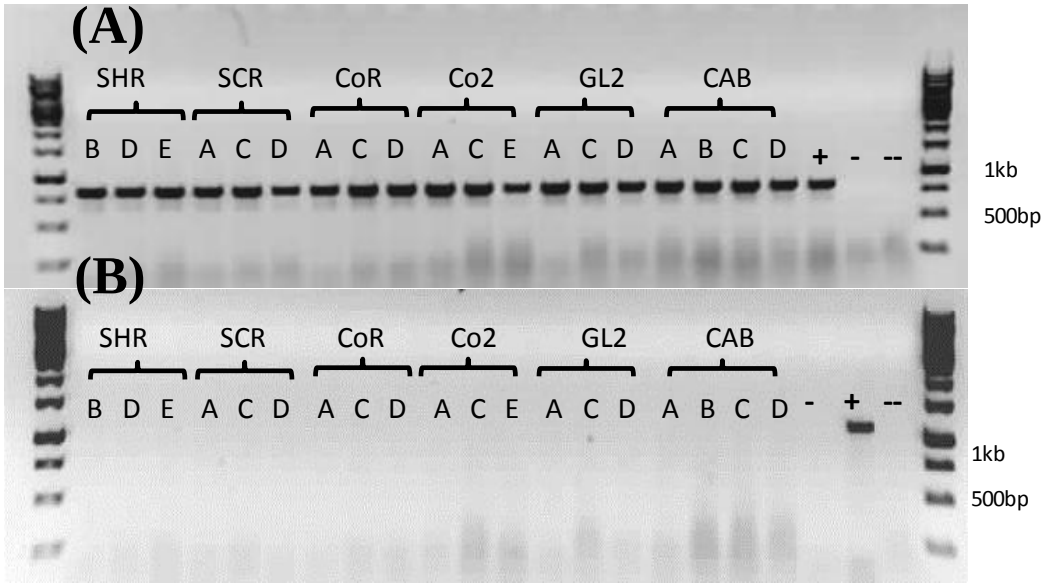

Figure 3-30: **Identification of the presence of the T-DNA insertion within Atga3ox2 and the lack of a functional *AtGA3ox2* in transgenic lines by gDNA PCR. (A).** Amplification product of 750-bp confirms the presence of the *atga3ox2* allele within transgenic lines. **(B)** Amplification product of 1-Kb confirms the presence of a functional *GA3ox2* in transgenic lines. Negative *ga3ox1,-2* control (-), positive WT Col-0 control (+), and water (--) are also included. For primer sequences used see Table 2-1 and for primer combinations used see Table 3-3

3.5.5 PCR to show successful integration of *AtGID1a:YFP* transgenes into the gDNA of *gid1aa,bb,cc* and that a functional *AtGID1a, AtGID1b* and *AtGID1c* are not present.

After *Agrobacterium*-mediated floral dip transformation of *gid1A,a,b,b,c,c* with the *AtGID1a:YFP* constructs, T1 transformants were selected on kanamycin, and segregation analysis was performed on the T2 and T3 generations to generate T3 single insertion homozygous lines that were incapable of germinating and could therefore be selected for embryo excision to ensure they were homozygous for g*id1a* knock out allele. The presence of *AtGID1a:YFP* in all the lines selected for primary analysis was confirmed by PCR primers designed internally to both the YFP and the GID1a gene (Figure 3-31-A). The presence of the mutant *AtGID1a* containing a T-DNA insertion was further confirmed by PCR using primers designed for the T-DNA insertion (Figure 3-31, Figure 3-32, Figure 3-33). PCR was also used to confirm the presence of a functional *AtGID1a* allele linked to the YFP insert thus distinguishing it from the inactive version found within the *gid1a,-b,-c* triple mutant in the transgenic lines, although this would not distinguish between the transgenic *AtGID1a:YFP* and wild-type *AtGID1a* (with no T-DNA insertion) if it were present (Figure 3-31-B). The presence of the mutant *atgid1b* (Figure 3-31) and *atgib1c* (Figure 3-33), containing T-DNA insertions, and the absence of functional *AtGID1b* (Figure 3-32) and *AtGID1C* alleles (Figure 3-33) in the transgenic lines were confirmed by PCR. This demonstrated that all transgenic lines contained the appropriate insert to complement the mutated GA related genes they contained.

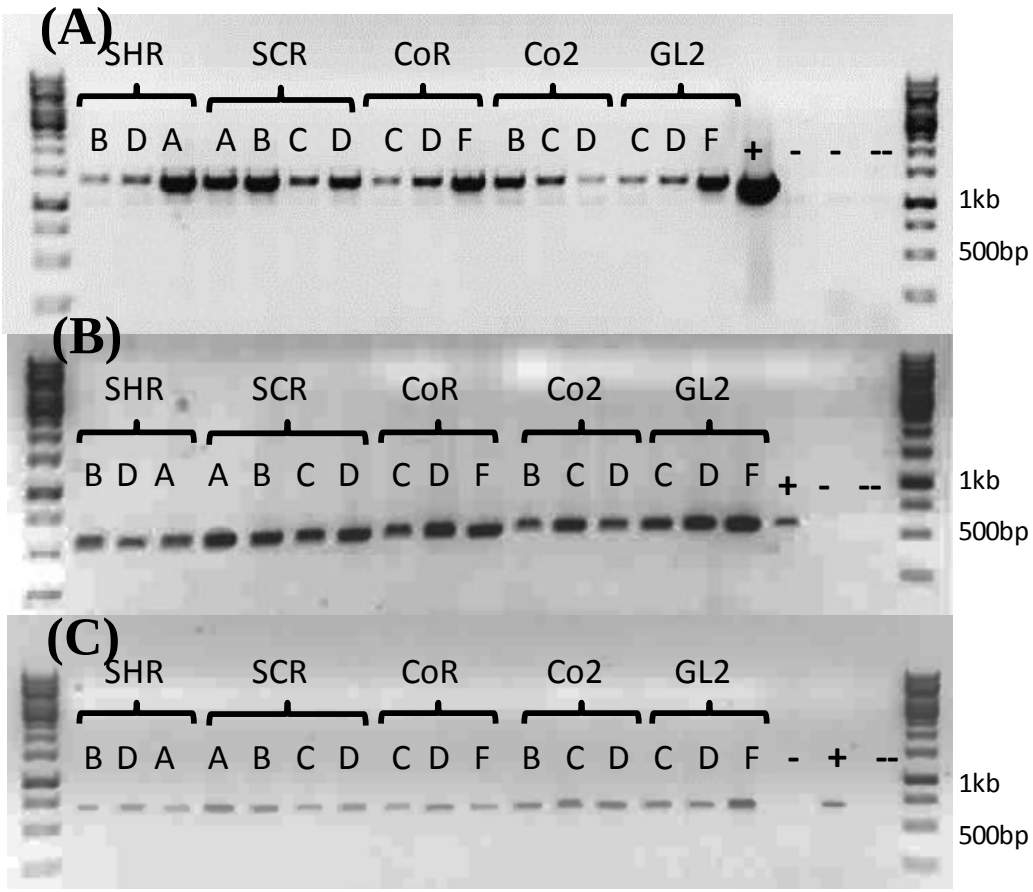

Figure 3-31**: Identification of *AtGID1a:YFP* and to confirm the presence of both the transgenic *AtGID1a* and *Atgid1a* alleles in transgenic lines by gDNA PCR. (A)** Amplification product of 1300-bp confirms integration of *GID1a:YFP* gene fusion in transgenic lines. **(B)** Amplification product of 500-bp confirms the presence of a functional *GID1a* gene either endogenously or due to the integration of *GID1a:YFP* gene fusion in transgenic lines. **(C)** Amplification product of 700-bp confirms the presence of a T-DNA insertion within the *gid1a* allele. Negative WT Col-0 control (-), positive *gid1a,-b,-c* control (+) and water (--) are also included. For primer sequences used see Table 2-1 and for primer combinations used see Table 3-3

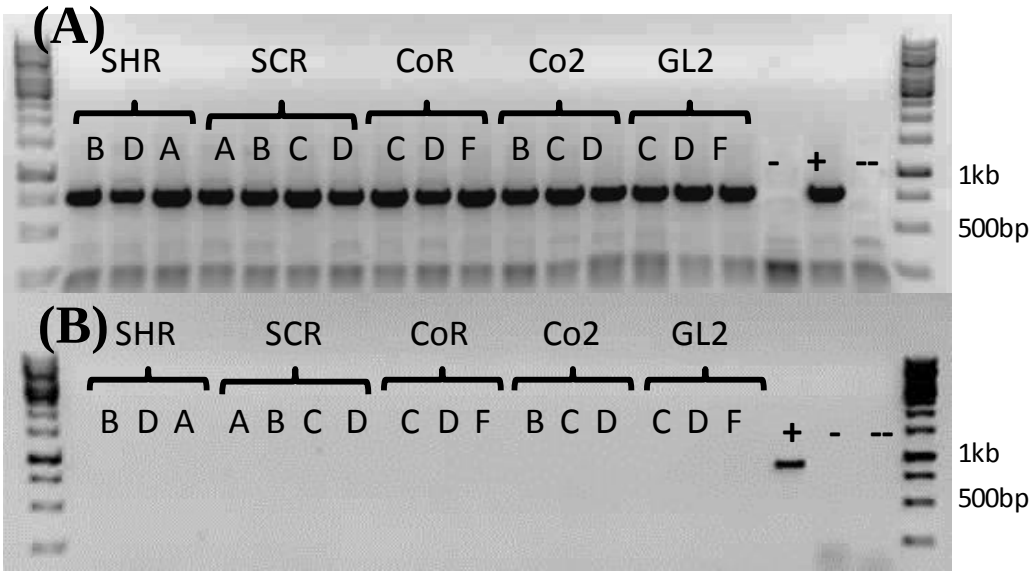

Figure 3-32**: Identification of Atgid1b and lack of *AtGID1B* within transgenic lines. (A)** Amplification product of 700-bp confirms the presence of a T-DNA insertion creating non-functional *gid1b* allele. **(B)** Amplification product of 900-bp would indicate the presence of *GID1B*. Positive WT Col-0 control (+), negative *gid1a,-b,-c* (-) and water (--) are also included. For primer sequences used see Table 2-1 and for primer combinations used see Table 3-3.

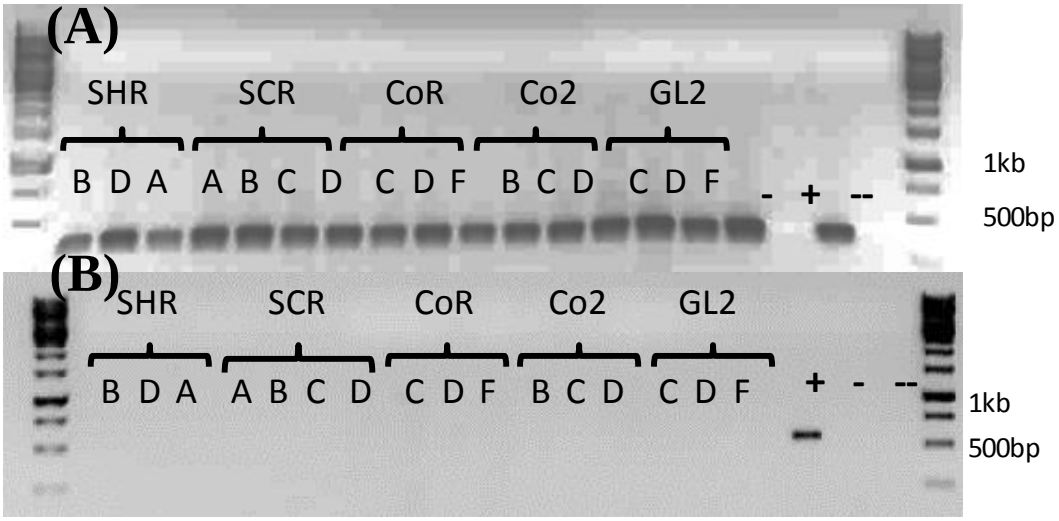

Figure 3-33**: Identification of Atgid1c and lack of *AtGID1c* within transgenic lines. (A)** Amplification product of 700-bp confirms the presence of a T-DNA insertion creating a non-functional *gid1c* allele. **(B)** Amplification product of 500-bp would indicate the presence of *GID1c*. Positive WT Col-0 control (+), negative *gid1a,-b,-c* (-) and water (--) are also included. For primer sequences used see Table 2-1 and for primer combinations used see Table 3-3

3.6 Conclusion of construct construction and Arabidopsis transformation

The C and N terminal YFP AtGA2ox2 constructs were successfully made in pET-32a, subsequent GA enzymatic assays demonstrated that both were functional allowing either to be used to degrade C_{19}-GAs in *Arabidopsis* (section 3.1 and section 3.2). AtGA2ox7 expression in *E. coli* and subsequent GA assay demonstrated that AtGA2ox7 cannot deactivate C_{19}-GAs and that GA_{24} is also a potential substrate. YFP fusions were then constructed in pENTR11 for each of the metabolic genes to be transformed into *Arabidopsis* under the control of the tissue specific promoters (section 3.3).

4 TISSUE-SPECIFIC GA INACTIVATION

4.1 INTRODUCTION TO 2β-HYDROYLATION

The 2β-hydroxylation of GA molecules either before or after they have been activated is an important mechanism for regulating GA content, allowing control of development in response to environmental cues (Achard et al., 2008a, Achard et al., 2008b). Since 2β-hydroxy GAs, formed by the action of GA2ox enzymes are found widely in many plant species, 2β-hydroxylation is likely to be a ubiquitous mechanism for GA inactivation (MacMillan, 2001). Its effectiveness was clearly demonstrated by Rieu *et al.,* (2008a) in a quintuple *GA2ox* knock-out mutants of *Arabidopsis* which confirmed a role for GA deactivation in a range of developmental processes such as limiting the number of flowers produced on each inflorescence.

There are currently two distinct clades of GA 2-oxidase enzymes: in *Arabidopsis*, five genes encode enzymes that are capable of deactivating bioactive C_{19}-GAs, such as GA_4 and GA_1 (Thomas et al., 1999), while another two GA2ox enzymes specifically hydroxylate C_{20}-GA precursors, such as GA_{12} and GA_{53} preventing them subsequently being converted to bioactive GAs (Schomburg et al., 2003) (Figure 4-1). Jiang *et al*. (2007) demonstrated that plants grown on high and low phosphate media exhibit variations in GA2ox expression levels depending on the environmental conditions, while studies involving the quintuple *GA2ox* knock-out mutant highlighted the fact that many developmental processes, including limiting elongation of the main stem and side shoots or the transition from vegetative to floral growth are redundantly regulated by the various C_{19}-GA 2-oxidases (Rieu et al., 2008a).

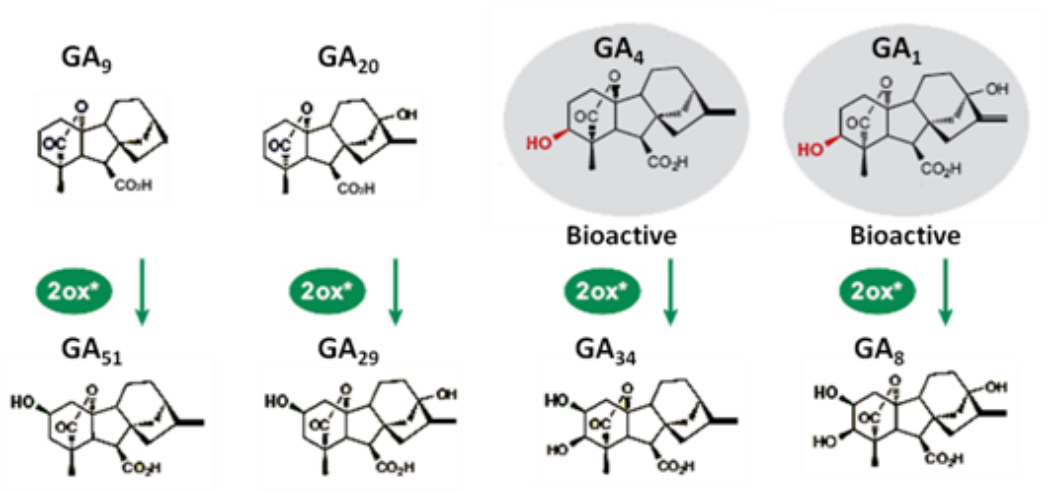

Figure 4-1: **Bioactive GAs and their immediate C_{19} precursors are inactivated by GA 2-oxidases.** A class of GA 2-oxidases can catalyse the oxidation of C-2 on C_{19}-GA precursors, such as GA_9 and GA_{20}, before activation and on C_{19}-GAs, such as GA_4 and GA_1, after activation by 3β-oxidation. Figure adapted with permission from Yamaguchi (2008).

Results from microarray studies demonstrate that the different GA2ox enzymes are expressed in all organs throughout the plant, while studies on the *Arabidopsis* root showed that their expression varies in a tissue-specific manner (Dugardeyn et al., 2008). Meta-analysis of multiple microarray studies by the Benfy group (Brady et al., 2007), Serres lab (Mustroph et al., 2009) and the CPIB group (unpublished data) of different stages of root development demonstrated that developmental regulation is important for determining the expression levels of the different GA2ox's. These data show much higher expression of *GA2ox6* in the differentiation zone (DZ), the mature region and the lateral root zone. In addition, expression of *GA2ox8*, which according to the analysis of Dugardeyn *et al.*, (2008) is present in the cortex and endodermis, is 2-fold greater in the DZ than in other regions of the root. Taken together these data suggest that the deactivation of bioactive GAs and C_{20}-GA precursors in the ground tissue is important for the normal homeostasis of the differentiation zone (DZ).

Tissue-specific inactivation of C_{19}-GAs or their C_{20} precursors was performed in order to locate the sites of GA biosynthesis and perception. These experiments rely on the fact that there are two classes of GA 2-oxidases (GA2ox) which inactivate GAs: those that act on bioactive GAs and their

immediate C_{19} precursors (e. g. AtGA2ox2), and those which act only on C_{20} precursor GAs earlier in the biosynthesis pathway (e.g. AtGA2ox7) (Schomburg et al., 2003, Hedden and Phillips, 2000). These experiments involve the transformation of wild type *Arabidopsis* Col-0 with constructs allowing the targeted expression of both YFP-AtGA2ox2 and YFP-AtGA2ox7 fusion proteins to the root epidermis, cortex, endodermis and stele. Homozygous transgenic lines were subsequently analysed for defects in root growth and development. Inhibition of growth through cell-type specific inactivation of C_{20}-GAs should indicate sites of biosynthesis, while inactivation of C_{19}-GAs should indicate sites of biosynthesis and perception. Complementation of the ga2ox2 and ga2ox7 mutants was not attempted as they are part of a large semi-redundant gene family so any phenotypes under normal growth conditions are generally insufficiently robust for statistically significant analysis (Rieu et al., 2008a, Schomburg et al., 2003). In addition, to see if the expression or stability of the transgenes is regulated by GA, plants were grown on GA_3 and a GA biosynthesis inhibitor paclobutrazol (PAC).

In order to determine if GAs moving from the shoot influence root growth, YFP-AtGA2ox2 and YFP-AtGA2ox7 expression was also targeted solely to photosynthetic tissues using the *CAB* promoter (Yadav et al., 2002). As the promoters used to target specific tissues and stages of development in the root are also expressed in aerial tissues this may complicate interpretation of root phenotypes potentially due to the movement of GA, however by using the photosynthetic tissue specific promoter of the *CAB* gene to drive the expression of the transgenes this will also allow the effect of any aerial expression to be accounted for. *SHR, SCR* and *GL2* promoters will be used to drive the expression of the transgene within the root stele, endodermis and epidermis respectfully (Heidstra et al., 2004, Hung et al., 1998, Di Laurenzio et al., 1996). In addition, the *Co2* and *CoR* promoters will be used to investigate the importance of GA metabolism within the ground tissue of the root meristematic and elongation zones (Dinneny et al., 2008, Heidstra et al., 2004).

4.1.1 Characterisation of *AtGA2ox2* targeted expression lines

The effect of targeting the expression of *AtGA2ox2* with tissue specific promoters on the phenotype of wild-type Col-0 was initially monitored in terms of effects on the root length of seven day-old seedlings grown on vertical plates, as well as the vegetative growth of the rosette after three weeks and the growth of the inflorescence after six weeks. The AtGA2ox2 gene was used as it had been previous shown to catabolise only C_{19}-GAs and was therefore present in the laboratory (Thomas et al., 1999). Three independently transformed lines were then selected for further detailed analysis of root growth, involving measuring root lengths, meristem lengths, and final cell sizes were all measured at seven days. Seven days was chosen as it has been previously shown by Achard *et al*., (2009) that by 7 days GA deficient mutants, such as *ga1-3,* have reached their maximum meristem length and therefore maximum growth rate. In all experiments the transgenic lines were compared with Col-0 and *ga1-3 as ga1-3 i*s known to be completely GA deficient and Col-0 was the ecotype that was genetically modified.

4.1.2 *Col-0;SHR::YFP:AtGA2ox2* does not affect root length or vegetative development

To investigate whether removing bioactive GA from the root stele would have an effect on root growth, expression of YFP-AtGA2ox2 was driven using the *SHR* promoter (Di Laurenzio et al., 1996). Root lengths of lines expressing *SHR::YFP:AtGA2ox2* compared with Col-0 and *ga1-3* are shown in Figure 4-2. The root length of lines A, D and E were shorter than Col-0 and larger than *ga1-3* making them significantly different from both Col-0 and *ga1-3* ($p<0.01$) but the root length of lines B and C were not significantly different from Col-0 ($p>0.05$). As the effect of the transgene on root lengths was small for all the lines and these lines did not display any obvious vegetative phenotypes, line D, showing the largest effect on root growth, was chosen for further analysis (Figure 4-3). Lines B and E were not significantly different from line D so were also selected for further analysis.

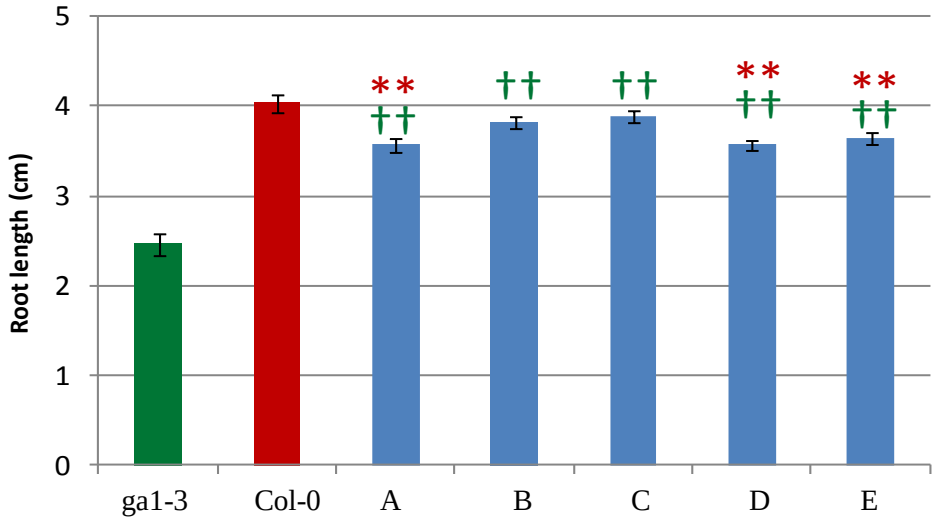

Figure 4-2**: Primary root length ±SE for *Col-0;SHR::YFP:AtGA2ox2* lines (A-E) compared to *ga1-3* and Col-0 at seven days**. Seedlings were grown on vertical plates and lengths calculated using ImageJ. Green crucifixes indicate the root lengths significantly different from *ga1-3* and the red asterisks indicate they are significantly different from Col-0. 30 plants for each line were analysed **=p<0.01, and ††=p<0.01. Error bars indicate standard error. The least significant differences (LSD) are given in Table 11-2.

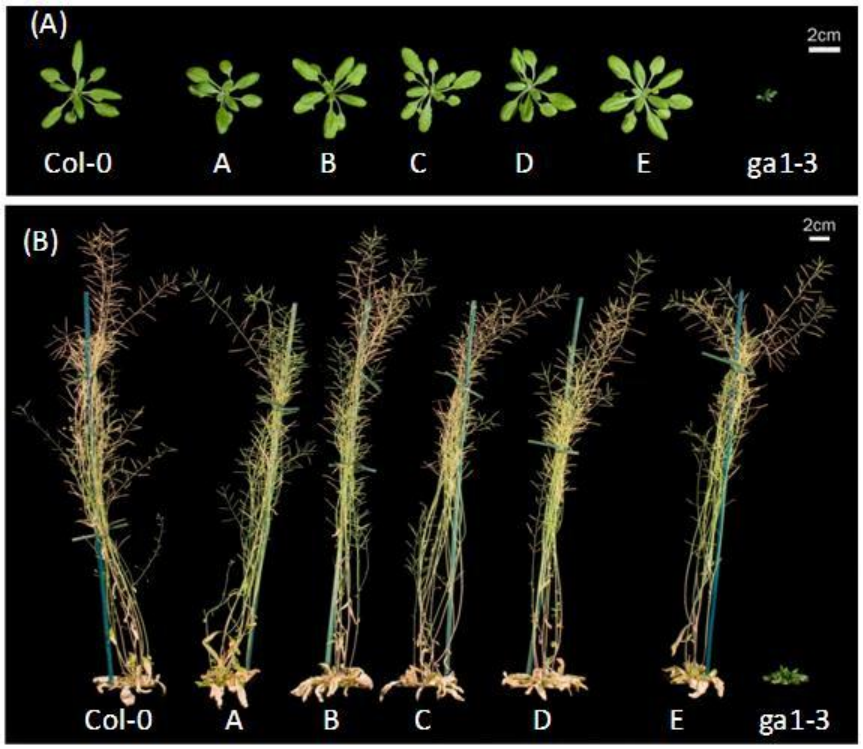

Figure 4-3: **Vegetative phenotypes are shown for Col-0;*SHR::YFP:AtGA2ox2* lines (A-E) compared to *ga1-3* and Col-0.** Plants were grown on Levingtons compost in 5.5 cm pots under long days at three (A) and six weeks (B).

4.1.3 *Col-0;SHR::YFP:AtGA2ox2*: root length, meristem length, cell length and transgene expression profile.

To determine whether the transgene was expressed in the expected tissue-specific localisation, confocal microscopy was performed on the five roots from the selected representative lines when the seedlings were 7 day old after being grown simultaneously on different vertical Gelrite plates. In all three *SHR::YFP:AtGA2ox2* lines, the transgene appeared to be expressed within the pericycle and vasculature of the meristematic region at a low level and in the endodermis of the differentiation zone at a relatively high level (Figure 4-4). In addition when plants were sown on plates containing 1 µM GA_3, expression of *SHR::YFP:AtGA2ox2* within the vasculature and pericycle increased relative to plants grown on control medium. In contrast, no *SHR::YFP:GA2ox2* expression could be observed when the plants were grown on medium containing 1 µM PAC (Figure 4-5), a GA biosynthesis inhibitor.

Primary root growth for 15 plants from each of the three selected lines expressing YFP-AtGA2ox2 under the *SHR* promoter were compared with *ga1-3* and Col-0. In addition to root length the meristem size of five plants and final cell length of 5 cells of each of the 5 plants was measured for further analysis (Figure 4-6). In agreement with the previous characterisation (section 0) *SHR::YFP:AtGA2ox2* did not affect root growth significantly in lines B and D, although there was moderate reduction in meristem size and root length in line E. Root lengths, meristem lengths and final cell lengths of lines B and D were not significantly different from Col-0 ($p>0.05$), whereas the significant reduction in final root length in line E compared with Col-0 ($p<0.05$) may be attributed to the reduced cell division since its meristem size, but not final cell length was significantly different from Col-0 ($p<0.05$).

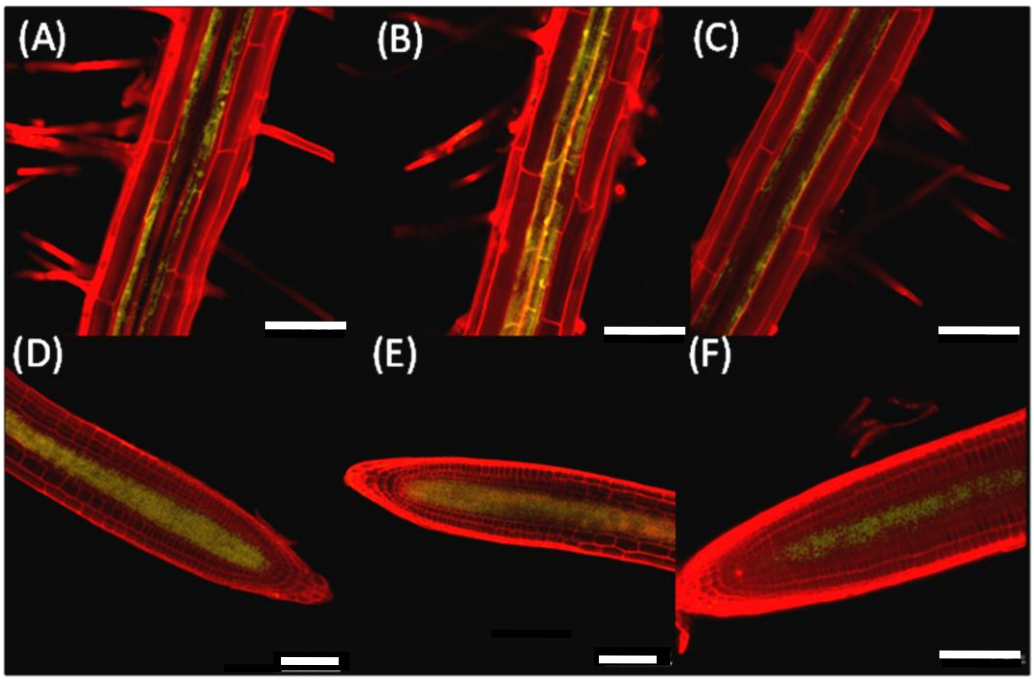

Figure 4-4: ***Col-0;SHR::YFP:AtGA2ox2*** **expression in vasculature is shown for lines B, D and E. (A-C)** YFP fluorescence in the differentiation zone. **(D-F)** YFP fluorescence in the meristematic region. Confocal microscopy was performed on the five roots of seven day old seedlings after being grown on vertical Gelrite plates. The YFP and the propidium iodide emission images are overlaid. Bars are 50 μm or 100 μm in length.

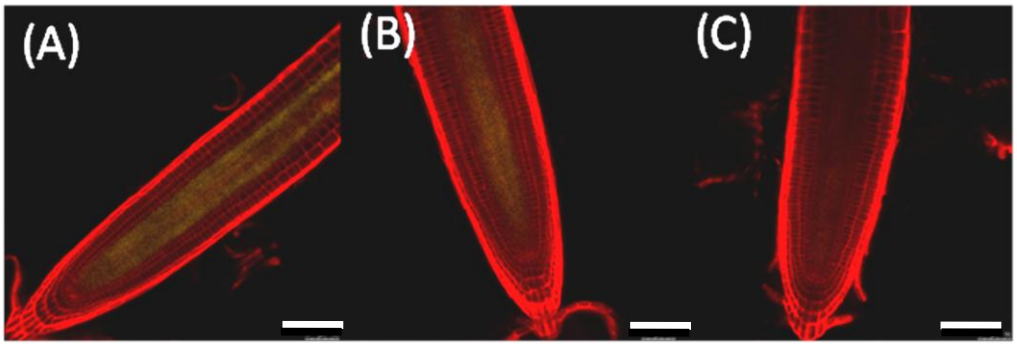

Figure 4-5: ***Col-0;SHR::YFP:AtGA2ox2*** **fluorescence response to GA_3 and PAC treatment. (A)** YFP expression in the meristematic region is shown for line D grown on Gelrite containing 1 μM GA_3, **(B)** when grown on control Gelrite, (C) when grown on Gelrite containing 1 μM PAC. Confocal microscopy was performed on the five roots of seven day old seedlings after being grown on vertical Gelrite plates. The YFP and the propidium iodide emission images are overlain. Bars are 100 μm in length.

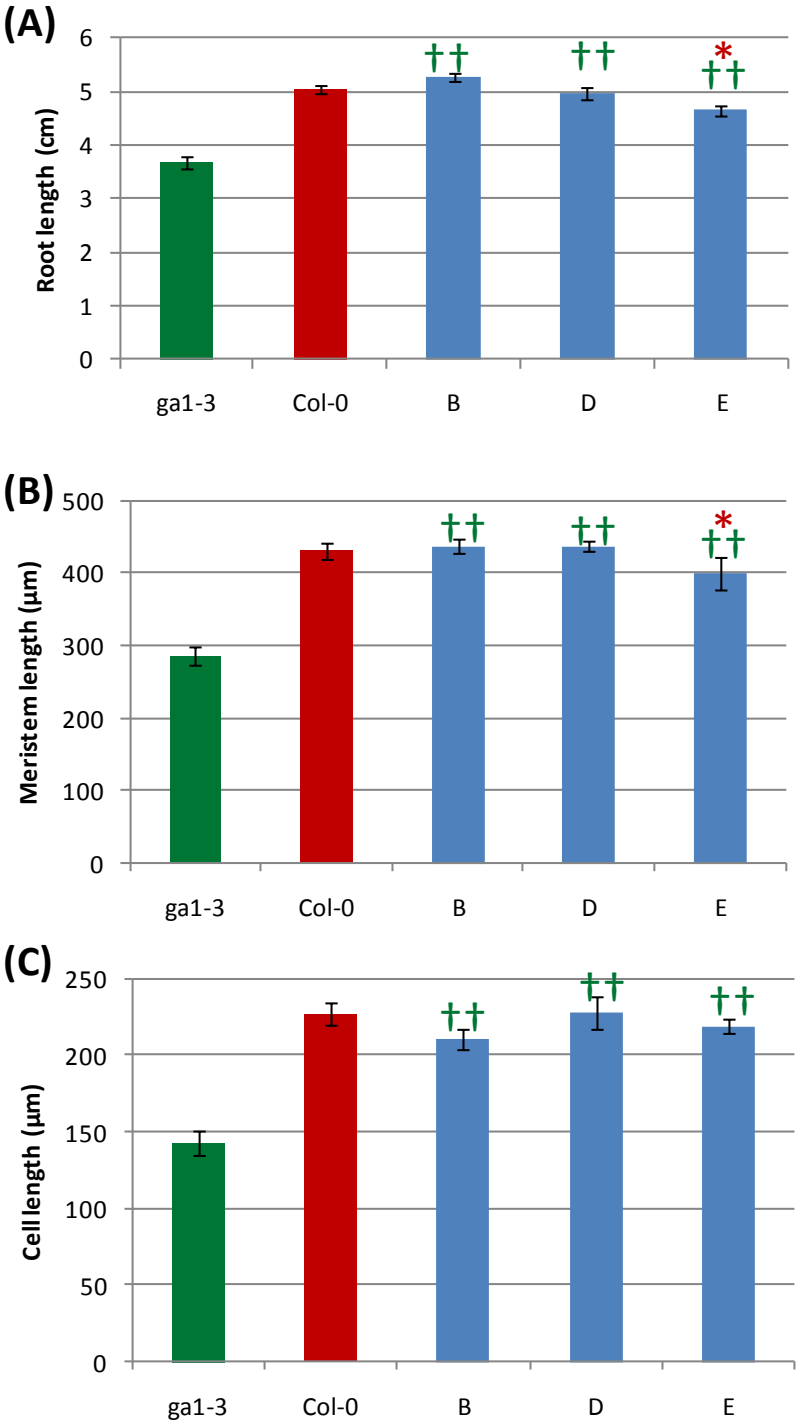

Figure 4-6**: Parameters for the primary root at 7 days in Col-0 lines B, D and E expressing *SHR::YFP:AtGA2ox2* compared with Col-0 and *ga1-3*.** **(A)** Primary root length ±SE. **(B)** Proximal meristem length ±SE. **(C)** Final cortical cell length ±SE. Seedlings were grown on vertical plates and lengths calculated using ImageJ. Green crucifixes indicate the transgenic lines are significantly different from *ga1-3* and the red asterisks indicate they are significantly different from Col-0. 15 plants for each line were measured for root length, 5 plants had their meristem and 5 cells measured *=$p<0.05$ and ††=$p<0.01$. Error bars indicate standard error. Restricted maximum likelihood (REML) was used to generate the LSD given in Table 11-7.

4.1.4 *Col-0;SCR::YFP:AtGA2ox2* severely reduces root length and retards vegetative development

To investigate whether removing bioactive GA from the root endodermis (Figure 4-12) would have an effect on root growth, YFP-AtGA2ox2 was driven using the *SCR* promoter (Di Laurenzio et al., 1996). Root lengths of Col-0 transgenic lines expressing *SCR::YFP:AtGA2ox2* compared with Col-0 and *ga1-3* are shown in Figure 4-7. Roots for all six transgenic lines were shorter than Col-0, lines A, B and F were significantly smaller than both Col-0 ($p<0.01$) and *ga1-3* (A and B at $p<0.01$, F at $p<0.05$). Lines C, D and E were significantly shorter than Col-0 (C and D at $p<0.01$, E at $p<0.05$) but were not significantly different from *ga1-3* ($p>0.05$). Interestingly, transgenic lines with primary root lengths that were significantly different from *ga1-3* displayed shorter roots than *ga1-3*. All transgenic lines displayed reduced stem and leaf elongation compared to Col-0 (Figure 4-8), with lines E and F being only mildly dwarfed, whereas the stem lengths of lines A-D were more severely reduced. Since line E displayed only a mild root and shoot phenotype, which was less consistent than the others, it was not selected for further analysis. Although line F vegetative phenotype was not as reduced as lines A-D, it was selected on the basis of its reduced root length. Since line A had the most severely reduced primary root length and the root length of line C was closest to the mean of all the lines, these lines were also selected for further analysis.

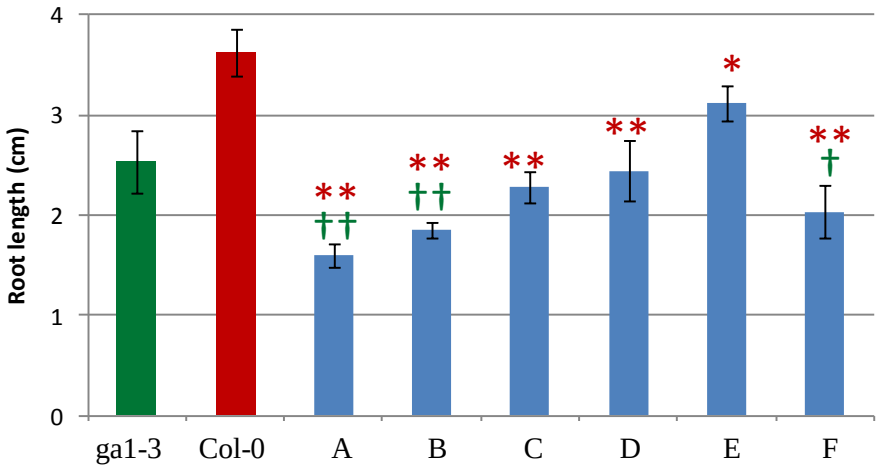

Figure 4-7**: Primary root length ±SE are shown for *Col-0;SCR::YFP:AtGA2ox2* lines (A-F) compared to *ga1-3* and Col-0 at seven days.** Seedlings were grown on vertical plates and lengths calculated using ImageJ. Green crucifixes indicate the transgenic lines are significantly different from *ga1-3* and the red asterisks indicate they are significantly different from the Col-0. 30 plants for each line were analysed *=p<0.05, **=p<0.01, †=p<0.05 and ††=p<0.01. Error bars indicate standard error. REML was used to generate the LSD given in Table 11-2.

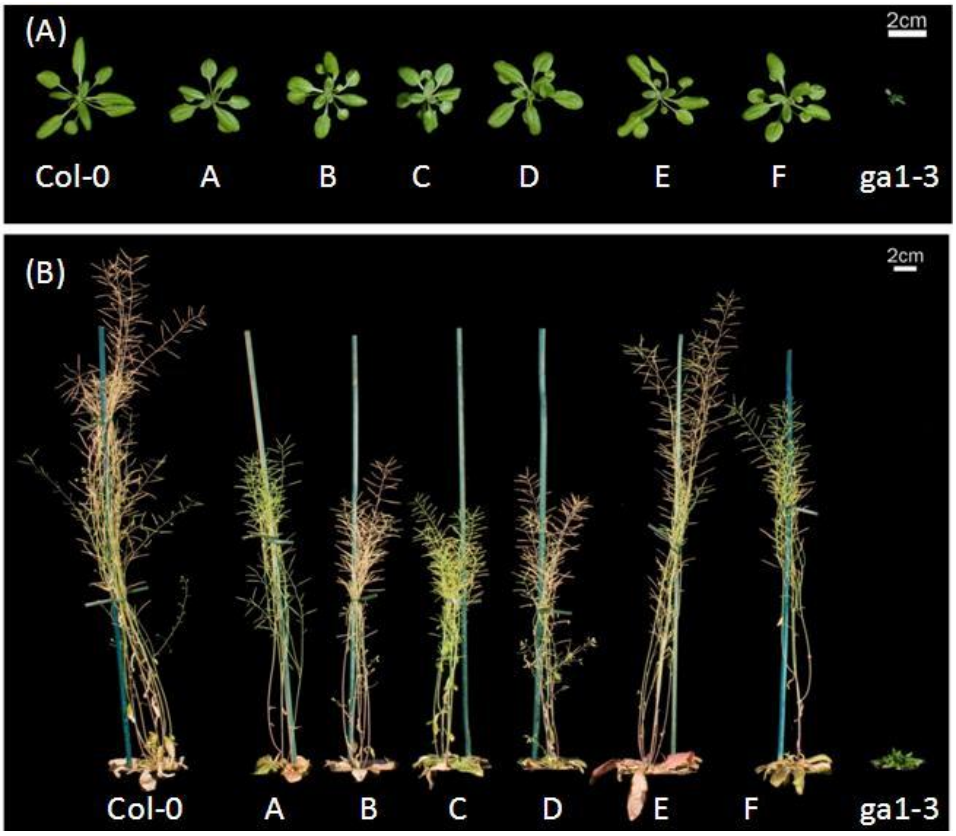

Figure 4-8: **Vegetative phenotypes are shown for *Col-0;SCR::YFP:AtGA2ox2* lines (A-F) compared to *ga1-3* and Col-0 at three and six weeks.** Plants were grown on Levingtons compost in 5.5 cm pots under long days.

4.1.5 *Col-0;SCR::YFP:AtGA2ox2*: root length, meristem length, cell length and transgene expression profile.

The primary root parameters for the three representative *Col-0;SCR::YFP:AtGA2ox2* lines were compared with those of *ga1-3* and Col-0 (Figure 4-9). In agreement with the previous characterisation (section 4.1.4), root growth was retarded in all three *Col-0;SCR::YFP:AtGA2ox2* lines: root lengths, meristem lengths and final cell lengths of these lines were significantly different from Col-0 ($p<0.01$, except line C in which root length was significantly different at $p<0.05$). Only line C had a final root length that was significantly different from *ga1-3* ($p<0.05$), due to cell length that was significantly different from both *ga1-3* and Col-0 ($p<0.01$).

On the basis of YFP fluorescence, expression of YFP-AtGA2ox2 in all three *SCR::YFP:AtGA2ox2* lines within the meristematic region was extremely low, so that it was difficult to be sure of its exact location (Figure 4-10); although expression within the endodermis was clear, it is also possible that there was some expression in the cortex and pericycle. Within the differentiation region fluorescence was higher and was localised to the endodermis and the occasional pericycle cell. When plants were sown on plates containing 1 µM GA_3, expression of *SCR::YFP:AtGA2ox2* increased dramatically, allowing fluorescence to be observed within the cortex, vasculature, pericycle as well as the endodermis, where it was most highly expressed. In the same experiment, the lines grown on control medium showed YFP fluorescence within the endodermis and to a lower extent in the cortex, while in plants on Gelrite containing 1 µM PAC no YFP fluorescence could be observed (Figure 4-11). In addition nuclear localisation of YFP-AtGA2ox2 can clearly be seen in the cortical cells of the elongation zone.

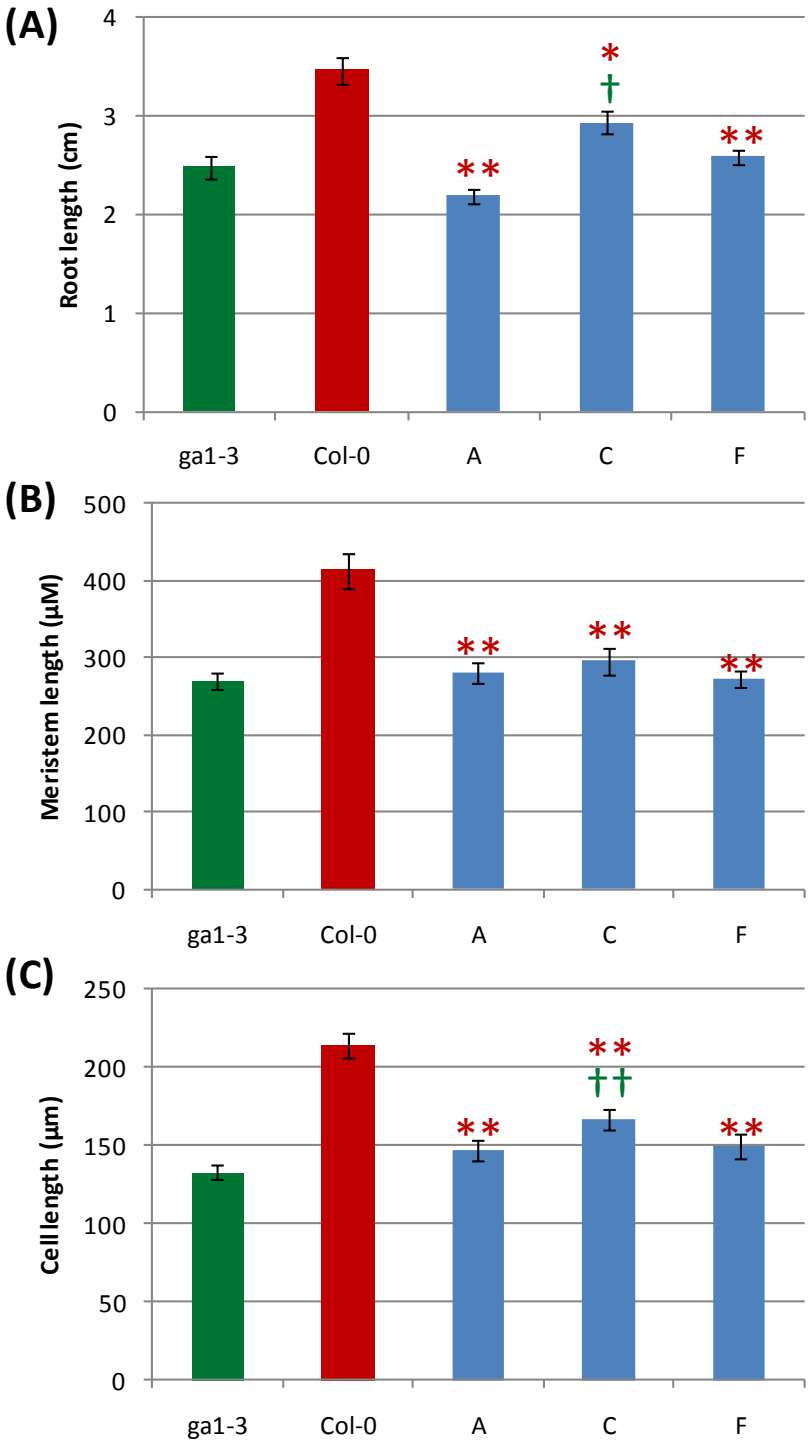

Figure 4-9**: Parameters for the primary root at 7 days in Col-0 lines A, C and F expressing *SCR::YFP:AtGA2ox2* compared with Col-0 and *ga1-3*.** **(A)** Primary root length ±SE. **(B)** Proximal meristem length ±SE. **(C)** Final cortical cell length ±SE. Seedlings were grown on vertical plates and lengths calculated using ImageJ. Green crucifixes indicate the transgenic lines are significantly different from *ga1-3* and the red asterisks indicate they are significantly different from Col-0. 15 plants for each line were measured for root length; 5 plants had their meristem and 5 cells measured *=p<0.05, **=p<0.01, †=p<0.05 and ††=p<0.01. Error bars indicate standard error. REML was used to generate the LSD given in Table 11-7.

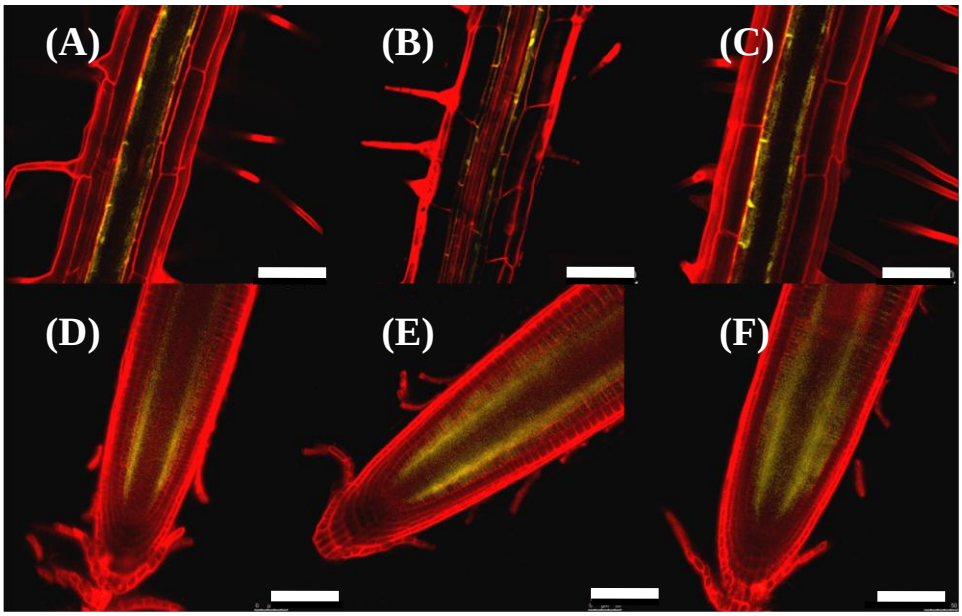

Figure 4-10: **YFP fluorescence in the meristem and differentiation zone of *Col-0;SCR::YFP:AtGA2ox2* line. (A-C)** YFP fluorescence is present in the differentiation zone of lines A, D and F, respectively; **(D-F)** YFP fluorescence is present in the meristematic region of lines A, D and F, respectively. Confocal microscopy was performed on the five roots of seven day old seedlings after being grown on vertical Gelrite plates. The YFP and the propidium iodide emission images are overlain. Bars are 100 μm in length.

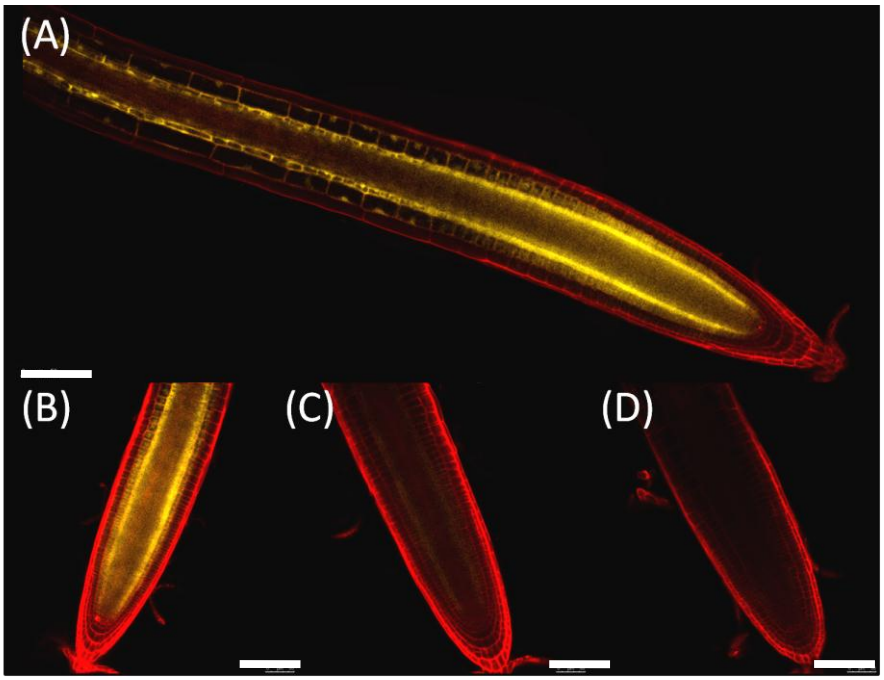

Figure 4-11: ***Col-0;SCR::YFP:AtGA2ox2* fluorescence response to GA_3 and PAC treatment. (A-B)** YFP fluorescence in roots of *SCR::YFP:AtGA2ox2* line D plants grown on Gelrite containing 1 μM GA_3, **(C)** plants grown without GA_3, **(D)** plants grown on Gelrite containing 1 μM PAC. Confocal microscopy was performed on the five roots of seven day old seedlings after being grown on vertical Gelrite plates. The YFP and the propidium iodide emission images are overlain. Bars are 100 μm in length.

4.1.6 Investigating the effect of PAC and GA_4 on *SHR* and *SCR* expression

Due to the increase in fluorescence in the *Col-0;SCR::YFP:AtGA2ox2* lines in response to GA_3 treatment, a decrease in response to treatment with PAC and the fluorescence observed within the cortex, the expression of *SCR* was investigated using *SCR::GFP* and *SCR::SCR:GFP* lines. Figure 4-12 shows that increasing or decreasing GA levels had no affect on *SCR* expression levels or domains, thus demonstrating that the changes in *YFP:AtGA2ox2* fluorescence in response to changes in GA content are due to effects on AtGA2ox2 stability or post transcriptional processing. It has been shown that correct *SCR* expression with the endodermis as the result of normal endodermal/cortical initial cell division cannot take place without the correct expression of the GRAS family transcription factor *SHR* (Benfey et al., 1993).

SHR has been shown to have multiple direct targets including a network of transcription factors (Levesque et al., 2006). *SHR* is transcribed and translated within the stele from which it accumulates in the endodermal cells, where it binds to the SCR protein, causing it to then enter the nucleus (Di Laurenzio et al., 1996). *SHR* then helps to activates multiple transcription factors including *SCR*, *NUTTCRACKER (NUC*), *JACKDAW* (*JKD*), and *MAGPIE* (*MGP*) which in turn assist on importing SHR into the nucleus (Welch et al., 2007). This transcriptional network of C2H2 zinc finger and GRAS family transcription factors help to establish cellular identity, promote cell division and SHR nuclear localisation (Welch et al., 2007). The GRAS and IDD proteins induce the nuclear localisation of the SHR protein consequently reducing SHR movement by confining it to the endodermis. This provides positional information about the cells proximity to vascular tissue, (Cui et al., 2007, Sena et al., 2004, Nakajima et al., 2001).

To investigate if the cortical expression of *SCR::YFP:AtGA2ox2* was due to alterations in SHR movement, the *SHR:GFP* reporter lines were grown on 1 μM PAC and 1 μM GA (Figure 4-13). No alteration to *SHR* expression could be observed on control plate or in response to either 1 μM PAC or 1 μM GA_3, so in order to investigate whether or not *SHR* expression might be regulated within the endodermis in a tissue specific manner, the *SHR* transcriptional and translational reporters were crossed into *SCR::YFP:AtGA2ox2* lines (Figure 4-14). No difference in *SHR::GFP* expression could be observed, although it was difficult to detect the nuclear localisation of the *SHR::SHR:GFP* protein in the endodermal nucleus when expressed in the *SCR::YFP:AtGA2ox2* background. It is unclear whether this is the result of reduced endodermal localisation of *SHR::SHR:GFP* or alternatively if it is due to YFP interference with the GFP fluorescence transmission.

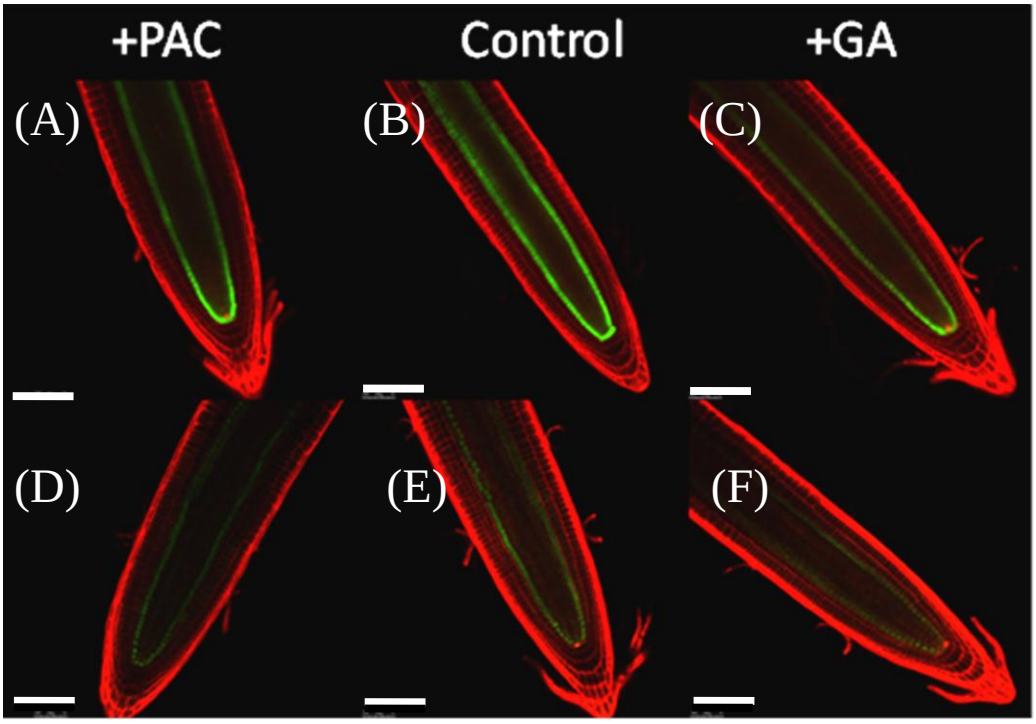

Figure 4-12: ***SCR::GFP* and *SCR::SCR:GFP* fluorescence response to GA and PAC treatments. (A-C)** *SCR::GFP* and **(D-F)** *SCR::SCR:GFP* lines. Plants were grown for 5 days on control Gelrite plates and then transferred to plates containing either 1 μM GA_3 or 1 μM PAC. Confocal microscopy was performed on the five roots of seven day old seedlings after being grown on vertical Gelrite plates. The GFP and the propidium iodide emission images are overlain. Bars are 50 μm in length.

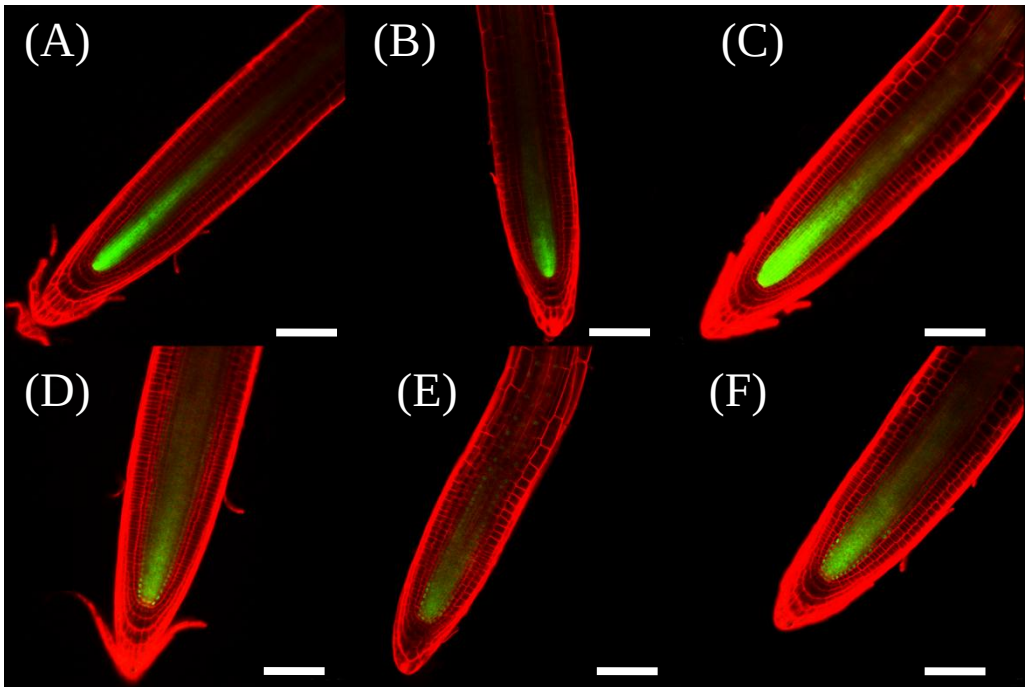

Figure 4-13: ***SHR::GFP* and *SHR::SHR:GFP* fluorescence response to GA and PAC treatments. (A-C)** *SHR::GFP* and **(D-F)** *SHR::SHR:GFP* lines. Plants were grown for 5 days on control Gelrite plates and then transferred to plates containing either 1 µM GA_3 or 1 µM PAC. Confocal microscopy was performed on the five roots of seven day old seedlings after being grown on vertical Gelrite plates. The GFP and the propidium iodide emission images are overlain. Bars are 100 µm in length.

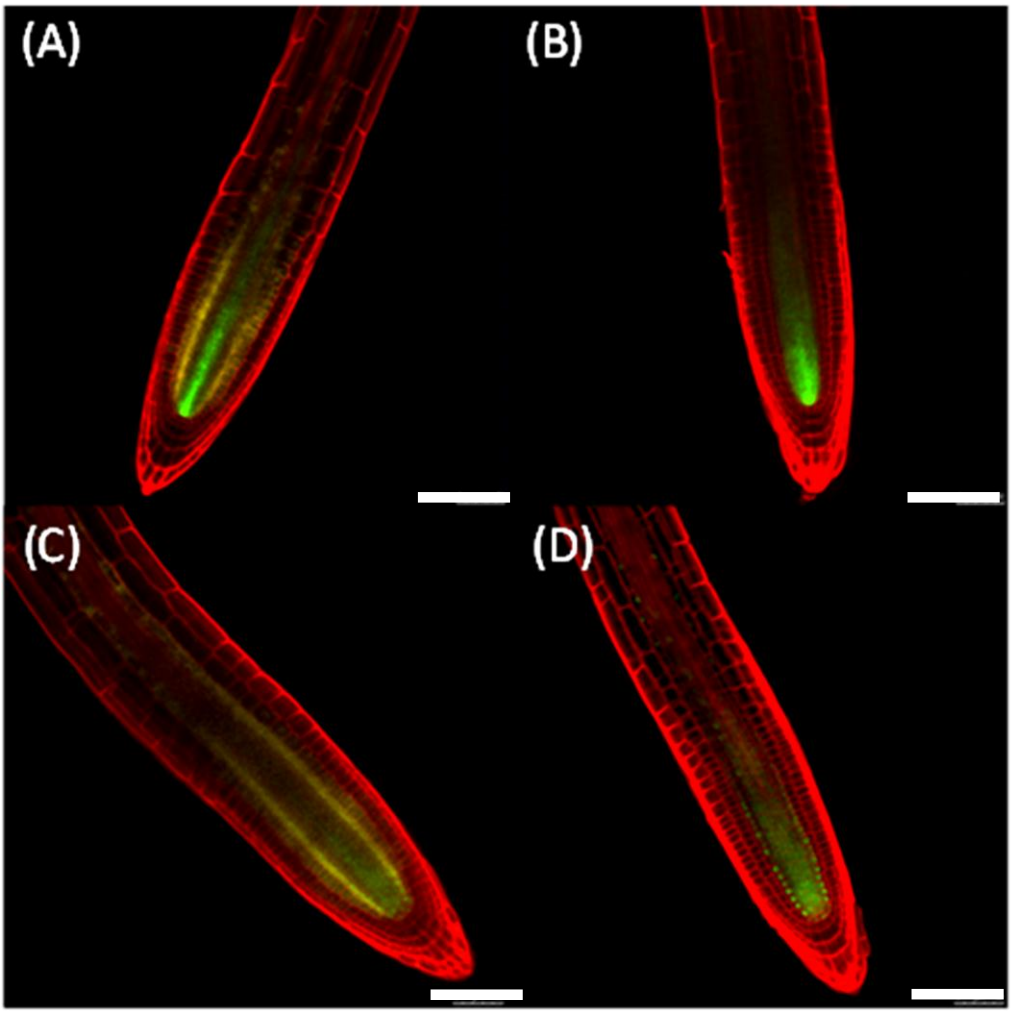

Figure 4-14: ***SHR::GFP*** **and** ***SHR::SHR:GFP*** **in Col-0 or** ***SCR::YFP:AtGA2ox2*** **backgrounds. (A)** *SHR:GFP* x *SCR::YFP:AtGA2ox2*. **(B)** *SHR:GFP*. **(C)** *SHR:SHR:GFP x SCR::YFP:AtGA2ox2*. **(D)** *SHR:SHR:GFP*. Confocal microscopy was performed on the five roots of seven day old seedlings after being grown on vertical Gelrite plates. The GFP, YFP and the propidium iodide emission images are overlaid. Bars are 100 μm in length.

4.1.7 *Col-0;CoR::YFP:AtGA2ox2* severely reduces root length and retards vegetative development

To investigate whether removing bioactive GA from the ground tissue of the elongation zone would have an effect on root growth, YFP-AtGA2ox2 was driven using the *CoR* promoter (Dinneny et al., 2008). Four *Col-0;CoR::YFP:GA2ox2* lines were obtained, from which three representative lines needed to be chosen for further analysis. In order to do this, root lengths for the four were compared with Col-0 and *ga1-3* (Figure 4-15). The root length of line A is significantly larger than *ga1-3* ($p<0.01$), and not significantly smaller than Col-0 ($p>0.05$). Lines B and C were significantly different from both *ga1-3* ($p<0.05$ and $p<0.01$, respectively) and Col-0 ($p<0.05$), while line D was significantly smaller than Col-0 ($p<0.01$), and not significantly different from *ga1-3* ($p>0.05$). The aerial phenotypes of the transgenic lines gave a range from mildly dwarfed, such as in line A, to severely dwarfed, such as line D (Figure 4-16). Since line A was the outlier in terms of root growth and had the least stunted aerial phenotype, lines B, C and D were chosen for further analysis.

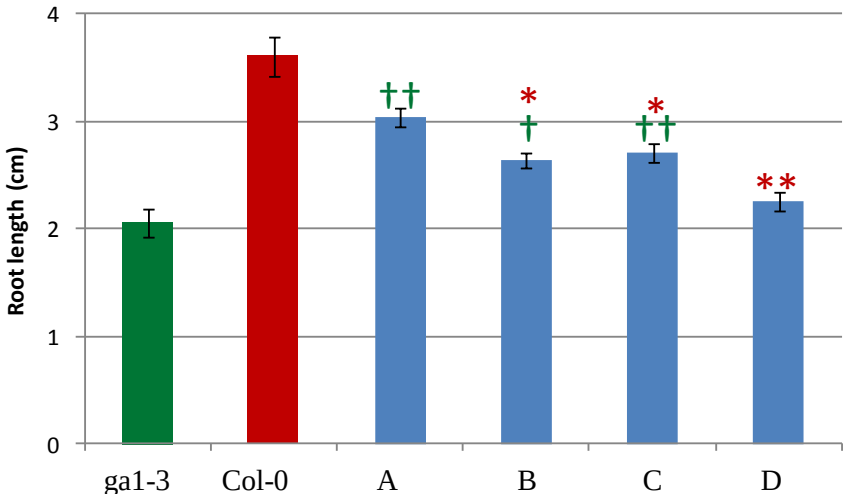

Figure 4-15**: Primary root length ±SE for *Col-0;CoR::YFP:AtGA2ox2* lines (A-D) compared to *ga1-3* and Col-0 at seven days.** Seedlings were grown on vertical plates and lengths calculated using ImageJ. Green crucifixes indicate the transgenic lines are significantly different from *ga1-3* and the red asterisks indicate if they are significantly different from Col-0. 30 plants for each line were analysed *=p<0.05, **=p<0.01, †=p<0.05 and ††=p<0.01. Error bars indicate standard error. REML was used to generate the LSD given in Table 11-2.

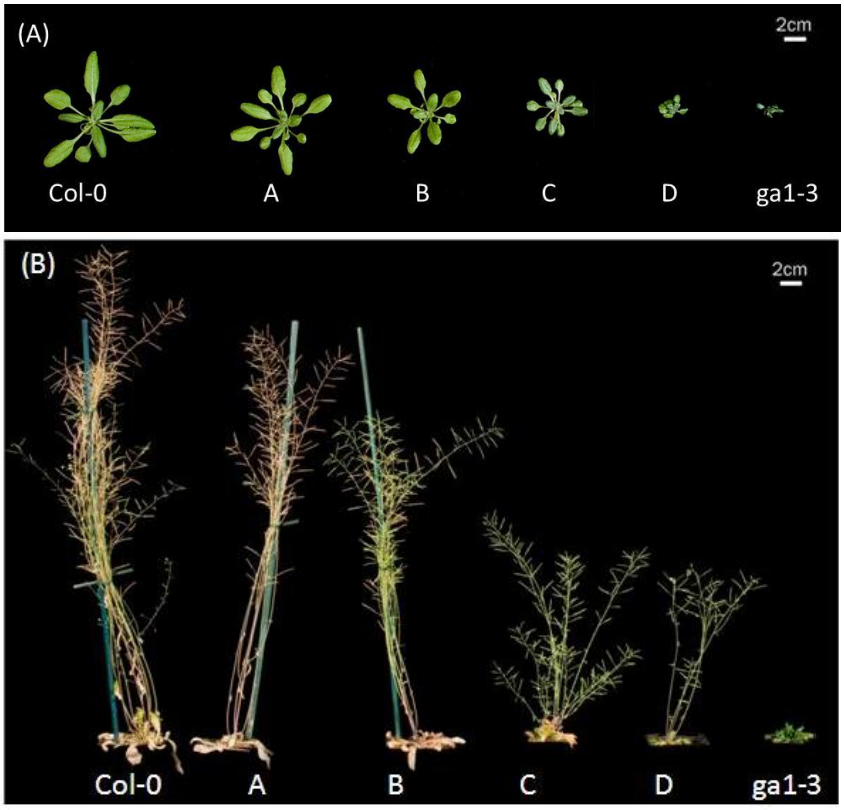

Figure 4-16: **Vegetative phenotypes are shown for *Col-0;CoR::YFP:AtGA2ox2* lines (A-D) compared to *ga1-3* and Col-0.** Plants were grown on Levingtons compost in 5.5 cm pots under long days at three (A) and six weeks (B).

4.1.8 *Col-0;CoR::YFP:AtGA2ox2*: root length, meristem length, cell length and transgene expression profile.

In all three *Col-0;CoR::YFP:AtGA2ox2* lines selected, YFP fluorescence was detected in the endodermis and cortex of the elongation zones (Figure 4-17). The primary root parameters for the three representative Col-0 lines expressing YFP-AtGA2ox2 with the *CoR* promoter were compared with *ga1-3* and wild-type Col-0 (Figure 4-18). *CoR::YFP:AtGA2ox2* expression did not affect the size of the root meristem in any of the three transgenic lines as it was not significantly different from that in Col-0. However, expression of this gene stunted root growth by reducing final cortical cell size. The root, meristem and final cell lengths of all three lines were significantly larger than for *ga1-3* ($p<0.01$). In agreement with the previous characterisation (section 4.1.7) root lengths were also significantly shorter from Col-0 ($p<0.01$) which was due to final cell lengths that were also significantly smaller than in Col-0 ($p<0.01$).

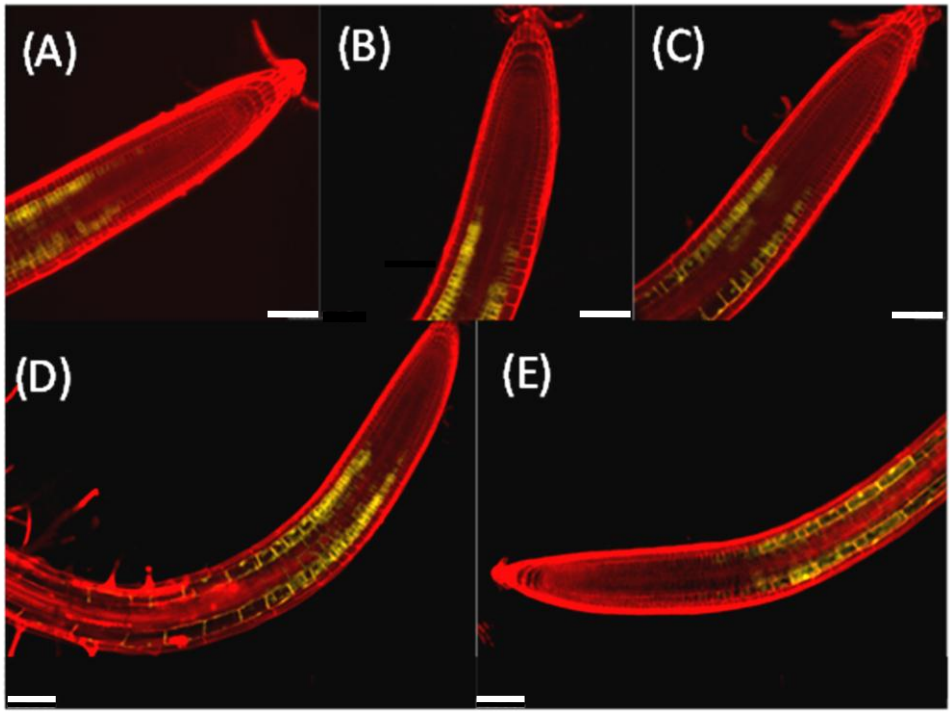

Figure 4-17: ***Col-0;CoR::YFP:AtGA2ox2* expression in roots. (A-C)** Lines B, C and D, respectively. **(D-E)** are composite images of multiple confocal images for line B and C respectively. Confocal microscopy was performed on the five roots of seven day old seedlings after being grown on vertical Gelrite plates. The YFP and the propidium iodide emission images are overlaid. Bars are 100 μm in length.

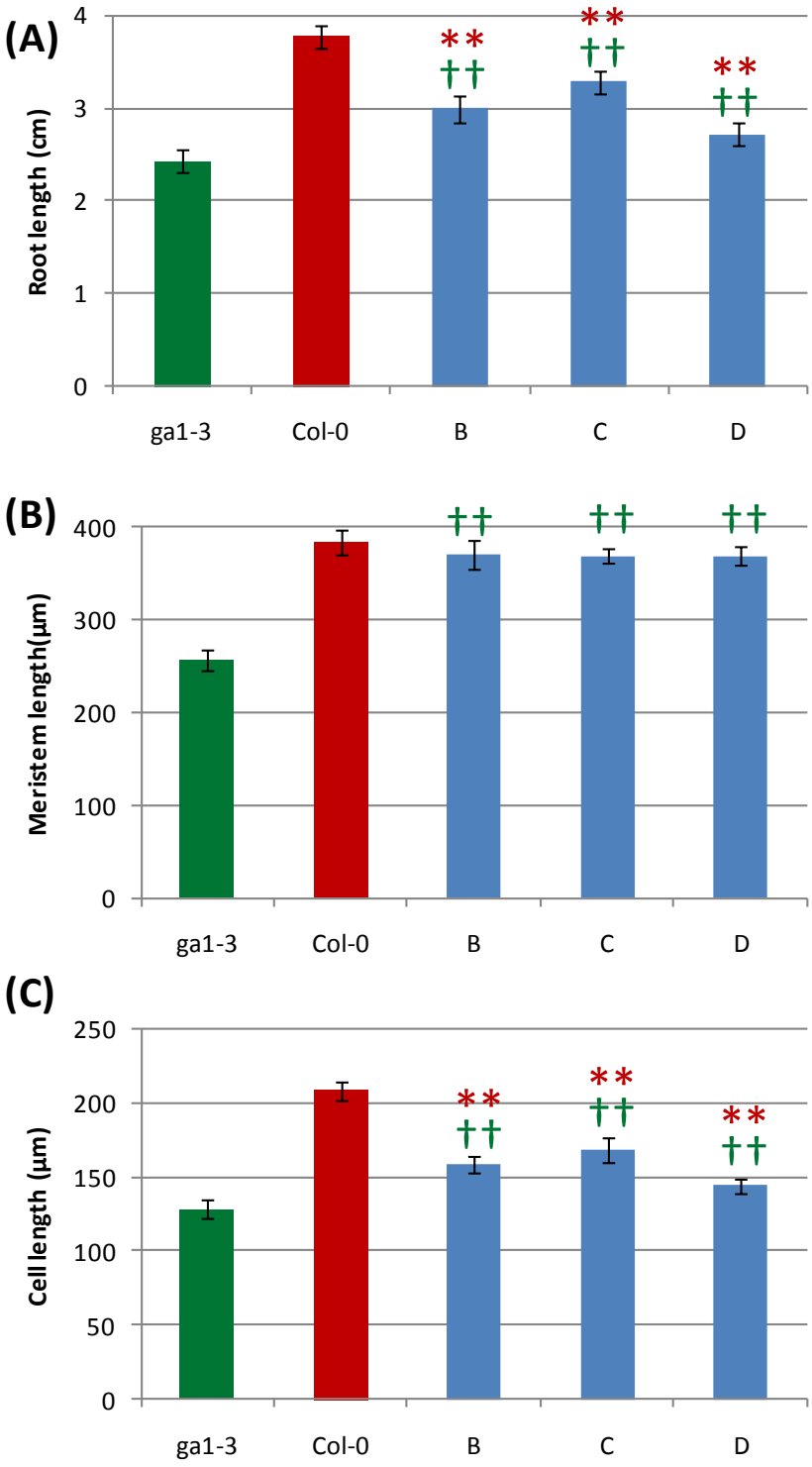

Figure 4-18**: Parameters for primary root growth at 7 days in Col-0 lines B, C and D expressing *CoR::YFP:AtGA2ox2* compared with Col-0 and *ga1-3*.** **(A)** Primary root length ±SE. **(B)** Proximal meristem length ±SE. **(C)** Final cortical cell length ±SE. Seedlings were grown on vertical plates and lengths calculated using ImageJ. Green crucifixes indicate the transgenic lines are significantly different from *ga1-3* and the red asterisks indicate if they are significantly different from Col-0. 15 plants were measured for root length, 5 plants had their meristem and 5 cells measured. **=$p<0.01$ and ††=$p<0.01$. Error bars indicate standard error. REML was used to generate the LSD given in Table 11-7.

4.1.9 *Col-0;Co2::YFP:AtGA2ox2* reduces root length and retards vegetative development

To investigate the importance of the cortical cells of the root apical meristem (RAM) and the endodermal/cortical initial (ECI) cells for GA biosynthesis and/or action, YFP-AtGA2ox2 expression was driven using the *Co2* promoter (Sozzani et al., 2010, Heidstra et al., 2004). Root lengths of lines expressing *Col-0;Co2::YFP:AtGA2ox2* were compared with Col-0 and *ga1-3*, as shown in Figure 4-19. The root length of lines A and D were significantly different from both Col-0 and *ga1-3* ($p<0.01$), while roots of lines B and C were significantly smaller from that in Col-0 ($p<0.01$) and not significantly different from that in *ga1-3* ($p>0.05$). The rosette leaves and florescence of all transgenic lines were mildly dwarfed, with line B being the smallest and line D the largest (Figure 4-20). As line D appeared to be the least affected by the expression of the transgene in both its root and shoot phenotypes, lines A, B and C were chosen for further analysis.

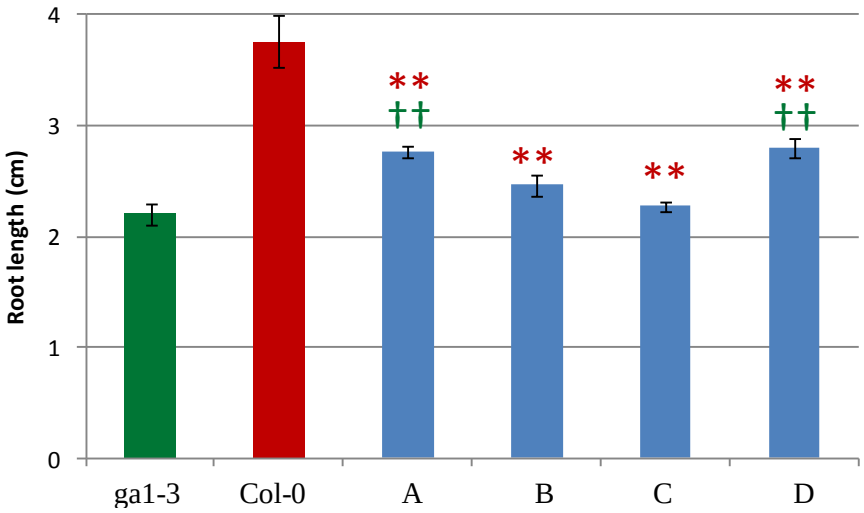

Figure 4-19**: Primary root length ±SE for *Col-0;Co2::YFP:AtGA2ox2* lines (A-D) compared to *ga1-3* and Col-0 at seven days.** Seedlings were grown on vertical plates and lengths calculated using ImageJ. Green crucifixes indicate the transgenic lines are significantly different from *ga1-3* and the red asterisks indicate they are significantly different from the Col-0. 30 plants were analysed **=p<0.01, and ††=p<0.01. Error bars indicate standard error. REML was used to generate the LSD given in Table 11-2.

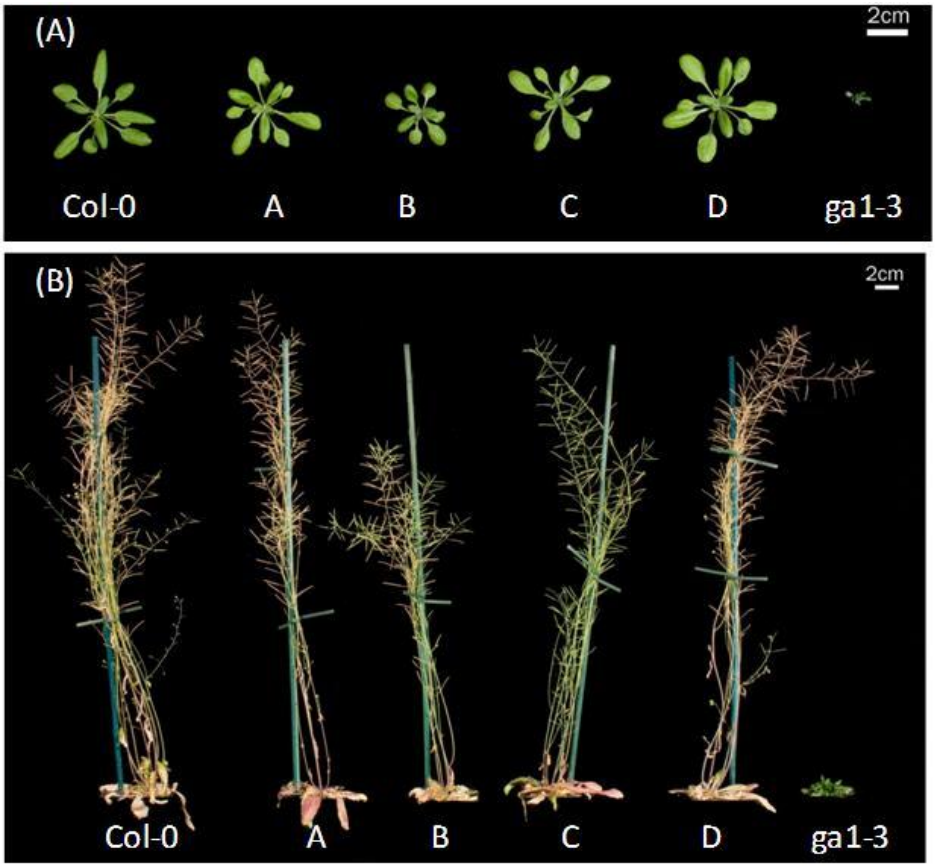

Figure 4-20: **Vegetative phenotypes for *Col-0;Co2::YFP:AtGA2ox2* lines (A-D) compared to *ga1-3* and Col-0.** Plants were grown on Levingtons compost in 5.5 cm pots under long days at three (A) and six weeks (B).

4.1.10 *Col-0;Co2::YFP:AtGA2ox2*: root length, meristem length, cell length and transgene expression profile.

All three *Col-0;Co2::YFP:AtGA2ox2* lines showed YFP fluorescence in the cortical cells of the meristematic region, as predicted (Figure 4-21). The primary root parameters for the three representative Col-0 lines expressing *YFP-AtGA2ox2* with the *Co2* promoter were compared with *ga1-3* and Col-0 (Figure 4-22). In agreement with the previous analysis (section 4.1.9), all three lines had greatly reduced root length as the result of significantly smaller meristems. The root lengths of all three lines were significantly shorter than Col-0 ($p<0.01$), and line C was also significantly shorter than *ga1-3* ($p<0.01$). This was not because of reduced cell length, which was not significantly different from that of Col-0 for all three lines ($p>0.05$). The reduced root length was due to reduced meristem lengths, such that they were not significant different from that in *ga1-3* ($p>0.05$).

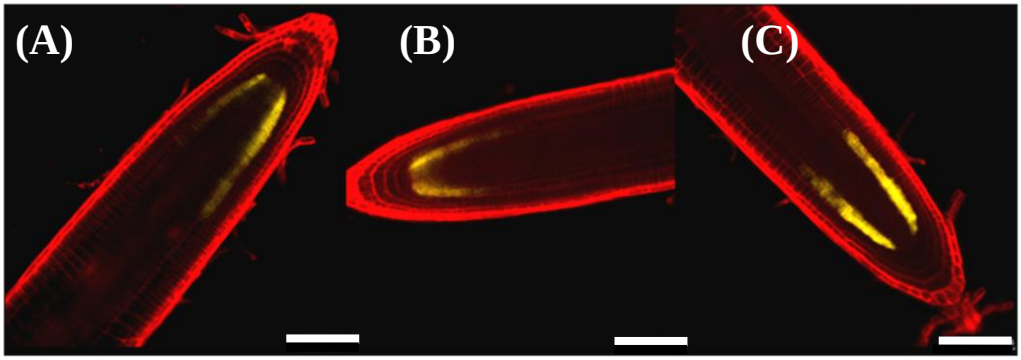

Figure 4-21: ***Col-0;Co2::YFP:AtGA2ox2* fluorescence in cortical cells of the meristematic region. (A-C)** Lines A, B and C, respectively**.** Confocal microscopy was performed on the five roots of seven day old seedlings after being grown on vertical Gelrite plates. The YFP and the propidium iodide emission images are overlaid. Bars are 100 μm in length.

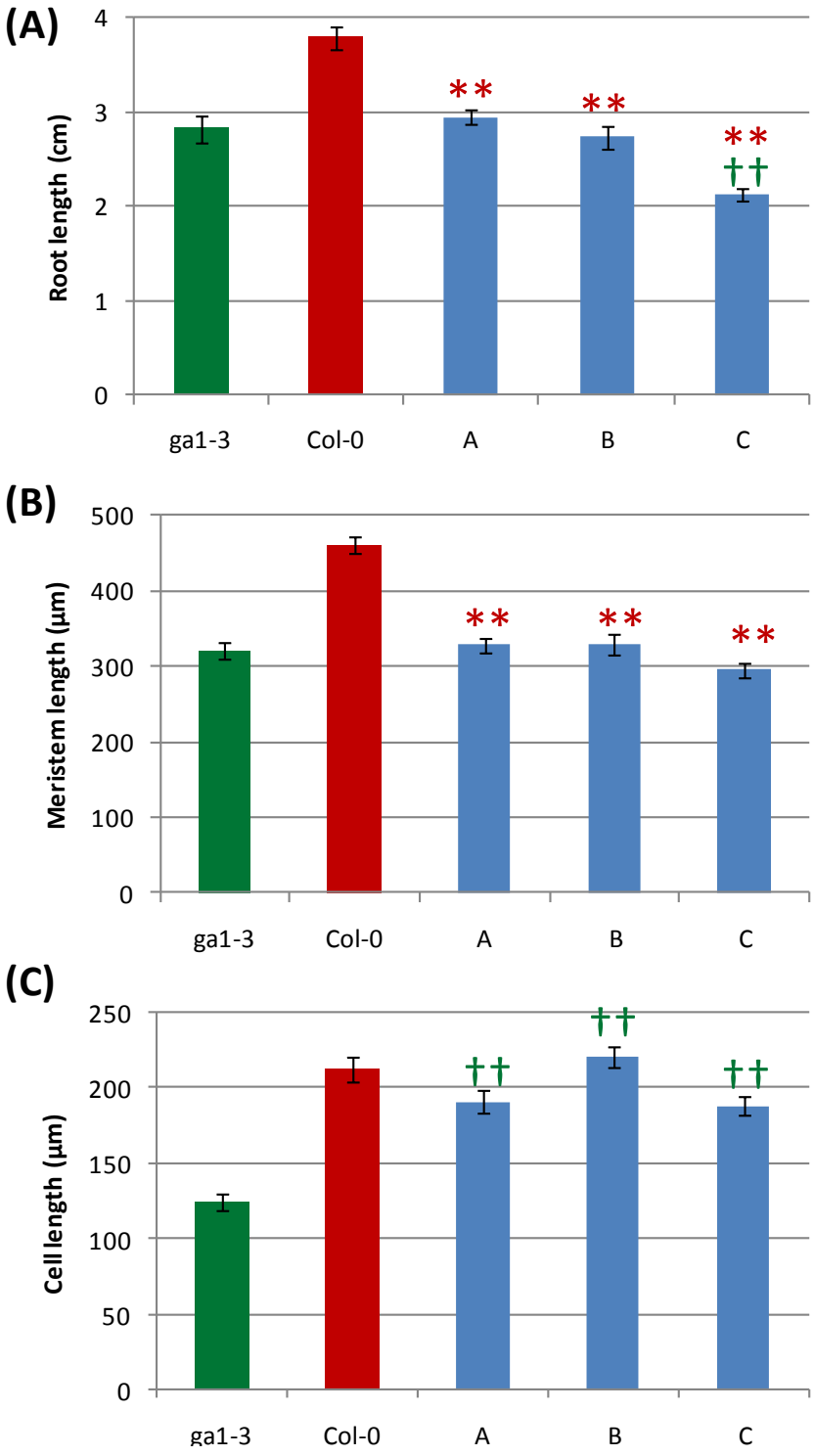

Figure 4-22**: Parameters for the primary root at 7 days in lines Col-0 A-C expressing *Co2::YFP:AtGA2ox2* compared with Col-0 and *ga1-3*. (A)** Primary root length ±SE. **(B)** Proximal meristem length ±SE. **(C)** Final cortical cell length ±SE. Seedlings were grown on vertical plates and lengths calculated using ImageJ. Green crucifixes indicate the transgenic lines are significantly different from *ga1-3* and the red asterisks indicate they are significantly different from the Col-0. 15 plants for each line were measured for root length, 5 plants had their meristems and 5 cells measured **=p<0.01 and ††=p<0.01. Standard errors used for error bars. REML was used to generate the LSD shown in Table 11-7.

4.1.11 *Col-0;GL2::YFP:AtGA2ox2* severely reduces root length and retards vegetative development

To investigate removing bioactive GA from the epidermis, the *GL2* promoter was used to drive expression of YFP-AtGA2ox2 in the atrichoblast non-hair forming cells of the root epidermis (Hung et al., 1998). Root lengths of lines expressing *Col-0;GL2::YFP:AtGA2ox2* were significantly different from Col-0 ($p<0.01$) and not significantly different from *ga1-3* ($p>0.05$) (Figure 4-24). Lines A, B and E, the root lengths for which were not significantly different ($p<0.01$), were selected for further analysis. Expression of *GL2::YFP:AtGA2ox2* produced mildly dwarfed rosette and inflorescence phenotypes that were consistent across all transgenic lines (Figure 4-24).

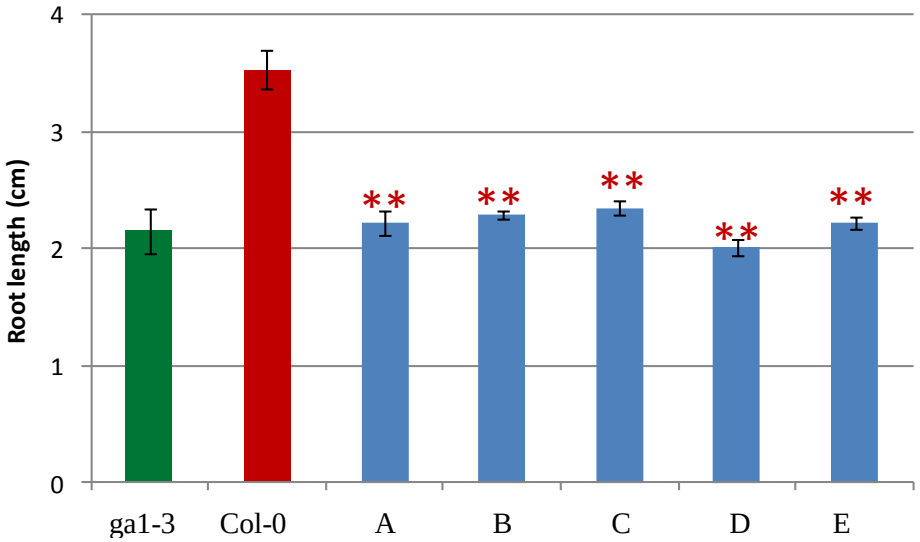

Figure 4-23**: Primary root length ±SE for *Col;GL2::YFP:AtGA2ox2* lines (A-E) compared to *ga1-3* and Col-0 at seven days.** Seedlings were grown on vertical plates and lengths calculated using ImageJ. The red asterisks indicate they are significantly different from the Col-0 control. 30 plants were analysed **= p<0.01. Error bars indicate standard error. REML was used to generate the LSD given in Table 11-2.

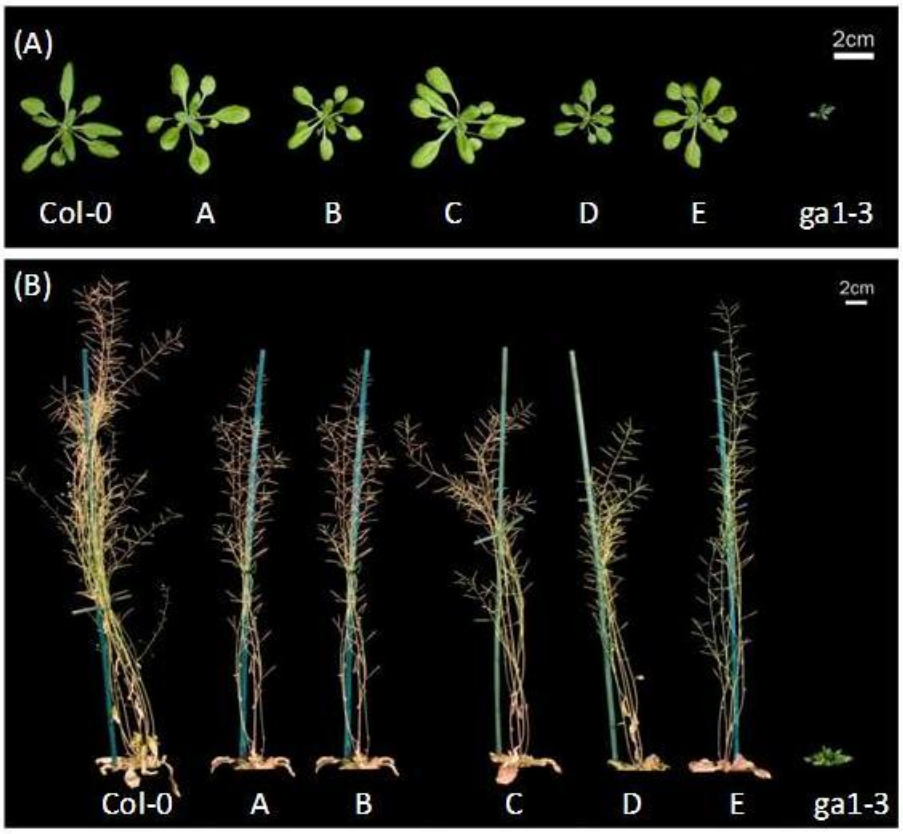

Figure 4-24: **Vegetative phenotypes of *Col-0;GL2::YFP:AtGA2ox2* lines (A-E) compared to *ga1-3* and Col-0.** Plants were grown on Levingtons compost in 5.5 cm pots under long days at three (A) and six weeks (B).

4.1.12 *Col-0;GL2::YFP:AtGA2ox2*: root length, meristem length, cell length and transgene expression profile.

In all three *GL2::YFP:AtGA2ox2* lines YFP fluorescence was detected within the epidermal atrichoblast cell in the meristematic region, elongation zone and, to a lesser extent, differentiation zone (Figure 4-25). The primary root parameters for the three representative Col-0 lines expressing YFP-AtGA2ox2 with the *GL2* promoter were compared with *ga1-3* and Col-0 (Figure 4-26). Col-0;*GL2::YFP:AtGA2ox2* expression resulted in reduced root growth which was consistent with the previous experiment (section 4.1.11). Interestingly, the main reason for this appeared to be a reduction in meristem size for all three transgenic lines, which were significantly different from both *ga1-3* and Col-0 ($p<0.01$, except meristem size in lines A and E for which $p<0.05$). However, the final cell lengths for each line were not significantly different from that of Col-0 ($p>0.05$). Thus, the reduced root length is predominantly due to the smaller meristem in these lines.

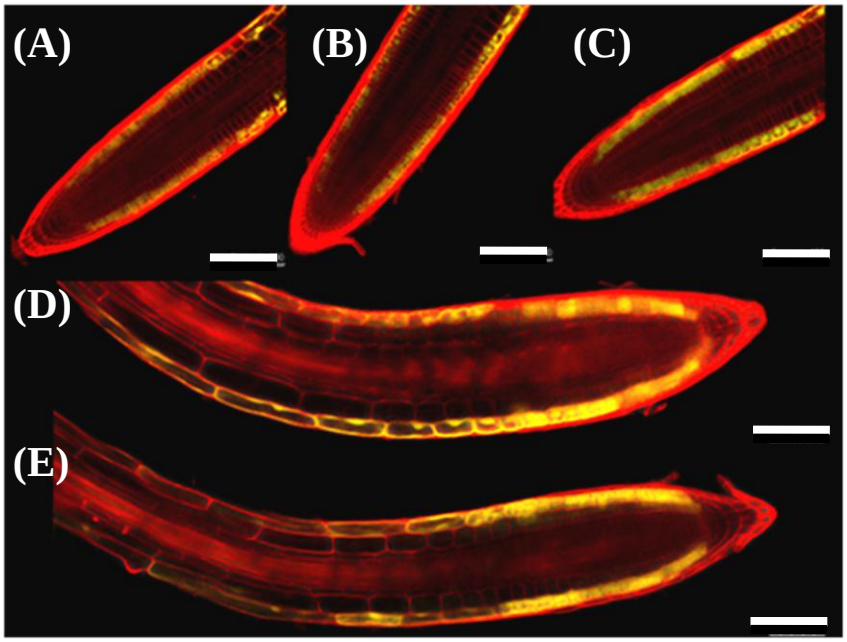

Figure 4-25: **YFP fluorescence in the epidermis of the *Col-0;GL2::YFP:AtGA2ox2* lines. (A-C)** Transgenic lines A, B and E, respectively. **(D-E)** Composite images from the QC to the elongation zone showing YFP fluorescence in epidermal cells. Confocal microscopy was performed on the five roots of seven day old seedlings after being grown on vertical Gelrite plates. The YFP and the propidium iodide emission images are overlain. Bars are 100 μm in length.

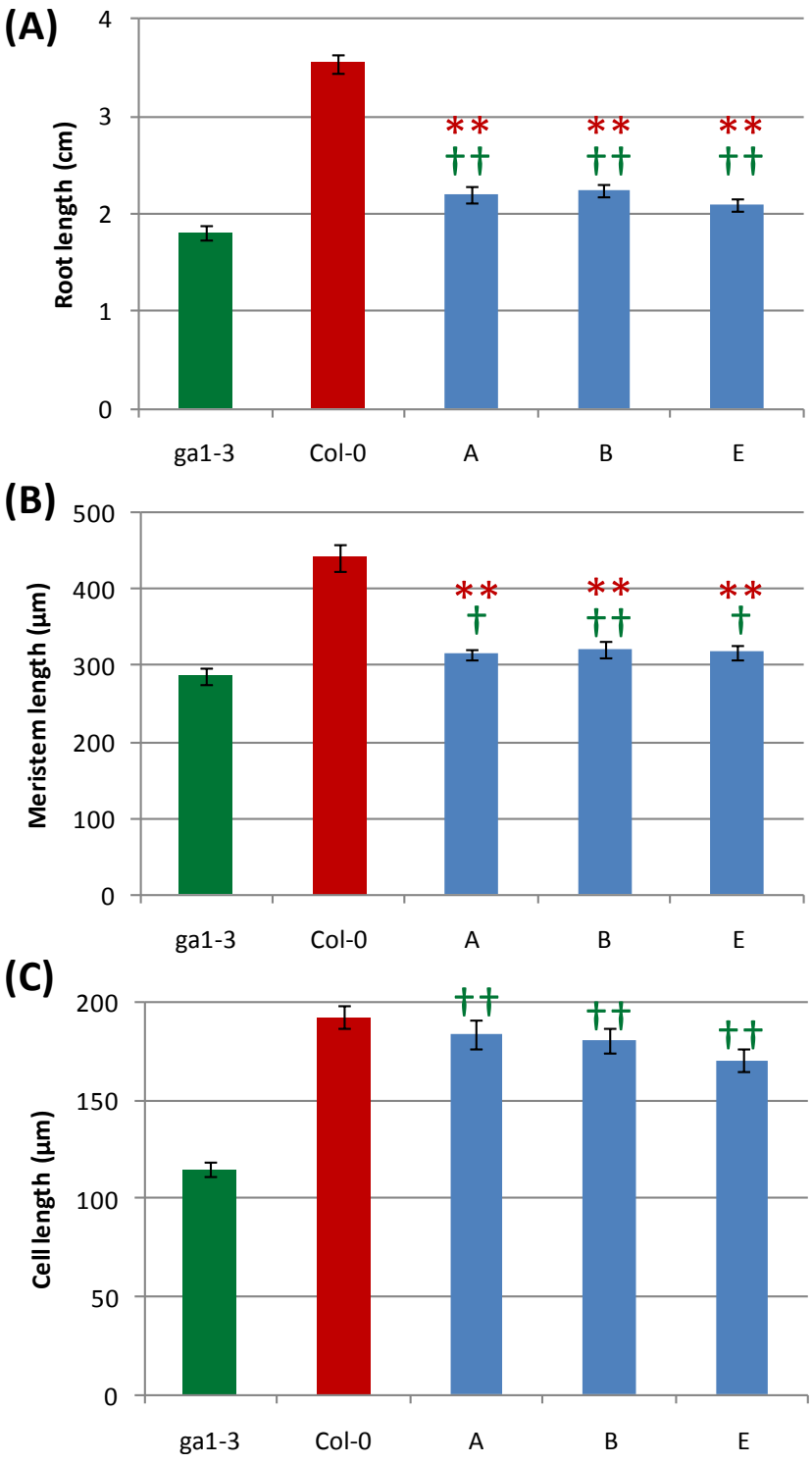

Figure 4-26**: Parameters for the primary root at 7 days in Col-0 lines A-E expressing *GL2::YFP:AtGA2ox2* compared with Col-0 and *ga1-3*. (A)** Primary root length ±SE. **(B)** Proximal meristem length ±SE. **(C)** Final cortical cell length ±SE. REML was used to generate the LSD. Seedlings were grown on vertical plates and lengths calculated using ImageJ. Green crucifixes indicate the transgenic lines are significantly different from *ga1-3* and the red asterisks indicate they are significantly different from the Col-0. 15 plants were measured for root length, 5 plants had their meristems and 5 cell lengths measured **=p<0.01, †=p<0.05 and ††=p<0.01. Error bars indicate standard error. The LSD are given in Table 11-7.

4.1.13 *Col-0;CAB::YFP:AtGA2ox2* does not affect root length and severely retards vegetative development

To investigate whether removing bioactive GA from photosynthetic tissues is capable of affecting root growth, YFP-AtGA2ox2 was driven using the *CAB* promoter (Yadav et al., 2002). Root lengths of Col-0 lines expressing *CAB::YFP:AtGA2ox2* compared with Col-0 and *ga1-3* are shown in Figure 4-27. The targeted expression of YFP-AtGA2ox2 with the *CAB* promoter produced extremely dwarfed shoots, although less so than in the *ga1-3* mutant (Figure 4-28). The primary root lengths for all lines were significantly longer from that of *ga1-3* ($p<0.01$) and not significantly different from that of Col-0 ($p>0.05$). Root lengths in lines A, B and C were not significantly different from each other ($p<0.01$) despite differences in their vegetative phenotypes, so that these lines were selected for further analysis.

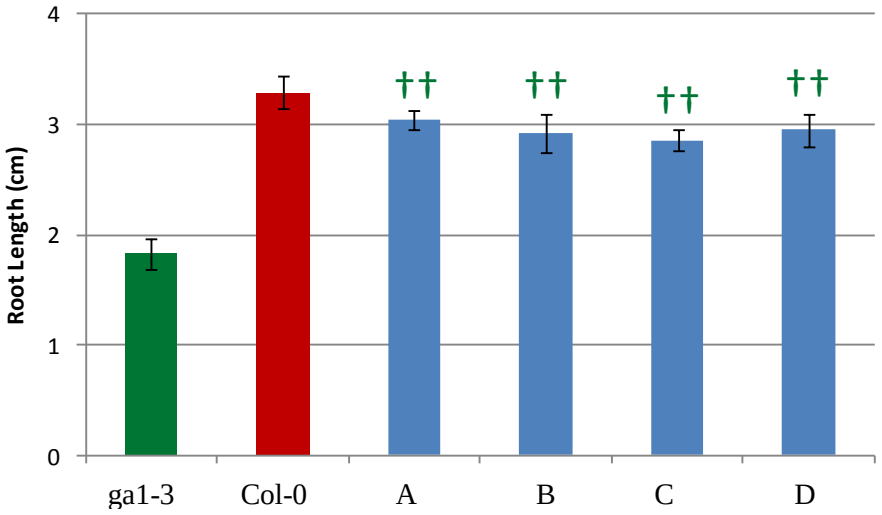

Figure 4-27**: Primary root length ±SE for *Col-0;CAB::YFP:AtGA2ox2* lines (A-D) compared to *ga1-3* and Col-0 at seven days.** Seedlings were grown on vertical plates and lengths calculated using ImageJ. Green crucifixes indicate the transgenic lines are significantly different from *ga1-3* control. 30 plants were analysed ††=p<0.01. Error bars indicate standard error. The LSD are given in Table 11-2.

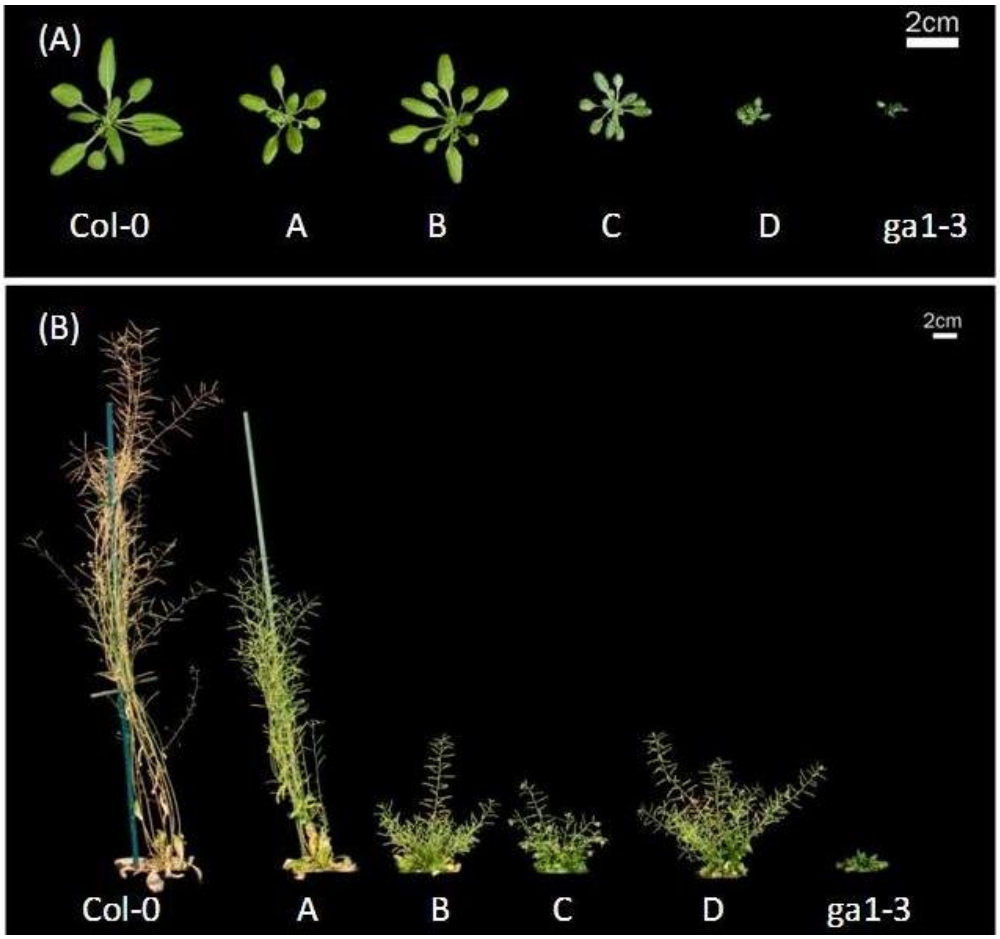

Figure 4-28: **Vegetative phenotypes shown for Col-0;*CAB::YFP:AtGA2ox2* lines (A-D) compared to *ga1-3* and Col-0.** Plants were grown on Levingtons compost in 5.5 cm pots under long days at three (A) and six weeks (B).

4.1.14 *Col-0;CAB::YFP:AtGA2ox2*: root length, meristem length, cell length and transgene expression profile.

The primary root parameters for the three representative Col-0 lines expressing YFP-AtGA2ox2 with the *CAB* promoter were compared with *ga1-3* and Col-0 (Figure 4-29). Col-0*;CAB::YFP:AtGA2ox2* expression resulted in slightly stunted root growth in one of the lines, line A, which had significantly shorter roots than those of Col-0 ($p>0.01$). However, consistent with the previous characterisation (section 4.1.13), the roots of the other lines were not significantly shorter from those of Col-0 ($p<0.05$), and all lines had significantly longer roots than *ga1-3* ($p>0.01$). The cell and meristem lengths for roots of all three lines were not significantly different from those in Col-0 ($p<0.05$).

Confocal microscope cross sections showed all three Col-0*;CAB::YFP:AtGA2ox2* lines had YFP fluorescence within young green vegetative shoot tissue (Figure 4-30). YFP was clearly visible in the first true leaves emerging at the base of the cotyledons, but none could be observed within the cotyledons, hypocotyl or roots. Auto-fluorescence could also easily be observed in the seed testa (Figure 4-30-C).

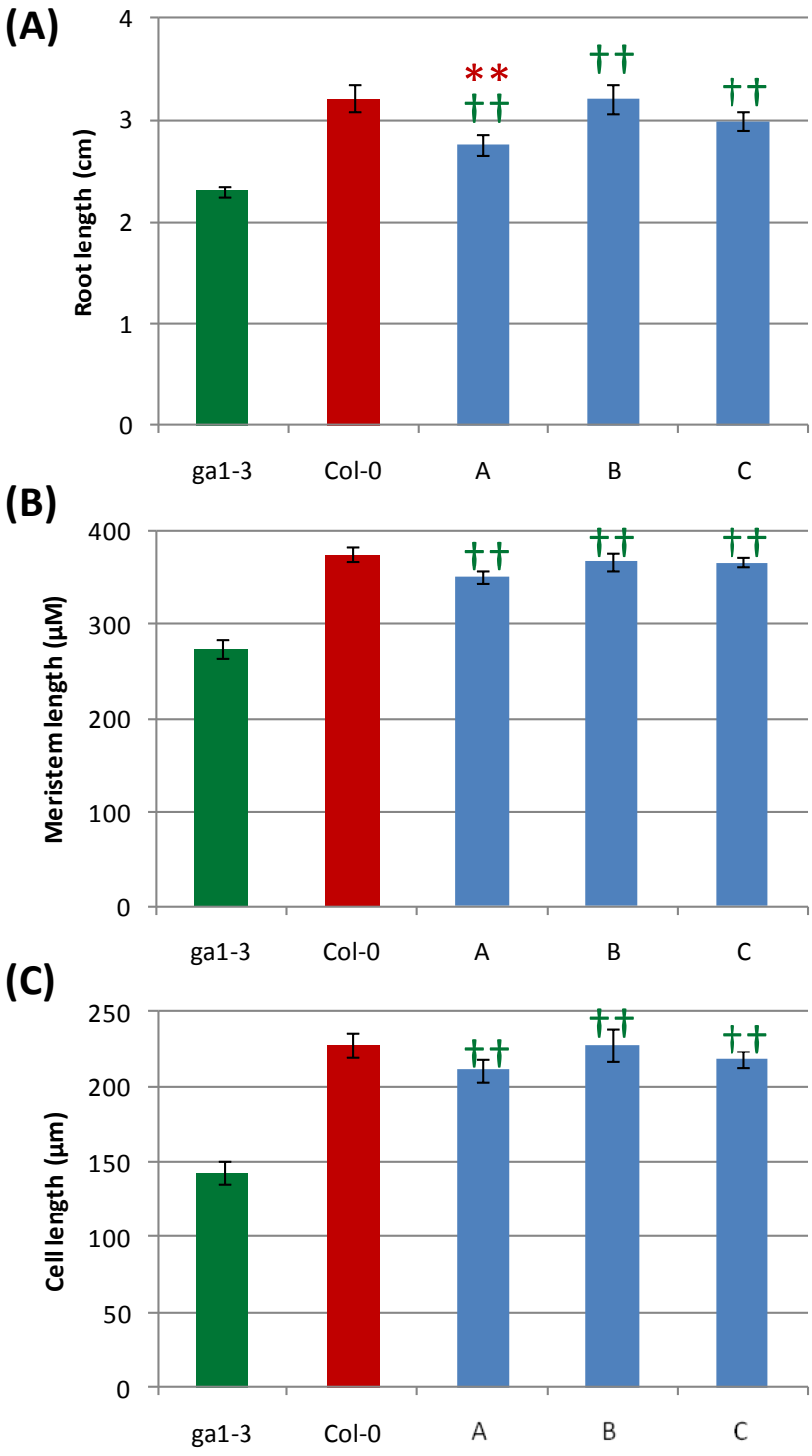

Figure 4-29**: Parameters for the primary root at 7 days in Col-0 lines A-C expressing *CAB::YFP:AtGA2ox2* compared with Col-0 and *ga1-3*. (A)** Primary root length ±SE. **(B)** Proximal meristem length ±SE. **(C)** Final cortical cell length ±SE. Seedlings were grown on vertical plates and lengths calculated using ImageJ. Green crucifixes indicate the transgenic lines are significantly different from *ga1-3* and the red asterisks indicate they are significantly different from the Col-0. 15 plants were measured for root length, 5 plants had their meristems and 5 cells measured **=p<0.01, and ††=p<0.01. The LSD used to generate standard errors used for error bars are shown in Table 11-7.

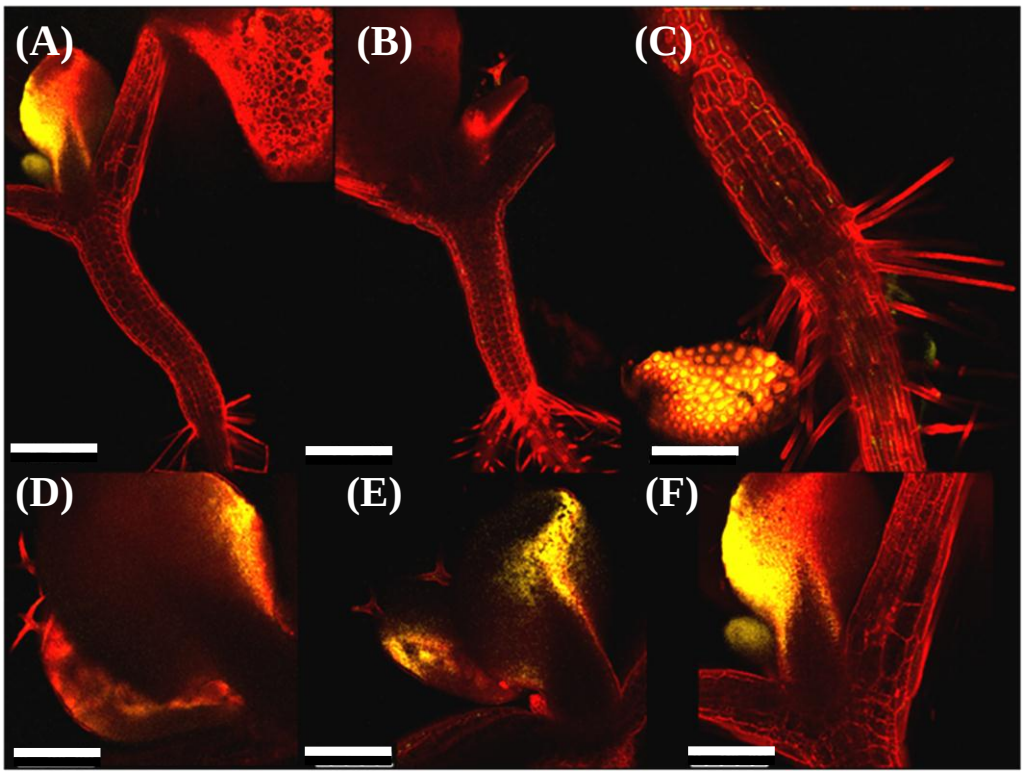

Figure 4-30: ***Col-0;CAB::YFP:AtGA2ox2*** **expression in the young vegetative tissue compared with auto-fluorescence in Col-0 and *ga1-3* lines. (A-C)** Transgenic line A, Col-0 and *ga1-3* respectively. **(D-F)** Fluorescence in the young vegetative tissue for lines A, B and C, respectively. Confocal microscopy was performed on the five roots of seven day old seedlings after being grown on vertical Gelrite plates. The YFP and the propidium iodide emission images are overlaid. Bars in (A-B) are 100 μm and bars in (C-F) are 50 μm in length.

4.1.15 Comparison of each promoter driving the expression of *YFP:AtGA2ox2* on the primary root, meristem and final cell length.

The median lines values for the primary root parameters for each *promoter::YFP-AtGA2ox2* are compared with *ga1-3* and Col-0 in Figure 4-43. Expression of YFP-AtGA2ox2 from the *SCR* promoter had the greatest effect on root length, producing a meristem that was not significantly different from that in the dwarf *ga1-3*, although final cell length was significantly larger than in *ga1-3*, but smaller than in Col-0 ($p>0.05$). Expression from *Co2* and *GL2* lines produced roots of very similar lengths ($p<0.01$) that, although less dwarfed than in the *Col-0;SCR::YFP:AtGA2ox2* line, are significantly shorter than in Col-0 ($p>0.01$). This was due to reduced meristem size as both lines had final cells lengths that were not significantly different from those in Col-0 ($p>0.05$). In contrast, reduced root length in the *Col-0;CoR::YFP:AtGA2ox2* was due to its reduced final cell length, which was not significantly different from that in *ga1-3* ($p>0.05$), while its meristem length was not significantly reduced ($p>0.05$). Although the root length of the *Col-0;SHR::YFP:AtGA2ox2* line was significantly different from that of both Col-0 (<0.01) and *ga1-3* (<0.05), neither final cell nor meristem lengths were significantly different from Col-0 ($p>0.05$). The *CAB* promoter driving YFP-AtGA2ox2 had no significant effect on root, meristem or final cell lengths. Figure 4-32 shows representative images for the root tip for the *SHR*, *SCR*, *CoR*, *Co2* and *GL2* YFP:AtGA2ox2 lines, as no fluorescence was observed at the root tip for the *CAB* lines photosynthetic tissue near the SAM is shown.

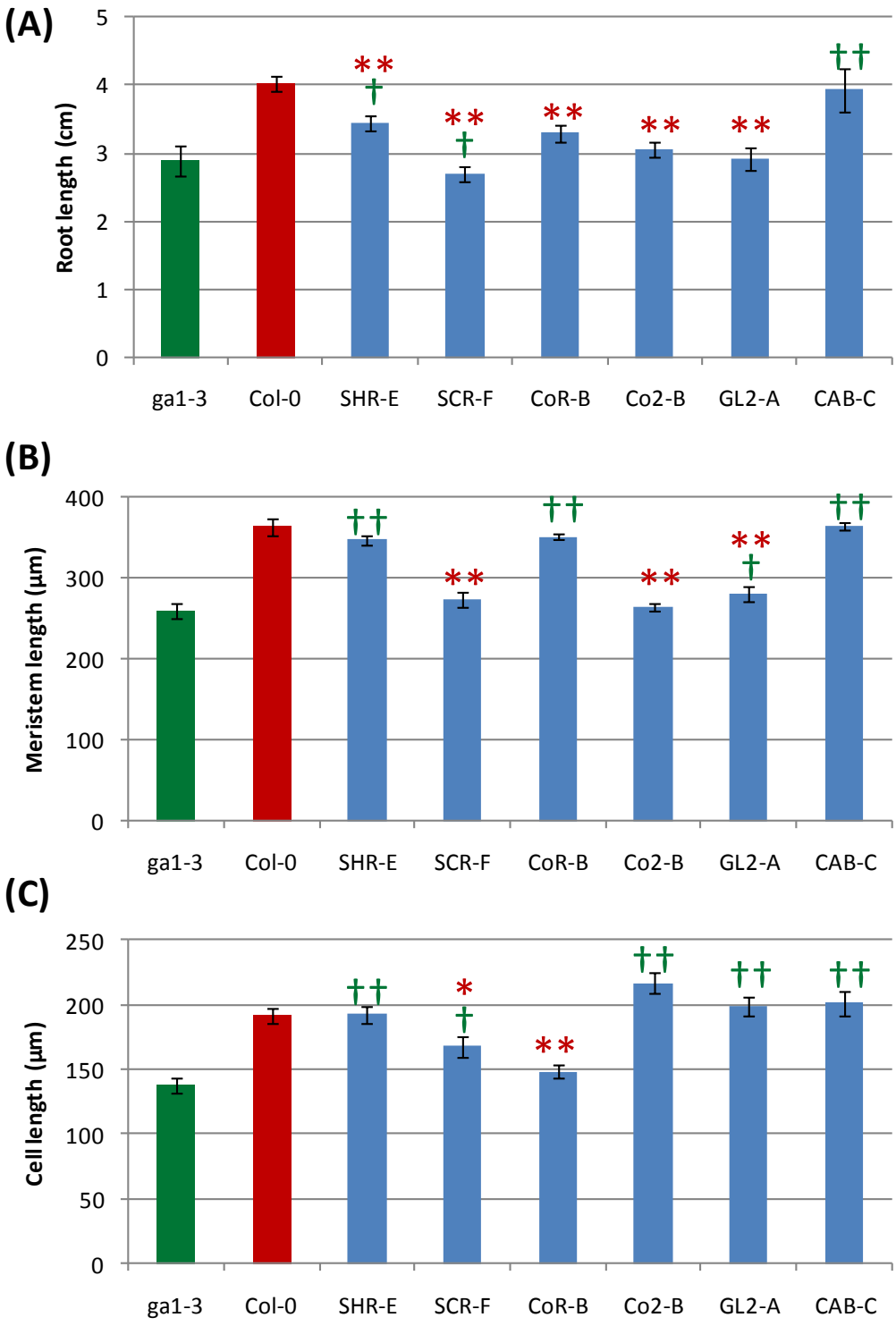

Figure 4-31**: Comparison of the primary root parameters for median lines for each *YFP:AtGA2ox2* construct with Col-0 and *ga1-3* at seven days. (A)** Primary root length ±SE. **(B)** Proximal meristem length ±SE. **(C)** Final cortical cell length ±SE. Seedlings were grown on vertical plates and lengths calculated using ImageJ. Green crucifixes indicate the transgenic lines are significantly different from *ga1-3* and the red asterisks indicate they are significantly different from the Col-0. 15 plants were measured for root length, 5 plants had their meristems and 5 cells measured *=p<0.05, **=p<0.01, †=p<0.05 and ††=p<0.01. Error bars indicate standard error. The LSD are given in Table 11-11.

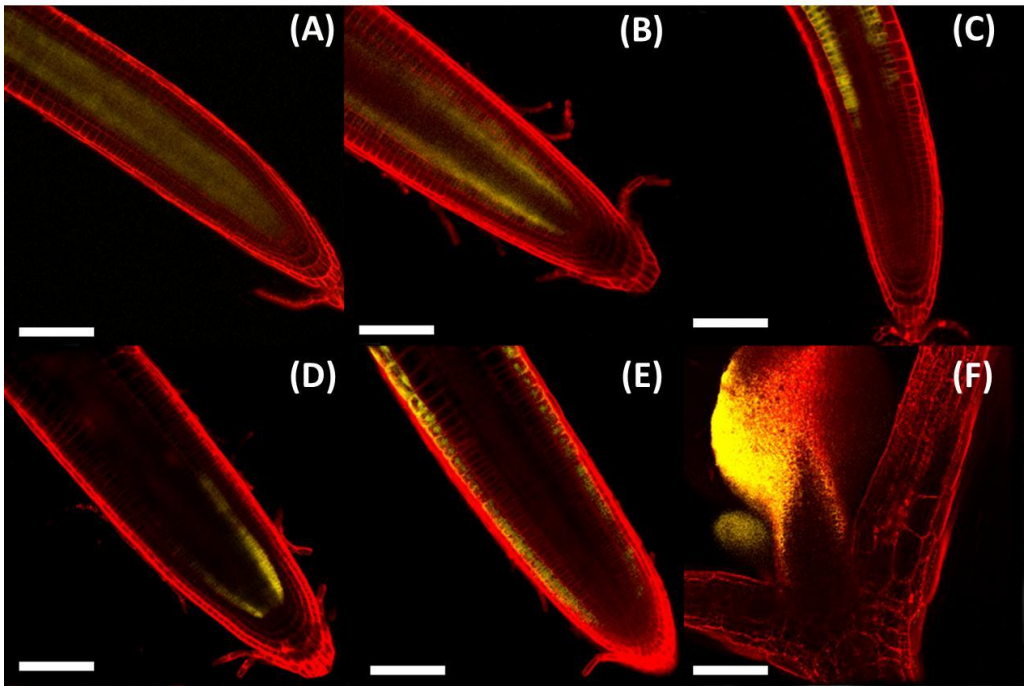

Figure 4-32: **Representative images for YFP fluorescence in the GA2ox2 lines. (A-F)** YFP-AtGA2ox2 attached to *SHR, SCR, CoR, Co2, GL2* and *CAB* promoters, respectively. Confocal microscopy was performed on seven day-old seedlings grown on vertical Gelrite plates. The YFP and the propidium iodide emission images are overlain. Bars are 100 μm in length.

In summary (Figure 4-33), *YFP-AtGA2ox2* expression was expected to stunt root growth by inactivating C_{19}-GAs and either reduce meristem size or final cell size at important sites of GA biosynthesis and/or signalling. Ectopic expression of AtGA2ox2 was able to completely stunt all aspects of root growth when expressed in the endodermis. *YFP-AtGA2ox2* expression in the epidermal or cortical cells of the meristematic region reduced meristem length. Interestingly expression in the epidermal cells did not reduce cell elongation while in contrast expression in the ground tissue did. The *SHR::YFP:AtGA2ox2* lines were inconsistent but suggest that the stele is not an important site of C20-GA biosynthesis or movement.

Figure 4-33: **Schematic diagram highlighting which tissues YFP-AtGA2ox2 was able to retard growth within.** The yellow lateral root cap and columella cells were not studied during this project. The torques meristematic endodermal, cortical and epidermal cells are sites of C_{19}-GA biosynthesis and/or perception required for cell division. The white ground tissue cells in the elongation zone are sites of C_{19}-GA biosynthesis and/or perception required for cellular elongation. The blue epidermal cells in the elongation zone are not important sites of C_{19}-GA biosynthesis and/or perception required for cellular elongation. The green vasculature cells are not sites of C_{19}-GA biosynthesis and/or perception required for either cell elongation or cell division.

4.2 TRANSGENIC LINES WITH TISSUE-SPECIFIC EXPRESSION OF YFP-ATGA2OX7

4.2.1 Characterisation of *AtGA2ox7* targeted expression lines

The effect of targeting the expression of YFP-AtGA2ox7 with tissue specific promoters on the phenotype of wild-type Col-0 plants was characterised. The characterisation initially measured the final root length after seven days growth and assessed the vegetative growth of the rosette after three weeks growth and the floral growth after six weeks growth. Three independently transformed lines were then selected for further analysis of root growth, involving measuring their root lengths, meristem lengths, and final cell sizes were all measured. Throughout all experiments the transgenic lines were compared to *ga1-3* and Col-0.

4.2.2 *Col-0;SHR::YFP:GA2ox7* does not affect root length but retards vegetative development

To investigate whether removing GA precursors from the stele of the RAM and elongation zone would have an effect on root growth, YFP-AtGA2ox7 expression was driven from the *SHR* promoter (Di Laurenzio et al., 1996). Root lengths of *Col-0* lines expressing *SHR::YFP:AtGA2ox7* compared with Col-0 and *ga1-3* are shown in Figure 4-34. The primary root length of all the lines were not significantly different from Col-0 ($p>0.05$), except for line E, which was significantly shorter from Col-0 ($p<0.05$). The lines displayed a variety of vegetative phenotypes that ranged from the severe dwarf of line D that was comparable to *ga1-3*, to the intermediate dwarfs such as line A (Figure 4-35). The root lengths of lines A and D were not significantly different from E ($p<0.05$) and as they also displayed a range of aerial phenotypes they were selected for further analysis.

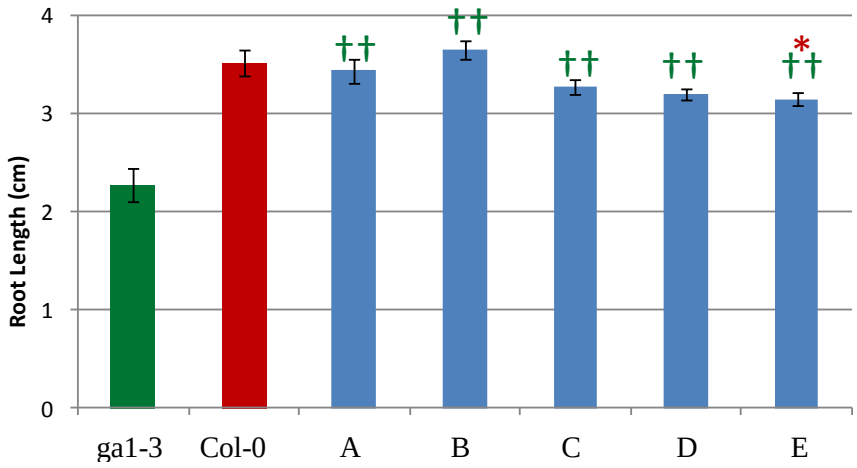

Figure 4-34**: Primary root length ±SE for *Col-0;SHR::YFP:AtGA2ox7* lines (A-E) compared to *ga1-3* and Col-0 at seven days.** Seedlings were grown on vertical plates and lengths calculated using ImageJ. Green crucifixes indicate the transgenic lines are significantly different from *ga1-3* and the red asterisks indicate they are significantly different from the Col-0. 30 plants were analysed *=p<0.05, and ††=p<0.01. Error bars indicate standard error. The LSD are given in Table 11-3.

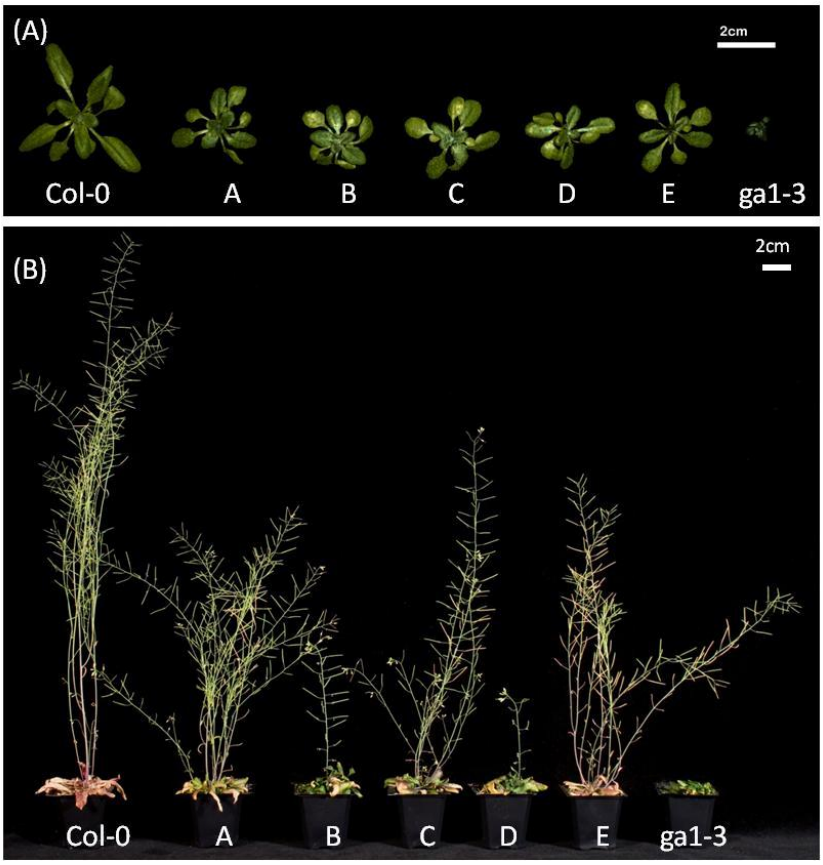

Figure 4-35: **Vegetative phenotypes shown for *Col-0;SHR::YFP:AtGA2ox7* lines (A-E) compared to *ga1-3* and Col-0.** Plants were grown on Levingtons compost in 5.5 cm pots under long days at three (A) and six weeks (B).

4.2.3 Col-0;*SHR::YFP:AtGA2ox7*: root length, meristem length, cell length and transgene expression profile.

The primary root parameters for the three representative Col-0 lines expressing *YFP-AtGA2ox7* with the *SHR* promoter were compared with *ga1-3* and Col-0 (Figure 4-35). The results agreed with the previous characterisation (section 4.2.2), except that root length for line D was significantly shorter than it was in the previous experiment. *Col-0;SHR::YFP:AtGA2ox7* expression was able to significantly affect the root growth of lines D and E ($p<0.01$), but not of line A. The meristem and final cell lengths of all three lines were not significantly different from Col-0 ($p>0.05$).

In all three *Col-0;SHR::YFP:AtGA2ox7* lines YFP fluorescence was present within pericycle and vasculature of the meristematic region at a low level and in the endodermis of the differentiation zone at a relatively high level (Figure 4-36). In addition, when plants were sown on plates containing 1 µM GA_3, fluorescence *SHR::YFP:AtGA2ox7* within the vasculature and pericycle was similar to that in plants grown on control Gelrite, but when grown on Gelrite containing 1 µM PAC no *SHR::YFP:AtGA2ox7* expression could be observed (Figure 4-37).

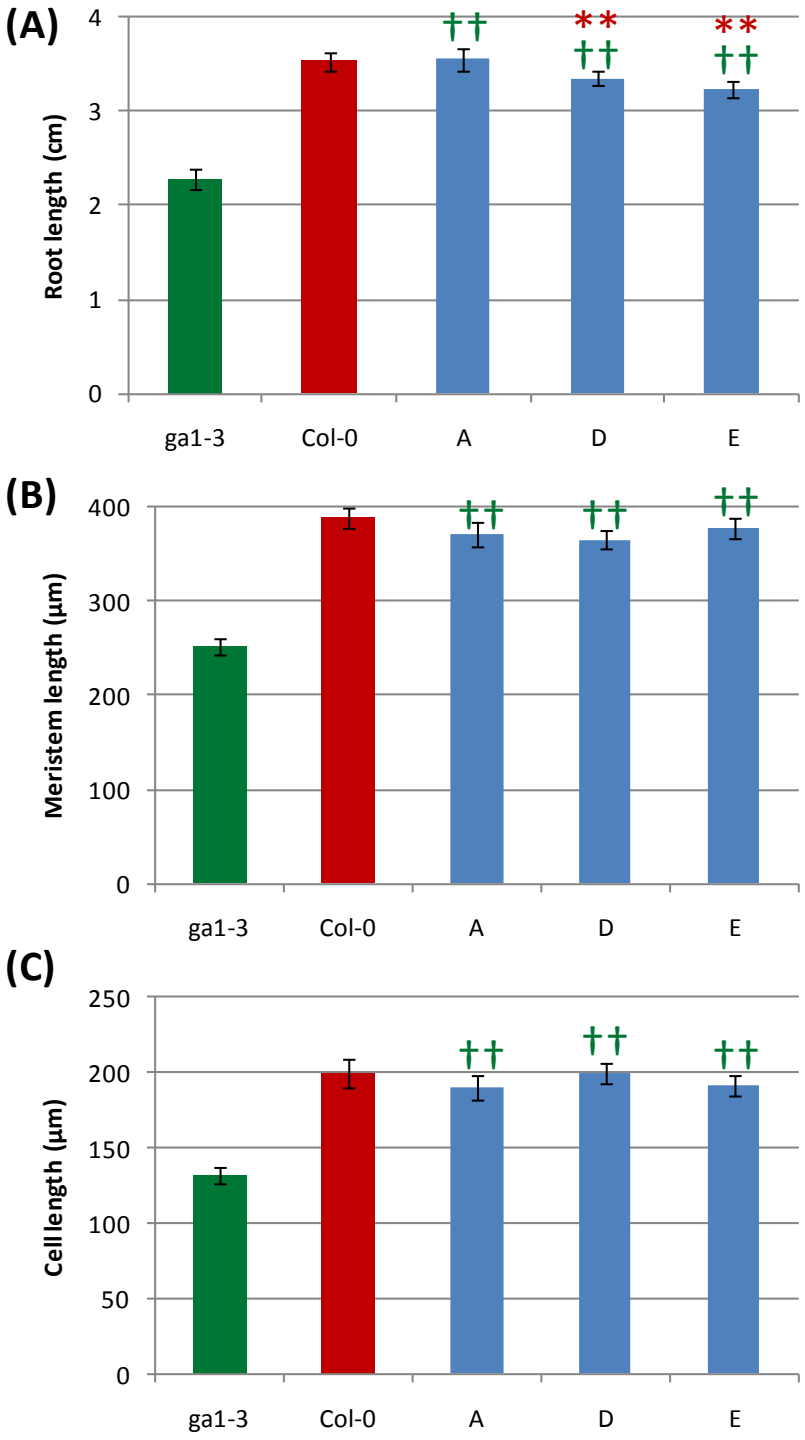

Figure 4-36**: Parameters for the primary root at 7 days in Col-0 lines A, D and E expressing *SHR::YFP:AtGA2ox7* compared with Col-0 and *ga1-3*.** **(A)** Primary root length ±SE. **(B)** Proximal meristem length ±SE. **(C)** Final cortical cell length ±SE. Seedlings were grown on vertical plates and lengths calculated using ImageJ. Green crucifixes indicate the transgenic lines are significantly different from *ga1-3* and the red asterisks indicate they are significantly different from the Col-0. 15 plants were measured for root length, 5 plants were measured for meristem and cell length **=p<0.01, and ††=p<0.01. Error bars indicate standard error. The LSD are given in Table 11-8.

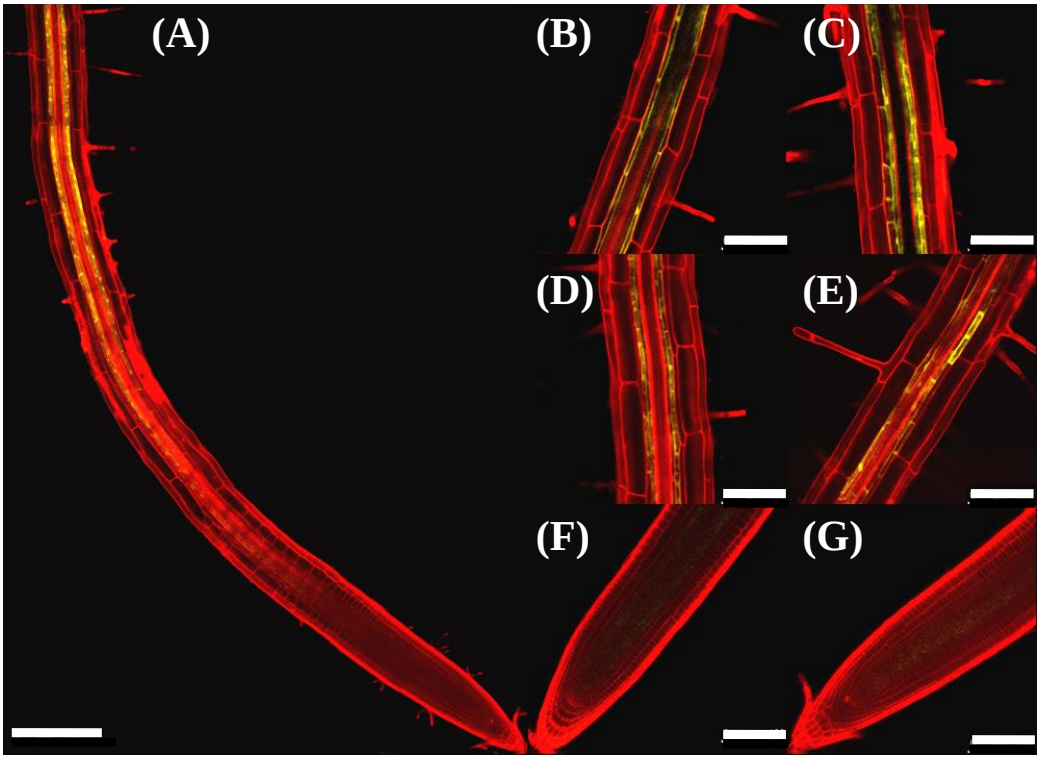

Figure 4-37: **YFP fluorescence in the root of *Col-0;SHR::YFP:AtGA2ox7* lines. (A)** Composite images showing fluorescence for line B. **(B-C)** line D expression within the differentiation zone, **(D-E)** line E fluorescence within the differentiation zone. **(F-G)** fluorescence within the meristematic region for line D and E. Confocal microscopy was performed on the five roots of seven day old seedlings after being grown on vertical Gelrite plates. The YFP and the propidium iodide emission images are overlain. The bar in 100 μm in length.

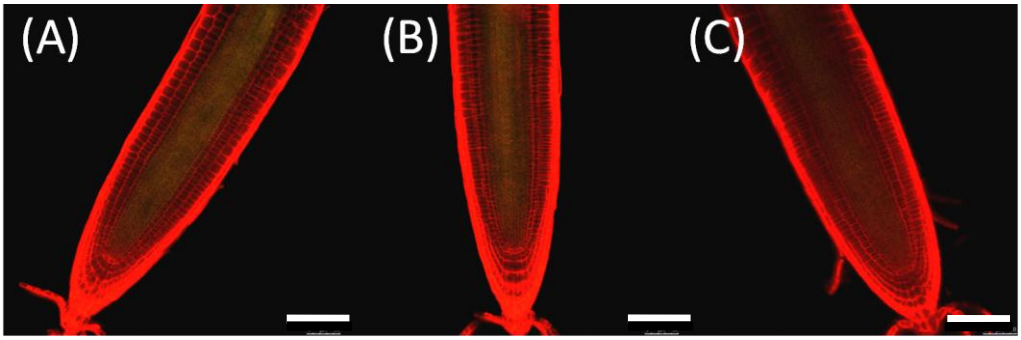

Figure 4-38: **YFP fluorescence in the meristematic region of *Col-0;SHR::YFP:AtGA2ox7* line D in response to GA and PAC treatment. (A)** YFP expression in the meristematic region is shown for plants grown on Gelrite containing 1 μM GA_3, **(B)** when grown on Gelrite, **(C)** when grown on Gelrite containing 1 μM PAC. Confocal microscopy was performed on the five roots of seven day old seedlings after being grown on vertical Gelrite plates. The YFP and the propidium iodide emission images are overlain. Bars are 100 μm in length.

4.2.4 *Col-0;SCR::YFP:AtGA2ox7* mildly reduces root length and severely retards leaf expansion and stem elongation

To investigate whether removing GA precursors from the endodermal cells of the RAM and elongation zone would have an effect on root growth *YFP-AtGA2ox7* expression was driven from the *SCR* promoter (Di Laurenzio et al., 1996). Root lengths of *Col-0* lines expressing *SCR::YFP:AtGA2ox7* compared with Col-0 and *ga1-3* are shown in Figure 4-39. The targeted expression of *YFP-AtGA2ox7* with the *SCR* promoter produced extremely dwarfed vegetative phenotypes (Figure 4-40). The root lengths of lines A, B, C and E were significantly different from both *ga1-3* and Col-0 ($p<0.01$ (except E compared to Col-0 where $p<0.05$)). The root length of line D was significantly different from Col-0 ($p>0.01$) and not from *ga1-3* ($p>0.05$). As the root lengths of lines A and D were not significantly different from E ($p<0.01$) and as they displayed the most variation amongst relatively consistent lines in both root and vegetative phenotypes they were chosen for further analysis.

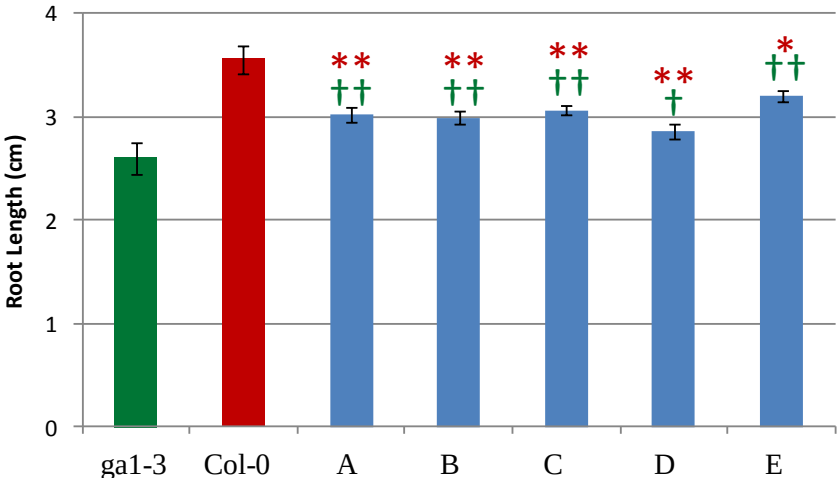

Figure 4-39**: Primary root length ±SE for *Col-0;SCR::YFP:AtGA2ox7* lines (A-E) compared to *ga1-3* and Col-0 at seven days.** Seedlings were grown on vertical plates and lengths calculated using ImageJ. Green crucifixes indicate the transgenic lines are significantly different from *ga1-3* and the red asterisks indicate they are significantly different from Col-0. 30 plants for each line were analyzed *=p<0.05, **=p<0.01, †=p<0.05 and ††=p<0.01. Error bars indicate standard error. The LSD are given in Table 11-3.

Figure 4-40: **Vegetative phenotypes shown for Col-0;*SCR::YFP:AtGA2ox7* lines (A-E) compared to *ga1-3* and Col-0.** Plants were grown on Levingtons compost in 5.5 cm pots under long days at three (A) and six weeks (B).

4.2.5 *Col-0;SCR::YFP:AtGA2ox7*: root length, meristem length, cell length and transgene expression profile.

The primary root parameters for the three representative Col-0 lines expressing *YFP-AtGA2ox7* from the *SCR* promoter were compared with *ga1-3* and Col-0 (Figure 4-41). As in the previous experiment (section 4.2.4), *SCR::YFP:AtGA2ox7* expression in *Col-0* retarded root growth in all three transgenic lines analysed; The root lengths, meristem lengths and final cell lengths of all three lines were significantly different from *ga1-3* ($p<0.01$), although meristem lengths were significantly different also from Col-0 ($p<0.05$). Only line A had a final cell length that was significantly different from Col-0 ($p<0.05$).

YFP fluorescence could be observed for all three *Col-0;SCR::YFP:AtGA2ox7* lines within the endodermis and to a lesser extent cortical cells of the meristematic region (Figure 4-42). Within the differentiation region expression was localised to the endodermis and the pericycle cell. When plants were sown on plates containing 1 µM GA_3, fluorescence in the meristematic region increased and could be observed within cortex, vasculature and pericycle, although it was strongest in the endodermis. During the same experiment YFP fluorescence in lines grown on Gelrite without treatment was visible in the endodermis and to a lower extent the cortex, and in plants grown on Gelrite containing 1 µM PAC, no fluorescence could be observed (Figure 4-43).

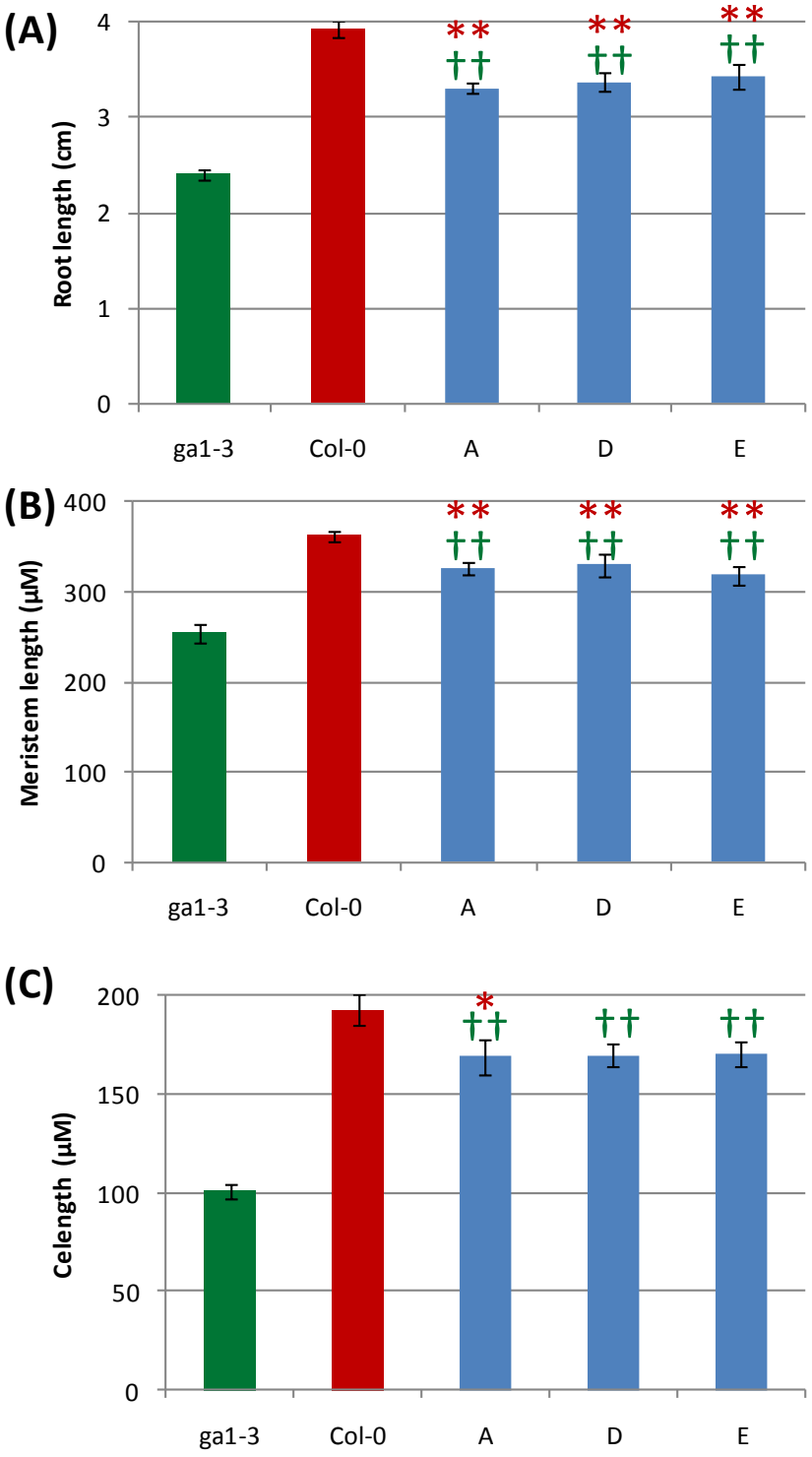

Figure 4-41**: Parameters for the primary root at 7 days in Col-0 lines A, D and E expressing *SCR::YFP:AtGA2ox7* compared with Col-0 and *ga1-3*. (A)** Primary root length ±SE. **(B)** Proximal meristem length ±SE. **(C)** Final cortical cell length ±SE. Seedlings were grown on vertical plates and lengths calculated using ImageJ. Green crucifixes indicate the transgenic lines are significantly different from *ga1-3* and the red asterisks indicate that they are significantly different from Col-0. 15 plants for each line were measured for root length, 5 plants for meristem and cell length, for which 5 cells were measured *= p<0.05, **= p<0.01, and ††=p<0.01. Error bars indicate standard error. The LSD are given in Table 11-8.

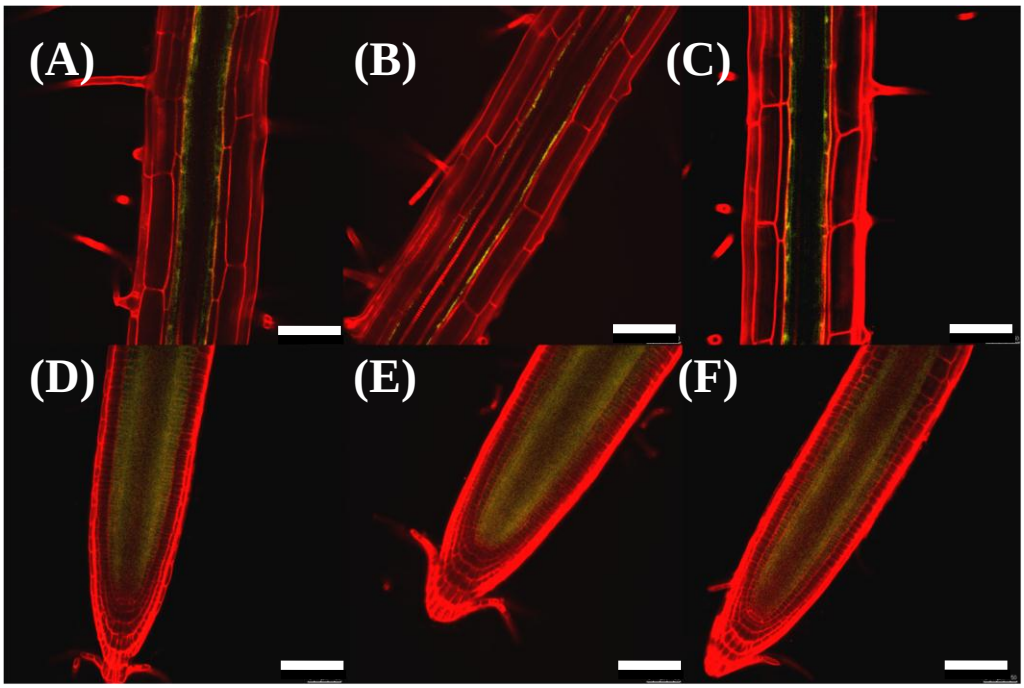

Figure 4-42: **YFP fluorescence in the meristematic and elongation zones of *SCR::YFP:AtGA2ox7* lines. (A-C)** Differentiation zones of lines A, D and E respectively. **(D-F)** Meristematic region for lines A, D and E respectively. Confocal microscopy was performed on the five roots of seven day old seedlings after being grown on vertical Gelrite plates. The YFP and the propidium iodide emission images are overlaid. Bars are 100 μm in length.

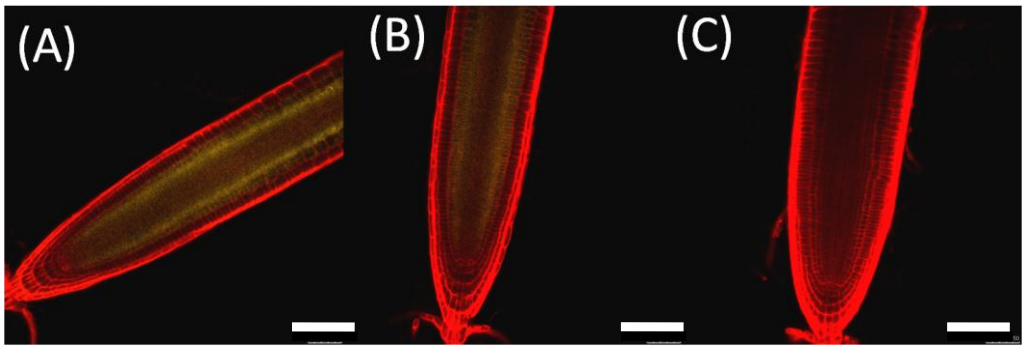

Figure 4-43: **YFP fluorescence in the meristematic zones of *Col-0;SCR::YFP:AtGA2ox7* lines treated with GA and PAC. (A)** *SCR::YFP:AtGA2ox7* line D grown on Gelrite containing 1 μM GA_3. **(B)** Grown on Gelrite. **(C)** Grown on Gelrite containing 1 μM PAC. Confocal microscopy was performed on the five roots of seven day old seedlings after being grown on vertical Gelrite plates. The YFP and the propidium iodide emission images are overlain. Bars are 100 μm in length.

4.2.6 *Col-0;CoR::YFP:AtGA2ox7* severely reduces root length and vegetative development

The effect of inactivating C_{20}-GA precursors in the ground tissue of the elongation zone was investigated by expressing *YFP-AtGA2ox7* under the *CoR* promoter (Dinneny et al., 2008). Six lines were generated and their root lengths are compared with those of Col-0 and *ga1-3* in Figure 4-44. The root length of all the lines A-F were significantly different from Col-0 ($p<0.01$) and were not significantly different from *ga1-3* ($p>0.05$). Lines C and D were not significantly different from line F ($p<0.01$) and were chosen for further analysis as they displayed the most variation amongst relatively consistent lines. All six lines generated had severely dwarfed rosettes that were similar to *ga1-3* and only lines B and D produced dwarf inflorescences (Figure 4-45).

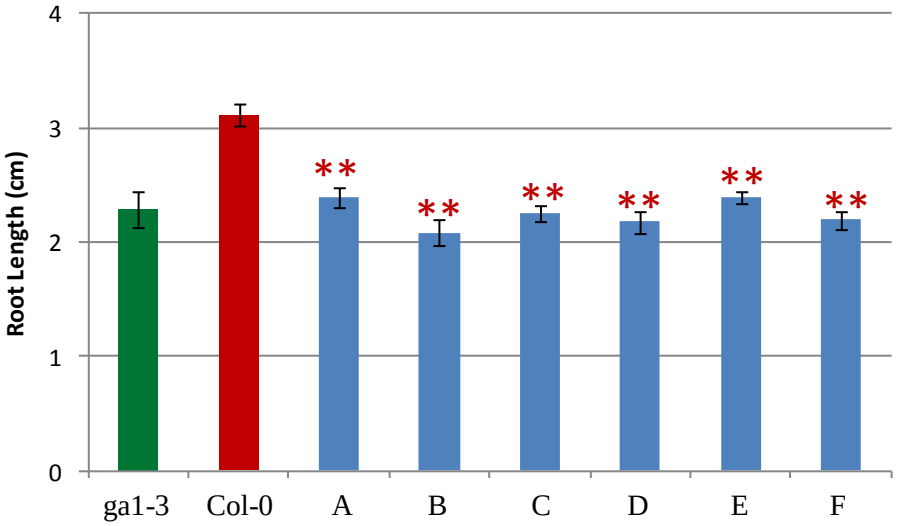

Figure 4-44**: Primary root length ±SE shown for *Col-0;CoR::YFP:AtGA2ox7* lines (A-F) compared to *ga1-3* and Col-0 at seven days.** Seedlings were grown on vertical plates and lengths calculated using ImageJ. The red asterisks indicate they are significantly different from Col-0. 30 plants for each line were analyzed **=p<0.01. Error bars indicate standard error. The LSD are given in Table 11-3.

Figure 4-45: **Vegetative phenotypes for *Col-0;CoR::YFP:AtGA2ox7* lines (A-F) compared to *ga1-3* and Col-0.** Plants were grown on Levingtons compost in 5.5 cm pots under long days at three (A) and six weeks (B).

4.2.7 *Col-0;CoR::YFP:AtGA2ox7*: root length, meristem length, cell length and transgene expression profile.

YFP fluorescence in all three *CoR::YFP:AtGA2ox7* lines was absent from the meristematic region, present within the ground tissue of the elongation zones and was not only in the cytosol but could also be seen in the nucleus (Figure 4-46). The primary root parameters for the three representative Col-0 lines expressing *YFP-AtGA2ox7* from the *CoR* promoter were compared with *ga1-3* and Col-0 (Figure 4-47). As in the previous experiment (section 4.2.6), root length was greatly reduced, but in this case the lengths were significantly larger than in *ga1-3*. *CoR::YFP:AtGA2ox7* expression stunted root growth by reducing the final cell size; since meristem size was not significantly different from Col-0 ($p<0.01$), while root length and final cell size, although larger than in *ga1-3* ($p<0.01$) were significantly less than in Col-0 ($p<0.01$).

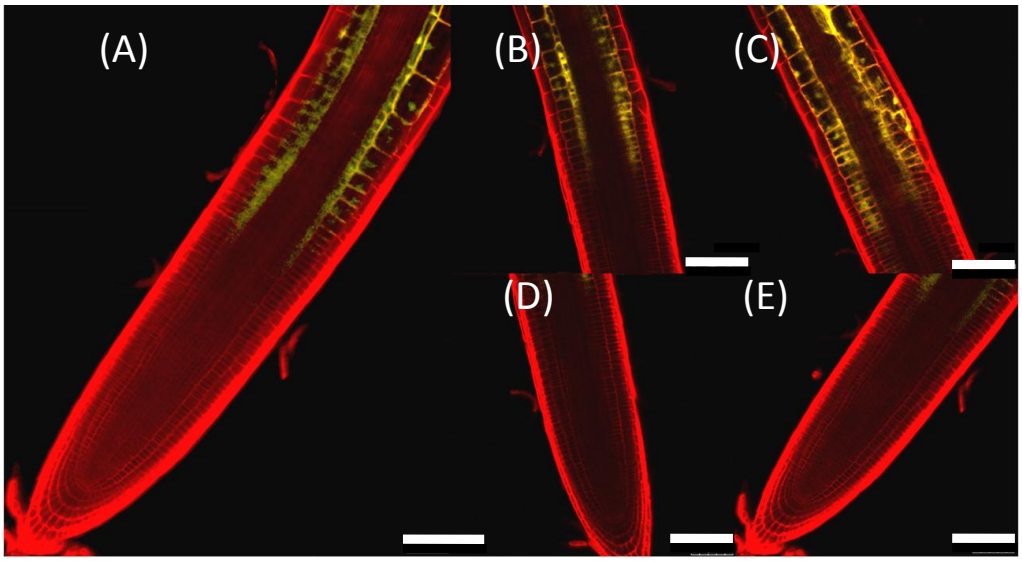

Figure 4-46: ***Col-0;CoR::YFP:AtGA2ox7* fluorescence in the elongation zones. (A-C)** Elongation zones of lines C, D and F, respectively. **(D-E)** Meristematic regions of lines D and F, respectively. Confocal microscopy was performed on the five roots of seven day old seedlings after being grown on vertical Gelrite plates. The YFP and the propidium iodide emission images are overlaid. Bars are 100 μm in length.

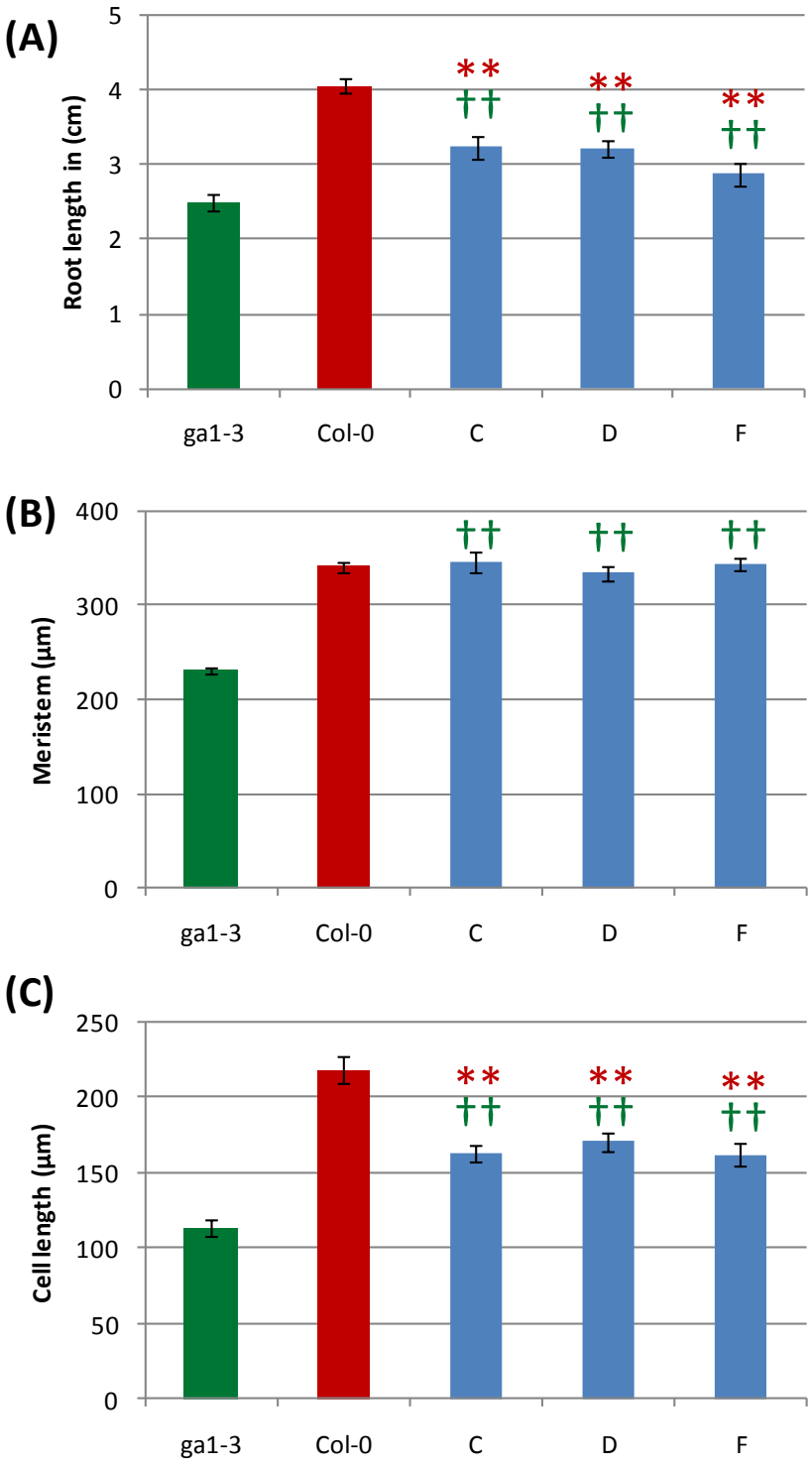

Figure 4-47**: Parameters for the primary root at 7 days in Col-0 lines C, D and F expressing *CoR::YFP:AtGA2ox7* compared with Col-0 and *ga1-3*.** **(A)** Primary root length ±SE. **(B)** Proximal meristem length ±SE. **(C)** Final cortical cell length ±SE. Seedlings were grown on vertical plates and lengths calculated using ImageJ. Green crucifixes indicate that the transgenic lines are significantly different from *ga1-3* and the red asterisks indicate they are significantly different from Col-0. 15 plants for each line were measured for root length, 5 plants were measured for meristem and cell size, with 5 cells being measured **=p<0.01, and ††=p<0.01. Error bars indicate standard error. The LSD are given in Table 11-8.

4.2.8 *Col-0;Co2::YFP:AtGA2ox7* mildly reduces root length and severely retards vegetative development

YFP-AtGA2ox7 was expressed from the *Co2* promoter to localise expression to the cortical cell of the RAM (Heidstra et al., 2004). Root lengths of *Col-0* lines expressing *Co2::YFP:AtGA2ox7* compared with Col-0 and *ga1-3* are shown in Figure 4-48. Lines A, B, E and F were not significantly different from *ga1-3* ($p>0.05$) and were significantly different from Col-0 ($p<0.05$ (except F where $p<0.01$)). Lines C and D were not significantly different from Col-0 ($p>0.05$) and were significantly different from *ga1-3* (C $p<0.01$ and D $p<0.05$). Root lengths in lines A, D and E were not significantly different ($p<0.01$) and were chosen for further analysis. The targeted expression of *YFP-AtGA2ox7* with the *Co2* promoter produced plants with variable amounts of shoot dwarfing (Figure 4-49), line D having the most stunted aerial phenotype and line E being closest to the mean of all the lines, which also contributed to their selection for further analysis.

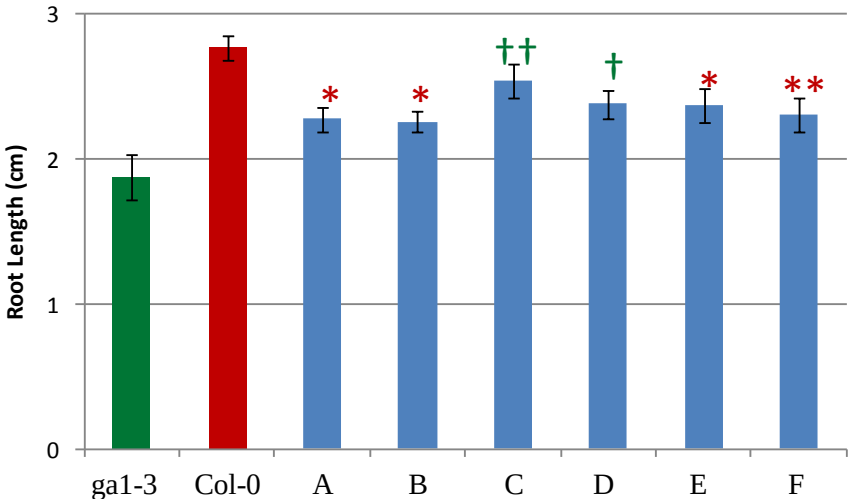

Figure 4-48**: Primary root length ±SE for *Col-0;Co2::YFP:AtGA2ox7* lines (A-F) compared to *ga1-3* and Col-0 at seven days.** Seedlings were grown on vertical plates and lengths calculated using ImageJ. Green crucifixes indicate that the transgenic lines are significantly different from *ga1-3* and the red asterisks indicate they are significantly different from Col-0. 30 plants for each line were analyzed *= $p<0.05$, **= $p<0.01$, †=$p<0.05$ and ††=$p<0.01$. The LSD used to generate standard errors used for error bars are shown in Table 11-3.

Figure 4-49: **Vegetative phenotypes of *Col-0;Co2::YFP:AtGA2ox7* lines (A-F) compared to *ga1-3* and Col-0.** Plants were grown on Levingtons compost in 5.5 cm pots under long days at three (A) and six weeks (B).

4.2.9 *Col-0;Co2::YFP:AtGA2ox7*: root length, meristem length, cell length and transgene expression profile.

In all three *Col-0;Co2::YFP:AtGA2ox7* lines, YFP fluorescence was visible only in the cortical cells of the meristematic region of primary and lateral roots (Figure 4-50). The primary root parameters for the three representative Col-0 lines expressing *YFP-AtGA2ox7* with the *Co2* promoter were compared with *ga1-3* and Col-0 (Figure 4-51). As in the previous experiment (section 4.2.8), all three lines had greatly reduced root length as the result of both reduced meristem and final cell lengths. The root lengths of all three lines were not significantly different from that of *ga1-3* ($p>0.05$), except for line A, for which root length was significantly different from both *ga1-3* and Col-0 ($p<0.05$). Meristem length in all three lines were significantly different from both Col-0 and *ga1-3* ($p>0.05$); while cell length in lines D and E were significantly shorter than in Col-0 ($p<0.01$), but all three lines had significantly larger cells than *ga1-3* ($p<0.01$).

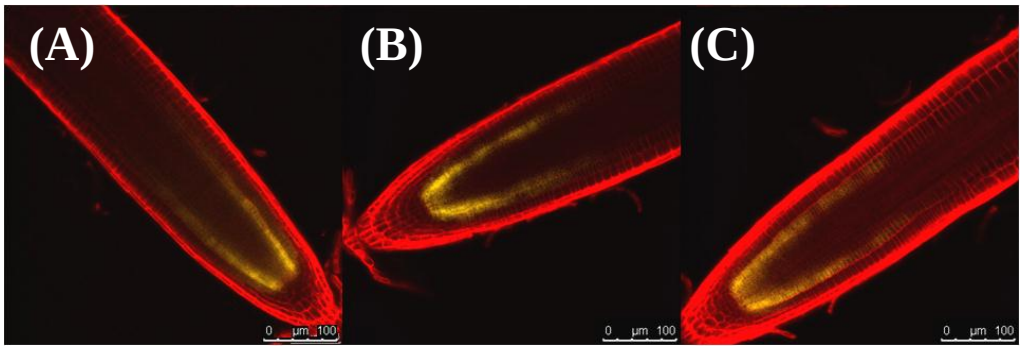

Figure 4-50: ***YFP* fluorescence in the cortical cells of the meristematic region of *Col-0;Co2::YFP:AtGA2ox7* lines. (A-C)** Meristematic region of lines A, D and E, respectively. Confocal microscopy was performed on the five roots of seven day old seedlings after being grown on vertical Gelrite plates. The YFP and the propidium iodide emission images are overlain. Bars are 100 µm in length.

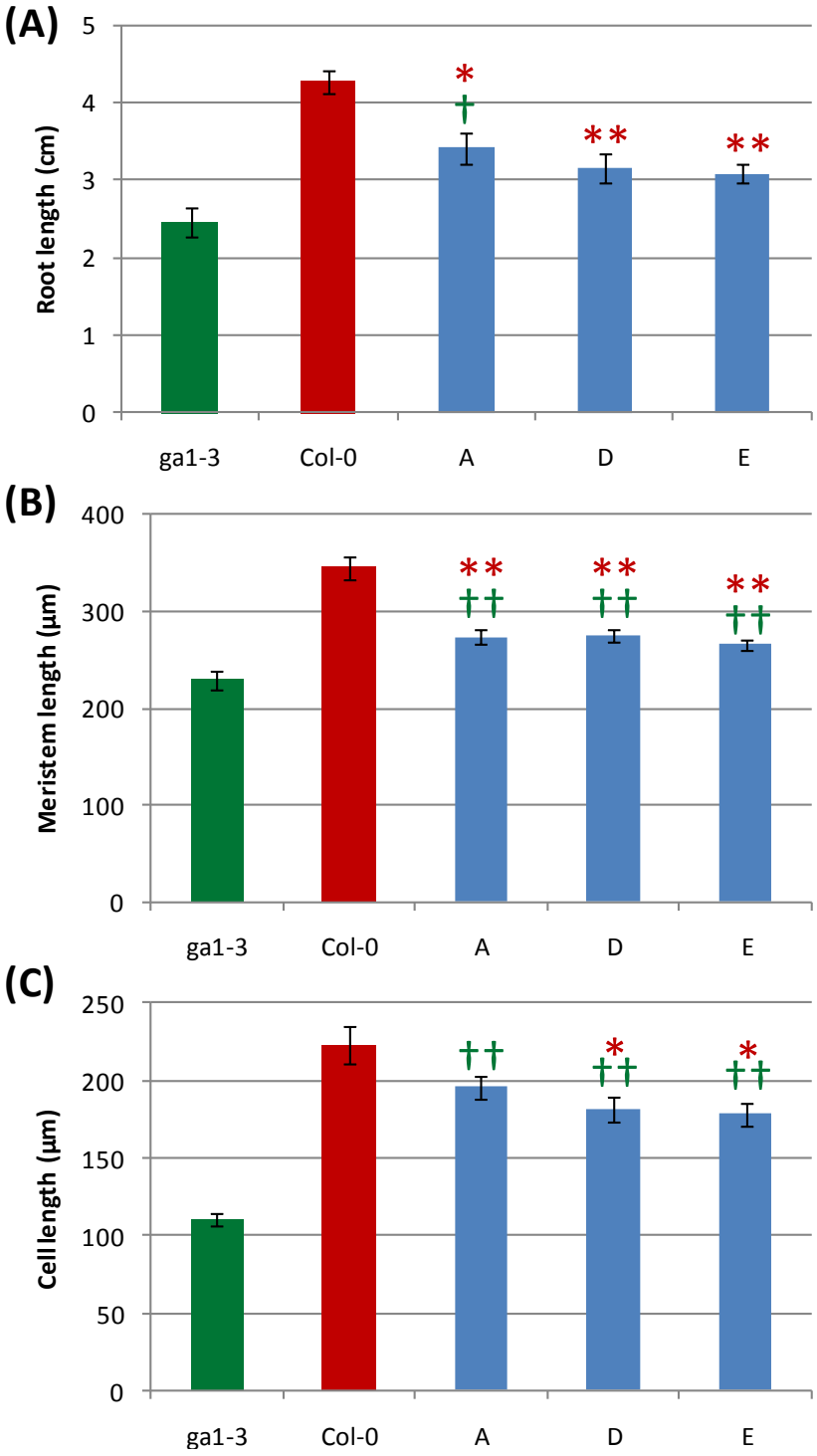

Figure 4-51**: Parameters for the primary root at 7 days in Col-0 lines A, D and E expressing *Co2::YFP:AtGA2ox7*, compared with Col-0 and *ga1-3*.** **(A)** Primary root length ±SE. **(B)** Proximal meristem length ±SE. **(C)** Final cortical cell length ±SE. Seedlings were grown on vertical plates and lengths calculated using ImageJ. Green crucifixes indicate that the transgenic lines are significantly different from *ga1-3* and the red asterisks indicate they are significantly different from Col-0. 15 plants for each line were measured for root length, 5 plants for meristem and cell size, for which 5 cells were measured *= $p<0.05$, **= $p<0.01$ and ††=$p<0.01$. Error bars indicate standard error. The LSD are given in Table 11-8.

4.2.10 *Col-0;GL2::YFP:AtGA2ox7* mildly reduces root length and severely retards vegetative development

To investigate whether removing C_{20}-GA precursors from the epidermis would have an effect on root growth YFP-AtGA2ox7 was driven in the atrichoblast cells using the *GL2* promoter (Hung et al., 1998). Root lengths of Col-0 lines expressing *GL2::YFP:AtGA2ox2* compared with Col-0 and *ga1-3* are shown in Figure 4-52. The transgenic insertion created semi-dwarf rosette leaves and inflorescence phenotypes shown in Figure 4-54. The root length of four lines A to D were significantly different from *ga1-3* ($p<0.01$ (except D where $p<0.05$)) and were not significantly different from Col-0 ($p>0.05$) except line D which was significantly different ($p<0.01$). Line A did not display any root or aerial phenotype, and was subsequently shown to be a null-segregant by a genomic PCR that could not detect the *YFP:AtGA2ox7* construct (Figure 3-25). Consequently line A was disregarded as a null-segregant and lines B, C and D were chosen for further analysis.

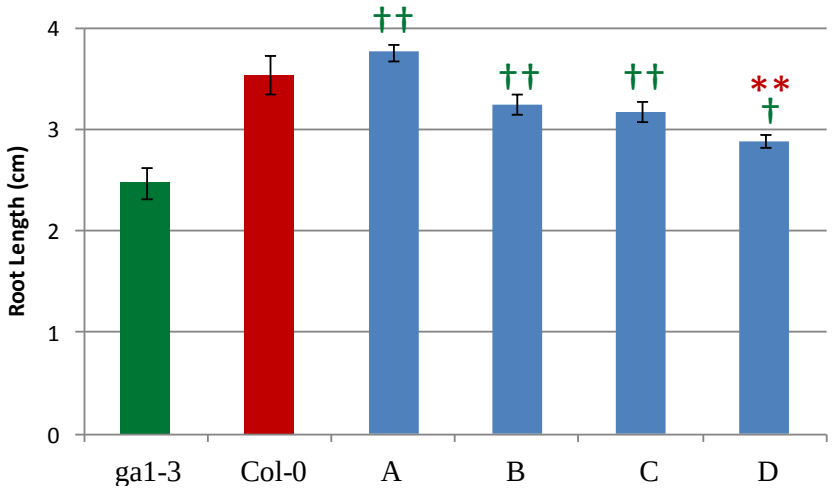

Figure 4-52**: Primary root lengths ±SE for *Col-0;GL2::YFP:AtGA2ox7* lines (A-D) compared to *ga1-3* and Col-0 at seven days.** Seedlings were grown on vertical plates and lengths calculated using ImageJ. Green crucifixes indicate that the transgenic lines are significantly different from *ga1-3* and the red asterisks indicate that they are significantly different from Col-0. 30 plants per line were analysed **=p<0.01, †=p<0.05 and ††=p<0.01. Error bars indicate standard error. The LSD are given in Table 11-3.

Figure 4-53: **Vegetative phenotypes for Col-0;*GL2::YFP:AtGA2ox7* lines (A-D) compared to *ga1-3* and Col-0.** Plants were grown on Levingtons compost in 5.5 cm pots under long days at three (A) and six weeks (B).

4.2.11 *Col-0;GL2::YFP:AtGA2ox7*: root length, meristem length, cell length and transgene expression profile.

In all three *Col-0;GL2::YFP:AtGA2ox7* lines, YFP fluorescence was present within the epidermal atrichoblast cell in the meristematic region, elongation zone and to a lesser extent differentiation zone (Figure 4-54). The primary root parameters for these lines compared with those of *ga1-3* and Col-0 are shown in Figure 4-55. As in the previous characterisation (section 4.2.10), Col-0;*GL2::YFP:AtGA2ox7* expression reduced root growth of all three transgenic lines, but the difference from wild type was significant only for one line (D). The root lengths of lines B and C were not significantly different from Col-0 ($p>0.05$), while root length in line D was not significantly different from that of *ga1-3* ($p>0.05$). The meristem lengths of all three lines were significantly different from both Col-0 and *ga1-3* ($p<0.05$), while the final cell length for only line C was significantly different from Col-0 ($p>0.05$), with all lines having larger cells than *ga1-3* ($p<0.01$).

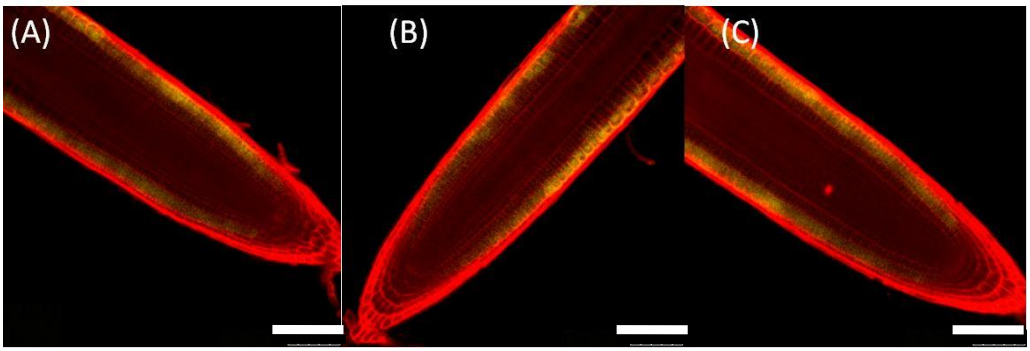

Figure 4-54: **YFP fluorescence in the meristematic region of *Col-0;GL2::YFP:AtGA2ox2* lines (A-C).** Fluorescence transgenic lines B, C and D respectively. Confocal microscopy was performed on the five roots of seven day old seedlings after being grown on vertical Gelrite plates. The YFP and the propidium iodide emission images are overlaid. Bars are 100 μm in length.

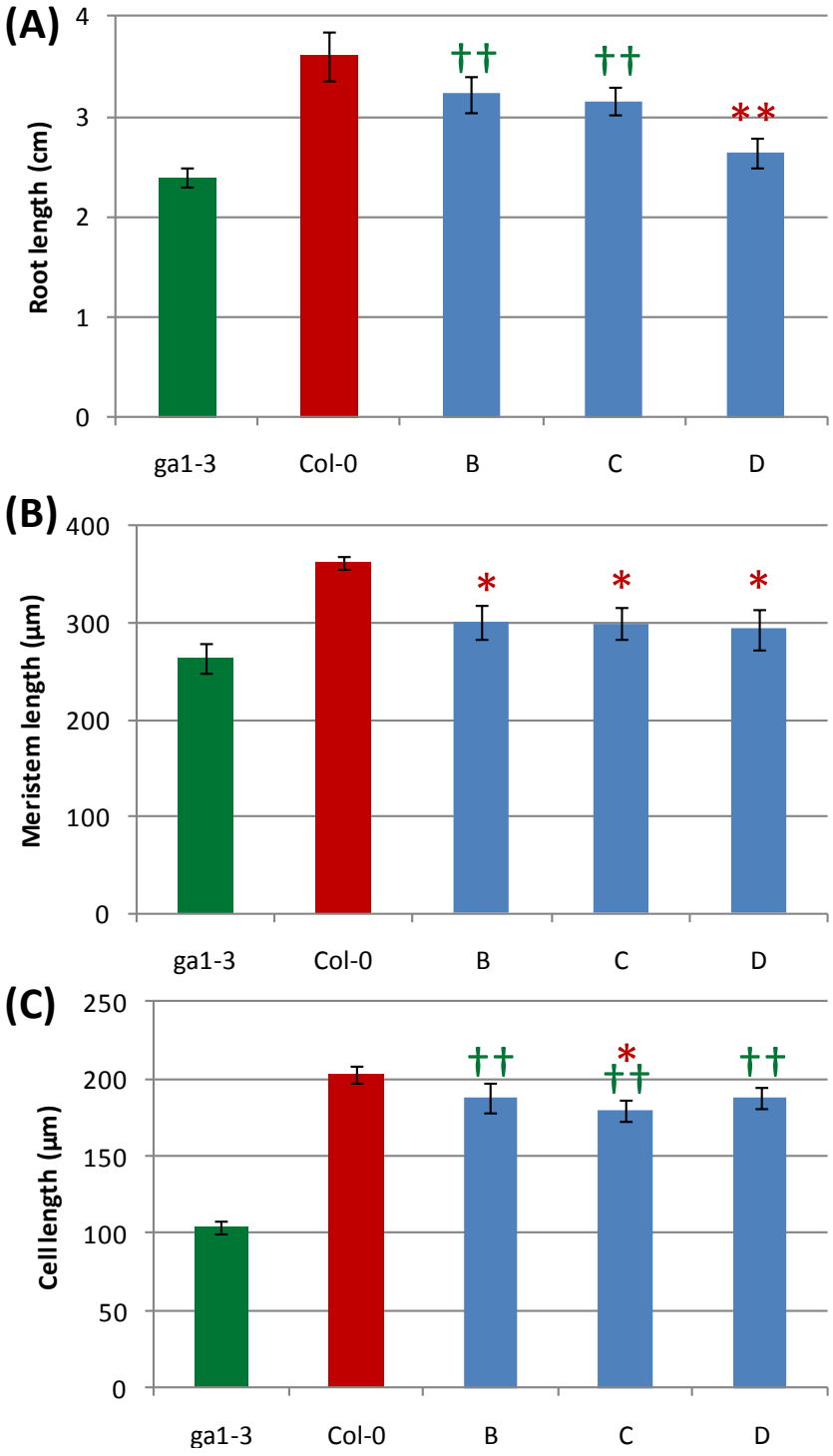

Figure 4-55**: Parameters for the primary root at 7 days in Col-0 lines B, C and D expressing *GL2::YFP:AtGA2ox7* compared with Col-0 and *ga1-3*.** **(A)** Primary root length ±SE. **(B)** Proximal meristem length ±SE. **(C)** Final cortical cell length ±SE. Seedlings were grown on vertical plates and lengths calculated using ImageJ. Green crucifix indicates that the transgenic lines are significantly different from *ga1-3* and the red asterisks indicate that they are significantly different from Col-0. 15 plants for each line were measured for root length, 5 plants were measured for meristem and cell, size, with the final length of 5 cells determined. *=p<0.05, **=p<0.01 and ††=p<0.01. Error bars indicate standard error. The LSD are given in Table 11-8.

4.2.12 Col-0;*CAB::YFP:AtGA2ox7* mildly reduced root length and severely retarded vegetative development

The shoots are a potential source of GA precursors for the roots and modifying the GA metabolism in the shoot may influence shoot and root growth. The importance of this contribution was assessed by expressing *YFP-AtGA2ox7* from the CAB promoter (Puente et al., 1996). In addition, this experiment was also used to investigate if the aerial expression of the root tissue specific promoters would affect root growth. Root lengths of *Col-0* lines expressing *CAB::YFP:AtGA2ox2* compared with Col-0 and *ga1-3* are shown in Figure 4-56. Shoot-targeted expression of *AtGA2ox7* severely dwarfed the aerial tissue (Figure 4-57). Root lengths of the lines A-F were variable, with roots of lines A, B, E and F being significantly shorter than Col-0 ($p>0.01$ (except E where $p<0.05$)), while lines C and D were not significantly different from Col-0 ($p>0.05$). Line A was severely dwarfed and produced few seeds. Since it could not be rescued by GA_3 application it was not analysed further. Lines D, E and F, which showed the greatest variation in shoot growth, were chosen for further analysis since their root lengths were not significantly different and were close to the mean of all the root lengths.

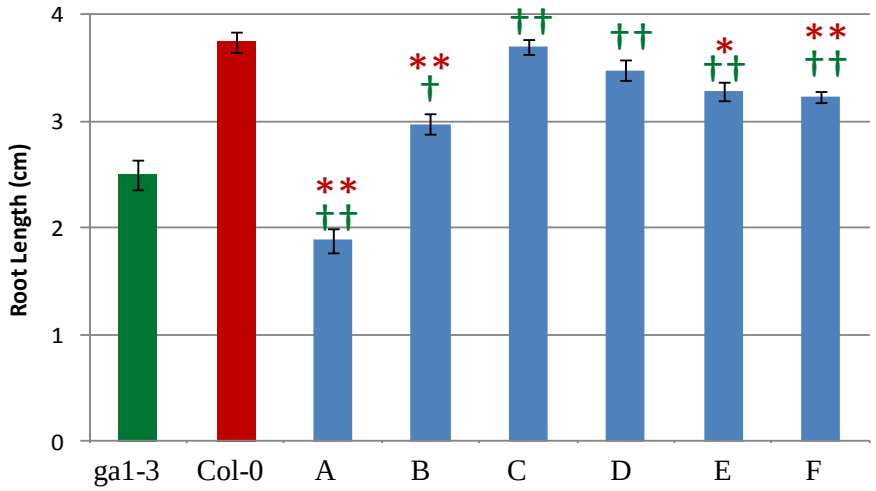

Figure 4-56**: Primary root length ±SE for *Col-0;CAB::YFP:AtGA2ox7* lines (A-F) compared to *ga1-3* and Col-0 at seven days.** Seedlings were grown on vertical plates and lengths calculated using ImageJ. Green crucifix indicates that the transgenic lines are significantly different from *ga1-3* and the red asterisk indicates that they are significantly different from Col-0. 30 plants per line were analysed *=p<0.05, **=p<0.01 and ††=p<0.01. Error bars indicate standard error. The LSD are given in Table 11-3.

Figure 4-57: **Vegetative phenotypes for *Col-0;CAB::YFP:AtGA2ox7* lines (A-F) compared to *ga1-3* and Col-0.** Plants were grown on Levingtons compost in 5.5 cm pots under long days at three (A) and six weeks (B).

4.2.13 Col-0*;CAB::YFP:AtGA2ox7*: root length, meristem length, cell length and transgene expression profile.

The primary root parameters for the three representative Col-0 lines expressing *YFP-AtGA2ox7* from the *CAB* promoter were compared with *ga1-3* and Col-0 (Figure 4-59). In agreement with the previous analysis (section 4.2.12), *Col-0;CAB::YFP:AtGA2ox7* produced mild stunting of root growth for two lines E and F. Roots of all three lines were significantly longer than those of *ga1-3* ($p>0.01$), while line E and F roots were also significantly shorter than Col-0 (E = $p<0.01$ and F= $p<0.05$), Cell and meristem lengths of all three lines were not significantly different from those in Col-0 ($p<0.05$), except line D that was significantly different from both Col-0 and *ga1-3* ($p>0.01$). All three *Col-0;CAB::YFP:AtGA2ox7* lines had YFP fluorescence in young green primary leaves, while no fluorescence could be observed within the root, hypocotyl or the cotyledons (Figure 4-58).

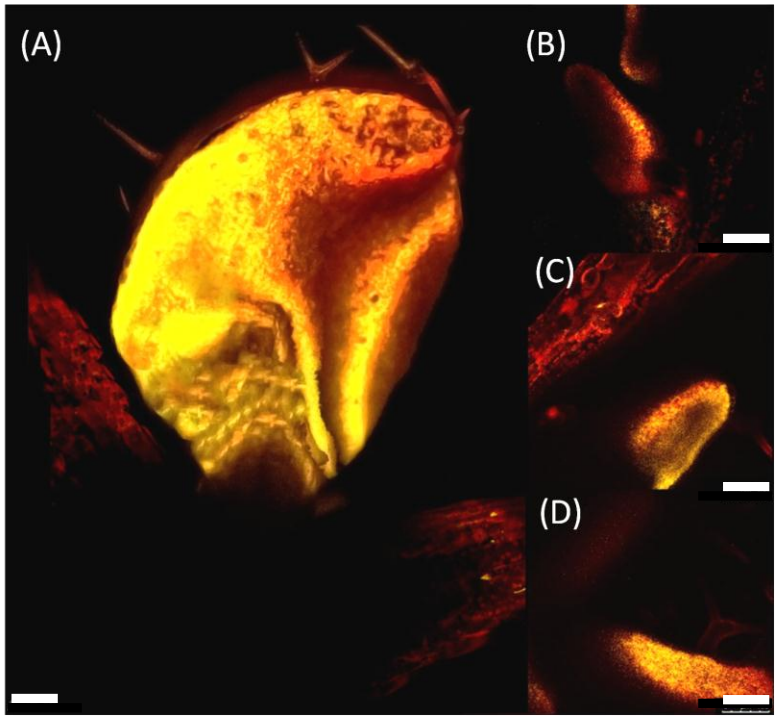

Figure 4-58**: YFP fluorescence in Col-0;*CAB::YFP:AtGA2ox7*. (A)** Shoots of line D showing YFP fluorescence in young leaves **(B-D)** Young shoot tissue emerging from the shoot apical meristem (SAM) for lines D, E and F, respectively. The YFP and the propidium iodide emission images are overlaid. Bars are 100 μm in length.

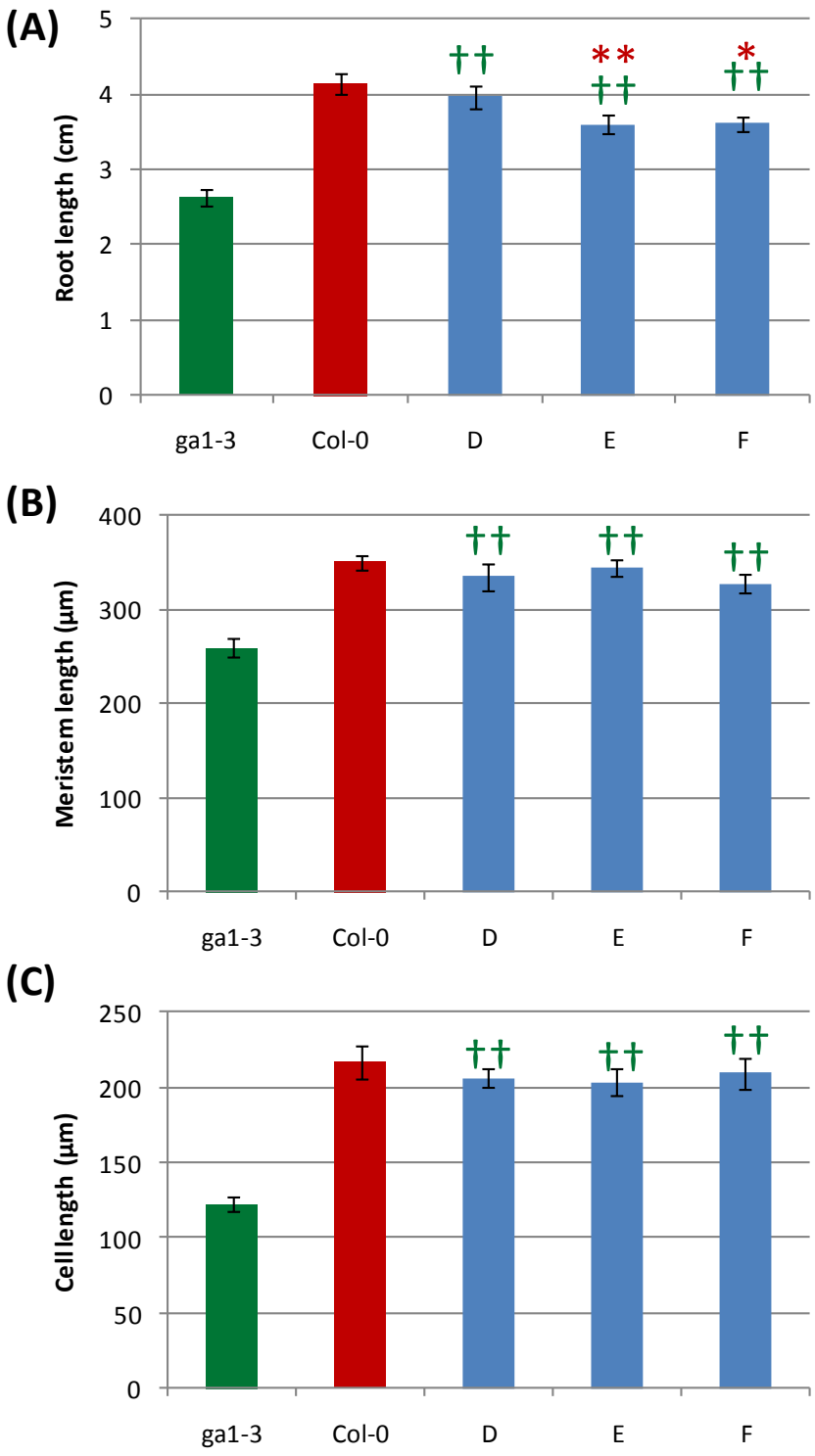

Figure 4-59**: Parameters for the primary root at 7 days in Col-0 lines D-F expressing *CAB::YFP:AtGA2ox7* compared with Col-0 and *ga1-3*. (A)** Primary root length ±SE. **(B)** Proximal meristem length ±SE. **(C)** Final cortical cell length ±SE. Seedlings were grown on vertical plates and lengths calculated using ImageJ. Green crucifixes indicate the transgenic lines are significantly different from *ga1-3* and the red asterisks indicate they are significantly different from Col-0. 15 plants for each line were measured for root length, and 5 for meristem and cell length, with 5 cells measured *=p<0.05, **=p<0.01, and ††=p<0.01. Error bars indicate standard error. The LSD are given in Table 11-8.

4.2.14 Comparison of the effects of each promoter driving expression of *YFP:AtGA2ox7*.

The primary root parameters for the median representative lines expressing *promoter::YFP-AtGA2ox7* compared with *ga1-3* and Col-0 (Figure 4-60). The root, cell and meristem lengths when the gene was expressed from *SHR* and *CAB* were not significantly different from each other and Col-0 ($p<0.05$). Expression from *SCR*, *Co2*, *GL2* and *CoR* reduced root growth ($p<0.05$) with expression from *SCR* and *CoR* producing roots that were not significantly different from *ga1-3* ($p<0.05$). Expression from *SCR* and *GL2* caused reductions in both meristem size and cell length (significantly different from Col-0 at $p<0.01$), while expression from the *CoR* promoter reduced only cell length (different from Col-0 at $p<0.01$). In contrast, the dwarf root from expression with the *Co2* promoter was due to a smaller meristem (different from Col-0 at p,0.05) and not reduced cell size, which was similar to that in Col-0 ($p>0.05$). Figure 4-61 shows representative images for the root tip for the *SHR*, *SCR*, *CoR*, *Co2* and *GL2* YFP:AtGA2ox7 lines, as no fluorescence was observed at the root tip for the *CAB* lines photosynthetic tissue near the SAM is shown.

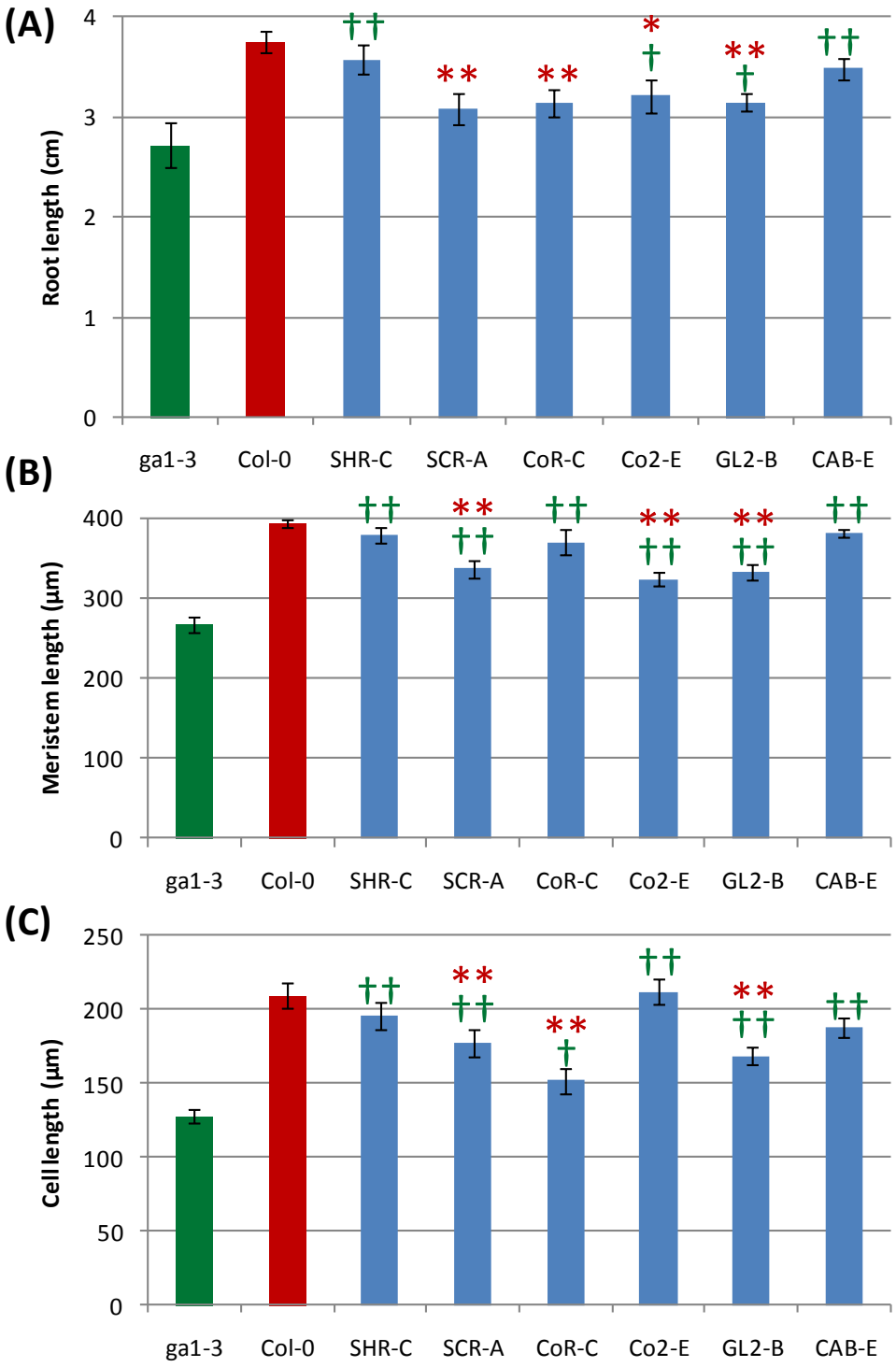

Figure 4-60**: Comparison of the primary root parameters for median lines for each *YFP:AtGA2ox7* construct with Col-0 and *ga1-3* at seven days. (A)** Primary root length ±SE. **(B)** Proximal meristem length ±SE. **(C)** Final cortical cell length ±SE. Seedlings were grown on vertical plates and lengths calculated using ImageJ. Green crucifixes indicate that the transgenic lines are significantly different from *ga1-3* and the red asterisks indicate that they are significantly different from Col-0. 15 plants for each line were measured for root length, 5 plants for meristem and cell size, with 5 cells measured *=p<0.05, **=p<0.01, †=p<0.05 and ††=p<0.01. Error bars indicate standard error. The LSD are given in Table 11-11.

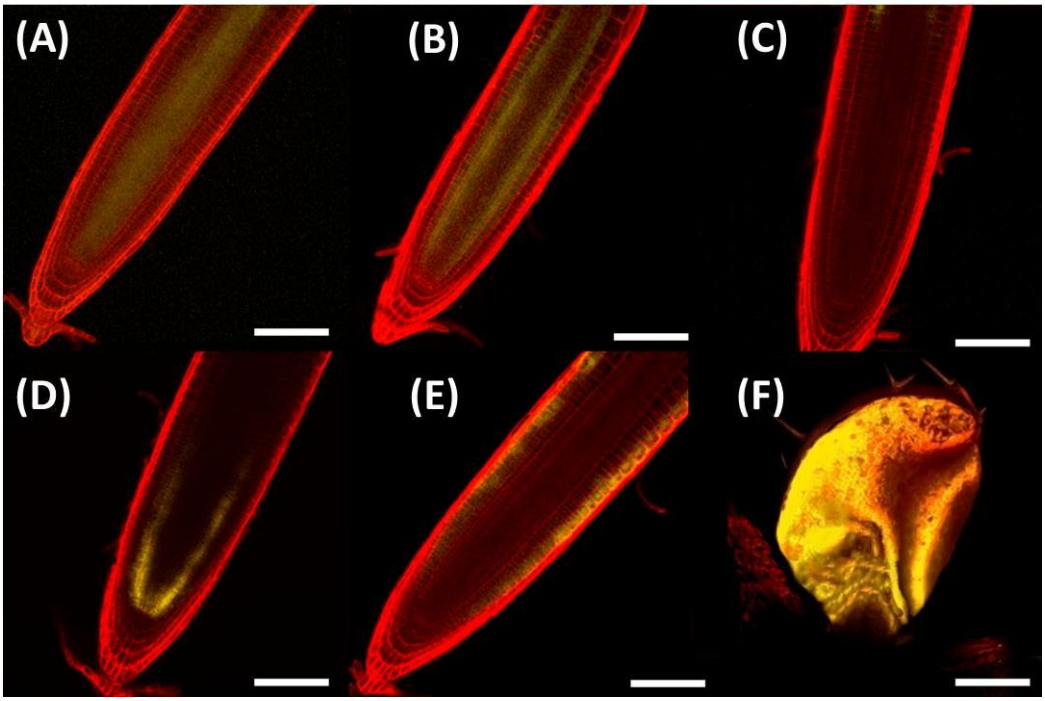

Figure 4-61: **Representative images for YFP fluorescence in the GA2ox7 lines. (A-F)** YFP-AtGA2ox7 attached to *SHR, SCR, CoR, Co2, GL2* and *CAB* promoters, respectively. Confocal microscopy was performed on seven day-old seedlings grown on vertical Gelrite plates. The YFP and the propidium iodide emission images are overlain. Bars are 100 μm in length.

In summary (Figure 4-62), *YFP-AtGA2ox7* expression was expected to stunt root growth by inactivating C_{20}-GAs and subsequently reduce meristem size or final cell size by removing GA precursors at their site of synthesis and/or by deactivating them on transit to their site of activation. Ectopic expression of AtGA2ox7 was able to partially stunt root growth when expressed in the endodermis, epidermis and the cortex of either the meristematic region or elongation zone. Expression of *YFP-AtGA2ox7* within photosynthetic or any aerial tissues dramatically stunted shoot growth. The *CoR::YFP:AtGA2ox7* lines had semi-dwarf final cortical cell lengths demonstrating the importance of either C_{20}-GA biosynthesis or movement within this tissue.

Figure 4-62: **Schematic diagram highlighting which tissues YFP-AtGA2ox7 was able to retard growth within.** The yellow lateral root cap and columella cells were not studied during this project. The torques meristematic endodermal, cortical and epidermal cells are sites of C_{20}-GA biosynthesis and/or movement required for cell division. The white ground tissue and epidermal cells in the elongation zone are sites of C_{20}-GA biosynthesis and/or movement required for cellular elongation. The green vasculature cells are not sites of C_{20}-GA biosynthesis and/or movement required for either cell elongation or cell division.

4.3 DISCUSSION OF THE EFFECTS OF TISSUE-SPECIFIC *YFP-GA2ox2* AND *YFP-GA2ox7* EXPRESSION IN Col-0

Recent work has shown that preventing GA signalling in the endodermis reduced cell division rates and cell elongation (Ubeda-Tomás et al., 2009, Ubeda-Tomas et al., 2008). The aim of the current work was to investigate how sites of GA biosynthesis and activation relate to this demonstrated site of action and if GA movement plays an important role. It has previously been shown that over-expression of GA2ox can create dwarf plants (Schomburg et al., 2003, Thomas et al., 1999) and that knocking out different combinations of GA2ox enzymes can modify certain growth characteristics (Rieu et al., 2008a). Expression of *YFP-AtGA2ox2* and *YFP-AtGA2ox7* from different tissue-specific promoters produced a range of phenotypes that have provided insights into GA metabolism and signalling. In addition to identifying the cells that are likely sources of the precursor GA_{12} and indicating the importance of movement of C_{20}-GA precursors from the meristematic region to the elongation zone, the results also suggest that post transcriptional regulation of GA2oxs may be controlled by GA concentrations.

4.3.1 Ectopic aerial expression of tissue specific YFP-AtGA2ox2 and YFP-AtGA2ox7 transgenes

The photosynthetic tissue specific *Col-0;CAB::YFP:AtGA2ox7* and *Col-0;CAB::YFP:atGA2ox2* transgenic lines had wild type root growth and had severely dwarfed aerial growth (Figure 4-30 and Figure 4-60). This demonstrates that root growth can be independent from either C_{20}-GAs or C_{19}-GAs moving down from aerial tissues. In addition, this also demonstrates that ectopic expression of the YFP-AtGA2ox7 and YFP-AtGA2ox2 transgene in aerial tissues will not affect root growth when driven from the other root tissue specific promoters. Therefore root growth can be driven solely from GAs derived from the root tip.

4.3.2 GA activation and movement within the elongation zone

Expression of *YFP-AtGA2ox2* within the ground tissue of the elongation zone from the *CoR* promoter reduced root growth by restricting cell elongation, but did not alter meristem length (Figure 4-18). *YFP-AtGA2ox7* expression from the *CoR* promoter partially reduced final cell size suggesting that synthesis of C_{20}-GAs in the elongation zone or their movement into this zone is required for normal cell elongation and correct growth (Figure 4-47).

4.3.3 GA activation and mobilisation in the meristematic region

Expression of *YFP-AtGA2ox2* within the epidermal cells of the meristematic region and elongation zone from the *GL2* promoter reduced root length by restricting meristem size, but had no effect on cell length, suggesting that GA perception within the epidermis and/or the epidermal/lateral root cap (ELRC) initial daughter cells has an important role in cell division while cell elongation does not require bioactive GA within the epidermis (Figure 4-26). Similarly expression of *YFP-AtGA2ox2* within cortical cells of the meristematic region and the cortical/endodermal initial daughter (CEID) cells using the *Co2* promoter also stunted root growth by shrinking the size of the meristematic region, but had no effect on cell elongation (Figure 4-22). Expression of *YFP-AtGA2ox7* from the same promoters also reduced root growth, due to a partial reduction in both meristem and cell length (Figure 4-60). This is probably caused by inactivation of C_{20}-GA precursors in the meristematic region reducing the amount of C_{20}-GAs available for GA synthesis within this region and therefore reducing the amount that can travel to the elongation zone (Figure 4-51). Thus the meristem is a source of GAs or GA precursors that are required for normal cell division and expansion.

4.3.4 C_{20}-GA and C_{19}-GA inactivation in the stele has no effect on root growth but dwarfed roots when it occurs in the endodermis/ground tissue

When *YFP-AtGA2ox2* was expressed within the stele from the *SHR* promoter there was no effect on root growth, while expression of *YFP-AtGA2ox7* within this tissue gave a slight reduction in root length, but had no significant effect on either meristem size or final cell length (Figure 4-6 and Figure 4-36). This suggests that the stele is not a significant source of C_{20}-GAs and that the presence of C_{19}-GAs within this tissue is not required for normal cell division and elongation to occur. Expression of *YFP-AtGA2ox2* in the endodermis from the *SCR* promoter led to severely suppressed primary root growth, suggesting that the endodermis is an important site of GA perception and/or synthesis for

both cell elongation and meristem length (Figure 4-9). In addition, expression of *YFP-AtGA2ox7* in the endodermis reduced root growth due to a partial reduction in both meristem and final cell size, indicating that the endodermis is an important source or transit route of C_{20}-GAs (Figure 4-41). The observation that both final cell size and meristem size in the *Col-0;SCR::YFP:AtGA2ox7* lines were larger than in the *Col-0;SCR::YFP:AtGA2ox2* lines suggests that normal root growth requires some movement of C_{19}-GAs (GA_4 or GA_9) into the endodermis and that it is a source or transit route of C_{20}-GAs.

4.3.5 C_{20}-GA and C_{19}-GA pools, and movement within root tissues

Expression of *YFP-AtGA2ox2* and *YFP-AtGA2ox7* within photosynthetic tissue using the *CAB* promoter had no affect on root growth, suggesting that roots are normally autonomous for GA production (Figure 4-34 and Figure 4-59). Thus the *Arabidopsis* root may have its own pool of C_{20}-GAs and C_{19}-GAs capable of driving root growth independently of shoot GA pools. Therefore the dwarfing of root meristems by expressing *YFP-AtGA2ox2* in the root epidermis, cortex or endodermis may be because each cell layer requires its own bioactive GA for cell division to occur correctly or alternatively might be due to depletion of an overall meristematic pool of the C_{19}-GAs GA_9 or GA_4. In the case of the second scenario it is likely that a putative GA transporter or the movement of GA through the plasmodesmata would be required (Dobson, 2009, Kramer, 2006).

The decrease of final cell size by expressing *YFP-AtGA2ox7* in the epidermis, cortex or endodermis suggests a pool of C_{20}-GAs that is capable of moving between cells. Calculations made by Kramer (2006) suggest that the C_{20}-GAs GA_{15} and GA_{24} would be able to cross cell membranes; however the pH of the apoplast would only allow small quantities to re-enter the cell by diffusion, and therefore an import transporter would be needed for GAs to re-enter the cells in large quantities. This is relevant if the media the plants are growing in influences the apoplastic pH of the root, as this could influence how much GA can re-enter the cell by diffusion. Thus the importance of a transporter would depend on the environmental conditions, which can modify apoplastic pH, as

has been demonstrated for drought and the ABA transporters (Kuromori et al., 2010, Kang et al., 2010). Therefore, the dwarfing of root growth caused by expressing *YFP-AtGA2ox7* within the elongation zone from the *CoR* promoter suggests the existence of a pool of C_{20}-GAs that are capable of moving to the elongation zone in order to promote full cell elongation.

4.3.6 Homeostatic mechanisms control AtGA2ox2 and AtGA2ox7 stability in a tissue specific manner

The expression of the metabolic enzymes that control GA biosynthesis and inactivation are control by complex feedback mechanisms (Thomas et al., 1999, Chiang et al., 1995, Phillips et al., 1995). When the *SHR* and *SCR* promoters were used to drive the expression of *YFP-AtGA2ox2* and *YFP-AtGA2ox7*, YFP fluorescence levels were increased upon application of 1 μM GA_3 and were decreased by application of 1 μM PAC (Figure 4-5 and Figure 4-11). As both the transcriptional and translational GFP fusions to the *SHR* and *SCR* promoters were not affected by either 1 μM GA_3 or 1 μM PAC application, this implies that AtGA2ox2 and AtGA2ox7 levels may be regulated either via RNA turnover through the action of miRNAs or via modification of protein stability in order to optimise GA homeostasis (Figure 4-12 and Figure 4-13). In addition, the increased levels of YFP-AtGA2ox2 after GA_3 application was much more extreme then the increased levels of YFP-AtGA2ox7, suggesting that different feedback mechanisms regulate the stability of these enzymes (Figure 4-11 and Figure 4-43).

The difference between YFP-AtGA2ox7 driven by the *SHR* promoter in the vasculature of the meristematic region and the elongation zone varied between developmental zones, with the fluorescence appearing brighter in the differentiation zone then the meristematic region (Figure 4-37). This reflects microarray data that showed the closely related *AtGA2ox8* was most highly expressed within the differentiation zone, although *AtGA2ox7* doesn't appear to be highly expressed in root its close homology to the *AtGA2ox8* might allow molecular mechanisms that act on both homologues. This suggests that the endodermal cells of the differentiation zone may have mechanisms that

promote the stability of members of the GA2ox clade that prefer C_{20}-GA substrates. In addition, homeostatic regulation of the *AtGA2ox2* and *AtGA2ox7* genes could also function in the other tissues at different stages of development. It would be interesting to see how *35S::YFP:AtGA2ox2* and *35S::YFP:AtGA2ox7* respond to PAC, C_{20}-GAs and C_{19}-GAs with particular emphasis on the potential variations between the different tissues and stages of development.

4.3.7 Aerial phenotypes from expression of the GA2ox genes

Expression of *YFP-AtGA2ox7* in photosynthetic tissues from the *CAB* promoter produced a far more severe dwarf aerial phenotype than when *YFP-AtGA2ox2* was expressed from this promoter. This was also true regardless of the promoter, with *YFP-GA2ox7* expression giving more severe dwarfing of the shoot than *YFP-GA2ox2*. This could be due to the importance of the movement of C_{20}-GAs for correct growth; however, it could also be due to the relative stabilities of the GA 2-oxidase enzymes with the stability of *AtGA2ox2* being more effectively down-regulated.

King and Evans (2003) proposed that the action of a GA2ox enzyme prevents bioactive GA from entering the shoot apical meristem (SAM) and inducing flowering. However this blockade would only be effective against the symplastic pathway and it is therefore possible that C_{20}-GAs reach the SAM via the apoplastic pathway. In addition, these routes of C_{20}-GA entry may be required in order to provide low concentrations of GA to promote cell division (Achard et al., 2009), but without promoting the floral transition. This is supported by experiments that show relatively high levels of GA_4 and GA_1 in leaves prior to the floral transition, but these are undetectable in the SAM (Gocal et al., 1999). Therefore it is possible that C_{20}-GAs such as GA_{15} and/or GA_{24} may be capable of moving to the SAM from their site of synthesis in order to promote cell division after activation. Although there is no support for this hypothesis in the literature this may be because only long-distance movement through the vasculature has been investigated.

The promoters used for cell specific expression in roots are also expressed within specific cell types in aerial tissues, providing insights into GA metabolism throughout the rest of the plant (Dhondt et al., 2010, Wysocka-Diller et al., 2000, Puente et al., 1996, Rerie et al., 1994). The *SCR* promoter is the best characterized of these promoters and has been shown to be active in the stem cambium and leaf bundle sheath cells (Wysocka-Diller et al., 2000). Expressing *YFP-AtGA2ox2* within these tissues produced a semi-dwarf, while shoot growth in the lines expressing *YFP-AtGA2ox7* was severely reduced, suggesting that production of C_{20}-GAs or their movement into, or through these shoot tissues is critical for plant growth and development (Figure 4-8 and Figure 4-40). The *SHR* promoter used to drive expression within the root stele is also expressed within the shoot vasculature (Dhondt et al., 2010). As SHR is known to promote *SCR* expression in the root endodermis, it may have a similar role in the stem cambium, the leaf bundle sheath cells (Wysocka-Diller et al., 2000) and potentially any cell surrounding vasculature bundles. Expression of *YFP-AtGA2ox2* from this promoter had no effect on shoot growth, but expression of *YFP-AtGA2ox7* caused stunting of the shoot, indicating that movement of C_{20}-GAs within the shoot vasculature and endodermis is important for leaf expansion and inflorescence elongation (Figure 4-3 and Figure 4-35). These data suggest that the movement of C_{19}-GAs to the stem cambium and the leaf bundle sheath cells does not require movement through the vasculature (Eriksson et al., 2006).

The *GL2* promoter used to drive expression within the root epidermis is also expressed throughout young leaf primordia, during early trichome development and persists in mature trichomes (Szymanski et al., 1998). In addition results from microarray analyses suggest that *GL2* is expressed in the stem epidermis and leaf stomata guard cells. Driving expression of *YFP-AtGA2ox2* with this promoter produced a mildly dwarfed shoot (Figure 4-24). In contrast, driving expression of *YFP-AtGA2ox7* with the same promoter created a severely dwarfed aerial phenotype, providing further evidence indicating that movement of C_{20}-GAs in aerial tissues is important (Figure 4-53). Taken together these data suggests that the epidermis, trichomes, and guard cells may be important

sources of C_{20}-GA precursors or are a route of C_{20}-GA and/or C_{19}-GA movement.

The exact aerial expression profile of the *CoR* and *Co2* promoters that were used to drive the expression within the ground tissue of the elongation zone and meristemic regions, respectively, is unknown. However microarray data suggest that both are highly expressed in the peripheral region of the SAM (Figure 3-16 and Figure 3-19). Interestingly expression of *YFP-AtGA2ox2* within this region produced a semi-dwarf phenotype, while expressing *YFP-AtGA2ox7* within these tissues created a severe dwarf. This suggests that the movement of C_{20}-GAs into and/or out from the central SAM is critical for plant growth and development (Figure 4-20 and Figure 4-49).

The *GL2* promoter used to drive expression within the root epidermis is also expressed throughout young leaf primordia, during early trichome development and persists in mature trichomes (Szymanski et al., 1998). In addition results from microarray analyses suggest that *GL2* is expressed in the stem epidermis and leaf stomata guard cells. Driving expression of *YFP-AtGA2ox2* with this promoter produced a mildly dwarfed shoot (Figure 4-24). In contrast, driving expression of *YFP-AtGA2ox7* with the same promoter created a severely dwarfed aerial phenotype, providing further evidence indicating that movement of C_{20}-GAs in aerial tissues is important (Figure 4-53). Taken together these data suggests that the epidermis, trichomes, and guard cells may be important sources of C_{20}-GA precursors or are a route of C_{20}-GA and/or C_{19}-GA movement.

5 TISSUE SPECIFIC RESCUE OF THE *ga20ox1,-2,-3* TRIPLE MUTANT USING *YFP:AtGA20ox1*

5.1 INTRODUCTION TO GA 20-OXIDATION

Gibberellin 20-oxidation, catalysed by GA20ox, results in the conversion of the early GA precursors GA_{12} and GA_{53} in preparation for the final step of the biosynthetic pathway (Figure 5-1). This 20-oxidation is necessary before activation as it removes the 20-carbon (C-20) atom, subsequently allowing the 3β-hydroxylation to activate the molecule (Yamaguchi, 2008). The potential sites of GA20ox activity in the plant were investigated by attempting to rescue the growth of the *Arabidopsis* GA-deficient mutant *ga20ox1 ga20ox2 ga20ox3* (hereafter referred to as *ga20ox1,-2,-3*) by targeting the expression of a YFP-AtGA20ox1 fusion protein to specific cell types, including the epidermis, cortex, endodermis, stele and photosynthetic tissue.

The effect of tissue-specific expression of YFP-AtGA20ox1 on the phenotypic rescue of root and aerial tissue the *ga20ox1,-2,-3* triple mutant will provide important information that will assist in mapping the sites C-20-oxidation. Rescue of growth will indicate that the targeted cells contain GA_{12}, GA_{15} and/or GA_{24} and that GA_9 is capable of becoming activated by C-3-oxidation in the same cells or by movement to cells expressing *GA3ox* genes. In contrast, lack of rescue could indicate limited availability of GA_{12} or alternatively GA_9 not getting to its site of activation. In addition, to investigate the potential significance of transport of GAs from the shoot to promote root growth, *YFP-AtGA20ox1* expression will also be targeted to the photosynthetic tissue in the *ga20ox1-,2,-3* triple mutant; if the root growth can be rescued by expression of *YFP-AtGA20ox1* in photosynthetic tissue then it will suggest that either GA_9 or GA_4 are capable of travelling to the roots to promote growth.

Gibberellin 20-oxidation, which is the rate-limiting step in GA biosynthesis in many species, performs three sequential oxidations with the GA substrate leaving the active site so it can re-enter with a fresh 2-oxoglutarate molecule (Fleet et al., 2003, Coles et al., 1999). Biosynthetic steps that occur

immediately before the 20-oxidation are not rate limiting (Fleet et al., 2003) and are catalysed by terpene cyclases CPS and KS then by the cytochrome P450s KO and KAO which microarrays studies have shown to be expressed around the QC and proximal meristematic region of the root (Figure 11-1). The three-step sequential oxidation of C-20 by GA20ox eventually results in the creation of the C_{19}-GA_{20} or C_{19}-GA_9 and the release of a CO_2 molecule. There are two potential products of this reaction as GA_{12} can undergo 13β-hydroxylation resulting in the creation of GA_{53}. If this occurs then there are subsequently two parallel sequences of reactions catalysed by GA20ox, the conversion of GA_{12} to GA_9 via the two intermediates GA_{15} and GA_{24} and the conversion of GA_{53} to GA_{20} via the two intermediates GA_{44} and GA_{19} (Figure 5-1).

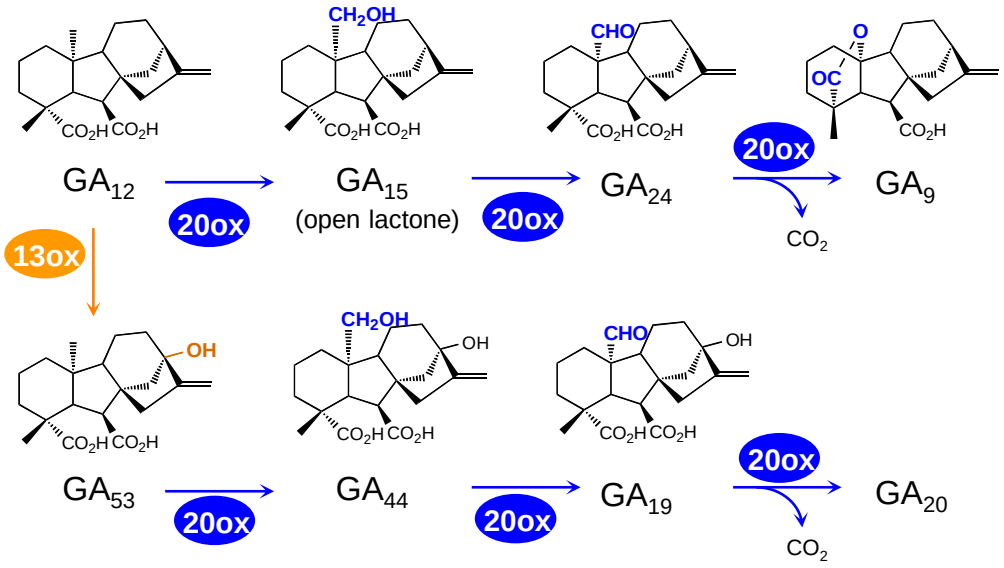

Figure 5-1**: Reactions catalysed by the GA 20-oxidase and GA 13β-hydroxylase enzymes.** A putative GA 13β-hydroxylase catalyses the conversion of GA_{12} to GA_{53}. There are subsequently two parallel sequences of reactions catalysed by AtGA20ox, the conversion of GA_{12} to GA_9 via the two intermediates GA_{15} and GA_{24} and the conversion of GA_{53} to GA_{20} via the two intermediates GA_{44} and GA_{19}. (Figure adapted with permission from Shinjiro Yamaguchi (2008)).

There are at least five paralogous genes encoding GA20ox enzymes in Arabidopsis; these genes act partially redundantly due to their distinct but overlapping expression patterns. Interestingly *AtGA20ox5* can only catalyse the first two 20-oxidation steps creating either GA_{24} or the 13-hydroxylated GA_{19}

in *in-vitro* assays (personal communication Peter Hedden). Reverse genetic approaches to uncover the roles of *GA20ox1* and *GA20ox2* have highlighted their involvement in hypocotyl growth, anther filament extension, stem internode elongation, silique development and male fertility (Rieu et al., 2008b). In contrast, loss of *GA20ox1* and *GA20ox2* do not cause a defect in root elongation (Rieu et al., 2008), indicating that other *GA20ox* genes have a role in controlling root elongation. The study by Rieu and colleagues (2008) used qRT-PCR to monitor the expression of the five *GA20ox* genes in several tissues including roots. They demonstrated that *GA20ox1*, *GA20ox2*, and *GA20ox3* are the most highly expressed *GA20ox* genes within the root. This is supported by meta-analysis of three recent microarray studies (Figure 11-1) performed in the Benfy lab (Brady et al., 2007), the Serres lab (Mustroph et al., 2009), The University of Nottingham's Centre for plant integrative biology (CPIB) group (unpublished data) and was also demonstrated by Dugardeyn et al., 2008. *AtGA20ox1*, *AtGA20ox2*, and *AtGA20ox3* expression peaks within the MS and gradually decreases with distance from the QC. The cell type-specific rescue experiments rely on the fact that the *ga20ox1,-2,-3* triple mutant plant has a dwarf root phenotype (Figure 5-2).

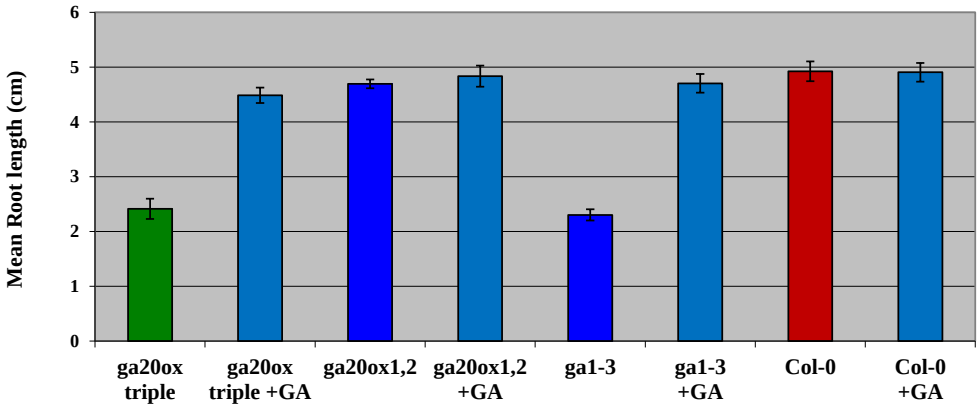

Figure 5-2**: Comparison of the root length ±SE of *ga20ox* mutants.** Primary root length are shown for *ga20ox1,-2,-3* triple mutants, *ga20ox1,2* double mutants, *ga1-3* and Col-0 at seven days when grown with and without GA. 30 plants were analysed, seedlings were grown on vertical Gelrite plates and lengths calculated using ImageJ. The error bars show the standard error for each line.

5.1.1 Characterisation of root growth in the *ga20ox* mutants

The *ga20ox1,-2,-3* triple mutant was generated by Omar Nilsson, Nieves Fernandez and Andy Plackett and contains two previously characterised null mutations in *GA20ox1* and *GA20ox2* (Rieu et al., 2008b) and a point mutation in *GA20ox3*, identified by Targeting Induced Local Lesions in Genomes (TILLinG), introducing a stop codon which in *in vitro* assays abolishes *GA20ox3* activity (personal correspondence with Andy Plackett). The triple mutant has reduced root length that is comparable to that in the GA-deficient mutant *ga1-3* (Figure 5-2), indicating it is highly deficient in GA and suitable for the targeted expression study. The effect of targeting the expression of *AtGA20ox1* with tissue specific promoters on the phenotype of *ga20ox1,-2,-3* plants was initially monitored by observing effects on the final root length after seven days growth, as well as on the vegetative growth of the rosette after three weeks growth, and the inflorescence growth after six weeks. The median line and closest lines were then selected for a further more detailed analysis of root growth, measuring root lengths, meristem lengths, and final cell sizes. In all experiments the transgenic lines were compared with Col-0 as this was the original ecotype that the *ga20ox1,-2,-3* was generated in and *ga20ox1,-2,-3* as this was the GA deficient mutant that was genetically modified for the targeted YFP-GA20ox1 rescue.

5.1.2 Expression of *SHR::YFP:AtGA20ox1* failed to rescue root length and vegetative development of the *ga20ox1,-2,*-3 mutant

To investigate the effect of targeting YFP-GA20ox1 to the root stele in *ga20ox1,-2,-3,* expression of this transgene was driven by the *SHR* promoter (Di Laurenzio et al., 1996). The final root lengths of six homozygous lines expressing the transgene were compared with Col-0 and *ga20ox1,-2,*-3 following 7 days growth on vertical plates. In all six independent transgenic lines no rescue of either the root growth or the vegetative growth was observed compared to the controls (Figure 5-3 and Figure 5-4). The root length of line A was not significantly larger than *ga20ox1,-2,-3* ($p>0.05$), while line B was not significantly different from lines A and C ($p>0.05$). The root length of Line F was significantly shorter than all the other genotypes ($p>0.01$) and its vegetative growth could not be rescued by exogenous GA_3 indicating that the transformation may have disrupted the function of another important gene so this line was not used for further analysis. Lines A, B and C had the most consistent phenotypes so were chosen for further analysis.

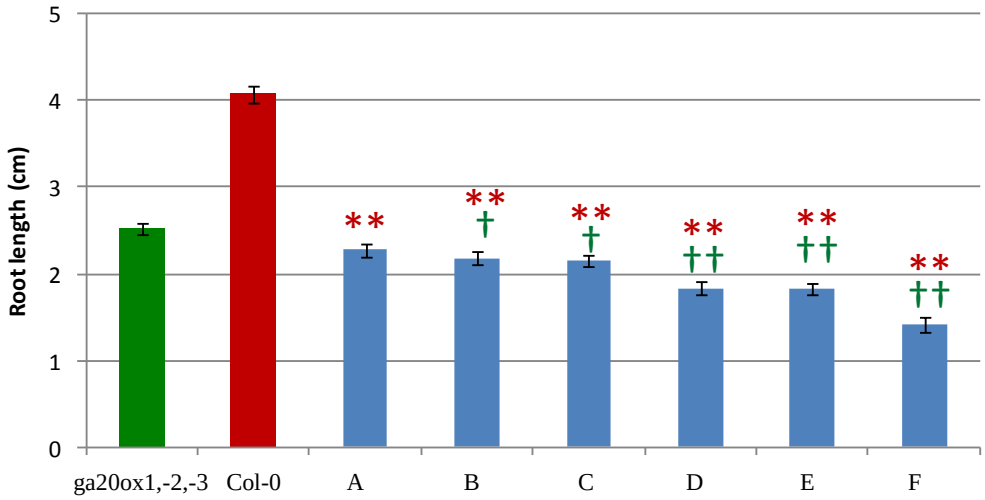

Figure 5-3**: Primary root lengths ±SE of *ga20ox1,-2,-3;SHR::YFP:AtGA20ox1* transgenic lines (A-F) compared to *ga20ox1,-2,-3* and Col-0 at seven days.** Seedlings were grown on vertical plates and lengths calculated using ImageJ. Values shown represent the average of 30 seedlings ±SE. Green crucifix indicates the transgenic lines are significantly different from *ga20ox1,-2,-3* and the red asterisk indicates if they are significantly different from Col-0. 30 plants for each line were analysed. **= p<0.01, †=p<0.05 and ††=p<0.01. Error bars are standard error. REML was used to generate the LSD given in Table 11-5.

Figure 5-4: **Vegetative phenotypes of *ga20ox1,-2,-3;SHR::YFP:AtGA20ox1* lines compared to *ga1-3, ga20ox1,-2,-3* and Col-0.** Plants were grown on Levingtons compost in 5.5-cm pots under long days for 3weeks (A) or 6 weeks (B).

5.1.3 *ga20ox1,-2,-3;SHR::YFP:AtGA20ox1:* root length, meristem length, cell length and transgene expression profile.

To determine whether the transgene was expressed in the expected tissue-specific localisation, confocal microscopy was performed on the five roots from the selected representative lines when the seedlings were 7 days old. YFP fluorescence could only be observed within the stele of the meristematic region if image enhancement was used (Figure 2-2). In contrast, the YFP signal within the endodermis of the differentiation zone was observed at a higher level (Figure 2-2 A-C).

A detailed analysis of the primary root growth characteristics was subsequently performed on the three selected independent *ga20ox1,-2,-3;SHR::YFP-AtGA20ox1* lines. Initially, the primary root lengths for 15 plants from each line were compared with *ga20ox1,-2,-3* and Col-0. In good correlation with the initial characterisation described above (section 0; Figure 5-3), there was no rescue of root growth compared to *ga20ox1,-2,-3.* In addition to root length, the meristem size and cortical cell lengths were determined for five plants (five cortical cells were measured for each plant) from each of these lines and compared to the *ga20ox1,-2,-3* and Col-0 controls. The meristem and final cortical cell lengths of all three lines were not significantly different from *ga20ox1,-2,-3* ($p>0.05$), but were significantly smaller than in Col-0 ($p<0.01$).

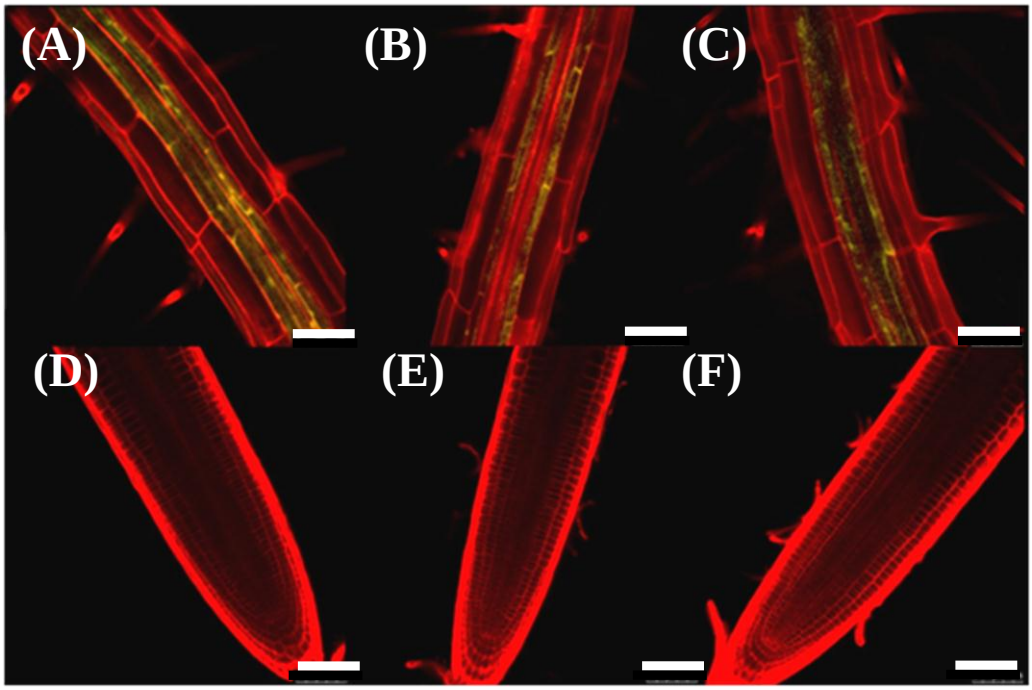

Figure 5-5**:** ***ga20ox1,-2,-3;SHR::YFP:AtGA20ox1*** **fluorescence in the meristematic region and the differentiation zone. (A-C)** Florescence in the differentiation zone is shown for lines A, B and C, respectively. **(D-F)** Fluorescence in the meristematic region for lines A, B and C, respectively. Confocal microscopy was performed on the five roots of seven day old seedlings after being grown on vertical Gelrite plates. The YFP and the propidium iodide emission images are overlain. Bars are 50 μm in length.

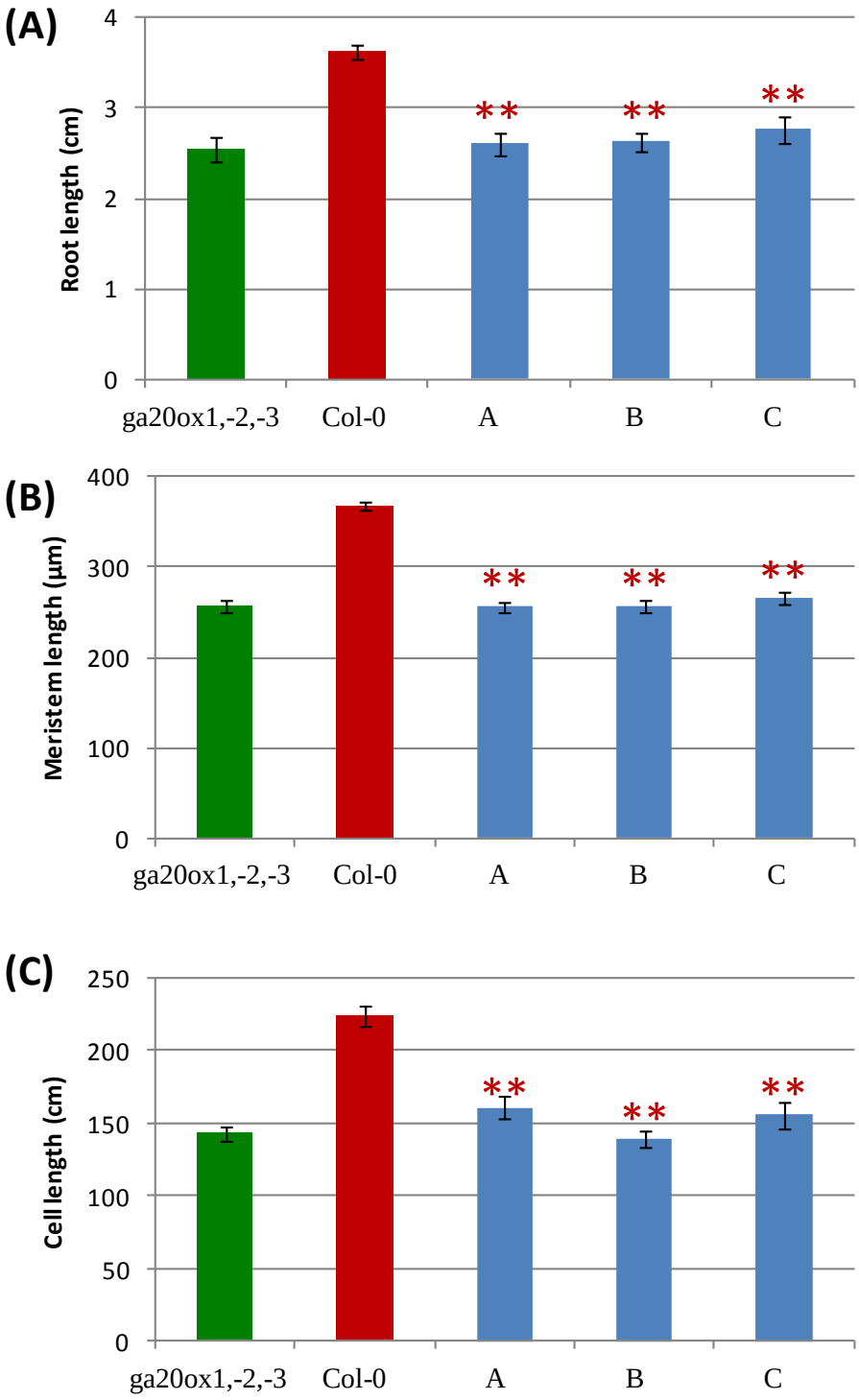

Figure 5-6**: Primary root parameters for *ga20ox1,-2,-3;SHR::YFP:AtGA20ox1* lines A, B and C compared with Col-0 and *ga20ox1,-2,-3* at seven days. (A)** Primary root length ±SE. **(B)** Proximal meristem length ±SE. **(C)** Final cortical cell length ±SE. Seedlings were grown on vertical plates for 7 days and lengths calculated using ImageJ. The red asterisks indicate that the transgenic lines are significantly different from Col-0. 15 plants for each line were measured for root length, and 5 for meristem size and final cell length, with the lengths of 5 cells being measured **= $p<0.01$. Error bars are standard error. REML was used to generate the LSD given in Table 11-9.

5.1.4 Expression of *SCR::YFP:AtGA20ox1* partially rescued root length and completely rescued vegetative development of the *ga20ox1,-2,-3* mutant

To investigate the effect of performing the oxidation of C-20 specially within the endodermis, the *SCR* promoter was used to drive the expression of *YFP-AtGA20ox1* in the *ga20ox1,-2,-3* mutant background (Di Laurenzio et al., 1996). Subsequent analysis of six transgenic lines revealed that the root length of line E was not significantly different from *ga20ox1,-2,-3* ($p>0.05$) (Figure 5-7), while in contrast the root length of lines A and D were not significantly different from Col-0 ($p>0.05$). In addition, the vegetative growth of line E could not be rescued by application of exogenous GA_3 (qualitative data not shown) so this line was discounted from further analysis. The root length of line C was closest to the median, while lines B and F were not significantly different from line C ($p>0.01$) so they were chosen for further analysis (Figure 5-7). The incorporation of the *SCR::YFP:AtGA20ox1* transgene was able to partially rescued the shoot growth of *ga20ox1,-2,-3* in lines A and F, completely rescue the shoot growth of line B and even made lines C and D larger than Col-0 (Figure 5-8).

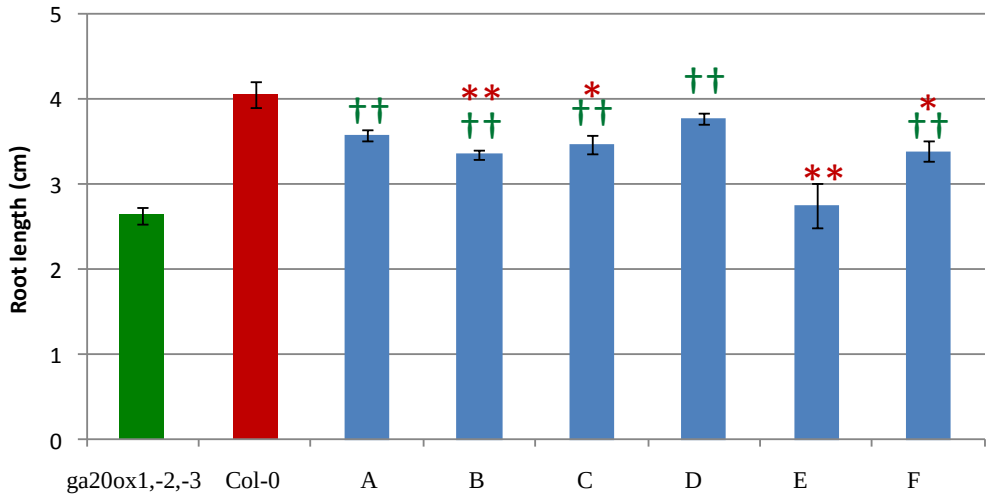

Figure 5-7**: Primary root length for *ga20ox1,-2,-3;SCR::YFP:AtGA20ox1* lines (A-F) compared to *ga20ox1,-2,-3* and Col-0 after seven days growth.** Green crucifixes indicate the transgenic lines are significantly different from *ga20ox1,-2,-3* and the red asterisks indicate they are significantly different from Col-0. 30 plants for each line were analysed *=p<0.05, **=p<0.01, †=p<0.05 and ††=p<0.01. Error bars are standard error. REML was used to generate the LSD given in Table 11-5.

Figure 5-8**: Vegetative phenotypes for *ga20ox1,-2,-3;SCR::YFP:AtGA20ox1* lines (A-F) compared to *ga1-3, ga20ox1,-2,-3* and Col-0.** Plants were grown on Levingtons compost in 5.5cm pots under long day at three (A) and six weeks (B).

5.1.5 *ga20ox1,-2,-3;SCR::YFP:AtGA20ox1:* root length, meristem length, cell length and transgene expression profile

To investigate the effect of expressing *YFP-AtGA20ox1* under control of the *SCR* promoter in the *ga20ox1,-2,-3* triple mutant background, plants from three representative lines were compared to *ga20ox1,-2,-3* and Col-0. In agreement with the previous characterisation (section 5.1.4), root growth of the *ga20ox1,-2,-3* triple mutant was partially rescued. The meristem and final cortical cell lengths of lines C and F were not significantly different from Col-0 ($p>0.05$) but the root lengths were both slightly shorter than Col-0 ($p<0.05$) although significantly longer than *ga20ox1,-2,-3* ($p<0.01$). Line B was more variable and had a root length that was significantly shorter than Col-0 ($p>0.05$) due to a reduction its final cell length. However, similar to the other two lines that were analysed, line B was found to have a longer root than *ga20ox1,-2,-3* ($p<0.01$).

In all three *ga20ox1,-2,-3*;*SCR::YFP:AtGA20ox1* lines, YFP fluorescence could be observed within the endodermis of the meristematic, elongation and differentiation zones (Figure 5-10). However, it appeared to be variable and could occasionally be observed within the cortical cells or disappear from the meristematic region completely. When plants were sown on plates containing 1 µM PAC, YFP fluorescence increased dramatically within both the endodermal and cortical cells of the meristematic region while mildly decreasing in the elongation zone. Interestingly, the changes in fluorescence also appeared to be distributed asymmetrically. When plants were grown on control plates or those containing 1 µM GA no YFP fluorescence could be observed within the proximal meristematic region (Figure 5-11).

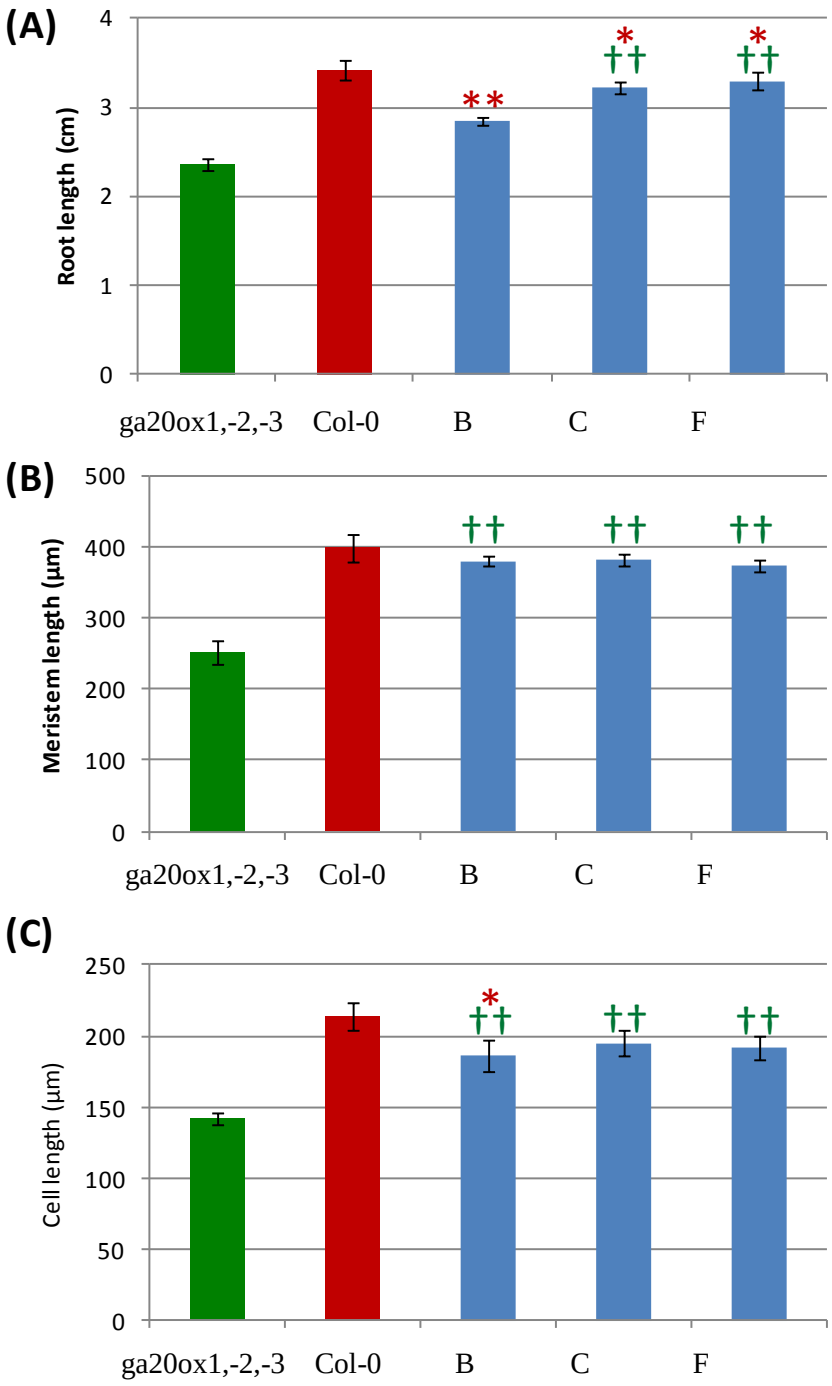

Figure 5-9**: Primary root parameters for *ga20ox1,-2,-3;SCR::YFP:AtGA20ox1* lines B, C and F compared with Col-0 and *ga20ox1,-2,-3* at seven days. (A)** Primary root length ±SE. **(B)** Proximal meristem length ±SE. **(C)** Final cortical cell length ±SE. Seedlings were grown on vertical plates and lengths calculated using ImageJ. Green crucifixes indicate the transgenic lines are significantly different from *ga20ox1,-2,-3* and the red asterisks indicate they are significantly different from Col-0. 15 plants for each line were measured for root length, and 5 for meristem size and final cell length, with the lengths of 5 cells being measured. *= $p<0.05$, **= $p<0.01$, and ††=$p<0.01$. Error bars are standard error. REML was used to generate the LSD given in Table 11-9.

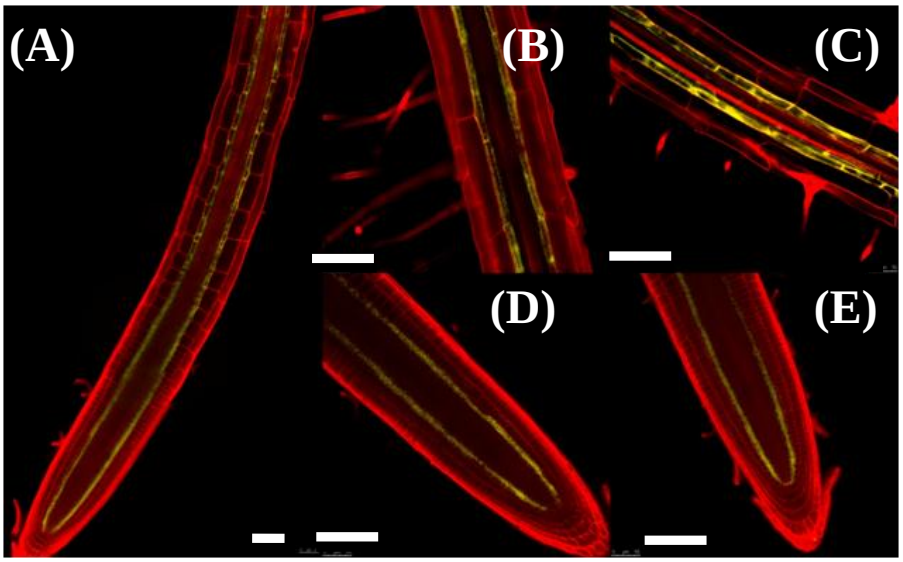

Figure 5-10**:** ***ga20ox1,-2,-3;SCR::YFP:AtGA20ox1*** **fluorescence in the endodermal meristematic region and the differentiation zone. (A)** Fluorescence in the meristematic and elongation zones for line B. **(B-C)** *SCR::YFP:AtGA20ox1* expression within the differentiation zone for lines C and F, respectively. (D-E) Fluorescence in the meristematic region for lines B and F, respectively. Confocal microscopy was performed on the five roots of seven day old seedlings after being grown on vertical Gelrite plates. The YFP and the propidium iodide emission images are overlain. Bars are 100 μm in length.

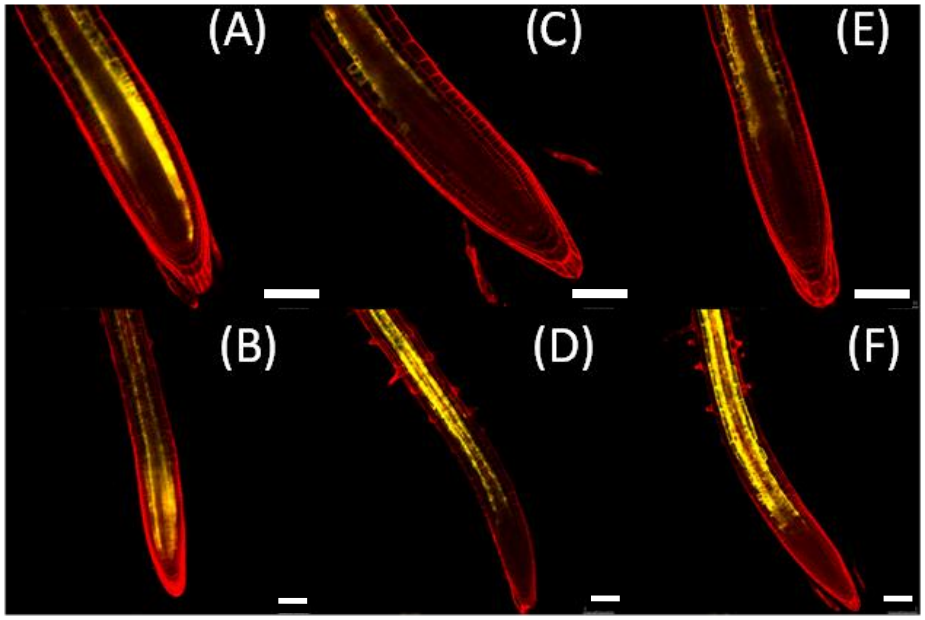

Figure 5-11: ***ga20ox1,-2,-3;SCR::YFP:AtGA20ox1*** **fluorescence responding to GA and PAC treatment. (A-B)** YFP florescence in the meristematic region of *SCR::YFP:AtGA2ox2* line D is shown for plants grown on Gelrite containing 1μM PAC. **(C-D)** when grown on control Gelrite. **(E-F)** when grown on Gelrite containing 1μM GA_3. The YFP and the propidium iodide emission images are overlain. Confocal microscopy was performed on the five roots of seven day old seedlings after being grown on vertical Gelrite plates. Bars are 100 μm in length.

5.1.6 Expression of *CoR::YFP:AtGA20ox1* failed to rescue root length and vegetative development of the *ga20ox1,-2,-3* mutant

To investigate the effect of confining GA 20-oxidation to the cortex cells of the elongation zone, *YFP-AtGA20ox1* expression was driven using the *CoR* promoter (Dinneny et al., 2008) in the *ga20ox1,-2,-3* mutant background, and the primary root length measured. The transgene was unable to rescue either the root or shoot growth of any of the four *ga20ox1,-2,-3;CoR::YFP:AtGA20ox1* transgenic lines (Figure 5-12 and Figure 5-13). The root length of all lines A-D were significantly shorter than Col-0 ($p<0.01$) and lines A-C were also significantly shorter from *ga20ox1,-2,-3* ($p>0.01$ (except C where $p<0.05$)). Line C was the median line for root length and was not significantly different from lines B and D ($p>0.01$) so they were chosen for further detailed analysis.

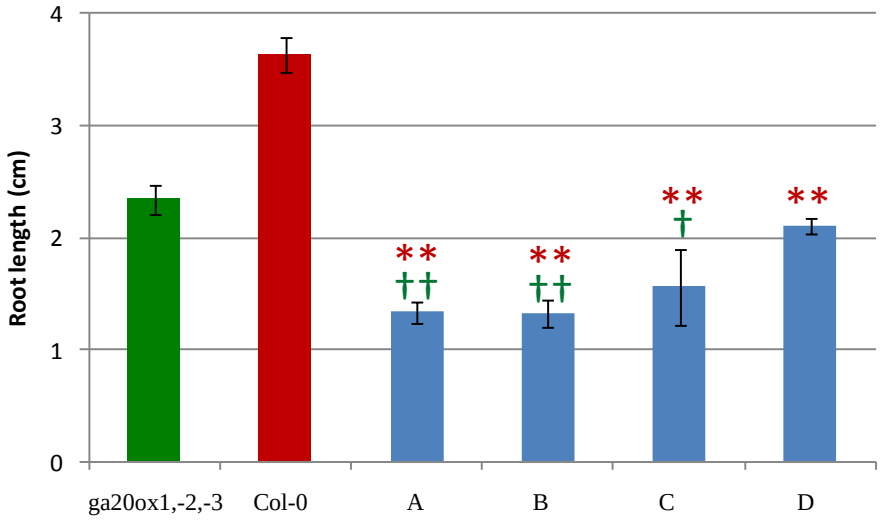

Figure 5-12**: Primary root length for *ga20ox1,-2,-3;CoR::YFP:AtGA20ox1* lines (A-D) compared to *ga20ox1,-2,-3* and Col-0 at seven days.** Seedlings were grown on vertical plates and lengths calculated using ImageJ. Green crucifixes indicate the transgenic lines are significantly different from *ga20ox1,-2,-3* and the red asterisks indicate they are significantly different from Col-0. 30 plants for each line were analysed **=p<0.01, †=p<0.05 and ††=p<0.01. Error bars are standard error. REML was used to generate the LSD given in Table 11-5.

Figure 5-13**: Vegetative phenotypes for *ga20ox1,-2,-3;CoR::YFP:AtGA20ox1* lines (A-D) compared to *ga1-3, ga20ox1,-2,-3* and Col-0.** Plants were grown on Levingtons compost in 5.5-cm pots under long day at three (A) and six weeks (B).

5.1.7 *ga20ox1,-2,-3;CoR::YFP:AtGA20ox1:* root length, meristem length, cell length and transgene expression profile

The characteristics of the primary root for the three representative lines were compared with those of *ga20ox1,-2,-3* and Col-0. The transgene in all three lines had flouresence within the cortex and endodermis (the ground tissue tissue) of the elongation zone, and to a lesser extent in the cortical cells of the differentiation zone, but was always completely excluded from the meristematic region (Figure 5-14). Interestingly, the YFP floresence was observed not only in the cytoplasm but also within the nucleus and was often stronger on one side of the root (Figure 5-14 (B)). In good correlation with the previous characterisation (section 5.1.6), expression of the *CoR::YFP:AtGA20ox1* transgene was unable to rescue the root growth of the *ga20ox1,-2,-3* triple mutant. The root, meristem and final cell lengths of all three lines were all identical to *ga20ox1,-2,-3* ($p>0.05$) (Figure 5-15).

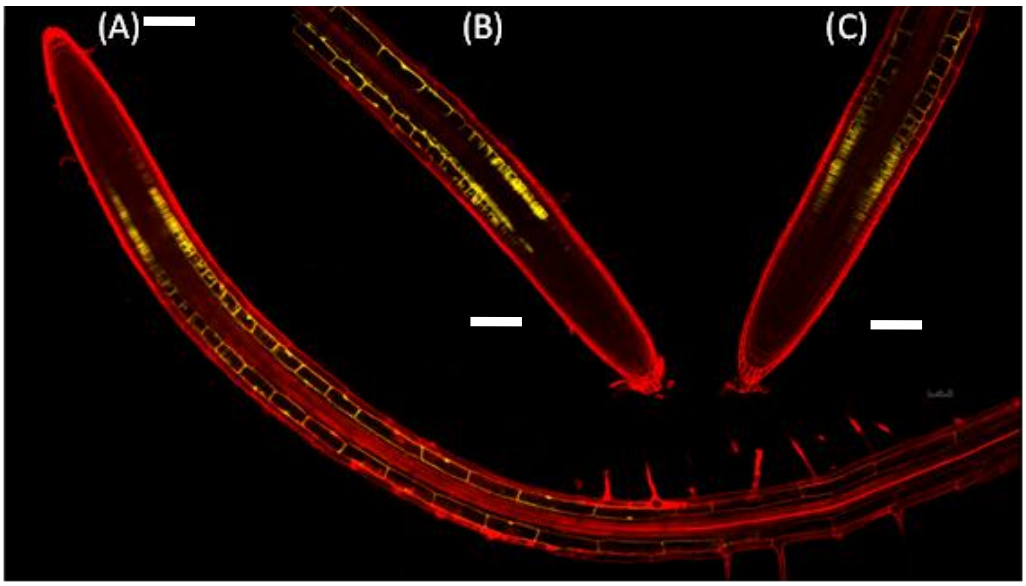

Figure 5-14**: YFP fluorescence in the roots of *ga20ox1,-2,-3;CoR::YFP:AtGA20ox1* lines. (A)** Florescence in the meristematic, elongation and differentiation zones for line B. **(B-C)** Fluorescence within the meristematic and elongation zones for lines C and D respectively. Confocal microscopy was performed on the five roots of seven day old seedlings after being grown on vertical Gelrite plates. The YFP and the propidium iodide emission images are overlain. Bar is 100 μm in length.

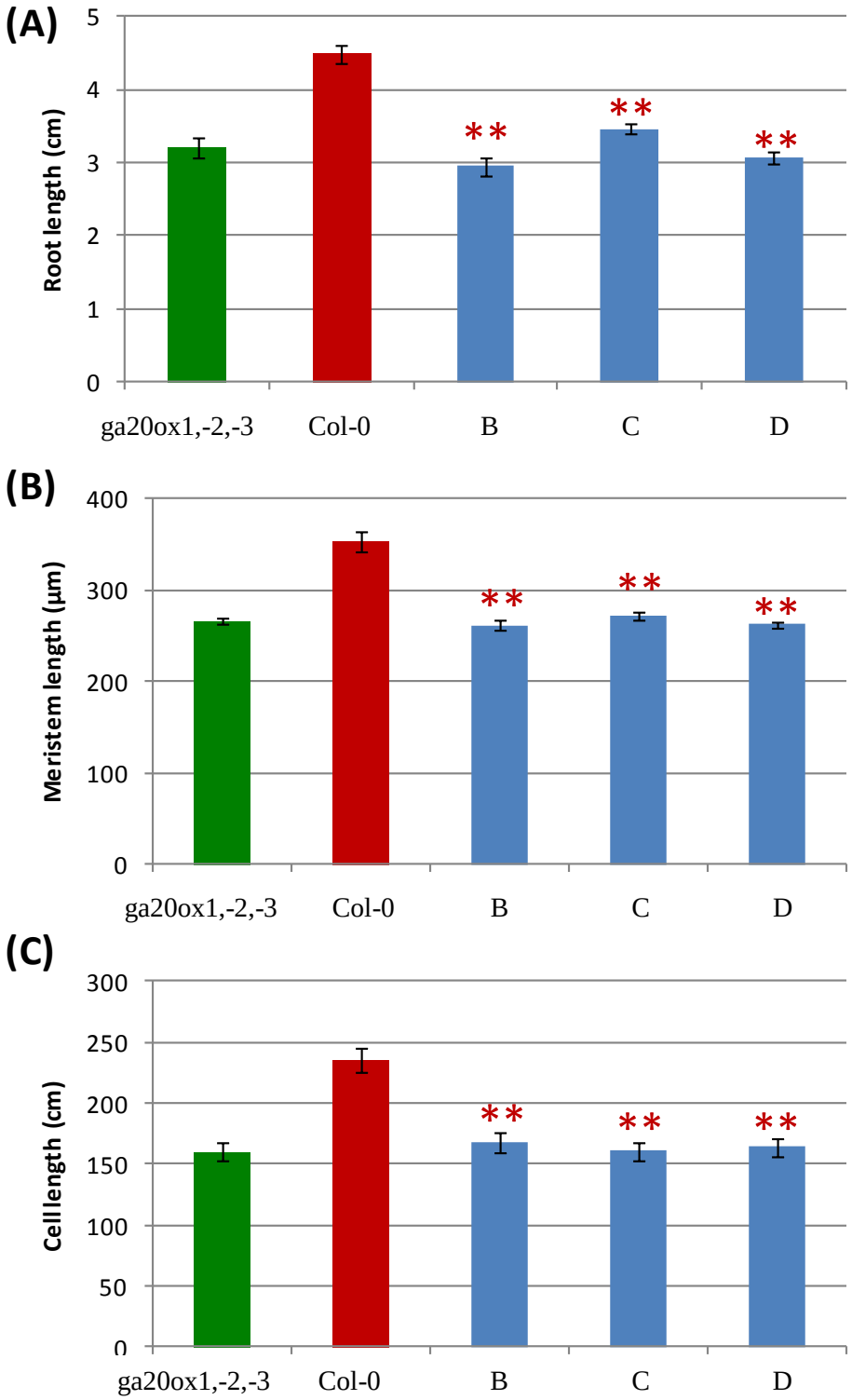

Figure 5-15**: Primary root parameters for *ga20ox1,-2,-3;CoR::YFP:AtGA20ox1* lines compared with Col-0 and *ga20ox1,-2,-3* at seven days. *3.*** **(A)** Primary root length ±SE. **(B)** Proximal meristem length ±SE. **(C)** Final cortical cell length ±SE. Seedlings were grown on vertical plates and lengths calculated using ImageJ. The red asterisks indicate the transgenic lines are significantly different from Col-0. 15 plants for each line were measured for root length, and 5 for meristem size and final cell length, with the lengths of 5 cells being measured **= $p<0.01$. Error bars are standard error. REML was used to generate the LSD given in Table 11-9.

5.1.8 Expression of *Co2::YFP:AtGA20ox1* partially recued root length and vegetative development of the ga20ox1,-2,-3 mutant

In order to investigate the effect of specifically performing 20-oxidation within the meristematic cortical cells, the targeted expression of *YFP-AtGA20ox1* from the *Co2* promoter (Heidstra et al., 2004) was performed in the *ga20ox1,-2,-3* mutant background. Six transgenic lines expressing this construct had partially rescued root and vegetative growth (Figure 5-16 andFigure 5-17). Line A had a variable phenotype that was occasionally giant and sometimes dwarf. Subsequent PCR analysis of gDNA revealed that this line was segregating for the three *ga20ox* mutations (Figure 3-26, Figure 3-27 and Figure 3-28) so was discounted from further analysis. The root length of line E was not significantly different from *ga20ox1,-2,-3* ($p<0.05$); lines B, C, D, and F were all significantly larger than *ga20ox1,-2,-3* ($p<0.01$) and significantly smaller than Col-0 ($p<0.01$). As lines B, C and D were not significantly different from one another they were chosen for further analysis.

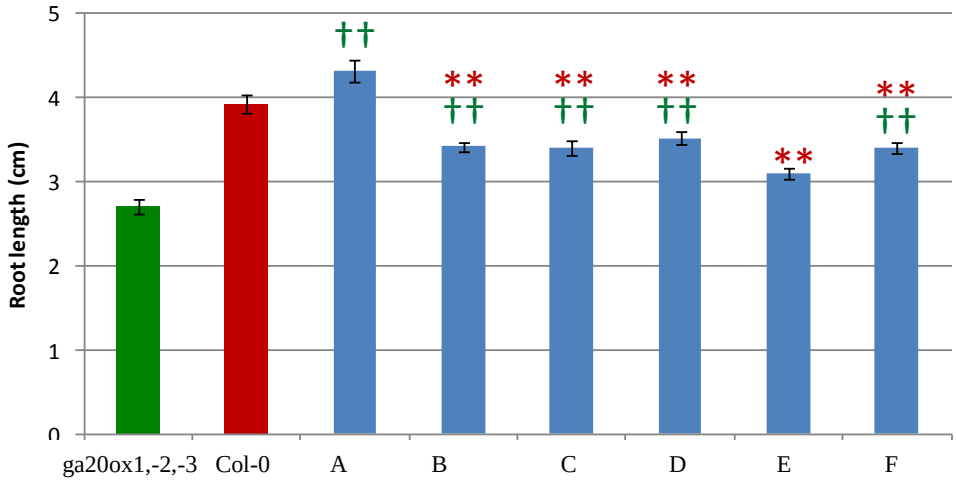

Figure 5-16**: Primary root length ±SE for *ga20ox1,-2,-3;Co2::YFP:AtGA20ox1* lines (A-F) compared to *ga20ox1,-2,-3* and Col-0 at seven days.** Seedlings were grown on vertical plates and lengths calculated using ImageJ. Green crucifixes indicate the transgenic lines are significantly different from *ga20ox1,-2,-3* and the red asterisks indicate they are significantly different from Col-0. 30 plants for each line were analysed **= $p<0.01$ and ††=$p<0.01$. Error bars are standard error. LSD are given in Table 11-5.

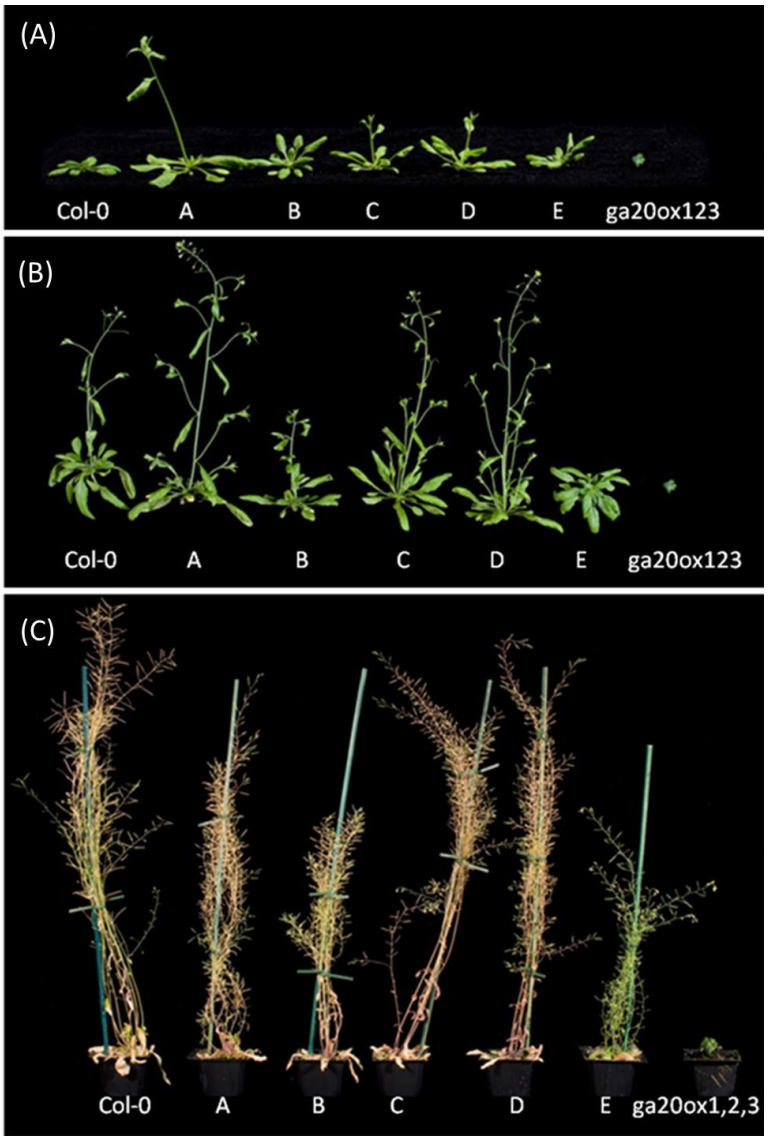

Figure 5-17: **Vegetative phenotypes for *ga20ox1,-2,-3;Co2::YFP:AtGA20ox1* lines (A-E) compared to *ga20ox1,-2,-3* and Col-0.** Plants were grown on Levingtons compost in 5.5-cm pots under long day for three (A), four (B), and six weeks (C).

5.1.9 *ga20ox1,-2,-3;Co2::YFP:AtGA20ox1:* root length, meristem length, cell length and transgene expression profile

To investigate the effect of expressing YFP-AtGA20ox1 with the *Co2* promoter in the *ga20ox1,-2,-3* triple mutant background, plants from three representative lines were compared with *ga20ox1,-2,-3* and Col-0. Confocal microscopy demonstrated that all three lines displayed YFP fluoresence within the cortical cells throughout the meristematic region (Figure 5-18). In agreement with the previous characterisation (section 5.1.8), *Co2::YFP:AtGA20ox1* expression partially rescued root growth of the *ga20ox1,-2,-3* triple mutant. Root lengths, meristem lengths and final cell lengths of all three lines were significantly larger than *ga20ox1,-2,-3* ($p<0.01$), but were also significantly smaller than Col-0 ($p<0.01$), except the final cell length of line D that was not significantly different *ga20ox1,-2,-3* ($p>0.05$) (Figure 5-19).

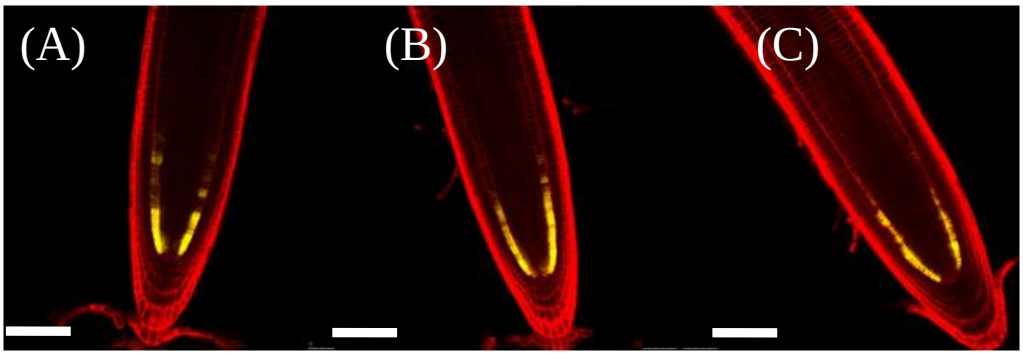

Figure 5-18**: YFP fluorescence in the cortical meristematic cells of *ga20ox1,-2,-3;Co2::YFP:AtGA20ox1* lines. (A-C)** Fluorescence in the meristematic zones for lines B, C and D. Confocal microscopy was performed on the five roots of seven day old seedlings after being grown on vertical Gelrite plates. The YFP and the propidium iodide emission images are overlain. Bars are 50 μm in length.

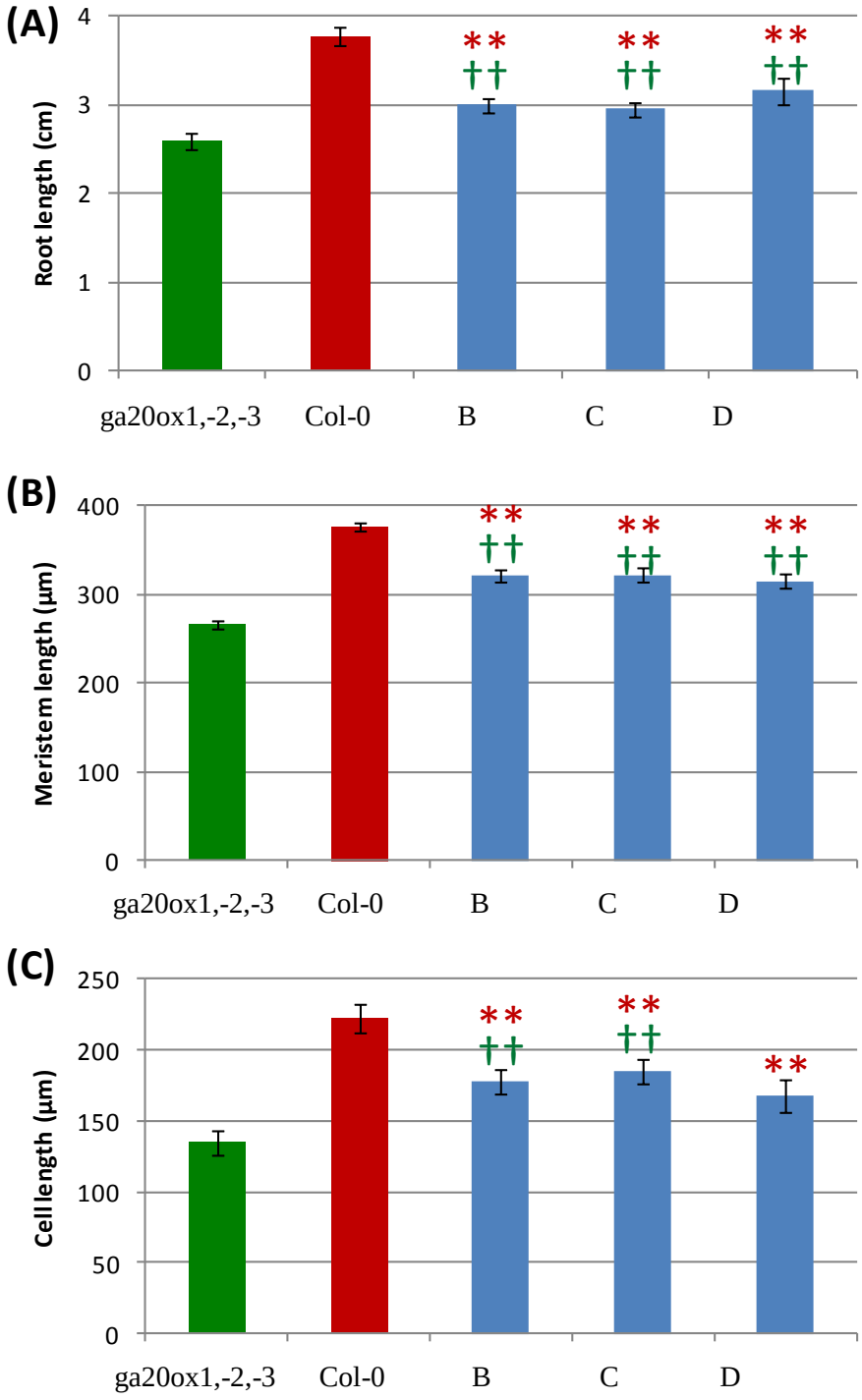

Figure 5-19**: Primary root parameters for *ga20ox1,-2,-3;Co2::YFP:AtGA20ox1* lines B, C and D compared with Col-0 and *ga20ox1,-2,-3* at seven days. (A)** Primary root length ±SE. **(B)** Proximal meristem length ±SE. **(C)** Final cortical cell length ±SE. Seedlings were grown on vertical plates and lengths calculated using ImageJ. Green crucifixes indicate the transgenic lines are significantly different from *ga20ox1,-2,-3* and the red asterisks indicate they are significantly different from Col-0. 15 plants for each line were measured for root length, 15 plants for each line were measured for root length, and 5 for meristem size and final cell length, with the lengths of 5 cells being measured **= $p<0.01$ and ††=$p<0.01$. Error bars are standard error. REML was used to generate the LSD shown Table 11-9.

5.1.10 *ga20ox1,-2,-3;Co2::YFP:AtGA20ox1* x *ga20ox1,-2,-3;CoR::YFP:AtGA20ox1:* root length, meristem length, cell length and transgene expression profile

To investigate the effect of expressing *YFP-AtGA20ox1* within both the elongation zone and meristematic region of the cortex *ga20ox1,-2,-3*;*Co2::YFP:AtGA20ox1* line D was crossed with *ga20ox1,-2,-3*;*CoR::YFP:AtGA20ox1* line C. Confocal microscopy on F2 homozygotes showed YFP fluoresence in the cortical cells of both the elongation and meristematic zones (

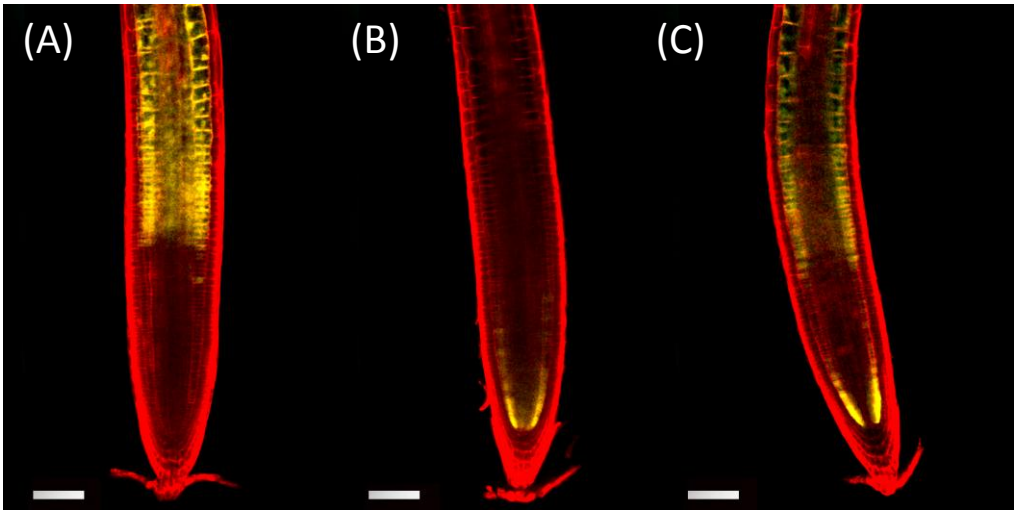

Figure 5-20C). The root length of the crossed line was not significantly different from Col-0 ($p>0.05$). In good agreement with the previous characterisation (section 5.1.8) of the *ga20ox1,-2,-3*;*Co2::YFP:AtGA20ox1* lines, the *ga20ox1,-2,-3*;*Co2::YFP:AtGA20ox1* /*CoR::YFP:AtGA20ox1* line had a partial rescue of meristem length that was significantly longer than *ga20ox1,-2,-3* ($p<0.01$) and statistically indistinguishable from the *Co2::YFP:AtGA20ox1* lines ($p>0.05$). However, in contrast to both the *ga20ox1,-2,-3*;*Co2::YFP:AtGA20ox1* and *ga20ox1,-2,-3*;*CoR::YFP:AtGA20ox1* lines (section 5.1.7 and section 5.1.8), final cell length in the *ga20ox1,-2,-3*;*Co2::YFP:AtGA20ox1*/*CoR::YFP:AtGA20ox1* lines was completely rescued and not significantly different from Col-0 ($p>0.05$) (Figure 5-21).

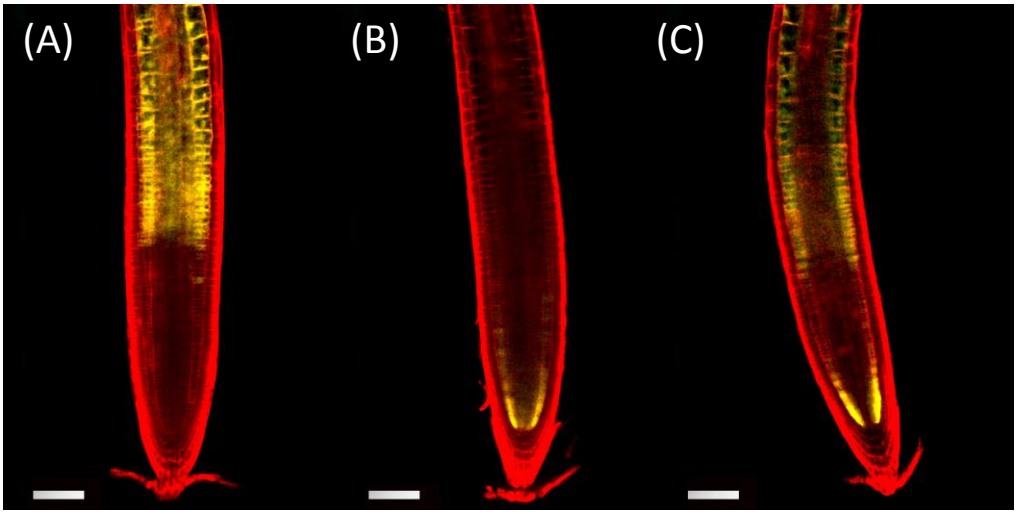

Figure 5-20**: YFP fluorescence *in ga20ox1,-2,-3;Co2::YFP:AtGA20ox1, CoR::YFP:20ox1* and a cross of both lines. (A)** *CoR::YFP:AtGA20ox1*, showing fluorescence in the elongation zone. **(B)** *Co2::YFP:AtGA20ox1*, showing fluorescence in the meristematic zone. **(C)** Fluorescence in both the meristematic region and elongation zone of the F2 cross containing both *Co2::YFP:AtGA20ox1* and *CoR::YFP:20ox1* transgenes. Confocal microscopy was performed on the five roots of seven day old seedlings after being grown on vertical Gelrite plates. The YFP fluorescence and the propidium iodide emission images are overlain. Bars are 100 μm in length.

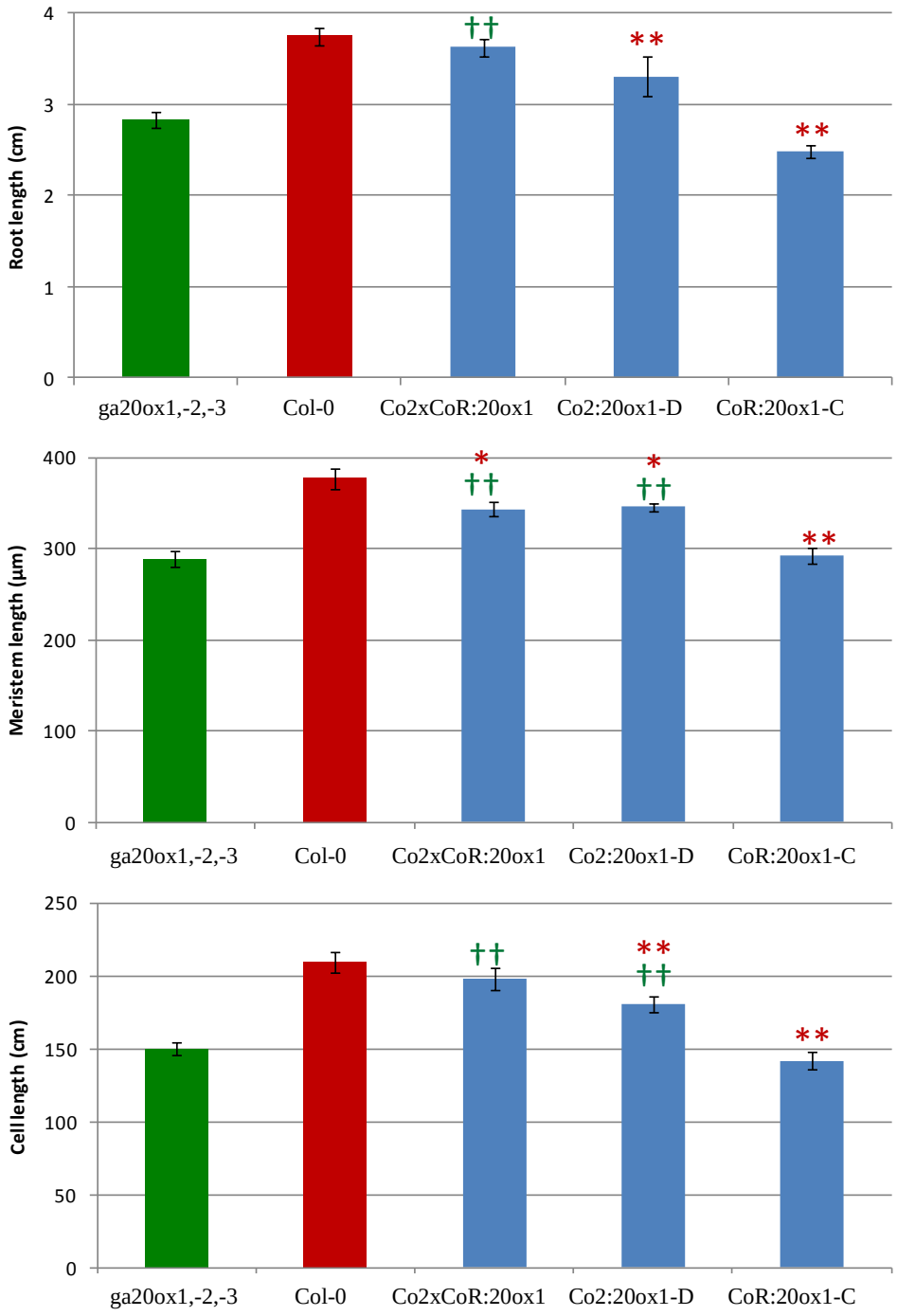

Figure 5-21**: Primary root parameters at 7 days for *ga20ox1,-2,-3;Co2::YFP:AtGA20ox1, ga20ox1,-2,-3;CoR::YFP:AtGA20ox1* and *Co2::YFP:AtGA20ox1 x CoR::YFP:*AtGA20ox1 in the *ga20ox1,-2,-3* background compared with Col-0 and *ga20ox1,-2,-3.* (A)** Primary root length ±SE. **(B)** Proximal meristem length ±SE. **(C)** Final cortical cell length ±SE. Seedlings were grown on vertical plates and lengths calculated using ImageJ. Green crucifixes indicate the transgenic lines are significantly different from *ga20ox1,-2,-3* and the red asterisks indicate they are significantly different from Col-0. 15 plants for each line were measured for root length, and 5 for meristem size and final cell length, with the lengths of 5 cells being measured. **= $p<0.01$ and ††=$p<0.01$. Error bars are standard error. REML was used to generate the LSD given in Table 11-9

5.1.11 Expression of *GL2::YFP:AtGA20ox1* partially rescued root length and vegetative development of the *ga20ox1,-2,-3* mutant

In order to investigate if the specific expression of *AtGA20ox1* within the atrichoblast cells of the root epidermis is important for root growth, *YFP-AtGA20ox1* expression was driven using the *GL2* promoter in the *ga20ox1,-2,-3* triple mutant (Masucci et al., 1996). Subsequent analysis of six transgenic lines indicated that incorporation of the *GL2::YFP:AtGA20ox1* transgene was able to partially rescue root and shoot growth defects in the *ga20ox1,-2,-3* background (Figure 5-22 and 1-24). There was a range of rescue of stem elongation and leaf expansion, although neither were completely rescued, but the plants appeared semi-dwarf with fertile flowers (Figure 5-23). The root lengths of all lines were significantly different from both Col-0 and *ga20ox1,-2,-3* ($p<0.01$). The root lengths of lines B and D were not significantly different from line C ($p<0.01$), which was the line that was closest to the mean of all the transgenic root lengths. Lines B, C and D were therefore chosen for further detailed analysis.

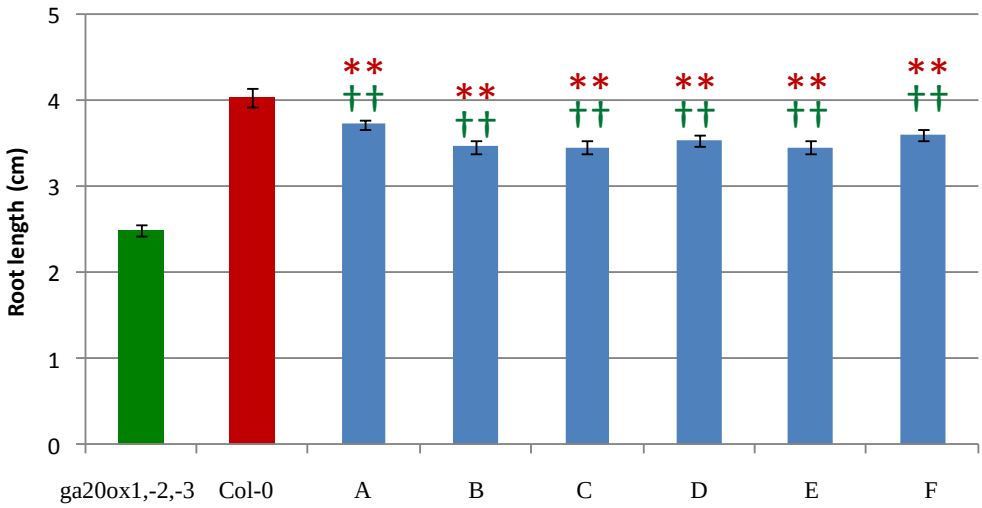

Figure 5-22**: Primary root length ±SE for *ga20ox1,-2,-3;GL2::YFP:AtGA20ox1* lines (A-F) compared to *ga20ox1,-2,-3* and Col-0 at seven days.** Seedlings were grown on vertical plates and lengths calculated using ImageJ. Green crucifixes indicate the transgenic lines are significantly different from *ga20ox1,-2,-3* and the red asterisks indicate if they are significantly different from Col-0. 30 plants for each line were analyzed **= p<0.01 and ††=p<0.01. Error bars are standard error. LSD given in Table 11-5.

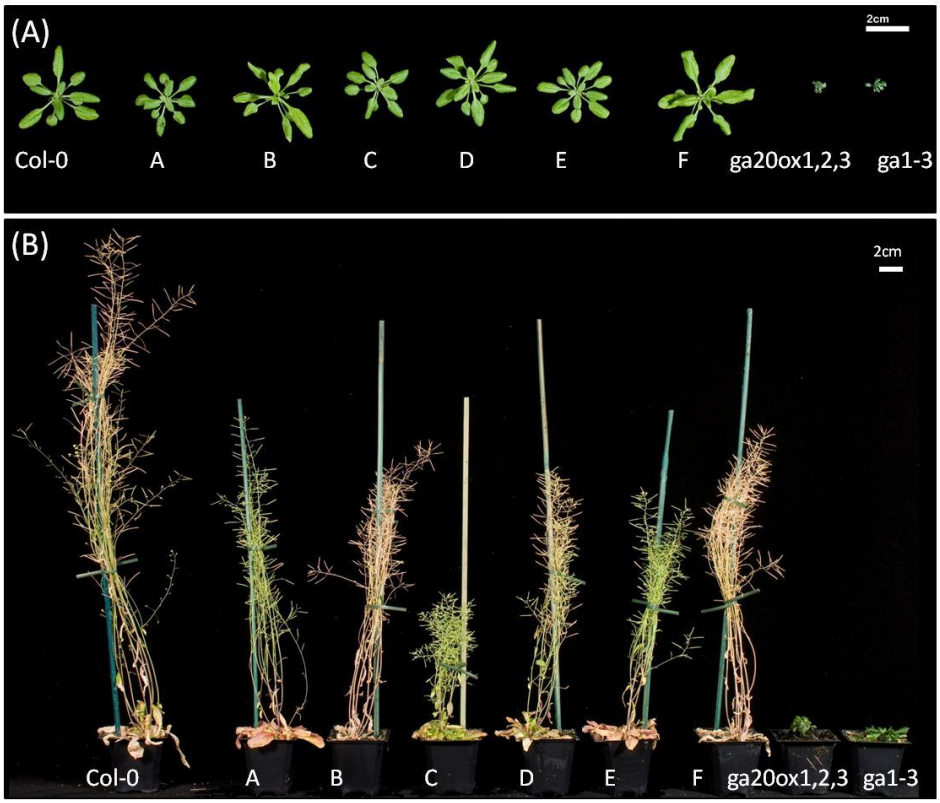

Figure 5-23**: Vegetative phenotypes for *ga20ox1,-2,-3;GL2::YFP:AtGA20ox1* lines (A-F) compared to *ga1-3, ga20ox1,-2,-3* and Col-0.** Plants were grown on Levingtons compost in 5.5cm pots under long days for three (A) and six weeks (B).

5.1.12 *ga20ox1,-2,-3;GL2::YFP:AtGA20ox1* root length, meristem length, cell length and transgene expression profile

Plants from the three representative lines were compared with *ga20ox1,-2,-3* and Col-0. In all three transgenic lines YFP fluorescence was observed within the epidermal atrichoblast cells of the meristematic region, elongation zone and to a lesser extent differentiation zone; in addition, the fluorescence occasionally seemed to be stronger on one side of the root when compared to the other (Figure 5-24A).

In good agreement with the previous characterisation (section 5.1.11), the transgene partially rescued the root growth of *ga20ox1,-2,-3*. The root and meristem lengths of all three lines were significantly smaller than Col-0, but significantly larger than *ga20ox1,-2,-3* ($p<0.01$ (except the meristem length of line D where the meristem is more similar to Col-0 $p<0.05$)) and the final cell lengths of all three lines were not significantly different from Col-0 ($p>0.05$) (Figure 5-25).

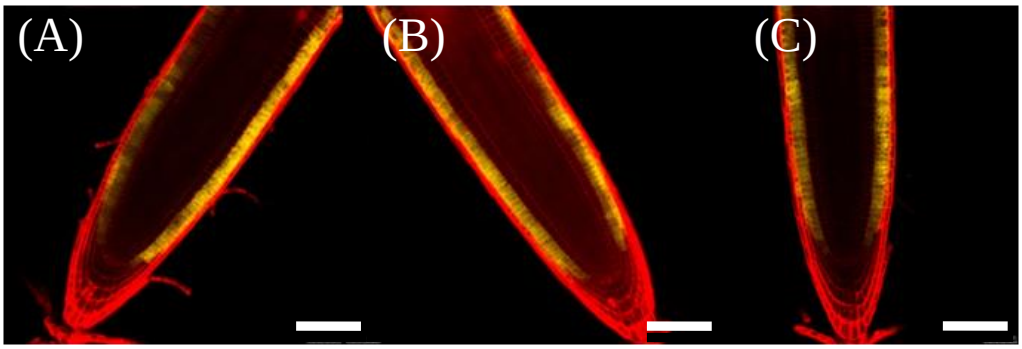

Figure 5-24**: YFP fluorescence in the meristematic epidermal atrichoblast cells of *ga20ox1,-2,-3;GL2::YFP:AtGA20ox1* lines. (A-C)** Fluorescence in the meristematic zones for lines B, C and D. Confocal microscopy was performed on the five roots of seven day old seedlings after being grown on vertical Gelrite plates. The YFP fluorescence and the propidium iodide emission images are overlain. Bars are 100 μm in length.

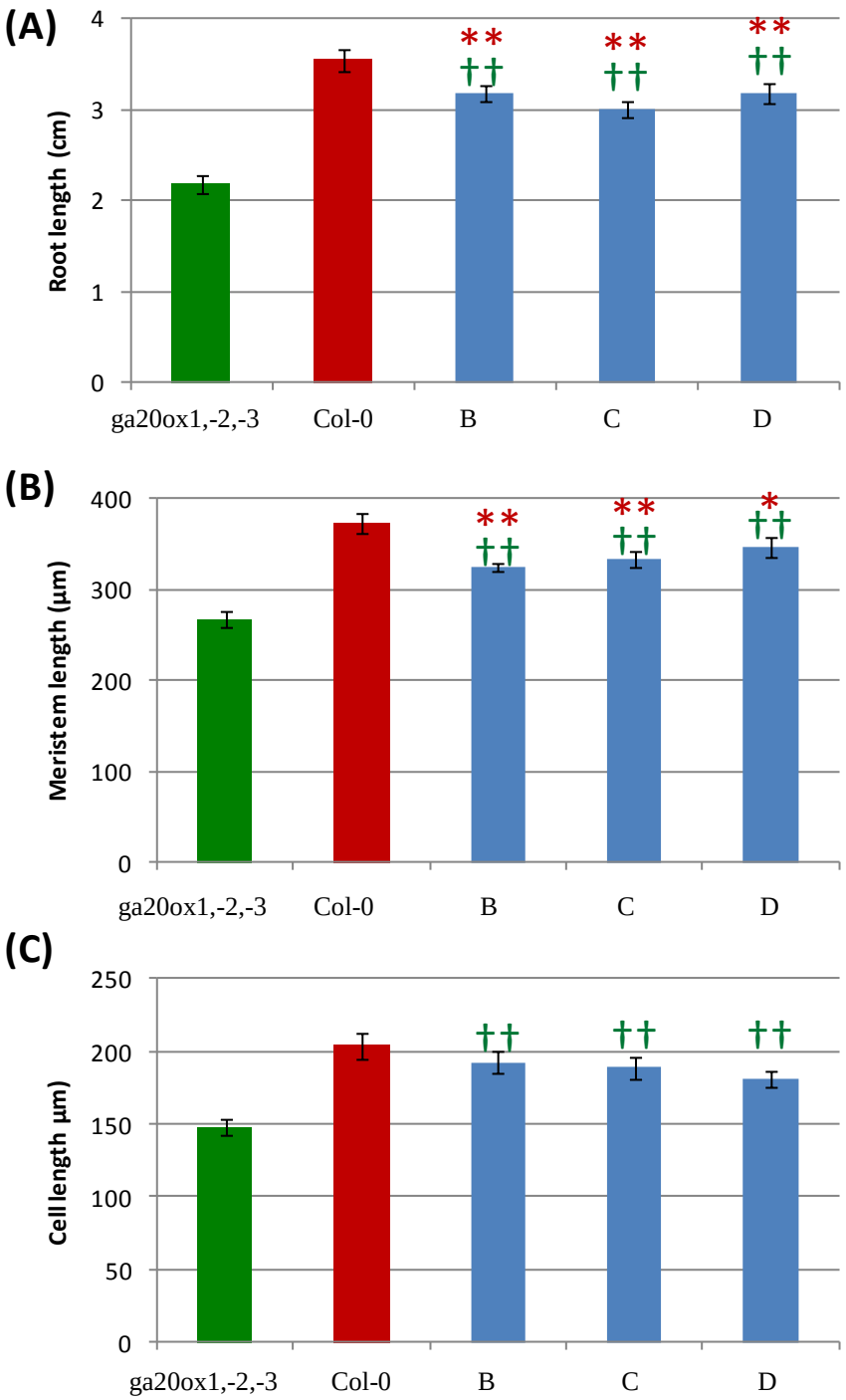

Figure 5-25: **Primary root parameters for *ga20ox1,-2,-3;Co2::YFP:AtGA20ox1* lines B, C and D compared with Col-0 and *ga20ox1,-2,-3* at seven days. (A)** Primary root length ±SE. **(B)** Proximal meristem length ±SE. **(C)** Final cortical cell length ±SE. Seedlings were grown on vertical plates and lengths calculated using ImageJ. Green crucifixes indicate the transgenic lines are significantly different from *ga20ox1,-2,-3* and the red asterisks indicate they are significantly different from Col-0. 15 plants for each line were measured for root length, and 5 for meristem size and final cell length, with the lengths of 5 cells being measured. *= $p<0.05$, **= $p<0.01$ and ††=$p<0.01$. Error bars are standard error. REML was used to generate the LSD given in Table 11-9.

5.1.13 Expression of *CAB::YFP:AtGA20ox1* partially rescued root length and completely rescued vegetative development of the *ga20ox1,-2,-3* mutant

To determine whether bioactive GAs or their precursors moving from the shoot can influence root growth, *AtGA20ox1* was expressed in green aerial tissues of the *ga20ox1,-2,-3* triple mutant. This was achieved by driving *YFP-AtGA20ox1* expression under the *CAB* promoter in the *ga20ox1,-2,-3* mutant background (Puente et al., 1996). Subsequent analysis of six homozygous transgenic lines demonstrated that expression of the transgene partially rescued root growth and completely rescued the shoot growth of lines A-D, but was unable to rescue the root growth of lines E and F (Figure 5-26 and Figure 5-27). Roots of all lines were significantly smaller than those of Col-0 ($p<0.01$) and those of lines A, B, C and D were also significantly larger than *ga20ox1,-2,-3* roots ($p<0.01$). Roots of lines E and F were not significantly different from those of *ga20ox1,-2,-3* ($p>0.05$). Root length in lines A and C was not significantly different ($p>0.05$) so these lines were chosen for further analysis along with line E (Figure 5-26), which was chosen to see if the lack of rescue observed in this line was due to a lower level of expression or altered expression domains.

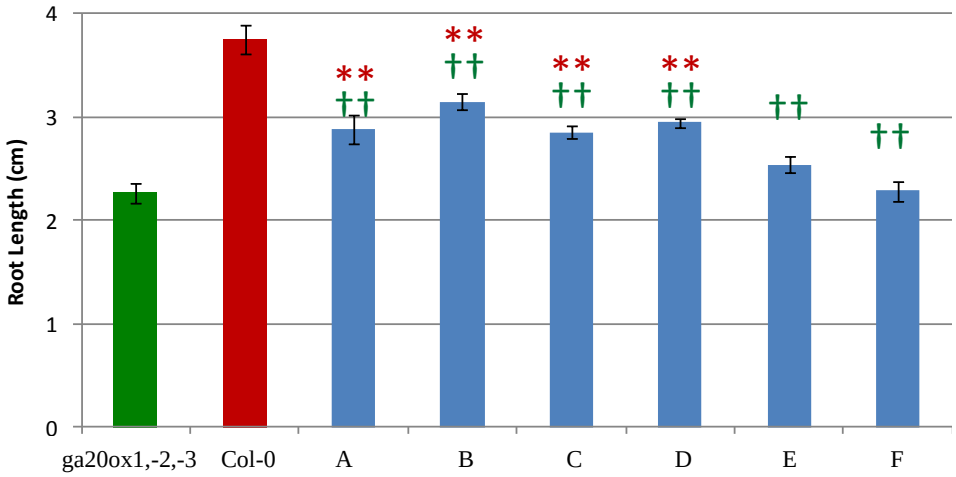

Figure 5-26**: Primary root length ±SE for *ga20ox1,-2,-3;CAB::YFP:AtGA20ox1* lines (A-F) compared to *ga20ox1,-2,-3* and Col-0 at seven days.** Seedlings were grown on vertical plates and lengths calculated using ImageJ. Green crucifixes indicate the transgenic lines are significantly different from *ga20ox1,-2,-3* and the red asterisks indicate they are significantly different from Col-0. 30 plants for each line were analyzed **=p<0.01 and ††=p<0.01. Error bars are standard error.

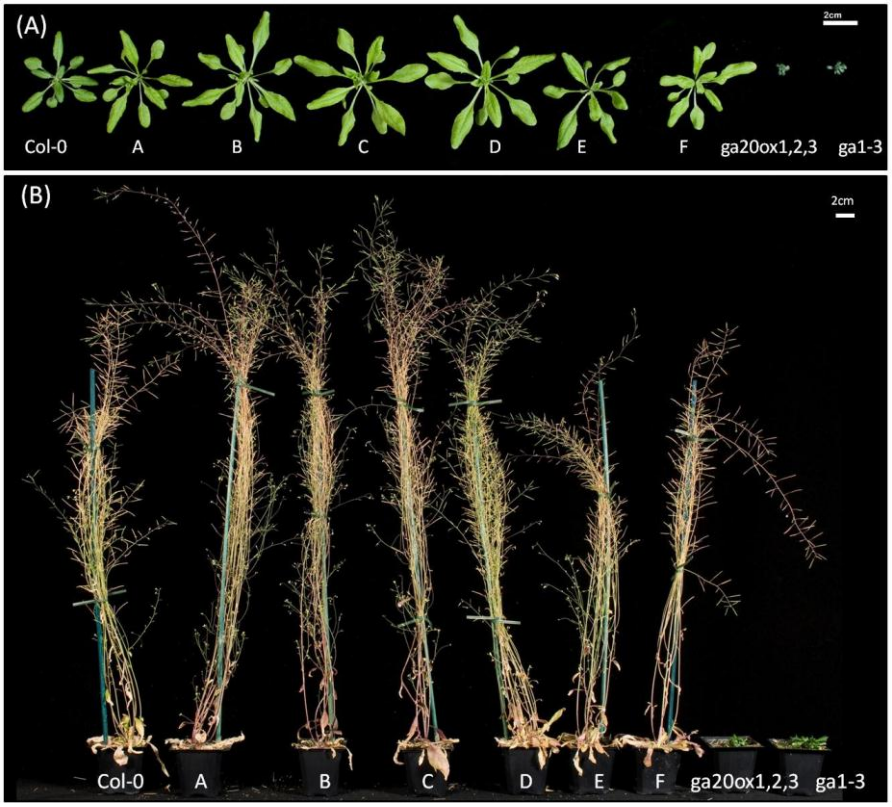

Figure 5-27**: Vegetative phenotypes for *ga20ox1,-2,-3;CAB::YFP:AtGA20ox1* lines (A-F) compared to *ga1-3, ga20ox1,-2,-3* and Col-0.** Plants were grown on Levingtons compost in 5.5cm pots under long day for three (A) and six weeks (B).

5.1.14 *ga20ox1,-2,-3;CAB::YFP:AtGA20ox1:* root length, meristem length, cell length and transgene expression profile

To investigate the effect of expressing *YFP-AtGA20ox1* from the *CAB* promoter in the *ga20ox1,-2,-3* triple mutant background, plants from three representative lines were compared with *ga20ox1,-2,-3* and Col-0. In all three *ga20ox1,-2,-3;CAB::YFP:AtGA20ox1* lines, YFP fluorescence was observed within young green shoot tissue after 7 days of growth (Figure 5-28) and no expression could be observed within any root tissue (data not shown). Inset images show the bright field light microscope image overlaid with the fluorescent image to demonstrate the edge of the leaf and the position of the fluorescence within it. In agreement with the previous characterisation (section 5.1.13), root growth was partially rescued in lines A and C predominantly due to a partial rescue of cell elongation, as shown in Figure 5-29. Line A had a root and final cell length that was significantly different from *ga20ox1,-2,-3* ($p<0.01$ (cell length $p<0.05$)), although its meristem length was not significantly different from that in the triple mutant ($p>0.05$). Root, cell and meristem lengths of lines C and E were all significantly different from Col-0 ($p>0.01$) and not significantly different from *ga20ox1,-2,-3* ($p>0.05$), except that the root length of line C was significantly different from both Col-0 and *ga20ox1,-2,-3* ($p<0.05$).

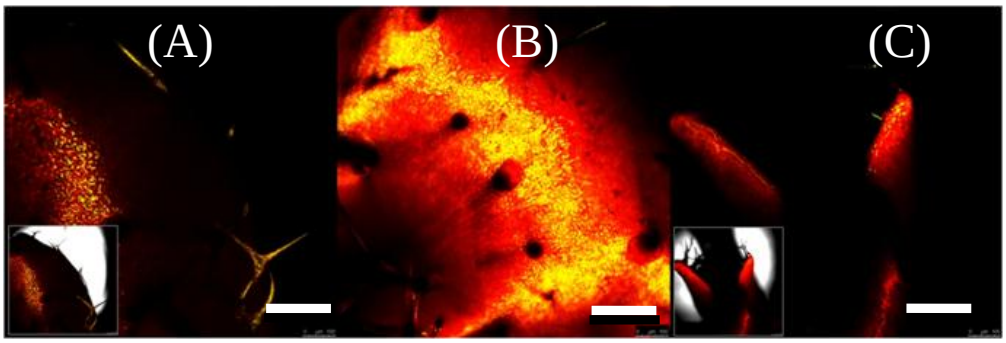

Figure 5-28**: YFP fluorescence in the first true leaves of *ga20ox1,-2,-3;CAB::YFP:AtGA20ox1* lines. (A-C)** Fluorescence in young photosynthetic tissue for lines A, C and E, respectively. Confocal microscopy was performed on the five roots of seven day old seedlings after being grown on vertical Gelrite plates. The YFP fluorescence and the propidium iodide emission images are overlaid; **(A)** & **(C)** have small inset images with the bright field emission overlaid. Bars are 100 μm in length.

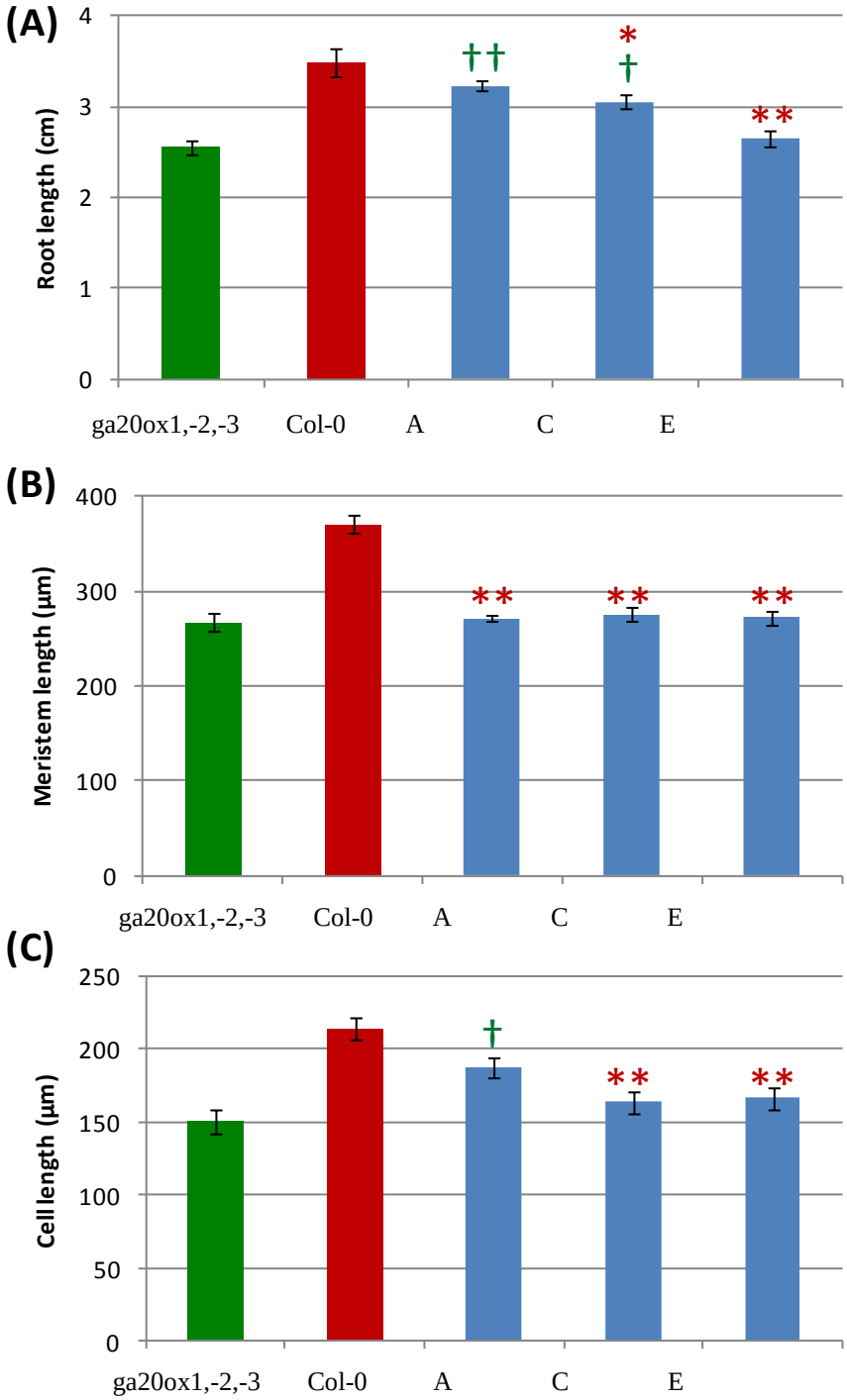

Figure 5-29**: Primary root parameters for *ga20ox1,-2,-3;CAB::YFP:AtGA20ox1* lines A, C and E compared with Col-0 and *ga20ox1,-2,-3* at seven days. (A)** Primary root length ±SE. **(B)** Proximal meristem length ±SE. **(C)** Final cortical cell length ±SE. Seedlings were grown on vertical plates and lengths calculated using ImageJ. Green crucifixes indicate the transgenic lines are significantly different from *ga20ox1,-2,-3* and the red asterisks indicate they are significantly different from Col-0. 15 plants for each line were measured for root length, and 5 for meristem size and final cell length, with the lengths of 5 cells being measured. *=p<0.05, **=p<0.01, †=p<0.05 and ††=p<0.01. Error bars are standard error. REML was used to generate the LSD given in Table 11-9.

5.1.15 Comparison of each promoter driving the expression *YFP:AtGA20ox1* on the primary root, meristem and final cell lengths.

The primary root parameters for the median representative *ga20ox1,-2,-3* transgenic lines expressing *YFP-AtGA20ox1* from each of the different promoters were compared with *ga20ox1,-2,-3* and Col-0. The *SCR*, *Co2*, *GL2* and the *CAB* promoters driving the expression of *YFP-AtGA20ox1* gave partial rescue of root growth, indicating that the endodermis, cortex, epidermis and aerial tissues are likely sites of GA_{12} mobilization (Figure 5-32 and Figure 5-30). The *SHR* and *CoR* promoters gave no rescue of meristem, cell or root size, which were not significantly different from *ga20ox1,-2,-3* ($p<0.01$). The root lengths of the lines expressing the transgenes from *SCR*, *Co2*, *GL2* and *CAB* promoters were all significantly larger than in *ga20ox1,-2,-3* ($p<0.01$). The partial rescue of root growth by the *CAB* promoter was due to a partial rescue of cell elongation as the meristem length was not significantly different from that in *ga20ox1,-2,-3* ($p>0.05$). The partial rescue of root growth by the *Co2::YFP:AtGA20ox1* and *GL2::YFP:AtGA20ox1* constructs was due to a partial rescue of both cell and meristem elongation; the *Co2* and *GL2* cortical cell lengths were significantly larger than in *ga20ox1,-2,-3* ($p<0.05$). However, the rescue was not complete as the cells were also significantly shorter than in Col-0 (*Co2*, $p<0.01$; *GL2*, $p<0.05$). The root, meristem and final cell lengths of the *ga20ox1,-2,-3;SCR::YFP:AtGA20ox1* line were not significantly different from Col-0 ($p>0.05$). Figure 5-31 shows representative images for the root tip for the *SHR*, *SCR*, *CoR*, *Co2* and *GL2* YFP:AtGA20ox1 lines, as no fluorescence was observed at the root tip for the *CAB* lines photosynthetic tissue near the SAM is shown.

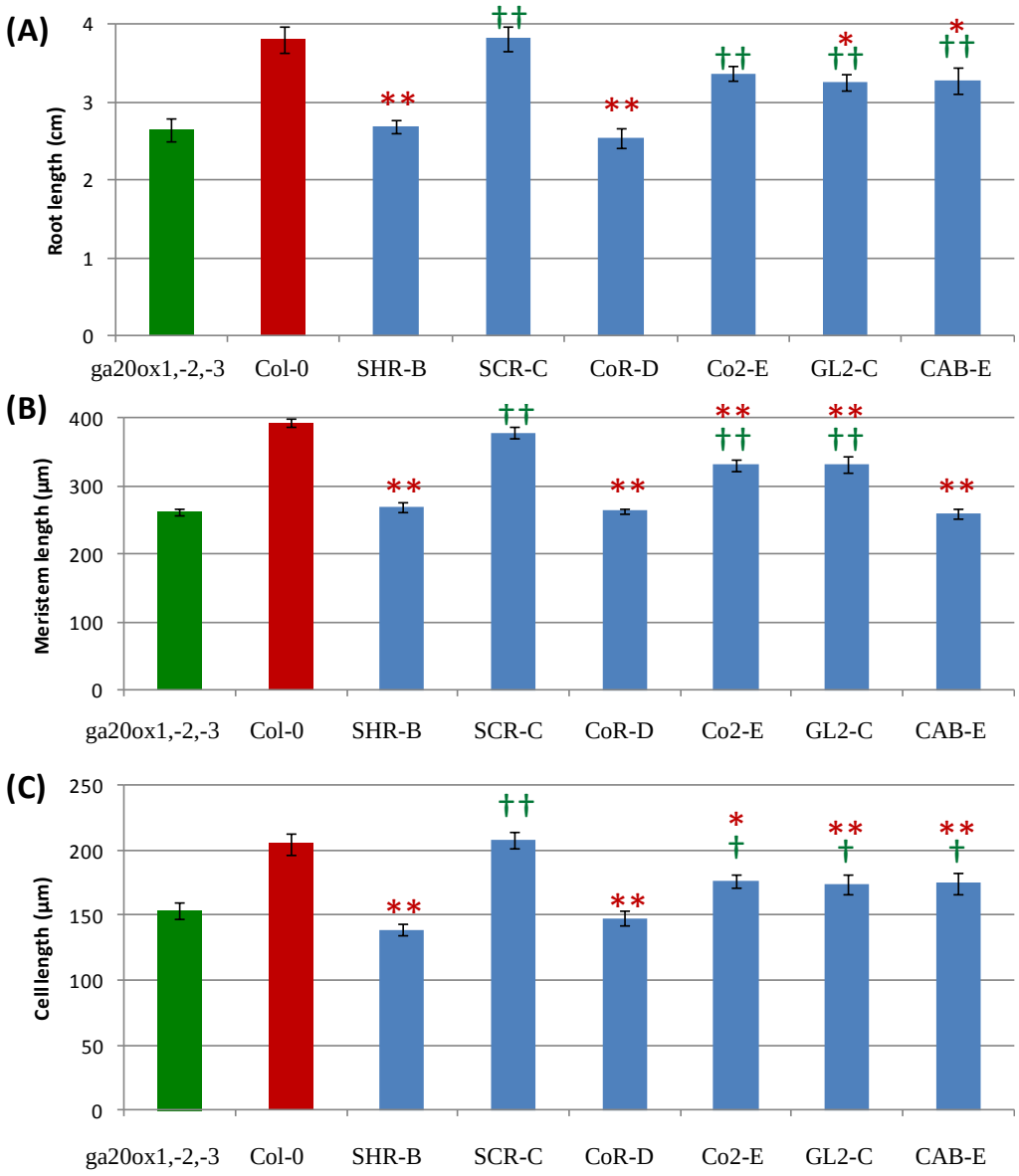

Figure 5-30**: Primary root parameters for the median lines harbouring each *YFP:AtGA20ox1* construct compared with Col-0 and *ga20ox1,-2,-3* at seven day. (A)** Primary root length ±SE. **(B)** Proximal meristem length ±SE. **(C)** Final cortical cell length ±SE. Seedlings were grown on vertical plates and lengths calculated using ImageJ. Green crucifixes indicate the transgenic lines are significantly different from *ga20ox1,-2,-3* and the red asterisks indicate if they are significantly different from Col-0. 15 plants for each line were measured for root length, and 5 for meristem size and final cell length, with the lengths of 5 cells being measured. *=p<0.05, **=p<0.01, †=p<0.05 and ††=p<0.01. Error bars are standard error. LSD are given in Table 11-11.

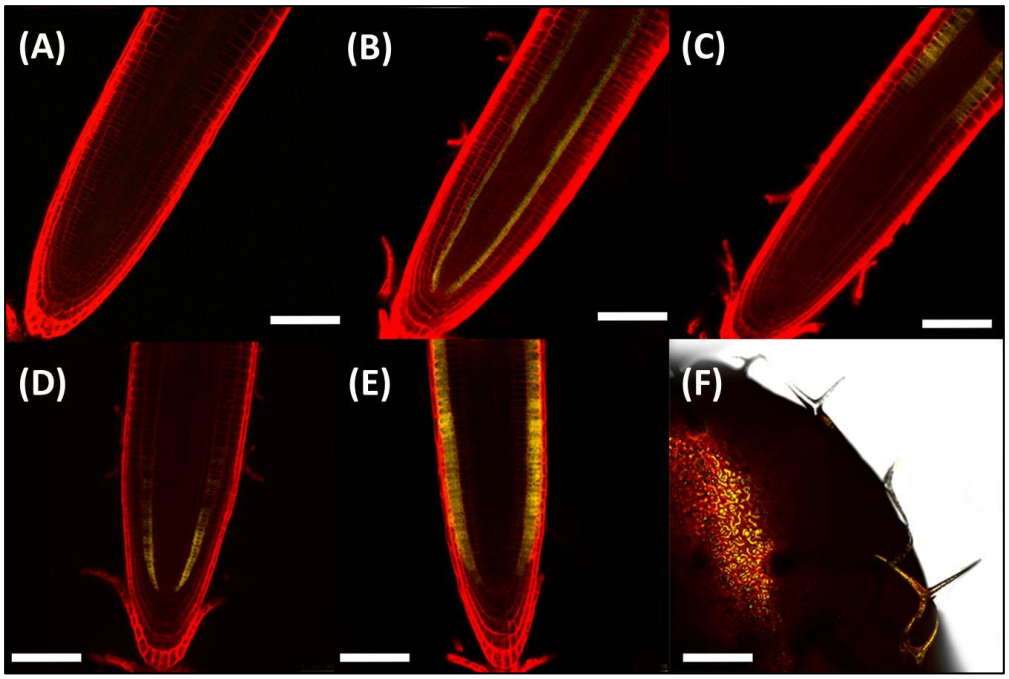

Figure 5-31: **Representative images for YFP fluorescence in the GA20ox1 lines. (A-F)** YFP-AtGA20ox1 attached to *SHR, SCR, CoR, Co2, GL2* and *CAB* promoters, respectively. Confocal microscopy was performed on seven day-old seedlings grown on vertical Gelrite plates. **(A-E)** The YFP and the propidium iodide emission images are overlain. **(F)** The YFP, propidium iodide and bright-field emission images are overlain. Bars are 100 μm in length.

In summary, *YFP-AtGA20ox1* expression was able to partially rescue root growth when expressed within the endodermis cortex or epidermis. *Co2::YFP:AtGA20ox1* was able to partially rescue growth of the *ga20ox1,-2,-3* mutant suggesting that the meristematic region is a site of GA_{12} C20-oxidation, in contrast, *CoR::YFP:AtGA20ox1* did not rescue any aspect of growth suggesting the elongation zone is not a site of GA_{12} C20-oxidation. In addition, the lack of rescue of the *ga20ox1,-2,-3;SHR::YFP:AtGA20ox1* lines demonstrates that the stele is also not a potential site of GA_{12} mobilisation. The partial rescue of cell elongation in the *ga20ox1,-2,-3;CAB::YFP:AtGA20ox1* lines demonstrates that after C20-oxidation GAs can become mobile and travel from the shoot to the root. Increased root growth is seen in the *ga20ox1,-2,-3* triple mutant by expression of YFP-AtGA20ox1 under different promoters. Previous experiments (Andy Plackett, unpublished data) have indicated that expression of AtGA20ox1 under the control of its native promoter fully complements the *ga20ox1,-2,-3* triple mutant. Therefore, it seems likely that this complementation provides only partial rescue of the phenotype. Additional controls such as the *ga20ox2,-3* double mutant, or transgenic *ga20ox1,-2,-3* triple mutants complemented with YFP-AtGA20ox1 under the native promoter could be used to confirm this.

5.2 DISCUSSION OF THE TARGETED EXPRESSION OF *YFP-AtGA20ox1* IN THE *ga20ox1,-2,-3* TRIPLE MUTANT

The aim of this experiment was to deduce important sites of GA biosynthesis and more precisely the site of GA_{12} production in the endoplasmic reticulum which leads to its eventual conversion to GA_{15}, GA_{24} and then finally to the C_{19}-GA GA_9 with the release of CO_2 (Yamaguchi, 2008). It has previously been shown that over-expression of GA 20-oxidases mildly increase the size of plants (Coles et al., 1999) and that knocking them out can produce dwarf mutants (Rieu et al., 2008b). The *ga20ox1,-2,-3* triple mutant has severely dwarfed roots comparable to *ga1-3*, due to reduced final cell length and meristem size (Figure 5-2 and Figure 5-6). The GA -deficient dwarf root of the *ga20ox1,-2,-3* triple mutant allowed the restoration of GA20ox activity in specific cells to determine the effect on meristem size and final cortical cell length that should provide insights into the main sights of GA 20-oxidation. Rescue of growth will indicate that the targeted cells have access to GA_{12}, GA_{15} or GA_{24}, that the GA_9 produced is capable of reaching a GA3ox enzyme and that the final bioactive GA_4 is then able to interact with a GID1 receptor; these reactions may all occur in one cell or the intermediates may be able to move between cells. In contrast, lack of rescue would indicate that the tissue does not contain GA_{12} and has no access to GA_{15} and GA_{24} through movement from other tissues, or that the tissue does not contain GA3ox activity or GID1 receptors and the GA20ox products are unable to move to tissues that does contain them.

5.2.1 Ectopic aerial expression of tissue specific YFP-AtGA20ox1 transgenes

The photosynthetic tissue specific *ga20ox1,-2,-3;CAB::YFP:AtGA20ox1* transgenic lines had semi-dwarf root growth and had complete aerial growth. Closer examination demonstrated that final cell size was partially rescued while meristem length was not (Figure 5-30). This indicates that cell elongation during root growth can be promoted by either C_{20}-GAs or C_{19}-GAs moving

down from aerial tissues. In addition, this also demonstrates that ectopic expression of the YFP-AtGA20ox1 transgene in aerial tissues may partially rescue cell elongation. Therefore, the complete cell elongation rescue of the *ga20ox1,-2,-3;SCR::YFP:AtGA20ox1* lines and the partial cell elongation rescue of the *ga20ox1,-2,-3;Co2::YFP:AtGA20ox1* and *ga20ox1,-2,-3;GL2::YFP:AtGA20ox1* lines may be due to GAs moving to the root from the shoot. However, the complete or partial rescue of meristem length in these lines implies that the endodermis, cortex and epidermis are all potential sites of C_{20}-GA biosynthesis. Therefore, aerial tissues can potentially produce excess C_{20}-GAs in order to boost cell elongation.

5.2.2 Expression of *YFP-AtGA20ox1* within the ground tissue and epidermis of the *ga20ox1,-2,-3* mutant rescues root growth

The tissue-specific expression of *YFP-AtGA20ox1* in the *ga20ox1,-2,-3* mutant produced a range of phenotypes that have provided insights into the sites of GA 20-oxidation that are necessary for promoting root growth. One of the main findings of this study was that GA 20-oxidation within the ground tissue of the meristem or the epidermis was capable of restoring root growth in the *ga20ox1,-2,-3* mutant. The rescue that was observed was through an increase in both meristem size and cell elongation. These findings demonstrate that GA_{12} (or conceivably GA_{15} or GA_{24}) are present in these locations and the GA_9 product is capable of being converted to GA_4 which is then able to interact with GID1 receptor leading to the rescue of root growth. It is possible that the GAs produced by the GA 20-oxidase and subsequently activated to GA_4 are acting locally, or alternatively movement to the site of action could be occurring.

Expressing *YFP-AtGA20ox1* within the endodermal cells of *ga20ox1,-2,-3* with the *SCR* promoter (Di Laurenzio et al., 1996) completely rescued meristem length, final cell length and therefore root length, indicating the importance of the conversion of C_{20}-GAs to C_{19}-GAs in the meristematic region and/or the elongation zone (Figure 5-19). This is supported by *YFP-AtGA20ox1* expression within the cortical cells of the meristematic region with the *Co2* promoter (Heidstra et al., 2004) which partially rescued meristem length, but not final cell length or root length, suggesting that these cells contain a pool of GA_{12}. Expressing *YFP-AtGA20ox1* within the epidermal cells of the elongation and meristematic region with the *GL2* promoter (Masucci et al., 1996) also produced partial rescue of meristem size and final cell length, suggesting that these tissues contain a pool of GA_{12} that can be converted to GA_9, activated and reach sites of perception, although the amount of GA produced and reaching the important sites of action is insufficient to fully restore growth (Figure 5-19 and Figure 5-25). Taken together, these results suggest that the endodermis, cortical and epidermal cells all contain GA_{12}. In addition, these data suggest that the endodermis and/or CEI cells produce sufficient GA_{12} for

the plant to grow normally, and that GA20ox activity is required in both the meristematic region and elongation zone for normal root growth.

Expressing YFP-AtGA20ox1 within the pericycle and vasculature cells of the *ga20ox1,-2,-3* using the *SHR* promoter (Di Laurenzio et al., 1996) provided no rescue of any aspect of root growth (Figure 5-6). Similarly, when YFP-*AtGA20ox1* was expressed within the ground tissue of the elongation zones with the *CoR* promoter (Dinneny et al., 2008), there was no rescue of root growth (Figure 5-15) unless GA20ox was also expressed in the meristematic region using the *Co2* promoter (Figure 5-21). These observations suggest that the GA 20-oxidase substrate, GA_{12} is not present in these locations and that GA20ox1 substrates must be capable of moving there. Alternatively it is possible that GA_9 is being produced but is not being further converted to GA_4 due to the lack of GA 3-oxidase activity, or alternatively, that GA_4 is produced but is not gaining access to the site of action. These questions could be addressed by performing GA analysis on the transgenic lines to determine whether GA_9 or GA_4 accumulate within the elongation zone.

In summary, the targeted expression of *YFP-AtGA20ox1* in the root of *ga20ox1,-2,-3* has demonstrated that the epidermis, cortex and endodermis all contain pools of GA_{12}, that after 20-oxidation are capable of being converted to bioactive GAs, which are perceived at a site of action. While conversely the stele and ground tissues of the elongation zone do not contain GA_{12} or the GA20ox1 products cannot reach either a GA3oxidase or a site of action (Figure 5-32).

Figure 5-32: **Schematic diagram highlighting which tissues rescued root growth when *YFP-AtGA20ox1* was targeted to them in the *ga20ox1,-2,-3* triple mutant.** The yellow lateral root cap and columella cells were not studied during this project. The torques meristematic endodermal, cortical and epidermal cells are sites of GA_{12} C20-oxidation. The white ground tissue cells in the elongation zone are sites of GA C20-oxidation required for cellular elongation but do not contain GA_{12}. The blue epidermal cells in the elongation zone are potential sites of GA C20-oxidation. The green vasculature cells are not sites of GA C20-oxidation

5.2.3 Potential movement of C_{20}-GAs from the meristematic region to the elongation zone

The targeted expression of *AtGA20ox1* to two distinct zones of the cortex in *ga20ox1,-2,-3* provided some further important insights into the regions in which GA 20-oxidation is necessary for promoting root growth. *YFP-AtGA20ox1* expression within the cortical cells of the meristematic region with the *Co2* promoter (Heidstra et al., 2004) partially rescued meristem length, cell length and root length (Figure 5-19), whereas , as discussed above, no rescue was obtained, even of cell elongation, when the transgene was expressed in the cortical cells of the elongation zone from the *CoR* promoter. When *ga20ox1,-2,-3;CoR::YFP:AtGA20ox1* was crossed with *ga20ox1,-2,-3;Co2::YFP:AtGA20ox1* a complete rescue of cell length and meristem length was achieved, indicating that the lack of rescue in the *CoR* lines was due to the absence of GA_{12} in the elongation zone and that the C_{19}-GAs produced in the meristematic region are not able to completely rescue cell elongation (Figure 5-21). This suggests that the elongation zone is dependent on the meristem as a source of C_{20}-GA precursors, which may move to the elongation zone or remain in the dividing cells until they elongate. Interestingly *GA20ox1:GUS* data (Figure 1-17), also demonstrates two distinct stages where *GA20ox1* expression occurs, one within the meristem and the other within the elongation zone consistent with GA20ox activity occurring at these different stages of development. Support for the meristem acting as the primary site of early GA biosynthesis is provided by microarray data showing the highest expression of the early GA biosynthesis genes in this region (Figure 5-1).

In summary, these experiments have also indicated that 20-oxidation is required in the meristematic region where GA_9 is subsequently activated to promote meristem growth. Either GA_9 or GA_4 then moves to the elongation zone where they partially promote cell elongation. These data also suggest that GA_{15} and/or GA_{24} may move from the meristematic region to the elongation zone to complete 20-oxidation and be activated to promote full cell elongation. The movement may be mediated by the symplastic, apoplastic pathways or

alternatively the C_{20}- and C_{19}-GAs may accumulate within the cells of the meristematic region then remain inside until they promote elongation.

5.2.4 Targeted expression of *YFP-AtGA20ox1* under the control of the *SCR, Co2* and *GL2* promoters rescues shoot growth in *ga20ox1,-2,-3*

The promoters used to drive the tissue-specific expression of *YFP-AtGA20ox1* within specific root tissues of *ga20ox1,-2,-3* are also expressed within the shoot (section 3.3). What was particularly striking about this study was that the same promoters which led to rescue of *ga20ox1,-2,-3* root growth when driving expression of *YFP-AtGA20ox1* had the same effect on shoot growth. Whilst a detailed phenotypic characterisation of shoot growth in these lines was not performed the effects were perhaps more striking than those observed for root growth. For example, neither root nor shoot growth were rescued in the *ga20ox1,-2,-3;CoR::YFP:AtGA20ox1* lines and *ga20ox1,-2,-3;SHR::YFP:AtGA20ox1* lines (Figure 5-4 and Figure 5-13). In contrast, the *SCR::YFP:AtGA20ox1, Co2::YFP:AtGA20ox1* and *GL2::YFP:AtGA20ox1* lines displayed considerable rescue of aerial growth compared to *ga20ox1,-2,-3*. Therefore these lines could provide some insights into the location of GA 20-oxidation required for shoot growth. Lack of rescue of the *CoR* and *SHR* lines demonstrates that the cells where these promoters are expressed either lack GA_{12}, GA3ox activity or there is lack of movement of GA_9 or GA_4 to the sites of activation or perception, respectively However, without GUS reporter or other data on the spatial expression from the *Co2* and *CoR* promoters no firm conclusions can be made from this study. Although GUS reporter lines do exist for *SHR* and *GL2* their description in the literature is limited. However the *SCR* promoter is well studied and was shown to be active in the stem cambium and the leaf bundle sheath cells (Wysocka-Diller et al., 2000). The targeted expression of *YFP-AtGA20ox1* with the *SCR* promoter rescued both leaf expansion and inflorescence elongation completely suggesting that the cell layer that surrounds the vasculature maybe an important site of GA_{12} metabolism.

5.2.5 GA20ox stability or post-transcriptional processing is subject to tissue-specific feedback regulation

GA biosynthesis is feedback regulated by the GA signalling pathway, both by the activation of GA-inactivation genes and by the suppression of GA-biosynthetic genes, such as *AtGA20ox1* (Rieu et al., 2008b, Phillips et al., 1995). It has been shown using a luciferase reporter gene that the *AtGA20ox1* promoter contains a 500-bp region that is required for GA-dependant feedback regulation (Meier et al., 2001). The research described here shows that, as well as being transcriptionally regulated, there is post-transcriptional regulation of GA20ox1, either at the level of protein or mRNA stability, or both, and this appears to occur in a tissue specific and GA dependant manner. In the *ga20ox1,-2,-3;SHR::YFP:AtGA20ox1* lines, YFP fluorescence was expected within the stele from the meristematic region to the mature zone, but could not be observed anywhere within the meristematic region. As *SHR::GFP* fluorescence was not affected by PAC and GA_3 application (Figure 4-13) this suggests that the vasculature may contain molecular components that reduce AtGA20ox1 stability. However, when the differentiation zone was examined fluorescence could clearly be seen in both the stele and endodermis, suggesting both tissue-specific and developmental control of AtGA20ox1 post-transcriptional expression (Figure 2-2).

Fluorescence in *ga20ox1,2,3;SCR::YFP:AtGA20ox1* lines was not confined to the endodermis as seen in the *SCR::GFP* reporter line shown in Figure 4-12, but could also occasionally be observed within the cortical cell layer. In addition, the fluorescence patterns varied considerably: it was usually only present in the endodermis of the elongation zone, but occasionally could be observed within the ground tissues of both the meristematic region and the elongation zone. To investigate if this was due to post-transcriptional regulation of *YFP-AtGA20ox1* in response to changes in GA signalling, plants were treated with PAC and GA_3. Fluorescence was not observed in the meristematic region when *ga20ox1,2,3;SCR::YFP:AtGA20ox1* plants were

grown on control plates and plates containing 1 μM GA_3, but appeared to have increased fluorescence within the elongation and differentiation zones.

Plants grown on 1 μM GA_3 had increased fluorescence within the cortical cells of the elongation zone. Furthermore, the opposite occurred when plant were grown on 1 μM PAC, when fluorescence increased within the meristematic region and decreased within the elongation and differentiation zones; this caused the fluorescence to be visible, not only in the endodermal cells of the meristematic region, but also in cortical cells (Figure 5-11). This suggests that due to reduced GA signalling YFP-AtGA20ox1 stability is increased in a tissue- and stage-specific manner. Fluorescence within the cortex was not observed within the *SCR::GFP* and *SCR::SCR:GFP* lines when these lines were treated with GA and PAC and there was no change in the fluorescence pattern (Figure 4-12), indicating that GA does not regulate *SCR* expression profiles. These observations suggest that *SCR* is expressed in the cortex at a low level which became apparent when YFP-AtGA20ox1 was stabilised; this hypothesis is supported by publicly available microarray data (Figure 3-13) and work performed by Susana Ubeda-Tomás at the University of Nottingham (Personal communication with Malcolm Bennett), which also indicated *SCR* expression could be observed in the cortex when a dexamethasone inducible non-degradable gai protein was expressed with the *SCR* promoter. However the potential mechanism for increasing YFP-AtGA20ox1 stability at the protein or transcript level is unclear.

In summary, YFP fluorescence profiles in the *SCR::YFP:AtGA20ox1* and *SHR::YFP:AtGA20ox1* lines did not match those of the *SCR::GFP* and *SHR::GFP* reporters. When treated with GA_3 and PAC, *SCR::YFP:AtGA20ox1* fluorescence profiles could be seen to fluctuate in a tissue- and developmental stage-specific manner. Therefore the stability of GA20ox1 enzyme or its transcript appears to be regulated by a GA-dependent and cell type-specific mechanism.

6 TISSUE SPECIFIC RESCUE OF *ga3ox1,-2* DOUBLE MUTANT USING *YFP-GA3ox1*

6.1 Introduction to GA 3β-hydroxylation

Gibberellin 3β-hydroxylation, catalysed by GA3ox, results in the conversion of the inactive GA_9 and GA_{20} to the active GA_4 and GA_1, respectively, in the final step of the biosynthetic pathway. This 3β-hydroxyl group is necessary for GA activity due to formation of a hydrogen bond within the binding pocket of the GID1 receptor via a bridging water molecule (Shimada et al., 2008, Murase et al., 2008). Potential sites of GA3ox activity within the *Arabidopsis* root were investigated by tissue-specific expression of *AtGA3ox1* in the *ga3ox1 ga3ox2* double mutant *(ga3ox1,-2)*, which has a short root phenotype (Figure 6-1).

Mutant plants were transformed with constructs allowing the expression of the *YFP:AtGA3ox1* fusion protein targeted to the root epidermis, cortex, endodermis and stele. Homozygous transgenic lines were generated and root growth and shoot development were analysed. Rescue of growth will occur if the cells expressing the transgene contain the main GA3ox substrate GA_9 and are sites of GA perception, or the bioactive GA_4 product is capable of moving to a site of perception. In addition, to investigate the importance for root growth of the transport of active GAs from the shoot, *AtGA3ox1* expression was targeted to the photosynthetic tissue using the *CAB* promoter; rescue of root growth using this promoter will suggest that bioactive GA_4 is capable of moving to the roots to promote growth. In some species GA3ox activity can convert GA_9 to 2β 3β-epoxy GA_9, GA_7 or GA_5 (Ward et al., 2010); however GA_{20} can also be converted by GA3ox enzymes to GA_5, which may be further converted by GA3ox to GA_6 or GA_3 (Figure 6-2). However these reactions do not appear to be important in *Arabidopsis* as AtGA3ox1 does not catalyse these reactions (Yamaguchi, 2008, Williams et al., 1998, Hedden and Kamiya, 1997).

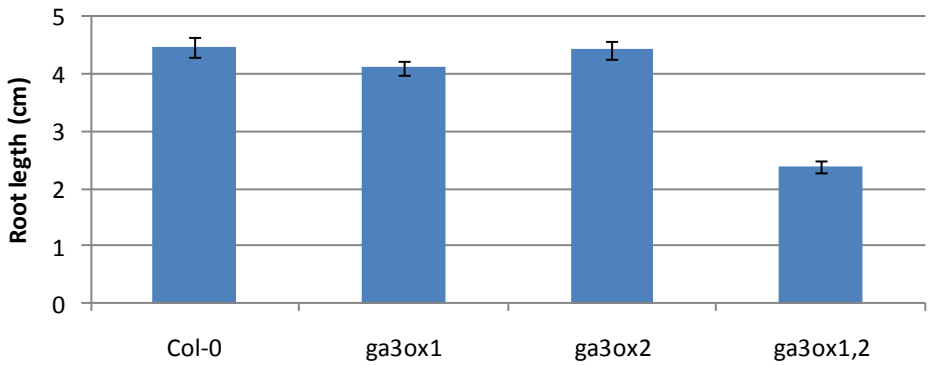

Figure 6-1**: Comparison of the root length of *ga3ox* mutants.** Primary root lengths ±SE are shown for *ga3ox1*, *ga3ox2*, *ga3ox1,-2* and Col-0 at seven days after germination. 30 plants were analyzed, seedlings were grown on vertical Gelrite plates and lengths calculated using ImageJ. Error bars indicate the standard error.

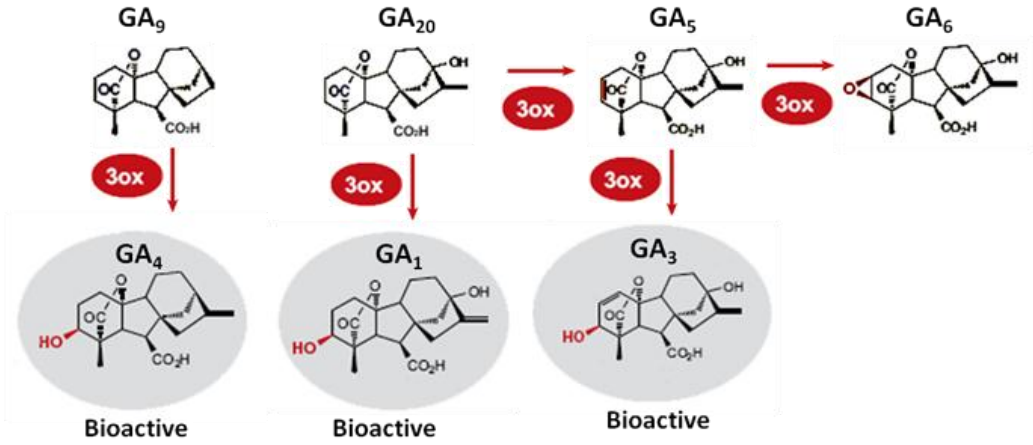

Figure 6-2**: Activation of GA by 3β-hydroxylation.** GA3ox catalyses the conversion of GA_9 to the biologically active GA_4, and GA_{20} to the biologically active GA_1. GA_{20} can be converted by some GA3ox enzymes to GA_5 and then to GA_6 or GA_3. (Adapted with permission from Shinjiro Yamaguchi., (2008)).

Within *Arabidopsis*, four *GA3ox* paralogues have been identified, each with distinct spatial and temporal expression patterns (Mitchum et al., 2006). A deficiency of bioactive GA_4 is known to stunt root growth by reducing DELLA degradation rates (Mitchum et al., 2006, Fu and Harberd, 2003). Although loss of GA3ox1 or GA3ox2 has no effect on root length the double *ga3ox1,-2* mutant has severely dwarfed roots demonstrating that these enzymes are completely redundant and at least one is required for correct root growth (Mitchum et al., 2006, Fu and Harberd, 2003). Supporting this, meta-analysis of microarray data produced by the Benfy lab, Serres lab (Mustroph et al., 2009) and CPIB group (unpublished data) suggest that *AtGA3ox1* and *AtGA3ox2* are the most highly expressed *GA3ox* genes at all stages of root growth with lowest expression in the differentiation zone (Figure 11-2). *GA3ox1* is the most highly expressed gene within the meristematic region.

6.1.1 Characterisation of *YFP:AtGA3ox1* expression lines

The effect of targeting the expression of *YFP:GA3ox1* with tissue specific promoters on the phenotype of *ga3ox1,-2* plants was initially monitored in terms of root length of seven day old seedlings grown on plates, as well as the vegetative growth of the rosette after three weeks and the inflorescence after six weeks. Three lines were then selected for further detailed analysis of root growth: root lengths, meristem lengths, and final cell sizes were measured. In all experiments the transgenic lines were compared with Col-0 as this was the original ecotype that the *ga3ox1,-2* was generated in and *ga3ox1,-2* as this was the GA deficient mutant that was genetically modified for the targeted YFP-GA3ox1 rescue.

6.1.2 *SHR::YFP:AtGA3ox1* partially rescues root length and completely rescues vegetative growth of the *ga3ox1,-2* mutant

The effect of GA3ox activity in the stele was examined by expressing *YFP-AtGA3ox1* from the *SHR* promoter (Di Laurenzio et al., 1996). Root lengths of lines expressing the transgene compared with Col-0 and *ga3ox1,-2* are shown in Figure 6-3. The targeted expression of the transgene partially rescued root growth and completely rescued the vegetative growth of all the lines (Figure 6-3 and Figure 6-4). The root lengths were significantly shorter than for Col-0 ($p<0.01$), but significantly longer than for *ga3ox1,-2* ($p<0.01$). The root length of line B was closest to the mean, with lines D and E not significantly different ($p<0.01$), so these lines were selected for further analysis.

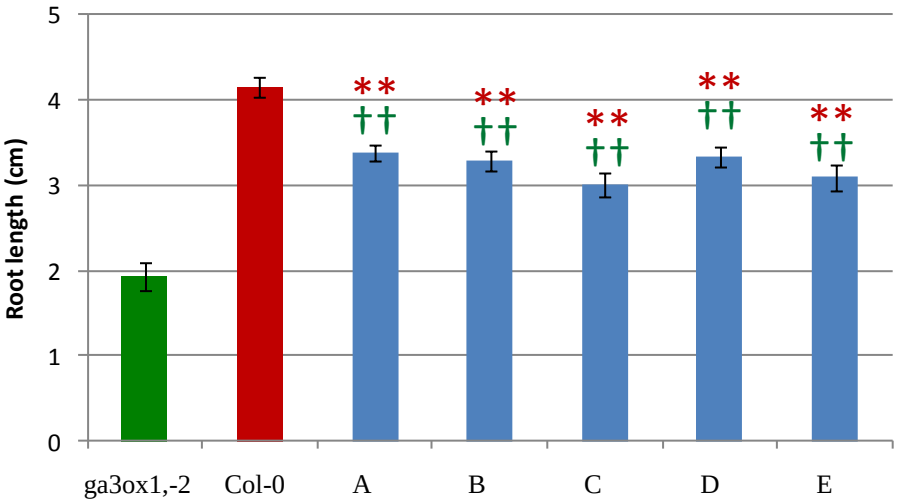

Figure 6-3**: Primary root length ±SE for *ga3ox1,-2;SHR::YFP:AtGA3ox1* lines (A-E) compared to *ga3ox1,-2* and Col-0 at seven days.** Seedlings were grown on vertical plates and lengths calculated using ImageJ. Green crucifixes indicate that the transgenic lines are significantly different from *ga1-3* and the red asterisks indicate they are significantly different from Col-0. 30 plants were analyzed **= p<0.01 and ††=p<0.01. Error bars indicate the standard error. REML was used to generate the LSD shown in Table 11-4.

Figure 6-4**: Vegetative phenotypes for *ga3ox1,-2;SHR::YFP:AtGA3ox1* lines (A-E) compared to *ga1-3*, ga3ox1,-2 and Col-0.** Plants were grown on Levingtons compost in 5.5 cm pots under long days for three (A) and six weeks (B).

6.1.3 *ga3ox1,-2;SHR::YFP:AtGA3ox1*: root length, meristem size, cell length and transgene expression profile.

The primary root growth for 15 plants from each of the three *SHR::YFP:AtGA3ox1* lines in the *ga3ox1,-2* background was compared with that of *ga3ox1,-2* and Col-0, measuring in addition to root length, meristem size in five plants and the final length of five cells in these five plants (Figure 6-5). There was a good agreement with the preliminary growth analysis (section 6.1.2), with line D having the longest roots and E the shortest. However, in this case the rescue was more complete, with root length in lines B and D not significantly different from that in Col-0 ($p>0.05$). The near complete rescue of root growth was also reflected in the rescue of meristem length and final cortical cell size: only line E had a final root length that was significantly smaller than Col-0 ($p<0.01$), which is likely to be due to reduced cell division as its meristem length was significantly smaller than in Col-0 ($p<0.05$).

To determine whether the transgene was expressed with the expected tissue-specific localisation, confocal microscopy was performed on the five roots from the selected representative lines when the seedlings were 7 day old after being grown simultaneously on different vertical Gelrite plates. All three *ga3ox1,-2;SHR::YFP:AtGA3ox1* lines showed fluorescence within the stele in the meristematic region, but interestingly fluorescence could also be observed in the endodermis of the differentiation zone (Figure 6-6).

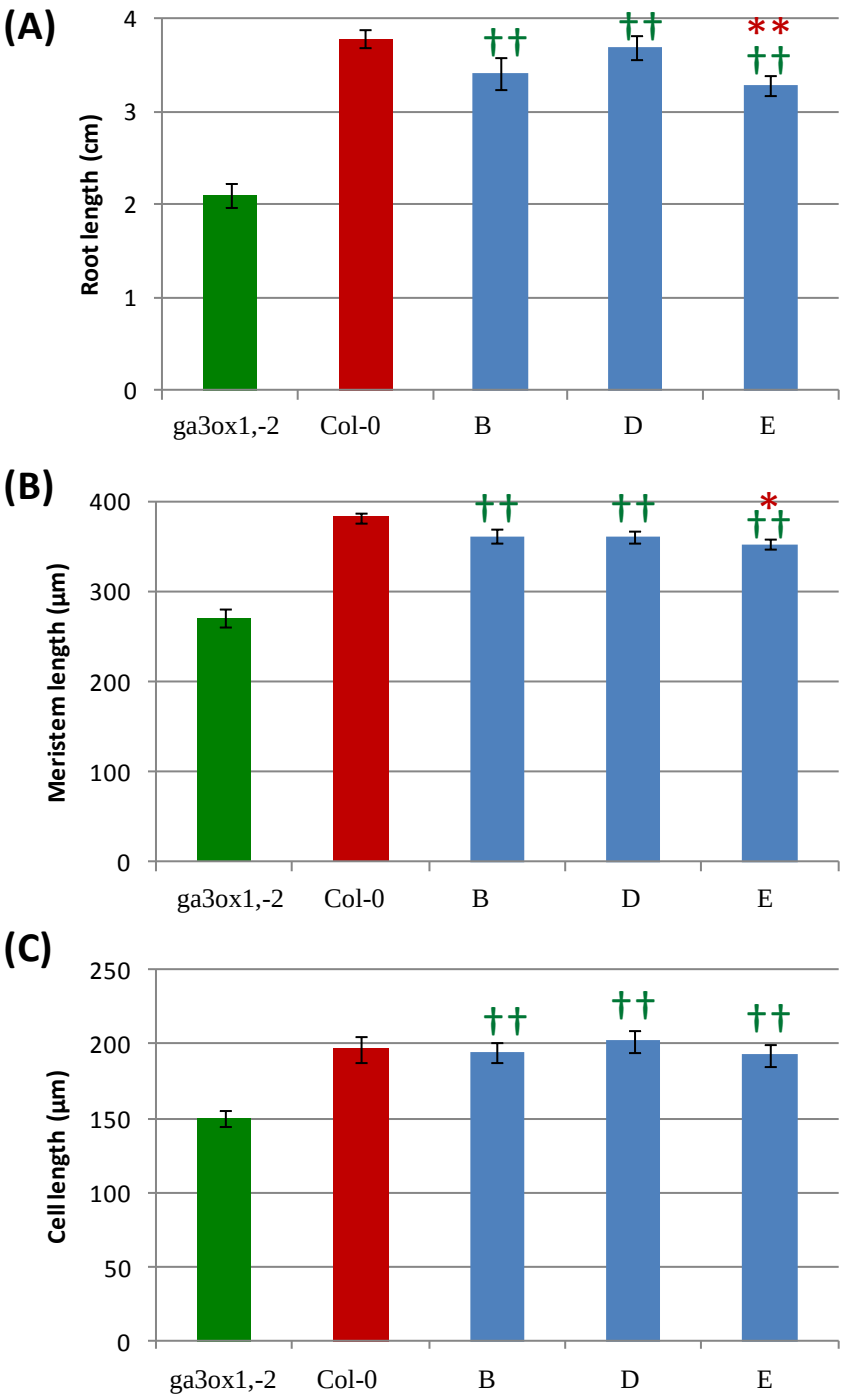

Figure 6-5**: Parameters for the primary root at 7 days in *ga3ox1,-2* lines B, D and E expressing *SHR::YFP:AtGA3ox1* compared with Col-0 and *ga3ox1,-2*. (A)** Primary root length ±SE. **(B)** Proximal meristem length ±SE. **(C)** Final cortical cell length ±SE. Seedlings were grown on vertical plates and lengths calculated using ImageJ. Green crucifixes indicate that the transgenic lines are significantly different from *ga3ox1,-2* and the red asterisks indicate that they are significantly different from Col-0. 15 plants were measured for root length, Meristem length is the mean from 5 plants, from which the lengths of 5 cells were measured *= $p<0.05$, **= $p<0.01$, and ††=$p<0.01$. Error bars indicate the standard error. REML was used to generate the LSD given in Table 11-10.

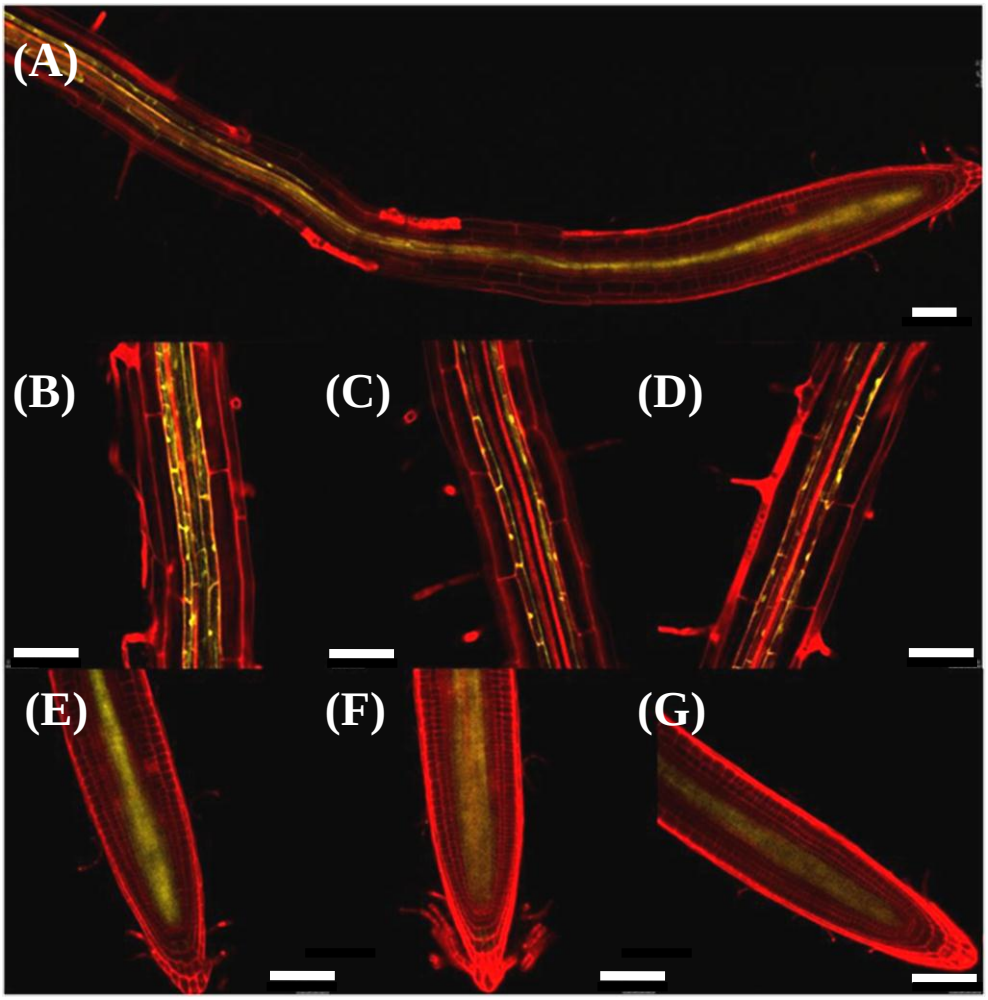

Figure 6-6**: *YFP* fluorescence in the meristematic region, elongation and differentiation zones of *ga3ox1,-2;SHR::YFP:AtGA3ox1* lines. (A)** Fluorescence from the QC to the DZ. **(B-D)** Fluorescence in the differentiation zone is shown for lines A, B and C. **(E-G)** Fluorescence in the meristematic region for lines A, B and C. Confocal microscopy was performed on the five roots of seven day old seedlings after being grown on vertical Gelrite plates. The YFP and the propidium iodide emission images are overlaid. Bars are 100 μm in length.

6.1.4 *SCR::YFP:AtGA3ox1* partially rescues root length and completely rescues vegetative development of the *ga3ox1,-2* mutant

To investigate the effect of GA activation in the endodermis, *YFP-AtGA3ox1* expression was driven from the *SCR* promoter in the *ga3ox1,-2* double mutant background (Di Laurenzio et al., 1996). Root lengths of four *ga3ox1,-2* transgenic lines expressing *SCR::YFP:AtGA3ox1* compared with Col-0 and *ga3ox1,-2* are shown in Figure 6-7. Preliminary analysis revealed that expression of the transgene partially rescued root growth and completely rescued the vegetative growth of all the lines (Figure 6-8). Although primary root lengths of all lines were significantly smaller than Col-0, they were significantly larger than *ga3ox1,-2* ($p<0.01$). Since root length of line C was closest to the mean, while lines A and D were not significantly different from line C ($p<0.01$), these lines were selected for further analysis.

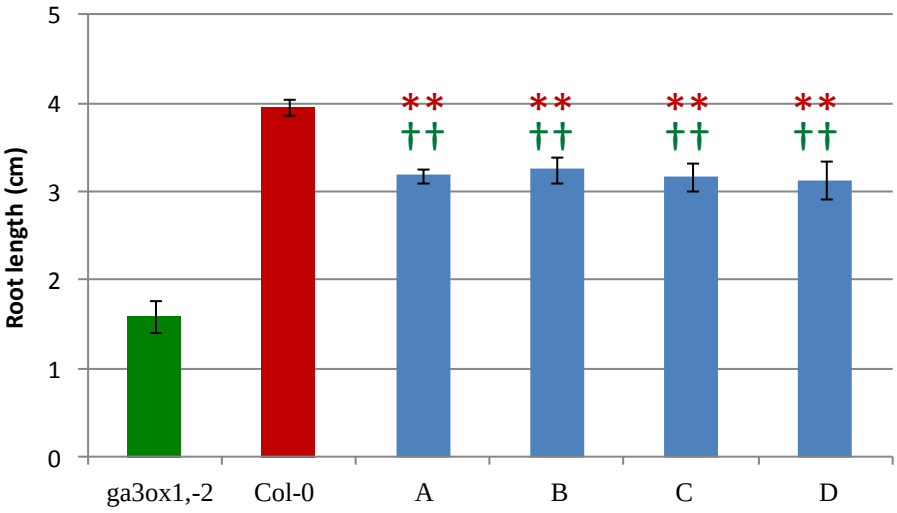

Figure 6-7**: Primary root length ±SE for *ga3ox1,-2;SCR::YFP:AtGA3ox1* lines (A-D) compared to *ga3ox1,-2* and Col-0 at seven days.** Seedlings were grown on vertical plates and lengths calculated using ImageJ. Green crucifixes indicate the transgenic lines are significantly different from *ga3ox1,-2* and the red asterisks indicate they are significantly different from Col-0. 30 plants were analyzed **= p<0.01 and ††=p<0.01. Error bars indicate the standard error. REML was used to generate the LSD given in Table 11-4.

Figure 6-8**: Vegetative phenotypes for *ga3ox1,-2;SCR::YFP:AtGA3ox1* lines (A-D) compared to *ga1-3,* ga3ox1,-2 and Col-0.** Plants were grown on Levingtons compost in 5.5-cm pots under long day for three **(A)** and six weeks **(B)**.

6.1.5 *ga3ox1,-2;SCR::YFP:AtGA3ox1*: root length, meristem length, cell length and transgene expression profile.

Growth parameters for the primary roots of the three representative *ga3ox1,-2* lines expressing *SCR::YFP:AtGA3ox1* were compared with *ga3ox1,-2* and Col-0 (Figure 6-9). As found in the preliminary analysis (section 6.1.4), the transgene was able to rescue root growth of the *ga3ox1,-2* double mutant completely for two of the three transgenic lines analysed; the root, meristem and final cell lengths of all three lines were significantly larger than in *ga3ox1,-2* ($p<0.01$ (except the meristem of line D, where $p<0.05$)). Only line D had a final root length that was significantly smaller than Col-0 ($p<0.01$), due to a reduction in both meristem size length ($p<0.01$) and cell length ($p<0.05$), which were also significantly smaller than Col-0.

All three transgenic lines showed fluorescence within the endodermis and occasionally, but always to a much lesser extent, the cortical cells of the proximal meristematic, elongation, and differentiation zones. Interestingly, YFP fluorescence could never be observed near the QC, ECI or their daughter cells (Figure 6-10). However, when the differentiation zone was examined in plants grown on plates containing 1 µM GA, fluorescence could be observed at a much higher level within the cortex. For lines grown on control Gelrite, expression was observed within the endodermis, and when grown on Gelrite containing 1 µM PAC, expression could be observed weakly in the endodermis and brightly within the pericycle (Figure 6-11). Despite these changes in YFP fluorescence in the differentiation zone in response to GA and PAC treatments, no such changes could be observed within the meristematic region (Figure 6-12).

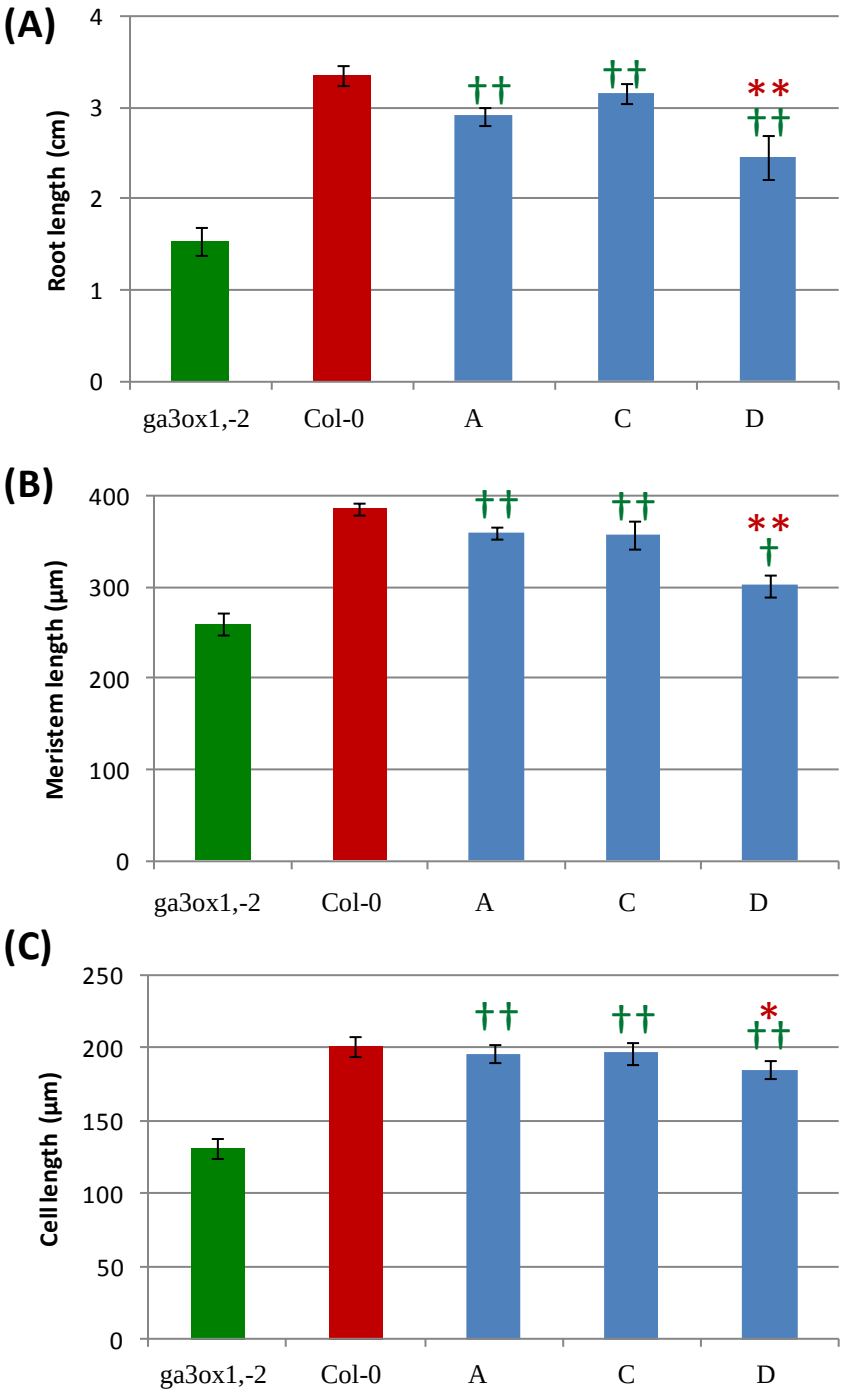

Figure 6-9**: Parameters for the primary root at 7 days in *ga3ox1,-2* lines A, C and D expressing *ga3ox1,-2;SCR::YFP:AtGA3ox1* compared with Col-0 and *ga3ox1,-2*.** **(A)** Primary root length ±SE. **(B)** Proximal meristem length ±SE. **(C)** Final cortical cell length ±SE. Seedlings were grown on vertical plates and lengths calculated using ImageJ. Green crucifixes indicate that the transgenic lines are significantly different from *ga3ox1,-2* and the red asterisks indicate that they are significantly different from Col-0. 15 plants were measured for root length, 5 plants meristem size and cell length *=p<0.05, **=p<0.01 and ††=p<0.01. REML was used to generate the LSD given in Table 11-10.

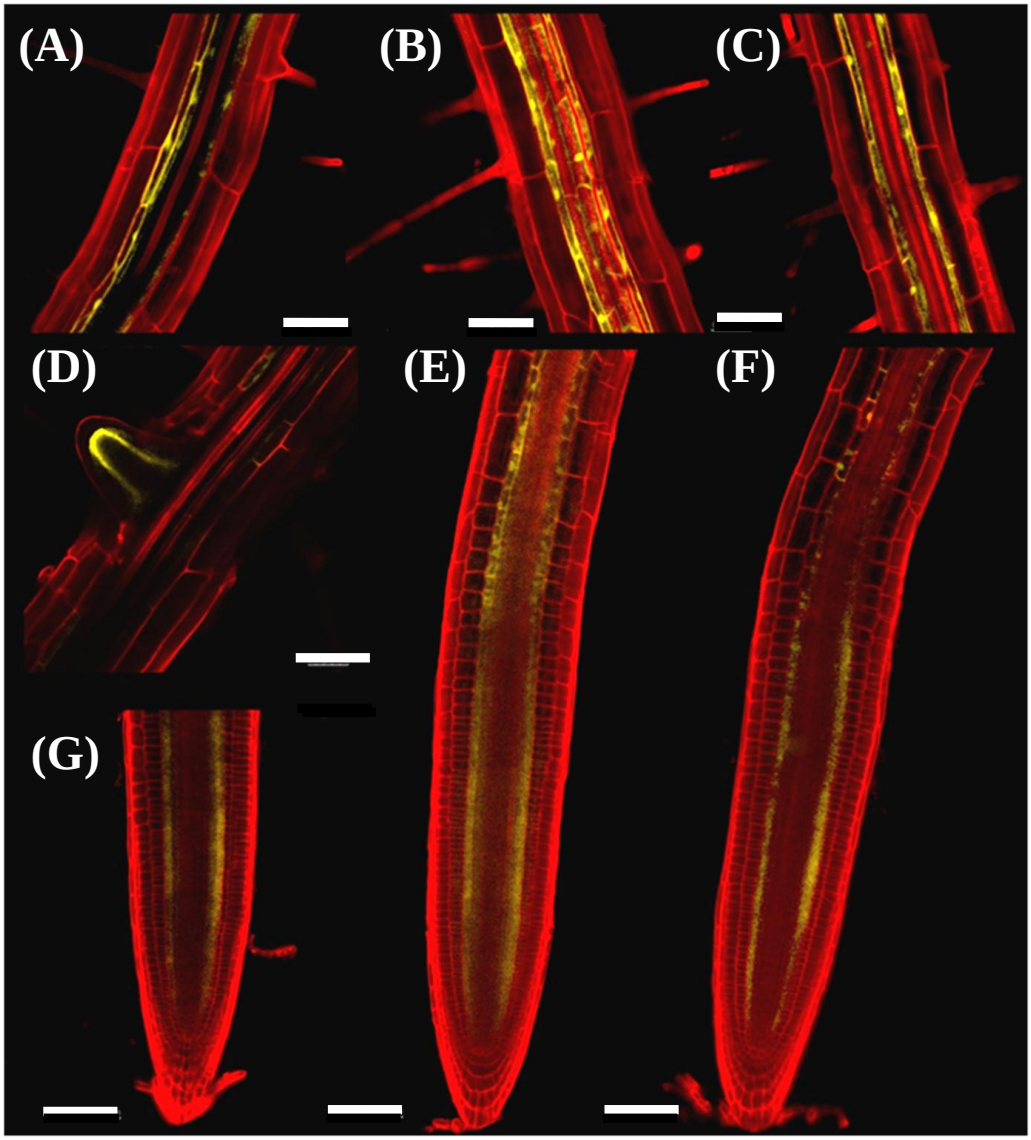

Figure 6-10: **YFP fluorescence in roots of the *ga3ox1,-2;SCR::YFP:AtGA3ox1* lines. (A-C)** Fluorescence in the differentiation zone for lines A, C and D, respectively; **(D)** Fluorescence in an emerging lateral root. **(E-F)** Fluorescence in the meristematic and elongation zones for lines C and D. **(G)** Fluorescence in the meristematic region for line A. Confocal microscopy was performed on the five roots of seven day old seedlings after being grown on vertical Gelrite plates. The YFP and the propidium iodide emission images are overlaid. Bars are 50 μm in length.

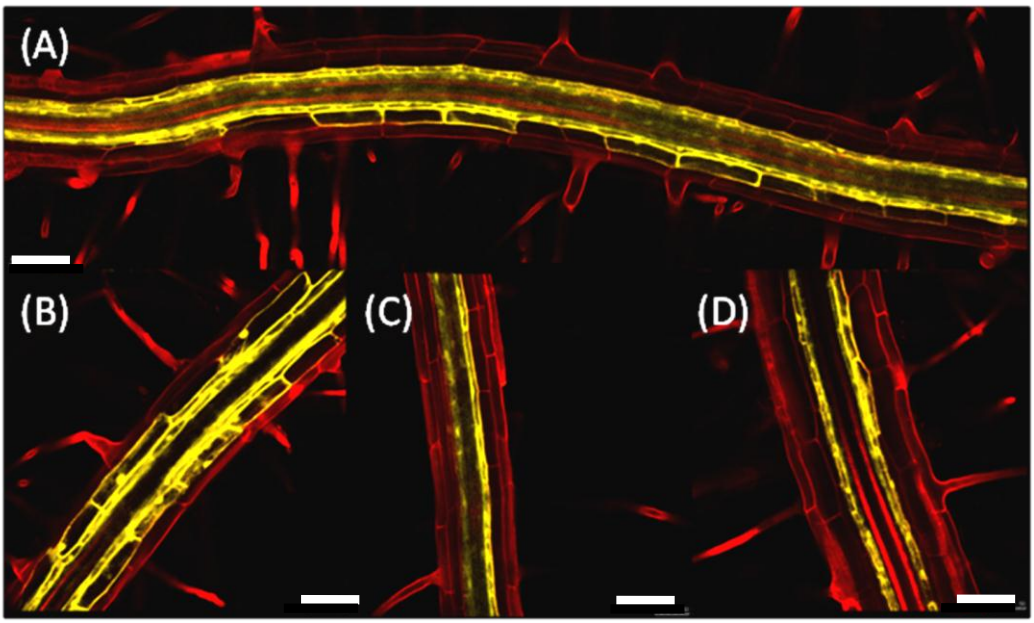

Figure 6-11**: YFP fluorescence in the differentiation zone of *ga3ox1,-2;SCR::YFP:AtGA3ox1* line C in response to GA status. (A-B)** Fluorescence in plants grown on Gelrite containing 1 µM GA_3. **(C)** Grown on Gelrite. **(D)** Grown on Gelrite containing 1 µM PAC. Confocal microscopy was performed on the five roots of seven day old seedlings after being grown on vertical Gelrite plates. The YFP and the propidium iodide emission images are overlaid. Bars are 100 µm in length.

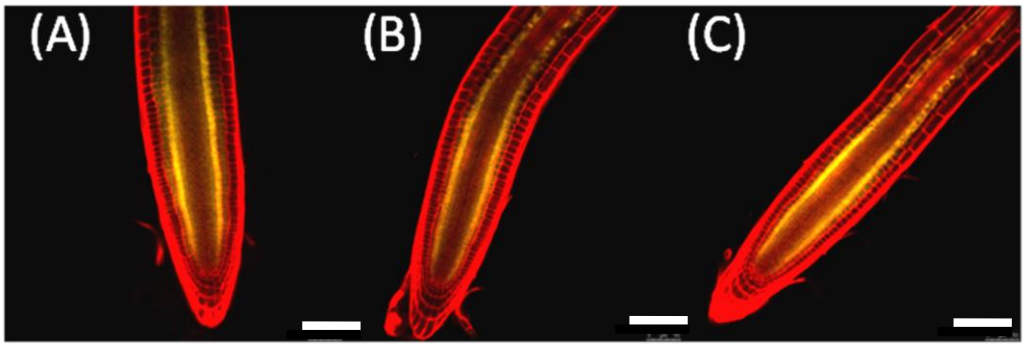

Figure 6-12**: *ga3ox1,-2;SCR::YFP:AtGA3ox1* line C expression in the meristematic and elongation zones. (A)** Plants grown on Gelrite containing 1 µM PAC. **(B)** Grown on Gelrite. **(C)** Grown on Gelrite containing 1 µM GA_3. Confocal microscopy was performed on the five roots of seven day old seedlings after being grown on vertical Gelrite plates. The YFP and the propidium iodide emission images are overlain. Bars are 100 µm in length.

6.1.6 *CoR::YFP:AtGA3ox1* partially rescues root length and completely rescues vegetative development of the *ga3ox1,-2* mutant

To investigate the effects on root growth of *YFP:AtGA3ox1* expression in the ground tissue of the elongation zone, gene expression was driven using the *CoR* promoter in the *ga3ox1,-2* background (Dinneny et al., 2008). Subsequently the root lengths of five transgenic lines were compared with Col-0 and *ga3ox1,-2* (Figure 6-13). This targeted expression of *YFP-AtGA3ox1* completely rescued shoot growth and produced a variegated leaf bleaching pattern on the centre of the rosette leaves of lines B and to a greater extent line D (Figure 6-14). The primary root lengths of all lines, although still significantly smaller than Col-0 ($p<0.01$), were significantly larger than *ga3ox1,-2* ($p<0.01$). The three lines with root lengths closest to the mean (lines A, C and D) were chosen for further analysis.

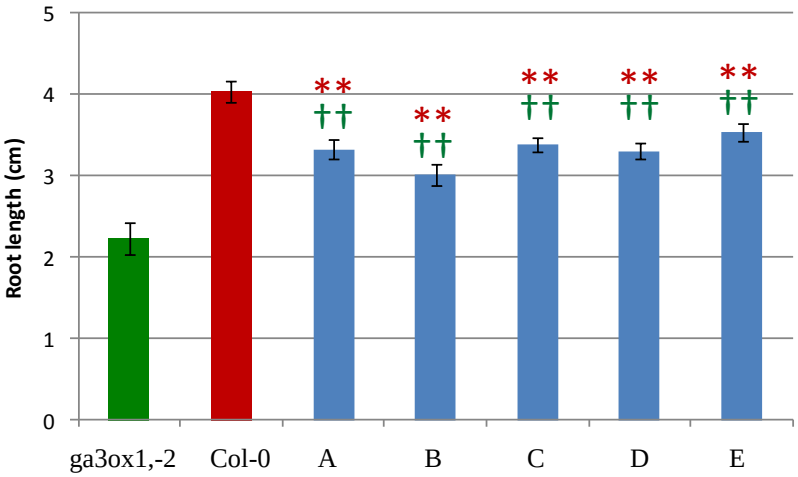

Figure 6-13**: Primary root length ±SE for *ga3ox1,-2;CoR::YFP:AtGA3ox1* lines (A-E) compared to *ga3ox1,-2* and Col-0 at seven days**. Seedlings were grown on vertical plates and lengths calculated using ImageJ. Green crucifixes indicate that the transgenic lines are significantly different from *ga3ox1,-2* and the red asterisks indicate that they are significantly different from Col-0. 30 plants were analyzed **=p<0.01 and ††=p<0.01. Error bars indicate the standard error. REML was used to generate the LSD given in Table 11-4.

Figure 6-14**: Vegetative phenotypes for *ga3ox1,-2;CoR::YFP:AtGA3ox1* lines (A-E) compared to *ga1-3*, ga3ox1,-2 and Col-0.** Plants were grown on Levingtons compost in 5.5cm pots under long days for three (A) and six weeks (B).

6.1.7 *ga3ox1,-2;CoR::YFP:AtGA3ox1:* root length, meristem length, cell length and transgene expression profile.

The primary root parameters of the three representative *ga3ox1,-2* lines expressing *CoR::YFP:AtGA3ox1* compared with *ga3ox1,-2* and Col-0 are shown in Figure 6-15. In agreement with the previous characterisation (section 6.1.6), the transgene rescued root growth of the *ga3ox1,-2* double mutant; the root and final cell lengths of all three lines were significantly larger than *ga3ox1,-2* ($p<0.01$) and the meristem length was not significantly different from both Col-0 ($p>0.01$) but not *ga3ox1,-2* ($p>0.05$). Only line A had a final root length that was significantly shorter than Col-0 ($p<0.01$), due to its reduced meristem size, since its cell length was not significantly shorter than Col-0 ($p>0.05$).

All three transgenic lines displayed fluorescence within the endodermis and cortex of the elongation zone, but, in addition and unusually, there was also low level fluorescence within the columella cells (Figure 6-16). When plants were sown on plates containing 1 µM GA_3, fluorescence appeared to be higher compared with untreated plants, while treatment with 1 µM PAC appeared to reduce fluorescence levels (Figure 6-17). Interestingly, *YFP:AtGA3ox1* fluorescence could be observed within the cytoplasm and the nucleus of all cells, but this was particularly clear within the elongation zone (Figure 6-16).

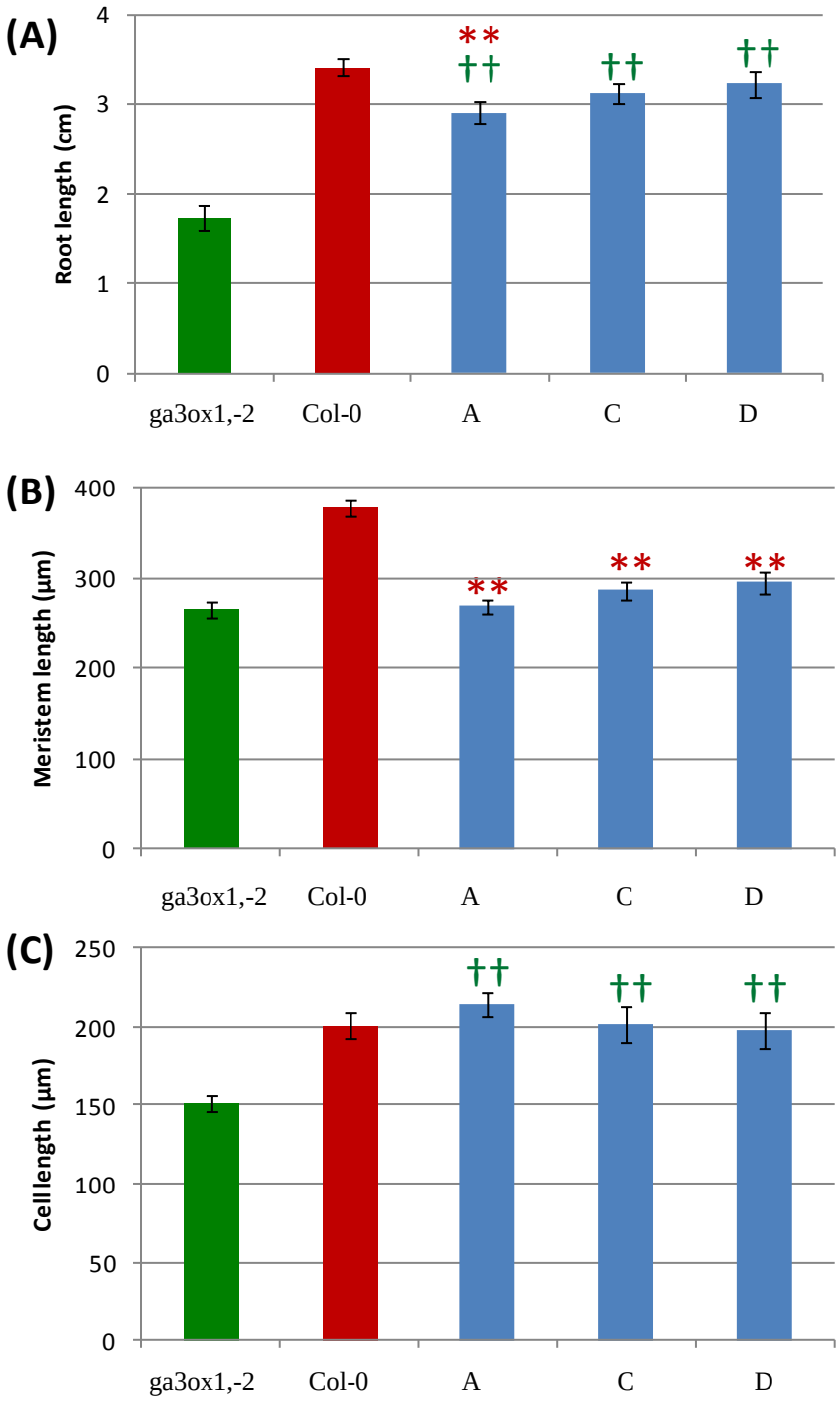

Figure 6-15**: Parameters for the primary root at 7 days in *ga3ox1,-2* lines A, C and D expressing *CoR::YFP:AtGA3ox1* compared with Col-0 and *ga3ox1,-2*.** **(A)** Primary root length ±SE. **(B)** Proximal meristem length ±SE. **(C)** Final cortical cell length ±SE. Seedlings were grown on vertical plates and lengths calculated using ImageJ. Green crucifixes indicate that the transgenic lines are significantly different from *ga3ox1,-2* and the red asterisks indicate that they are significantly different from Col-0. 15 plants were measured for root length, 5 plants for meristem size and cell lengths, with 5 cortical cells being measured **= $p<0.01$, and ††=$p<0.01$. Error bars indicate the standard error. REML was used to generate the LSD given in Table 11-10.

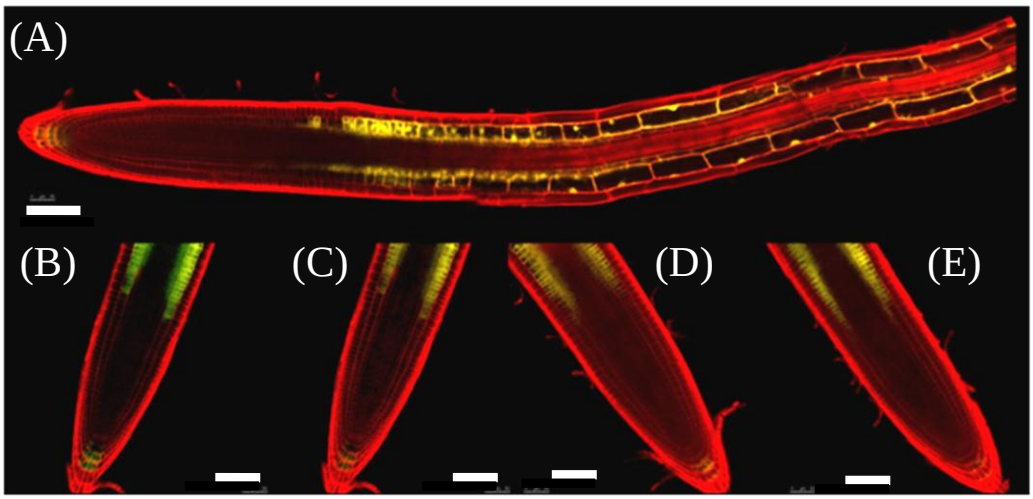

Figure 6-16**: *YFP:AtGA3ox1* fluorescence in the meristematic and elongation zones. (A)** Fluoresence in the meristematic and elongation zones for line A. **(B)** The red pigment has been reduced in the meristematic region of line A to make the columella fluorescence more visible. **(C-D)** *CoR::YFP:AtGA3ox1* expression in the meristematic for lines A, C and D, respectively. Confocal microscopy was performed on the five roots of seven day old seedlings after being grown on vertical Gelrite plates. The YFP and the propidium iodide emission images are overlaid. Bars are 100 μm in length.

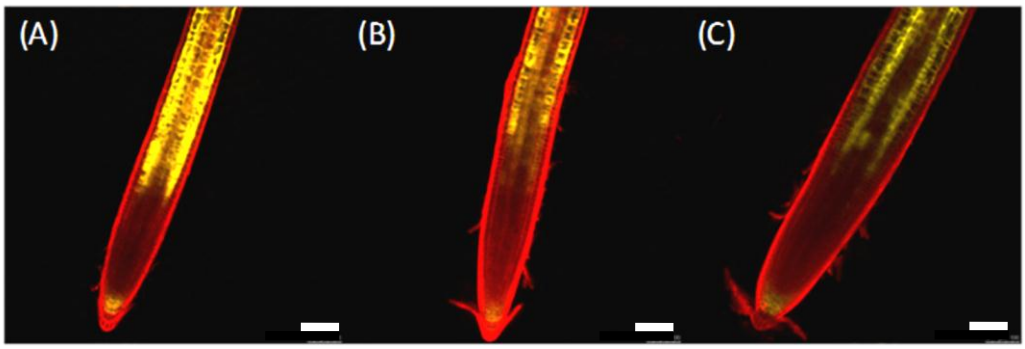

Figure 6-17**: *YFP:AtGA3ox1* fluorescence after treatment with GA and PAC treatment. (A)** *ga3ox1,-2;CoR::YFP:AtGA3ox1* line D showing fluorescence in the meristematic region for plants grown on Gelrite containing 1 μM GA_3, **(B)** when grown on Gelrite, **(C)** when grown on Gelrite containing 1 μM PAC. Confocal microscopy was performed on the five roots of seven day old seedlings after being grown on vertical Gelrite plates. The YFP and the propidium iodide emission images are overlaid. Bars are 100 μm in length.

6.1.8 *Co2::YFP:AtGA3ox1* partially rescues root length and completely rescues vegetative development of the *ga3ox1,-2* mutant

The *Co2* promoter was used to drive *YFP:AtGA3ox1* expression in the meristematic cortical cells and cortical/endodermal initial cells of the *ga3ox1,-2* mutant background (Heidstra et al., 2004). Root lengths of five transgenic lines were compared with Col-0 and *ga3ox1,-2* (Figure 6-18). The primary root lengths of all lines were significantly shorter than Col-0 ($p<0.01$), but also significantly longer than *ga3ox1,-2* ($p<0.01$). The three lines with root lengths closest to the mean (lines A, D and E) were chosen for further analysis. The targeted expression of *YFP:AtGA3ox1* completely rescued shoot growth, producing plants that were larger than WT Col-0 (Figure 6-19).

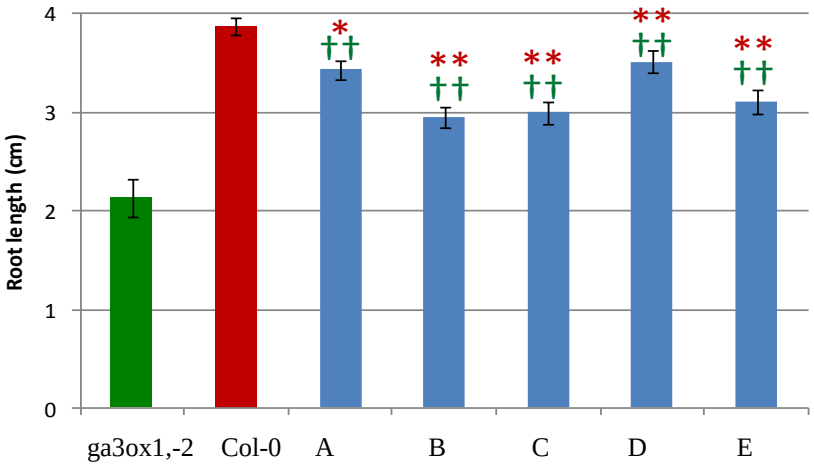

Figure 6-18**: Primary root length ±SE for *ga3ox1,-2;Co2::YFP:AtGA3ox1* lines (A-E) compared to *ga3ox1,-2* and Col-0 at seven days.** Seedlings were grown on vertical plates and lengths calculated using ImageJ. Green crucifixes indicate that the transgenic lines are significantly different from *ga3ox1,-2* and the red asterisks indicate that they are significantly different from Col-0. 30 plants were analyzed **= p<0.01, and ††=p<0.01. Error bars indicate the standard error. REML was used to generate the LSD given in Table 11-4.

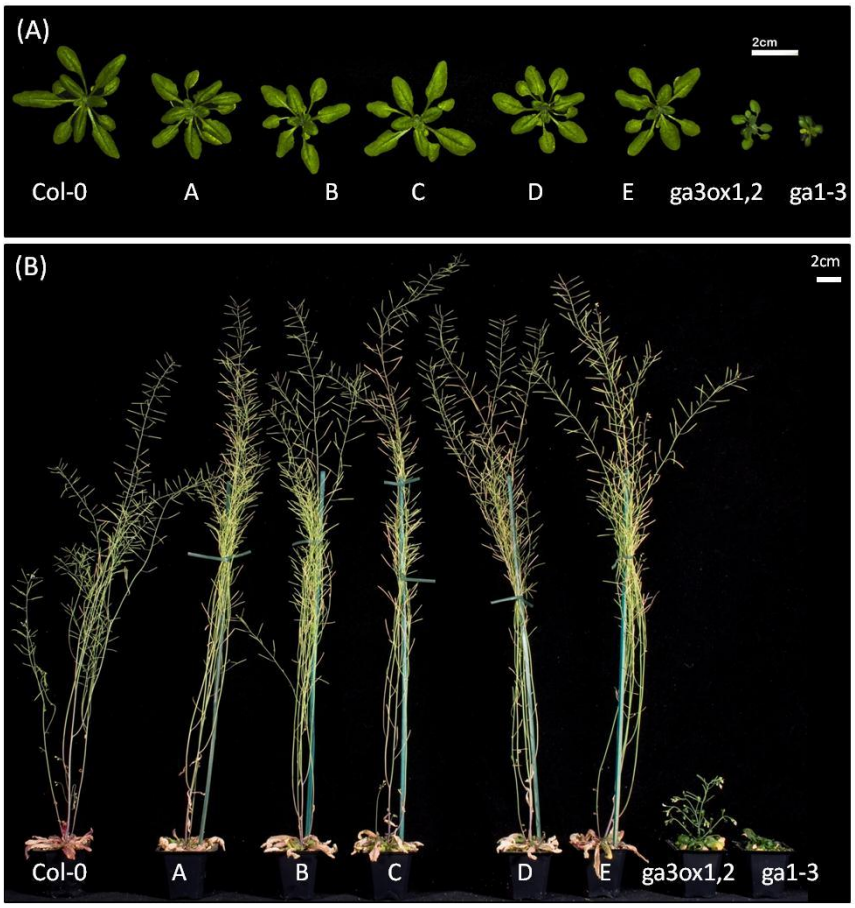

Figure 6-19**: Vegetative phenotypes for *ga3ox1,-2;Co2::YFP:AtGA3ox1* lines (A-E) compared to *ga1-3*, ga3ox1,-2 and Col-0.** Plants were grown on Levingtons compost in 5.5 cm pots under long days for three (A) and six weeks (B).

6.1.9 *ga3ox1,-2;Co2::YFP:AtGA3ox1*: root length, meristem length, cell length and transgene expression profile.

The primary root parameters of three representative *ga3ox1,-2* lines expressing *Co2::YFP:AtGA2ox2* compared with *ga3ox1,-2* and Col-0 are shown in Figure 6-20. In agreement with the previous characterisation (section 6.1.8), the extent of rescue of root length varied, ranging from partial to almost complete rescue of the *ga3ox1,-2* double mutant. However, the meristem sizes and cell lengths of the lines were not significantly different from Col-0 ($p>0.05$), except for cell length in line D which was significantly less than for Col-0 ($p<0.05$).

In all three lines YFP fluorescence was present in the cortical cells of the meristematic region, but confined to a few cells close to the QC (Figure 6-21). When plants were sown on plates containing 1 µM PAC, fluorescence intensity and domain increased compared to that in untreated plants or those grown on 1 µM GA_3 (Figure 6-22). This is consistent with the restricted expression profile observed on control plates being due to post transcriptional regulation in the proximal meristem, although promoter responses cannot be completely ruled out without testing *Co2* transcriptional reporter lines responses to GA_3 and PAC.

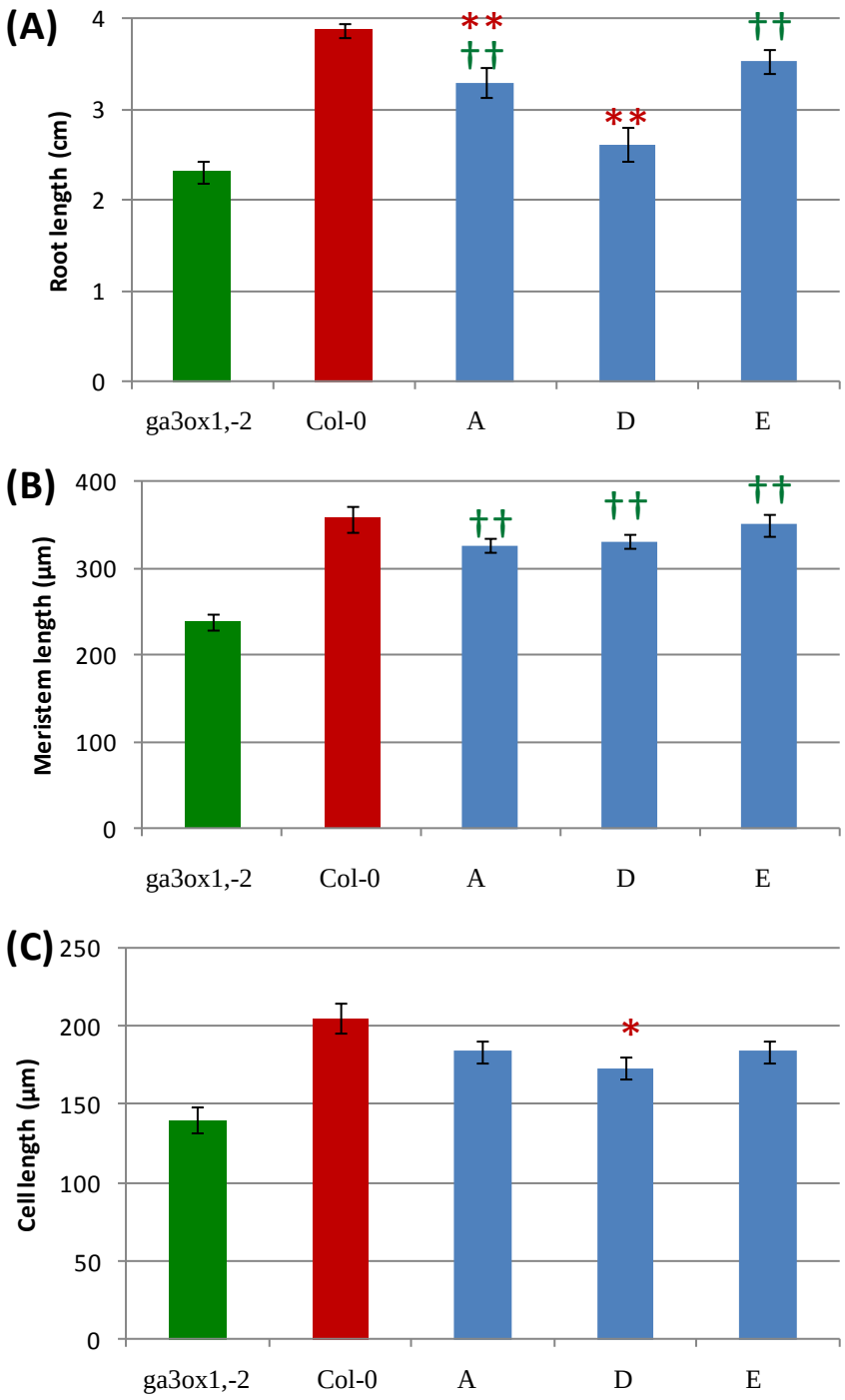

Figure 6-20**: Parameters for the primary root at 7 days in *ga3ox1,-2* lines A, D and E expressing *Co2::YFP:AtGA3ox1* compared with Col-0 and *ga3ox1,-2*.** **(A)** Primary root length ±SE. **(B)** Proximal meristem length ±SE. **(C)** Final cortical cell length ±SE. Seedlings were grown on vertical plates and lengths calculated using ImageJ. Green crucifixes indicate that the transgenic lines are significantly different from *ga3ox1,-2* and the red asterisks indicate that they are significantly different from Col-0, **=p<0.01, and ††=p<0.01. Error bars indicate the standard error. REML was used to generate the LSD given in Table 11-10.

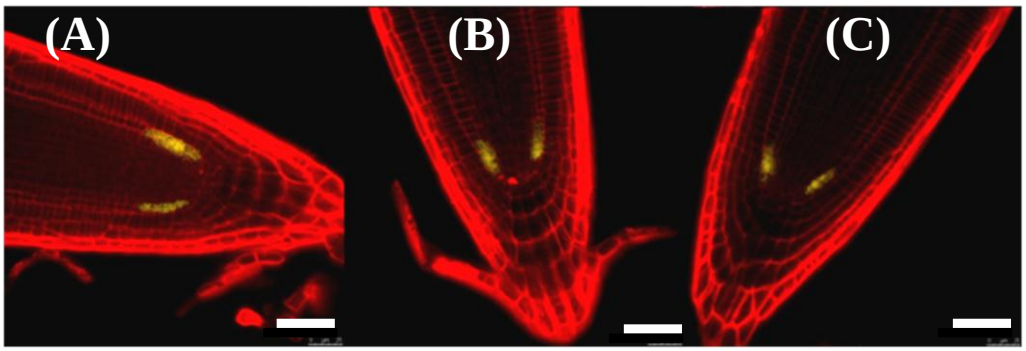

Figure 6-21**: YFP:AtGA3ox1 fluorescence within the meristematic region. (A-C)** Fluorescence in the meristematic zones for *ga3ox1,-2;Co2::YFP:AtGA3ox1* lines A, D and E, respectively. Confocal microscopy was performed on the five roots of seven day old seedlings after being grown on vertical Gelrite plates. The YFP and the propidium iodide emission images are overlaid. Bars are 100 μm in length.

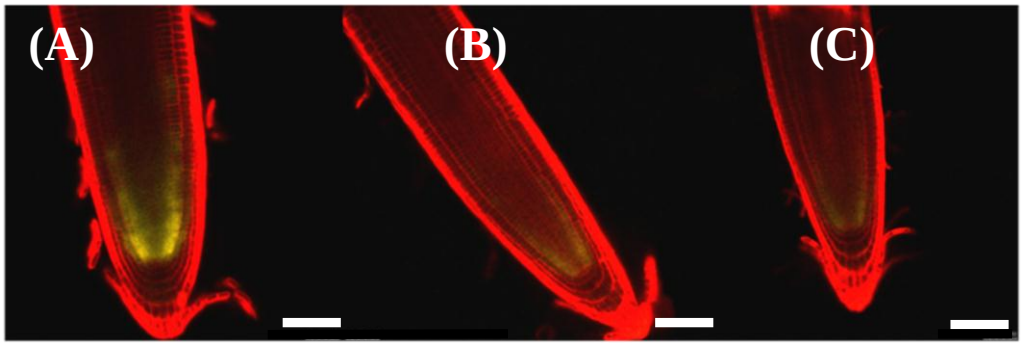

Figure 6-22**: YFP:AtGA3ox1 fluorescence in response to PAC and GA treatment. (A)** *ga3ox1,-2;Co2::YFP:AtGA3ox1* line D showing YFP fluorescence in the meristematic region for plants grown on Gelrite containing 1 μM PAC, **(B)** when grown on Gelrite, **(C)** when grown on Gelrite containing 1 μM GA_3. Confocal microscopy was performed on the five roots of seven day old seedlings after being grown on vertical Gelrite plates. The YFP and the propidium iodide emission images are overlaid. Bars are 100 μm in length.

6.1.10 *GL2::YFP:AtGA3ox1* partially rescues root length and completely rescues vegetative development of the *ga3ox1-2* mutant

Expression of *YFP:AtGA3ox1* in the root epidermis of the *ga3ox1,-2* mutant was achieved using the *GL2* promoter, which directs expression to the atrichoblast non-root hair epidermal cells (Masucci et al., 1996). The root lengths of five transgenic lines were compared with Col-0 and *ga1-3* (Figure 6-23); root lengths of all lines were significantly larger than *ga3ox1,-2* ($p<0.01$), although they were all also significantly smaller than Col-0 (lines A, C, D and E, $p<0.01$; line B, $p<0.05$). Lines A, C and D, for which roots lengths were closest to the mean, were chosen for further analysis. The targeted mis-expression construct completely rescued the shoot growth of all lines, except line E which was partially rescued (Figure 6-24).

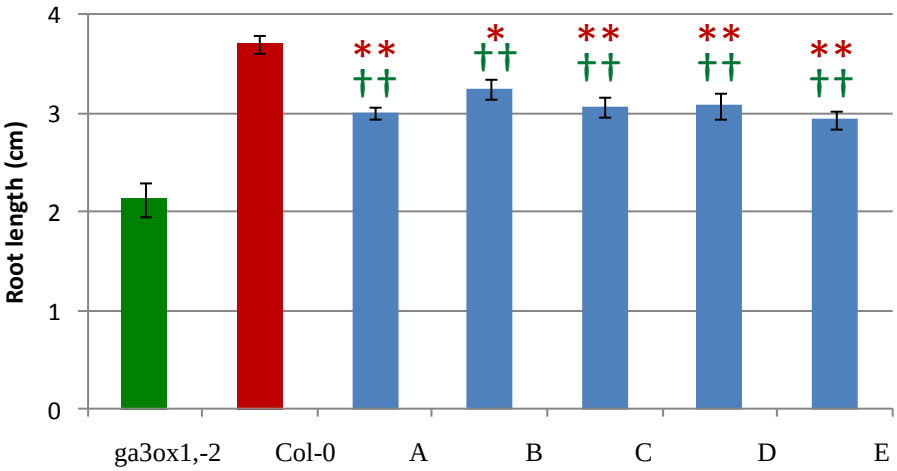

Figure 6-23**: Primary root length ±SE for *ga3ox1,-2;GL2::YFP:AtGA3ox1* lines (A-E) compared to *ga3ox1,-2* and Col-0 at seven days.** Seedlings were grown on vertical plates and lengths calculated using ImageJ. Green crucifixes indicate that the transgenic lines are significantly different from *ga3ox1,-2* and the red asterisks indicate that they are significantly different from Col-0. 30 plants were analyzed *=p<0.05, **=p<0.01, and ††=p<0.01. Error bars indicate the standard error. REML was used to generate the LSD given in Table 11-4.

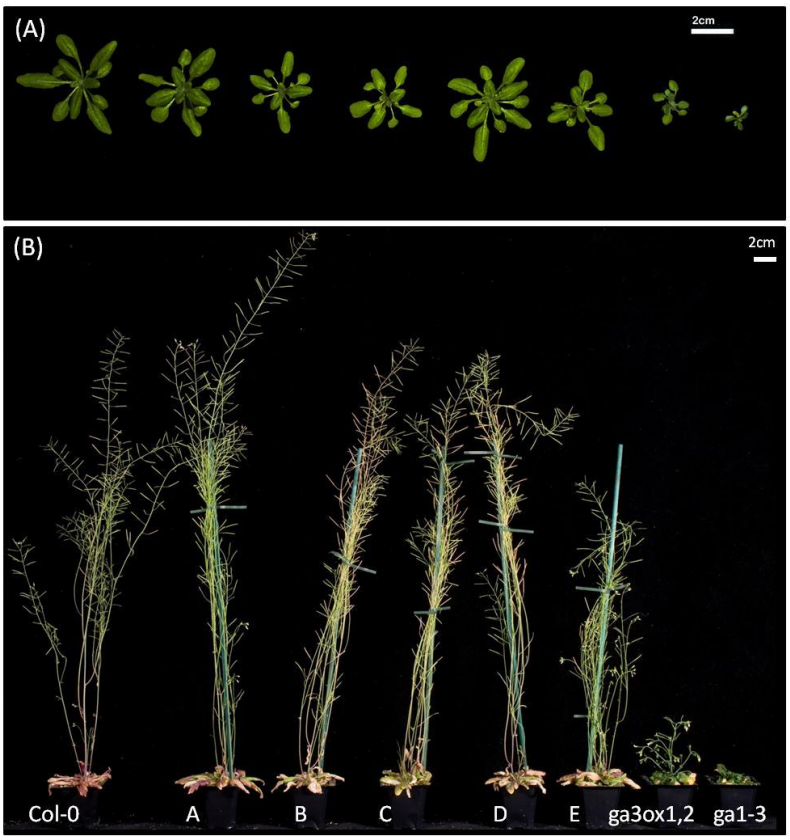

Figure 6-24**: Vegetative phenotypes for *ga3ox1,-2;GL2::YFP:AtGA3ox1* lines (A-E) compared to *ga1-3, ga3ox1,-2* and Col-0.** Plants were grown on Levingtons compost in 5.5 cm pots under long days for at three (A) and six weeks (B).

6.1.11 *ga3ox1,-2;GL2::YFP:AtGA3ox1*: root length, meristem length, cell length and transgene expression profile.

The primary root parameters of the three representative *ga3ox1,-2* lines expressing *GL2::YFP:AtGA3ox1* compared with *ga3ox1,-2* and Col-0 are shown in Figure 6-25. In contrast with the previous characterisation (section 6.1.10), *GL2::YFP:AtGA3ox1* completely rescued root growth of the *ga3ox1,-2* double mutant, with root lengths not significantly different from Col-0 ($p>0.05$). However, the meristem size and final cell lengths for each line were significantly smaller than in Col-0 ($p<0.01$), although they were larger than in *ga3ox1,-2* ($p>0.01$) (Figure 6-25).

Fluorescence could be observed for all three *ga3ox1,-2;GL2::YFP:AtGA3ox1* lines in the epidermal atrichoblast cells within the meristematic region, elongation zone and, to a lesser extent, differentiation zone (Figure 6-26). However, expression was occasionally brighter in one epidermal cells compared to its neighbour, creating a mosaic affect. This was easier to see in lateral roots or when the confocal microscope was focused on the surface of the epidermis (Figure 6-26). Growing plants on plates containing 1 µM GA_3 or 1 µM PAC did not alter the fluorescence domain although fluorescence intensity did appear to decrease with PAC treatment (Figure 6-27).

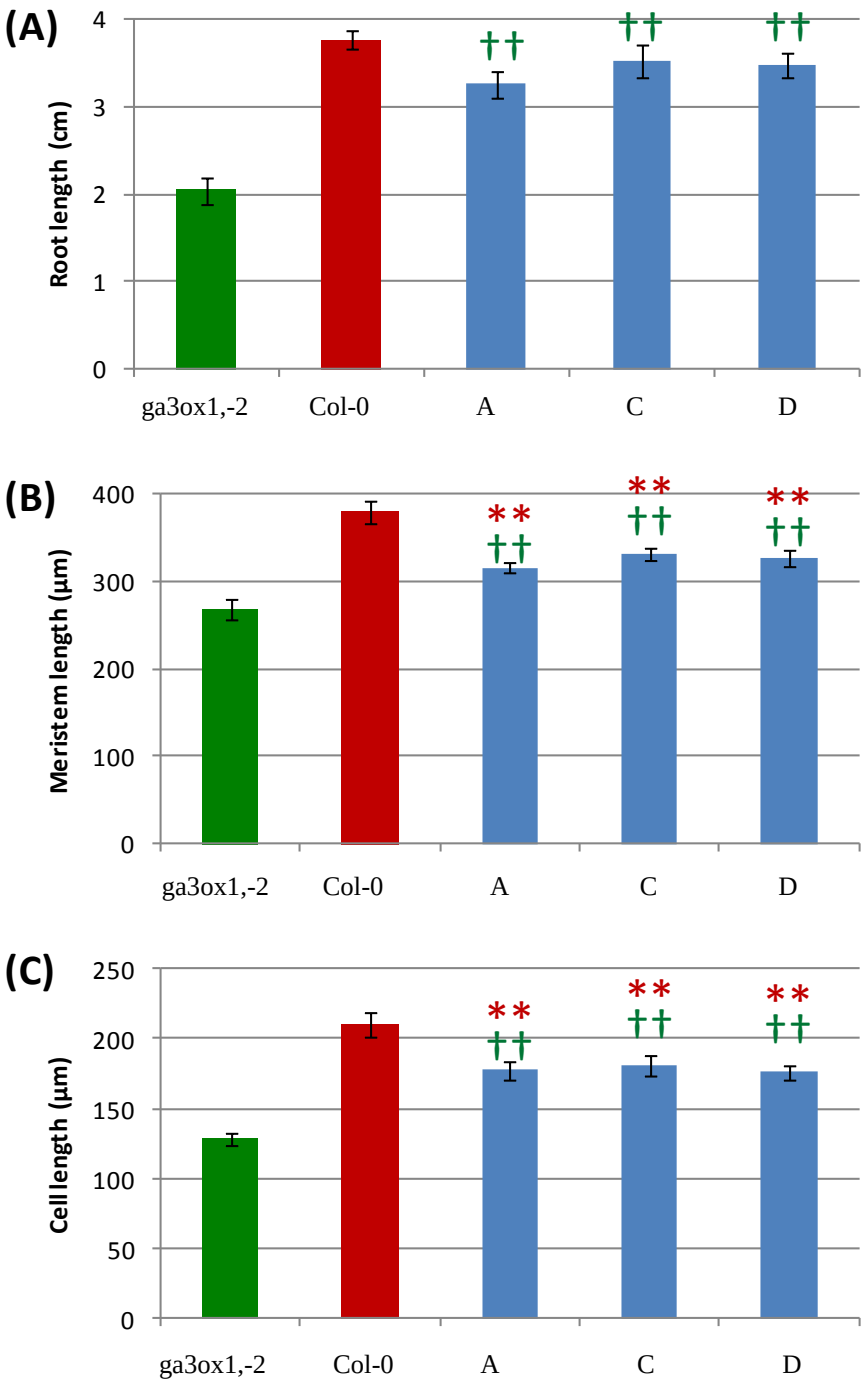

Figure 6-25**: Parameters for the primary root at 7 days in *ga3ox1,-2* lines A, C and D expressing *GL2::YFP:AtGA3ox1* compared with Col-0 and *ga3ox1,-2*. (A)** Primary root length ±SE. **(B)** Proximal meristem length ±SE. **(C)** Final cortical cell length ±SE. Seedlings were grown on vertical plates and lengths calculated using ImageJ. Green crucifixes indicate the transgenic lines that are significantly different from *ga3ox1,-2* and the red asterisks indicate that they are significantly different from Col-0. 15 plants were measured for root length, 5 plants for meristem size and cell length, with 5 cells measured **=p<0.01, and ††=p<0.01. Error bars indicate the standard error. REML was used to generate the LSD given in Table 11-10.

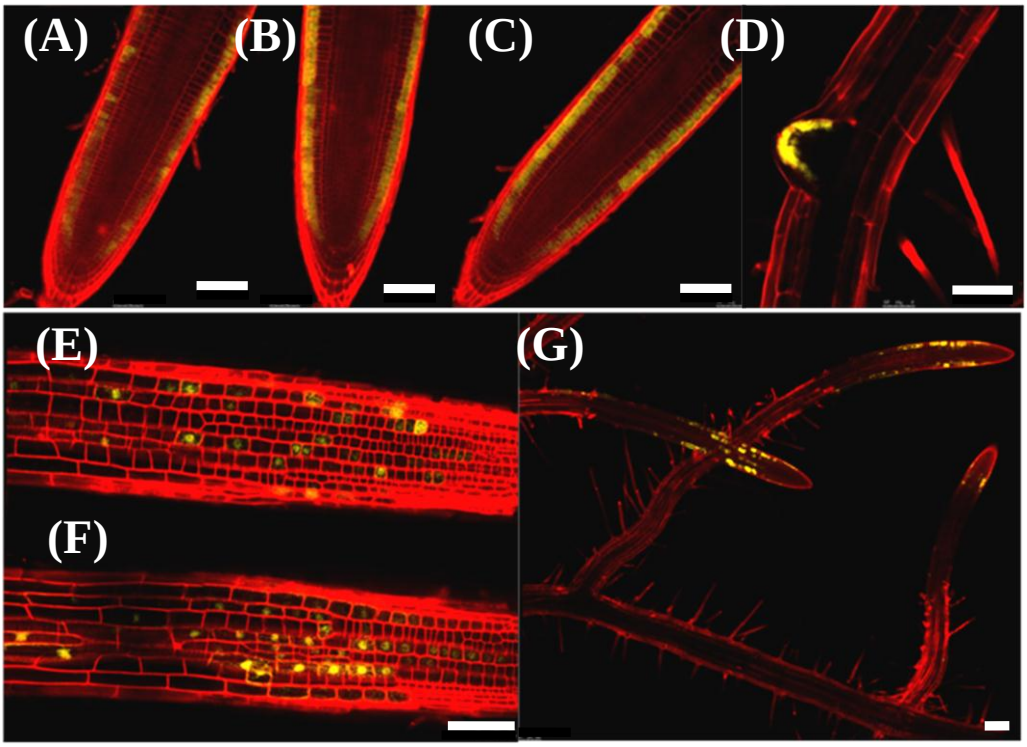

Figure 6-26: **YFP fluorescence in epidermal cells of the root meristem and lateral roots of *ga3ox1,-2;GL2::YFP:AtGA3ox1* lines. (A-C)** Expression in the meristematic region for line A, C and D, respectively. **(D)** Lateral root from line B emerging from the primary. **(E, F)** Epidermal YFP fluorescence on the roots of lines A and C, respectively. **(G)** Lateral roots of line A. Confocal microscopy was performed on the five roots of seven day old seedlings after being grown on vertical Gelrite plates. The YFP and the propidium iodide emission images are overlaid. Bars are 100 μm in length.

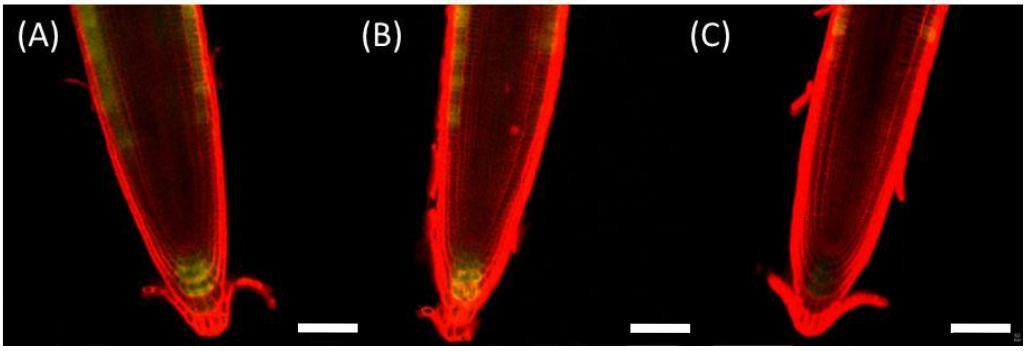

Figure 6-27**: YFP fluorescence in the meristem of *ga3ox1,-2;GL2::YFP:AtGA3ox1* line D. (A)** plant grown on Gelrite containing 1 μM GA_3, **(B)** when grown on Gelrite, **(C)** when grown on Gelrite containing 1 μM PAC. Confocal microscopy was performed on the five roots of seven day old seedlings after being grown on vertical Gelrite plates. The YFP and the propidium iodide emission images are overlaid. Bars are 100 μm in length.

6.1.12 *CAB::YFP:AtGA3ox1* partially rescues root length and completely rescues vegetative development of the *ga3ox1,-2* mutant

The effect of restoring GA biosynthesis in green tissues was investigated by driving expression of *YFP:AtGA3ox1* from the *CAB* promoter in the *ga3ox1,-2* mutant background (Puente et al., 1996). Comparison of the root lengths of four transgenic lines with Col-0 and *ga3ox1,-2* revealed a range of root phenotypes, from no rescue to complete rescue (Figure 6-28). In addition, shoot growth was completely rescued in all lines, except line C, for which there was only partial rescue (Figure 6-29). The root length of line A was not significantly different from *ga3ox1,-2* ($p>0.05$), while the root lengths of lines B and C were not significantly different from Col-0 ($p>0.05$). The root length of Line D was significantly different from both Col-0 and *ga3ox1,-2* ($p>0.01$). As there was such variability in root length amongst the transgenic lines, the largest line (C), the smallest line (A) and the closest to the mean line (D) were chosen for further analysis.

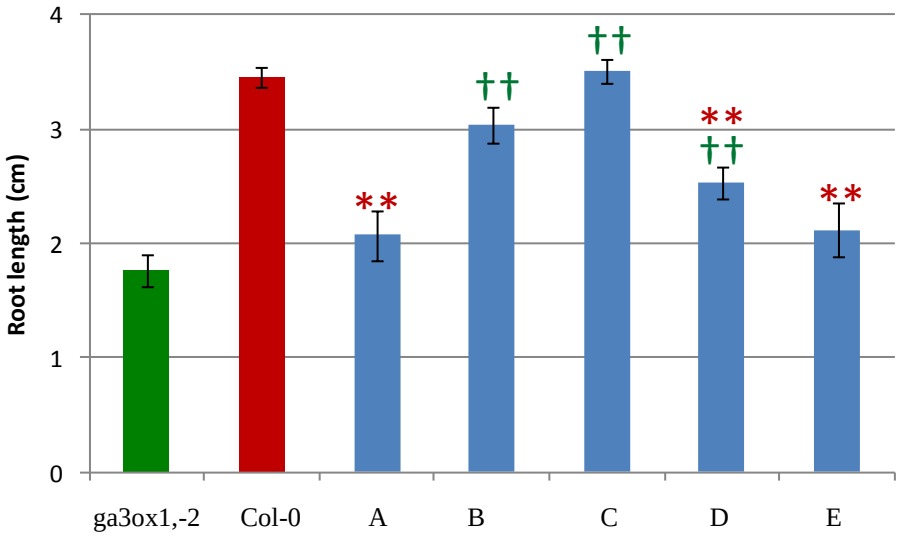

Figure 6-28**: Primary root length ±SE for *ga3ox1,-2;CAB::YFP:AtGA3ox1* lines (A-E) compared to *ga3ox1,-2* and Col-0 at seven days.** Seedlings were grown on vertical plates and lengths calculated using ImageJ. Green crucifixes indicate that the transgenic lines are significantly different from *ga3ox1,-2* and the red asterisks indicate that they are significantly different from Col-0. 30 plants were analyzed **=p<0.01, and ††=p<0.01. Error bars indicate the standard error. REML was used to generate the LSD given in Table 11-4.

Figure 6-29**: Vegetative phenotypes for *ga3ox1,-2;CAB::YFP:AtGA3ox1* lines (A-D) compared to *ga1-3, ga3ox1,-2* and Col-0.** Plants were grown on Levingtons compost in 5.5 cm pots under long days for three (A) and six weeks (B).

6.1.13 *ga3ox1,-2;CAB::YFP:AtGA3ox1*: root length, meristem length, cell length and transgene expression profile.

The primary root parameters of the three representative *ga3ox1,-2* lines expressing *CAB::YFP:AtGA3ox1* compared with *ga3ox1,-2* and Col-0 are shown in Figure 6-30. There was less variability in root growth than found in the previous characterisation (section 6.1.12). *CAB::YFP:AtGA3ox1* expression partially rescued root length, with almost complete rescue of cell size, but only partial rescue of meristem size. Thus, the root and meristem lengths of all three lines were significantly different from both *ga3ox1,-2* and Col-0 ($p<0.01$), whereas only line D had a final cell length that was significantly different from Col-0 ($p>0.05$). The final cell lengths of all three lines were also significantly larger than in *ga3ox1,-2*.

All three *CAB::YFP:AtGA3ox1* lines exhibited fluorescence in young green vegetative shoot tissues (Figure 6-31), and interestingly fluorescence could also be observed within columella cells. This had not been noticed for any of the other YFP constructs (Figure 6-32). When plants were sown on plates containing 1 µM GA_3 and 1 µM PAC, the YFP fluorescence could still be observed within the columella cells (Figure 6-32).

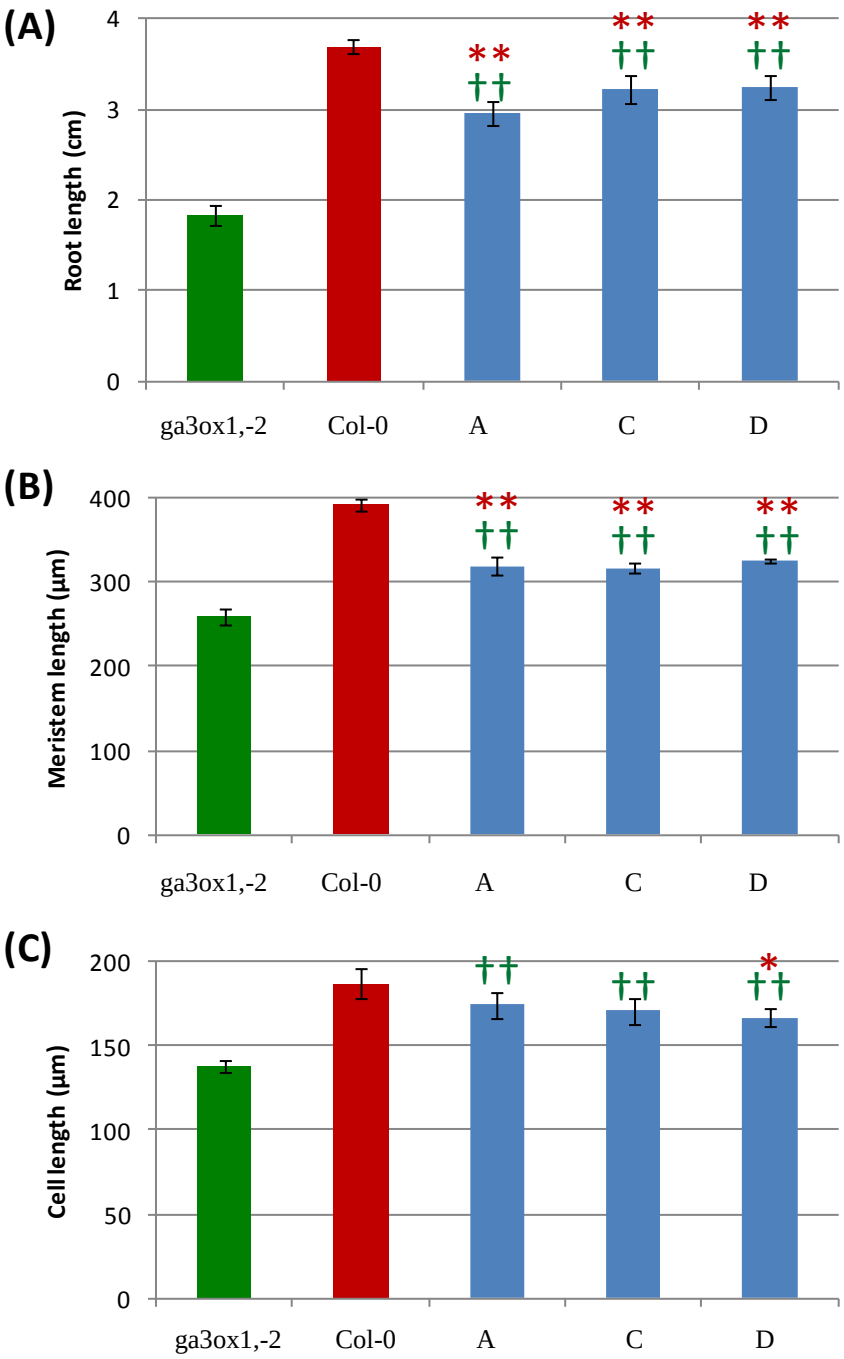

Figure 6-30**: Parameters for the primary root at 7 days in lines A-D expressing *CAB::YFP:AtGA3ox1* compared with Col-0 and *ga3ox1,-2*. (A)** Primary root length ±SE. **(B)** Proximal meristem length ±SE. **(C)** Final cortical cell length ±SE. Seedlings were grown on vertical plates and lengths calculated using ImageJ. Green crucifixes indicate the transgenic lines that are significantly different from *ga3ox1,-2* and the red asterisks indicate that they are significantly different from Col-0. 15 plants were measured for root length, 5 plants had their meristems and 5 cells measured *=p<0.05, **=p<0.01, and ††=p<0.01. Error bars indicate the standard error. REML was used to generate the LSD given in Table 11-10.

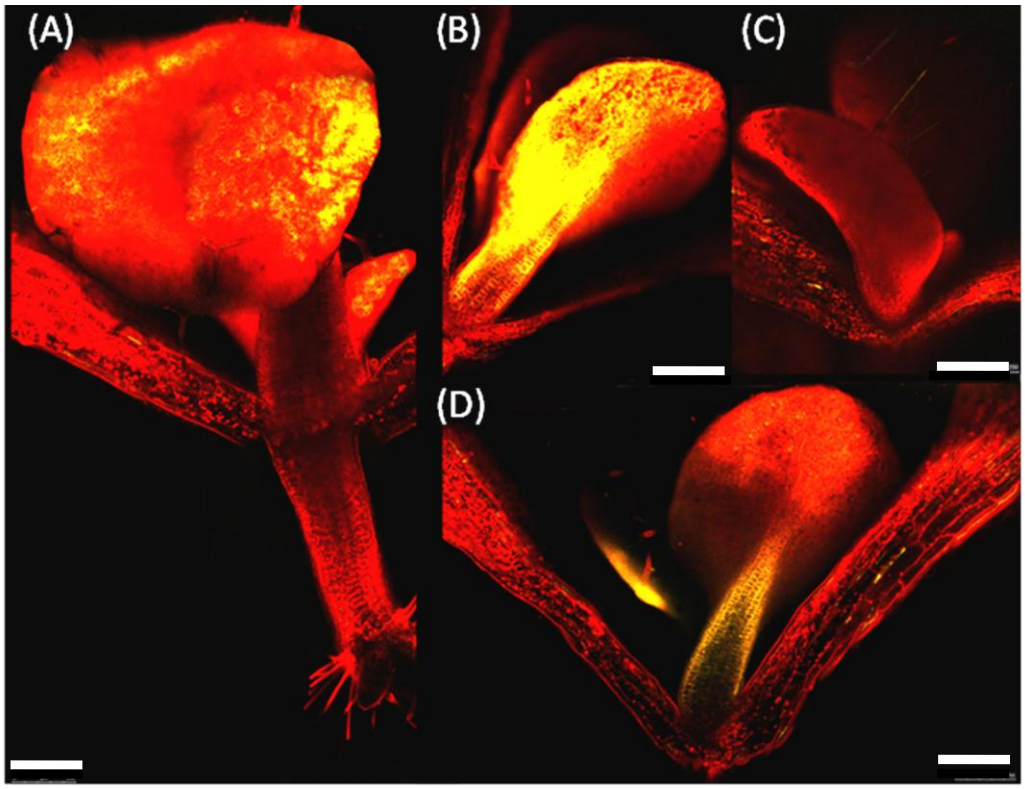

Figure 6-31: **YFP fluorescence in green tissue of *ga3ox1,-2;CAB::YFP:AtGA3ox1* lines. (A, B and D).** Photosynthetic tissue of lines A, C and D, respectively. **(C)** Photosynthetic tissue for the *ga3ox1,-2* mutant showing slight auto-fluorescence in the cotyledon stem. Confocal microscopy was performed on the five roots of seven day old seedlings after being grown on vertical Gelrite plates. The YFP and the propidium iodide emission images are overlaid. Bars are 100 μm in length.

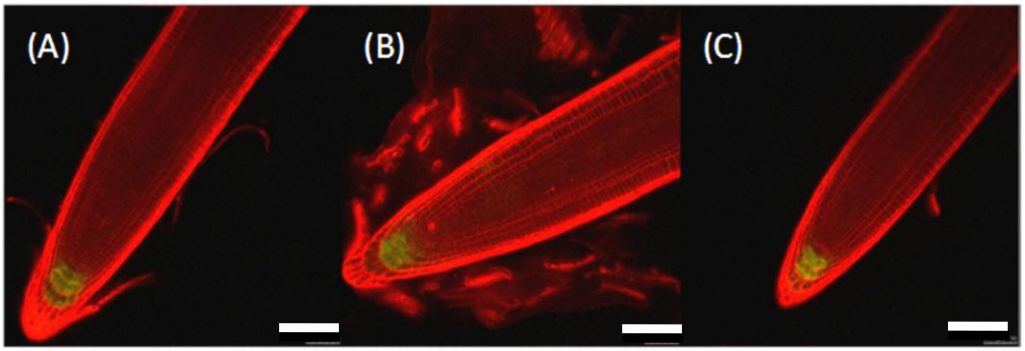

Figure 6-32**: YFP fluorescence within columella cells of *ga3ox1,-2;CAB::YFP:AtGA3ox1* line D. (A)** the meristematic region of plants grown on Gelrite containing 1 μM GA_3, **(B)** when grown on Gelrite, **(C)** when grown on Gelrite containing 1 μM PAC. Confocal microscopy was performed on the five roots of seven day old seedlings after being grown on vertical Gelrite plates. The YFP and the propidium iodide emission images are overlaid. Bars are 100 μm in length.

6.1.14 Comparison of the promoters driving *YFP:AtGA3ox1* expression on the primary root, meristem and final cell lengths.

Root growth parameters were compared for the median lines for each *promoter::YFP:AtGA3ox1* construct (Figure 6-33). When driven from the *SHR, SCR, CoR* and *GL2* promoters, *YFP:AtGA3ox1* expression rescued root growth in the *ga3ox1,-2* mutant, producing root lengths that were not significantly different from Col-0 ($p>0.05$). In the *SHR* and *SCR* lines, meristem and final cell lengths were also not significantly different from Col-0 ($p>0.05$). Final cell lengths in the *CoR* and *GL2* were also not significantly different from Col-0 ($p>0.05$), but meristem size for these lines was significantly smaller than in Col-0 ($p<0.01$), although significantly larger than in *ga3ox1,-2* ($p<0.01$). Expression of *YFP:AtGA3ox1* from the *CAB* promoter mildly rescued root growth producing root lengths that were significantly larger than in *ga3ox1,-2*, although significantly smaller than in Col-0 ($p<0.01$). Meristem size in this line was not significantly different from that in *ga3ox1,-2* ($p>0.05$) while cell length was not significantly different from Col-0 ($p>0.05$). The least rescue of root length was obtained from the *Co2* promoter, with root length in this line being significantly different from both controls ($p<0.01$). Although meristem size in the *ga3ox1,-2;Co2::YFP:AtGA3ox1* line was not significantly different from Col-0 ($p>0.05$), final cell length was significantly smaller than in Col-0 ($p<0.05$), if significantly larger than *ga3ox1,-2* ($p<0.01$). Figure 6-34 shows representative images for the root tip for the *SHR*, *SCR*, *CoR*, *Co2* and *GL2* YFP:AtGA20ox1 lines, as fluorescence was observed at the root tip for the *CAB* lines both the root tip and photosynthetic tissue near the SAM are shown.

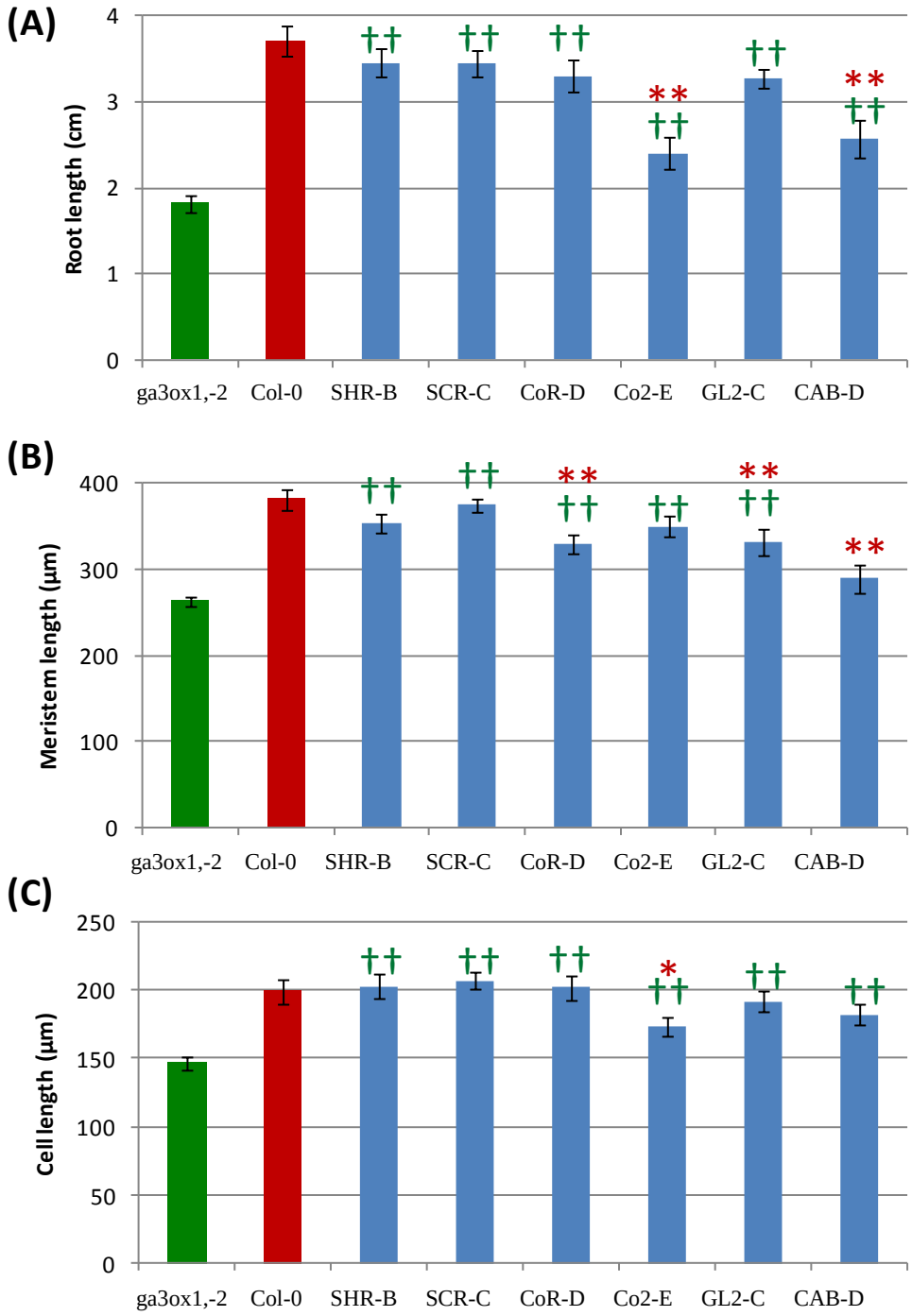

Figure 6-33**: Primary root parameters for the median lines for each *YFP:AtGA3ox1* construct compared with Col-0 and *ga3ox1,-2* at seven days. (A)** Primary root length ±SE. **(B)** Proximal meristem length ±SE. **(C)** Final cortical cell length ±SE. Seedlings were grown on vertical plates and lengths calculated using ImageJ. Green crucifixes indicate that the transgenic lines are significantly different from *ga3ox1,-2* and the red asterisks indicate that they are significantly different from Col-0. 15 plants were measured for root length and 5 plants for meristem size and cell length, with 5 cortical cells measured per plant *=p<0.05, **=p<0.01, and ††=p<0.01. Error bars indicate the standard error. LSD given in Table 11-11.

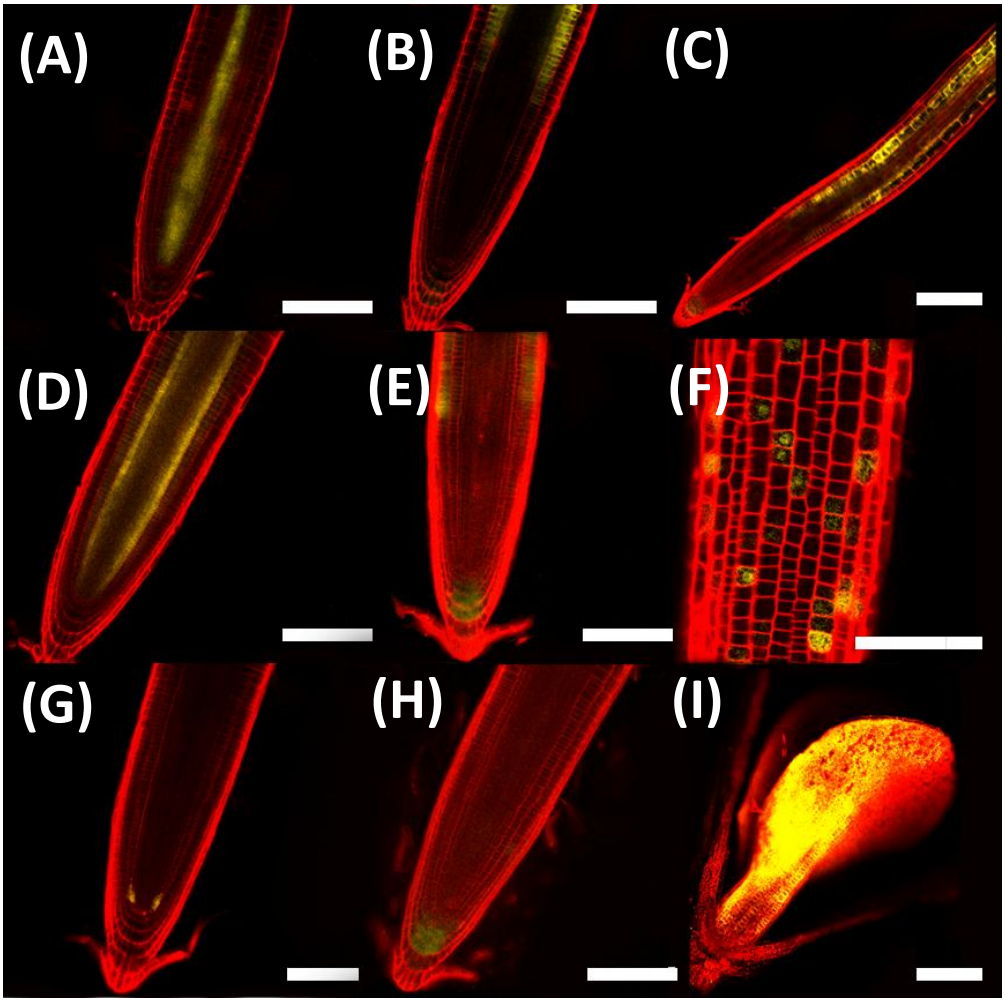

Figure 6-34: **Representative images for YFP fluorescence in the GA3ox1 lines. (A)** YFP-AtGA3ox1 attached to *SHR*, **(B-C)** *CoR*, **(D)** *SCR*, **(E-F)** *GL2*, **(G)** *Co2*, **(H-I)** *CAB* promoters. Confocal microscopy was performed on seven day-old seedlings grown on vertical Gelrite plates. The YFP and the propidium iodide emission images are overlain. Bars are 100 μm in length

In summary, *YFP-AtGA3ox1* expression was able to rescue root growth when expressed within the stele, endodermis cortex or epidermis (Figure 6-33). Although the columella cells were not intentionally targeted they may also have contributed to the rescue of root growth in the *CAB::YFP:AtGA3ox1*, *GL2::YFP:AtGA3ox1* and *CoR::YFP:AtGA3ox1* lines. The partial rescue of cortical cell length of the *Co2::YFP:AtGA3ox1* lines despite the transgene not being expressed in the elongation zone may suggest either short distance movement of GA_4 or bioactive GA being locked in the cells as they move from the meristem. Here we show partial rescue of the *ga3ox1,-2* double mutant by expression of YFP-AtGA3ox1 under different promoters. However, potentially YFP-AtGA3ox1 under the control of its native promoter may only partially complement the *ga3ox1,-2* double mutant. This could be confirmed using the *ga3ox2* mutant, or transgenic *ga3ox1,-2* double mutants complemented with YFP-AtGA3ox1 under the native promoter as additional controls. This would demonstrate the level of complementation compared to the level of rescue when GA3ox1 alone is in its native expression state.

6.2 DISCUSSION OF THE RESCUE OF *ga3ox1,-2* BY TARGETED EXPRESSION OF YFP-*ATGA3OX1*

Previous work has shown that GA signalling within the endodermis is required for GA-dependent cell division and cell elongation within the *Arabidopsis* root (Ubeda-Tomás et al., 2009, Ubeda-Tomas et al., 2008). Mitchum *et al.*, (2006) showed that *AtGA3ox1* and *AtGA3ox2* are partially redundant and that the double mutant produced dwarf roots. They also used promoter GUS fusions to demonstrate that expression of *AtGA3ox1* and *AtGA3ox2* is tightly regulated within the *Arabidopsis* root and is restricted to specific tissues and stages of development (Mitchum et al., 2006). Interestingly expression of these genes did not occur just in the endodermis but also appeared to be expressed within the vasculature, the QC, the initial daughter cells and the columella cells. In the current study, the site of GA activation was investigated by tissue-specific expression of *YFP:AtGA3ox1* in the *ga3ox1,-2* mutant, which produced a range

of phenotypes and demonstrated that GA activation is required both in the meristematic region and in the elongation zone for normal meristem and cell elongation to occur. As discussed below, this study demonstrates that GA can be activated in the stele, endodermis, cortex, epidermis and columella and promote GA dependant root growth (Figure 6-35).

6.2.1 Ectopic aerial expression of tissue specific YFP-AtGA3ox1 transgenes

The photosynthetic tissue specific *ga3ox1,-2;CAB::YFP:AtGA3ox1* transgenic lines had semi-dwarf root growth and had complete aerial growth. Closer examination demonstrates that final cell size was partially rescued while meristem length was not (Figure 6-30). This indicates that cell elongation during root growth can be promoted by either bioactive C_{19}-GAs moving down from aerial tissues. In addition, this also demonstrates that ectopic expression of the YFP-AtGA3ox1 transgene in aerial tissues may partially rescue cell elongation. Therefore, the complete cell elongation rescue of the *SHR::YFP:AtGA3ox1, SCR::YFP:AtGA3ox1, CoR::YFP:AtGA3ox1* and *GL2::YFP:AtGA3ox1 ga3ox1,-,2* mutant lines and the partial cell elongation rescue of the *ga3ox1,-,2;Co2::YFP:AtGA3ox1* lines may be due to bioactive GAs moving to the root from the shoot. Interestingly the *ga3ox1,-2;CAB::YFP:AtGA3ox1* lines displayed a partial rescue of meristem growth, which could suggest that bioactive GAs may be able to promote root tips cell division rates. However, the *ga3ox1,2;CAB::YFP:AtGA3ox1, ga3ox1,2;CoR::YFP:AtGA3ox1,* and *ga3ox1,2;GL2::YFP:AtGA3ox1*, lines also had ectopic expression within the columella cells which may have contributed to a meristematic pool of bioactive GA that partially rescued meristem length. Therefore, aerial tissues may be able produce excess bioactive C_{19}-GAs in order to promote both cell elongation and cell division, but due to abnormal fluorescence patterns this is inconclusive.

Therefore, aerial tissues can potentially produce excess C_{20}-GAs in order to boost cell elongation and/or produce excess bioactive C_{19}-GAs in order to promote both cell elongation and cell division.

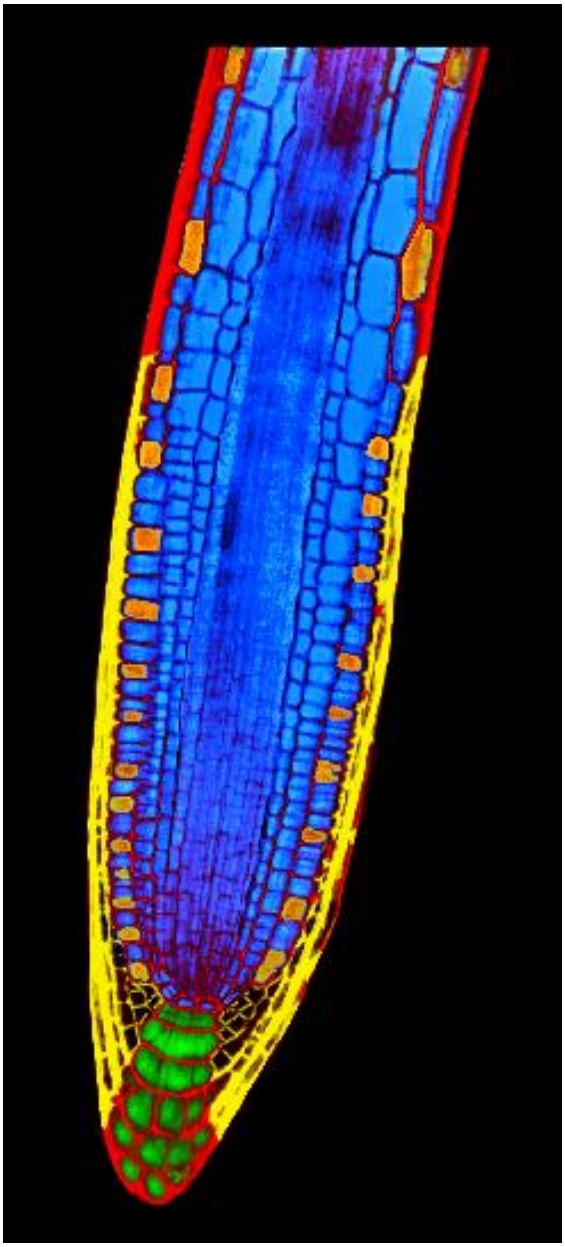

Figure 6-35: **Schematic diagram highlighting which tissues were able to rescue root growth when YFP-AtGA3ox1 was targeted to them in the *ga3ox1,-2* double mutant.** The blue vasculature, endodermal, cortical and epidermal cells are all potential sites of GA_9 3-oxidation. The orange epidermal cells demonstrate abnormal fluorescence patterns within the atrichoblast cell file. The yellow lateral root cap cells were not studied during this project. The green columella cells were not targeted during this experiment but ectopic fluorescence was observed within them suggesting they are an important site of GA_9 3-oxidation.

6.2.2 The complete aerial rescue of the *ga3ox1,-2* mutant using tissue specific expression of *YFP-GA3ox1*

The complete aerial rescue and partial root elongation rescue with every promoter also demonstrated that the GA3ox substrate GA_9 is either produced in every cell or is not sufficiently mobile to access the GA3ox enzyme in any tissue. Furthermore, the bioactive GA_4 must be able to move to its sites of perception or every cell is capable of promoting growth in response to it. Interestingly, expressing *YFP-AtGA20ox1* in photosynthetic tissue with the *CAB* promoter (Puente et al., 1996) was able to partially rescue root growth via increased cell elongation indicating that the products of this enzyme, either the C_{20}-GA_{15} or -GA_{24}, or the C_{19}-GAs, GA_9 and/or C_{19}-GA_4, are capable of moving down from green tissue to influence cell elongation (Figure 6-30). Interestingly, the *CAB::YFP-AtGA3ox1* lines also partially rescued meristem length, indicating that GAs are capable of moving down from aerial tissue (Figure 6-30), or alternatively as YFP-AtGA3ox1 fluorescence could be observed within the columella cells and this may be the source of the bioactive GA that partially rescued meristem length. However, it is unlikely that columella expression of *GA3ox1* would rescue cell length since the *Co2::YFP:AtGA3ox1* lines rescued final cell length to a lesser extent than the *CAB::YFP:atGA3ox1* lines (Figure 6-33). Therefore it is possible that the root tissue specific promoter's activity within photosynthetic tissue might partially rescue the cell elongation and this should be taken into consideration when interpreting the results.

These data indicate that bioactive GA_4 is capable of moving down from photosynthetic tissues to influence cell elongation, but has little effect on cell division, possibly suggesting the presence of GA import mechanism within in the elongation zone. This long distance transport may be via mass flow in the vasculature and the eventual movement into a cell could suggest the need for a directional cellular transport mechanism as has been previously demonstrated with auxin or perhaps via aquaporins (Maurel et al., 2008, Vieten et al., 2007, Kramer, 2006).

6.2.3 GA activation is required in both the meristematic region and the elongation zone for normal root growth

When *YFP:AtGA3ox1* was expressed in the elongation zone ground tissue with the *CoR* promoter (Dinneny et al., 2008), it completely rescued cell elongation and partially rescued meristem size (Figure 6-15). Conversely, expression of this construct within the cortical cells of the meristem with the *Co2* (Heidstra et al., 2004) promoter only partially rescued root growth. This was mediated primarily by rescue of cell division, but also partially of cell elongation (Figure 6-20). These findings suggest that *GA3ox* expression within the meristematic region is required for normal cell division and its expression within the elongation zone is required for full cell elongation. Thus, these processes require a local activation site to provide a source of bioactive GA, i.e. GA_4. In summary, normal root growth requires 3β-hydroxylation of GA_9 to occur within the cells of both the meristematic region and the elongation zone.

6.2.4 GA_9 and/or GA_4 are mobile within the root over short distances

The partial rescue of the *ga3ox1,-2* mutant by YFP-AtGA3ox1 when expressed from the zone-specific promoters *CoR* and *Co2* demonstrated that both the meristematic and elongation zones contain GA_9 (Figure 6-15 and Figure 6-20). Expressing YFP-AtGA3ox1 within the endodermis or stele cells of both the meristematic and elongation zones with the *SHR* and *SCR* promoters (Figure 6-5 and Figure 6-9) was able to rescue both meristem size and final cell length, demonstrating that these cells contain GA_9 and that the bioactive GA is able to reach important sites of perception by either diffusion, active transport or both (Ubeda-Tomás et al., 2009, Dobson, 2009, Ubeda-Tomas et al., 2008, Kramer, 2006). Expressing *AtGA3ox1* within the epidermis of both the meristematic and elongation zones with the *GL2* promoter (Masucci et al., 1996) partially rescued root, meristem, and final cell lengths (Figure 6-25), demonstrating that all root tissues have access to GA_9 and that the bioactive GA_4 is able to

promote growth in any root tissue or is capable of moving to the sites of GA perception (Ubeda-Tomás et al., 2009, Ubeda-Tomas et al., 2008).

In summary, C_{19}-GA_9 is likely to be mobile or can be synthesised in every cell as it is available in every tissue tested in this experiment, the activated GA_4 is capable of moving from one stage of development to another in both acropetal and basipetal directions. This short distance movement would have to be via plasmodesmata or active transport across the membrane protein channel as diffusion across a membrane is unlikely according to recent systems biology modelling and calculations based on auxin membrane mobility (Dobson, 2009, Kramer, 2006, Eriksson et al., 2006).

6.2.5 Post-transcriptional regulation of AtGA3ox in the QC and differentiation zone

The *AtGA3ox1::GUS* data produced by Mitchum *et al.,* (2006) demonstrated expression only within the vasculature and ground tissue of the differentiation zone, while *AtGA3ox2::GUS* was confined to the QC, columella cells, the vasculature of the elongation zone of the *Arabidopsis* root, with GA3ox expression completely absent from the proximal meristem region. This suggested GA can naturally be activated in the QC, its initial daughter cells, the columella cells and then later on in development within the vasculature and ground tissue of the elongation zone. This study showed that the columella cells contain molecular components that appear to be capable of stabilizing the GA3ox protein (Figure 6-16 and Figure 6-32). The *CAB::YFP-AtGA3ox1*, *GL2::YFP-AtGA3ox1* and *CoR::YFP-AtGA3ox1* lines all had fluorescence within the columella cells, indicating expression of these genes in a location that was not previously described by Puente *et al.,* (1996), Mascui *et al.,* (1996) or Dinney *et al.,* (2006). It is possible that these promoters drive expression in the columella at a low level and that YFP-AtGA3ox1 is stabilised in these cells (Figure 6-16, Figure 6-27 and Figure 6-32). This suggests that there might be mechanisms that stabilise the YFP-AtGA3ox1 protein fusions or some form of post-transcriptional or post-translational regulation.

The epidermal fluorescence of the YFP-AtGA3ox1 expressed under the *GL2* promoter did not give the expected traditional strips of atrioblast cell files (Masucci et al., 1996). Instead fluorescence appeared to be irregular (Figure 6-26). This might suggest a role for GA activation of pre-existing GA precursors in cells that will differentiate into root hairs. Further evidence for tissue specific regulation of GA3ox stability comes from the *Co2::YFP-AtGA3ox1* lines in which fluorescence was restricted to just a few cells near the QC (Figure 6-21) and did not extend along the proximal meristem like other Co2 transgene fusions (Figure 4-21 and/or Figure 4-50). This potentially implies that within the cortical cells of the proximal meristem there are post-transcriptional and/or -translational regulatory mechanisms dependent on GA signalling (Figure 6-22). Taken together these data suggest that AtGA3ox1 stability and/or expression may be regulated in a tissue-specific, GA-dependant and stage-specific manner. In addition, this experiment also provides evidence for the existence of a molecular mechanism that promotes YFP-AtGA3ox1 stability within columella cells.

7 MAPPING THE SITE OF GA PERCEPTION IN ROOTS AND SHOOTS

7.1 INTRODUCTION TO GA PERCEPTION

GA perception is mediated by the GID1 receptor, which was first identified in rice (Ueguchi-Tanaka et al., 2005). Three GID1 receptor genes were subsequently identified in *Arabidopsis* and were named: *AtGID1a*, *AtGID1b* and *AtGID1c* (Nakajima et al., 2006). These paralogues, which are partially redundant, bind to DELLA proteins in the presence of GA, causing them to be polyubiquitinated and subsequently degraded by the 26S proteosome. Interestingly GID1b has a substitution that allows it to bind to GAI independently of GA, the substitution responsible for this is also found in the GA receptors found within rice (*Oryza sativa*), soybean (*Glycine max*) and oil seed rape (*Brassica napus*) (Yamamoto et al., 2010). It has recently been shown that bioactive GA enters a pocket within the GA receptor (Figure 7-1), the N-terminus then closes over the binding pocket, trapping the GA molecule within the receptor. This allosterically activates GID1 by exposing the hydrophobic surface of the N-terminus lid, which binds to DELLA proteins (Shimada et al., 2008, Murase et al., 2008). In addition, it has recently been shown in rice that the OsSLR1 proteins DELLA/TVHYNP motif also binds with the GID1 receptor, this enables the GRAS domain of SLR1 to interact with the GID1 N-terminus and the then stable GID1-SLR1 complex is more efficiently recognized by GID2, the F-box responsible for targeting SLR1 for degradation (Hirano et al., 2010). Although all GA receptors function via the same mechanism, the genes appear to have distinct expression profiles and therefore possibly also exhibit some distinct roles (Iuchi et al., 2007, Ueguchi-Tanaka et al., 2007, Griffiths et al., 2006). Recent research has provided insights into the molecular interactions that control GA signalling and many of the genes involved have been discovered (Gallego-Bartolomé et al., 2010, Feng et al., 2008, de Lucas et al., 2008, Oh et al., 2004); however less is known about the cellular and tissue scale mechanisms that allow GA signalling to influence plant growth and development.

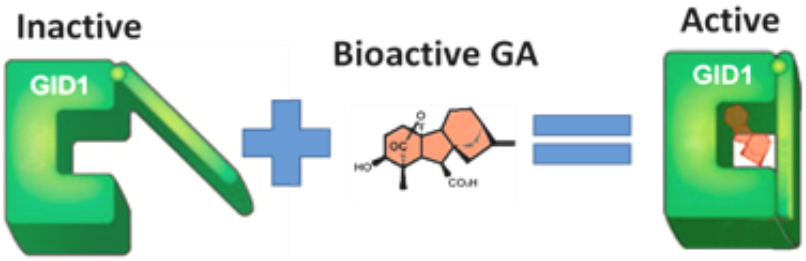

Figure 7-1: **Bioactive GA binds inside a pocket on the GID1 receptor.** When GA binds to the GID1 receptor it is enclosed within a pocket causing a conformational change, trapping the GA molecule inside. Adapted with permission from Hedden (2008).

7.1.1 Tissue specific GA perception

Recent work has shown that in *Arabidopsis* roots regulation of meristem size and final cell length by GA is mediated via DELLA degradation within the endodermis (Ubeda-Tomás et al., 2009, Ubeda-Tomas et al., 2008). These authors targeted a non-degradable form of DELLA to specific root tissues, observing that root growth was blocked when expressed in endodermal cells, but not in other root tissues. To investigate if this DELLA-mediated repression of root growth requires GA perception within the root endodermis, a targeted rescue of the *gid1a gid1b gid1c* triple mutant (*gid1a,-b,-c*) was employed using root tissue specific promoters to express a functional GID1a receptor in specific tissues and stages of development. These experiments rely on the fact that the *gid1a,-b,-c* triple mutant has a dwarf root phenotype (Figure 7-2) (Griffiths et al., 2006).

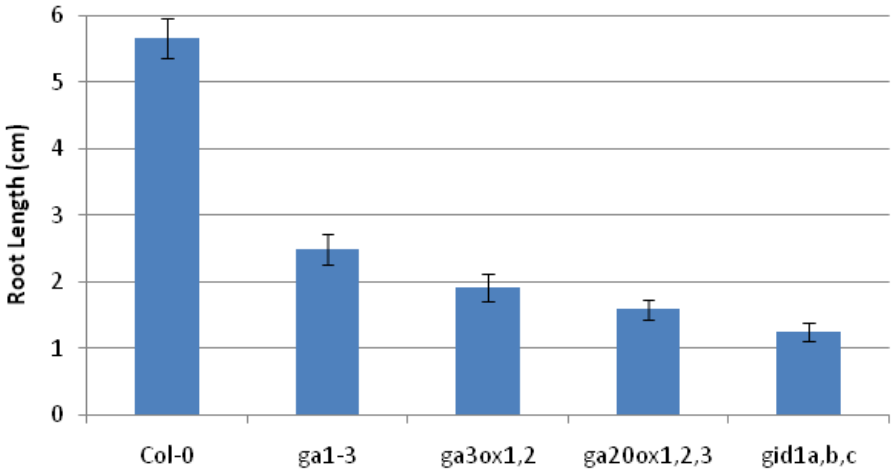

Figure 7-2: **Root length ±SE of GA biosynthetic and signalling mutants.** Primary root lengths are shown for the *gid1a,-b,-c* triple mutant, *ga20ox1,-2,-3* triple mutant, *ga3ox1,-2* double mutant, *ga1-3* and Col-0 seven days after embryo excision. 30 plants were analyzed, seedlings were grown on vertical Gelrite plates and lengths calculated using ImageJ. Error bars indicate standard error.

Plants homozygous for the *gid1a* and *gid1b* knock out mutations and heterozygous for the *gid1c* knockout were transformed to allow the expression of a functional *AtGID1a* receptor to be targeted to the specific tissues and stages of root cell development. Restoration of growth due to the expression of a functional *GID1A* in specific cell-types will be indicative of site(s) of perception. Transgenic lines with homozygous single insertions were generated and genotyped to select lines homozygous for all three *gid1* knockout mutations (See section 3.5.5). It was originally intended to express a GID1a-YFP fusion, but no YFP fluorescence was detected in any of the transgenic lines and it was subsequently found that, due to the presence of a stop codon at the end of the GID1a open reading frame, only the GID1a receptor would be translated.

7.2 CHARACTERISATION OF *ATGID1A* TARGETED EXPRESSION LINES

The effect of targeting the expression of *AtGID1a* with tissue specific promoters on the phenotype of *gid1a,-b,-c* triple mutant plants was initially monitored in terms of effects on the final root length after seven days growth on vertical agar plates after embryo excision of all lines including the Col-0 controls. In addition, the vegetative growth of the rosette after three weeks and the inflorescence after six weeks was also photographed. The median transgenic line was then selected for more detailed analysis of root growth, measuring root length, meristem lengths, and final cell sizes. In all experiments the transgenic lines were compared to the triple *gid1a,-b,-c* mutant and Col-0. In all experiments the transgenic lines were compared with Col-0 as this was the original ecotype that the *gid1a,-b,-c* mutant was generated in and *gid1a,-b,-c* as this was the GA deficient mutant that was genetically modified for the targeted GID1a rescue.

7.2.1 *SHR::GID1a* partially rescues root length and vegetative development of the *gid1a,-b,-c* mutant

To investigate the effect of expressing *GID1a* in the root stele, *AtGID1a* expression was driven from the *SHR* promoter (Di Laurenzio et al., 1996) in the *gid1a,-b,-c* triple mutant background. The root lengths of the transgenic lines compared with Col-0 and *gid1a,-b,-c* shown in Figure 7-3 demonstrate that GA perception in the stele alone is not sufficient to completely rescue root growth. Furthermore, expression of the transgene also partially rescued shoot growth (Figure 7-4): rosettes contained dark spiralling leaves, and after six to eight weeks, produced long thin inflorescences with no lateral branches and infertile flowers. Root lengths for all lines were significantly different from Col-0 ($p<0.01$) and *gid1a,-b,-c* ($p<0.01$). The root length of Line D was closest to the mean of all lines so was chosen for further analysis.

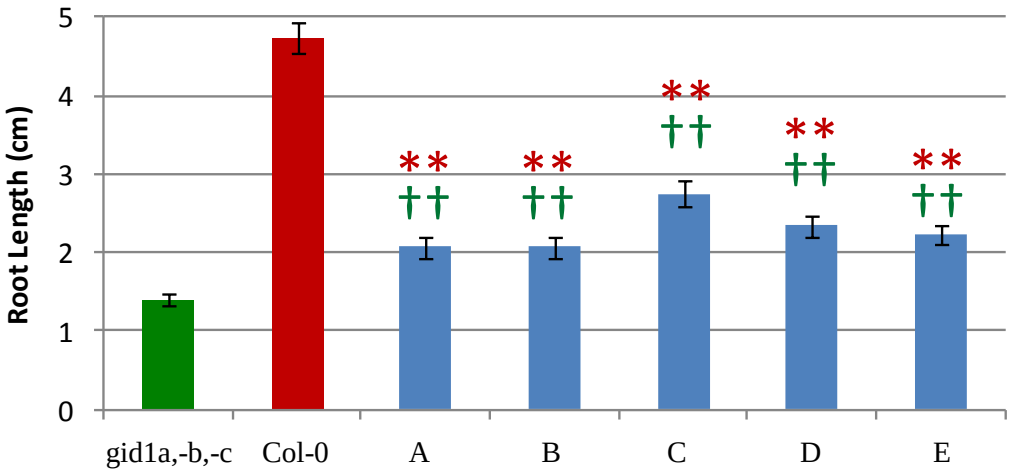

Figure 7-3**: Primary root length ±SE at seven days post embryo excision for *gid1a,-b,-c;SHR:GID1a* lines (A-E) compared to *gid1a,-b,-c* and Col-0.** Seedlings were grown on vertical plates and lengths calculated using ImageJ. Green crucifixes indicate the transgenic lines are significantly different from *gid1a,-b,-c* and the red asterisks indicate they are significantly different from the Col-0. 30 plants for each line were analyzed **=p<0.01, and ††=p<0.01. Error bars indicate standard error. REML was used to generate the LSD given in Table 11-6.

Figure 7-4**: Vegetative phenotype of *gid1a,-b,-c;SHR::AtGID1a* lines (A-E) compared to *gid1a,-b,-c* and Col-0**. Plants were grown on Levingtons compost in 5.5-cm pots under long day for four weeks **(A)** and the floral phenotype of *gid1a,-b,-c;SHR::AtGID1a* line C compared to *gid1a,-b,-c* at eight weeks **(B)**.

7.2.2 *SCR::GID1a* rescues root length and vegetative development of the *gid1a,-b,-c* mutant

To investigate the effect of GA perception only in the endodermis, *AtGID1a* expression was driven from the *SCR* promoter (Di Laurenzio et al., 1996) in the *gid1a,-b,-c* triple mutant background. Root lengths of transgenic lines compared with Col-0 and *gid1a,-b,-c* are shown in Figure 7-5. In mutant lines expressing the transgene root and rosette growth were almost completely rescued, while there was partial rescue of inflorescence stem growth in lines A, C and D (Figure 7-6). Although inflorescence stem elongation was only partially rescued for line B, there was complete rescue of the fertility and seed germination in this line (qualitative data not shown). Despite lines A, C and D being rescued to a greater extent than line B in terms of inflorescence size, restoration of fertility and germination was only partial for these lines. The primary root growth of all lines was significantly greater than for *gid1a,-b,-c*, but less than for Col-0 ($p<0.01$ (except A compared to Col-0 where $p<0.05$)). The root length of line D was closest to the mean of all lines so this line was chosen for further analysis.

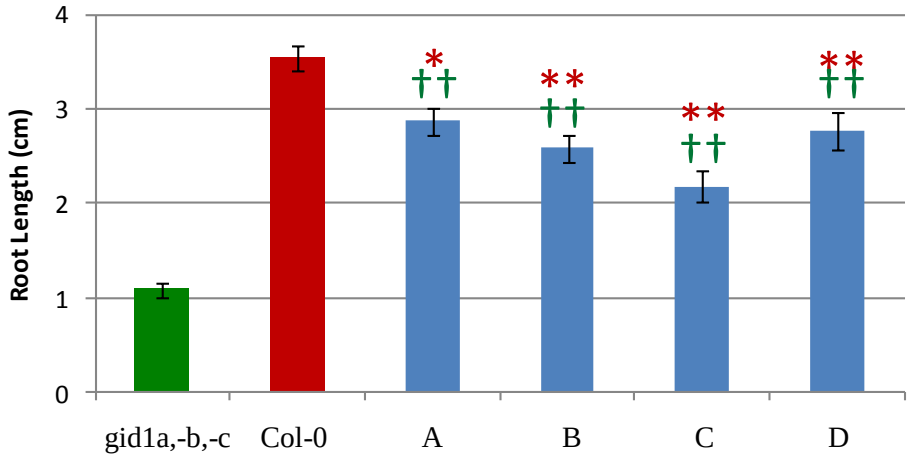

Figure 7-5: **Primary root length ±SE at seven days post embryo excision for *gid1a,-b,-c;SCR:GID1a* lines (A-D) compared to *gid1a,-b,-c* and Col-0.** Seedlings were grown on vertical plates and lengths calculated using ImageJ. Green crucifixes indicate the transgenic lines are significantly different from *gid1a,-b,-c* and the red asterisks indicate they are significantly different from the Col-0. 30 plants for each line were analyzed **=$p<0.01$, and ††=$p<0.01$. Error bars indicate standard error. REML was used to generate the LSD given in Table 11-6.

Figure 7-6**: Vegetative phenotypes shown for *gid1a,-b,-c;SCR::GID1a* lines (A-D) compared to *gid1a,-b,-c* and Col-0.** Plants were grown on Levingtons compost in 5.5-cm pots under long day conditions at three weeks (A-B) and six weeks (C).

7.2.3 *CoR:AtGID1a* rescues root length and vegetative development of the *gid1a,-b,-c* mutant

The effect of GA perception only in the ground tissue of the elongation zones was investigated by expressing *AtGID1a* from the *CoR* promoter (Dinneny et al., 2008) in the *gid1a,-b,-c* triple mutant background. Root lengths of six transgenic lines compared with Col-0 and *gid1a,-b,-c* are shown in Figure 7-7. The root lengths of lines C, D and F were not significantly different from Col-0 ($p>0.05$), while roots of lines A, B and E were smaller than Col-0 (A = $p<0.01$ (B and E =$p<0.05$)). Line C had a vegetative phenotype that was closest to Col-0 and the greatest recovery of root length so was chosen for further analysis.

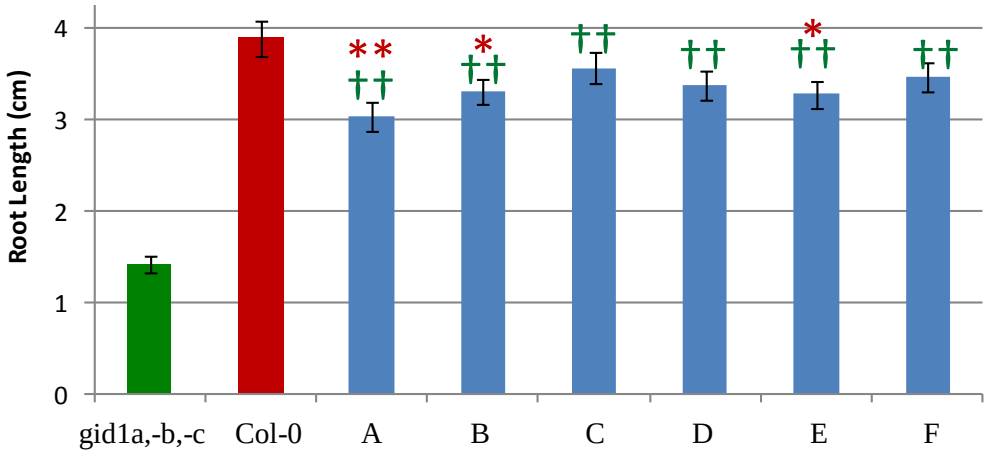

Figure 7-7**: Primary root length ±SE at seven days post embryo excision for *gid1a,-b,-c;CoR:GID1a* lines (A-F) compared to *gid1a,-b,-c* and Col-0.** Seedlings were grown on vertical plates and lengths calculated using ImageJ. Green crucifixes indicate the transgenic lines are significantly different from *gid1a,-b,-c* and the red asterisks indicate they are significantly different from the Col-0. 30 plants for each line were analyzed *=$p<0.05$, **=$p<0.01$, and ††=$p<0.01$. Error bars indicate standard error. REML was used to generate the LSD given in Table 11-6.

As the *CoR* promoter had previously been shown to respond to ABA (Figure 3-17) its response to 1 µM GA and 1 µM PAC was tested (Figure 7-8). The decrease in GA as a result of PAC application appeared to cause *CoR::GFP* to be ectopically expressed within the endodermis. The application of GA_3 caused expression to remain in the cortex but also extend down into the meristem transition zone. Hence, when expressed in the *gid1a,-b,-c* triple mutant background, the *CoR* promoter could be expressing the functional GID1a in endodermal cells of the elongation zone and the cortical cells of the proximal meristem transition zone.

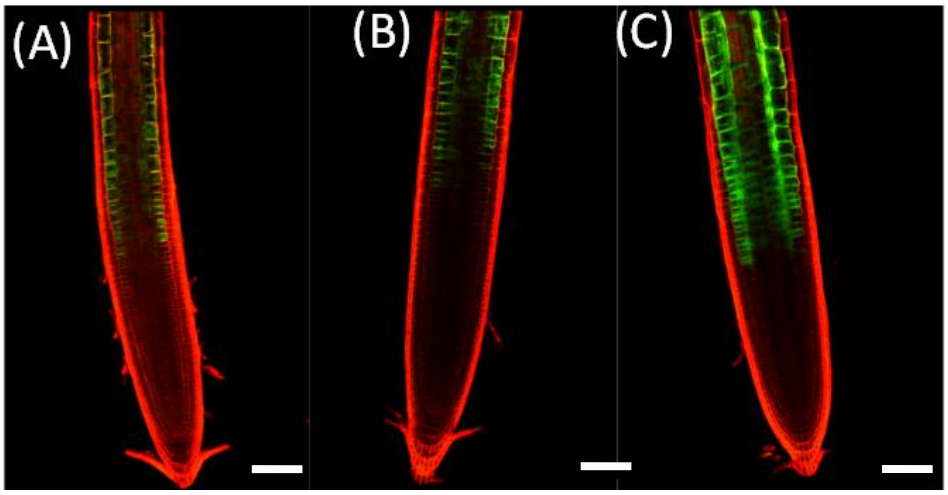

Figure 7-8: ***CoR::GFP* fluorescence responding to GA and PAC treatment.** **(A)** *CoR::GFP* fluorescence in the elongation zone is shown for plants grown on Agar containing 1 µM GA, **(B),** control Agar, **(C)** and Agar containing 1 µM PAC_3. Confocal microscopy was performed on the five roots of seven day old seedlings after being grown on vertical Gelrite plates. The GFP and the propidium iodide emission images are overlain. Bars are 100 µm in length.

The targeted expression of the *CoR::AtGID1a* transgene was able to completely rescue vegetative growth of the *gid1a,-b,-c* triple mutant (Figure 7-9). Rosettes of all lines grew faster and for longer than WT Col-0, producing larger leaves before forming floral inflorescences. Lines A, C, D and F all eventually produced inflorescences that were taller than Col-0 and lines C and F were also fertile. Lines B and E had thin cauline leaves produced prolifically at the base of the primary inflorescence, while no secondary inflorescences emerged; the primary inflorescence grew slowly with faster growing side branches.

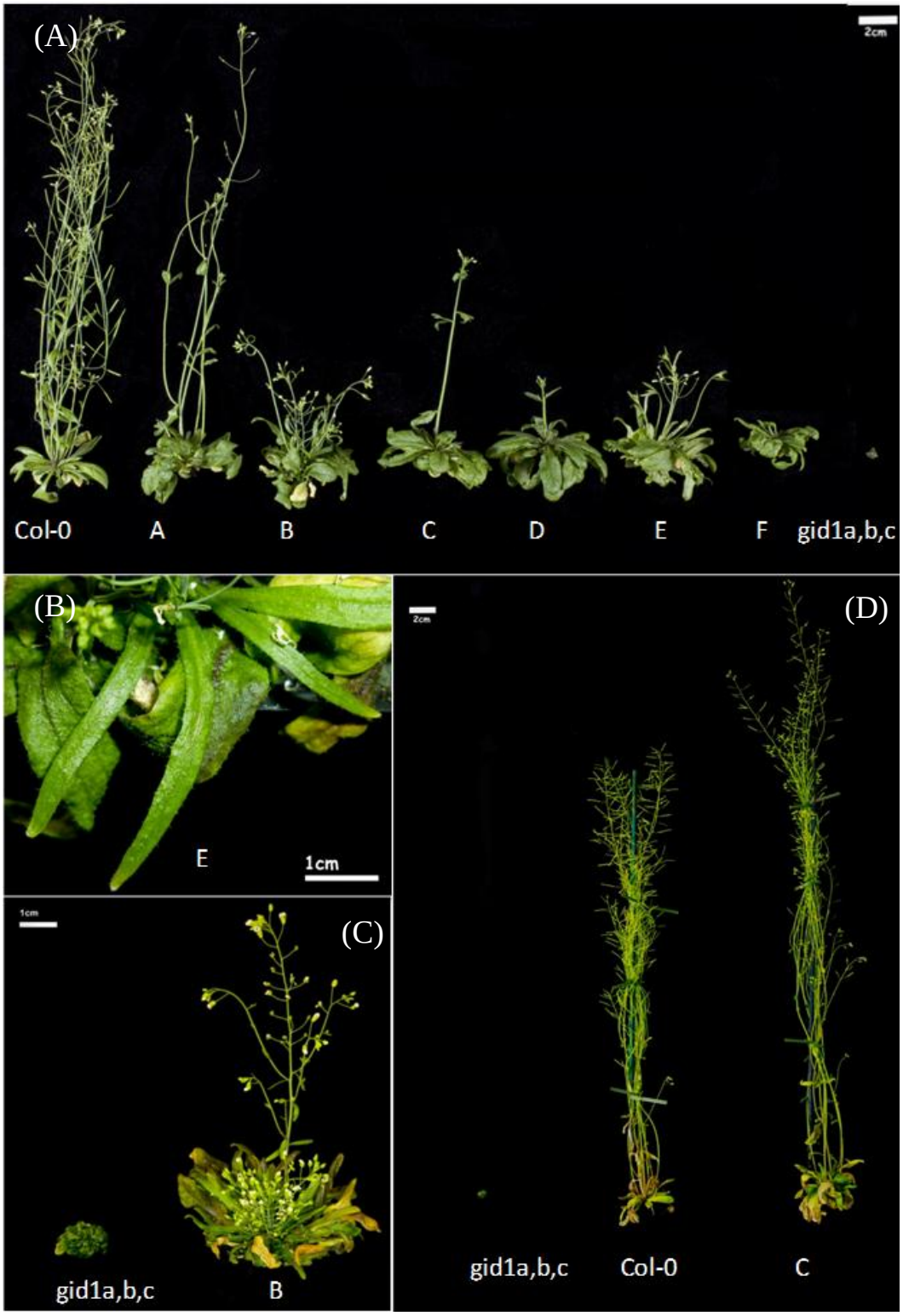

Figure 7-9**: Vegetative phenotype of *gid1a,-b,-c;CoR::GID1a* (lines F, D and C) compared to *gid1a,-b,-c* and Col-0.** Plants were grown on Levingtons compost in 5.5-cm pots under long day for 4 weeks (A), vegetative phenotype of *gid1a,-b,-c;CoR::GID1a* lines E (B) and B (C) compared to *gid1a,-b,-c* at three weeks. Vegetative phenotype of *gid1a,-b,-c;CoR:GID1a* line C compared to *gid1a,-b,-c* and Col-0 at six weeks (D).

7.2.4 *Co2:GID1a* failed to rescue root length and vegetative development of the *gid1a,-b,-c* mutant

GA-perception limited to the cortical and endodermal/cortical initial daughter (ECID) cells of the meristematic region was investigated by expressing *AtGID1a* from the *Co2* promoter (Heidstra et al., 2004) in the *gid1a,-b,-c* triple mutant background. This targeted expression weakly rescued shoot growth and after six weeks the plants sent out multiple inflorescences with infertile flowers (Figure 7-10). Similarly, the root lengths of all the transgenic lines were significantly smaller than Col-0 ($p<0.01$), and while lines B and D were significantly larger than *gid1a,-b,-c* ($p<0.01$ and $p<0.05$ respectfully), lines A and C were not significantly different from the triple mutant ($p>0.05$) (Figure 7-11). The root length of line D was closest to the mean of all lines and so this line was chosen for further analysis.

Figure 7-10**: Vegetative phenotype of *gid1a,-b,-c;Co2:GID1a* lines (A-D) compared to *gid1a,-b,-c* and Col-0.** Plants were grown on Levingtons compost in 5.5-cm pots under long day for four weeks (A) and the floral phenotype of *gid1a,-b,-c;Co2:GID1a* line D compared to *gid1a,-b,-c* at eight weeks (B).

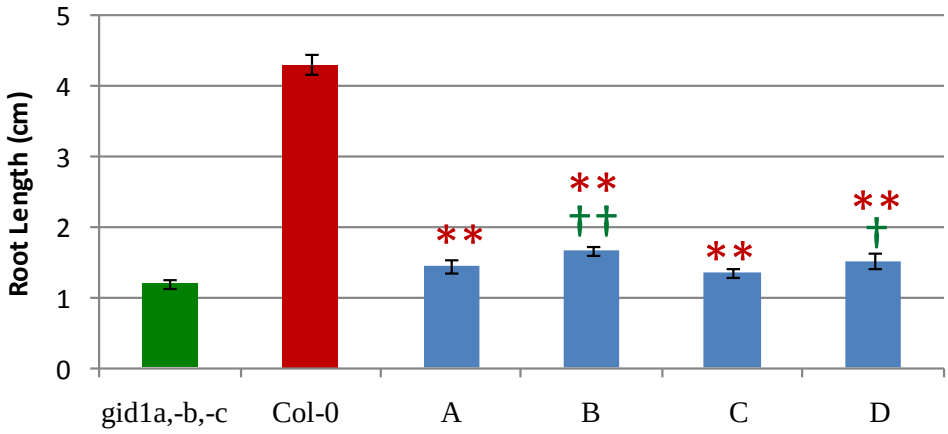

Figure 7-11**: Primary root length ±SE after seven days growth post embryo excision for *gid1a,-b,-c;Co2:GID1a* lines (A-D) compared to *gid1a,-b,-c* and Col-0.** Seedlings were grown on vertical plates and lengths calculated using ImageJ. Green crucifixes indicate the transgenic lines are significantly different from *gid1a,-b,-c* and the red asterisks indicate they are significantly different from the Col-0. 30 plants for each line were analyzed **=p<0.01, †=p<0.05 and ††=p<0.01. Error bars indicate standard error. REML was used to generate the LSD given in Table 11-6.

7.2.5 *GL2::GID1a* partially rescued root length and vegetative development of the *gid1a,-b,-c* mutant

AtGID1a was expressed from the *GL2* promoter in order to allow GA perception in the epidermal non-hair atrichoblast cells (Masucci et al., 1996). Expression of the transgene partially rescued shoot growth, although the rosette grew more slowly, with dark green leaves, with a convex curve and crinkled edges (Figure 7-12). After six weeks a few short inflorescences emerged and lines A and C eventually produced small siliques containing seeds that would not germinate unless embryos were excised. Similarly, the root lengths of all the lines were significantly smaller than Col-0 ($p<0.01$) (Figure 7-13), although roots of lines A, B, C, E and F were significantly larger than *gid1a,-b,-c* ($p<0.01$ (except E compared to Col-0, where $p<0.05$)). The root of line D was not significantly longer than that of *gid1a,-b,-c* ($p>0.05$). Line B, for which root length was closest to the mean of all lines was chosen for further analysis.

Figure 7-12**: Vegetative phenotype of *gid1a,-b,-c;GL2::GID1a* lines (A-E) compared to *gid1a,-b,-c* and Col-0.** Plants were grown on Levingtons compost in 5.5-cm pots under long day for four weeks (A) and floral phenotype of *gid1a,-b,-c;GL2:GID1a* line C compared to *gid1a,-b,-c* at eight weeks (B).

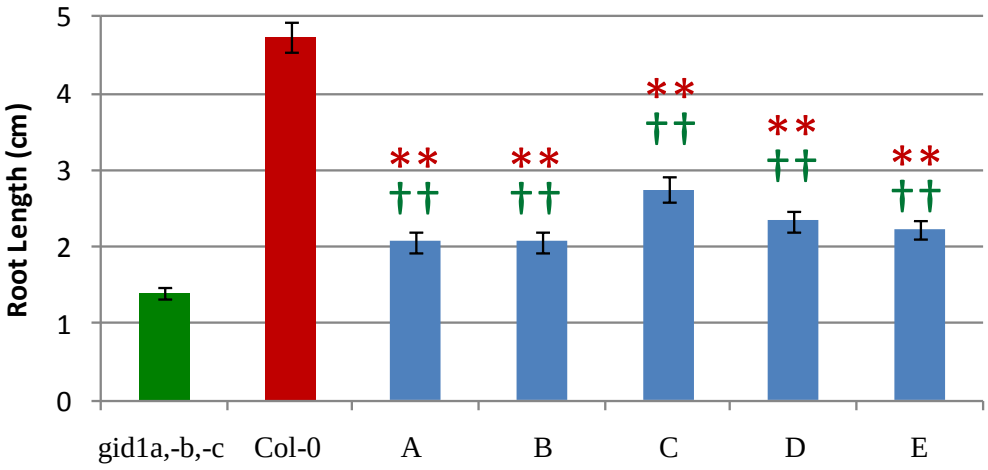

Figure 7-13**: Primary root length ±SE after seven days growth post embryo excision for *gid1a,-b,-c;GL2:GID1a* lines (A-E) compared to *gid1a,-b,-c* and Col-0.** Seedlings were grown on vertical plates and lengths calculated using ImageJ. Green crucifixes indicate the transgenic lines are significantly different from *gid1a,-b,-c* and the red asterisks indicate they are significantly different from the Col-0. 30 plants for each line were analyzed **=$p<0.01$, and ††=$p<0.01$. Error bars indicate standard error. REML was used to generate the LSD given in Table 11-6.

7.2.6 Comparison of primary root parameters for lines targeting tissue-specific expression of *GID1a*

The primary root growth for 18 plants from the median line selected from each *Promoter:: AtGID1a:YFP* construct in the *gid1a,-b,-c* background were compared with *gid1a,-b,-c* and Col-0 after embryo excision to allow germination. In addition to root length measurements, the meristem size of five plants and final cell length of 5 cortical cells from the differentiation zone from of each of these 5 plants were used for further analysis (Figure 7-14).

The *SCR* promoter provided the most complete rescue of root growth, allowing the growth of roots that were significantly larger than *gid1a,b,*c ($p<0.01$), although final root length was significantly smaller than in Col-0 ($p<0.01$). Final cell length was not significantly different from that in Col-0 ($p>0.05$), but there was only partial rescue of meristem size (significantly larger than *gid1a,-b,-c* ($p<0.01$), but significantly smaller than Col-0 ($p<0.01$)). Expression from the *SHR* and *CoR* promoters resulted in similar root lengths ($p>0.05$) which were significantly different from both Col-0 and *gid1a,b,*c ($p<0.01$). Although roots of the *SHR* and *CoR* lines had final cell lengths that were not significantly different from Col-0 ($p>0.05$), meristem lengths were significantly smaller than Col-0 but significantly larger than *gid1a,-b,-c* ($p<0.01$) (Figure 7-14).

The *Co2* and *GL2* lines had similar root lengths ($p>0.05$) that were significantly different from both *gid1a,-b,-c* ($p<0.01$) and Col-0 ($p<0.01$). However, while the final cell length in the *GL2* line was not significantly different from that in Col-0 ($p<0.01$), cell size in the *Co2* line was the same as in the *gid1a,-b,-c* mutant ($p<0.01$). These results are difficult to reconcile with the finding that meristem lengths in the *Co2* and *GL2* lines were not significantly different from one another ($p>0.05$), being significantly larger than in *gid1a,-b,-c* ($p<0.05$) and smaller than in Col-0 ($p<0.01$) (Figure 7-14).

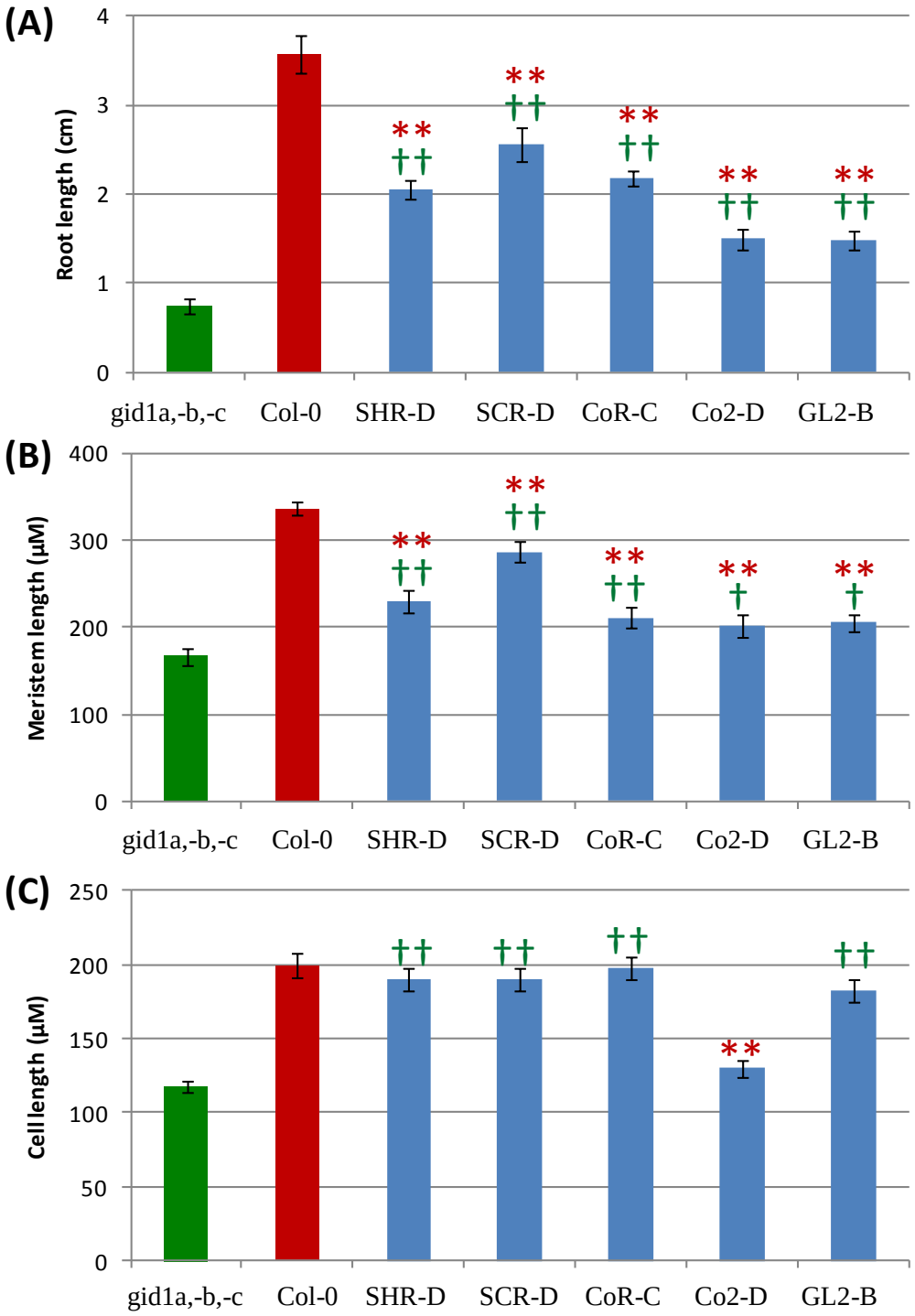

Figure 7-14**: Mean values of primary root parameters for selected lines for each *gid1a,-b,-c ;promoter:GID1a* construct compared with *gid1a,-b,-c* and Col-0 at seven days. (A)** Primary root length ±SE. **(B)** Proximal meristem length ±SE. **(C)** Final cortical cell length ±SE. Seedlings were grown on vertical plates and lengths calculated using ImageJ. Green crucifixes indicate the transgenic lines are significantly different from *gid1a,-b,-c* and the red asterisks indicate if they are significantly different from Col-0. 18 plants for each line were measured for root length; 5 plants had their meristems and 5 cells measured from each plant that had its meristem measured **=p<0.01, †=p<0.05 and ††=p<0.01. Error bars indicate standard error. LSD given in Table 11-11.

7.1 DISCUSSION OF SITES OF GA PERCEPTION WITHIN ARABIDOPSIS TISSES

The aim of the experiments described in this chapter was to investigate the sites of GA perception in the elongating root and to test if the endodermis is either one of many or the only site of GA perception (Ubeda-Tomás et al., 2009, Ubeda-Tomas et al., 2008). Each of the different promoters *SHR, SCR, CoR, Co2* and *GL2* were all able to increase meristem size so it was statistically significantly different from the *gid1a,-b,-c* triple mutant. In addition, all promoters except *Co2* which is only expressed in the meristematic region were able to completely rescue cell elongation. As discussed later, GA perception in just the stele, endodermis, cortex and epidermis can partially rescue meristem size and completely rescue cell elongation (Figure 7-15).

Figure 7-15: **Schematic diagram highlighting which tissues were able to rescue root growth when *AtGID1a* was targeted to them in the *gid1a,-b,-c* triple mutant.** The yellow lateral root cap and columella cells were not studied during this project. The green epidermal, cortical, endodermal and vasculature cells of the elongation zone are all capable of promoting cellular elongation. The black epidermal, cortical and vasculature cells of the meristematic region are all capable of perceiving GA in order to promote cell division. The blue endodermal cells of the meristematic region have a disproportionately large role in promoting GA dependant cell division.

7.1.3 Investigating GA perception in the endodermis

Ubeda-Tomás *et al.,* (2008, 2009) demonstrated that the expression of a non-degradable DELLA protein within the endodermis reduced cell division rates and final cortical cell length, producing dwarf roots. In support of these findings, we found that expressing a functional *AtGID1a* transgene within the endodermis of the *gid1a,-b,-c* triple mutant using the *SCR* promoter partially rescued root growth (Figure 7-5). Final cell length was completely rescued, although there was incomplete rescue of meristem length (Figure 7-14). This could be due to the expression of the *SCR::GID1a* transgene in the *gid1a,-b,-c* triple mutant being lower than that of the endogenous *GID1* genes. However this is not supported by the Birnbaum *et al.,* (2006) data set, which indicates that *SCR* is more highly expressed than the *GID1a*, *GID1b* or *GID1c* genes. Alternatively, it could be due to only partial functional redundancy between the different *GID1* family members and that *GID1a* alone cannot interact with all the downstream molecular components required for correct growth. It is also possible that the endodermis is the main site of GA perception that drives root elongation, but perception in additional cell types is required for normal cell division. Perazza *et al.,* (1997) showed that GA signalling is also required for normal epidermal root hair growth and if this tissue cannot directly perceive GA this might result in reduced meristem size via some as yet uncharacterised mechanism.

SCR::GID1a expression either completely or partially rescued germination in the *gid1a,-b,-c* triple mutant; *SCR* is known to be expressed within the endodermis and QC of the radicle, but is also present in the endosperm of the seed coat (Figure 3-13 and Figure 3-14) (Wysocka-Diller et al., 2000). Hence, it is likely that the rescue of germination is due to the restoration of GA-dependant RGL2 degradation in the endosperm, reducing the germination inhibition mediated by RGL2 and an ABA positive feedback loop (Lee et al., 2010). It is also likely that RGA/GAI degradation within the QC and endodermis promoting cell division and cell elongation in the growing radicle has an important role (Lee et al., 2010, Achard et al., 2009, Ubeda-Tomas et al., 2008).

7.1.4 GA signalling in QC initial cells may have a role in regulating meristem size

It has previously been shown that by expressing a non-degradable DELLA in all tissues of the meristem that cell division rates can be reduced (Achard et al., 2009). Expressing *AtGID1a* expression within the proximal meristematic cortical and endodermal/cortical initial daughter (ECID) cells of the *gid1a,-b,-c* triple mutant using the *Co2* promoter was able to partially rescue root growth via a mild increase in meristem length and the same was true when *AtGID1a* was expressed in epidermal/lateral root cap (ELRC) initial cells and atrichoblast epidermal cells using the *GL2* promoter (Figure 7-14). Interestingly, there was no significant difference between *gid1a,-b,-c;Co2:GID1a* and *gid1a,-b,-c;GL2:GID1a* meristem sizes ($p<0.01$), suggesting there is a common mechanism linking their meristem rescue phenotypes.

Another common feature of these two lines is that the promoters of the transgenes are both active in initial cells neighbouring the QC, although in different initial cells. This suggests GA signalling in the initial cells may be required for correct meristem development. This hypothesis is supported by the observation that meristem size is partially rescued in *gid1a,-b,-c;SCR:GID1a* (Figure 7-14). The lack of complete meristem rescue in these lines may be due to the inability to perceive GA in the ELRC initial cells. It would be interesting to see the effect of expressing a functional GID1a receptor in the endodermis as well as the QC and its initial cells (by crossing selected lines) to produce a similar expression pattern to that of the GA-biosynthetic gene *AtGA3ox2*, as indicated by the GUS staining around the QC in the *AtGA3ox2-GUS* lines (Mitchum et al., 2006).

7.1.5 GA signalling is important within the ground tissue

As shown in Figure 7-14, when the *CoR* promoter was used to express *AtGID1a* within the ground tissue of the elongation zone it enabled a complete rescue of cell elongation and a partial, yet significant rescue, of meristem

length. However, when *CoR::GFP* was grown on plates containing 1 μM PAC, expression could be observed also within the endodermis of the elongation zone, while after treatment with 1 μM GA_3, expression could be observed within the cortical cells of the proximal meristem transition zone (Figure 7-8), demonstrating that the expression domain of the *CoR* promoter is sensitive to GA signalling. In addition, it has been shown that the *gid1a,-b,-c* mutant has elevated levels of GA (Griffiths et al., 2006), so it is possible that this would influence the *CoR::GID1a* expression causing it become expressed within the cortical cells of the proximal meristem transition zone. However, the *gid1,-2,-3* triple mutant does not respond to GA so that, even if GA levels are elevated, the GA-induced extension of the *CoR* expression domain into the meristem as seen when the *CoR::GFP* line is grown on GA_4 would not occur, unless GA action is sufficiently restored in the relevant cells of the meristem. Furthermore, ,the *CoR* expression profile in the triple mutant background would be similar to that in PAC-treated plants may thus may also be present in the endodermis of the elongation zone and transition zone, potentially causing the partial rescue of meristem length shown in Figure 7-14. The greatest rescue of meristem length in the mutant was achieved by expressing *GID1a* in the endodermis with the *SCR* promoter, supporting the findings of Ubeda-Tomas *et al.* (2009), who showed that DELLA degradation within the endodermis and QC is essential for correct cell division and elongation to occur and is therefore the most important site of GA perception for primary root growth (Figure 7-14).

7.1.6 Cell elongation can be rescued by *GID1a* expression in any tissue of the *gid1a,-b,-c* mutant elongation zone

Expression of a functional *AtGID1a* transgene within the meristematic cortical cells of the *gid1a,-b,-c* triple mutant using the *Co2* promoter (Heidstra et al., 2004) did not rescue cell elongation. In contrast *gid1a,-b,-c;CoR:GID1a, gid1a,-b,-c;SHR::AtGID1a, gid1a,-b,-c;SCR::AtGID1a* and *gid1a,-b,-c;GL2::AtGID1a* lines exhibited a complete rescue of cell elongation. Taken together it could be concluded that GA perception in any tissue of the

elongation zone is sufficient to promote cell elongation (Figure 7-14). However, this is hard to reconcile with the results of Ubeda-Tomas et al. (2008), who demonstrated inhibition of cell elongation when a non-degradable DELLA protein was expressed in the endodermis. The restoration of GA signalling in the cortex, stele or epidermis in the *GID1* transgenic lines may cause the production of a mobile hormonal, miRNA or small peptide signal that is capable of moving to the endodermis to cause DELLA degradation or activate a downstream signal thus coordinate cell expansion rates. It would be interesting to use DELLA antibodies or cross *RGA::RGA:GFP* lines with the *gid1a,-b,-c;SHR::GID1a*, *gid1a,-b,-c;CoR::GID1a*, or *gid1a,-b,-c;GL2::GID1a* lines to investigate if and where DELLA stability is being affected.

7.1.7 Expression of *GID1a* from the *SCR* and *CoR* promoter rescues growth of aerial tissues

Expression of *SCR::GID1a* and *CoR::GID1a* in the *gid1a,-b,-c* triple mutant provided the greatest rescue of aerial growth and both also rescued floral fertility. The *gid1a,-b,-c;CoR::GID1a* lines were the most variable, producing relatively large rosette leaves and large inflorescences or normal sized rosette leaves that sent out thin cauline leaves at the base of the slow growing inflorescence (Figure 7-9). In contrast the *gid1a,-b,-c;SCR::GID1a* lines maintained aerial phenotypes that were similar to WT Col-0 although of variable size (Figure 7-6). When microarray data are considered (Figure 3-15 and Figure 3-16), the *gid1a,-b,-c;CoR::GID1a* aerial rescue is not surprising as *CoR* appears to be highly expressed in many tissues and throughout most stages of development. However the *gid1a,-b,-c;SCR::GID1a* aerial rescue is much more striking as *SCR* expression is confined to one cell layer that surrounds the vasculature throughout the plant (Wysocka-Diller et al., 2000). When taken together with recent work showing that the endodermis is the main site of GA perception within the root (Ubeda-Tomás et al., 2009, Ubeda-Tomas et al., 2008), these current findings suggest that this hypothesis may also apply to the rest of the plant. However, as in the case of roots, the aerial rescue of the

gid1a,-b,-c;SCR::GID1a lines was not complete, demonstrating that the endodermis or its aerial equivalents (the leaf bundle sheath and stem cambium cells) are not the sole site of GA perception, but represents the most important tissue for driving organ growth.

7.1.8 GA signalling within the vascular and epidermal aerial tissues cause differential growth affecting leaf curvature.

The *gid1a,-b,-c;SHR::GID1a* and *gid1a,-b,-c;GL2::GID1a* lines possessed very similar aerial phenotypes with two clear distinctions, the different angles of leaf curvature and only the *gid1a,-b,-c;GL2::GID1a* lines set seed. Microarray data showed that *GL2* is highly expressed within siliques during the early stages of seed set while *SHR* is expressed only at very low levels early on in silique development (Figure 3-11 and Figure 3-12). In terms of leaf curvature, *gid1a,-b,-c;SHR::GID1a* lines exhibited concave curves while the *gid1a,-b,-c;GL2::GID1a* leaves had a convex curve. Microarray analysis suggests that *GL2* is expressed in some aerial epidermal tissues and it is possible that SHR is expressed in the vasculature of the stem, as in leaves, but it has not been definitively demonstrated in the literature. However, it is well documented that SHR movement regulates *SCR* expression in root tissues, and, if this is also true for aerial tissue, then on the basis of data produced by Wysocka-Diller *et al.,* (2000) showing *SCR* expression in the tissues surrounding the vasculature it is reasonable to assume that *SHR* will also be expressed throughout the stem vasculature, as has recently been demonstrated in developing leaves (Dhondt et al., 2010). Taken together with the knowledge that leaf curvature is caused by differential abaxial and adaxial growth then these data suggest GA response in epidermal and vascular tissues may play an important role in regulating leaf shape.

8 DISCUSSION

8.1 TISSUE-SPECIFIC EXPRESSION OF GA METABOLIC OR SIGNALING COMPONENTS IN WT AND MUTANT COL-0

Gibberellins regulate many aspects of plant growth and development, including root elongation (Yaxley et al., 2001). The role of GAs in controlling *Arabidopsis* root growth is clearly illustrated in severe GA-biosynthetic and signalling mutants, which display dramatically reduced root elongation (Fu and Harberd, 2003). In which tissue(s) GA is synthesised and where it acts to control root growth has been the focus of several earlier studies. Using targeted expression of a constitutively active repressor of GA signalling Ubeda-Tomas *et al.*, (2008; 2009) demonstrated that GA action in endodermal cells is necessary for promoting cell division in the meristematic region and cell extension within the elongation zone. In contrast, promoter GUS reporter studies have shown the GA-biosynthetic genes necessary for the two final steps in the production of bioactive GAs are expressed in cells adjacent to the endodermis (Nieves Fernandez-Garcia, unpublished data Figure 1-17), indicating that movement of GAs from their site of synthesis to site of action may be required (Yamaguchi et al., 2001, Mitchum et al., 2006).

The aim of this project was to localise where the final biosynthetic steps that create bioactive GAs take place and to explore the site of GA perception within *Arabidopsis* root tissues. The *SHR*, *SCR*, *Co2*, *CoR*, *GL2* and *CAB* genes have been shown to be expressed in specific cell types, so were employed to drive the expression of selected GA biosynthesis, inactivation and receptor proteins in the root (Di Laurenzio et al., 1996, Heidstra et al., 2004, Dinneny et al., 2008, Masucci et al., 1996, Puente et al., 1996). These promoters were used to drive the expression of YFP-AtGA2ox2, YFP-AtGA2ox7, YFP-AtGA20ox1, YFP-AtGA3ox1 and *AtGID1a* within the targeted cells. The GA-inactivating enzymes AtGA2ox2, and AtGA2ox7 were expressed in Col-0 *Arabidopsis* to investigate the effect of inactivating either C_{19} or C_{20}-GAs in specific root tissues. YFP-AtGA20ox1, YFP-AtGA3ox1 and AtGID1a were expressed in the *ga20ox1,-2,-3*, *ga3ox1,-2* and *gid1a,-b,-c* mutants, respectively, to

investigate sites of GA 20-oxidation, 3β-hydroxylation and perception. The transgenic lines produced were compared to WT and mutant controls. These studies provide insights into the mechanisms by which GA controls the growth and development of the *Arabidopsis* root (Figure 8-1). It would have been useful to create a quantative root map describing important tissues involved in GA metabolism using measurements of the effect that the various transgenes have in each tissue however qRTPCR would be required to validate the results. However qualitative diagrams describing which tissues are important such as Figure 8-1 and Figure 8-2 have been created based on the data generated during this study to illustrate which sections of the root that will be discussed below, their role in GA metabolism and which are likely to have conserved function.

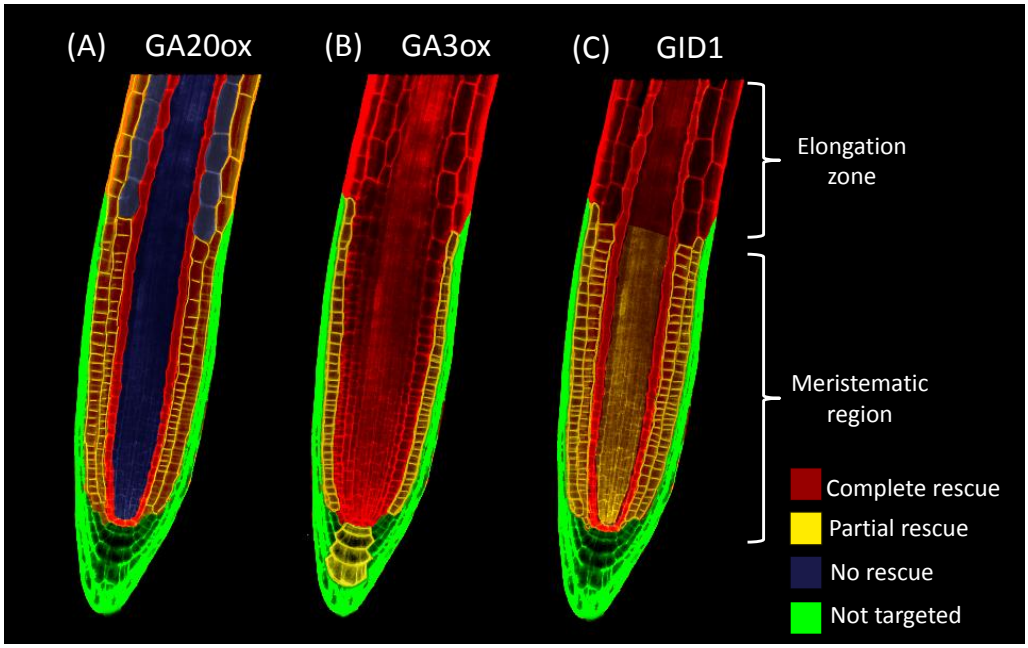

Figure 8-1: **Schematic diagram illustrating the extent of mutant rescue by ectopic expression of genes encoding GA-biosynthetic enzymes or the GID1 receptor. (A)** Expression of *YFP-AtGA20ox1* in the *ga20ox1,-2,-3* triple mutant. **(B)** Expression of *YFP-AtGA3ox1* in the *ga3ox1, -2* double mutant. **(C)** Expression of *AtGID1A-YFP* in the triple *atgid1a, -1b, 1c* mutant. Tissues in which transgene expression produced almost complete rescue of root growth are coloured red, whereas partial rescue is denoted by yellow and no effect by blue. Tissues coloured green were not studied during this project.

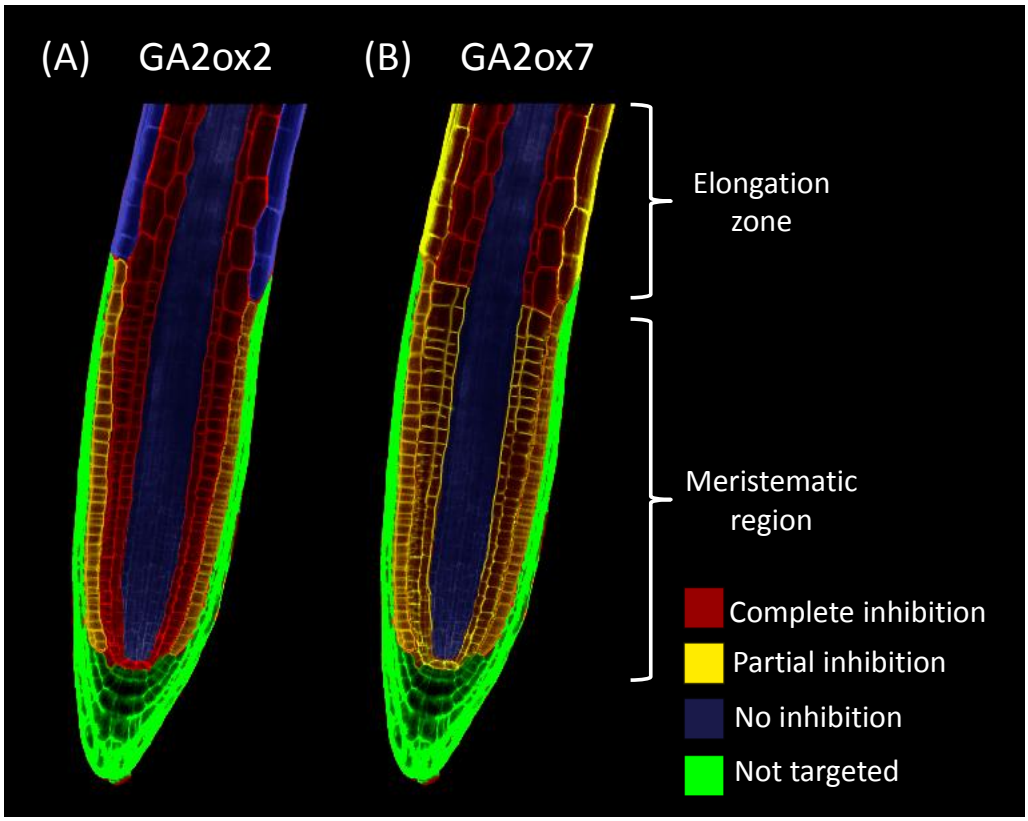

Figure 8-2: **Schematic diagram illustrating the effects on root growth of ectopic expression of genes encoding GA-inactivating enzymes. (A)** and (**B)** Expression of *YFP-AtGA2ox1* and *YFP-AtGA2ox7*, respectively, in Col-0. Tissues in which *GA2ox* expression resulted in the most severe growth reduction are coloured red, while yellow denotes milder effects and blue no inhibition of root growth. Tissues coloured green were not studied.

8.1.1 Ectopic aerial expression of tissue specific YFP-AtGA2ox2, YFP-AtGA2ox7, YFP-AtGA20ox1 and AtGA3ox1 transgenes effect on root growth

The photosynthetic tissue specific *Col-0;CAB::YFP:AtGA2ox7* and *Col-0;CAB::YFP:atGA2ox2* transgenic lines had wild type root growth and both had severely dwarfed aerial growth (Figure 4-30 and Figure 4-60). This demonstrates that root growth can be driven solely from GAs derived from the root, allowing it to grow independently from either C_{20}-GAs or C_{19}-GAs moving down from aerial tissues. However, *ga20ox1,-2,-3;CAB::YFP:AtGA20ox1* lines had a complete rescue of aerial growth and a partial rescue of root growth due to a partial rescue of cortical cell elongation (Figure 5-30). This indicates that cell elongation during root growth can be promoted by either C_{20}-GAs or C_{19}-GAs moving down from aerial tissues. Therefore, aerial tissues can potentially produce excess C_{20}-GAs in order to boost cell elongation.

The *ga3ox1,-2;CAB::YFP:AtGA3ox1* transgenic lines had a complete aerial rescue and semi-dwarf root growth due to a partial rescue meristem length and a complete of final cortical cell length (Figure 6-30). This indicates that cell elongation during root growth may be promoted by bioactive C_{19}-GAs moving down from aerial tissues. However, the *ga3ox1,2;CAB::YFP:AtGA3ox1* lines also had ectopic expression within the columella cells which may have contributed to a meristematic pool of bioactive GA that partially rescued meristem length. Therefore, it is unclear whether excess bioactive C_{19}-GAs produced within aerial tissues are able promote cell division due to abnormal fluorescence patterns within the *ga3ox1,2;CAB::YFP:AtGA3ox1* lines and it would be interesting to repeat this experiment with another photosynthetic specific tissue promoter for clarification. In summary the *CAB* lines have demonstrated that GA dependant root growth can occur independently of shoot derived GAs, however it is possible that shoot derived C_{20}-GAs are capable of promoting cell elongation and that shoot derived bioactive GA are capable of promoting both cell elongation and cell division. This would provide the shoot

with mechanisms to regulate root growth rates so that both the aerial and below ground canopies are proportional to one another. There is also the potential that the promoters show low levels of expression in other tissues, which are sufficient to drive GA biosynthetic pathway.

8.1.2 The endodermis is the primary site of GA perception controlling cell division

Firstly the expression of genes encoding GA-inactivating enzymes that specifically act on C_{20}-GA precursors (AtGA2ox7) or C_{19}-GAs (AtGA2ox2) were targeted to the endodermis. Expressing *YFP-AtGA2ox7* or *YFP-AtGA2ox2* using the *SCR* promoter in the neighbouring endodermal/ground tissue (Di Laurenzio et al., 1996) created a semi-dwarf root phenotype suggesting that the transgenic lines were GA-deficient by removing either inactive C_{20}-GA precursors, such as GA_{12}, GA_{15} and GA_{24}, the C_{19}-GA precursor GA_9 and/or the bioactive GA_4. The dwarf phenotype of the Col-0;*SCR::YFP:AtGA2ox2* lines indicates that the endodermis/ground tissue is an important site of C_{19}-GA movement, activation, and/or perception.

When a functional YFP-AtGA20ox1 was expressed using the *SCR* promoter, it partially rescued root growth of the *ga20ox1,-2,-3* mutant. This suggests that the endodermal cells contain the GA20ox substrate(s) GA_{12}, GA_{15} or GA_{24} and are potentially sites of GA_9 biosynthesis. Furthermore, the resulting products are activated and reach sites of GA perception. Transgenic lines containing *SCR::YFP:AtGA3ox1* only partially rescued root growth of the *ga3ox1,-2* double mutant, confirming that the *GA3ox1* substrate GA_9 is present in the endodermis but suggesting that it is not the only source. The lack of complete rescue could indicate that GA activated in the endodermis is unable to reach an important site of GA perception. However, *SCR::GID1a* expression produced significant rescue of root growth in the *gid1a,-b,-c* mutant, demonstrating the importance of GA perception within the endodermis. In addition, the partial rescue of root growth demonstrates that the root endodermis also contains an important network that coordinates root growth. However, the lack of complete

meristem rescue demonstrates that the endodermis is not the only important site of GA perception for regulating meristem size.

8.1.3 GA activation and perception within the stele can promote root growth despite its lack of GA_{12}

Expressing YFP-GA2ox7 within the vasculature and pericycle using the *SHR* promoter (Di Laurenzio et al., 1996) did not inhibit root growth, suggesting that that the stele does not contain an essential source or represent a route of transport for GA_{12} or other C_{20}-GAs. The *ga20ox1,-2,-3;SHR::YFP:AtGA20ox1* lines displayed no rescue of growth either, further supporting the notion that the vasculature is incapable of producing the GA20ox substrates GA_{12}, GA_{15} and GA_{24} or receiving them via movement. Alternatively the lack of rescue in the *ga20ox1,-2,-3;SHR::YFP:AtGA20ox1* lines could mean that the GA20ox product GA_9 is incapable of reaching a GA3ox for activation; however, the partial rescue of the *ga3ox1,-2* mutant by *SHR::YFP:AtGA3ox1* shows that the vasculature contains the GA3ox C_{19}-substrate GA_9, which is capable of reaching a site of action. Thus taken together this demonstrates that GA_9 must be capable of moving into the stele and that bioactive GAs in the stele can reach important sites of action. Interestingly, expressing *YFP-AtGA2ox2* in the stele had no effect on root growth, meristem length or cell elongation, indicating that the vasculature is not an essential source or transport route for C_{19}-GAs involved in promoting cell division and elongation. Finally, there was significant rescue of root growth in the *gid1a,-b,-c;SHR::AtGID1a* lines via partial restoration of cell division and complete rescue of cell elongation, demonstrating that the vasculature contains bioactive GA and a transcriptional network that is capable of responding to GA to promote cell elongation and division.

8.1.4 GA perception and biosynthesis within the epidermis has a role in promoting root growth

The *GL2* promoter is expressed within the trichoblast cells of the root epidermis from the QC to the hypocotyl. The trichoblast cells differentiate from epidermal daughter cells produced by division of epidermal/lateral root cap (ELRC) initial cells. The Col-0;*GL2::YFP:AtGA2ox7* lines exhibited significantly reduced root lengths, with smaller meristems, but normal final cell sizes, suggesting the epidermis is a potential source of GA_{12} and/or C_{20}-GAs must travel through this tissue for correct meristem growth to occur. The *GL2*::*YFP:AtGA20ox1* construct was capable of partially rescuing the root growth of *ga20ox1,-2,-3,* providing further evidence for the epidermal cells acting as a source of C_{20}-GAs. Supporting this, the *ga3ox1,-2;GL2::YFP:AtGA3ox1* lines exhibited partial rescue of root growth demonstrating that the *GA3ox1* substrate GA_9 can be synthesised within the epidermis or is mobile enough to reach the epidermis and, after activation to GA_4, is able to reach a site of action. However, failure to completely rescue either meristem or final cell length suggests that the activated GA is incapable of reaching an important site of action in sufficient quantities.

In contrast to the report by Ubeda-Tomás *et al*., (2008), who found that blocking GA signalling within the endodermis was necessary and sufficient to block cell elongation, the *gid1a,-b,-c;GL2:GID1a* lines showed significant rescue of root growth due to the complete restoration of cell elongation and partial rescue of cell division. The present data suggest that the epidermis contains transcriptional networks that can induce cell elongation and promote cell division, but play a minor role in GA-mediated cell division in comparison to the endodermis (Ubeda-Tomás et al., 2009, Achard et al., 2009). It is possible that the cause of this discrepancy may be due to a functional specificity of the GAI within the endodermis that would not have been observed if another non-degradable mutant DELLA protein had been used or as Moubayin *et al.,* (2010) showed that RGA-GFP stability in root cells varied in a tissue and stage of development specific manner.

8.1.5 GA activation, GA 20-oxidation and perception are required in both the meristematic region and the elongation zone

When GA 20-oxidation was confined within the meristematic cortical cells and endodermal/cortical initial daughter (ECID) cells by expressing YFP-AtGA20ox1 with the *Co2* promoter (Heidstra et al., 2004) partially rescued root growth of the *ga20ox1,-2,-3* mutant, demonstrating that these cells contain a source of C_{20}-GAs (Figure 8-4). As both meristem and cell elongation rescue were partial, there may be other potential sites of C_{20}-GA biosynthesis/mobilisation that contribute to GA-dependent root growth. However, the lack of rescue of the *ga20ox1,-2,-3* mutant when *YFP:AtGA20ox1* by the *CoR* promoter demonstrates that the elongation zone ground tissue of the *ga20ox1,-2,-3* does not produce GA_{12}, meaning any C_{20}-GAs in this region must have travelled from either aerial tissue and/or the root tip or remained within the cells as they matured. This is supported by microarray data for different *Arabidopsis* root tissues show that the expression of the early biosynthetic genes *KS* and *KAO* is highest within the meristematic region and columella cells (Birnbaum et al., 2003, Dugardeyn et al., 2008) suggesting that are these are the primary sites for early GA-biosynthesis.

However, *AtGA20ox1* promoter::GUS reporter lines demonstrate expression specifically within these cells (Figure 1-17), and the reduced cell lengths of Col-0;*CoR::YFP:AtGA2ox7* lines indicate that correct cell elongation requires C_{20}-GA metabolism and eventual activation within the ground tissue of the elongation zone. *AtGA2ox7* and *AtGA2ox8* have previously been shown to degrade GA_{12} (Schomburg et al., 2003); in this study we show that GA2ox7 also degrades GA_{24}. Taken together the reduced cell length of the *CoR::YFP:AtGA2ox7* lines suggests that the cortical cells of the elongation zone are transit routes for GA_{12}, GA_{15} or GA_{24} movement that is required for cell elongation. The smaller meristems and final cortical cell length of the Col-0;*Co2::YFP:AtGA2ox7* lines also demonstrate that the meristematic cortical cells are also a site of early C_{20}-GA biosynthesis and that GA transport from this region to the elongation zone is required.

Expression of *Co2::YFP:AtGA3ox1* fully rescued meristem length, but only partially rescued final cell length of the *ga3ox1,-2* mutant, suggesting that the cortical cells near the QC contain GA_9 and, after activation, GA_4 can reach sites of perception that regulate cell division, but has limited access to sites of action that regulate cell elongation. The complete rescue of cell elongation in the *ga3ox1,-2;CoR::YFP:AtGA3ox1* lines supports the presence of GA_9 within the elongation zone and demonstrates GA activated in this region can reach a site of perception (Figure 8-3). The partial meristem rescue of the *ga3ox1,-2;CoR::YFP:AtGA3ox1* lines may indicate that bioactive GA can move from the elongation zone to the meristematic region, however YFP-AtGA3ox1 fluorescence was observed within the columella cells and this is cannot be ruled out as the source of bioactive GA that partially rescued meristem length.

GA-inactivation in the meristematic region within the Col-0;*Co2::YFP:AtGA2ox2* lines reduced meristem size, but had no effect on final cell length, suggesting that the production or movement of GA_9 or GA_4 within these cells is important for regulation of GA-dependent cell division and that C20-GAs must be capable of moving from the meristematic region in order to promote cell elongation. The severe reduction in cell length that is observed in the Col-0;*CoR::YFP:AtGA2ox2* lines, demonstrates that the cortex of the elongation zone is an important movement route for C_{19}-GAs and/or GA perception and that the meristematic region does not require C_{19}-GA movement from the elongation zone for correct cell division to occur.

Finally, expressing *Co2::AtGID1a* in the *gid1a,-b,-c* mutant did not significantly rescue final cell length, suggesting that cortical cells in the root meristem are not important sites for GA perception for cell elongation but the mild meristem rescue does suggest they have transcriptional networks that can promote cell division (Figure 8-1). Expressing the *AtGID1a* receptor with the *CoR* promoter in the *gid1a,-b,-c* mutant completely rescued cell elongation, demonstrating that the ground tissue cells of the elongation zone contain transcriptional networks capable of promoting cell elongation. There was also partial rescue of meristem size which could suggest a signal from this region is capable of moving from the elongation zone to promote growth. Since

CoR::GFP was shown to also be expressed in the periphery of the proximal meristem in response of GA and PAC, *CoR::GID1a* expression may be within the meristematic region, however if this was the case then you would expect to see reductions on the meristem size in the Col-0;*CoR::YFP:AtGA2ox2* lines.

The separation of GA biosynthesis and signalling in germinating cereal seeds is well documented: GAs produced in the embryo move to the aleurone where they induce α-amylase expression (Jones and Jacobsen, 1991, Kaneko et al., 2003). The separation of the site of biosynthesis and perception is also supported by experiments in rice that demonstrated the expression of the GA signalling component *OsSLR1* could be found within both the scutellum and aleurone layer (Kaneko et al., 2002). Taken together these data tell us that both the meristematic region and the site where cells undergo rapid expansion require GA signalling. We also demonstrate that both GA 20-oxidation and subsequent GA activation is required within both these regions for correct root growth to occur. In addition, they also demonstrate that the elongation zone does not contain GA_{12} and requires a source of both C_{19}- and C_{20}-GA for correct growth and development to occur.

8.1.6 Vegetative tissues can promote GA-dependant cell elongation in roots

Constitutive over-expression of *AtGA2ox2* and *AtGA2ox7* have long been known to produce dwarf phenotypes (Schomburg et al., 2003, Thomas et al., 1999). The targeting of YFP-AtGA2ox2 to YFP-AtGA2ox7 to the photosynthetic tissues using the *CAB* promoter severely dwarfed the aerial organs and yet had no affect on root growth. This suggests that under the experimental conditions used, *Arabidopsis* root growth is autonomous for GA production. Thus aerial architecture can be manipulated by modifying GA metabolism without affecting primary root length.

Interestingly, expressing *YFP-AtGA3ox1* in the *ga3ox1,-2* background or expressing *YFP-AtGA20ox1* in the *ga20ox1,-2,-3* background with the *CAB* promoter partially rescued root cell elongation, suggesting that some form(s) of GA are able to move to the root to promote cell elongation. As YFP-AtGA3ox1 fluorescence was observed within the columella cells this confuses interpretation of these data particularly regarding the partial meristem rescue. However, the partial rescue of cortical cell length of the *ga20ox1,-2,-3* mutant by *CAB::YFP:AtGA20ox1* suggests that GAs from the shoot may be able to promote cell elongation. Due to its natural abundance it is conceivable that GA_{24} may be a mobile form of GA. However, it is likely that GA_{24} would be converted to GA_9 which would undergo activation *en route* from the shoot due to GA3ox expression within the root vasculature/pericycle cells (Mitchum et al., 2006). The experiments in potato indicated that GA_{20}, but not GA_1, moved from the shoots to the stolons (Jackson, 1999). However, the results of the present experiment suggest that GA_{24} as well as GA_9 may be mobile in *Arabidopsis*.

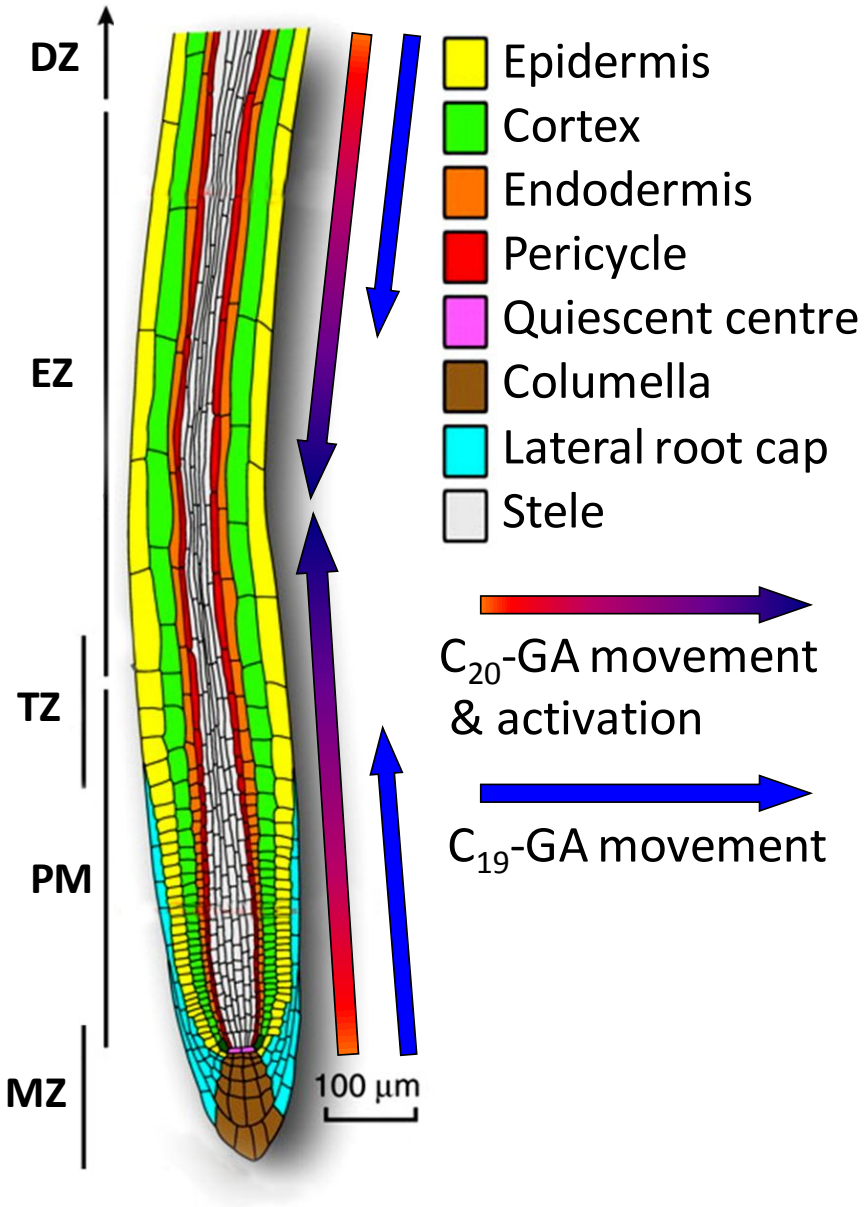

Figure 8-3: **Schematic diagram of the *Arabidopsis* root showing proposed GA_{20} and C_{19} movement routes.** Indicated on the left are the meristematic zone (MZ), proximal meristem (PM), transition zone (TZ), elongation zone (EZ), and the differentiation zone (DZ). The blue arrow demonstrates movement of either the C_{19}-GAs, GA_9 or GA_4. The red and purple arrows indicate movement of the C_{20}-GAs GA_{15} and/or GA_{24} and likely site of bioactive perception. Figure adapted from Overvoorde *et al*. (2010) with permission from Tom Beeckman.

8.1.7 Is GA being transported, diffusing across membranes or trapped within ageing cells?

Kramer (2006) showed that the membrane mobility of hormones could be predicted by taking into account a few characteristics such as the thickness of the cell wall, permeability of membrane, proportion of protonated form of the hormone on each side of membrane and presence of transports within the membrane. Known measurements for auxin were used to develop an algorithm to predict membrane permeability for a small number of GAs (See appendix Table 11-1). The C-20-oxidation of GA_{12} into GA_{15}-open lactone changes its $P_{AH}{}^{b}$ to 5.78 theoretically releasing the C_{20}-GA precursors from being trapped inside the cells. If the sequential 20-oxidation continues then GA_{15} will be converted to GA_{24}, the most abundant form of GA found within *Arabidopsis*, which has a $P_{AH}{}^{b}$ (cm/hr) of 12.33 thus suggesting a further increase in membrane permeability, potentially increasing the amount that can cross the membrane into the apoplast. After completion of the 20-oxidation, the loss of CO_2 is predicted to cause a reduction in membrane mobility, which is further decreased by its activation by 3β-hydroxylation. Interestingly the membrane permeability when the solution pH is at apoplastic levels the P_eff (cm/hr) suggests that only a small proportion of GA_{15}, GA_{24}, GA_9, and GA_4 should be capable of crossing a membrane into a cell.

This leaves three interesting possibilities. First, membrane transporters may facilitate the uptake of one or all of these GAs. Second, the amount of GA that crosses the membrane is heavily dependent on the apoplast pH. The P_eff prediction (See appendix GA membrane permeability estimates
Table 11-1) assumes that the apoplastic pH is 5.5, but any change in apoplastic pH by, for example, environmental factors, would impact GA uptake capacity. Third, both GA transporters and C_{20}-GA diffusion across a membrane may have important roles. Previous work has demonstrated that GA_4 is capable of moving from leaves to the shoot apical meristem (SAM), where it induces *LFY* during the floral transition under non-inductive short day conditions (Eriksson et al., 2006). However, it is still unclear how GA_4 applied to or produced in the

leaves reaches the SAM, without the discovery of a GA transporter it leaves passive diffusion and mass flow though the vasculature as the most likely mode of transport.

Results using the transgenic lines produced in this study suggest that GA_{12} is mobilised during conversion to the C_{20}-GA_{15}, C_{20}-GA_{24} and C_{19}-GA_9 by GA20ox enzymes within the epidermis, cortex and endodermis of the meristematic region of the *Arabidopsis* root (Figure 8-4). The GA may be released as an intermediate during 20-oxidation or alternatively after the 20-oxidation has removed CO_2 creating GA_9. The mobilised GA precursors may then be capable of moving to its site of activation. The bioactive GA precursor GA_9 can then move to sites of activation and perception around the plant via the vasculature, thus ensuring coordination of growth rates between the different plant tissues and organs. The tight regulation of bioactive GA distribution is also mediated by GA2ox enzymes that are specifically targeted to key tissues and developmental stages (Jasinski et al., 2005). If GA_9 enters a cell that is not a key site of perception the C_{19}-GA-specific 2-oxidases can deactivate it. However the mobile C_{20}-GAs can move through these tissues and promote GA-dependent responses in other tissues.

When the cell size dwarfing obtained with Col-0;*CoR::YFP:AtGA2ox7* lines compared with lack of an effect in Col-0;*SHR::YFP:AtGA2ox7* is also taken into consideration this could suggest that the movement of C_{20}-GAs through ground and potentially epidermal tissue play an important role by moving from their site of synthesis to their site of activation. GA movement has also been demonstrated in a grafting experiment using *Pisum sativum* where a *na-1* mutant scion was grafted onto an *le-3* (a *GA3ox* mutant) rootstock indicating that a non-active GA precursor is capable of crossing the graft to promote growth (Ingram et al., 1984, Davidson et al., 2003, Proebsting et al., 1992). The *na-1* mutation is in the *PsKAO* which is before GA_{12} in the pathway thus suggesting that the mobile GA is either a C_{20}-GA or C_{19}-GA later in the pathway. In addition, grafting experiments with the *le-1* mutants and WT plants suggested that GA_1/GA_4 is not the mobile factor capable of promoting growth; taken together this implies that it is a C_{20}-GA and/or GA_{20} (In

Arabidopsis GA_9) that is likely to be the mobile factor (Davidson et al., 2003, Proebsting et al., 1992).

However, recent work by Dobson *et al*. (2009) suggests that the traditional view of small molecules passively diffusing across membranes due to their lipophilicity may be naive. They suggest that the biophysical forces that small molecules encounter when they interact with the phospholipid bilayer are the same as those involved with protein lipid interactions. This suggests that carrier-mediated active or passive uptake of small molecules is likely to be the more commonly used mode of uptake and passive diffusion more rare (Dobson and Kell, 2008). Assuming that GA has similar characteristics to the small molecules discussed by Dobson *et al.* (2009), then bioactive GA or precursors should have specific or non-specific transporters that assist their movement across membranes as have recently been identified for ABA (Kang et al., 2010, Kuromori et al., 2010). Another interesting possibility is that the movement of C_{20}-GAs from the meristematic region to the elongation zone that is required for complete cell elongation (as described in section 4.3.5 and Figure 8-3) could be via plasmodesmata and the symplastic pathway through the ground and epidermal tissue.

AtGA3ox2::GUS activity was found in cells around the QC, within the columella cells and the elongation zone, while *AtGA3ox1::GUS* lines staining was excluded from the meristematic region and the root cap and is only expressed within the vasculature of the differentiation zone (Mitchum et al., 2006). It is possible that some GA_9 is activated in cells surrounding the columella, trapping it inside the cells in order to promote cell division and once the cells have aged enough eventually promoting cell elongation. In support of the QC/columella being a major site of GA activation, experiments in peas have shown that auxin increases the expression of *PsGA3ox1* while simultaneously suppressing the expression of *PsGA2ox1/2* (O'Neill and Ross, 2002), GA3ox up regulation has also been demonstrated in barley where auxin was shown to regulate expression of *HvGA3ox2* (Wolbang et al., 2004). In addition, experiments in *Arabidopsis* also clearly demonstrate that auxin and

GA metabolism are intermately linked (Frigerio et al., 2006), thus it is possible that the auxin maxima at the root apex generated by auxin biosynthesis and transport (Grieneisen et al., 2007) would activate *GA3ox* and *GA20ox* expression. The bioactive GA consequentially destabilizing DELLA proteins in a manner that coordinates not only cell division but also auxin transport and therefore is also likely to influence cell elongation in epidermal tissue and gravitropic curvature (Swarup et al., 2005, Fu and Harberd, 2003, Barlow, 2003) (Figure 8-4).

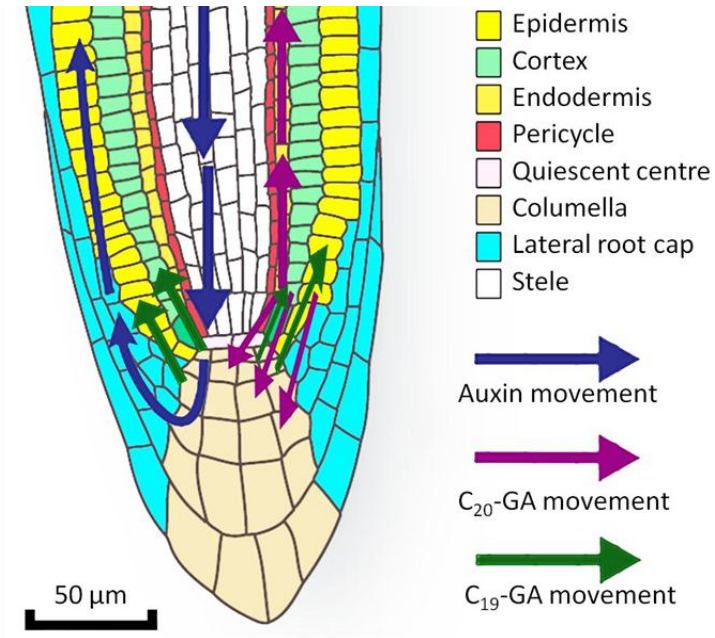

Figure 8-4: **Hormonal control of root growth and gravitropism.** The blue arrow indicates the reverse fountain of auxin flow. The purple arrow indicates the movement route of inactive C_{20}-GA precursors. The green arrow indicates the likely route of C_{19}-GA movement or the movement of the cells containing bioactive C_{19}-GAs within them. Figure adapted from Overvoodre *et al*., (2010) with permission from Tom Beeckman.

8.1.8 Post-transcriptional regulation of GA metabolism

Plants have homeostatic regulatory mechanisms that involve both feedback and feedforward transcriptional regulation of GA metabolism genes in order to maintain optimum growth rates (Figure 1-14). This homeostatic mechanism is clearly illustrated by comparing GA levels in GA3ox mutants with wild type plants (Hedden and Croker, 1991). There is considerable evidence for feedback

regulation occurring at the transcript level (Thomas *et al.,* 1999). Confocal analysis of the transgenic lines demonstrated many changes in the fluorescence distribution from the original published expression patterns for the promoters used in the present study. In addition, growing the transgenic plants on GA and PAC had different effects depending on the GA-metabolic enzyme attached to YFP. In the case of Col-0;*SCR::YFP:AtGA2ox2* lines, it was shown using a *SCR:GFP* line that the promoter was not sensitive to GA, whereas fluorescence in Col-0;*SCR::YFP:AtGA2ox2* was strongly GA-inducible. This suggests that the fluorescence variations observed may be due to post-transcriptional regulation of the transgene or modifications to protein stability.

It has long been known that elevating GA levels causes an up-regulation of the expression of GA degrading enzymes like *AtGA2ox1* and *AtGA2ox2* (Thomas et al., 1999). This positive feed-forward regulation is not exclusive to *AtGA2ox1* and *AtGA2ox2,* with *AtGA2ox4, AtGA2ox6* and *AtGA2ox8* mRNA abundance are also shown to be up-regulated by GA (Rieu et al., 2008a). However regulation at the post transcriptional level has not previously been reported. Here fluorescence in both Col-0;*SCR::YFP-AtGA2ox2* and Col-0;*SCR::YFP-AtGA2ox7* lines was suppressed in response to PAC, although unlike YFP-AtGA2ox2, YFP-AtGA2ox7 fluorescence did not increase dramatically in response to GA_3 treatment. This may suggest that the abundance of each individual GA2ox enzyme is controlled by a different regulatory mechanism that may function in a tissue specific manner.

Other enzymes in the GA biosynthesis and inactivation pathway may also be subject to post-transcriptional regulation. Chiange *et al.,* (1995) and Philips *et al.,* (1995) have shown that both *AtGA3ox1* and *AtGA20ox1* expression are under positive feedback control. Interestingly, *ga3ox1,-2;Co2::YFP:AtGA3ox1* showed restricted fluorescence profiles and YFP fluorescence appeared to be GA responsive in a few cells close to the QC. In addition, when the differentiation zone of these lines was examined after GA_3 treatment, fluorescence could be observed within the endodermis and cortex, whereas it appeared only in the endodermis of untreated plants and in the endodermis and pericycle cells after PAC treatment. This suggests that the homeostatic

regulation of GA metabolism may be controlled in a tissue specific manner. YFP-AtGA3ox1 expressed from the *CoR*, *CAB*, and *GL2* promoters was visible in the columella cells, which was surprising as this was not observed with any of *AtGA2ox2*, *AtGA2ox7* or *AtGA20ox1* lines. Mitchum *et al.* (2006) produced GUS data indicating *GA3ox2* expression within the columella cells, so it is possible that these cells contain molecular mechanisms that increase YFP-AtGA3ox1 stability enabling low expression levels to be visible. To investigate this further, fluorescent protein fusions with each of the GA-oxidases could be compared after being expressed by their natural and the *35S* tulip mosaic virus promoters.

Supporting this, it has been shown that the enzyme regulating the penultimate step in ethylene biosynthesis ACC synthesis, ACS is regulated at the protein level. Experiments in tomato first demonstrated that phosphorylation/dephosphorylation of the ACS protein regulated its turnover and not its function (Spanu et al., 1994). It was then shown in *Arabidopsis* that ACS stability was regulated by protein interactions at the C-terminus of the protein with an $ETO1^{CUL3A}$ RBX1-E2 ubiquitin ligase complex that caused polyubiquitination and was subsequently degraded by a 26S proteosome complex (Chae et al., 2003, Wang et al., 2004). Hence, later steps of hormone biosynthesis are often regulated at both the transcriptional, the post-transcriptional and post-translational level.

However, the changes in abundance observed for the GA biosynthesis and inactivation enzymes may reflect regulation at the post-transcriptional level or at both the post-transcriptional and post-translational levels. These transcripts may be targets for regulation by microRNA (miRNAs). Adai *et al.,* (2005) used a comparative genomic computational algorithm to predict likely miRNAs in the *Arabidopsis* genome; then they used experimental verification to demonstrate their algorithms accuracy and in the process also revealed that some miRNAs are under developmental control. The predicted miRNAs candidate precursor sequences that had corresponding target sites within transcripts were deposited in a database online (http://sundarlab.ucdavis.edu/mirna/). Searching the database for the GA

metabolic genes used during this study revealed that *AtGA2ox2*, *AtGA2ox7*, *AtGA20ox1* and *AtGA3ox1* are likely to be subject to miRNA regulation (Table 12). Interestingly it has recently been shown that the site of miRNA expression is important and that their movement between cells can play a role in cellular development and differentiation (Carlsbecker et al., 2010). It is therefore possible that the genes used in this study may be subject to miRNA regulation and may be affected by temporal, spatial and environmental control feeding back on the GA metabolic and signalling components. In order to test if the regulation is at the transcript or protein level transgenic plants could be grown on a chemical proteasome inhibitor such as MG132, if the GA metabolic genes are being destabilised by the presence or absence of GA via a protesome mediated pathway then no change of fluorescence would be observed. In addition qRT-PCR could be used to test if the expression levels is fluctuating which in combination could be used to further investigate if miRNA's play a role.

8.1.9 Tissue specific expression of GID1a reveals

GA control over meristem size is mediated by DELLA proteins both directly via transcriptional networks and also by modifying other hormones movement and biosynthesis. Auxin, which is the major determinant of meristem size, is known to influence many GA responses (Swarup and Bennett, 2003, Fu and Harberd, 2003). It has recently been shown that GA can affect auxin flow, mediated via PIN proteins, resulting in a change in the balance between ARR1 and ARR12 that affects *SHY2* stability, cytokinin signalling and subsequently the balance of cell division, differentiation and ultimately meristem length (Ioio et al., 2008, Moubayidin et al., 2010). Exactly which downstream targets of GA signalling control growth and development remains unclear, although Moubayidin *et al.*, (2010) demonstrated that the questions of where and when GA signalling takes place may be as important while describing growth and development.

In previous studies it has been demonstrated that GID1a-1c receptors perform functionally redundant roles in regulating root growth (Griffiths et al., 2006).

In their absence, GA-dependent root growth is completely abolished. Expressing a *GID1a* receptor within the vasculature using the *SHR* promoter in the *gid1a,-b,-c* background partially, but significantly rescued root growth. Similarly the root growth was partially restored in *gid1a,-b,-c*;*GL2:GID1a* lines, in which expressing occurred in the epidermis. As this partial rescue was primarily due to restoration of cell elongation in both cases, the vasculature and epidermis are both potential sites of GA action within the elongation zone. Interestingly both the *gid1a,-b,-c*;*GL2:GID1a* and *gid1a,-b,-c*;*SHR:GID1a* lines also exhibited partial rescue of meristem length suggesting that there are transcriptional networks within the stele and epidermis of the meristematic region (Achard et al., 2009) that can promote GA dependant cell division.

In agreement with Ubeda-Tomas *et al*., (2008 and 2009), *SCR::AtGID1a* provided the greatest rescue of meristem size and final cell length, confirming that the endodermis is a major site of GA perception. The *gid1a,-b,-c;Co2::AtGID1a* lines did not have a significant rescue of root growth, suggesting that the cortical cells of the root meristem are not major sites for GA perception. This demonstrates that GA signalling within the elongation zone is required for cortical cell elongation, which was supported by the complete restoration of cell elongation in the *gid1a,-b,-c*;*CoR::AtGID1a* lines suggesting that the ground tissue cells of the elongation zone are the main sites of GA perception for GA-dependent cell elongation.

8.2 THE TARGETED EXPRESSION LINES PROVIDE INSIGHTS INTO SIGHTS OF GA BIOSYNTHESIS AND PERCEPTION WITHIN AERIAL TISSUES

The primary objective of this project was to investigate the sites of GA metabolism and perception in the root. However, the promoters used were also expressed in aerial tissues and produced a range of interesting phenotypes that provided further insights into GA action. Due to auto-fluorescence of chloroplasts it was not possible to observe where the transgenes were expressed in the aerial tissue; however, many microarray studies have been

performed on the various *Arabidopsis* organs and tissues which provide some information on gene expression profiles.

The aerial expression profiles revealed by GUS and microarray studies are discussed in section 3.3.2. The *Col-0;SHR::YFP:AtGA2ox2* lines did not display any aerial phenotypes, suggesting that the vasculature tissues are not an essential site of production or action, and is not normally an important route for the transport of bioactive GAs. The *ga3ox1,-2:SHR::YFP:AtGA3ox1* lines had a complete rescue of vegetative growth demonstrating that the vasculature contains GA_9 which must be capable of moving there and reaching an important site of signalling. The partial rescue of vegetative growth of the *gid1a,-b,-c;SHR::AtGID1a* lines demonstrating that the aerial vasculature does contain transcriptional networks that can promote GA dependant growth but that GA activated in the vasculature must be able to reach other sites of GA perception. In addition not only the bioactive GA must be capable of moving but also its precursors, as the *ga20ox1,-2,-3;SHR::YFP:AtGA20ox1* lines had dwarf aerial phenotypes demonstrating that the vasculature doesn't contain any GA_{12}. However, dwarf phenotype of the Col-0;*SHR::YFP:AtGA2ox7* lines and the rescue of the *ga3ox1,-2:SHR::YFP:AtGA3ox1* lines, suggest that the movement of C_{20}-GAs and GA_9 within the aerial vasculature are important for vegetative growth.

The expression profile of *SCR* in aerial tissue as described by anti-body, GFP and microarray studies is described in section 3.3.3. Expression of *AtGA2ox2* with the *SCR* promoter produced a semi dwarf aerial phenotype suggest that the bundle sheath and stem cambium cells may be important sites of GA_9 or GA_4 biosynthesis, transport or perception. The fact that expressing *AtGA2ox7* from this promoter produced a more severe dwarf aerial phenotype indicates that these cells are important sites of GA_{12} conversion to GA_9 and/or C_{20}-GA movement. However, none of the vegetative phenotypes of the Col-0;*SCR::YFP:AtGA2ox2* lines were as extreme as the *ga1-3* mutant, suggesting that either other sites of GA biosynthesis, movement and/or perception must exist. Alternatively if both C_{20}-GAs and C_{19}-GAs were mobile in vegetative

tissue inactivation of both types of GA would be needed to obtain a phenotype as severe as the *ga1-3* mutant.

The *ga20ox1,-2,-3*;*SCR::YFP:AtGA20ox1* lines had a partial rescue the aerial growth and the *ga3ox1,-2;SCR::YFP:AtGA3ox1* lines had a complete rescue of aerial growth. Suggesting that the associated tissues have access to a pool of C_{20}-GAs and that GA_9 can be activated and reach a site(s) of perception. However, as the *ga20ox1,-2,-3* mutant rescue was incomplete there must also be other tissues where the mobilisation of C_{20}-GAs is required for normal vegetative growth. The almost complete rescue of shoot growth in the *gid1a,-b,-c;SCR::AtGID1a* lines indicates that, as the endodermis of the root, the cambium cells of the stem and the bundle sheath of the leaves are major sites of GA perception. The aerial phenotypes of the *gid1a,-b,-c*;*SCR::AtGID1a* lines extends Ubeda Tomás *et al.*, (2008, 2009) discovery of the importance of the DELLA-mediated endodermal transcriptional network from root and suggests their findings can be extended to aerial tissues.

No published papers describe the expression profile of the *CoR* gene however the aerial expression profiles demonstrated by mircroarray studies is discussed in section 3.3.4. The *Col-0;CoR::YFP:AtGA2ox2* lines produced dwarf aerial phenotypes, suggesting that *CoR* is expressed in aerial tissues at a site essential for GA biosynthesis and/or transport of GA_9 and/or GA_4. This is supported by the complete vegetative rescue of the *gid1a,-b,-c*;*CoR::AtGID1a* lines. However, the lack of rescue in the *ga20ox1,-2,-3*;*CoR::YFP:AtGA20ox1* lines and the dwarf stature of the Col-0;*CoR::YFP:AtGA2ox7* lines suggest that these cells are also not capable of producing GA_{12} and are dependent on import of C_{20}- and/or C_{19}-GAs.

8.3 Improvements and future work

Partial rescue of the *ga20ox1,-2,-3* triple and *ga3ox1,-2* mutants by expression of YFP-AtGA20ox1 and YFP-AtGA3ox1 under different promoters has been demonstrated. However, potentially these constructs under the control of their native promoter may also only partially complement

the *ga20ox1,-2,-3* and *ga3ox1,-2* mutants. Therefore, further controls such as the *ga20ox2,-3* and ga3ox2 mutants, or transgenic lines complemented with YFP fusions under their native promoters, could be used. These controls are needed to show complementation since otherwise it is unclear what the level of rescue is when GA20ox1 is in its native expression state.

GA promotes germination, so many of the GA biosynthetic and signalling mutants have difficulty in germinating. During this project this was overcome by treating all the mutants and controls with GA4 to ensure uniform germination. However, it would have been more effective if plant growth had been monitored by time-lapse photography so that root growth rates could be measured precisely from the moment of radicle emergence to a specific end time point and any time points in between. This would prevent the age of the seed and resulting germination time increasing variability amongst the results.

If more time was available qRT-PCR would have been performed in order to demonstrate the levels of transgene expression and to allow comparison of the expression levels between the transgenes. It would also have been useful to compare transgenic lines containing the same constructs to check if any variability was due to level of expression, or due to the position of insertion. In addition, it would have been useful to see if driving the different metabolic genes in the same tissues has different expression levels depending on the transgene. This could reveal if RNAi is reducing specific genes transcript abundance in a tissue specific manner. In addition, it would have been useful to perform qRT-PCR on the *Col-0;SCR::YFP:AtGA2ox2* lines when grown on GA, PAC and control agar plates in order to reveal if the changes in fluorescence were due to changes in transcript abundance or post-translation processing.

9 CONCLUDING REMARKS

The targeted expression strategies used here have demonstrated that GA biosynthesis and perception are controlled in a tissue specific manner and that GA metabolism is not only regulated at the transcriptional level but also post-translationally. This project has generated more questions than it has answered, some of which will require further targeted expression experiments and the localisation of the GID1a transgene in both root and shoot tissues. Others, such as the proposed model of GA movement and potential tissue-specific regulation of transcript or protein stability for the metabolic enzymes, will require qRT-PCR to determine relative levels of gene expression and further investigation of the effect of GA on the RNA and/or protein stability for the enzymes. In addition the integration with systems biology modelling data to include interactions with other hormonal networks will provide further exciting insights into GA movement and metabolism (Liu et al., 2010). In conclusion data generated during this project support the conclusions of Ubeda Tomás *et al.,* (2008 and 2009) that the endodermis is the primary site of GA signalling that drives primary root growth by increasing cell division rates and final cortical cell length. However, this project also demonstrated that other tissues require GA signalling for normal growth and development to occur.

10 REFERENCES

ACHARD, P., CHENG, H., DE GRAUWE, L., DECAT, J., SCHOUTTETEN, H., MORITZ, T., VAN DER STRAETEN, D., PENG, J. R. & HARBERD, N. P. 2006. Integration of plant responses to environmentally activated phytohormonal signals. *Science,* 311**,** 91-94.

ACHARD, P. & GENSCHIK, P. 2009. Releasing the brakes of plant growth: how GAs shutdown DELLA proteins. *Journal of Experimental Botany,* 60**,** 1085-1092.

ACHARD, P., GONG, F., CHEMINANT, S., ALIOUA, M., HEDDEN, P. & GENSCHIK, P. 2008a. The Cold-Inducible CBF1 Factor-Dependent Signaling Pathway Modulates the Accumulation of the Growth-Repressing DELLA Proteins via Its Effect on Gibberellin Metabolism. *THE PLANT CELL,* 20**,** 2117-2129.

ACHARD, P., GUSTI, A., CHEMINANT, S., ALIOUA, M., DHONDT, S., COPPENS, F., BEEMSTER, G. T. S. & GENSCHIK, P. 2009. Gibberellin Signaling Controls Cell Proliferation Rate in Arabidopsis.

ACHARD, P., LIAO, L. L., JIANG, C. F., DESNOS, T., BARTLETT, J., FU, X. D. & HARBERD, N. P. 2007. DELLAs contribute to plant photomorphogenesis. *Plant Physiology,* 143**,** 1163-1172.

ACHARD, P., RENOU, J. P., BERTHOME, R., HARBERD, N. P. & GENSCHIK, P. 2008b. Plant DELLAs restrain growth and promote survival of adversity by reducing the levels of reactive oxygen species. *Current Biology,* 18**,** 656-660.

ACHARD, P., VRIEZEN, W. H., VAN DER STRAETEN, D. & HARBERD, N. P. 2003. Ethylene regulates Arabidopsis development via the modulation of DELLA protein growth repressor function. *Plant Cell,* 15**,** 2816-2825.

APPLEFORD, N. E. J. & LENTON, J. R. 1991. GIBBERELLINS AND LEAF EXPANSION IN NEAR-ISOGENIC WHEAT LINES CONTAINING RHT1 AND RHT3 DWARFING ALLELES. *Planta,* 183**,** 229-236.

ARIIZUMI, T., MURASE, K., SUN, T.-P. & STEBER, C. M. 2008. Proteolysis-Independent Downregulation of DELLA Repression in Arabidopsis by the Gibberellin Receptor GIBBERELLIN INSENSITIVE DWARF1. *THE PLANT CELL,* 20**,** 2447-2459.

ARMENGAUD, P., ZAMBAUX, K., HILLS, A., SULPICE, R., PATTISON, R. J., BLATT, M. R. & AMTMANN, A. 2009. EZ-Rhizo: integrated software for the fast and accurate measurement of root system architecture. *Plant Journal,* 57**,** 945-956.

BARLOW, P. 2003. The Root Cap: Cell Dynamics, Cell Differentiation and Cap Function. *Journal of Plant Growth Regulation,* 21**,** 261-286.

BENFEY, P. N., LINSTEAD, P. J., ROBERTS, K., SCHIEFELBEIN, J. W., HAUSER, M. T. & AESCHBACHER, R. A. 1993. Root development in Arabidopsis: four mutants with dramatically altered root morphogenesis. *Development,* 119**,** 57-70.

BENFEY, P. N. & SCHERES, B. 2000. Primer - Root development. *Current Biology,* 10**,** R813-R815.

BIRNBAUM, K., JUNG, J. W., WANG, J. Y., LAMBERT, G. M., HIRST, J. A., GALBRAITH, D. W. & BENFEY, P. N. 2005. Cell type-specific expression profiting in plants via cell sorting of protoplasts from fluorescent reporter lines. *Nature Methods,* 2**,** 615-619.

BIRNBAUM, K., SHASHA, D. E., WANG, J. Y., JUNG, J. W., LAMBERT, G. M., GALBRAITH, D. W. & BENFEY, P. N. 2003. A gene expression map of the Arabidopsis root. *Science,* 302**,** 1956-1960.

BOUQUIN, T., MEIER, C., FOSTER, R., NIELSEN, M. E. & MUNDY, J. 2001. Control of specific gene expression by gibberellin and brassinosteroid. *Plant Physiology,* 127**,** 450-458.

BRADY, S. M., ORLANDO, D. A., LEE, J. Y., WANG, J. Y., KOCH, J., DINNENY, J. R., MACE, D., OHLER, U. & BENFEY, P. N. 2007. A high-resolution root spatiotemporal map reveals dominant expression patterns. *Science,* 318**,** 801-806.

CARLSBECKER, A., LEE, J.-Y., ROBERTS, C. J., DETTMER, J., LEHESRANTA, S., ZHOU, J., LINDGREN, O., MORENO-RISUENO, M. A., VATÉN, A., THITAMADEE, S., CAMPILHO, A., SEBASTIAN, J., BOWMAN, J. L., HELARIUTTA, Y. & BENFEY, P. N. 2010. Cell signalling by microRNA165/6 directs gene dose-dependent root cell fate. *Nature,* 465**,** 316-321.

CHAE, H. S., FAURE, F. & KIEBER, J. J. 2003. The eto1, eto2, and eto3 Mutations and Cytokinin Treatment Increase Ethylene Biosynthesis in Arabidopsis by Increasing the Stability of ACS Protein. *The Plant Cell Online,* 15**,** 545-559.

CHEN, J. G., PANDEY, S., HUANG, J. R., ALONSO, J. M., ECKER, J. R., ASSMANN, S. M. & JONES, A. M. 2004. GCR1 can act independently of heterotrimeric G-protein in response to brassinosteroids and gibberellins in Arabidopsis seed germination. *Plant Physiology,* 135**,** 907-915.

CHIANG, H. H., HWANG, I. & GOODMAN, H. M. 1995. ISOLATION OF THE ARABIDOPSIS GA4 LOCUS. *Plant Cell,* 7**,** 195-201.

CLOUGH, S. J. & BENT, A. F. 1998. Floral dip: a simplified method for Agrobacterium-mediated transformation of Arabidopsis thaliana. *Plant Journal,* 16**,** 735-743.

COLES, J. P., PHILLIPS, A. L., CROKER, S. J., GARCIA-LEPE, R., LEWIS, M. J. & HEDDEN, P. 1999. Modification of gibberellin production and plant development in Arabidopsis by sense and antisense expression of gibberellin 20-oxidase genes. *Plant Journal,* 17**,** 547-556.

CUI, H., LEVESQUE, M. P., VERNOUX, T., JUNG, J. W., PAQUETTE, A. J., GALLAGHER, K. L., WANG, J. Y., BLILOU, I., SCHERES, B. & BENFEY, P. N. 2007. An Evolutionarily Conserved Mechanism Delimiting SHR Movement Defines a Single Layer of Endodermis in Plants. *Science,* 316**,** 421-425.

CZECHOWSKI, T., STITT, M., ALTMANN, T., UDVARDI, M. K. & SCHEIBLE, W. R. 2005. Genome-wide identification and testing of superior reference genes for transcript normalization in Arabidopsis. *Plant Physiology,* 139**,** 5-17.

DAVIDSON, S. E., ELLIOTT, R. C., HELLIWELL, C. A., POOLE, A. T. & REID, J. B. 2003. The Pea Gene NA Encodes ent-Kaurenoic Acid Oxidase. *Plant Physiology,* 131**,** 335-344.

DE GRAUWE, L., CHAERLE, L., DUGARDEYN, J., DECAT, J., RIEU, I., VRIEZEN, W. H., BAGHOUR, M., MORITZ, T., BEEMSTER, G. T. S., PHILLIPS, A. L., HARBERD, N. P., HEDDEN, P. & VAN DER STRAETEN, D. 2008. Reduced gibberellin response affects ethylene biosynthesis and responsiveness in the Arabidopsis gai eto2-1 double mutant (vol 177, pg 128, 2008). *New Phytologist,* 178**,** 457-457.

DE LUCAS, M., DAVIERE, J. M., RODRIGUEZ-FALCON, M., PONTIN, M., IGLESIAS-PEDRAZ, J. M., LORRAIN, S., FANKHAUSER, C., BLAZQUEZ, M. A., TITARENKO, E. & PRAT, S. 2008. A molecular framework for light and gibberellin control of cell elongation. *Nature,* 451**,** 480-U11.

DELLO IOIO, R., LINHARES, F. S., SCACCHI, E., CASAMITJANA-MARTINEZ, E., HEIDSTRA, R., COSTANTINO, P. & SABATINI, S. 2007. Cytokinins Determine Arabidopsis Root-Meristem Size by Controlling Cell Differentiation. 17**,** 678-682.

DESHAIES, R. J. 1999. SCF and cullin/RING H2-based ubiquitin ligases. *Annual Review of Cell and Developmental Biology,* 15**,** 435-467.

DHONDT, S., COPPENS, F., DE WINTER, F., SWARUP, K., MERKS, R. M. H., INZE, D., BENNETT, M. J. & BEEMSTER, G. T. S. 2010. SHORT-ROOT and SCARECROW

Regulate Leaf Growth in Arabidopsis by Stimulating S-Phase Progression of the Cell Cycle. *Plant Physiology,* 154**,** 1183-1195.

DI LAURENZIO, L., WYSOCKA-DILLER, J., MALAMY, J. E., PYSH, L., HELARIUTTA, Y., FRESHOUR, G., HAHN, M. G., FELDMANN, K. A. & BENFEY, P. N. 1996. The SCARECROW Gene Regulates an Asymmetric Cell Division That Is Essential for Generating the Radial Organization of the Arabidopsis Root. *Cell,* 86**,** 423-433.

DINNENY, J. R. & BENFEY, P. N. 2008. Plant stem cell niches: Standing the test of time. *Cell,* 132**,** 553-557.

DINNENY, J. R., LONG, T. A., WANG, J. Y., JUNG, J. W., MACE, D., POINTER, S., BARRON, C., BRADY, S. M., SCHIEFELBEIN, J. & BENFEY, P. N. 2008. Cell identity mediates the response of Arabidopsis roots to abiotic stress. *Science,* 320**,** 942-945.

DOBSON, P. D. & KELL, D. B. 2008. Carrier-mediated cellular uptake of pharmaceutical drugs: an exception or the rule? *Nat Rev Drug Discov,* 7**,** 205-220.

DOBSON, P. D. L., KARIN. OLIVER, STEPHEN G. KELL, DOUGLAS B. 2009. Implications of the Dominant Role of Transporters in Drug Uptake by Cells (Supplementary Material). *Current Topics in Medicinal Chemistry,* 9**,** 163-181.

DOLAN, L. 2001. Root patterning: SHORT ROOT on the move. *Current Biology,* 11**,** R983-R985.

DUGARDEYN, J., VANDENBUSSCHE, F. & VAN DER STRAETEN, D. 2008. To grow or not to grow: what can we learn on ethylene-gibberellin cross-talk by in silico gene expression analysis? *Journal of Experimental Botany,* 59**,** 1-16.

ECKARDT, N. A. 2007. Gibberellins are modified by methylation in planta. *Plant Cell,* 19**,** 3-6.

ELLIOTT, R. C., ROSS, J. J., SMITH, J. L., LESTER, D. R. & REID, J. B. 2001. Feed-forward regulation of gibberellin deactivation in pea. *Journal of Plant Growth Regulation,* 20**,** 87-94.

ERIKSSON, S., BOHLENIUS, H., MORITZ, T. & NILSSON, O. 2006. GA(4) is the active gibberellin in the regulation of LEAFY transcription and Arabidopsis floral initiation. *Plant Cell,* 18**,** 2172-2181.

FARRAS, R., FERRANDO, A., JASIK, J., KLEINOW, T., OKRESZ, L., TIBURCIO, A., SALCHERT, K., DEL POZO, C., SCHELL, J. & KONCZ, C. 2001. SKP1-SnRK protein kinase interactions mediate proteasomal binding of a plant SCF ubiquitin ligase. *Embo Journal,* 20**,** 2742-2756.

FENG, S. H., MARTINEZ, C., GUSMAROLI, G., WANG, Y., ZHOU, J. L., WANG, F., CHEN, L. Y., YU, L., IGLESIAS-PEDRAZ, J. M., KIRCHER, S., SCHAFER, E., FU, X. D., FAN, L. M. & DENG, X. W. 2008. Coordinated regulation of Arabidopsis thaliana development by light and gibberellins. *Nature,* 451**,** 475-U9.

FLEET, C. M., YAMAGUCHI, S., HANADA, A., KAWAIDE, H., DAVID, C. J., KAMIYA, Y. & SUN, T.-P. 2003. Overexpression of AtCPS and AtKS in Arabidopsis Confers Increased ent-Kaurene Production But No Increase in Bioactive Gibberellins. *Plant Physiology,* 132**,** 830-839.

FRENCH, A., UBEDA-TOMAS, S., HOLMAN, T. J., BENNETT, M. J. & PRIDMORE, T. 2009. High throughput quantification of root growth using a novel image analysis tool. *Plant Physiology***,** pp.109.140558.

FRIGERIO, M., ALABADI, D., PEREZ-GOMEZ, J., GARCIA-CARCEL, L., PHILLIPS, A. L., HEDDEN, P. & BLAZQUEZ, M. A. 2006. Transcriptional regulation of gibberellin metabolism genes by auxin signaling in arabidopsis. *Plant Physiology,* 142**,** 553-563.

FU, X. D. & HARBERD, N. P. 2003. Auxin promotes Arabidopsis root growth by modulating gibberellin response. *Nature,* 421**,** 740-743.

FUJIOKA, S., YAMANE, H., SPRAY, C. R., GASKIN, P., MACMILLAN, J., PHINNEY, B. O. & TAKAHASHI, N. 1988. QUALITATIVE AND QUANTITATIVE-ANALYSES OF GIBBERELLINS IN VEGETATIVE SHOOTS OF NORMAL, DWARF-1, DWARF-2, DWARF-3, AND DWARF-5 SEEDLINGS OF ZEA-MAYS-L. *Plant Physiology,* 88**,** 1367-1372.

GAGNE, J. M., DOWNES, B. P., SHIU, S. H., DURSKI, A. M. & VIERSTRA, R. D. 2002. The F-box subunit of the SCF E3 complex is encoded by a diverse superfamily of genes in Arabidopsis. *Proceedings of the National Academy of Sciences of the United States of America,* 99**,** 11519-11524.

GALLEGO-BARTOLOMÉ, J., MINGUET, E. G., MARÍN, J. A., PRAT, S., BLÁZQUEZ, M. A. & ALABADÍ, D. 2010. Transcriptional Diversification and Functional Conservation between DELLA Proteins in Arabidopsis. *Molecular Biology and Evolution,* 27**,** 1247-1256.

GAPPER, C. & DOLAN, L. 2006. Control of Plant Development by Reactive Oxygen Species. *Plant Physiology,* 141**,** 341-345.

GOCAL, G. F. W., POOLE, A. T., GUBLER, F., WATTS, R. J., BLUNDELL, C. & KING, R. W. 1999. Long-Day Up-Regulation of a GAMYB Gene duringLolium temulentum Inflorescence Formation. *Plant Physiology,* 119**,** 1271-1278.

GOLDBERG, R. B. 1986. REGULATION OF PLANT GENE-EXPRESSION. *Philosophical Transactions of the Royal Society of London Series B-Biological Sciences,* 314**,** 343-353.

GREENBOIM-WAINBERG, Y., MAYMON, I., BOROCHOV, R., ALVAREZ, J., OLSZEWSKI, N., ORI, N., ESHED, Y. & WEISS, D. 2005. Cross Talk between Gibberellin and Cytokinin: The Arabidopsis GA Response Inhibitor SPINDLY Plays a Positive Role in Cytokinin Signaling. *THE PLANT CELL,* 17**,** 92-102.

GRIENEISEN, V. A., XU, J., MAREE, A. F. M., HOGEWEG, P. & SCHERES, B. 2007. Auxin transport is sufficient to generate a maximum and gradient guiding root growth. *Nature,* 449**,** 1008-1013.

GRIFFITHS, J., MURASE, K., RIEU, I., ZENTELLA, R., ZHANG, Z.-L., POWERS, S. J., GONG, F., PHILLIPS, A. L., HEDDEN, P., SUN, T.-P. & THOMAS, S. G. 2006. Genetic Characterization and Functional Analysis of the GID1 Gibberellin Receptors in Arabidopsis. *THE PLANT CELL,* 18**,** 3399-3414.

HA, S. B. & AN, G. H. 1988. IDENTIFICATION OF UPSTREAM REGULATORY ELEMENTS INVOLVED IN THE DEVELOPMENTAL EXPRESSION OF THE ARABIDOPSIS-THALIANA CAB1 GENE. *Proceedings of the National Academy of Sciences of the United States of America,* 85**,** 8017-8021.

HANSON, H., BORLAUG, N. & ANDERSON, R. 1982. *Wheat in the Third World,* Boulder, Westview Press.

HARBERD, N. P. & FREELING, M. 1989. GENETICS OF DOMINANT GIBBERELLIN-INSENSITIVE DWARFISM IN MAIZE. *Genetics,* 121**,** 827-838.

HEDDEN, P. 1997. The oxidases of gibberellin biosynthesis: Their function and mechanism. *Physiologia Plantarum,* 101**,** 709-719.

HEDDEN, P. 2003. The genes of the Green Revolution. *Trends in Genetics,* 19**,** 5-9.

HEDDEN, P. & CROKER, S. J. REGULATION OF GIBBERELLIN BIOSYNTHESIS IN MAIZE SEEDLINGS. *In:* KARSSEN, C. M., VANLOON, L. C. & VREUGDENHIL, D., eds. 14th International Conf on Plant Growth Substances, Jul 21-26 1991 Amsterdam, Netherlands. Kluwer Academic Publ, 534-544.

HEDDEN, P., HOAD, G. V., GASKIN, P., LEWIS, M. J., GREEN, J. R., FURBER, M. & MANDER, L. N. 1993. KAURENOIDS AND GIBBERELLINS, INCLUDING THE

NEWLY CHARACTERIZED GIBBERELLIN-A88, IN DEVELOPING APPLE SEEDS. *Phytochemistry,* 32**,** 231-237.

HEDDEN, P. & KAMIYA, Y. 1997. GIBBERELLIN BIOSYNTHESIS: Enzymes, Genes and Their Regulation. *Annual Review of Plant Physiology and Plant Molecular Biology,* 48**,** 431.

HEDDEN, P. & PHILLIPS, A. L. 2000. Manipulation of hormone biosynthetic genes in transgenic plants. *Current Opinion in Biotechnology,* 11**,** 130-137.

HEIDSTRA, R., WELCH, D. & SCHERES, B. 2004. Mosaic analyses using marked activation and deletion clones dissect Arabidopsis SCARECROW action in asymmetric cell division. *Genes and Development,* 18**,** 1964-1969.

HELARIUTTA, Y., FUKAKI, H., WYSOCKA-DILLER, J., NAKAJIMA, K., JUNG, J., SENA, G., HAUSER, M.-T. & BENFEY, P. N. 2000. The SHORT-ROOT Gene Controls Radial Patterning of the Arabidopsis Root through Radial Signaling. *Cell,* 101**,** 555-567.

HELLIWELL, C. A., POOLE, A., JAMES PEACOCK, W. & DENNIS, E. S. 1999. Arabidopsis ent-Kaurene Oxidase Catalyzes Three Steps of Gibberellin Biosynthesis. *Plant Physiology,* 119**,** 507-510.

HIRANO, K., ASANO, K., TSUJI, H., KAWAMURA, M., MORI, H., KITANO, H., UEGUCHI-TANAKA, M. & MATSUOKA, M. 2010. Characterization of the Molecular Mechanism Underlying Gibberellin Perception Complex Formation in Rice. *The Plant Cell Online,* 22**,** 2680-2696.

HIRANO, K., UEGUCHI-TANAKA, M. & MATSUOKA, M. 2008. GID1-mediated gibberellin signaling in plants. *Trends in Plant Science,* 13**,** 192-199.

HOWELL, W. M., KELLER, G. E., KIRKPATRICK, J. D., JENKINS, R. L., HUNSINGER, R. N. & MCLAUGHLIN, E. W. 2007. Effects of the plant steroidal hormone, 24-epibrassinolide, on the mitotic index and growth of onion (Allium cepa) root tips. *Genetics and Molecular Research,* 6**,** 50-58.

HUANG, J., TANG, D., SHEN, Y., QIN, B., HONG, L., YOU, A., LI, M., WANG, X., YU, H., GU, M. & CHENG, Z. 2010. Activation of gibberellin 2-oxidase 6 decreases active gibberellin levels and creates a dominant semi-dwarf phenotype in rice (Oryza sativa L.). *Journal of Genetics and Genomics,* 37**,** 23-36.

HUNG, C. Y., LIN, Y., ZHANG, M., POLLOCK, S., MARKS, M. D. & SCHIEFELBEIN, J. 1998. A common position-dependent mechanism controls cell-type patterning and GLABRA2 regulation in the root and hypocotyl epidermis of Arabidopsis. *Plant Physiology,* 117**,** 73-84.

INGRAM, T. J., REID, J. B., MURFET, I. C., GASKIN, P., WILLIS, C. L. & MACMILLAN, J. 1984. INTERNODE LENGTH IN PISUM - THE LE GENE CONTROLS THE 3-BETA-HYDROXYLATION OF GIBBERELLIN-A20 TO GIBBERELLIN-A1. *Planta,* 160**,** 455-463.

IOIO, R. D., NAKAMURA, K., MOUBAYIDIN, L., PERILLI, S., TANIGUCHI, M., MORITA, M. T., AOYAMA, T., COSTANTINO, P. & SABATINI, S. 2008. A Genetic Framework for the Control of Cell Division and Differentiation in the Root Meristem. *Science,* 322**,** 1380-1384.

IUCHI, S., SUZUKI, H., KIM, Y. C., IUCHI, A., KUROMORI, T., UEGUCHI-TANAKA, M., ASAMI, T., YAMAGUCHI, I., MATSUOKA, M., KOBAYASHI, M. & NAKAJIMA, M. 2007. Multiple loss-of-function of Arabidopsis gibberellin receptor AtGID1s completely shuts down a gibberellin signal. *Plant Journal,* 50**,** 958-966.

JASINSKI, S., PIAZZA, P., CRAFT, J., HAY, A., WOOLLEY, L., RIEU, I., PHILLIPS, A., HEDDEN, P. & TSIANTIS, M. 2005. KNOX Action in Arabidopsis Is Mediated by Coordinate Regulation of Cytokinin and Gibberellin Activities. *Current Biology,* 15**,** 1560-1565.

JIANG, C. F., GAO, X. H., LIAO, L., HARBERD, N. P. & FU, X. D. 2007. Phosphate starvation root architecture and anthocyanin accumulation responses are modulated by the gibberellin-DELLA signaling pathway in Arabidopsis(1[OA]). *Plant Physiology,* 145**,** 1460-1470.

JONES, R. L. & JACOBSEN, J. V. 1991. REGULATION OF SYNTHESIS AND TRANSPORT OF SECRETED PROTEINS IN CEREAL ALEURONE. *International Review of Cytology-a Survey of Cell Biology,* 126**,** 49-88.

KANEKO, M., ITOH, H., INUKAI, Y., SAKAMOTO, T., UEGUCHI-TANAKA, M., ASHIKARI, M. & MATSUOKA, M. 2003. Where do gibberellin biosynthesis and gibberellin signaling occur in rice plants? *The Plant Journal,* 35**,** 104-115.

KANEKO, M., ITOH, H., UEGUCHI-TANAKA, M., ASHIKARI, M. & MATSUOKA, M. 2002. The α-Amylase Induction in Endosperm during Rice Seed Germination Is Caused by Gibberellin Synthesized in Epithelium. *Plant Physiology,* 128**,** 1264-1270.

KANG, J., HWANG, J.-U., LEE, M., KIM, Y.-Y., ASSMANN, S. M., MARTINOIA, E. & LEE, Y. 2010. PDR-type ABC transporter mediates cellular uptake of the phytohormone abscisic acid. *Proceedings of the National Academy of Sciences,* 107**,** 2355-2360.

KING, K. E., MORITZ, T. & HARBERD, N. P. 2001. Gibberellins are not required for normal stem growth in Arabidopsis thaliana in the absence of GAI and RGA. *Genetics,* 159**,** 767-776.

KLIEBENSTEIN, D. J., MONDE, R.-A. & LAST, R. L. 1998. Superoxide Dismutase in Arabidopsis: An Eclectic Enzyme Family with Disparate Regulation and Protein Localization. *Plant Physiology,* 118**,** 637-650.

KO, J. H., YANG, S. H. & HAN, K. H. 2006. Upregulation of an Arabidopsis RING-H2 gene, XERICO, confers drought tolerance through increased abscisic acid biosynthesis. *Plant Journal,* 47**,** 343-355.

KOORNNEEF, M., BENTSINK, L. & HILHORST, H. 2002. Seed dormancy and germination. *Current Opinion in Plant Biology,* 5**,** 33-36.

KOORNNEEF, M., ELGERSMA, A., HANHART, C. J., VANLOENENMARTINET, E. P., VANRIJN, L. & ZEEVAART, J. A. D. 1985. A GIBBERELLIN INSENSITIVE MUTANT OF ARABIDOPSIS-THALIANA. *Physiologia Plantarum,* 65**,** 33-39.

KOORNNEEF, M. & VANDERVEEN, J. H. 1980. INDUCTION AND ANALYSIS OF GIBBERELLIN SENSITIVE MUTANTS IN ARABIDOPSIS-THALIANA (L) HEYNH. *Theoretical and Applied Genetics,* 58**,** 257-263.

KRAMER, E. M. 2006. How Far Can a Molecule of Weak Acid Travel in the Apoplast or Xylem? *Plant Physiology,* 141**,** 1233-1236.

KURODA, H., TAKAHASHI, N., SHIMADA, H., SEKI, M., SHINOZAKI, K. & MATSUI, M. 2002. Classification and expression analysis of Arabidopsis F-box-containing protein genes. *Plant and Cell Physiology,* 43**,** 1073-1085.

KUROMORI, T., MIYAJI, T., YABUUCHI, H., SHIMIZU, H., SUGIMOTO, E., KAMIYA, A., MORIYAMA, Y. & SHINOZAKI, K. 2010. ABC transporter AtABCG25 is involved in abscisic acid transport and responses. *Proceedings of the National Academy of Sciences,* 107**,** 2361-2366.

KWAK, J. M., MORI, I. C., PEI, Z. M., LEONHARDT, N., TORRES, M. A., DANGL, J. L., BLOOM, R. E., BODDE, S., JONES, J. D. G. & SCHROEDER, J. I. 2003. NADPH oxidase AtrbohD and AtrbohF genes function in ROS-dependent ABA signaling in Arabidopsis. *Embo Journal,* 22**,** 2623-2633.

LE, J., VANDENBUSSCHE, F., VAN DER STRAETEN, D. & VERBELEN, J.-P. 2001. In the Early Response of Arabidopsis Roots to Ethylene, Cell Elongation Is Up- and Down-Regulated and Uncoupled from Differentiation. *Plant Physiology,* 125**,** 519-522.

LECHNER, E., XIE, D. X., GRAVA, S., PIGAGLIO, E., PLANCHAIS, S., MURRAY, J. A. H., PARMENTIER, Y., MUTTERER, J., DUBREUCQ, B., SHEN, W. H. & GENSCHIK, P. 2002. The AtRbx1 protein is part of plant SCF complexes, and its down-regulation causes severe growth and developmental defects. *Journal of Biological Chemistry,* 277**,** 50069-50080.

LEE, K. P., PISKUREWICZ, U., TUREČKOVÁ, V., STRNAD, M. & LOPEZ-MOLINA, L. 2010. A seed coat bedding assay shows that RGL2-dependent release of abscisic acid by the endosperm controls embryo growth in Arabidopsis dormant seeds. *Proceedings of the National Academy of Sciences*.

LEUBNER-METZGER, G. 2001. Brassinosteroids and gibberellins promote tobacco seed germination by distinct pathways. *Planta,* 213**,** 758-763.

LEVESQUE, M. P., VERNOUX, T., BUSCH, W., CUI, H., WANG, J. Y., BLILOU, I., HASSAN, H., NAKAJIMA, K., MATSUMOTO, N., LOHMANN, J. U., SCHERES, B. & BENFEY, P. N. 2006. Whole-Genome Analysis of the SHORT-ROOT Developmental Pathway in <italic>Arabidopsis</italic>. *PLoS Biol,* 4**,** e143.

LEYSER, O. 2006. Dynamic Integration of Auxin Transport and Signalling. 16**,** R424-R433.

LIU, J., MEHDI, S., TOPPING, J., TARKOWSKI, P. & LINDSEY, K. 2010. Modelling and experimental analysis of hormonal crosstalk in Arabidopsis. *Mol Syst Biol,* 6.

MACMILLAN, J. 1997. Biosynthesis of the gibberellin plant hormones. *Nat. Prod. Rep***,** 221 - 243.

MACMILLAN, J. 2001. Occurrence of Gibberellins in Vascular Plants, Fungi, and Bacteria. *Journal of Plant Growth Regulation,* 20**,** 387-442.

MACMILLAN, J. & TAKAHASHI, N. 1968. Proposed Procedure for the Allocation of Trivial Names to the Gibberellins. *Nature,* 217**,** 170-171.

MASUCCI, J. D., RERIE, W. G., FOREMAN, D. R., ZHANG, M., GALWAY, M. E., MARKS, M. D. & SCHIEFELBEIN, J. W. 1996. The homeobox gene GLABRA 2 is required for position-dependent cell differentiation in the root epidermis of Arabidopsis thaliana. *Development,* 122**,** 1253-1260.

MAUREL, C., VERDOUCQ, L., LUU, D. T. & SANTONI, V. 2008. Plant aquaporins: Membrane channels with multiple integrated functions. *Annual Review of Plant Biology,* 59**,** 595-624.

MCGINNIS, K. M., THOMAS, S. G., SOULE, J. D., STRADER, L. C., ZALE, J. M., SUN, T.-P. & STEBER, C. M. 2003. The Arabidopsis SLEEPY1 Gene Encodes a Putative F-Box Subunit of an SCF E3 Ubiquitin Ligase. *THE PLANT CELL,* 15**,** 1120-1130.

MEIER, C., BOUQUIN, T., NIELSEN, M. E., RAVENTOS, D., MATTSSON, O., ROCHER, A., SCHOMBURG, F., AMASINO, R. M. & MUNDY, J. 2001. Gibberellin response mutants identified by luciferase imaging. *The Plant journal : for cell and molecular biology,* 25**,** 509-19.

MITCHUM, M. G., YAMAGUCHI, S., HANADA, A., KUWAHARA, A., YOSHIOKA, Y., KATO, T., TABATA, S., KAMIYA, Y. & SUN, T. P. 2006. Distinct and overlapping roles of two gibberellin 3-oxidases in Arabidopsis development. *Plant Journal,* 45**,** 804-818.

MOUBAYIDIN, L., PERILLI, S., DELLO IOIO, R., DI MAMBRO, R., COSTANTINO, P. & SABATINI, S. 2010. The Rate of Cell Differentiation Controls the Arabidopsis Root Meristem Growth Phase. *Current Biology,* 20**,** 1138-1142.

MOUCHEL, C. F., OSMONT, K. S. & HARDTKE, C. S. 2006. BRX mediates feedback between brassinosteroid levels and auxin signalling in root growth. *Nature,* 443**,** 458-461.

MURASE, K., HIRANO, Y., SUN, T.-P. & HAKOSHIMA, T. 2008. Gibberellin-induced DELLA recognition by the gibberellin receptor GID1. *Nature,* 456**,** 459-463.

MUSSIG, C., SHIN, G.-H. & ALTMANN, T. 2003. Brassinosteroids Promote Root Growth in Arabidopsis. *Plant Physiology,* 133**,** 1261-1271.

MUSTROPH, A., ZANETTI, M. E., JANG, C. J. H., HOLTAN, H. E., REPETTI, P. P., GALBRAITH, D. W., GIRKE, T. & BAILEY-SERRES, J. 2009. Profiling translatomes of discrete cell populations resolves altered cellular priorities during hypoxia in Arabidopsis. *Proceedings of the National Academy of Sciences,* 106**,** 18843-18848.

NAKAJIMA, K., SENA, G., NAWY, T. & BENFEY, P. N. 2001. Intercellular movement of the putative transcription factor SHR in root patterning. *Nature,* 413**,** 307-311.

NAKAJIMA, M., SHIMADA, A., TAKASHI, Y., KIM, Y. C., PARK, S. H., UEGUCHI-TANAKA, M., SUZUKI, H., KATOH, E., IUCHI, S., KOBAYASHI, M., MAEDA, T., MATSUOKA, M. & YAMAGUCHI, I. 2006. Identification and characterization of Arabidopsis gibberellin receptors. *Plant Journal,* 46**,** 880-889.

NAWY, T., LEE, J. Y., COLINAS, J., WANG, J. Y., THONGROD, S. C., MALAMY, J. E., BIRNBAUM, K. & BENFEY, P. N. 2005. Transcriptional profile of the Arabidopsis root quiescent center. *Plant Cell,* 17**,** 1908-1925.

O'NEILL, D. P. & ROSS, J. J. 2002. Auxin Regulation of the Gibberellin Pathway in Pea. *Plant Physiology,* 130**,** 1974-1982.

OGAWA, M., HANADA, A., YAMAUCHI, Y., KUWALHARA, A., KAMIYA, Y. & YAMAGUCHI, S. 2003. Gibberellin biosynthesis and response during Arabidopsis seed germination. *Plant Cell,* 15**,** 1591-1604.

OH, E., KIM, J., PARK, E., KIM, J.-I., KANG, C. & CHOI, G. 2004. PIL5, a Phytochrome-Interacting Basic Helix-Loop-Helix Protein, Is a Key Negative Regulator of Seed Germination in Arabidopsis thaliana. *THE PLANT CELL,* 16**,** 3045-3058.

PAQUETTE, A. J. & BENFEY, P. N. 2005. Maturation of the ground tissue of the root is regulated by gibberellin and SCARECROW and requires SHORT-ROOT. *Plant Physiology,* 138**,** 636-640.

PATTERSON, H. D. & THOMPSON, R. 1971. Recovery of inter-block information when block sizes are unequal. *Biometrika,* 58**,** 545-554.

PENG, J., RICHARDS, D. E., HARTLEY, N. M., MURPHY, G. P., DEVOS, K. M., FLINTHAM, J. E., BEALES, J., FISH, L. J., WORLAND, A. J., PELICA, F., SUDHAKAR, D., CHRISTOU, P., SNAPE, J. W., GALE, M. D. & HARBERD, N. P. 1999. /`Green revolution/' genes encode mutant gibberellin response modulators. *Nature,* 400**,** 256-261.

PENG, J. R. & HARBERD, N. P. 2002. The role of GA-mediated signalling in the control of seed germination. *Current Opinion in Plant Biology,* 5**,** 376-381.

PETERSSON, S. V., JOHANSSON, A. I., KOWALCZYK, M., MAKOVEYCHUK, A., WANG, J. Y., MORITZ, T., GREBE, M., BENFEY, P. N., SANDBERG, G. & LJUNG, K. 2009. An Auxin Gradient and Maximum in the Arabidopsis Root Apex Shown by High-Resolution Cell-Specific Analysis of IAA Distribution and Synthesis. *THE PLANT CELL***,** tpc.109.066480.

PHILLIPS, A. L. 1998. Gibberellins in Arabidopsis. *Plant Physiology and Biochemistry,* 36**,** 115-124.

PHILLIPS, A. L., WARD, D. A., UKNES, S., APPLEFORD, N. E. J., LANGE, T., HUTTLY, A. K., GASKIN, P., GRAEBE, J. E. & HEDDEN, P. 1995. ISOLATION AND EXPRESSION OF 3 GIBBERELLIN 20-OXIDASE CDNA CLONES FROM ARABIDOPSIS. *Plant Physiology,* 108**,** 1049-1057.

PROEBSTING, W. M., HEDDEN, P., LEWIS, M. J., CROKER, S. J. & PROEBSTING, L. N. 1992. Gibberellin Concentration and Transport in Genetic Lines of Pea : Effects of Grafting. *Plant Physiology,* 100**,** 1354-1360.

PUENTE, P., WEI, N. & DENG, X. W. 1996. Combinatorial interplay of promoter elements constitutes the minimal determinants for light and developmental control of gene expression in Arabidopsis. *Embo Journal,* 15**,** 3732-3743.

RERIE, W. G., FELDMANN, K. A. & MARKS, M. D. 1994. THE GLABRA2 GENE ENCODES A HOMEO DOMAIN PROTEIN REQUIRED FOR NORMAL TRICHOME DEVELOPMENT IN ARABIDOPSIS. *Genes & Development,* 8**,** 1388-1399.

RIEU, I., ERIKSSON, S., POWERS, S. J., GONG, F., GRIFFITHS, J., WOOLLEY, L., BENLLOCH, R., NILSSON, O., THOMAS, S. G., HEDDEN, P. & PHILLIPS, A. L. 2008a. Genetic Analysis Reveals That C-19-GA 2-Oxidation Is a Major Gibberellin Inactivation Pathway in Arabidopsis. *Plant Cell,* 20**,** 2420-2436.

RIEU, I., RUIZ-RIVERO, O., FERNANDEZ-GARCIA, N., GRIFFITHS, J., POWERS, S. J., GONG, F., LINHARTOVA, T., ERIKSSON, S., NILSSON, O., THOMAS, S. G., PHILLIPS, A. L. & HEDDEN, P. 2008b. The gibberellin biosynthetic genes AtGA20ox1 and AtGA20ox2 act, partially redundantly, to promote growth and development throughout the Arabidopsis life cycle. *Plant Journal,* 53**,** 488-504.

SANTES, C. M., HEDDEN, P., GASKIN, P. & GARCIAMARTINEZ, J. L. 1995. GIBBERELLINS AND RELATED-COMPOUNDS IN YOUNG FRUITS OF PEA AND THEIR RELATIONSHIP TO FRUIT-SET. *Phytochemistry,* 40**,** 1347-1355.

SAVALDI-GOLDSTEIN, S., PETO, C. & CHORY, J. 2007. The epidermis both drives and restricts plant shoot growth. *Nature,* 446**,** 199-202.

SCHOMBURG, F. M., BIZZELL, C. M., LEE, D. J., ZEEVAART, J. A. D. & AMASINO, R. M. 2003. Overexpression of a Novel Class of Gibberellin 2-Oxidases Decreases Gibberellin Levels and Creates Dwarf Plants. *THE PLANT CELL,* 15**,** 151-163.

SENA, G., JUNG, J. W. & BENFEY, P. N. 2004. A broad competence to respond to SHORT ROOT revealed by tissue-specific ectopic expression. *Development,* 131**,** 2817-2826.

SHEN, W. H., PARMENTIER, Y., HELLMANN, H., LECHNER, E., DONG, A. W., MASSON, J., GRANIER, F., LEPINIEC, L., ESTELLE, M. & GENSCHIK, P. 2002. Null mutation of AtCUL1 causes arrest in early embryogenesis in Arabidopsis. *Molecular Biology of the Cell,* 13**,** 1916-1928.

SHIMADA, A., UEGUCHI-TANAKA, M., NAKATSU, T., NAKAJIMA, M., NAOE, Y., OHMIYA, H., KATO, H. & MATSUOKA, M. 2008. Structural basis for gibberellin recognition by its receptor GID1. *Nature,* 456**,** 520-523.

SILVERSTONE, A. L., JUNG, H.-S., DILL, A., KAWAIDE, H., KAMIYA, Y. & SUN, T.-P. 2001. Repressing a Repressor: Gibberellin-Induced Rapid Reduction of the RGA Protein in Arabidopsis. *THE PLANT CELL,* 13**,** 1555-1566.

SMYTH, D. R., BOWMAN, J. L. & MEYEROWITZ, E. M. 1990. Early Flower Development in Arabidopsis. *Plant Cell,* 2**,** 755-767.

SOZZANI, R., CUI, H., MORENO-RISUENO, M. A., BUSCH, W., VAN NORMAN, J. M., VERNOUX, T., BRADY, S. M., DEWITTE, W., MURRAY, J. A. H. & BENFEY, P. N. 2010. Spatiotemporal regulation of cell-cycle genes by SHORTROOT links patterning and growth. *Nature,* 466**,** 128-132.

SPANU, P., GROSSKOPF, D. G., FELIX, G. & BOLLER, T. 1994. THE APPARENT TURNOVER OF 1-AMINOCYCLOPROPANE-1-CARBOXYLATE SYNTHASE IN TOMATO CELLS IS REGULATED BY PROTEIN-PHOSPHORYLATION AND DEPHOSPHORYLATION. *Plant Physiology,* 106**,** 529-535.

STOWE, B. B. & YAMAKI, T. 1957. The History and Physiological Action of the Gibberellins. *Annual Review of Plant Physiology,* 8**,** 181.

SUN, T., GOODMAN, H. M. & AUSUBEL, F. M. 1992. Cloning the Arabidopsis GA1 Locus by Genomic Subtraction. *The Plant Cell Online,* 4**,** 119-128.

SWARUP, R. & BENNETT, M. 2003. Auxin Transport: The Fountain of Life in Plants? *Developmental Cell,* 5**,** 824-826.

SWARUP, R., KRAMER, E. M., PERRY, P., KNOX, K., LEYSER, H. M. O., HASELOFF, J., BEEMSTER, G. T. S., BHALERAO, R. & BENNETT, M. J. 2005. Root gravitropism requires lateral root cap and epidermal cells for transport and response to a mobile auxin signal. *Nat Cell Biol,* 7**,** 1057-1065.

SWARUP, R., PERRY, P., HAGENBEEK, D., VAN DER STRAETEN, D., BEEMSTER, G. T. S., SANDBERG, G., BHALERAO, R., LJUNG, K. & BENNETT, M. J. 2007. Ethylene Upregulates Auxin Biosynthesis in Arabidopsis Seedlings to Enhance Inhibition of Root Cell Elongation. *THE PLANT CELL,* 19**,** 2186-2196.

SZYMANSKI, D. B., JILK, R. A., POLLOCK, S. M. & MARKS, M. D. 1998. Control of GL2 expression in Arabidopsis leaves and trichomes. *Development,* 125**,** 1161-1171.

TAKAHASHI, N., KITAMURA, H., KAWARADA, A., SETA, Y., TAKAI, M., TAMURA, S. & SUMIKI, Y. 1955. BIOCHEMICAL STUDIES ON BAKANAE FUNGUS .34. ISOLATION OF GIBBERELLINS AND THEIR PROPERTIES. *Bulletin of the Agricultural Chemical Society of Japan,* 19**,** 267-277.

TALON, M., KOORNNEEF, M. & ZEEVAART, J. A. D. 1990. ACCUMULATION OF C19-GIBBERELLINS IN THE GIBBERELLIN-INSENSITIVE DWARF MUTANT GAI OF ARABIDOPSIS-THALIANA (L) HEYNH. *Planta,* 182**,** 501-505.

TANAKA, H., DHONUKSHE, P., BREWER, P. & FRIML, J. 2006. Spatiotemporal asymmetric auxin distribution: a means to coordinate plant development. *Cellular and Molecular Life Sciences (CMLS),* 63**,** 2738-2754.

THE_ARABIDOPSIS_INITIATIVE 2000. Analysis of the genome sequence of the flowering plant Arabidopsis thaliana. *Nature,* 408**,** 796-815.

THOMAS, S. G., PHILLIPS, A. L. & HEDDEN, P. 1999. Molecular cloning and functional expression of gibberellin 2- oxidases, multifunctional enzymes involved in gibberellin deactivation. *Proceedings of the National Academy of Sciences,* 96**,** 4698-4703.

UBEDA-TOMÁS, S., FEDERICI, F., CASIMIRO, I., BEEMSTER, G. T. S., BHALERAO, R., SWARUP, R., DOERNER, P., HASELOFF, J. & BENNETT, M. J. 2009. Gibberellin Signaling in the Endodermis Controls Arabidopsis Root Meristem Size.

UBEDA-TOMAS, S., SWARUP, R., COATES, J., SWARUP, K., LAPLAZE, L., BEEMSTER, G. T. S., HEDDEN, P., BHALERAO, R. & BENNETT, M. J. 2008. Root growth in Arabidopsis requires gibberellin/DELLA signalling in the endodermis. *Nature Cell Biology,* 10**,** 625-628.

UEGUCHI-TANAKA, M., ASHIKARI, M., NAKAJIMA, M., ITOH, H., KATOH, E., KOBAYASHI, M., CHOW, T. Y., HSING, Y. I. C., KITANO, H., YAMAGUCHI, I. & MATSUOKA, M. 2005. GIBBERELLIN INSENSITIVE DWARF1 encodes a soluble receptor for gibberellin. *Nature,* 437**,** 693-698.

UEGUCHI-TANAKA, M., HIRANO, K., HASEGAWA, Y., KITANO, H. & MATSUOKA, M. 2008. Release of the Repressive Activity of Rice DELLA Protein SLR1 by Gibberellin Does Not Require SLR1 Degradation in the gid2 Mutant. *THE PLANT CELL,* 20**,** 2437-2446.

UEGUCHI-TANAKA, M., NAKAJIMA, M., MOTOYUKI, A. & MATSUOKA, M. 2007. Gibberellin receptor and its role in gibberellin signaling in plants. *Annual Review of Plant Biology,* 58**,** 183-198.

ULLAH, H., CHEN, J. G., WANG, S. C. & JONES, A. M. 2002. Role of a heterotrimeric G protein in regulation of Arabidopsis seed germination. *Plant Physiology,* 129**,** 897-907.

VARBANOVA, M., YAMAGUCHI, S., YANG, Y., MCKELVEY, K., HANADA, A., BOROCHOV, R., YU, F., JIKUMARU, Y., ROSS, J., CORTES, D., MA, C. J., NOEL, J. P., MANDER,

L., SHULAEV, V., KAMIYA, Y., RODERMEL, S., WEISS, D. & PICHERSKY, E. 2007. Methylation of Gibberellins by Arabidopsis GAMT1 and GAMT2. *THE PLANT CELL,* 19**,** 32-45.

VIETEN, A., SAUER, M., BREWER, P. B. & FRIML, J. 2007. Molecular and cellular aspects of auxin-transport-mediated development. *Trends in Plant Science,* 12**,** 160-168.

WANG, K. L. C., YOSHIDA, H., LURIN, C. & ECKER, J. R. 2004. Regulation of ethylene gas biosynthesis by the Arabidopsis ETO1 protein. *Nature,* 428**,** 945-950.

WARD, D. A., MACMILLAN, J., GONG, F., PHILLIPS, A. L. & HEDDEN, P. 2010. Gibberellin 3-oxidases in developing embryos of the southern wild cucumber, Marah macrocarpus. *Phytochemistry,* 71**,** 2010-2018.

WELCH, D., HASSAN, H., BLILOU, I., IMMINK, R., HEIDSTRA, R. & SCHERES, B. 2007. Arabidopsis JACKDAW and MAGPIE zinc finger proteins delimit asymmetric cell division and stabilize tissue boundaries by restricting SHORT-ROOT action. *Genes & Development,* 21**,** 2196-2204.

WILLIAMS, J., PHILLIPS, A. L., GASKIN, P. & HEDDEN, P. 1998. Function and substrate specificity of the gibberellin 3 beta-hydroxylase encoded by the Arabidopsis GA4 gene. *Plant Physiology,* 117**,** 559-563.

WOLBANG, C. M., CHANDLER, P. M., SMITH, J. J. & ROSS, J. J. 2004. Auxin from the Developing Inflorescence Is Required for the Biosynthesis of Active Gibberellins in Barley Stems. *Plant Physiology,* 134**,** 769-776.

WYSOCKA-DILLER, J. W., HELARIUTTA, Y., FUKAKI, H., MALAMY, J. E. & BENFEY, P. N. 2000. Molecular analysis of SCARECROW function reveals a radial patterning mechanism common to root and shoot. *Development,* 127**,** 595-603.

YADAV, R. K., GIRKE, T., PASALA, S., XIE, M. & REDDY, G. V. 2009. Gene expression map of the Arabidopsis shoot apical meristem stem cell niche. *Proceedings of the National Academy of Sciences,* 106**,** 4941-4946.

YADAV, V., KUNDU, S., CHATTOPADHYAY, D., NEGI, P., WEI, N., DENG, X. W. & CHATTOPADHYAY, S. 2002. Light regulated modulation of Z-box containing promoters by photoreceptors and downstream regulatory components, COP1 and HY5, in Arabidopsis. *Plant Journal,* 31**,** 741-753.

YAMAGUCHI, S. 2008. Gibberellin Metabolism and its Regulation. *Annual Review of Plant Biology,* 59**,** 225.

YAMAGUCHI, S., KAMIYA, Y. & SUN, T. P. 2001. Distinct cell-specific expression patterns of early and late gibberellin biosynthetic genes during Arabidopsis seed germination. *Plant Journal,* 28**,** 443-453.

YAMAGUCHI, S., SUN, T. P., KAWAIDE, H. & KAMIYA, Y. 1998. The GA2 locus of Arabidopsis thaliana encodes ent-kaurene synthase of gibberellin biosynthesis. *Plant Physiology,* 116**,** 1271-1278.

YAMAMOTO, Y., HIRAI, T., YAMAMOTO, E., KAWAMURA, M., SATO, T., KITANO, H., MATSUOKA, M. & UEGUCHI-TANAKA, M. 2010. A Rice gid1 Suppressor Mutant Reveals That Gibberellin Is Not Always Required for Interaction between Its Receptor, GID1, and DELLA Proteins. *The Plant Cell Online,* 22**,** 3589-3602.

YAXLEY, J. R., ROSS, J. J., SHERRIFF, L. J. & REID, J. B. 2001. Gibberellin biosynthesis mutations and root development in pea. *Plant Physiology,* 125**,** 627-633.

ZHANG, Z.-L., OGAWA, M., FLEET, C. M., ZENTELLA, R., HU, J., HEO, J.-O., LIM, J., KAMIYA, Y., YAMAGUCHI, S. & SUN, T.-P. 2011. SCARECROW-LIKE 3 promotes gibberellin signaling by antagonizing master growth repressor DELLA in Arabidopsis. *Proceedings of the National Academy of Sciences*.

ZHAO, X. Y., YU, X. H., FOO, E., SYMONS, G. M., LOPEZ, J., BENDEHAKKALU, K. T., XIANG, J., WELLER, J. L., LIU, X. M., REID, J. B. & LIN, C. T. 2007. A study of

gibberellin homeostasis and cryptochrome-mediated blue light inhibition of hypocotyl elongation. *Plant Physiology,* 145**,** 106-118.

ZHENG, N., SCHULMAN, B. A., SONG, L., MILLER, J. J., JEFFREY, P. D., WANG, P., CHU, C., KOEPP, D. M., ELLEDGE, S. J., PAGANO, M., CONAWAY, R. C., CONAWAY, J. W., HARPER, J. W. & PAVLETICH, N. P. 2002. Structure of the Cul1-Rbx1-Skp1-F boxSkp2 SCF ubiquitin ligase complex. *Nature,* 416**,** 703-709.

ZHU, Y., NOMURA, T., XU, Y., ZHANG, Y., PENG, Y., MAO, B., HANADA, A., ZHOU, H., WANG, R., LI, P., ZHU, X., MANDER, L. N., KAMIYA, Y., YAMAGUCHI, S. & HE, Z. 2006. ELONGATED UPPERMOST INTERNODE Encodes a Cytochrome P450 Monooxygenase That Epoxidizes Gibberellins in a Novel Deactivation Reaction in Rice. *THE PLANT CELL,* 18**,** 442-456.

11 APPENDIX

11.1 GA metabolism microarray meta-analysis

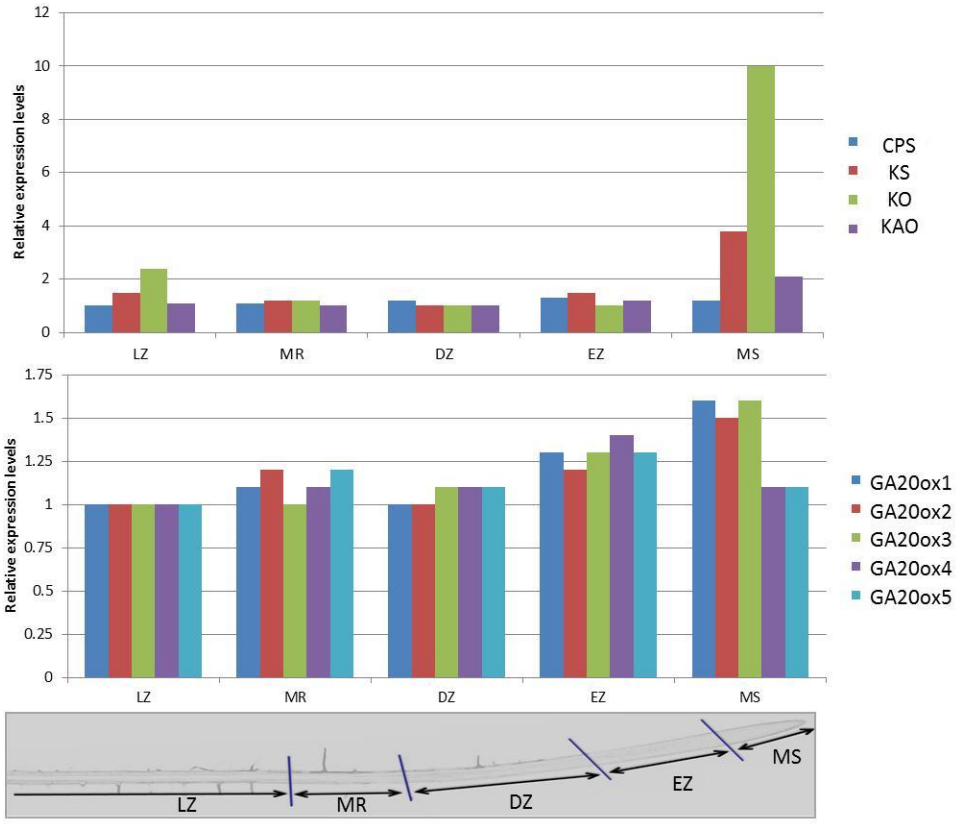

Figure 11-1: **The relative expression levels of the early GA-biosynthetic and AtGA20ox genes in different zones of an elongating Arabidopsis root.** Lateral root zone (LZ), mature region (MR), differentiation zone (DZ), the elongation zone (EZ) and the meristematic zone (MS). Schematic diagram of the different developmental zones as distance from the QC increases MS =~350 µm, DZ =~900 µm, DZ=~1.2 mm, MR =~500 µm, LZ=~2.5 cm (courtesy of CPIB). These data are assembled from microarray experiments from the laboratories of Drs Benfey, Serres and the CPIB group which was provided courtesy of Michael Wilson.

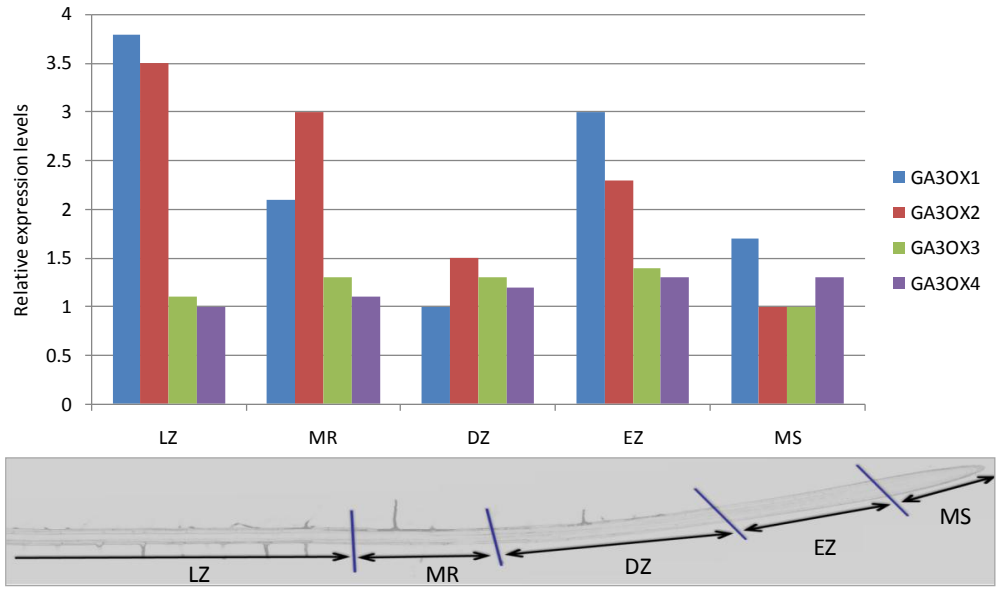

Figure 11-2**: The relative expression levels of the *GA3ox* genes in the lateral root zone (LZ), the mature region (MR), the differentiation zone (DZ), the elongation zone (EZ) and the meristematic zone (MS).** Schematic diagram of the different developmental zones as distance from the QC increases MS =~350 µm, DZ =~900 µm, DZ =~1.2 mm, MR =~500 µm, LZ =~2.5 cm (courtesy of CPIB). These data are assembled from microarray experiments from the Drs Benfey, Serres and the CPIB lab which was provided courtesy of Michael Wilson.

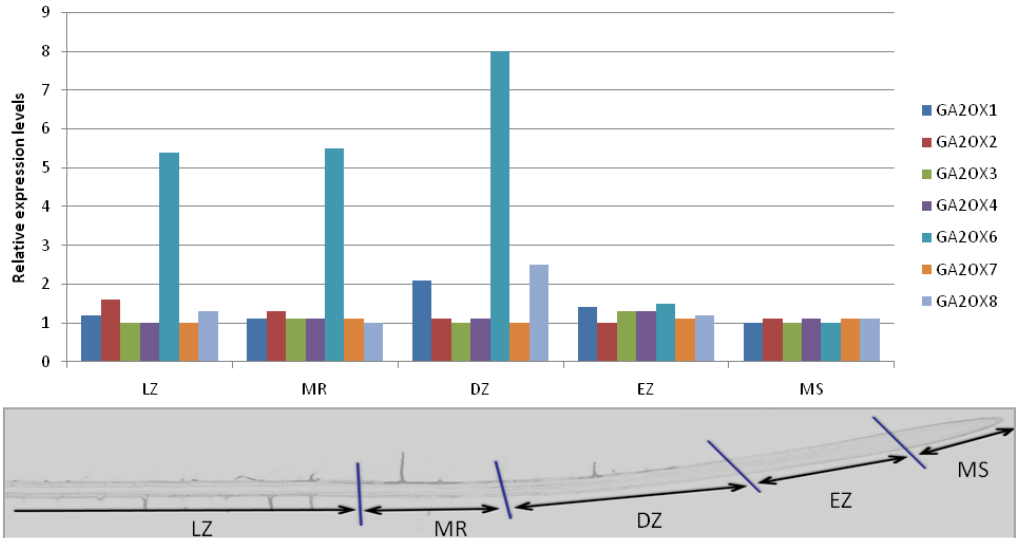

Figure 11-3: **The relative expression levels of the *GA2ox* genes in the lateral root zone (LZ), the mature region (MR), the differentiation zone (DZ), the elongation zone (EZ) and the meristematic zone (MS).** Schematic diagram of the different developmental zones as distance from the QC increases MS =~350 µm, DZ =~900 µm, DZ=~1.2 mm, MR~500 µm, LZ=~2.5 cm (courtesy of CPIB). These data are assembled from microarray experiments from the laboratories of Drs Benfey, Serres and CPIB, which was provided courtesy of Michael Wilson.

11.2 GA membrane permeability estimates

Table 11-1: **Predicted membrane mobility of important *Arabidopsis GAs*.** Estimates of pKa, pKa2, membrane permeability at cellular pH 7.2 (P_AH), and at apoplastic pH 5.5 (P_eff). Courtesy of Prof Eric Kramer.

	pKa	pKa2	P_AH (cm/hr)	P_eff (cm/hr)
IAA	4.85		0.20	0.04
GA_{12}	4.2	5.08	269.79	3.67
GA_{15}-open lactone	4.13	5.01	5.77	0.06
GA_{15}-closed lactone	4.45		10.74	0.88
GA_{24}	3.95	4.83	12.33	0.06
GA_9	4.34		4.28	0.28
GA_4	4.22		0.37	0.02

11.3 GID1a root hair phenotypes

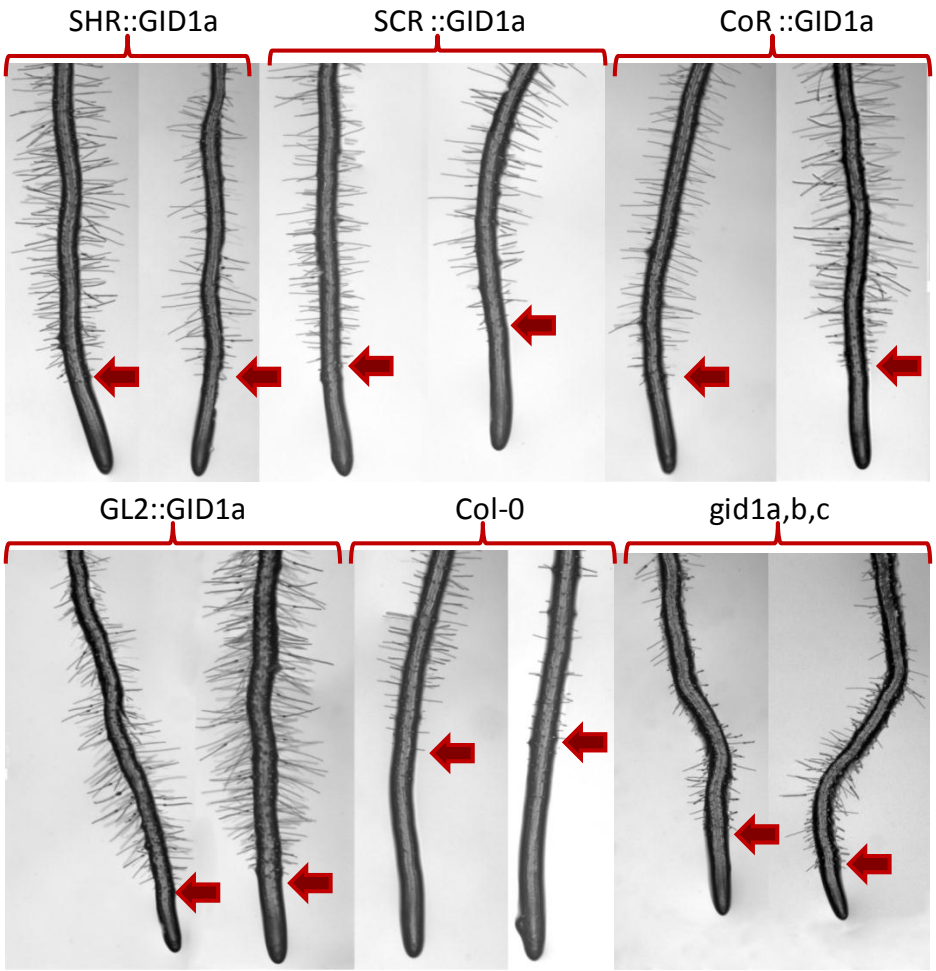

Figure 11-4: **Root hair phenotypes of *gid1a,-b,-c* triple mutants carrying tissue specific promoters expressing functional GID1a GA receptors.** The red arrow indicates the site of root hair elongation. Plants were grown for 7 days under normal conditions. Images are composites and are not to scale but are relative to one another.

11.4 Construct design diagrams

SHR::YFP:AtGA2ox2 (arrows indicate digestion and ligation)

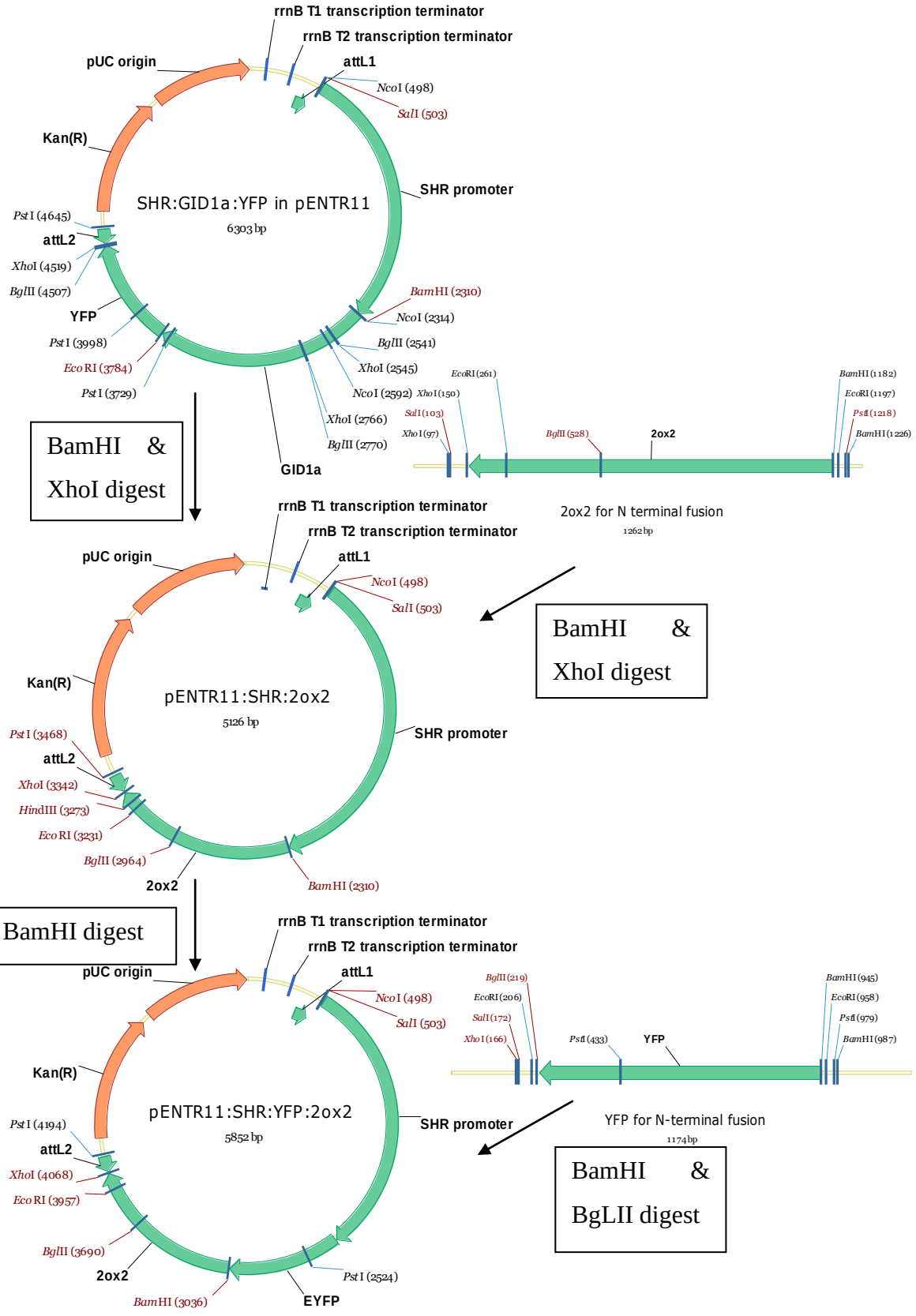

SCR::YFP:AtGA2ox2

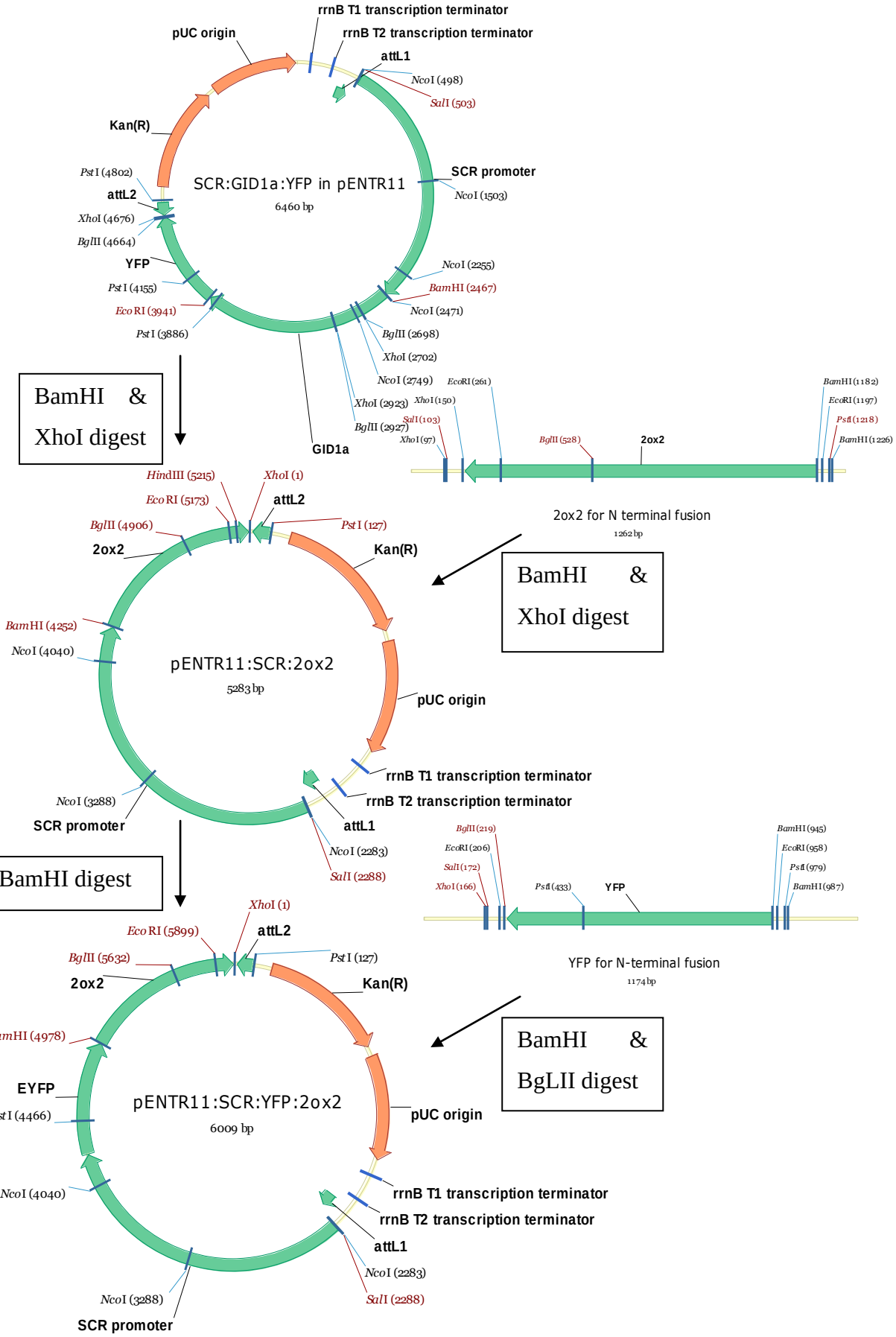

CAB::YFP:AtGA2ox2

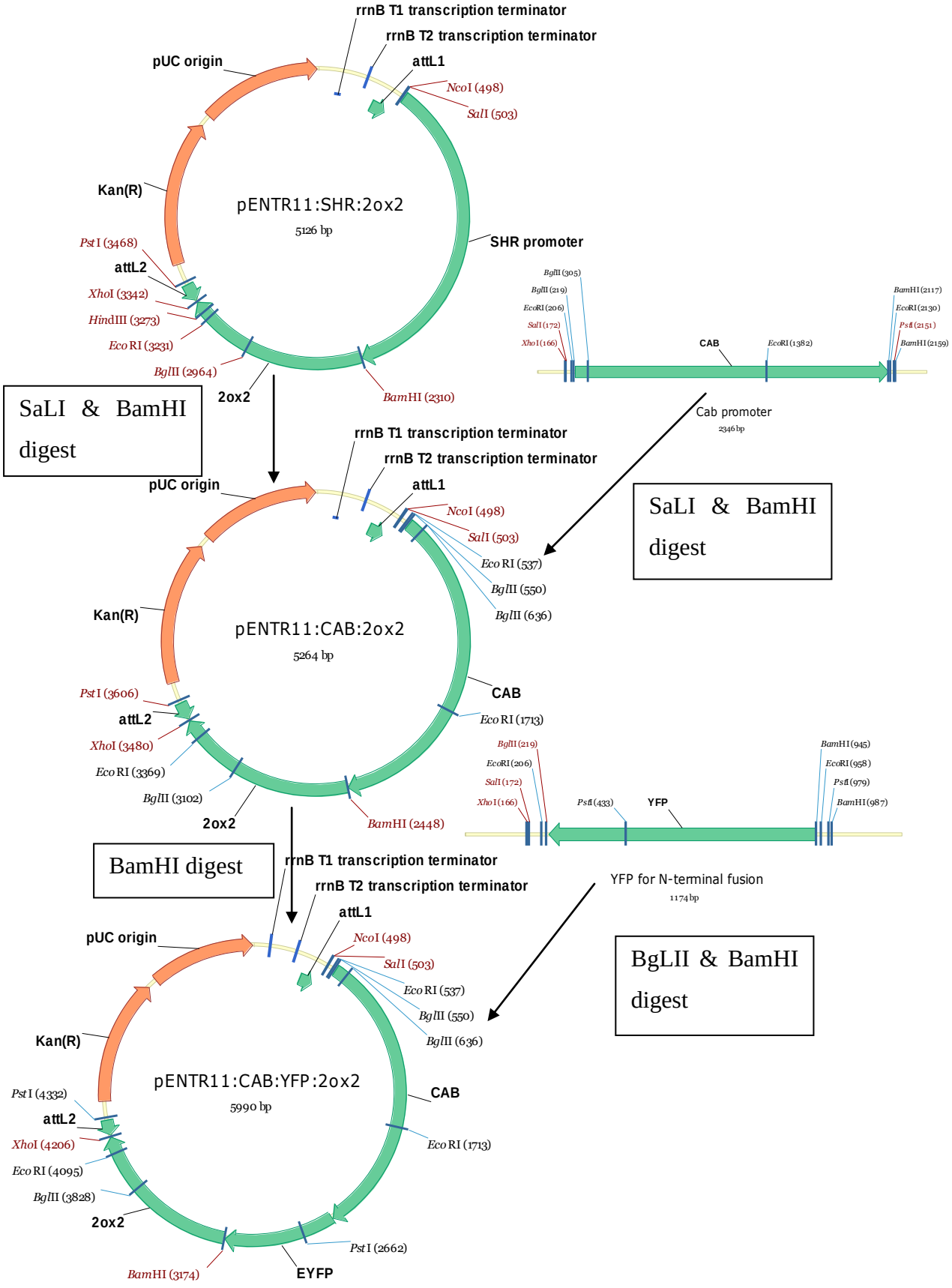

Co2::AtGID1a:YFP

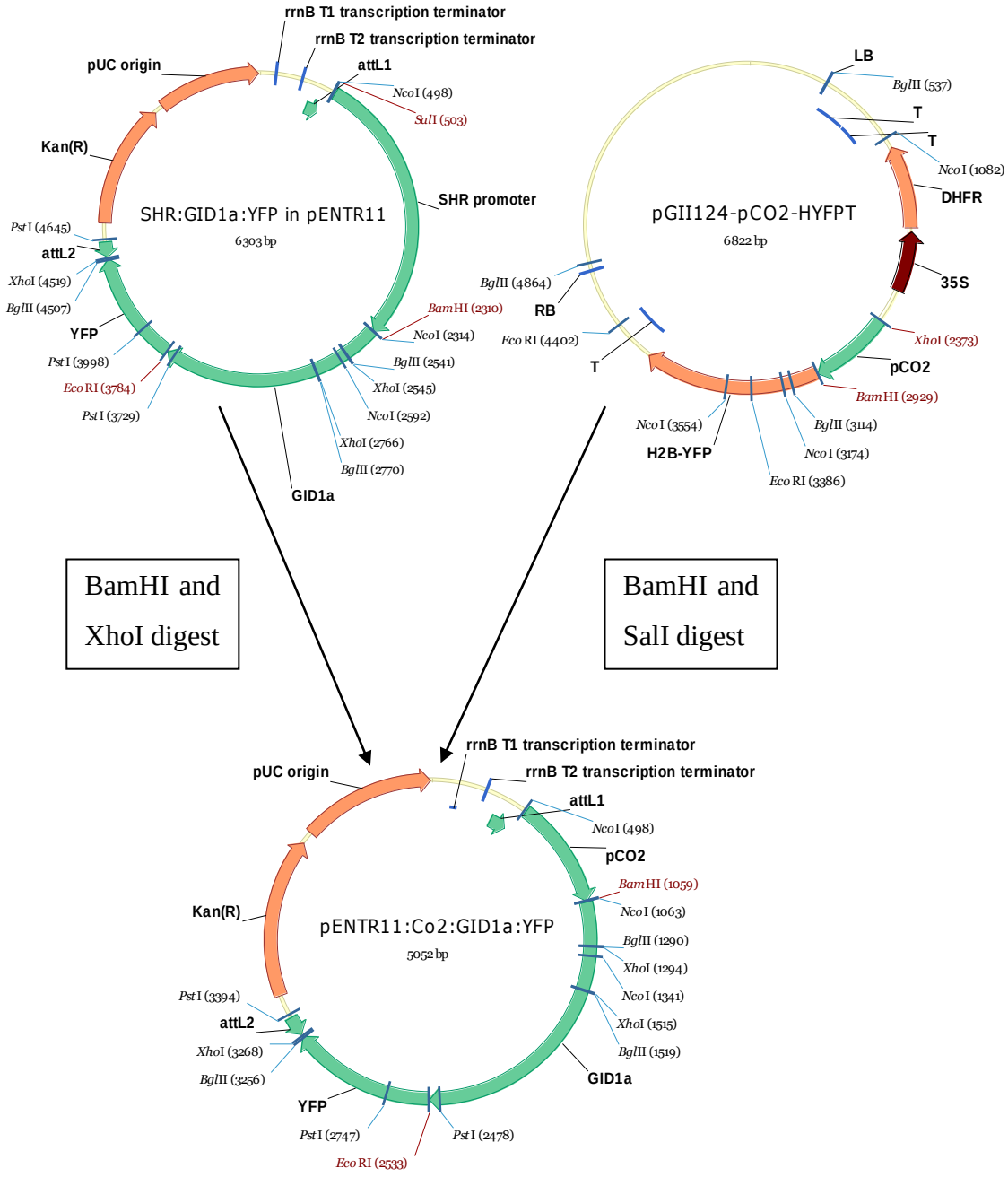

Co2::YFP:AtGA2ox2

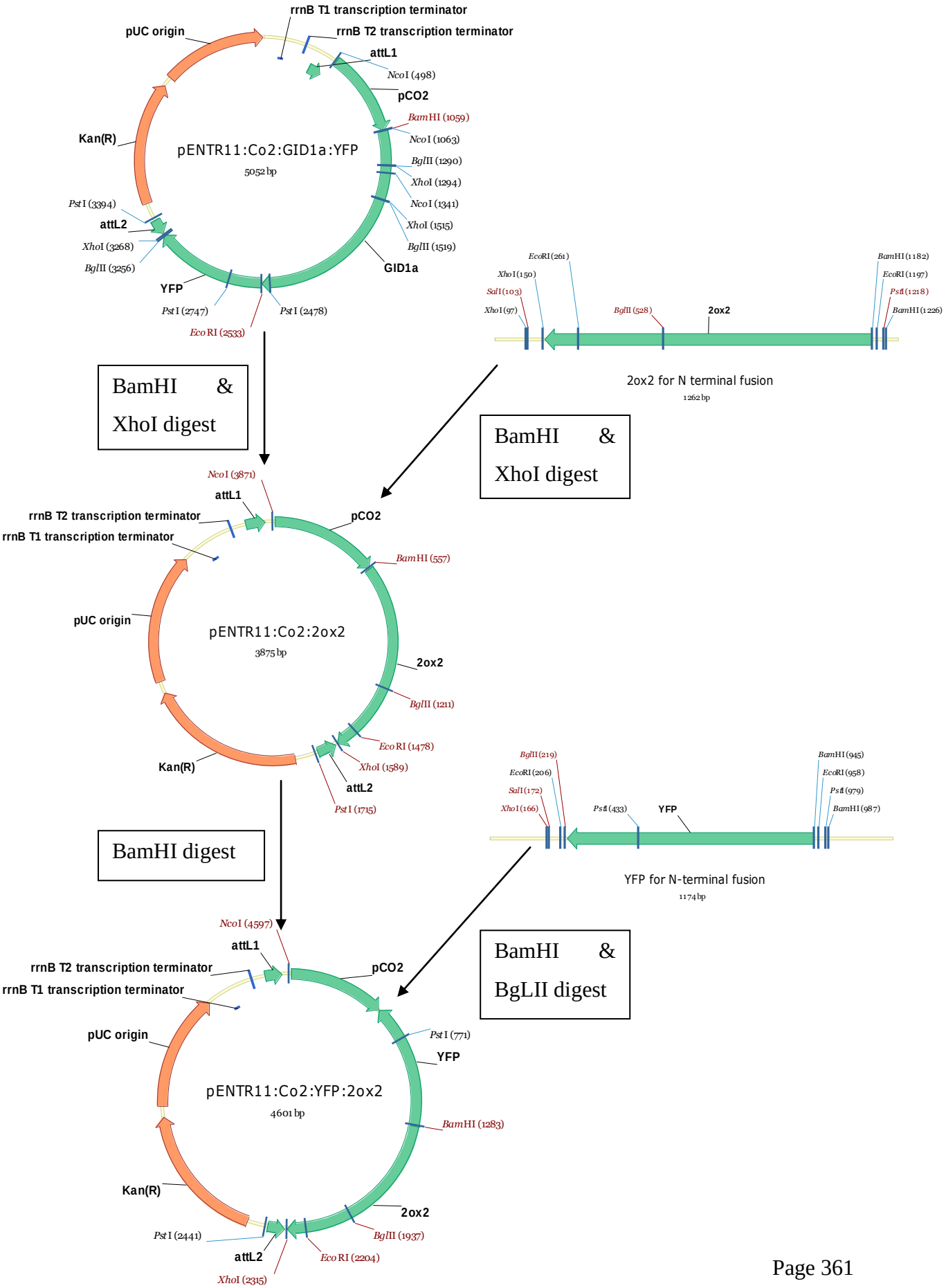

GL2::YFP:AtGA2ox2

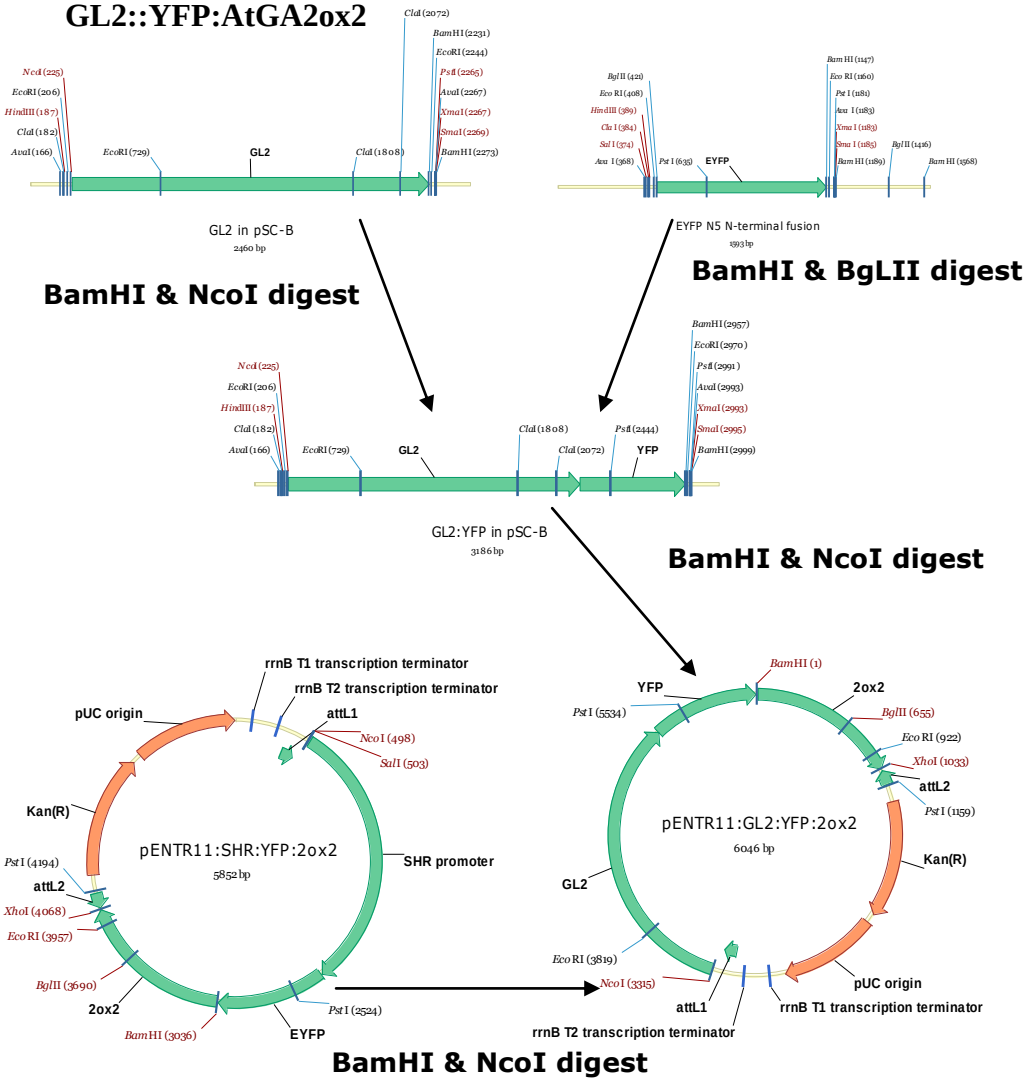

GL2::AtGID1a:YFP

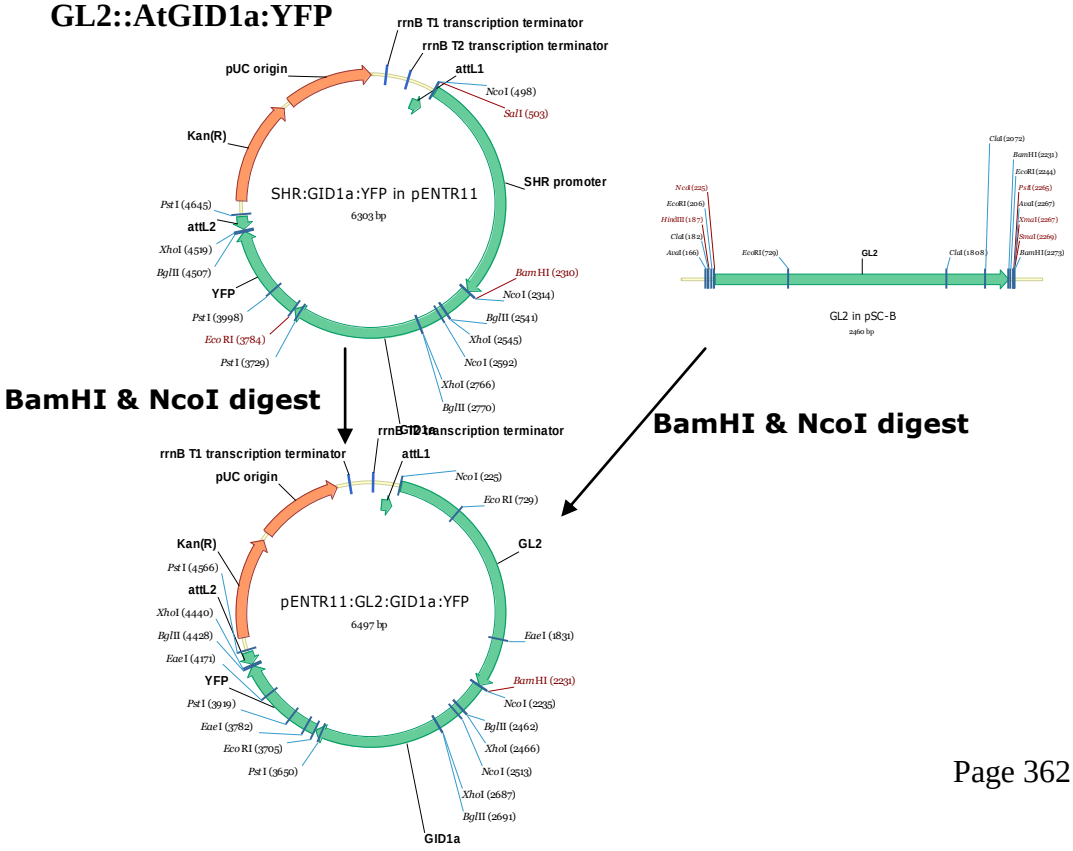

11.5 Statistics from preliminary characterisation

Table 11-2: AtGA2ox2 EXP1

Promo	a	b	c	d	e	f	Col-0	ga1-3	SED ($_{ave}$)	LSD($_{5\%}$)	LSD($_{1\%}$)
SHR	3.57	3.81	3.89	3.57	3.64		4.03	2.47	0.13	0.26	0.35
SCR	1.5	1.74	2.13	2.29	2.91	1.92	3.39	2.38	0.21	^{T}0.46	^{T}0.62
CoR	2.87	2.49	2.56	2.12			3.01	1.95	0.18	^{T}0.42	^{T}0.56
Co2	2.61	2.31	2.12	2.65			3.29	2.05	0.14	^{T}0.32	^{T}0.42
GL2	2.07	2.15	2.18	1.86	2.09		3.24	2.01	0.18	^{T}0.38	^{T}0.52
CAB	2.87	2.56	2.7	2.75			2.95	1.69	0.21	^{T}0.49	^{T}0.67

^{T} means Reml was used to generate the LSD

Note: When Reml LSD values were used the highest LSD from the table was selected.

Table 11-3: AtGA2ox7 EXP1

Promoter	a	b	c	d	e	f	Col-0	ga1-3	SED($_{ave}$)	LSD($_{5\%}$)	LSD($_{1\%}$)
SHR	3.431	3.643	3.261	3.199	3.145		3.547	2.238	0.1692	0.3491	0.4732
SCR	3.021	2.994	3.067	2.867	3.198		3.536	2.619	0.1334	0.2754	0.3732
CoR	2.391	2.087	2.255	2.176	2.395	2.197	3.121	2.218	0.1374	0.2814	0.3796
Co2	2.278	2.259	2.519	2.384	2.369	2.288	2.788	1.877	0.2102	0.4508	0.6256
GL2	3.761	3.249	3.177	2.888			3.529	2.5	0.1775	0.3702	0.505
CAB	1.886	2.967	3.704	3.482	3.28	3.23	3.712	2.535	0.1624	0.3326	0.4487

^{T} means REML was used to generate the LSD

Note: In order to be to be conservative when using REML LSD values, the highest LSD from the table was selected.

Table 11-4: AtGA3ox1 EXP1

Promoter	a	b	c	d	e	Col-0	ga1-3	ga3ox,1,2	SED($_{ave}$)	LSD($_{5\%}$)	LSD($_{1\%}$)
SHR	3.38	3.29	3.012	3.326	3.089	4.157	2.709	1.928	0.1908	^{T}0.4355	^{T}0.5876
SCR	3.184	3.248	3.175	2.629		3.948	2.728	1.595	0.2235	^{T}0.4835	^{T}0.6555
CoR	3.325	3.01	3.393	3.318	3.548	4.047	2.499	2.215	0.1809	^{T}0.4250	^{T}0.5737
Co2	3.432	2.966	2.998	3.511	3.128	3.883	2.479	2.054	0.1851	^{T}0.3963	^{T}0.5353
GL2	3.003	3.249	3.069	3.733	2.936	3.096	2.562	2.086	0.1982	^{T}0.4341	^{T}0.5866
CAB	2.07	3.036	3.512	2.529	2.115	3.459	2.282	1.763	0.2177	^{T}0.4761	^{T}0.6284

^{T} means REML was used to generate the LSD

Note: In order to be to be conservative when using REML LSD values, the highest LSD from the table was selected.

Table 11-5: AtGA20ox1 EXP1

Promoter	a	b	c	d	e	f	Col-0	ga1-3	ga20ox1	SED($_{ave}$)	LSD($_{5\%}$)	LSD($_{1\%}$)
SHR	2.276	2.184	2.15	1.827	1.829	1.411	4.072	2.899	2.521	0.1243	^{T}0.2880	^{T}0.3874
SCR	3.582	3.362	3.476	3.778	2.835	3.392	4.045	2.961	2.641	0.2298	^{T}0.4918	^{T}0.6618
CoR	1.342	1.338	1.45	2.103			3.741	2.289	2.337	0.2192	^{T}0.6591	^{T}0.8922
Co2	4.322	3.432	3.404	3.522	3.093	3.412	4.154	2.796	2.701	0.1934	0.394	0.5296
GL2	3.724	3.464	3.463	3.546	3.467	3.61	4.047	2.607	2.499	0.103	0.2097	0.2819
CAB	2.877	3.151	2.852	2.942	2.574	2.288	3.76	2.652	2.273	0.1671	0.3404	0.4577

^{T} means REML was used to generate the LSD

Note: In order to be to be conservative when using REML LSD values, the highest LSD from the table was selected.

Table 11-6: AtGID1a EXP1

Promoter	a	b	c	d	e	f	Col-0	gid1a,b,c	$SED_{(ave)}$	$LSD_{(5\%)}$	$LSD_{(1\%)}$
SHR	2.064	2.063	2.739	2.338	2.221		4.735	1.401	0.1964	$^{T}0.4111$	$^{T}0.5428$
SCR	2.931	2.674	2.166	2.742			3.542	1.085	0.2717	$^{T}0.5928$	$^{T}0.7981$
CoR	3.052	3.307	3.637	3.394	3.311	3.475	3.894	1.439	0.2549	$^{T}0.5404$	$^{T}0.7245$
Co2	1.46	1.656	1.36	1.533			4.317	1.199	0.1333	$^{T}0.2968$	$^{T}0.3923$
GL2	2.324	2.029	2.472	1.529	1.608	2.358	4.043	1.143	0.1859	0.3959	0.5297

T means REML was used to generate the LSD

Note: In order to be to be conservative when using REML LSD values, the highest LSD from the table was selected.

11.6 Statistics from secondary root characterisation; root length, meristem length, final cortical cell length.

Table 11-7: AtGA2ox2 EXP2

Promoter - SHR:AtGA2ox2	B	D	E	Col-0	ga1-3	$SED_{(ave)}$	$LSD_{(5\%)}$	$LSD_{(1\%)}$
Root length	4.394	4.15	3.875	4.2	3.243	$^{T}0.1427$	$^{T}0.2976$	$^{T}0.406$
Meristem length	432	423	400.2	441.2	285.6	16.38	34.73	47.85
Cell length	5.338	5.384	5.413	5.415	4.934	0.06072	0.1329	0.1811

Promoter - SCR:AtGA2ox2	A	C	F	Col-0	ga1-3	$SED_{(ave)}$	$LSD_{(5\%)}$	$LSD_{(1\%)}$
Root length	2.193	2.933	2.591	3.465	2.48	$^{T}0.1957$	$^{T}0.4149$	$^{T}0.5717$
Meristem length	281	296	272.6	413.8	270.4	22.99	48.74	67.15
Cell length	4.969	5.102	4.983	5.354	4.872	0.0588	0.1264	0.1724

Promoter - CoR:AtGA2ox2	B	C	D	Col-0	ga1-3	$SED_{(ave)}$	$LSD_{(5\%)}$	$LSD_{(1\%)}$
Root length	3.052	3.285	2.724	3.791	2.429	0.1472	0.2999	0.4032
Meristem length	375.2	373.4	371.2	384	256.4	17.62	37.35	51.46
Cell length	5.035	5.093	4.946	5.347	4.983	0.05689	0.1222	0.1666

Promoter - Co2:AtGA2ox2	A	B	C	Col-0	ga1-3	$SED_{(ave)}$	$LSD_{(5\%)}$	$LSD_{(1\%)}$
Root length	2.966	2.735	2.136	3.792	2.81	0.1518	0.3219	0.4435
Meristem length	328.2	329.6	295.2	460.2	321.4	13.05	27.66	38.11
Cell length	5.231	5.378	5.225	5.341	4.796	$^{T}0.06323$	$^{T}0.137$	$^{T}0.1871$

Promoter - GL2:AtGA2ox2	A	B	E	Col-0	ga1-3	$SED_{(ave)}$	$LSD_{(5\%)}$	$LSD_{(1\%)}$
Root length	2.201	2.248	2.091	3.546	1.807	0.1343	0.2848	0.3924
Meristem length	315.8	322.2	318	441.8	286.6	11.2	23.74	32.7
Cell length	5.179	5.175	5.125	5.242	4.718	0.06559	0.1496	0.2071

Promoter - CAB:AtGA2ox2	A	B	C	Col-0	ga1-3	$SED_{(ave)}$	$LSD_{(5\%)}$	$LSD_{(1\%)}$
Root length	2.755	3.232	2.968	3.21	2.017	0.1339	0.2838	0.3911
Meristem length	349.8	367.2	366	374.6	274	11.79	24.99	34.43
Cell length	5.284	5.22	5.226	5.272	4.802	0.0588	0.1247	0.1718

T means REML was used to generate the LSD

Note: In order to be to be conservative when using REML LSD values, the highest LSD from the table was selected.

Table 11-8: AtGA2ox7 EXP2

Promoter - SHR:AtGA2ox7	A	D	E	Col-0	ga1-3	$SED_{(ave)}$	$LSD_{(5\%)}$	$LSD_{(1\%)}$
Root length	3.55	3.35	3.24	3.54	2.28	0.12	0.25	0.34
Meristem length	5.92	5.90	5.93	5.96	5.53	0.04	0.09	0.13
Cell length	5.23	5.28	5.24	5.32	4.86	0.07	0.14	0.20

Promoter - SCR:AtGA2ox7	A	D	E	Col-0	ga1-3	$SED_{(ave)}$	$LSD_{(5\%)}$	$LSD_{(1\%)}$
Root length	3.31	3.37	3.42	3.93	2.41	0.16	0.34	0.46
Meristem length	5.78	5.80	5.76	5.89	5.53	0.03	0.06	0.08
Cell length	5.10	5.12	5.12	5.24	4.60	0.06	0.13	0.18

Promoter - CoR:AtGA2ox7	C	D	F	Col-0	ga1-3	$SED_{(ave)}$	$LSD_{(5\%)}$	$LSD_{(1\%)}$
Root length	3.24	3.24	2.88	4.06	2.47	0.13	0.28	0.39
Meristem length	5.85	5.81	5.84	5.83	5.44	0.02	0.05	0.07
Cell length	5.08	5.12	5.06	5.36	4.71	0.06	0.14	0.19

Promoter - Co2:AtGA2ox7	A	D	E	Col-0	ga1-3	$SED_{(ave)}$	$LSD_{(5\%)}$	$LSD_{(1\%)}$
Root length	3.41	3.16	3.08	4.27	2.54	0.31	0.66	0.91
Meristem length	5.61	5.62	5.58	5.84	5.43	0.04	0.08	0.11
Cell length	5.26	5.18	5.16	5.37	4.69	0.07	0.16	0.21

Promoter - GL2:AtGA2ox7	B	C	D	Col-0	ga1-3	$SED_{(ave)}$	$LSD_{(5\%)}$	$LSD_{(1\%)}$
Root length	3.22	3.16	2.79	3.61	2.37	0.25	0.54	0.74
Meristem length	5.70	5.70	5.67	5.89	5.57	0.08	0.17	0.23
Cell length	5.21	5.17	5.23	5.30	4.63	0.05	0.11	0.15

Promoter - CAB:AtGA2ox7	D	E	F	Col-0	ga1-3	$SED_{(ave)}$	$LSD_{(5\%)}$	$LSD_{(1\%)}$
Root length	3.96	3.60	3.63	4.13	2.66	0.17	0.37	0.51
Meristem length	5.81	5.84	5.79	5.86	5.56	0.05	0.10	0.13
Cell length	5.32	5.29	5.32	5.35	4.79	0.04	0.09	0.12

Table 11-9: AtGA20ox1 EXP2

Promoter - SHR:AtGA20ox1	A	B	C	Col-0	ga20ox1,2,3	$SED_{(ave)}$	$LSD_{(5\%)}$	$LSD_{(1\%)}$
Root length	2.60	2.57	2.76	3.63	2.76	0.24	0.50	0.69
Meristem length	255.80	256.80	265.80	368.20	257.20	10.01	21.22	29.24
Cell length	5.05	4.92	5.02	5.39	4.95	0.08	0.17	0.23

Promoter - SCR:AtGA20ox1	B	C	F	Col-0	ga20ox1,2,3	$SED_{(ave)}$	$LSD_{(5\%)}$	$LSD_{(1\%)}$
Root length	2.85	3.22	3.29	3.70	2.50	0.17	0.36	0.50
Meristem length	380.00	382.00	373.20	398.20	252.40	17.54	37.18	51.23
Cell length	5.19	5.25	5.23	5.34	4.95	0.05	0.11	0.15

Promoter - CoR:AtGA20ox1	B	C	D	Col-0	ga20ox1,2,3	$SED_{(ave)}$	$LSD_{(5\%)}$	$LSD_{(1\%)}$
Root length	2.95	3.47	3.06	4.49	3.21	0.18	0.39	0.53
Meristem length	262.00	272.20	262.40	353.40	266.20	6.74	14.29	19.69
Cell length	5.10	5.05	5.08	5.44	5.05	0.07	0.14	0.19

Promoter - Co2:AtGA20ox1	B	C	D	Col-0	ga20ox1,2,3	$SED_{(ave)}$	$LSD_{(5\%)}$	$LSD_{(1\%)}$
Root length	3.00	2.95	3.16	3.77	2.62	0.10	0.21	0.28
Meristem length	322.00	322.20	315.40	377.00	266.20	8.46	17.94	24.71
Cell length	5.15	5.20	5.06	5.38	5.00	0.05	0.10	0.14

Co2 X CoR AtGA20ox1	Co2xCoR	Co2-D	CoR-C	Col-0	ga20ox1,2,3	$SED_{(ave)}$	$LSD_{(5\%)}$	$LSD_{(1\%)}$
Root length	399.2	337.6	271.1	415.6	310.5	20.4	43.24	59.57
Meristem length	343.2	345.8	293.2	377	289.2	12.35	26.18	36.07
Cell length	198.5	181	142.2	209.6	149.9	8.35	17.71	24.4

Promoter - GL2:AtGA20ox1	B	C	D	Col-0	ga20ox1,2,3	$SED_{(ave)}$	$LSD_{(5\%)}$	$LSD_{(1\%)}$
Root length	3.18	3.01	3.15	3.54	2.18	0.12	0.26	0.35
Meristem length	324.20	332.60	346.80	372.60	267.00	11.01	23.34	32.15
Cell length	5.20	5.22	5.19	5.30	4.98	0.06	0.13	0.18

Promoter - CAB:20ox1	A	C	E	Col-0	ga20ox1,2,3	$SED_{(ave)}$	$LSD_{(5\%)}$	$LSD_{(1\%)}$
Root length	3.23	3.05	2.65	3.50	2.55	0.18	0.38	0.52
Meristem length	271.80	275.80	272.00	371.00	267.40	11.12	23.56	32.47
Cell length	5.22	5.07	5.09	5.35	5.03	0.07	0.15	0.20

Table 11-10: AtGA3ox1 EXP2

Promoter - SHR:AtGA3ox1	B	D	E	Col-0	ga3ox1,2	$SED_{(ave)}$	$LSD_{(5\%)}$	$LSD_{(1\%)}$
Root length	3.42	3.69	3.25	3.79	2.11	0.18	0.39	0.53
Meristem length	361.40	361.00	351.80	382.20	270.80	11.16	23.67	32.61
Cell length	194.60	202.00	192.50	196.60	150.40	10.15	21.51	29.64

Promoter - SCR:AtGA3ox1	A	C	D	Col-0	ga3ox1,2	$SED_{(ave)}$	$LSD_{(5\%)}$	$LSD_{(1\%)}$
Root length	2.91	3.17	2.51	3.37	1.58	0.29	0.61	0.84
Meristem length	359.60	357.40	302.60	387.40	260.20	14.71	31.19	42.97
Cell length	195.90	196.70	181.80	201.20	148.40	9.09	19.27	26.55

Promoter - CoR:AtGA3ox1	A	C	D	Col-0	ga3ox1,2	$SED_{(ave)}$	$LSD_{(5\%)}$	$LSD_{(1\%)}$
Root length	2.88	3.12	3.22	3.42	1.77	0.15	0.33	0.45
Meristem length	344.40	355.00	370.40	355.00	273.80	13.38	28.35	39.07
Cell length	214.20	201.60	198.40	200.80	151.10	13.07	27.70	38.16

Promoter - Co2:AtGA3ox1	A	d	E	Col-0	ga3ox1,2	$SED_{(ave)}$	$LSD_{(5\%)}$	$LSD_{(1\%)}$
Root length	3.30	2.58	3.53	3.88	2.32	0.19	0.41	0.56
Meristem length	326.40	330.80	350.20	357.40	239.40	15.83	33.55	46.22
Cell length	183.60	173.10	183.80	204.80	160.70	11.04	23.39	32.23

Promoter - GL2:AtGA3ox1	A	C	D	Col-0	ga3ox1,2	$SED_{(ave)}$	$LSD_{(5\%)}$	$LSD_{(1\%)}$
Root length	3.25	3.48	3.48	3.75	2.17	0.28	0.60	0.83
Meristem length	315.80	331.40	326.20	380.20	268.60	10.66	22.61	31.15
Cell length	177.60	181.60	176.00	210.10	147.30	9.43	19.99	27.54

Promoter - CAB:AtGA3ox1	A	C	D	Col-0	ga3ox1,2	$SED_{(ave)}$	$LSD_{(5\%)}$	$LSD_{(1\%)}$
Root length	2.96	3.18	3.25	3.66	1.93	0.22	0.22	0.65
Meristem length	318.80	316.80	325.00	393.00	259.80	11.52	24.43	33.65
Cell length	174.50	170.80	166.90	187.10	137.60	9.20	19.51	26.88

Table 11-11: Median lines EXP2

Effector - AtGA2ox2	SHR-E	SCR-F	CoR-B	Co2-B	GL2-A	CAB-C	Col-0	ga1-3	$SED_{(ave)}$	$LSD_{(5\%)}$	$LSD_{(1\%)}$
Root length	3.46	2.70	3.38	2.99	2.92	4.19	4.03	3.07	0.17	0.36	0.49
Meristem length	347.20	273.80	351.60	264.60	281.00	365.40	363.60	260.00	9.30	19.05	25.69
Cell length	5.25	5.10	4.99	5.36	5.27	5.28	5.24	4.95	0.06	0.12	0.17

Effector - AtGA2ox7	SHR-C	SCR-A	CoR-C	Co2-E	GL2-B	CAB-E	Col-0	ga1-3	$SED_{(ave)}$	$LSD_{(5\%)}$	$LSD_{(1\%)}$
Root length	3.58	3.08	3.14	3.21	3.15	3.48	3.75	2.72	0.20	0.41	0.55
Meristem length	5.94	5.82	5.91	5.78	5.80	5.94	5.98	5.59	0.04	0.07	0.10
Cell length	5.25	5.15	4.99	5.34	5.11	5.22	5.32	4.83	0.06	0.12	0.17

Effector - AtGA3ox1	SHR-B	SCR-C	CoR-D	Co2-E	GL2-C	CAB-D	Col-0	ga3ox1,2	$SED_{(ave)}$	$LSD_{(5\%)}$	$LSD_{(1\%)}$
Root length	3.45	3.45	3.24	2.60	3.27	2.88	3.71	1.77	0.25	0.50	0.67
Meristem length	353.60	374.60	328.60	350.20	331.60	289.20	381.20	263.40	16.86	34.54	46.59
Cell length	5.29	5.32	5.28	5.13	5.24	5.18	5.27	4.98	0.06	0.11	0.15

Effector - AtGA20ox1	SHR-D	SCR-B	CoR-C	Co2-D	GL2-D	CAB-E	Col-0	ga20ox1,2	$SED_{(ave)}$	$LSD_{(5\%)}$	$LSD_{(1\%)}$
Root length	2.68	3.82	2.55	3.37	3.26	3.28	3.80	2.64	0.22	0.44	0.59
Meristem length	269.40	378.40	263.40	331.00	332.20	259.80	393.40	262.20	10.78	22.07	29.78
Cell length	4.92	5.33	4.98	5.17	5.14	5.14	5.31	5.02	0.05	0.11	0.15

Effector - AtGID1a	SHR-D	SCR-D	CoR-C	Co2-D	GL2-B	Col-0	gid1a,	$SED_{(ave)}$	$LSD_{(5\%)}$	$LSD_{(1\%)}$
Root length	1.43	1.60	1.48	1.21	1.21	1.88	0.86	0.07	^{T}0.1567	^{T}0.211
Meristem length	229.70	286.80	211.30	202.50	205.30	336.70	166.80	15.84	32.35	43.56
Cell length	5.22	5.22	5.27	4.85	5.18	5.27	4.75	0.05	0.10	0.14

11.7 *In-silico* predictions of possible number if miRNAs

Table 12**: A computational prediction of the number of miRNAs likely to interfere with the expression of the GA metabolic genes used to generate transgenic lines.** The stringent filtering criteria had overlapping target sites and a miRNA candidate query overlap of > 15 nucleotides. (Accessed online 6/4/2011 from http://sundarlab.ucdavis.edu/mirna/).

Gene name	ATG code	Number of predicted miRNA stringent and relaxed criteria
AtGA3ox1	At1g15550	3-5
AtGA20ox1	At4g25420	5-6
AtGA2ox2	At1g30040	4-7
AtGA2ox7	At1g50960	0-3
AtGID1a	At3g05120	1-3

11.8 Extra comparison of tissues and YFP images

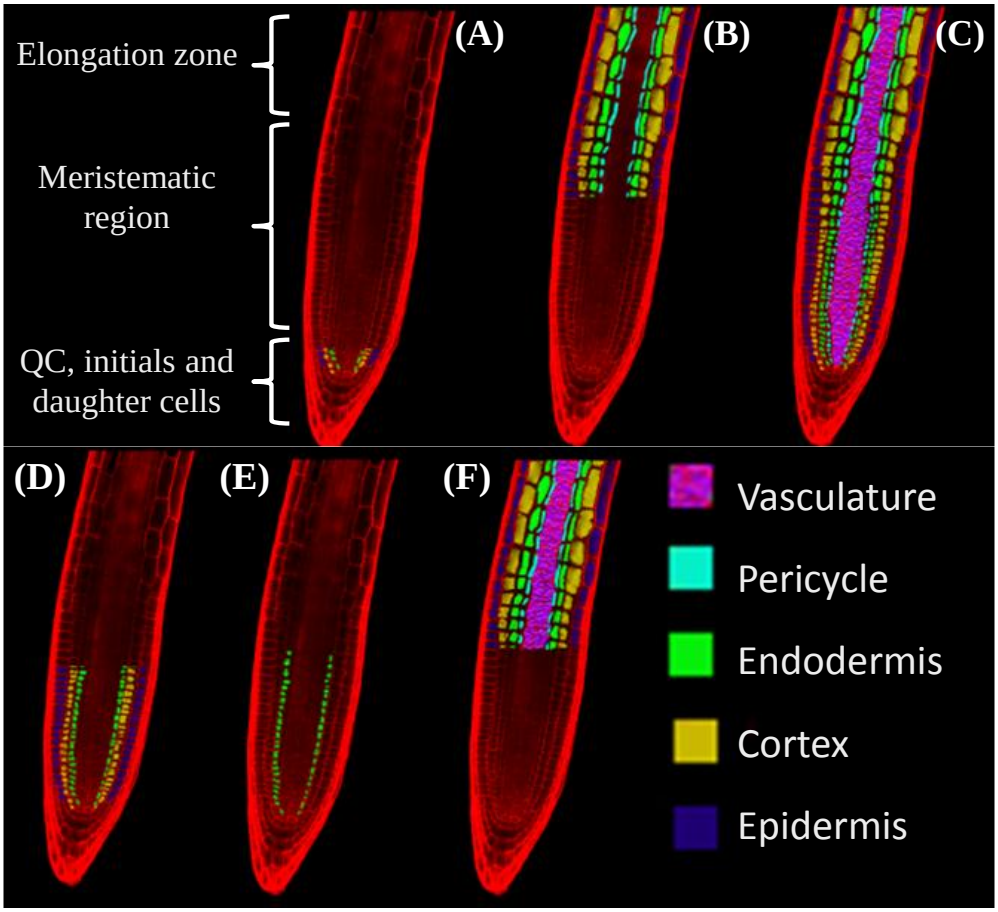

AtGA2ox2

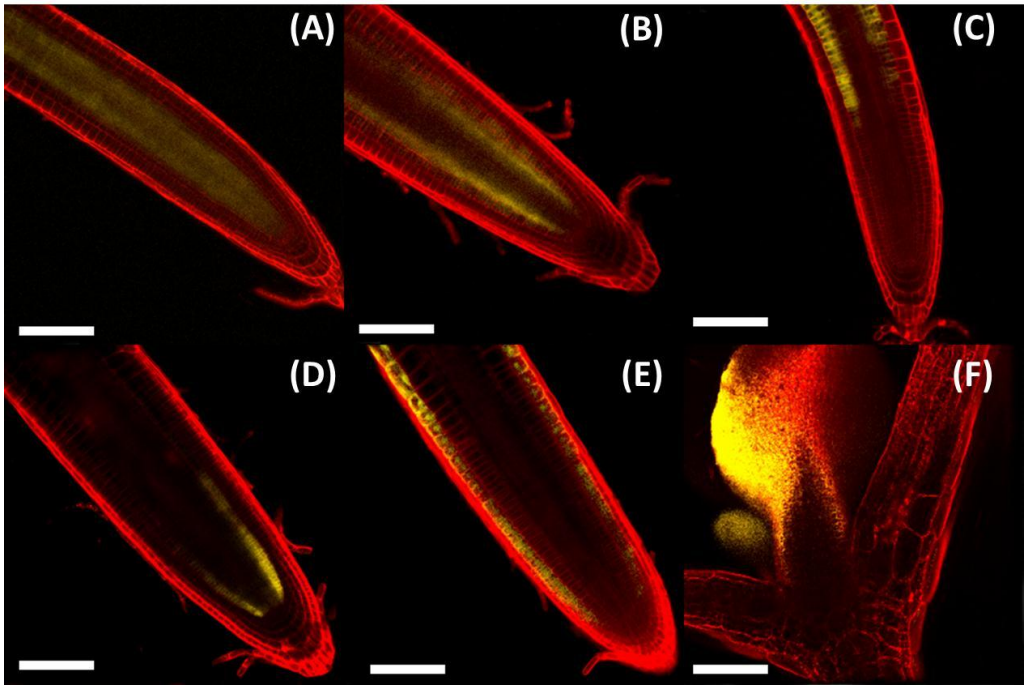

AtGA2ox7

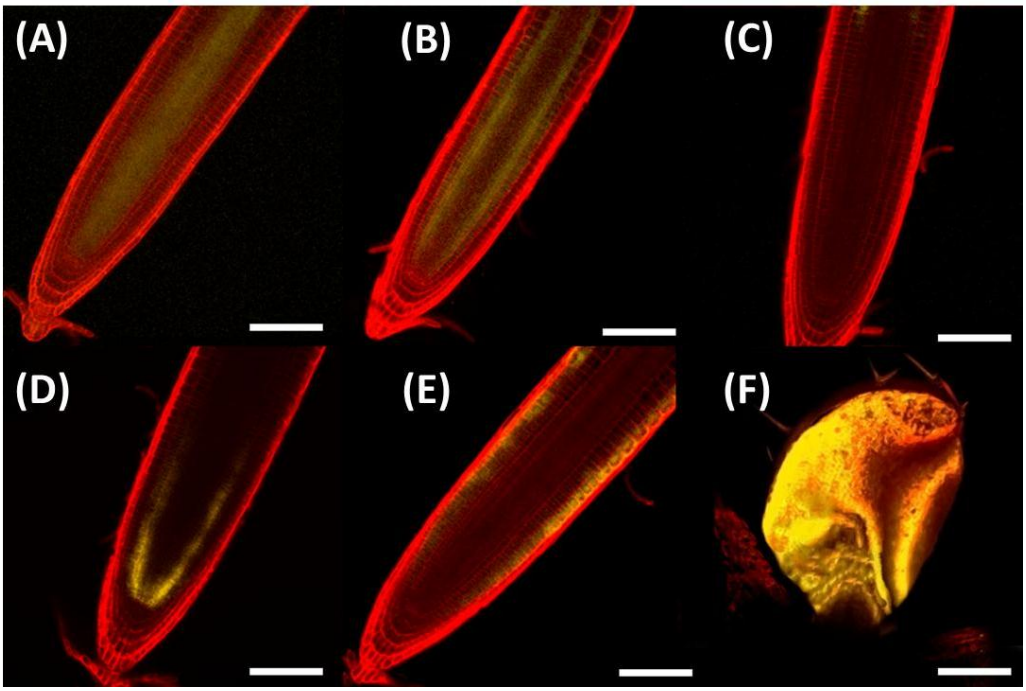

GA20ox1

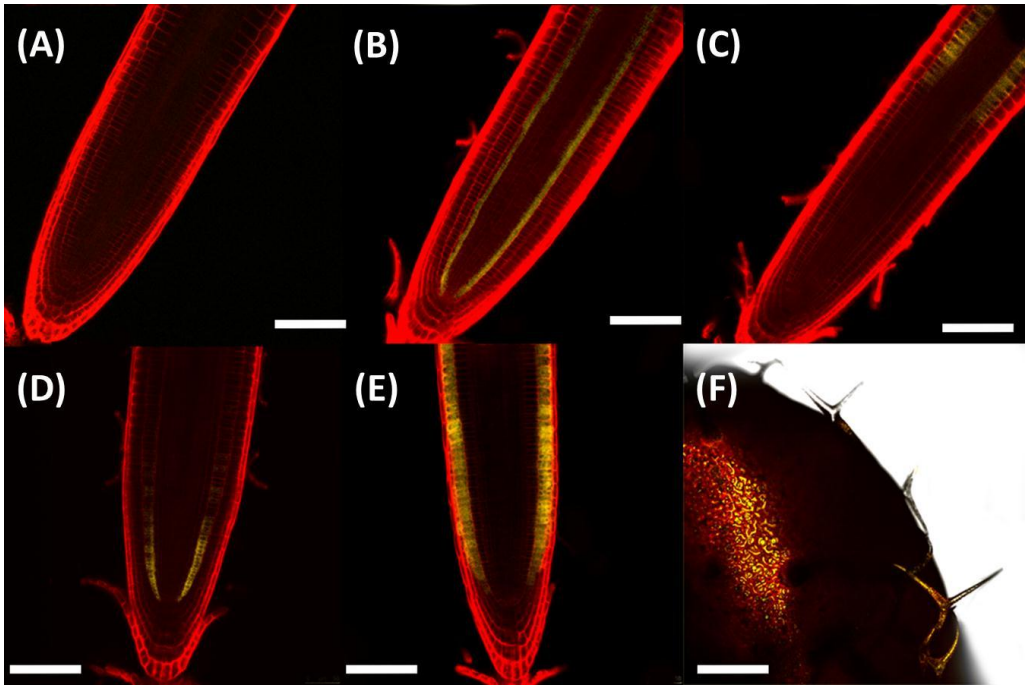

GA3ox1